



**EFFECT OF STEAM ENVIRONMENT ON CREEP BEHAVIOR OF
NEXTEL720/ALUMINA-MULLITE CERAMIC MATRIX
COMPOSITE AT ELEVATED TEMPERATURE**

THESIS

Tolga KUTSAL, First Lieutenant, TUAF

AFIT/GSS/ENY/09-M03

**DEPARTMENT OF THE AIR FORCE
AIR UNIVERSITY**

AIR FORCE INSTITUTE OF TECHNOLOGY

Wright-Patterson Air Force Base, Ohio

APPROVED FOR PUBLIC RELEASE; DISTRIBUTION UNLIMITED

The views expressed in this thesis are those of the author and do not reflect the official policy or position of the United States Air Force, Department of Defense, or the United States Government.

AFIT/GSS/ENY/09-M03

EFFECT OF STEAM ENVIRONMENT ON CREEP BEHAVIOR OF
NEXTEL720/ALUMINA-MULLITE CERAMIC MATRIX COMPOSITE
AT ELEVATED TEMPERATURE

THESIS

Presented to the Faculty

Department of Aeronautics and Astronautics

Graduate School of Engineering and Management

Air Force Institute of Technology

Air University

Air Education and Training Command

In Partial Fulfillment of the Requirements for the

Degree of Master of Science (Space Systems)

Tolga KUTSAL, B.S.

First Lieutenant, TUAF

March 2009

APPROVED FOR PUBLIC RELEASE; DISTRIBUTION UNLIMITED

AFIT/GSS/ENY/09-M03

EFFECT OF STEAM ENVIRONMENT ON CREEP BEHAVIOR OF
NEXTEL720/ALUMINA-MULLITE CERAMIC MATRIX COMPOSITE
AT ELEVATED TEMPERATURE

Tolga KUTSAL, B.S.

First Lieutenant, TUAF

Approved:

//signed//	13 Mar 09
_____ Dr. Marina B. Ruggles-Wrenn (Chairman)	_____ Date
//signed//	18 Mar 09
_____ Dr. Geoff E. Fair (Member)	_____ Date
//signed//	13 Mar 09
_____ Dr. Randall S. Hay (Member)	_____ Date

Abstract

The tensile creep behavior of an oxide-oxide ceramic matrix composite (CMC) was investigated at 1000 and 1100 °C in laboratory air and steam. The oxide-oxide CMC studied in this research was NextelTM720/alumina-mullite (N720/AM). The composite consists of N720 fibers with 0°/90° fiber orientation and a porous alumina-mullite matrix. There is no interface between fiber and matrix, and the material relies on porosity of matrix for damage tolerance.

Tensile-strain behavior was investigated and tensile properties were measured at 900, 1000 and 1100 °C. The effect of loading rate on tensile properties of N720/AM ceramic matrix composite at 1100 °C in steam was also examined and a strong dependence of tensile behavior on loading rate was observed. Creep-rupture tests were performed at 1100 °C in laboratory air and steam, and at 1000 °C only in steam. Creep run-out time was defined as 100 hours. Tests were performed at the creep stress levels of 109 and 131 MPa in laboratory air and stress levels of 87.5, 109 and 131 MPa in steam at 1100 °C. Creep run-out was achieved at both creep stresses conducted at 1100 °C in laboratory air. At 1100 °C in steam, creep run-out was achieved only at 87.5 MPa. At 1000 °C, tests were performed at the creep stress levels of 131 and 140 MPa only in steam and at both stress levels creep run-out was achieved. Retained strength properties were also measured for test specimens achieving creep run-out of 100 h. Presence of

steam caused larger creep strains and the higher stress levels decreased the creep life of the N720/AM ceramic matrix composite. After the mechanical tests, fracture surfaces of the failed specimens were examined using an optical microscope and a scanning electron microscope (SEM).

Acknowledgements

I would like to express my sincere appreciation to my faculty advisor, Dr. Marina Ruggles-Wrenn for her guidance throughout the course of this thesis effort. Her insight and support throughout this experience was greatly appreciated. I would like to thank Mr. Barry Paige, John Hixenbaugh and Chris Zickefoose for their help during the experimental process. I also would like to thank 1st Lt. Tufan Yeleser for his guidance during the orientation process and 1st Lt. Muzaffer Ozer for his companionship and most importantly, my wife for her unwavering support.

Tolga KUTSAL

Table of Contents

	Page
Abstract	iv
Acknowledgements	vi
Table of Contents	vii
List of Figures	ix
List of Tables	lxx
I. Introduction	1
II. Background and Applications	3
2.1 Ceramic Matrix Composites	3
2.2 Fibers	8
2.3 Matrix.....	11
2.4 Ceramic Matrix Composite Applications	12
2.5 Previous Research.....	16
2.6 Nextel™ 720/AM.....	18
2.7 Thesis Objective	20
III. Experimental Arrangements and Test Procedures	20
3.1 Testing Equipment	21
3.1.1 Mechanical Equipments.....	21
3.1.2 Environmental Equipments.....	23
3.1.3. Microstructural Characterization Equipments.....	26
3.2 Test Procedures	29
3.2.1 Temperature Calibration	29
3.2.2 Preparation Of Mechanical Testing	30
3.2.3 Monotonic Tensile Tests	33
3.2.4 Creep-Rupture Tests	33
3.2.5 Tensile Tests At Stress Rates 0.0025 And 25 Mpa/S.....	34
3.2.6 Microstructural Characterization.....	34
IV. Results and Analysis.....	36

4.1 Section Summary	36
4.2 Thermal Expansion	38
4.3 Monotonic Tension	40
4.4 Creep-Rupture	45
4.4.1 <i>Creep-Rupture Tests at 1100°C</i>	46
4.4.2 <i>Creep-Rupture Tests at 1000°C</i>	49
4.5 Effects of Temperature and Steam on Creep Rupture Behavior	52
4.6 Retained Tensile Properties	61
4.7 Microstructural Analysis	63
4.7.1 <i>Optical Microscopy Analysis</i>	63
4.7.2 <i>Scanning Electron Microscopy Analysis</i>	68
V. Conclusions	78
Appendix. Additional Micrographs	81
Bibliography	351
Vita	354

List of Figures

Figure	Page
Figure 1. Maximum Material Service Temperatures [3].	2
Figure 2. Failure of CMC as a function of interfacial bond strength.....	6
Figure 3. Typical stress strain curve for CMC with weak interface [8].	7
Figure 4. The classification of fibers [4].....	9
Figure 5. As-processed N720/A composite a) overview, optical microscope and b) porous nature of the matrix is evident [13].	11
Figure 6. Potential applications of CMCs [14].	14
Figure 7. Ratio of strength to weight as a function of temperature [15].....	16
Figure 8. Low magnification views showing dramatic difference between	19
Figure 9. MTS 810 Test Station.....	21
Figure 10. NESLAB Model HX-75 Chiller.....	22
Figure 11. Mechanical Test System.....	23
Figure 12. Heating Equipment: (a) AMTECO Hot-Rail Furnace.....	24
Figure 13. MTS Model 409.83B Temperature Controller.....	25
Figure 14. Susceptor a) front view and b) rear view.....	26
Figure 15. Zeiss Discovery V12 Optical Microscope.....	27
Figure 16. FEI FP 2011/11 Quanta 200 3D HV Scanning Electron Microscope.	28
Figure 17. Temperature Calibration Specimen.	29
Figure 18. Omega Engineering, Inc, OMNI-CAL-8A-110	30

Figure	Page
Figure 19. Uniaxial test specimen (dimensions in mm) [18].....	31
Figure 20. Mitutoyo Corporation Digital Micrometer	32
Figure 21. Tabbed Test Specimen.	32
Figure 22. Typical tensile test procedure.....	33
Figure 23. Typical creep test procedure.....	34
Figure 24. CNC Saw.	35
Figure 25. (a) SPI Carbon Coating Machine (b) Carbon-coated failed specimens in the storage box.	36
Figure 26. Tensile stress-strain curves for N720/AM composite obtained	41
Figure 27. Tensile stress vs. strain curves for the N720/AM with constant loading rates of 25 and 0.0025 MPa/s at 1100°C in steam. Effect of loading rate on stress-strain behavior and strength properties is evident.....	43
Figure 28. Creep strain vs. time curves for N720/AM composite at 1100°C in air and steam. Stress levels adjusted for $V_f = 0.44$ are shown in parentheses.....	48
Figure 29. Creep strain vs. time curves for N720/A composite at 1100°C in air and steam. Data from reference [18].....	49
Figure 30. Creep strain vs. time curves for the N720/AM ceramic matrix composite at 1000°C. Stress levels adjusted for $V_f = 0.44$ are shown in parentheses.....	51
Figure 31. Creep strain vs. time curves for the N720/A ceramic matrix composite at 1000°C. Data from reference [18].....	51

Figure	Page
Figure 32. Creep strain vs. time curves for N720/AM ceramic matrix composite at 1100 and 1200°C in laboratory air. Time scale is reduced to clearly show the creep curve at 150MPa. Data at 1200°C from Genelin [16]. Stress levels adjusted for $V_f = 0.44$ are shown in parentheses.....	53
Figure 33. Creep strain vs. time curves for N720/AM ceramic matrix composite at 1000, 1100 and 1200°C in steam. Data at 1200°C from Genelin [16]. Stress levels adjusted for $V_f = 0.44$ are shown in parentheses.	55
Figure 34. Creep strain vs. time curves for N720/A and N720/AM ceramic matrix composites at 150 MPa creep stress level at 1100°C. Stress level adjusted for $V_f = 0.44$ is shown in parentheses. Data for N720/A from reference [18].	57
Figure 35. Minimum creep rate as a function of applied stress for N720/AM.....	58
Figure 36. Minimum creep rate as a function of applied stress for N720/A	59
Figure 37. Creep stress vs. time to rupture for N720/AM ceramic matrix composite.....	60
Figure 38. Effect of prior creep on tensile stress-strain	62
Figure 39. Fracture surfaces of the N720/AM specimens tested in tension to failure in air at: (a) 900 (b) 1000 and (c) 1100°C and (d) 1200°C. Micrograph at 1200°C obtained from Genelin [22].....	64
Figure 40. Fracture surfaces of the N720/AM specimens obtained in creep tests at 1100°C in air at: (a-b) 131MPa (equivalent to 150 MPa for $V_f = 0.44$), $t_f = > 100$ h and (c-d) 109 MPa (equivalent to 125 MPa for $V_f = 0.44$), $t_f = > 100$ h.	65

Figure	Page
Figure 41. Fracture surfaces of the N720/AM specimens obtained in creep tests at 1100°C in steam at: (a-b) 87.5MPa (equivalent to 100 MPa for $V_f = 0.44$), $t_f = >100$ h and (c-d) 109 MPa (equivalent to 125 MPa for $V_f = 0.44$), $t_f = 35.2$ h (e-f) 131 MPa (equivalent to 150 MPa for $V_f = 0.44$), $t_f = 4.12$.	66
Figure 42. Fracture surfaces of the N720/AM specimens obtained in creep tests in steam at (a-b) 131 MPa (equivalent to 150 MPa for $V_f = 0.44$), $t_f = > 100$ h at 1000°C and (b) 131 MPa (equivalent to 150 MPa for $V_f = 0.44$), $t_f = 4.12$ h at 1100°C (c) 136 MPa (equivalent to 150 MPa for $V_f = 0.44$), $t_f = 0.012$ h at 1200°C in steam. Micrographs of the specimen tested in 1200°C from Genelin [16].	67
Figure 43. Fracture surfaces of the N720/AM specimens subjected to tensile test to failure in steam at 1100°C with the constant loading rates of: (a-b) 25 MPa/s, $t_f = 0.0017$ h and (c-d) 0.0025 MPa/s, $t_f = 10.38$ h.	68
Figure 44. Fracture surface of the N720/AM specimens tested in tension to failure	69
Figure 45. Fracture surfaces of specimens tested in tension to failure with displacement control at various magnifications in air at a) 1100°C b) 1000°C and (c-d) 900°C	71
Figure 46. Fracture surfaces of the N720/AM specimens obtained in creep tests at 1100°C in steam at: (a-b) 131MPa (c-d) 109 MPa	72
Figure 47. Detailed fracture surfaces of N720/AM specimens subjected to creep	73
Figure 48. Fracture surfaces of the N720/AM specimens subjected to creep	75

Figure	Page
Figure 49. Fracture surface of N720/A specimen subjected tensile to failure at 1100°C in steam with the constant loading rates of: (a-b-c) 25MPa/s and (d-e-f) 0.0025 MPa/s	77
Figure 50. Fracture surface of the N720/AM specimen tested in tension to failure at 900°C in laboratory air	81
Figure 51. Fracture surface of the N720/AM specimen tested in tension to failure at 900°C in laboratory air	81
Figure 52. Fracture surface of the N720/AM specimen tested in tension to failure at 900°C in laboratory air	82
Figure 53. Fracture surface of the N720/AM specimen tested in tension to failure at 900°C in laboratory air	82
Figure 54. Fracture surface of the N720/AM specimen tested in tension to failure at 900°C in laboratory air	83
Figure 55. Fracture surface of the N720/AM specimen tested in tension to failure at 900°C in laboratory air	83
Figure 56. Fracture surface of the N720/AM specimen tested in tension to failure at 900°C in laboratory air	84
Figure 57. Fracture surface of the N720/AM specimen tested in tension to failure at 900°C in laboratory air	84
Figure 58. . Fracture surface of the N720/AM specimen tested in tension to failure at 900°C in laboratory air	85

Figure	Page
Figure 59. Fracture surface of the N720/AM specimen tested in tension to failure at 900°C in laboratory air	85
Figure 60. Fracture surface of the N720/AM specimen tested in tension to failure at 900°C in laboratory air	86
Figure 61. Fracture surface of the N720/AM specimen tested in tension to failure at 900°C in laboratory air	86
Figure 62. Fracture surface of the N720/AM specimen tested in tension to failure at 900°C in laboratory air	87
Figure 63. Fracture surface of the N720/AM specimen tested in tension to failure at 900°C in laboratory air	87
Figure 64. Fracture surface of the N720/AM specimen tested in tension to failure at 900°C in laboratory air	88
Figure 65. Fracture surface of the N720/AM specimen tested in tension to failure at 900°C in laboratory air	88
Figure 66. Fracture surface of the N720/AM specimen tested in tension to failure at 900°C in laboratory air	89
Figure 67. Fracture surface of the N720/AM specimen tested in tension to failure at 900°C in laboratory air	89
Figure 68. Fracture surface of the N720/AM specimen tested in tension to failure at 900°C in laboratory air	90

Figure	Page
Figure 69. Fracture surface of the N720/AM specimen tested in tension to failure at 900°C in laboratory air.....	90
Figure 70. Fracture surface of the N720/AM specimen tested in tension to failure at 900°C in laboratory air.....	91
Figure 71. Fracture surface of the N720/AM specimen tested in tension to failure at 1000°C in laboratory air.....	91
Figure 72. Fracture surface of the N720/AM specimen tested in tension to failure at 1000°C in laboratory air.....	92
Figure 73. Fracture surface of the N720/AM specimen tested in tension to failure at 1000°C in laboratory air.....	92
Figure 74. Fracture surface of the N720/AM specimen tested in tension to failure at 1000°C in laboratory air.....	93
Figure 75. Fracture surface of the N720/AM specimen tested in tension to failure at 1000°C in laboratory air.....	93
Figure 76. Fracture surface of the N720/AM specimen tested in tension to failure at 1000°C in laboratory air.....	94
Figure 77. Fracture surface of the N720/AM specimen tested in tension to failure at 1000°C in laboratory air.....	94
Figure 78. Fracture surface of the N720/AM specimen tested in tension to failure at 1000°C in laboratory air.....	95

Figure	Page
Figure 79. Fracture surface of the N720/AM specimen tested in tension to failure at 1000°C in laboratory air.....	95
Figure 80. Fracture surface of the N720/AM specimen tested in tension to failure at 1000°C in laboratory air.....	96
Figure 81. Fracture surface of the N720/AM specimen tested in tension to failure at 1000°C in laboratory air.....	96
Figure 82. Fracture surface of the N720/AM specimen tested in tension to failure at 1000°C in laboratory air.....	97
Figure 83. Fracture surface of the N720/AM specimen tested in tension to failure at 1000°C in laboratory air.....	97
Figure 84. Fracture surface of the N720/AM specimen tested in tension to failure at 1000°C in laboratory air.....	98
Figure 85. Fracture surface of the N720/AM specimen tested in tension to failure at 1000°C in laboratory air.....	98
Figure 86. Fracture surface of the N720/AM specimen tested in tension to failure at 1000°C in laboratory air.....	99
Figure 87. Fracture surface of the N720/AM specimen tested in tension to failure at 1000°C in laboratory air.....	99
Figure 88. Fracture surface of the N720/AM specimen tested in tension to failure at 1000°C in laboratory air.....	100

Figure	Page
Figure 89. Fracture surface of the N720/AM specimen tested in tension to failure at 1000°C in laboratory air.....	100
Figure 90. Fracture surface of the N720/AM specimen tested in tension to failure at 1000°C in laboratory air.....	101
Figure 91. Fracture surface of the N720/AM specimen tested in tension to failure at 1000°C in laboratory air.....	101
Figure 92. Fracture surface of the N720/AM specimen tested in tension to failure at 1000°C in laboratory air.....	102
Figure 93. Fracture surface of the N720/AM specimen tested in tension to failure at 1000°C in laboratory air.....	102
Figure 94. Fracture surface of the N720/AM specimen tested in tension to failure at 1000°C in laboratory air.....	103
Figure 95. Fracture surface of the N720/AM specimen tested in tension to failure at 1000°C in laboratory air.....	103
Figure 96. Fracture surface of the N720/AM specimen tested in tension to failure at 1000°C in laboratory air.....	104
Figure 97. Fracture surface of the N720/AM specimen tested in tension to failure at 1000°C in laboratory air.....	104
Figure 98. Fracture surface of the N720/AM specimen tested in tension to failure at 1000°C in laboratory air.....	105

Figure	Page
Figure 99. Fracture surface of the N720/AM specimen tested in tension to failure at 1000°C in laboratory air.....	105
Figure 100. Fracture surface of the N720/AM specimen tested in tension to failure at 1000°C in laboratory air.....	106
Figure 101. Fracture surface of the N720/AM specimen tested in tension to failure at 1000°C in laboratory air.....	106
Figure 102. Fracture surface of the N720/AM specimen tested in tension to failure at 1000°C in laboratory air.....	107
Figure 103. Fracture surface of the N720/AM specimen tested in tension to failure at 1100°C in laboratory air.....	107
Figure 104. Fracture surface of the N720/AM specimen tested in tension to failure at 1100°C in laboratory air.....	108
Figure 105. Fracture surface of the N720/AM specimen tested in tension to failure at 1000°C in laboratory air.....	108
Figure 106. Fracture surface of the N720/AM specimen tested in tension to failure at 1000°C in laboratory air.....	109
Figure 107. Fracture surface of the N720/AM specimen tested in tension to failure at 1000°C in laboratory air.....	109
Figure 108. . Fracture surface of the N720/AM specimen tested in tension to failure at 1000°C in laboratory air.....	110

Figure	Page
Figure 109. Fracture surface of the N720/AM specimen tested in tension to failure at 1100°C in laboratory air.....	110
Figure 110. Fracture surface of the N720/AM specimen tested in tension to failure at 1100°C in laboratory air.....	111
Figure 111. Fracture surface of the N720/AM specimen tested in tension to failure at 1100°C in laboratory air.....	111
Figure 112. Fracture surface of the N720/AM specimen tested in tension to failure at 1100°C in laboratory air.....	112
Figure 113. Fracture surface of the N720/AM specimen tested in tension to failure at 1100°C in laboratory air.....	112
Figure 114. Fracture surface of the N720/AM specimen tested in tension to failure at 1100°C in laboratory air.....	113
Figure 115. Fracture surface of the N720/AM specimen tested in tension to failure at 1100°C in laboratory air.....	113
Figure 116. Fracture surface of the N720/AM specimen tested in tension to failure at 1100°C in laboratory air.....	114
Figure 117. Fracture surface of the N720/AM specimen tested in tension to failure at 1100°C in laboratory air.....	114
Figure 118. Fracture surface of the N720/AM specimen tested in tension to failure at 1100°C in laboratory air.....	115

Figure	Page
Figure 119. Fracture surface of the N720/AM specimen tested in tension to failure at 1100°C in laboratory air.....	115
Figure 120. Fracture surface of the N720/AM specimen tested in tension to failure at 1100°C in laboratory air.....	116
Figure 121. Fracture surface of the N720/AM specimen tested in tension to failure at 1100°C in laboratory air.....	116
Figure 122. Fracture surface of the N720/AM specimen tested in tension to failure at 1100°C in laboratory air.....	117
Figure 123. Fracture surface of the N720/AM specimen tested in tension to failure at 1100°C in laboratory air.....	117
Figure 124. Fracture surface of the N720/AM specimen tested in tension to failure at 1100°C in laboratory air.....	118
Figure 125. Fracture surface of the N720/AM specimen tested in tension to failure at 1100°C in laboratory air.....	118
Figure 126. Fracture surface of the N720/AM specimen tested in tension to failure at 1000°C in laboratory air.....	119
Figure 127. Fracture surface of the N720/AM specimen tested in tension to failure at 1000°C in laboratory air.....	119
Figure 128. Fracture surface of the N720/AM specimen tested in tension to failure at 1000°C in laboratory air.....	120

Figure	Page
Figure 129. Fracture surface of the N720/AM specimen tested in tension to failure at 1000°C in laboratory air.....	120
Figure 130. Fracture surface of the N720/AM specimen tested in tension to failure at 1000°C in laboratory air.....	121
Figure 131. Fracture surface of the N720/AM specimen tested in tension to failure at 1000°C in laboratory air.....	121
Figure 132. Fracture surface of the N720/AM specimen tested in tension to failure at 1000°C in laboratory air.....	122
Figure 133. Fracture surface of the N720/AM specimen tested in tension to failure at 1000°C in laboratory air.....	122
Figure 134. Fracture surface of the N720/AM specimen tested in tension to failure at 1100°C in laboratory air.....	123
Figure 135. Fracture surface of the N720/AM specimen tested in tension to failure with constant loading rate of 25MPa at 1100°C in steam.	123
Figure 136. Fracture surface of the N720/AM specimen tested in tension to failure with constant loading rate of 25MPa at 1100°C in steam.	124
Figure 137. Fracture surface of the N720/AM specimen tested in tension to failure with constant loading rate of 25MPa at 1100°C in steam.	124
Figure 138. Fracture surface of the N720/AM specimen tested in tension to failure with constant loading rate of 25MPa at 1100°C in steam.	125

Figure	Page
Figure 139. Fracture surface of the N720/AM specimen tested in tension to failure with constant loading rate of 25MPa at 1100°C in steam.	125
Figure 140. Fracture surface of the N720/AM specimen tested in tension to failure with constant loading rate of 25MPa at 1100°C in steam.	126
Figure 141. Fracture surface of the N720/AM specimen tested in tension to failure with constant loading rate of 25MPa at 1100°C in steam.	126
Figure 142. Fracture surface of the N720/AM specimen tested in tension to failure with constant loading rate of 25MPa at 1100°C in steam.	127
Figure 143. Fracture surface of the N720/AM specimen tested in tension to failure with constant loading rate of 25MPa at 1100°C in steam.	127
Figure 144. Fracture surface of the N720/AM specimen tested in tension to failure with constant loading rate of 25MPa at 1100°C in steam.	128
Figure 145. Fracture surface of the N720/AM specimen tested in tension to failure with constant loading rate of 25MPa at 1100°C in steam.	128
Figure 146. Fracture surface of the N720/AM specimen tested in tension to failure with constant loading rate of 25MPa at 1100°C in steam.	129
Figure 147. Fracture surface of the N720/AM specimen tested in tension to failure with constant loading rate of 25MPa at 1100°C in steam.	129
Figure 148. Fracture surface of the N720/AM specimen tested in tension to failure with constant loading rate of 25MPa at 1100°C in steam.	130

Figure	Page
Figure 149. Fracture surface of the N720/AM specimen tested in tension to failure with constant loading rate of 25MPa at 1100°C in steam.	130
Figure 150. Fracture surface of the N720/AM specimen tested in tension to failure with constant loading rate of 25MPa at 1100°C in steam.	131
Figure 151. Fracture surface of the N720/AM specimen tested in tension to failure with constant loading rate of 25MPa at 1100°C in steam.	131
Figure 152. Fracture surface of the N720/AM specimen tested in tension to failure with constant loading rate of 25MPa at 1100°C in steam.	132
Figure 153. Fracture surface of the N720/AM specimen tested in tension to failure with constant loading rate of 25MPa at 1100°C in steam.	132
Figure 154. Fracture surface of the N720/AM specimen tested in tension to failure with constant loading rate of 25MPa at 1100°C in steam.	133
Figure 155. Fracture surface of the N720/AM specimen tested in tension to failure with constant loading rate of 25MPa at 1100°C in steam.	133
Figure 156. Fracture surface of the N720/AM specimen tested in tension to failure with constant loading rate of 25MPa at 1100°C in steam.	134
Figure 157. Fracture surface of the N720/AM specimen tested in tension to failure with constant loading rate of 25MPa at 1100°C in steam.	134
Figure 158. Fracture surface of the N720/AM specimen tested in tension to failure with constant loading rate of 25MPa at 1100°C in steam.	135

Figure	Page
Figure 159. Fracture surface of the N720/AM specimen tested in tension to failure with constant loading rate of 25MPa at 1100°C in steam.	135
Figure 160. Fracture surface of the N720/AM specimen tested in tension to failure with constant loading rate of 25MPa at 1100°C in steam.	136
Figure 161. Fracture surface of the N720/AM specimen tested in tension to failure with constant loading rate of 25MPa at 1100°C in steam.	136
Figure 162. Fracture surface of the N720/AM specimen tested in tension to failure with constant loading rate of 25MPa at 1100°C in steam.	137
Figure 163. Fracture surface of the N720/AM specimen tested in tension to failure with constant loading rate of 25MPa at 1100°C in steam.	137
Figure 164. Fracture surface of the N720/AM specimen tested in tension to failure with constant loading rate of 25MPa at 1100°C in steam.	138
Figure 165. Fracture surface of the N720/AM specimen tested in tension to failure with constant loading rate of 25MPa at 1100°C in steam.	138
Figure 166. Fracture surface of the N720/AM specimen tested in tension to failure with constant loading rate of 25MPa at 1100°C in steam.	139
Figure 167. Fracture surface of the N720/AM specimen tested in tension to failure with constant loading rate of 25MPa at 1100°C in steam.	139
Figure 168. Fracture surface of the N720/AM specimen tested in tension to failure with constant loading rate of 25MPa at 1100°C in steam.	140

Figure	Page
Figure 169. Fracture surface of the N720/AM specimen tested in tension to failure with constant loading rate of 25MPa at 1100°C in steam.	140
Figure 170. Fracture surface of the N720/AM specimen tested in tension to failure with constant loading rate of 25MPa at 1100°C in steam.	141
Figure 171. Fracture surface of the N720/AM specimen tested in tension to failure with constant loading rate of 25MPa at 1100°C in steam.	141
Figure 172. Fracture surface of the N720/AM specimen tested in tension to failure with constant loading rate of 25MPa at 1100°C in steam.	142
Figure 173. Fracture surface of the N720/AM specimen tested in tension to failure with constant loading rate of 25MPa at 1100°C in steam.	142
Figure 174. Fracture surface of the N720/AM specimen tested in tension to failure with constant loading rate of 25MPa at 1100°C in steam.	143
Figure 175. Fracture surface of the N720/AM specimen tested in tension to failure with constant loading rate of 25MPa at 1100°C in steam.	143
Figure 176. Fracture surface of the N720/AM specimen tested in tension to failure with constant loading rate of 25MPa at 1100°C in steam.	144
Figure 177. Fracture surface of the N720/AM specimen tested in tension to failure with constant loading rate of 25MPa at 1100°C in steam.	144
Figure 178. Fracture surface of the N720/AM specimen tested in tension to failure with constant loading rate of 25MPa at 1100°C in steam.	145

Figure	Page
Figure 179. Fracture surface of the N720/AM specimen tested in tension to failure with constant loading rate of 25MPa at 1100°C in steam.	145
Figure 180. Fracture surface of the N720/AM specimen tested in tension to failure with constant loading rate of 25MPa at 1100°C in steam.	146
Figure 181. Fracture surface of the N720/AM specimen tested in tension to failure with constant loading rate of 25MPa at 1100°C in steam.	146
Figure 182. Fracture surface of the N720/AM specimen tested in tension to failure with constant loading rate of 25MPa at 1100°C in steam.	147
Figure 183. Fracture surface of the N720/AM specimen tested in tension to failure with constant loading rate of 25MPa at 1100°C in steam.	147
Figure 184. Fracture surface of the N720/AM specimen tested in tension to failure with constant loading rate of 25MPa at 1100°C in steam.	148
Figure 185. Fracture surface of the N720/AM specimen tested in tension to failure with constant loading rate of 25MPa at 1100°C in steam.	148
Figure 186. Fracture surface of the N720/AM specimen tested in tension to failure with constant loading rate of 25MPa at 1100°C in steam.	149
Figure 187. Fracture surface of the N720/AM specimen tested in tension to failure with constant loading rate of 0.0025MPa at 1100°C in steam.	149
Figure 188. Fracture surface of the N720/AM specimen tested in tension to failure with constant loading rate of 0.0025MPa at 1100°C in steam.	150

Figure	Page
Figure 189 Fracture surface of the N720/AM specimen tested in tension to failure with constant loading rate of 0.0025MPa at 1100°C in steam.	150
Figure 190 Fracture surface of the N720/AM specimen tested in tension to failure with constant loading rate of 0.0025MPa at 1100°C in steam.	151
Figure 191 Fracture surface of the N720/AM specimen tested in tension to failure with constant loading rate of 0.0025MPa at 1100°C in steam.	151
Figure 192 Fracture surface of the N720/AM specimen tested in tension to failure with constant loading rate of 0.0025MPa at 1100°C in steam.	152
Figure 193 Fracture surface of the N720/AM specimen tested in tension to failure with constant loading rate of 0.0025MPa at 1100°C in steam.	152
Figure 194 Fracture surface of the N720/AM specimen tested in tension to failure with constant loading rate of 0.0025MPa at 1100°C in steam.	153
Figure 195 Fracture surface of the N720/AM specimen tested in tension to failure with constant loading rate of 0.0025MPa at 1100°C in steam.	153
Figure 196. Fracture surface of the N720/AM specimen tested in tension to failure with constant loading rate of 0.0025MPa at 1100°C in steam.	154
Figure 197. Fracture surface of the N720/AM specimen tested in tension to failure with constant loading rate of 0.0025MPa at 1100°C in steam.	155
Figure 198. Fracture surface of the N720/AM specimen tested in tension to failure with constant loading rate of 0.0025MPa at 1100°C in steam.	155

Figure	Page
Figure 199. Fracture surface of the N720/AM specimen tested in tension to failure with constant loading rate of 0.0025MPa at 1100°C in steam.	156
Figure 200. Fracture surface of the N720/AM specimen tested in tension to failure with constant loading rate of 0.0025MPa at 1100°C in steam.	156
Figure 201. Fracture surface of the N720/AM specimen tested in creep at 109 MPa in laboratory air at 1100°C.	157
Figure 202. Fracture surface of the N720/AM specimen tested in creep at 109 MPa in laboratory air at 1100°C.	157
Figure 203. Fracture surface of the N720/AM specimen tested in creep at 109 MPa in laboratory air at 1100°C.	158
Figure 204. Fracture surface of the N720/AM specimen tested in creep at 109 MPa in laboratory air at 1100°C.	158
Figure 205. Fracture surface of the N720/AM specimen tested in creep at 109 MPa in laboratory air at 1100°C.	159
Figure 206. Fracture surface of the N720/AM specimen tested in creep at 109 MPa in laboratory air at 1100°C.	159
Figure 207. Fracture surface of the N720/AM specimen tested in creep at 109 MPa in laboratory air at 1100°C.	160
Figure 208. Fracture surface of the N720/AM specimen tested in creep at 109 MPa in laboratory air at 1100°C.	160

Figure	Page
Figure 209. Fracture surface of the N720/AM specimen tested in creep at 109 MPa in laboratory air at 1100°C.....	161
Figure 210. Fracture surface of the N720/AM specimen tested in creep at 109 MPa in laboratory air at 1100°C.....	161
Figure 211. Fracture surface of the N720/AM specimen tested in creep at 109 MPa in laboratory air at 1100°C.....	162
Figure 212. Fracture surface of the N720/AM specimen tested in creep at 109 MPa in laboratory air at 1100°C.....	162
Figure 213. Fracture surface of the N720/AM specimen tested in creep at 109 MPa in laboratory air at 1100°C.....	163
Figure 214. Fracture surface of the N720/AM specimen tested in creep at 109 MPa in laboratory air at 1100°C.....	163
Figure 215. Fracture surface of the N720/AM specimen tested in creep at 109 MPa in laboratory air at 1100°C.....	164
Figure 216. Fracture surface of the N720/AM specimen tested in creep at 109 MPa in laboratory air at 1100°C.....	164
Figure 217. Fracture surface of the N720/AM specimen tested in creep at 109 MPa in laboratory air at 1100°C.....	165
Figure 218. Fracture surface of the N720/AM specimen tested in creep at 109 MPa in laboratory air at 1100°C.....	165

Figure	Page
Figure 219. Fracture surface of the N720/AM specimen tested in creep at 109 MPa in laboratory air at 1100°C.....	166
Figure 220. Fracture surface of the N720/AM specimen tested in creep at 109 MPa in laboratory air at 1100°C.....	166
Figure 221. Fracture surface of the N720/AM specimen tested in creep at 109 MPa in laboratory air at 1100°C.....	167
Figure 222. Fracture surface of the N720/AM specimen tested in creep at 109 MPa in laboratory air at 1100°C.....	167
Figure 223. Fracture surface of the N720/AM specimen tested in creep at 109 MPa in laboratory air at 1100°C.....	168
Figure 224. Fracture surface of the N720/AM specimen tested in creep at 109 MPa in laboratory air at 1100°C.....	168
Figure 225. Fracture surface of the N720/AM specimen tested in creep at 109 MPa in laboratory air at 1100°C.....	169
Figure 226. Fracture surface of the N720/AM specimen tested in creep at 109 MPa in laboratory air at 1100°C.....	169
Figure 227. Fracture surface of the N720/AM specimen tested in creep at 109 MPa in laboratory air at 1100°C.....	170
Figure 228. Fracture surface of the N720/AM specimen tested in creep at 109 MPa in laboratory air at 1100°C.....	170

Figure	Page
Figure 229. Fracture surface of the N720/AM specimen tested in creep at 109 MPa in laboratory air at 1100°C.....	171
Figure 230. Fracture surface of the N720/AM specimen tested in creep at 109 MPa in laboratory air at 1100°C.....	171
Figure 231. Fracture surface of the N720/AM specimen tested in creep at 109 MPa in laboratory air at 1100°C.....	172
Figure 232. Fracture surface of the N720/AM specimen tested in creep at 109 MPa in laboratory air at 1100°C.....	172
Figure 233. Fracture surface of the N720/AM specimen tested in creep at 109 MPa in laboratory air at 1100°C.....	173
Figure 234. Fracture surface of the N720/AM specimen tested in creep at 109 MPa in laboratory air at 1100°C.....	173
Figure 235. Fracture surface of the N720/AM specimen tested in creep at 109 MPa in laboratory air at 1100°C.....	174
Figure 236. Fracture surface of the N720/AM specimen tested in creep at 109 MPa in laboratory air at 1100°C.....	174
Figure 237. Fracture surface of the N720/AM specimen tested in creep at 109 MPa in laboratory air at 1100°C.....	175
Figure 238. Fracture surface of the N720/AM specimen tested in creep at 109 MPa in laboratory air at 1100°C.....	175

Figure	Page
Figure 239. Fracture surface of the N720/AM specimen tested in creep at 131 MPa in laboratory air at 1100°C.....	176
Figure 240. Fracture surface of the N720/AM specimen tested in creep at 131 MPa in laboratory air at 1100°C.....	176
Figure 241. Fracture surface of the N720/AM specimen tested in creep at 131 MPa in laboratory air at 1100°C.....	177
Figure 242. Fracture surface of the N720/AM specimen tested in creep at 131 MPa in laboratory air at 1100°C.....	177
Figure 243. Fracture surface of the N720/AM specimen tested in creep at 131 MPa in laboratory air at 1100°C.....	178
Figure 244. Fracture surface of the N720/AM specimen tested in creep at 131 MPa in laboratory air at 1100°C.....	178
Figure 245. Fracture surface of the N720/AM specimen tested in creep at 131 MPa in laboratory air at 1100°C.....	179
Figure 246. Fracture surface of the N720/AM specimen tested in creep at 131 MPa in laboratory air at 1100°C.....	179
Figure 247. Fracture surface of the N720/AM specimen tested in creep at 131 MPa in laboratory air at 1100°C.....	180
Figure 248. Fracture surface of the N720/AM specimen tested in creep at 131 MPa in laboratory air at 1100°C.....	180

Figure	Page
Figure 249. Fracture surface of the N720/AM specimen tested in creep at 131 MPa in laboratory air at 1100°C.....	181
Figure 250. Fracture surface of the N720/AM specimen tested in creep at 131 MPa in laboratory air at 1100°C.....	181
Figure 251. Fracture surface of the N720/AM specimen tested in creep at 131 MPa in laboratory air at 1100°C.....	182
Figure 252. Fracture surface of the N720/AM specimen tested in creep at 131 MPa in laboratory air at 1100°C.....	182
Figure 253. Fracture surface of the N720/AM specimen tested in creep at 131 MPa in laboratory air at 1100°C.....	183
Figure 254. Fracture surface of the N720/AM specimen tested in creep at 131 MPa in laboratory air at 1100°C.....	184
Figure 255. Fracture surface of the N720/AM specimen tested in creep at 131 MPa in laboratory air at 1100°C.....	184
Figure 256. Fracture surface of the N720/AM specimen tested in creep at 131 MPa in laboratory air at 1100°C.....	185
Figure 257. Fracture surface of the N720/AM specimen tested in creep at 131 MPa in laboratory air at 1100°C.....	185
Figure 258. Fracture surface of the N720/AM specimen tested in creep at 131 MPa in laboratory air at 1100°C.....	186

Figure	Page
Figure 259. Fracture surface of the N720/AM specimen tested in creep at 131 MPa in laboratory air at 1100°C.....	186
Figure 260. Fracture surface of the N720/AM specimen tested in creep at 131 MPa in laboratory air at 1100°C.....	187
Figure 261. Fracture surface of the N720/AM specimen tested in creep at 131 MPa in laboratory air at 1100°C.....	187
Figure 262. Fracture surface of the N720/AM specimen tested in creep at 131 MPa in laboratory air at 1100°C.....	188
Figure 263. Fracture surface of the N720/AM specimen tested in creep at 131 MPa in laboratory air at 1100°C.....	188
Figure 264. Fracture surface of the N720/AM specimen tested in creep at 131 MPa in laboratory air at 1100°C.....	189
Figure 265. Fracture surface of the N720/AM specimen tested in creep at 131 MPa in laboratory air at 1100°C.....	189
Figure 266. Fracture surface of the N720/AM specimen tested in creep at 131 MPa in laboratory air at 1100°C.....	190
Figure 267. Fracture surface of the N720/AM specimen tested in creep at 131 MPa in laboratory air at 1100°C.....	190
Figure 268. Fracture surface of the N720/AM specimen tested in creep at 131 MPa in laboratory air at 1100°C.....	191

Figure	Page
Figure 269. Fracture surface of the N720/AM specimen tested in creep at 131 MPa in laboratory air at 1100°C.....	191
Figure 270. Fracture surface of the N720/AM specimen tested in creep at 131 MPa in laboratory air at 1100°C.....	192
Figure 271. Fracture surface of the N720/AM specimen tested in creep at 131 MPa in laboratory air at 1100°C.....	192
Figure 272. Fracture surface of the N720/AM specimen tested in creep at 131 MPa in laboratory air at 1100°C.....	193
Figure 273. Fracture surface of the N720/AM specimen tested in creep at 131 MPa in laboratory air at 1100°C.....	193
Figure 274. Fracture surface of the N720/AM specimen tested in creep at 131 MPa in laboratory air at 1100°C.....	194
Figure 275. Fracture surface of the N720/AM specimen tested in creep at 131 MPa in laboratory air at 1100°C.....	194
Figure 276. Fracture surface of the N720/AM specimen tested in creep at 131 MPa in laboratory air at 1100°C.....	195
Figure 277. Fracture surface of the N720/AM specimen tested in creep at 131 MPa in laboratory air at 1100°C.....	195
Figure 278. Fracture surface of the N720/AM specimen tested in creep at 131 MPa in laboratory air at 1100°C.....	196

Figure	Page
Figure 279. Fracture surface of the N720/AM specimen tested in creep at 131 MPa in laboratory air at 1100°C.	196
Figure 280. Fracture surface of the N720/AM specimen tested in creep at 131 MPa in laboratory air at 1100°C.	197
Figure 281. Fracture surface of the N720/AM specimen tested in creep at 131 MPa in laboratory air at 1100°C.	197
Figure 282. Fracture surface of the N720/AM specimen tested in creep at 131 MPa in laboratory air at 1100°C.	198
Figure 283. Fracture surface of the N720/AM specimen tested in creep at 131 MPa in laboratory air at 1100°C.	198
Figure 284. Fracture surface of the N720/AM specimen tested in creep at 131 MPa in laboratory air at 1100°C.	199
Figure 285. Fracture surface of the N720/AM specimen tested in creep at 131 MPa in laboratory air at 1100°C.	199
Figure 286. Fracture surface of the N720/AM specimen tested in creep at 131 MPa in laboratory air at 1100°C.	200
Figure 287. Fracture surface of the N720/AM specimen tested in creep at 131 MPa in laboratory air at 1100°C.	200
Figure 288. Fracture surface of the N720/AM specimen tested in creep at 131 MPa in steam at 1100°C.	201

Figure	Page
Figure 289. Fracture surface of the N720/AM specimen tested in creep at 131 MPa in steam at 1100°C.	202
Figure 290. Fracture surface of the N720/AM specimen tested in creep at 131 MPa in steam at 1100°C.	202
Figure 291. Fracture surface of the N720/AM specimen tested in creep at 131 MPa in steam at 1100°C.	203
Figure 292. Fracture surface of the N720/AM specimen tested in creep at 131 MPa in steam at 1100°C.	203
Figure 293. Fracture surface of the N720/AM specimen tested in creep at 131 MPa in steam at 1100°C.	204
Figure 294. Fracture surface of the N720/AM specimen tested in creep at 131 MPa in steam at 1100°C.	204
Figure 295. Fracture surface of the N720/AM specimen tested in creep at 131 MPa in steam at 1100°C.	205
Figure 296. Fracture surface of the N720/AM specimen tested in creep at 131 MPa in steam at 1100°C.	205
Figure 297. Fracture surface of the N720/AM specimen tested in creep at 131 MPa in steam at 1100°C.	206
Figure 298. Fracture surface of the N720/AM specimen tested in creep at 131 MPa in steam at 1100°C.	206

Figure	Page
Figure 299. Fracture surface of the N720/AM specimen tested in creep at 131 MPa in steam at 1100°C.	207
Figure 300. Fracture surface of the N720/AM specimen tested in creep at 131 MPa in steam at 1100°C.	207
Figure 301. Fracture surface of the N720/AM specimen tested in creep at 131 MPa in steam at 1100°C.	208
Figure 302. Fracture surface of the N720/AM specimen tested in creep at 131 MPa in steam at 1100°C.	208
Figure 303. Fracture surface of the N720/AM specimen tested in creep at 131 MPa in steam at 1100°C.	209
Figure 304. Fracture surface of the N720/AM specimen tested in creep at 131 MPa in steam at 1100°C.	209
Figure 305. Fracture surface of the N720/AM specimen tested in creep at 131 MPa in steam at 1100°C.	210
Figure 306. Fracture surface of the N720/AM specimen tested in creep at 131 MPa in steam at 1100°C.	210
Figure 307. Fracture surface of the N720/AM specimen tested in creep at 131 MPa in steam at 1100°C.	211
Figure 308. Fracture surface of the N720/AM specimen tested in creep at 131 MPa in steam at 1100°C.	211

Figure	Page
Figure 309. Fracture surface of the N720/AM specimen tested in creep at 131 MPa in steam at 1100°C.	212
Figure 310. Fracture surface of the N720/AM specimen tested in creep at 131 MPa in steam at 1100°C.	212
Figure 311. Fracture surface of the N720/AM specimen tested in creep at 131 MPa in steam at 1100°C.	213
Figure 312. Fracture surface of the N720/AM specimen tested in creep at 131 MPa in steam at 1100°C.	213
Figure 313. Fracture surface of the N720/AM specimen tested in creep at 131 MPa in steam at 1100°C.	214
Figure 314. Fracture surface of the N720/AM specimen tested in creep at 131 MPa in steam at 1100°C.	214
Figure 315. Fracture surface of the N720/AM specimen tested in creep at 131 MPa in steam at 1100°C.	215
Figure 316. Fracture surface of the N720/AM specimen tested in creep at 131 MPa in steam at 1100°C.	215
Figure 317. Fracture surface of the N720/AM specimen tested in creep at 131 MPa in steam at 1100°C.	216
Figure 318. Fracture surface of the N720/AM specimen tested in creep at 131 MPa in steam at 1100°C.	216

Figure	Page
Figure 319. Fracture surface of the N720/AM specimen tested in creep at 131 MPa in steam at 1100°C.	217
Figure 320. Fracture surface of the N720/AM specimen tested in creep at 109 MPa in steam at 1100°C.	217
Figure 321. Fracture surface of the N720/AM specimen tested in creep at 109 MPa in steam at 1100°C.	218
Figure 322. Fracture surface of the N720/AM specimen tested in creep at 109 MPa in steam at 1100°C.	218
Figure 323. Fracture surface of the N720/AM specimen tested in creep at 109 MPa in steam at 1100°C.	219
Figure 324. Fracture surface of the N720/AM specimen tested in creep at 109 MPa in steam at 1100°C..	219
Figure 325. Fracture surface of the N720/AM specimen tested in creep at 109 MPa in steam at 1100°C.	220
Figure 326. Fracture surface of the N720/AM specimen tested in creep at 109 MPa in steam at 1100°C.	220
Figure 327. Fracture surface of the N720/AM specimen tested in creep at 109 MPa in steam at 1100°C.	221
Figure 328. Fracture surface of the N720/AM specimen tested in creep at 109 MPa in steam at 1100°C.	221

Figure	Page
Figure 329. Fracture surface of the N720/AM specimen tested in creep at 109 MPa in steam at 1100°C.	222
Figure 330. Fracture surface of the N720/AM specimen tested in creep at 109 MPa in steam at 1100°C.	222
Figure 331. Fracture surface of the N720/AM specimen tested in creep at 109 MPa in steam at 1100°C.	223
Figure 332. Fracture surface of the N720/AM specimen tested in creep at 109 MPa in steam at 1100°C.	223
Figure 333. Fracture surface of the N720/AM specimen tested in creep at 109 MPa in steam at 1100°C.	224
Figure 334. Fracture surface of the N720/AM specimen tested in creep at 109 MPa in steam at 1100°C.	224
Figure 335. Fracture surface of the N720/AM specimen tested in creep at 109 MPa in steam at 1100°C.	225
Figure 336. Fracture surface of the N720/AM specimen tested in creep at 109 MPa in steam at 1100°C..	225
Figure 337. Fracture surface of the N720/AM specimen tested in creep at 109 MPa in steam at 1100°C.	226
Figure 338. Fracture surface of the N720/AM specimen tested in creep at 109 MPa in steam at 1100°C.	226

Figure	Page
Figure 339. Fracture surface of the N720/AM specimen tested in creep at 109 MPa in steam at 1100°C.	227
Figure 340. Fracture surface of the N720/AM specimen tested in creep at 109 MPa in steam at 1100°C.	227
Figure 341. Fracture surface of the N720/AM specimen tested in creep at 109 MPa in steam at 1100°C.	228
Figure 342. Fracture surface of the N720/AM specimen tested in creep at 109 MPa in steam at 1100°C.	228
Figure 343. Fracture surface of the N720/AM specimen tested in creep at 109 MPa in steam at 1100°C.	229
Figure 344. Fracture surface of the N720/AM specimen tested in creep at 109 MPa in steam at 1100°C.	229
Figure 345. Fracture surface of the N720/AM specimen tested in creep at 109 MPa in steam at 1100°C.	230
Figure 346. Fracture surface of the N720/AM specimen tested in creep at 109 MPa in steam at 1100°C.	230
Figure 347. Fracture surface of the N720/AM specimen tested in creep at 109 MPa in steam at 1100°C.	231
Figure 348. Fracture surface of the N720/AM specimen tested in creep at 109 MPa in steam at 1100°C.	231

Figure	Page
Figure 349. Fracture surface of the N720/AM specimen tested in creep at 109 MPa in steam at 1100°C.	232
Figure 350. Fracture surface of the N720/AM specimen tested in creep at 109 MPa in steam at 1100°C.	232
Figure 351. Fracture surface of the N720/AM specimen tested in creep at 109 MPa in steam at 1100°C.	233
Figure 352. Fracture surface of the N720/AM specimen tested in creep at 87.5 MPa in steam at 1100°C.	233
Figure 353. Fracture surface of the N720/AM specimen tested in creep at 87.5 MPa in steam at 1100°C.	234
Figure 354. Fracture surface of the N720/AM specimen tested in creep at 87.5 MPa in steam at 1100°C.	234
Figure 355. Fracture surface of the N720/AM specimen tested in creep at 87.5 MPa in steam at 1100°C.	235
Figure 356. Fracture surface of the N720/AM specimen tested in creep at 87.5 MPa in steam at 1100°C.	235
Figure 357. Fracture surface of the N720/AM specimen tested in creep at 87.5 MPa in steam at 1100°C.	236
Figure 358. Fracture surface of the N720/AM specimen tested in creep at 87.5 MPa in steam at 1100°C.	236

Figure	Page
Figure 359. Fracture surface of the N720/AM specimen tested in creep at 87.5 MPa in steam at 1100°C.	237
Figure 360. Fracture surface of the N720/AM specimen tested in creep at 87.5 MPa in steam at 1100°C.	237
Figure 361. Fracture surface of the N720/AM specimen tested in creep at 87.5 MPa in steam at 1100°C.	238
Figure 362. Fracture surface of the N720/AM specimen tested in creep at 87.5 MPa in steam at 1100°C.	238
Figure 363. Fracture surface of the N720/AM specimen tested in creep at 87.5 MPa in steam at 1100°C.	239
Figure 364. Fracture surface of the N720/AM specimen tested in creep at 87.5 MPa in steam at 1100°C.	239
Figure 365. Fracture surface of the N720/AM specimen tested in creep at 87.5 MPa in steam at 1100°C.	240
. Figure 366. Fracture surface of the N720/AM specimen tested in creep at 87.5 MPa in steam at 1100°C.	240
Figure 367. Fracture surface of the N720/AM specimen tested in creep at 87.5 MPa in steam at 1100°C.	241
Figure 368. Fracture surface of the N720/AM specimen tested in creep at 87.5 MPa in steam at 1100°C.	241

Figure	Page
Figure 369. Fracture surface of the N720/AM specimen tested in creep at 87.5 MPa in steam at 1100°C.	242
Figure 370. Fracture surface of the N720/AM specimen tested in creep at 87.5 MPa in steam at 1100°C.	242
Figure 371. Fracture surface of the N720/AM specimen tested in creep at 87.5 MPa in steam at 1100°C.	243
Figure 372. Fracture surface of the N720/AM specimen tested in creep at 87.5 MPa in steam at 1100°C.	243
Figure 373. Fracture surface of the N720/AM specimen tested in creep at 87.5 MPa in steam at 1100°C.	244
Figure 374. Fracture surface of the N720/AM specimen tested in creep at 87.5 MPa in steam at 1100°C.	244
Figure 375. Fracture surface of the N720/AM specimen tested in creep at 87.5 MPa in steam at 1100°C.	245
Figure 376. Fracture surface of the N720/AM specimen tested in creep at 87.5 MPa in steam at 1100°C.	245
Figure 377. Fracture surface of the N720/AM specimen tested in creep at 87.5 MPa in steam at 1100°C.	246
Figure 378. Fracture surface of the N720/AM specimen tested in creep at 87.5 MPa in steam at 1100°C.	246

Figure	Page
Figure 379. Fracture surface of the N720/AM specimen tested in creep at 87.5 MPa in steam at 1100°C.	247
Figure 380. Fracture surface of the N720/AM specimen tested in creep at 87.5 MPa in steam at 1100°C.	247
Figure 381. Fracture surface of the N720/AM specimen tested in creep at 87.5 MPa in steam at 1100°C.	248
Figure 382. Fracture surface of the N720/AM specimen tested in creep at 87.5 MPa in steam at 1100°C.	248
Figure 383. Fracture surface of the N720/AM specimen tested in creep at 87.5 MPa in steam at 1100°C.	249
Figure 384. Fracture surface of the N720/AM specimen tested in creep at 87.5 MPa in steam at 1100°C.	249
Figure 385. Fracture surface of the N720/AM specimen tested in creep at 87.5 MPa in steam at 1100°C.	250
Figure 386. Fracture surface of the N720/AM specimen tested in creep at 87.5 MPa in steam at 1100°C.	250
Figure 387. Fracture surface of the N720/AM specimen tested in creep at 87.5 MPa in steam at 1100°C.	251
Figure 388. Fracture surface of the N720/AM specimen tested in creep at 87.5 MPa in steam at 1100°C.	251

Figure	Page
Figure 389. Fracture surface of the N720/AM specimen tested in creep at 87.5 MPa in steam at 1100°C.	252
Figure 390. Fracture surface of the N720/AM specimen tested in creep at 87.5 MPa in steam at 1100°C.	252
Figure 391. Fracture surface of the N720/AM specimen tested in creep at 87.5 MPa in steam at 1100°C.	253
Figure 392. Fracture surface of the N720/AM specimen tested in creep at 87.5 MPa in steam at 1100°C.	253
Figure 393. Fracture surface of the N720/AM specimen tested in creep at 87.5 MPa in steam at 1100°C.	254
Figure 394. Fracture surface of the N720/AM specimen tested in creep at 87.5 MPa in steam at 1100°C.	254
Figure 395. Fracture surface of the N720/AM specimen tested in creep at 87.5 MPa in steam at 1100°C.	255
Figure 396. Fracture surface of the N720/AM specimen tested in creep at 87.5 MPa in steam at 1100°C.	255
Figure 397. Fracture surface of the N720/AM specimen tested in creep at 131 MPa in steam at 1000°C.	256
Figure 398. Fracture surface of the N720/AM specimen tested in creep at 131 MPa in steam at 1000°C.	256

Figure	Page
Figure 399. Fracture surface of the N720/AM specimen tested in creep at 131 MPa in steam at 1000°C.	257
Figure 400. Fracture surface of the N720/AM specimen tested in creep at 131 MPa in steam at 1000°C.	257
Figure 401. Fracture surface of the N720/AM specimen tested in creep at 131 MPa in steam at 1000°C.	258
Figure 402. Fracture surface of the N720/AM specimen tested in creep at 131 MPa in steam at 1000°C.	258
Figure 403. Fracture surface of the N720/AM specimen tested in creep at 131 MPa in steam at 1000°C.	259
Figure 404. Fracture surface of the N720/AM specimen tested in creep at 131 MPa in steam at 1000°C.	259
Figure 405. Fracture surface of the N720/AM specimen tested in creep at 131 MPa in steam at 1000°C.	260
Figure 406. Fracture surface of the N720/AM specimen tested in creep at 131 MPa in steam at 1000°C.	260
Figure 407. Fracture surface of the N720/AM specimen tested in creep at 131 MPa in steam at 1000°C.	261
Figure 408. Fracture surface of the N720/AM specimen tested in creep at 131 MPa in steam at 1000°C.	261

Figure	Page
Figure 409. Fracture surface of the N720/AM specimen tested in creep at 131 MPa in steam at 1000°C.	262
Figure 410. Fracture surface of the N720/AM specimen tested in creep at 131 MPa in steam at 1000°C.	262
Figure 411. Fracture surface of the N720/AM specimen tested in creep at 131 MPa in steam at 1000°C.	263
Figure 412. Fracture surface of the N720/AM specimen tested in creep at 131 MPa in steam at 1000°C.	263
Figure 413. Fracture surface of the N720/AM specimen tested in creep at 131 MPa in steam at 1000°C.	264
Figure 414. Fracture surface of the N720/AM specimen tested in creep at 131 MPa in steam at 1000°C.	264
Figure 415. Fracture surface of the N720/AM specimen tested in creep at 131 MPa in steam at 1000°C.	265
Figure 416. Fracture surface of the N720/AM specimen tested in creep at 131 MPa in steam at 1000°C.	265
Figure 417. Fracture surface of the N720/AM specimen tested in creep at 131 MPa in steam at 1000°C.	266
Figure 418. Fracture surface of the N720/AM specimen tested in creep at 131 MPa in steam at 1000°C.	266

Figure	Page
Figure 419. Fracture surface of the N720/AM specimen tested in creep at 131 MPa in steam at 1000°C.	267
Figure 420. Fracture surface of the N720/AM specimen tested in creep at 131 MPa in steam at 1000°C.	267
Figure 421. Fracture surface of the N720/AM specimen tested in creep at 131 MPa in steam at 1000°C.	268
Figure 422. Fracture surface of the N720/AM specimen tested in creep at 131 MPa in steam at 1000°C.	268
Figure 423. Fracture surface of the N720/AM specimen tested in creep at 131 MPa in steam at 1000°C.	269
Figure 424. Fracture surface of the N720/AM specimen tested in creep at 131 MPa in steam at 1000°C.	269
Figure 425. Fracture surface of the N720/AM specimen tested in creep at 131 MPa in steam at 1000°C.	270
Figure 426. Fracture surface of the N720/AM specimen tested in creep at 131 MPa in steam at 1000°C.	270
Figure 427. Fracture surface of the N720/AM specimen tested in creep at 131 MPa in steam at 1000°C.	271
Figure 428. Fracture surface of the N720/AM specimen tested in creep at 131 MPa in steam at 1000°C.	271

Figure	Page
Figure 429. Fracture surface of the N720/AM specimen tested in creep at 131 MPa in steam at 1000°C.	272
Figure 430. Fracture surface of the N720/AM specimen tested in creep at 131 MPa in steam at 1000°C.	272
Figure 431. Fracture surface of the N720/AM specimen tested in creep at 131 MPa in steam at 1000°C.	273
Figure 432. Fracture surface of the N720/AM specimen tested in creep at 131 MPa in steam at 1000°C.	273
Figure 433. Fracture surface of the N720/AM specimen tested in creep at 131 MPa in steam at 1000°C.	274
Figure 434. Fracture surface of the N720/AM specimen tested in creep at 131 MPa in steam at 1000°C.	274
Figure 435. Fracture surface of the N720/AM specimen tested in creep at 131 MPa in steam at 1000°C.	275
Figure 436. Fracture surface of the N720/AM specimen tested in creep at 131 MPa in steam at 1000°C.	275
Figure 437. Fracture surface of the N720/AM specimen tested in creep at 131 MPa in steam at 1000°C.	276
Figure 438. Fracture surface of the N720/AM specimen tested in creep at 131 MPa in steam at 1000°C.	276

Figure	Page
Figure 439. Fracture surface of the N720/AM specimen tested in creep at 131 MPa in steam at 1000°C.	277
Figure 440. Fracture surface of the N720/AM specimen tested in creep at 131 MPa in steam at 1000°C.	277
Figure 441. Fracture surface of the N720/AM specimen tested in creep at 131 MPa in steam at 1000°C.	278
Figure 442. Fracture surface of the N720/AM specimen tested in creep at 131 MPa in steam at 1000°C.	278
Figure 443. Fracture surface of the N720/AM specimen tested in creep at 131 MPa in steam at 1000°C.	279
Figure 444. Fracture surface of the N720/AM specimen tested in creep at 131 MPa in steam at 1000°C.	279
Figure 445. Fracture surface of the N720/AM specimen tested in creep at 131 MPa in steam at 1000°C.	280
Figure 446. Fracture surface of the N720/AM specimen tested in creep at 131 MPa in steam at 1000°C.	280
Figure 447. Fracture surface of the N720/AM specimen tested in creep at 131 MPa in steam at 1000°C.	281
Figure 448. Fracture surface of the N720/AM specimen tested in creep at 131 MPa in steam at 1000°C.	281

Figure	Page
Figure 449. Fracture surface of the N720/AM specimen tested in creep at 131 MPa in steam at 1000°C.	282
Figure 450. Fracture surface of the N720/AM specimen tested in creep at 131 MPa in steam at 1000°C.	282
Figure 451. Fracture surface of the N720/AM specimen tested in creep at 131 MPa in steam at 1000°C.	283
Figure 452. Fracture surface of the N720/AM specimen tested in creep at 131 MPa in steam at 1000°C.	283
Figure 453. Fracture surface of the N720/AM specimen tested in creep at 131 MPa in steam at 1000°C.	284
Figure 454. Fracture surface of the N720/AM specimen tested in creep at 131 MPa in steam at 1000°C.	284
Figure 455. Fracture surface of the N720/AM specimen tested in creep at 131 MPa in steam at 1000°C.	285
Figure 456. Fracture surface of the N720/AM specimen tested in creep at 131 MPa in steam at 1000°C.	285
Figure 457. Fracture surface of the N720/AM specimen tested in creep at 131 MPa in steam at 1000°C.	286
Figure 458. Fracture surface of the N720/AM specimen tested in creep at 131 MPa in steam at 1000°C.	286

Figure	Page
Figure 459. Fracture surface of the N720/AM specimen tested in creep at 131 MPa in steam at 1000°C.	287
Figure 460. Fracture surface of the N720/AM specimen tested in creep at 140 MPa in steam at 1000°C.	287
Figure 461. Fracture surface of the N720/AM specimen tested in creep at 140 MPa in steam at 1000°C.	288
Figure 462. Fracture surface of the N720/AM specimen tested in creep at 140 MPa in steam at 1000°C.	288
Figure 463. Fracture surface of the N720/AM specimen tested in creep at 140 MPa in steam at 1000°C.	289
Figure 464. Fracture surface of the N720/AM specimen tested in creep at 140 MPa in steam at 1000°C.	289
Figure 465. Fracture surface of the N720/AM specimen tested in creep at 140 MPa in steam at 1000°C.	290
Figure 466. Fracture surface of the N720/AM specimen tested in creep at 140 MPa in steam at 1000°C.	290
Figure 467. Fracture surface of the N720/AM specimen tested in creep at 140 MPa in steam at 1000°C.	291
Figure 468. Fracture surface of the N720/AM specimen tested in creep at 140 MPa in steam at 1000°C.	291

Figure	Page
Figure 469. Fracture surface of the N720/AM specimen tested in creep at 140 MPa in steam at 1000°C.	292
Figure 470. Fracture surface of the N720/AM specimen tested in creep at 140 MPa in steam at 1000°C.	292
Figure 471. Fracture surface of the N720/AM specimen tested in creep at 140 MPa in steam at 1000°C.	293
Figure 472. Fracture surface of the N720/AM specimen tested in creep at 140 MPa in steam at 1000°C.	293
Figure 473. Fracture surface of the N720/AM specimen tested in creep at 140 MPa in steam at 1000°C.	294
Figure 474. Fracture surface of the N720/AM specimen tested in creep at 140 MPa in steam at 1000°C.	294
Figure 475. Fracture surface of the N720/AM specimen tested in creep at 140 MPa in steam at 1000°C.	295
Figure 476. Fracture surface of the N720/AM specimen tested in creep at 140 MPa in steam at 1000°C.	295
Figure 477. Fracture surface of the N720/AM specimen tested in creep at 140 MPa in steam at 1000°C.	296
Figure 478. Fracture surface of the N720/AM specimen tested in creep at 140 MPa in steam at 1000°C.	296

Figure	Page
Figure 479. Fracture surface of the N720/AM specimen tested in creep at 140 MPa in steam at 1000°C.	297
Figure 480. Fracture surface of the N720/AM specimen tested in creep at 140 MPa in steam at 1000°C.	297
Figure 481. Fracture surface of the N720/AM specimen tested in creep at 140 MPa in steam at 1000°C.	298
Figure 482. Fracture surface of the N720/AM specimen tested in creep at 140 MPa in steam at 1000°C.	298
Figure 483. Fracture surface of the N720/AM specimen tested in creep at 140 MPa in steam at 1000°C.	299
Figure 484. Fracture surface of the N720/AM specimen tested in creep at 140 MPa in steam at 1000°C.	299
Figure 485. Fracture surface of the N720/AM specimen tested in creep at 140 MPa in steam at 1000°C.	300
Figure 486. Fracture surface of the N720/AM specimen tested in creep at 140 MPa in steam at 1000°C.	300
Figure 487. Fracture surface of the N720/AM specimen tested in creep at 140 MPa in steam at 1000°C.	301
Figure 488. Fracture surface of the N720/AM specimen tested in creep at 140 MPa in steam at 1000°C.	301

Figure	Page
Figure 489. Fracture surface of the N720/AM specimen tested in creep at 140 MPa in steam at 1000°C.	302
Figure 490. Fracture surface of the N720/AM specimen tested in creep at 140 MPa in steam at 1000°C.	302
Figure 491. Fracture surface of the N720/AM specimen tested in creep at 140 MPa in steam at 1000°C.	303
Figure 492. Fracture surface of the N720/AM specimen tested in creep at 140 MPa in steam at 1000°C.	303
Figure 493. Fracture surface of the N720/AM specimen tested in creep at 140 MPa in steam at 1000°C.	304
Figure 494. Fracture surface of the N720/AM specimen tested in creep at 140 MPa in steam at 1000°C.	304
Figure 495. Fracture surface of the N720/AM specimen tested in creep at 140 MPa in steam at 1000°C.	305
Figure 496. Fracture surface of the N720/AM specimen tested in creep at 140 MPa in steam at 1000°C.	305
Figure 497. Fracture surface of the N720/AM specimen tested in creep at 140 MPa in steam at 1000°C.	306
Figure 498. Fracture surface of the N720/AM specimen tested in creep at 140 MPa in steam at 1000°C.	306

Figure	Page
Figure 499. Fracture surface of the N720/AM specimen tested in creep at 140 MPa in steam at 1000°C.	307
Figure 500. Fracture surface of the N720/AM specimen tested in creep at 140 MPa in steam at 1000°C.	307
Figure 501. Fracture surface of the N720/AM specimen tested in creep at 140 MPa in steam at 1000°C.	308
Figure 502. Fracture surface of the N720/AM specimen tested in creep at 140 MPa in steam at 1000°C.	308
Figure 503. Fracture surface of the N720/AM specimen tested in tension to failure at 900°C in laboratory air.	309
Figure 504. Fracture surface of the N720/AM specimen tested in tension to failure at 900°C in laboratory air.	309
Figure 505. Fracture surface of the N720/AM specimen tested in tension to failure at 900°C in laboratory air.	310
Figure 506. Fracture surface of the N720/AM specimen tested in tension to failure at 900°C in laboratory air.	310
Figure 507. Fracture surface of the N720/AM specimen tested in tension to failure at 900°C in laboratory air (side view).	311
Figure 508. Fracture surface of the N720/AM specimen tested in tension to failure at 900°C in laboratory air (side view).	311

Figure	Page
Figure 509. Fracture surface of the N720/AM specimen tested in tension to failure at 900°C in laboratory air (side view).....	311
Figure 510. Fracture surface of the N720/AM specimen tested in tension to failure at 900°C in laboratory air (side view).....	311
Figure 511. Fracture surface of the N720/AM specimen tested in tension to failure at 1000°C in laboratory air.....	312
Figure 512. Fracture surface of the N720/AM specimen tested in tension to failure at 1000°C in laboratory air.....	312
Figure 513. Fracture surface of the N720/AM specimen tested in tension to failure at 1000°C in laboratory air.....	313
Figure 514. Fracture surface of the N720/AM specimen tested in tension to failure at 1000°C in laboratory air.....	313
Figure 515. Fracture surface of the N720/AM specimen tested in tension to failure at 1000°C in laboratory air (side view).....	314
Figure 516. Fracture surface of the N720/AM specimen tested in tension to failure at 1000°C in laboratory air (side view).....	314
Figure 517. Fracture surface of the N720/AM specimen tested in tension to failure at 1000°C in laboratory air (side view).....	314
Figure 518. Fracture surface of the N720/AM specimen tested in tension to failure at 1000°C in laboratory air (side view).....	314

Figure	Page
Figure 519. Fracture surface of the N720/AM specimen tested in tension to failure at 1100°C in laboratory air.....	315
Figure 520. Fracture surface of the N720/AM specimen tested in tension to failure at 1100°C in laboratory air.....	315
Figure 521. Fracture surface of the N720/AM specimen tested in tension to failure at 1100°C in laboratory air.....	316
Figure 522. Fracture surface of the N720/AM specimen tested in tension to failure at 1100°C in laboratory air.....	316
Figure 523. Fracture surface of the N720/AM specimen tested in tension to failure at 1100°C in laboratory air (side view).....	317
Figure 524. Fracture surface of the N720/AM specimen tested in tension to failure at 1100°C in laboratory air (side view).....	317
Figure 525. Fracture surface of the N720/AM specimen tested in tension to failure at 1100°C in laboratory air (side view).....	317
Figure 526. Fracture surface of the N720/AM specimen tested in tension to failure at 1100°C in laboratory air (side view).....	317
Figure 527. Fracture surface of the N720/AM specimen tested in tension to failure with constant loading rate of 25MPa at 1100°C in steam.....	318
Figure 528. Fracture surface of the N720/AM specimen tested in tension to failure with constant loading rate of 25MPa at 1100°C in steam.....	318

Figure	Page
Figure 529. Fracture surface of the N720/AM specimen tested in tension to failure with constant loading rate of 25MPa at 1100°C in steam.	319
Figure 530. Fracture surface of the N720/AM specimen tested in tension to failure with constant loading rate of 25MPa at 1100°C in steam.	319
Figure 531. Fracture surface of the N720/AM specimen tested in tension to failure with constant loading rate of 25MPa at 1100°C in steam (side view).	320
Figure 532. Fracture surface of the N720/AM specimen tested in tension to failure with constant loading rate of 25MPa at 1100°C in steam (side view).	320
Figure 533. Fracture surface of the N720/AM specimen tested in tension to failure with constant loading rate of 25MPa at 1100°C in steam (side view).	320
Figure 534. Fracture surface of the N720/AM specimen tested in tension to failure with constant loading rate of 25MPa at 1100°C in steam (side view).	320
Figure 535. Fracture surface of the N720/AM specimen(2) tested in tension to failure with constant loading rate of 25MPa at 1100°C in steam.	321
Figure 536. Fracture surface of the N720/AM specimen(2) tested in tension to failure with constant loading rate of 25MPa at 1100°C in steam.	321
Figure 537. Fracture surface of the N720/AM specimen(2) tested in tension to failure with constant loading rate of 25MPa at 1100°C in steam.	322
Figure 538. Fracture surface of the N720/AM specimen(2) tested in tension to failure with constant loading rate of 25MPa at 1100°C in steam.	322

Figure	Page
Figure 539. Fracture surface of the N720/AM specimen(2) tested in tension to failure with constant loading rate of 25MPa at 1100°C in steam (side view).	323
Figure 540. Fracture surface of the N720/AM specimen(2) tested in tension to failure with constant loading rate of 25MPa at 1100°C in steam (side view).	323
Figure 541. Fracture surface of the N720/AM specimen(2) tested in tension to failure with constant loading rate of 25MPa at 1100°C in steam (side view).	323
Figure 542. Fracture surface of the N720/AM specimen(2) tested in tension to failure with constant loading rate of 25MPa at 1100°C in steam (side view).	323
Figure 543. Fracture surface of the N720/AM specimen(2) tested in tension to failure with constant loading rate of 25MPa at 1100°C in steam (side view).	324
Figure 544. Fracture surface of the N720/AM specimen(2) tested in tension to failure with constant loading rate of 25MPa at 1100°C in steam (side view).	324
Figure 545. Fracture surface of the N720/AM specimen tested in tension to failure with constant loading rate of 0.0025MPa at 1100°C in steam.	325
Figure 546. Fracture surface of the N720/AM specimen tested in tension to failure with constant loading rate of 0.0025MPa at 1100°C in steam.	325
Figure 547. Fracture surface of the N720/AM specimen tested in tension to failure with constant loading rate of 0.0025MPa at 1100°C in steam (side view).	326
Figure 548. Fracture surface of the N720/AM specimen tested in tension to failure with constant loading rate of 0.0025MPa at 1100°C in steam (side view).	326

Figure	Page
Figure 549. Fracture surface of the N720/AM specimen tested in tension to failure with constant loading rate of 0.0025MPa at 1100°C in steam (side view).	326
Figure 550. Fracture surface of the N720/AM specimen tested in tension to failure with constant loading rate of 0.0025MPa at 1100°C in steam (side view).	326
Figure 551. Fracture surface of the N720/AM specimen(2) tested in tension to failure with constant loading rate of 0.0025MPa at 1100°C in steam.	327
Figure 552. Fracture surface of the N720/AM specimen(2) tested in tension to failure with constant loading rate of 0.0025MPa at 1100°C in steam.	327
Figure 553. Fracture surface of the N720/AM specimen(2) tested in tension to failure with constant loading rate of 0.0025MPa at 1100°C in steam.	328
Figure 554. Fracture surface of the N720/AM specimen(2) tested in tension to failure with constant loading rate of 0.0025MPa at 1100°C in steam.	328
Figure 555. Fracture surface of the N720/AM specimen(2) tested in tension to failure with constant loading rate of 0.0025MPa at 1100°C in steam (side view).	329
Figure 556. Fracture surface of the N720/AM specimen(2) tested in tension to failure with constant loading rate of 0.0025MPa at 1100°C in steam (side view).	329
Figure 557. Fracture surface of the N720/AM specimen(2) tested in tension to failure with constant loading rate of 0.0025MPa at 1100°C in steam (side view).	329
Figure 558. Fracture surface of the N720/AM specimen(2) tested in tension to failure with constant loading rate of 0.0025MPa at 1100°C in steam (side view).	329

Figure	Page
Figure 559. Fracture surface of the N720/AM specimen tested in creep at 109 MPa in laboratory air at 1100°C.	330
Figure 560. Fracture surface of the N720/AM specimen tested in creep at 109 MPa in laboratory air at 1100°C.	330
Figure 561. Fracture surface of the N720/AM specimen tested in creep at 109 MPa in laboratory air at 1100°C.	331
Figure 562. Fracture surface of the N720/AM specimen tested in creep at 109 MPa in laboratory air at 1100°C.	331
Figure 563. Fracture surface of the N720/AM specimen tested in creep at 109 MPa in laboratory air at 1100°C (side view).	332
Figure 564. Fracture surface of the N720/AM specimen tested in creep at 109 MPa in laboratory air at 1100°C (side view).	332
Figure 565. Fracture surface of the N720/AM specimen tested in creep at 109 MPa in laboratory air at 1100°C (side view).	332
Figure 566. Fracture surface of the N720/AM specimen tested in creep at 109 MPa in laboratory air at 1100°C (side view).	332
Figure 567. Fracture surface of the N720/AM specimen tested in creep at 131 MPa in laboratory air at 1100°C.	333
Figure 568. Fracture surface of the N720/AM specimen tested in creep at 131 MPa in laboratory air at 1100°C.	333

Figure	Page
Figure 569. Fracture surface of the N720/AM specimen tested in creep at 131 MPa in laboratory air at 1100°C.	334
Figure 570. Fracture surface of the N720/AM specimen tested in creep at 131 MPa in laboratory air at 1100°C.	334
Figure 571. Fracture surface of the N720/AM specimen tested in creep at 131 MPa in laboratory air at 1100°C (side view).	335
Figure 572. Fracture surface of the N720/AM specimen tested in creep at 131 MPa in laboratory air at 1100°C (side view).	335
Figure 573. Fracture surface of the N720/AM specimen tested in creep at 131 MPa in laboratory air at 1100°C (side view).	335
Figure 574. Fracture surface of the N720/AM specimen tested in creep at 131 MPa in laboratory air at 1100°C (side view).	335
Figure 575. Fracture surface of the N720/AM specimen tested in creep at 131 MPa in steam at 1100°C.	336
Figure 576. Fracture surface of the N720/AM specimen tested in creep at 131 MPa in steam at 1100°C.	336
Figure 577. Fracture surface of the N720/AM specimen tested in creep at 131 MPa in steam at 1100°C.	337
Figure 578. Fracture surface of the N720/AM specimen tested in creep at 131 MPa in steam at 1100°C.	337

Figure	Page
Figure 579. Fracture surface of the N720/AM specimen tested in creep at 131 MPa in steam at 1100°C (side view).	338
Figure 580. Fracture surface of the N720/AM specimen tested in creep at 131 MPa in steam at 1100°C (side view).	338
Figure 581. Fracture surface of the N720/AM specimen tested in creep at 131 MPa in steam at 1100°C (side view).	338
Figure 582. Fracture surface of the N720/AM specimen tested in creep at 131 MPa in steam at 1100°C (side view).	338
Figure 583. Fracture surface of the N720/AM specimen tested in creep at 109 MPa in steam at 1100°C.	339
Figure 584. Fracture surface of the N720/AM specimen tested in creep at 109 MPa in steam at 1100°C.	339
Figure 585. Fracture surface of the N720/AM specimen tested in creep at 109 MPa in steam at 1100°C.	340
Figure 586. Fracture surface of the N720/AM specimen tested in creep at 109 MPa in steam at 1100°C.	340
Figure 587. Fracture surface of the N720/AM specimen tested in creep at 109 MPa in steam at 1100°C (side view).	341
Figure 588. Fracture surface of the N720/AM specimen tested in creep at 109 MPa in steam at 1100°C (side view).	341

Figure	Page
Figure 589. Fracture surface of the N720/AM specimen tested in creep at 109 MPa in steam at 1100°C (side view).	341
Figure 590. Fracture surface of the N720/AM specimen tested in creep at 109 MPa in steam at 1100°C (side view).	341
Figure 591. Fracture surface of the N720/AM specimen tested in creep at 87.5 MPa in steam at 1100°C.	342
Figure 592. Fracture surface of the N720/AM specimen tested in creep at 87.5 MPa in steam at 1100°C.	342
Figure 593. Fracture surface of the N720/AM specimen tested in creep at 87.5 MPa in steam at 1100°C.	343
Figure 594. Fracture surface of the N720/AM specimen tested in creep at 87.5 MPa in steam at 1100°C.	343
Figure 595. Fracture surface of the N720/AM specimen tested in creep at 87.5 MPa in steam at 1100°C (side view).	344
Figure 596. Fracture surface of the N720/AM specimen tested in creep at 87.5 MPa in steam at 1100°C (side view).	344
Figure 597. Fracture surface of the N720/AM specimen tested in creep at 87.5 MPa in steam at 1100°C (side view).	344
Figure 598. Fracture surface of the N720/AM specimen tested in creep at 87.5 MPa in steam at 1100°C (side view).	344

Figure	Page
Figure 599. Fracture surface of the N720/AM specimen tested in creep at 131 MPa in steam at 1000°C.	345
Figure 600. Fracture surface of the N720/AM specimen tested in creep at 131 MPa in steam at 1000°C.	345
Figure 601. Fracture surface of the N720/AM specimen tested in creep at 131 MPa in steam at 1000°C.	346
Figure 602. Fracture surface of the N720/AM specimen tested in creep at 131 MPa in steam at 1000°C.	346
Figure 603. Fracture surface of the N720/AM specimen tested in creep at 131 MPa in steam at 1000°C (side view).	347
Figure 604. Fracture surface of the N720/AM specimen tested in creep at 131 MPa in steam at 1000°C (side view).	347
Figure 605. Fracture surface of the N720/AM specimen tested in creep at 131 MPa in steam at 1000°C (side view).	347
Figure 606. Fracture surface of the N720/AM specimen tested in creep at 131 MPa in steam at 1000°C (side view).	347
Figure 607. Fracture surface of the N720/AM specimen tested in creep at 140 MPa in steam at 1000°C.	348
Figure 608. Fracture surface of the N720/AM specimen tested in creep at 140 MPa in steam at 1000°C.	348

Figure	Page
Figure 609. Fracture surface of the N720/AM specimen tested in creep at 140 MPa in steam at 1000°C.	349
Figure 610. Fracture surface of the N720/AM specimen tested in creep at 140 MPa in steam at 1000°C.	349
Figure 611. Fracture surface of the N720/AM specimen tested in creep at 140 MPa in steam at 1000°C (side view).	350
Figure 612. Fracture surface of the N720/AM specimen tested in creep at 140 MPa in steam at 1000°C (side view).	350
Figure 613. Fracture surface of the N720/AM specimen tested in creep at 140 MPa in steam at 1000°C (side view).	350
Figure 614. Fracture surface of the N720/AM specimen tested in creep at 140 MPa in steam at 1000°C (side view).	350

List of Tables

Table	Page
Table 1. Important properties of selected fibers [1,22].....	10
Table 2. CMC Applications	15
Table 3. Summary of tensile data for N720/AM with 0°/90° fiber	37
Table 4. Summary of creep data for N720/AM with 0°/90° fiber	37
Table 5. Summary of retained properties for N720/AM with	38
Table 6. Summary of thermal properties for N720/AM composite.....	39
Table 7. Average thermal properties measured for the N720/A and N720/AM composites due to temperature rise from 23°C to	39
900, 1000 and 1100°C. Data for N720/A from Braun[10]	39
Table 8. The average tensile properties for the N720/A and N720/AM composites at various temperatures. Data for N720/A from Braun[10,17]	42
Table 9. The average tensile properties for N720/AM composite with constant loading rates at 25 and 0.0025MPa/s in steam. Data at 1200°C from Genelin [22]	44
Table 10. Results of Creep-Rupture tests for N720/AM.	45
Table 11. Results of Creep-Rupture tests for the N720/A and N720/AM composites with 0°/90° fiber orientation at 1100°C. Data for N720/A from Braun[10]	47
Table 12 Results of Creep-Rupture tests for the N720/A and N720/AM composites at 1000°C. Data for N720/A from Braun [10].	50
Table 13. Retained properties for the N720/AM specimen subjected to prior creep	61

EFFECT OF STEAM ENVIRONMENT ON CREEP BEHAVIOR OF NEXTEL720/ALUMINA-MULLITE CERAMIC MATRIX COMPOSITE AT ELEVATED TEMPERATURE

I. Introduction

Advancing aerospace technology is driving a need for structural materials with ever increasing thermal capabilities. For example, all types of engines benefit thermodynamically when materials permit operation at higher combustion temperatures and/or with reduced cooling requirements. Likewise future space/reentry vehicle designs will benefit greatly from improved thermal protection systems with the mechanical integrity to serve structural functions [1].

Strength and toughness have always been two major problems in a lot of areas such as aerospace industry. Furthermore, with the effect of severe environments including high temperature corrosion, these problems have become more complicated. The necessity for structural materials that have excellent mechanical properties under extreme conditions have been raised with developing technology. Ceramic matrix composites (CMCs) having long-term strength and fracture toughness properties at high temperatures are important materials for such aerospace applications. Additionally, lower densities of CMCs and their high use temperature, together with a reduced need for cooling air, allow for improved high-temperature performance when compared to conventional nickel based superalloys [2]. Ceramics are the only class of material that

can reliably be used at temperatures above 1100 °C. Figure 1 illustrates the maximum service temperatures of polymers, metals and ceramics.

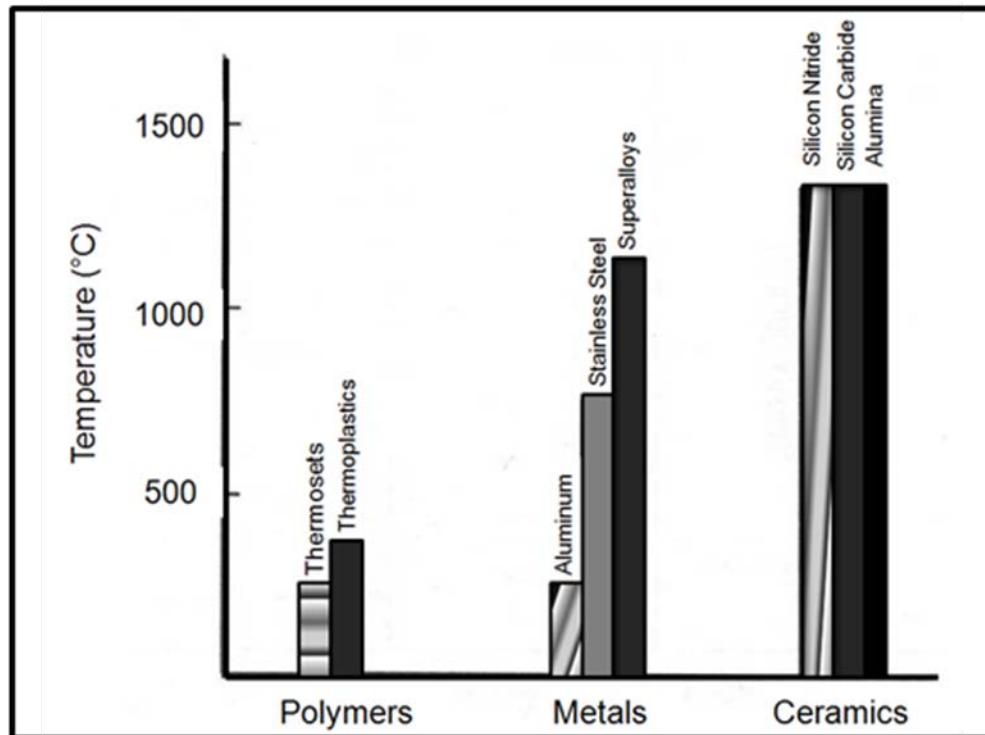


Figure 1. Maximum Material Service Temperatures [3].

The use of CMCs is not limited to aerospace applications. There are many other areas where CMCs will be of great value, including engine components operating at high temperatures and in corrosive environments, cutting tool inserts, wear resistant parts, nozzles, exhaust ducts, and energy-related applications [3].

This study is based on the effect of steam environment on creep behavior of Nextel 720/ Alumina-Mullite Ceramic Matrix Composite at elevated temperatures. The

objective is to identify the temperature range where steam environment causes degradation of creep resistance of Nextel720/Alumina-Mullite Ceramic Matrix Composite.

II. Background and Applications

2.1 Ceramic Matrix Composites

Ceramics are defined as inorganic, non-metallic materials which are typically crystalline in nature and contain metallic and non-metallic elements such as Al_2O_3 , CaO , ZrO_2 , SiC , and Si_3N_4 . There are several broad categories of ceramics classifying the industrial products as follows; clay products, white ware, refractories, cements, abrasives, and advanced ceramics [4].

Advanced ceramics are materials tailored to possess exceptional properties (superior mechanical properties, corrosion/oxidation resistance, thermal, electrical, optical or magnetic properties) by controlling their composition and internal structure [4].

Since the beginning of 1990's there has been a great interest in developing a new generation of ceramic composite which can withstand high temperatures in oxidative atmospheres over long periods. A further expectation is that the ceramic composite products show inelastic straining, in other terms, display graceful failure rather than brittle fracture as ceramics [5]. On the negative side, ceramics tend to be brittle, with low fracture toughness and damage tolerance. While metals can deform plastically before

fracture, a process that involves extensive energy dissipation, monolithic ceramics do not show signs of plastic deformation and fail in a catastrophic fashion [6].

The major scopes of CMCs can be divided into the areas of [4]:

- biological applications (bioceramics)
- high-temperature applications

Some of these scopes are partly related to each other, and in general they benefit from the low densities of CMCs compared to their metallic counterparts, leading to lightweight structures [4].

Ceramic matrix composites (CMCs) with fiber reinforcement provide the exemplary way to reduce the negative effects of brittleness of engineering ceramics, whilst retaining the further advantageous properties of ceramic structures. The behavior of CMCs is heavily dependent upon the components used, and a clever combination of reinforcements, interfaces and matrix materials leads to sophisticated composites achieving outstanding performances, especially under severe environmental conditions. This enables the designing engineer to adjust the composites' properties directly to various application requirements and load conditions [4].

Besides resistance to oxidation and corrosion, the mechanical properties of CMCs for example fracture toughness and damage tolerance, are of major interest. Thus, those mechanisms which are responsible for such tolerant behavior by CMCs must be adjusted to achieve crack deflection and high energy dissipation in general [4]. In all CMC variations-whether short-or-long-fiber-reinforced-either the interface or the matrix must

meet this challenge. In consequence, different CMC strategies have been followed, including weak interface composites (WIC) or weak matrix composites (WMC) [4].

Since the research performed in the early 80's with the first generation of ceramic fibers, CMCs have experienced an exceptional development throughout the last decade, mainly for short terms in the field of aerospace applications (missile, rocket propulsion) where there is a constant need to increase payloads and working temperatures [7].

After the beginning of 1990's, there has been a great interest in developing a new generation of ceramic composite which can withstand high temperatures in oxidative atmospheres over long periods. A further expectation is that the ceramic composite products show inelastic straining, in other terms, display graceful failure rather than brittle fracture as ceramics normally do. And, more importantly than this, that the high temperature damage tolerance should hold over several thousand hours, so that the composites exhibit minimized degradation in service. Instead, a moderately high mechanical strength and high toughness in the composites were given greater priority [5].

The fiber/matrix interface affects the behavior of composites. Specially, in CMCs, interfacial bonding affects the fracture behavior of the composite. A strong interfacial bond will allow an oncoming crack go unimpeded through the interface and the composite will fail in a brittle manner. The interaction of a crack in the matrix with a weak interfacial bond, on the other hand, is likely to lead to debonding at the interface through the fibers, followed by crack deflection, crack bridging, fiber fracture and finally fiber pull-out. All these additional energy absorbing phenomena lead to an enhanced toughness and a non-catastrophic failure mode [3].

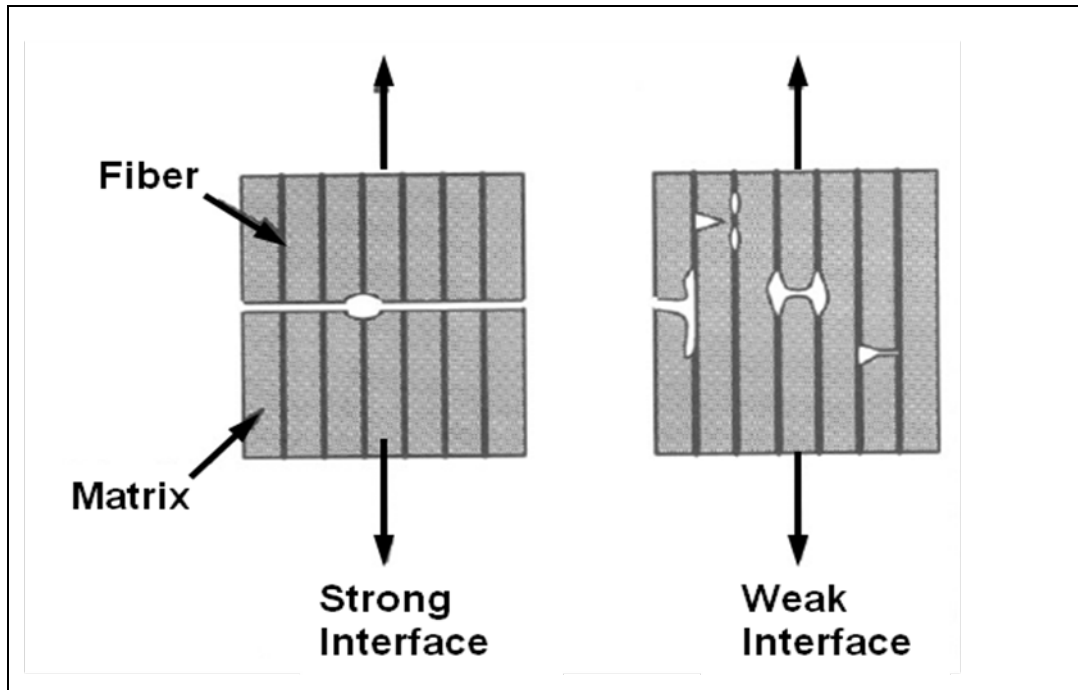


Figure 2. Failure of CMC as a function of interfacial bond strength
 (a) strong interfacial bond; (b) weak interfacial bond [3].

Ceramic Matrix Composites that rely on a weak interface for their toughness can be characterized by their stress strain curve. Initially the stress-strain curve is linear, as the matrix and fibers share the load. As micro-cracks start forming in the matrix, the curve slope starts to decrease. As the cracks in the matrix grow, and then start coalescing, a distinctive knee in the curve is seen. This happens when the cracks propagate through the thickness of the material and all load is transferred to the fibers. At this point the curve is dominated by individual fiber failure and subsequent load transfer to other fibers until the material fails [8]. A typical stress strain curve for a CMC with a weak interface is presented in Figure 3.

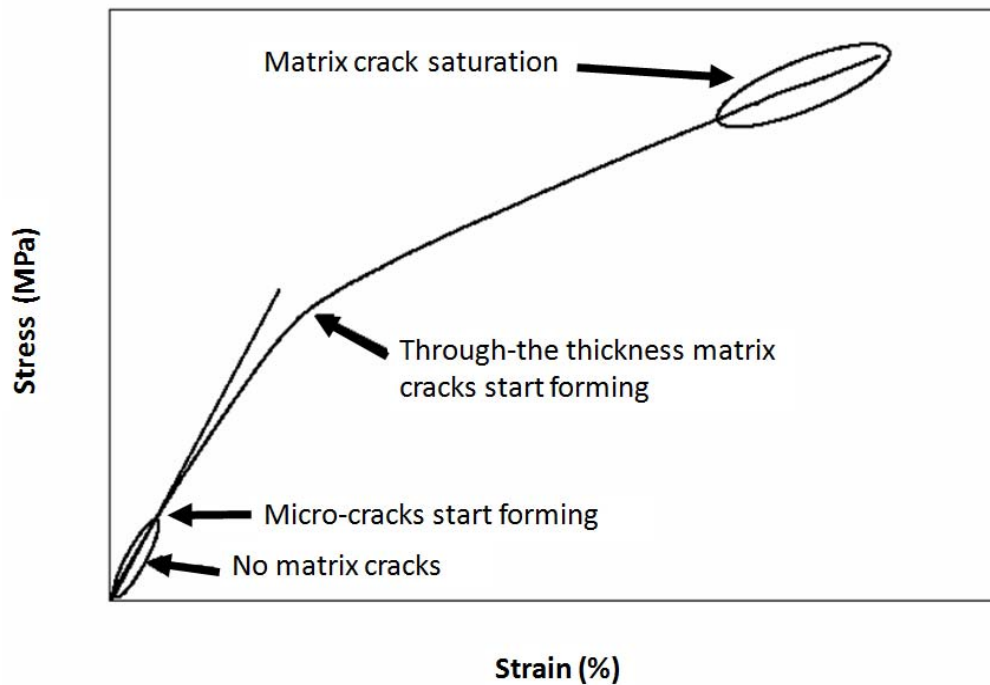


Figure 3. Typical stress strain curve for CMC with weak interface [8].

Ceramic matrix composites are designed to minimize the drawbacks of monolithic ceramics. Compared to monolithic ceramics, continuous fiber ceramic composites (CFCCs) exhibit reduced brittleness and decreased susceptibility to both flaws and thermal shock, while maintaining excellent properties at high temperatures [9].

Most important mechanical properties to classify the CMCs are elastic modulus, tensile strength (or flexural strength by bending), fracture toughness, interfacial stresses (thermal and radial stresses) and creep behavior [5]. Creep is deformation of a material over time, caused by a constant or very slightly varying applied load. In the case of ceramics, grain size, porosity, and impurities from processing also contribute to creep [7]. Basically, a stress/displacement curve contains a linear stress/strain behavior which

describes the details of elastic deformation behavior. Then, once the stress for matrix cracking has been reached, the CMC shows stress/strain behavior similar to plastic deformation demonstrated in metals [5].

2.2 Fibers

The main advantage of CMCs over monolithic ceramics is their superior toughness, tolerance to the presence of cracks and defects, and non-catastrophic mode of failure. It is widely accepted that to avoid brittle fracture behavior in CMCs and improve the damage tolerance, a weak fiber/matrix interface is needed, which serves to deflect matrix cracks and to allow subsequent fiber pullout [10].

Although the interaction between the fibers, interface and matrix determines the bulk composite performance, the fibers are of particular importance. This is based on several reasons. First, the reinforcing component determines the maximum properties achievable, and hence fibers are the first choice to develop a CMC. The nature of the fiber influences the production process to be selected and the composite design in terms of interface and matrix to be installed. Second, reinforcements offer various design possibilities as, for example, the type of fiber (long, short, filament diameter, aspect ratio, number of filaments per roving, etc.), fiber volume ratio, and the fiber architecture of the composite [4]. In general, fibers can be classified on the basis of their composition and structure that is shown in figure 4.

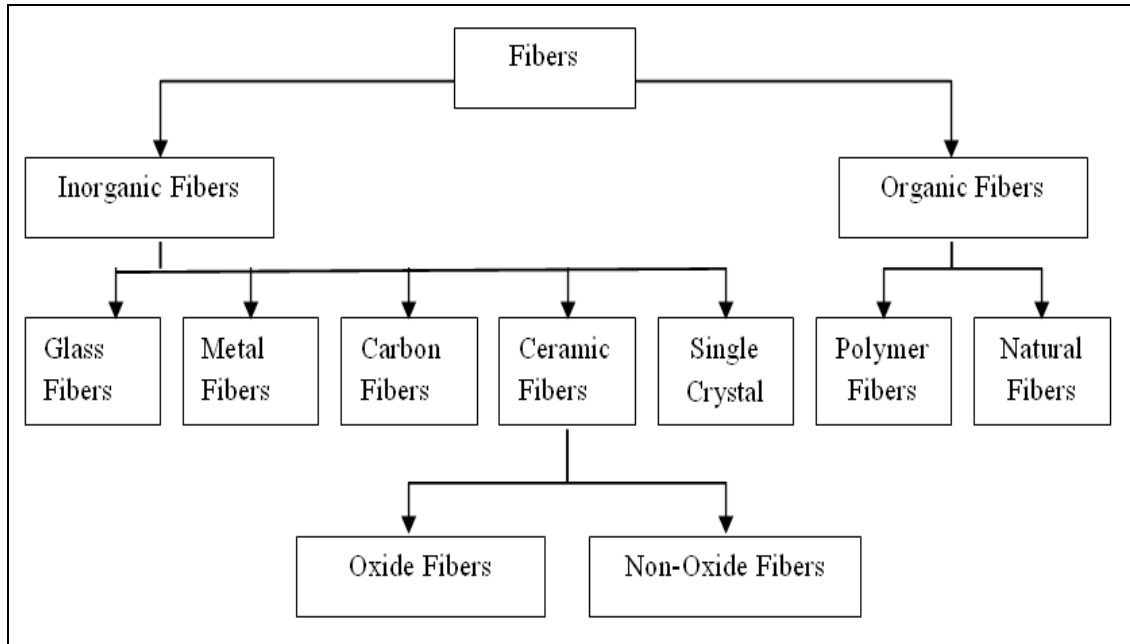


Figure 4. The classification of fibers [4].

Ceramic fibers are classified as oxide or non-oxide. Non-oxide fibers are made from silicon carbide (SiC). Nicalon, Tyranno, and Sylramic are examples of non-oxide fibers [2]. Table 1 shows important properties of selected oxide ceramic fibers.

Table 1. Important properties of selected fibers [4].

Fiber Type	Trademark (Nextel)	Composition (%)	Diameter (μm)	Density (gcm^{-3})	Young's Modulus (GPa)
$\text{Al}_2\text{O}_3 + \text{SiO}_2$	312	62 Al_2O_3 24 SiO_2 14 B_2O_3	8-12	2.7	1.7 / 150
$\text{Al}_2\text{O}_3 + \text{SiO}_2$	440	70 Al_2O_3 28 SiO_2	10-12	3.05	2.1 / 190
$\text{Al}_2\text{O}_3 + \text{SiO}_2$	550	73 Al_2O_3 27 SiO_2	10-12	3.0	2.0 / 190
$\text{Al}_2\text{O}_3 + \text{ZrO}_2$	650	89 Al_2O_3 10 ZrO_2 1 Y_2O_3	11	4.1	2.5 / 360
$\text{Al}_2\text{O}_3 + \text{SiO}_2$	720	85 Al_2O_3 15 SiO_2	12	3.4	2.1 / 260
$\alpha\text{-Al}_2\text{O}_3$	610	99 Al_2O_3 0.3 SiO_2 0.7 Fe_2O_3	10-12	3.75	2.6 / 370

Reinforcing components can be produced in form of continuous fibers, short fibers, and whiskers. High performance CMCs are mainly reinforced by continuous fibers, since distinct fiber arrangements have led to explicit changes in materials' properties. One of the most important attributes of fibers is their flexibility, this being a function of elastic modulus (E). Hence, reducing the fiber diameter to a sufficiently small value leads to very flexible fibers, even for ceramics with very high E and extreme brittleness. Thus, continuous fibers can be transferred in semi-finished fiber preforms, which today play a major role in the processing of CMCs [4].

The processing of oxide fibers began during the 1970s, and first commercial products contained SiO_2 besides the main component Al_2O_3 [4]. Later, pure $\alpha\text{-Al}_2\text{O}_3$ fibers were produced and embedded in alumina matrices in order to provide lightweight

ceramic structures with a high Young's modulus. α - Al_2O_3 -fibers with second phases were also developed with the objective to enhance the creep resistance for applications at high temperatures [4, 9, 11].

2.3 Matrix.

The matrix is the continuous phase that provides the shape of the material. The primary functions of the matrix are to transfer load between fibers, separates fibers to prevent adjacent filaments from failing, and to protect and house the fibers from environmental attack [12].

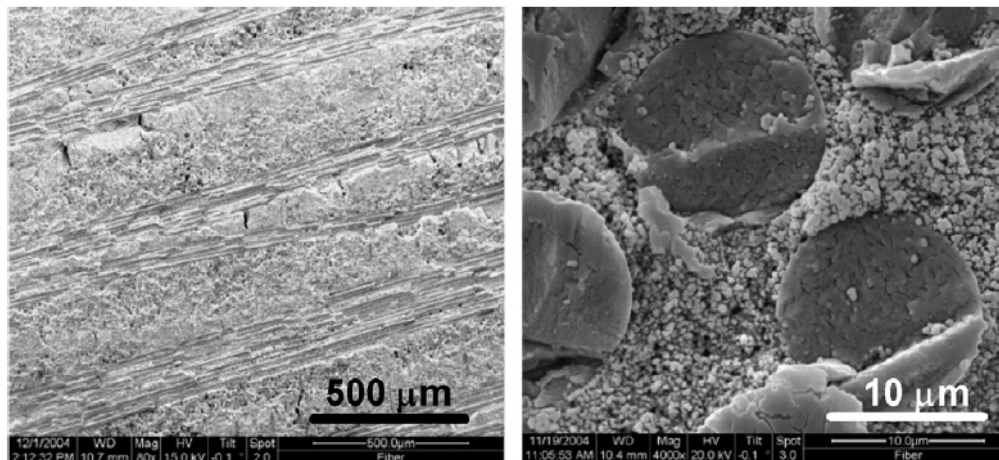


Figure 5. As-processed N720/A composite a) overview, optical microscope and b) porous nature of the matrix is evident [13].

Although no one ceramic is going to meet all the requirements, one can make a list of some desirable characteristics of a ceramic matrix. That is, what one would like to see in an ideal matrix material. In a real matrix, one can only hope for a large number of these characteristics, An ideal ceramic matrix material should:

- infiltrate a bundle of fibers, whiskers, or particulate perform.

- Form a mechanical or frictional bond with the reinforcement.
- Have no chemical reaction with the fiber reinforcement during fabrication or service.
- No damage to the fiber.
- Have a good resistance to creep, fatigue, and impact.
- Have a high toughness
- Should be chemically stable, i.e., it should be impermeable to moisture, resistant to oxidation, should not hydrate or volatilize, etc [3].

In an air or oxygen, oxide ceramics are inherently more stable than non-oxide ceramics [3].

2.4 Ceramic Matrix Composite Applications

Today, military and commercial aerospace vehicles desire to go higher, farther, and faster. This need has dramatically increased the demand for lightweight, high strength structural materials that can perform in aggressive operating environments at extremely high temperatures. Aircraft such as the F-22 and the Boeing 787 Dreamliner are pushing the technological limits in order to achieve faster cruising speeds, longer operating distances, and improved flight performance. “These goals translate into material requirements involving increased strength-to-weight, stiffness-to-density, and improved damage tolerance - all at significantly higher temperatures” [6]

The main advantage of all-oxide composites over non-oxide ones (e.g. SiC/SiC, C/SiC) is their superior resistance to oxidation under typical turbine engine conditions,

since non-oxide fiber-reinforced CMCs show no oxidation resistance at temperatures as far as above 1000°C. A remarkable research effort has been exerted in the development of non-oxide fiber-reinforced CMCs and the resulting composites exhibit high strength, high toughness in many applications. However, this is not the case for those which require oxidation resistance [5].

The application areas of composite are defined as:

1. aircraft engine components such as turbine combustors, compressors and exhaust nozzles.
2. ground based gas turbine and automotive components such as combustors, first and second stage turbine vanes and blades
3. aerospace engines and missiles and reusable space vehicles and
4. industrial applications such as heat exchangers and radiant burners where primarily high temperature and oxidation resistance of the material demanded [5].

Besides offering high temperature capability and eliminating cooling requirements, CMCs offer a significant weight reduction [14]. Figure 6 shows potential applications of CMCs, as non structural and structural parts of aero-engine components.

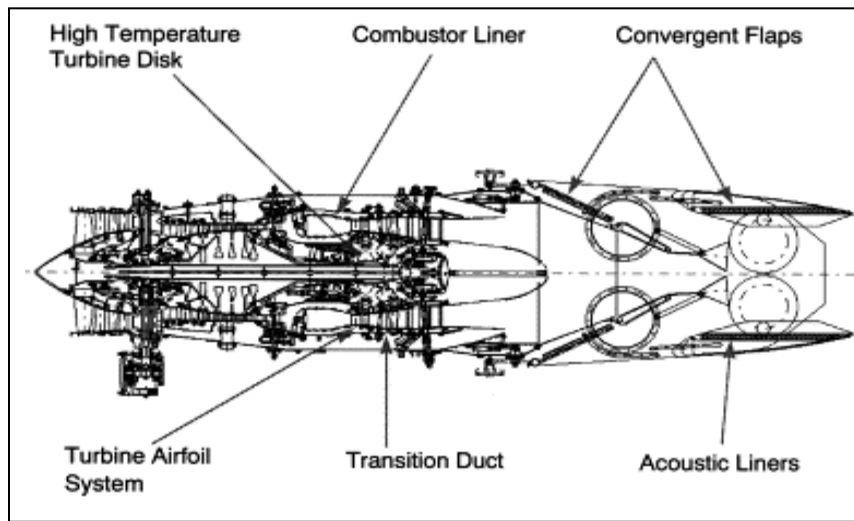


Figure 6. Potential applications of CMCs [14].

For applications in spacecraft, the major challenge is to provide new materials that will withstand the projected high temperatures and long-term conditions, where metallic or pure carbon materials are insufficiently stable. Moreover, with the availability of flexible manufacturing techniques such as winding, weaving, lay-up laminates and new jointing methods, CMCs become a particularly attractive for these purposes. For the development of new re-entry vehicles such as X38, Hermes, and others, the development of new complex components is vital [4]. However, in space applications, the material life requirements are less demanding and the environment in space is often non-oxidizing (Table 2.3). Therefore, non-oxide CMCs are hereby more convenient since they will not undergo oxidative embrittlement and display higher mechanical strength [5].

Another field of CMC use in space industry is the development of new propulsion systems. Radiation cooled nozzle extensions and combustion chambers are favorably fabricated from CMCs, the major advantages being the materials' high strength and light

weight, high applicable service temperatures, and chemical stability versus liquid propellant [4]. Aircraft, space and industrial application fields of CMCs are shown in Table 2.

Table 2. CMC Applications

2.1. Aircraft applications [5].

TYPE	COMPONENT	TYPICAL GOALS
Land based gas turbines	Combustor Turbine vanes	operating at $> 1600^{\circ}\text{C}$ for 25.000 hrs
Power Generation	Shrouds Combustor Thermophotovoltaic Cells	900°C for short For 25.000 hrs
Industrial Processing	Chemical Pumps Gas filters Furnace hardware	350°C For 30.000 hrs in chemical hazardous environment

2.2. Industrial and power generation applications [5].

AIRCRAFT TYPE	COMPONENT	TYPICAL GOALS
Civil Aircraft Gas Turbines	Compressor Combustor turbine	For both components $> 1300^{\circ}\text{C}$ for > 10.000 hrs
Commercial Supersonic Transport	Combustor Exhaust Nozzle	$> 1600^{\circ}\text{C}$ $> 800^{\circ}\text{C}$ for 10.000 hrs
Military	Combustor turbine Exhaust nozzle	For both components $> 1300^{\circ}\text{C}$ for over 1000 hrs

2.3. Space applications [5].

TYPE	COMPONENT	TYPICAL GOALS
Missile	Combustor Turbine rotors	Operating at $> 1400^{\circ}\text{C}$
Space Vehicles	Turbomachinery Nozzles Thrust chambers	Very high temperatures $> 1600^{\circ}\text{C}$ for short periods of time
Satellites	Maneuvering Thrusters	$> 1700^{\circ}\text{C}$ for > 10 hrs

As seen in figure 7, ceramic matrix composites are less dense than high temperature superalloys yet still have comparable strength to weight ratios and much greater temperature operating ranges [15].

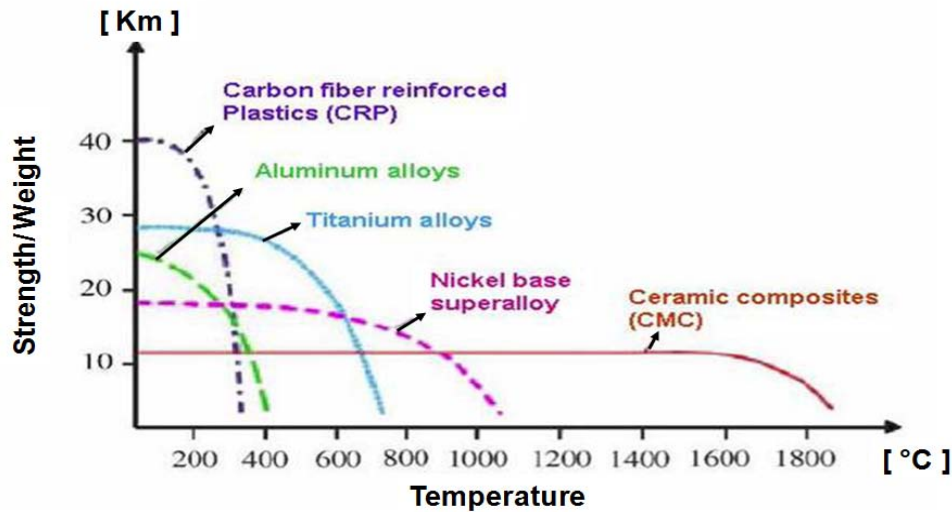


Figure 7. Ratio of strength to weight as a function of temperature [15].

2.5. Previous Research

There are some previous research efforts exist on the Nextel™ 720/Alumina-Mullite and Nextel™720/Alumina composites with 0°/90° fiber orientation in both air and steam environments at AFIT.

Genelin [16] studied the tensile creep behavior of the N 720/Alumina-Mullite ceramic matrix composite with 0°/90° fiber orientation at 1200 °C. Creep tests performed in air, steam and argon which is a non-oxidizing environment. He first investigated the stress-strain behavior of the composite. Additionally, the influence of the loading rate on tensile behavior of the material was explored. Creep tests were conducted at 1200 °C in

air, steam and argon. According to his results, the N720/AM composite exhibits primary and secondary creep regimes in air and steam. The largest creep strains were accumulated in steam. He observed that the presence of steam dramatically reduced creep lifetimes of the N720/AM and he also found that the presence of argon had a detrimental effect on creep performance of the N720/AM.

Harlan [17] examined creep-rupture behavior of the N720/Alumina ceramic matrix composite with 0/90° fiber orientation in both laboratory air and steam environments at 1200 and 1330 °C. Creep stress levels ranging from 80 to 154 MPa at 1200 °C and creep stress levels of 50 and 100 MPa at 1330 °C were investigated. According to his results, the material performed well during creep tests in air, but the material's creep performance in steam degraded at both temperatures.

Braun [18] studied the creep behavior of the N720/A composite with 0/90° fiber orientation. The creep behavior of the N720/A composite was characterized in air and in steam for different creep stress levels at 1000 and 1100 °C. According to his results the tensile properties were strongly influenced by the loading rate at 1100 °C in steam. Braun found that the N720/A ceramic matrix composite exhibits decreased damage tolerance and reduced creep lifetimes at temperatures ≥ 1100 °C. He explored the influence of loading rate at 1100 °C. The results of his study demonstrated that at temperatures ≥ 1100 °C the presence of steam causes degradation of creep resistance of the N720/A composite, as manifested by shortened creep lifetimes [18, 19].

Siegert [20] investigated the creep behavior of the N720/A composite with $\pm 45^\circ$ fiber orientation. In his effort, creep tests were performed in air, steam and argon. The

results showed that specimens tested in air produced lower creep rates than specimens tested at the same stress levels in other environments. He reported that environment did not appear to have a significant influence on the creep life of $\pm 45^\circ$ specimens.

2.6. Nextel™ 720/AM

The N720/AM is an oxide-oxide ceramic matrix composite consists of N720 fibers with $0^\circ/90^\circ$ fiber orientation and a porous alumina-mullite matrix. There is no interface between fiber and matrix, and the material relies on porosity of matrix for damage tolerance.

Fiber that exists in Nextel™720/Alumina-Mullite ceramic matrix composite is manufactured by Minnesota Mining and Manufacturing Company (3M™). This fiber is composed of 85% Al_2O_3 and 15% SiO_2 in the form of α -alumina [21].

Early investigations on alumina and mullite based fibers (e.g. Nextel™312, 450 and 550) showed that these fibers degrade in strength above 1250°C on long-term exposure (> 100 h). The loss of strength may arise from grain growth within the fiber and/or from chemical reaction of fiber with the matrix or interface material under high-temperatures. With Nextel™720, the first progress is reported. The superiority of this fiber relies on the grain growth inhibition of alumina, achieved by addition of mullite [5].

Mullite is a live compound of alumina and silica in the compositional range of 71-75 % alumina. Commonly mullite is represented by formula, $3\text{Al}_2\text{O}_3.2\text{SiO}_2$. It has excellent strength and creep resistance as well as low thermal expansion and conductivity [3].

The fiber Nextel™720 shows the highest thermal stability in the Nextel family. The fiber consists of alumina and mullite grains, and is manufactured via a sol-gel process. Small plate-like Al_2O_3 grains (70-100 nm) are distributed between and inside mullite grains (300-500 nm), which consist of smaller subgrains. At 1400 °C, 85% of the room-temperature strength is retained and the creep resistance is superior to that of all other Nextel fibers [4].

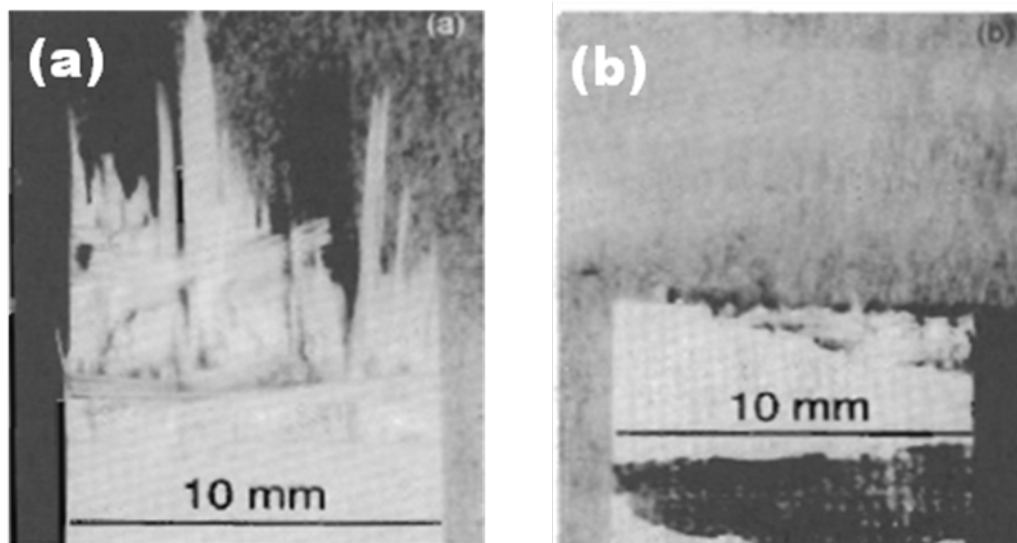


Figure 8. Low magnification views showing dramatic difference between a) fibrous failure normally seen with porous matrix composites and b) a brittle failure [1].

The composite manufactured by COI Ceramics (San Diego, CA), was supplied in a form of a 3.2 mm thick plate, comprised of 12 0°/90° woven layers [22] and the N720/Alumina-Mullite specimens used in this research had a fiber volume fraction of 38.5%.

2.7. Thesis Objective

The previous study revealed degrading effect of steam environments on material performance under both static and cyclic loadings. An additional matrix sintering was observed at 1200 °C, which led to the loss of matrix porosity and deterioration of composite toughness. This degradation process was accelerated in the presence of steam. In addition, the prior study revealed that at 1200 °C the creep performance of NextelTM720/Alumina-Mullite CMC, a material system which relies on a porous alumina/mullite matrix for damage tolerance, also deteriorates drastically in the presence of steam [16, 22]. The objective of this study is to identify the temperature range where steam environment causes degradation of creep resistance of the NextelTM720/Alumina-Mullite CMC.

III. Experimental Arrangements and Test Procedures

This chapter explains both the testing and supporting equipments used in this research. Additionally, detailed descriptions of all test procedures and microstructural analysis are presented.

3.1 Testing Equipment

3.1.1 Mechanical Equipments

A servo-hydraulic Material Test Systems (MTS) 810 machine was used for all tensile, creep and stress rate tests. The maximum loading capacity was 5.5 kip (25 kN). This vertically actuated machine is shown in Figure 9.



Figure 9. MTS 810 Test Station.

Water-cooled hydraulic wedge grips with surfalloy surfaces grip the test specimens. An MTS TestStar II digital controller was used for test control and data acquisition.

A grip pressure of 8 Mpa, prevents specimen slippage while keeping the gripped portion of the specimen from damage, was used in all tests. A NESLAB model HX-75 chiller provided 15 °C deionized water circulation through the wedges which ensured the grips to be cooled. It is shown in Figure 10.



Figure 10. NESLAB Model HX-75 Chiller.

Force measurement was acquired by a 25 kN (5.5 kip) maximum capacity MTS Force Transducer (Model 661.19E-04). A uniaxial, high-temperature, low contact force MTS Extensometer (Model 632.53E-14) with the 12.5 mm gage length performed the strain measurement. Displacement measurement was obtained by an LVDT internal to the MTS servo-hydraulic machine. Figure 11 shows the mechanical test system includes close-up view of the transducer, top wedge grips, and extensometer set-up.



Figure 11. Mechanical Test System.

3.1.2 Environmental Equipments

To maintain the elevated temperature and environment required for testing, the mechanical testing station was equipped with a dual zone Amteco Hot Rail Furnace System. The dual zone Amteco Hot Rail Furnace is shown in Figure 12a. Two heating elements, internally insulated with alumina, were established each sides of the furnace. The insulation was modified to enable the oven to close around the test specimens without any undesirable interference. Figure 12b shows the modified furnace insulation where heating elements and control thermocouple are visible. An R-type thermocouple,

fitted on each side of the furnace, provided temperature information of the chamber to the controller unit.

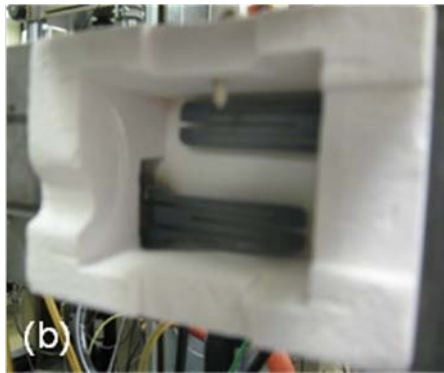


Figure 12. Heating Equipment: (a) AMTECO Hot-Rail Furnace
(b) Modified furnace insulation with heating elements and control thermocouple.
(c) Heating Element

The dual zone Amteco Hot Rail Furnace System (see Fig. 12) was controlled by an MTS Model 409.83B Temperature Controller that is shown in Figure 13.



Figure 13. MTS Model 409.83B Temperature Controller.

Continuous steam environment was obtained by an Amteco HRFS-STMGEN Steam Generation System during the tests conducted in steam. Steam Generation System supplied de-ionized water using a one-gallon water reservoir. An alumina susceptor, cylinder tube with end caps, which fits inside the furnace provided a positive pressure chamber around the specimen forcing out the dry air. The gauge section of the specimen was placed inside the susceptor while the ends passing through the slots. Note that the susceptor was not used during the tests in air. Figure 14 shows the front and rear view of the susceptor with the entrance slot for specimens, and holes for the extensometer and steam tube.

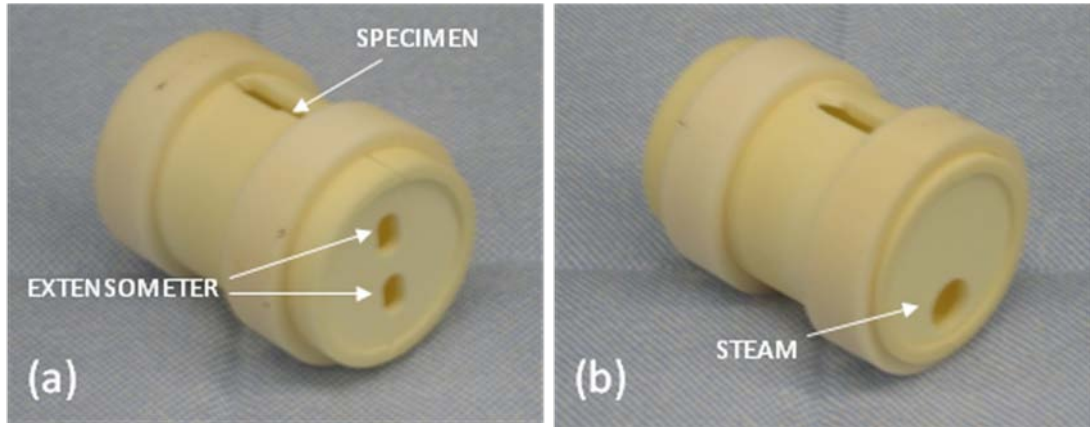


Figure 14. Susceptor a) front view and b) rear view

3.1.3. Microstructural Characterization Equipments

Both an optical microscope and a scanning electron microscope (SEM) were used for post test analysis of the failed specimens' fracture surfaces. A Zeiss Discovery V12 optical microscope equipped with a Zeiss AxiCam HRc digital camera was used to examine the damage zones of the specimens. Figure 15 shows a Zeiss Discovery V12 optical microscope. Micrographs were taken at various magnifications up to 100X by the optical microscope.



Figure 15. Zeiss Discovery V12 Optical Microscope.

An F E I F P 2011/ 11 Q uanta 200 H V S canning E lectron M icroscope s hown i n Figure 16 w as us ed t o e xamine t he s pecimen m icrostructure c haracterization a t magnifications of up to 20,000X.

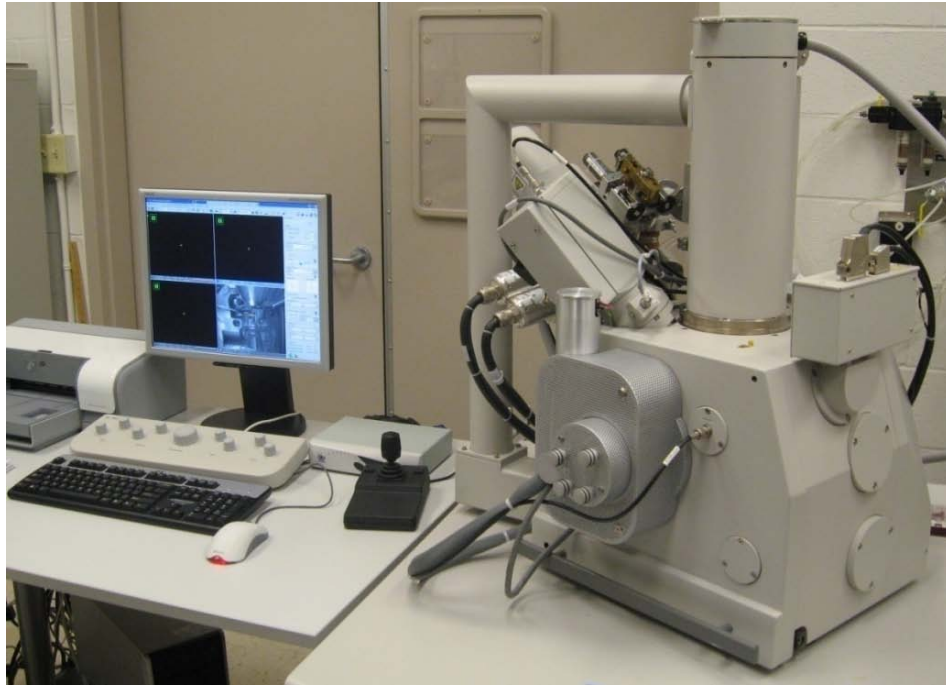


Figure 16. FEI FP 2011/11 Quanta 200 3D HV Scanning Electron Microscope.

The scanning electron microscope (SEM) is a type of electron microscope that images the sample surface by scanning it with a high-energy beam of electrons in a raster scan pattern. The electrons interact with the atoms that make up the sample producing signals that contain information about the sample's surface topography, composition and other properties such as electrical conductivity. The SEM produces images by probing the specimen with a focused electron beam that is scanned across a rectangular area of the specimen. At each point on the specimen the incident electron beam loses some energy, and that lost energy is converted into other forms, such as heat, emission of low-energy secondary electrons, light emission (cathodoluminescence) or x-ray emission. The signals result from interactions of the electron beam with atoms at or near the surface of the sample. The display of the SEM maps the varying intensity of any of these signals

into the image in a position corresponding to the position of the beam on the specimen when the signal was generated. The SEM micrographs have a very large depth of field yielding a characteristic three-dimensional appearance useful for understanding the surface structure of a sample [23].

3.2 Test Procedures

3.2.1 Temperature Calibration

To obtain the desired test temperature of the specimen, the furnace temperature controller was calibrated prior to mechanical testing. Calibration was performed by using a test specimen fitted with 2 R-type thermocouples shown in Figure 17. The thermocouples were wrapped with a high temperature wire to ensure contact with the specimen. This specimen was placed into the MTS machine following the same procedures during tests.

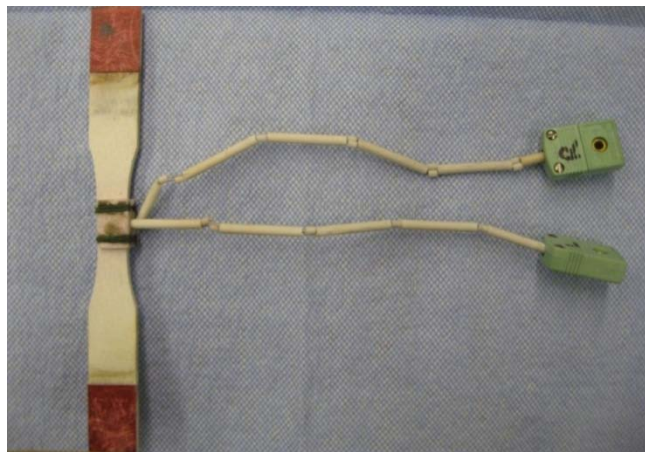


Figure 17. Temperature Calibration Specimen.

After placing the calibration specimen, the furnace temperature was raised until the specimen temperature reached the desired temperature level at a rate of $1\text{ }^{\circ}\text{C/s}$. To obtain the precise elevated temperature calibration, the thermocouple temperature readings were closely monitored while the oven temperatures were manually increased to establish the desired temperature of the test specimen. The temperature of the specimen was read by a portable temperature reader shown in Figure 18.



Figure 18. Omega Engineering, Inc, OMNI-CAL-8A-110
Portable Temperature Reader

3.2.2 Preparation of Mechanical Testing

Prior to mechanical testing, specimen fabrication process was completed. Specimens were cut from the composite panel by the AFIT machine shop technicians using a high pressure water-jet machine. The panel was sandwiched between two thin aluminum sheets to prevent possible edge wear. Water-jet machine has a computer-controlled nozzle that sprays water mixed with garnet particles at high pressures to precision-cut different kinds of materials.

After cutting process, three steps of cleaning process were followed to remove the debris from the water-jet process. The cut specimens were placed into an ultrasonic bath and exposed to de-ionized water for 20 min, then soaked in 200-proof ethyl alcohol for 20 min. The cleaning process was completed after drying the specimens in the Omegalux LMF-3550 Benchtop Muffler Furnace at 250 °C for at least 2 hours. Figure 19 shows the uniaxial test specimen geometry.

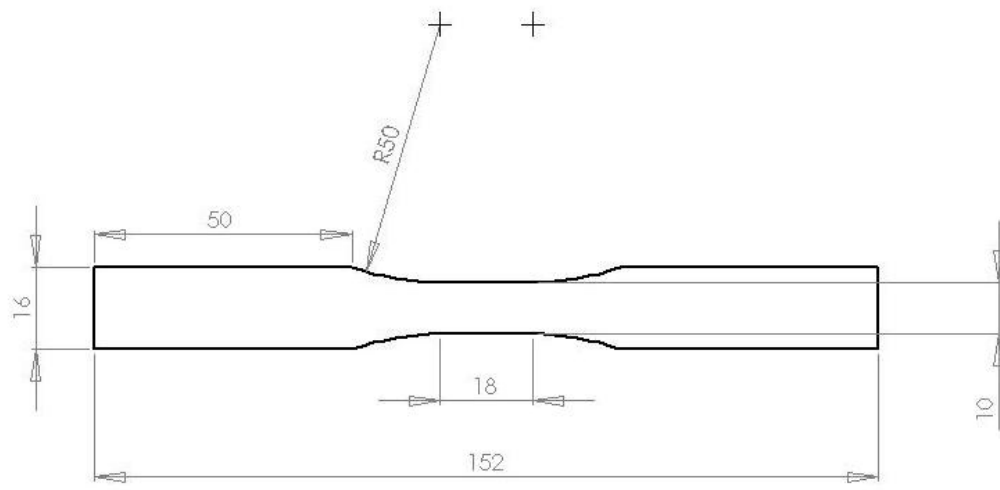


Figure 19. Uniaxial test specimen (dimensions in mm) [18].

Servo-hydraulic testing machine was warmed up in order to ensure the hydraulic fluid was at its operating temperature. The Function Generator mode of the MTS 810 Machine was used to cycle the actuator in displacement control for a minimum of 30 minutes. In this warm up process, square wave function with the frequency of 3 Hz and amplitude of 0.01 inches was used.

The sizes (width and thickness) of the specimen gauge section were measured at least three times by a Mitutoyo Corporation Digital Micrometer (Model NTD12-6”C) shown in figure 20 and an average was taken.



Figure 20. Mitutoyo Corporation Digital Micrometer

The cross-sectional area of the specimen was calculated using the measurements. The calculated cross-sectional area was used to find the load needed to achieve the desired test stress level, using the equation:

$$P = \sigma \times A$$

where P is load in Newtons (N), σ is stress in Pascals (Pa), and A is cross-sectional area in meters squared (m^2).

To protect the specimen from damaging by the pressure of the grips, the edges of the specimen were tabbed with rectangular fiberglass papers. (see Figure 21)



Figure 21. Tabbed Test Specimen.

3.2.3 Monotonic Tensile Tests

All monotonic tensile tests to failure were conducted at 900, 1000 and 1100 °C in laboratory air . The specimens were heated under zero load from room temperature to the elevated temperature at 1 °C/s and held at that temperature for 20 minutes. After the 20 minutes of dwell time, the specimen was loaded using displacement control at a constant rate of 0.05mm/s until failure. Load, strain, displacement, time data were recorded every 0.05 s from the beginning to the failure for all tensile tests.






Type	Name	Start	Interrupt
	Record Warm Up	<Procedure>.Start	Ramp Ovens to Temp.Done
	Ramp Ovens to Temp	<Procedure>.Start	
	Record Tensile Data	Ramp Ovens to Temp.Done	Shut Off Ovens.Done
	Load to Failure (Disp Ctrl)	Ramp Ovens to Temp.Done	
	Shut Off Ovens	Load to Failure (Disp Ctrl) Done	

Figure 22. Typical tensile test procedure.

3.2.4 Creep-Rupture Tests

Creep-rupture tests were conducted in load control at 1000 °C only in steam and at 1100 °C in both laboratory air and steam . Creep run-out was defined as 100 h at a given creep stress for all creep rupture tests. Specimens that achieved run-out in creep tests were unloaded to zero load and then they were subjected to tensile tests to failure in order to evaluate the retained tensile properties

Similar procedures were followed during the creep tests in steam except the addition of an alumina susceptor. Steam was pumped through a feeding tube into the rear section of the susceptor at a rate of 30 mL/minute expelling the dry air from the susceptor

and creating a near 100 % steam environment inside the susceptor. Figure 23 shows a typical creep test procedure.

Type	Name	Start	Interrupt
	Upper/Lower Disp Limits	<Procedure> Start	
	Record Warm Up	<Procedure> Start	Warm Up/Hold Ovens Done
	Warm Up/Hold Ovens	<Procedure> Start	Upper/Lower Disp Limits Done
	Record Load Up	Warm Up/Hold Ovens Done	Ramp Up (Load Ctrl) Done
	Ramp Up (Load Ctrl)	Warm Up/Hold Ovens Done	Upper/Lower Disp Limits Done
	Record Creep (0-5 min)	Ramp Up (Load Ctrl) Done	
	Record Creep (5-10 min)	Record Creep (0-5 min) Done	
	Record Creep (10 min -1 hr)	Record Creep (5-10 min) Done	
	Record Creep (1-3 hr)	Record Creep (10 min -1 hr) Done	
	Record Creep (3-5 hr)	Record Creep (1-3 hr) Done	
	Record Creep (5-25 hr)	Record Creep (3-5 hr) Done	
	Record Creep (25-100 hr)	Record Creep (5-25 hr) Done	Hold Load 100 Hrs (Load Ctrl) Done
	Hold Load 100 Hrs (Load Ctrl)	Ramp Up (Load Ctrl) Done	Upper/Lower Disp Limits Done
	Record Ramp Down	Hold Load 100 Hrs (Load Ctrl) Done	Ramp Down (Load Ctrl) Done
	Ramp Down (Load Ctrl)	Hold Load 100 Hrs (Load Ctrl) Done	Upper/Lower Disp Limits Done
	Record Tensile Test	Ramp Down (Load Ctrl) Done	Tensile Test (Disp Ctrl) Done
	Tensile Test (Disp Ctrl)	Ramp Down (Load Ctrl) Done	Upper/Lower Disp Limits Done
	Shut Down Ovens	Tensile Test (Disp Ctrl) Done	

Figure 23. Typical creep test procedure.

3.2.5 Tensile Tests at Stress Rates 0.0025 and 25 MPa/s

To observe the effects of both slow and fast stress rate during tensile, two repeated tests were conducted in force control at 1100 °C in steam environment. The tests were conducted at the stress rates of 0.0025 and 25 MPa/s.

3.2.6 Microstructural Characterization

Optical microscope and SEM were used for post-test microstructure examination. Various magnifications were used to examine the entire fracture surface of each half of the failed specimens.

Note that, one optical micrograph was taken per side of failed half specimens. After that, only one half of the each failed specimens was prepared to get a clear view in the SEM. During this preparation process, failed specimens were mounted on to

aluminum platforms by gluing with silver paste after they had been cut by CNC saw shown in Figure 24. The other half parts of the failed specimens were collected for documentation.

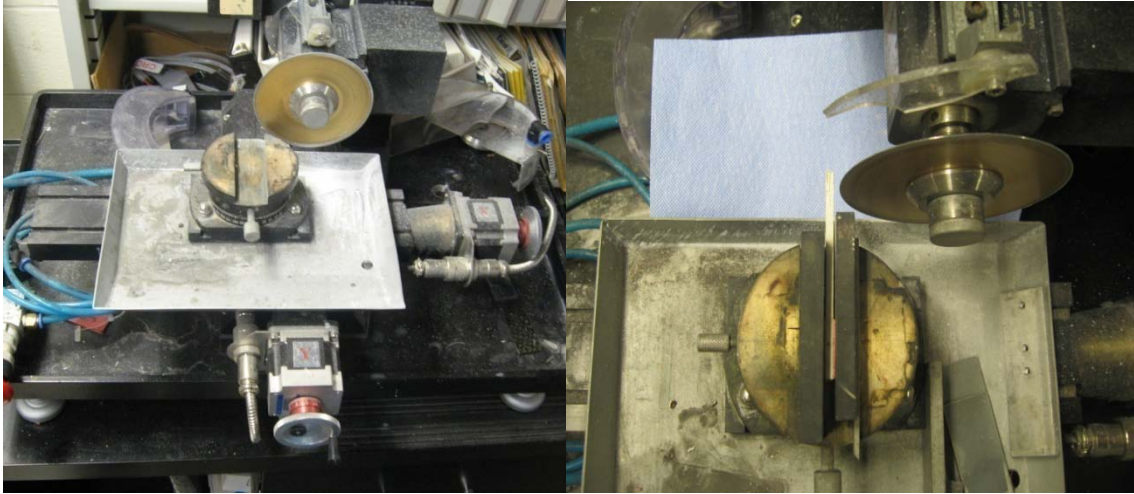


Figure 24. CNC Saw.

SEM, utilizing the process described in chapter 3.1.3, requires conductive materials that prevent charging in order to enable creating clear images. A non-conductive specimen cause a charge which obscures resolution capability and may damage the equipment. Since the CMCs are non-conductive materials, they were first coated with carbon using an SPI-Module Control and Carbon Coater to observe the fracture surfaces of the specimens. The SPI-Module Control and Carbon Coater and the storage box includes carbon coated samples are shown in Figure 25.



Figure 25. (a) SPI Carbon Coating Machine (b) Carbon-coated failed specimens in the storage box.

IV. Results and Analysis

4.1 Section Summary

This chapter explains the detailed experimental results of the all tests were performed in this research.

First, the chapter starts with the presentation and discussion about thermal properties of the N720/AM ceramic matrix composite. Then, the results of tensile tests with both displacement and constant loading rate control are presented. Next, the results of creep-rupture tests are explained and discussed. Effect of temperature and steam environment on creep-rupture behavior is widely discussed. Comparisons of the results from this research and previous efforts are also presented. Finally, fracture surfaces of failed N720/AM specimens are characterized. Micrographs obtained by using optical and

scanning electron microscope are discussed. Following tables represent the summary of the experimental tests performed in this research.

Table 3. Summary of tensile data for N720/AM with 0°/90° fiber orientation obtained in tensile tests.

Specimen (#)	Control Method	Environment	Temperature (°C)	Elastic Modulus (GPa)	UTS (MPa)
1	0.05mm/s	Air	900	67.5	146.4
2	0.05mm/s	Air	1000	65.5	161
4	0.05mm/s	Air	1100	63.5	160.2
13	25 MPa/s	Steam	1100	65.5	150
14	0.0025 MPa/s	Steam	1100	44.0	132
15	0.0025 MPa/s	Steam	1100	44.2	130
16	25 MPa/s	Steam	1100	62.3	155

Table 4. Summary of creep data for N720/AM with 0°/90° fiber orientation obtained in creep-rupture tests.

Specimen (#)	Environment	Temperature (°C)	Elastic Modulus (GPa)	Creep Stress (MPa)	Creep Strain (%)	Creep Life (h)
6*	Air	1100	65.2	109	0.2	>100
7*	Air	1100	64.7	131	0.23	>100
8	Steam	1100	62.9	131	0.42	4.12
9	Steam	1100	66.3	109	0.87	35.2
10*	Steam	1100	64.4	87.5	0.69	>100
11*	Steam	1000	65.4	131	0.20	>100
12*	Steam	1000	65.3	140	0.21	>100

* Run-out (100h)

Table 5. Summary of retained properties for N720/AM with 0°/90° fiber orientation subjected to prior creep.

Specimen (#)	Temperature (°C)	Environment	Creep Stress (MPa)	Retained Modulus (GPa)	Retained Strength
11	1000	Steam	131	58.7	166
12		Steam	140	60.6	173
6	1100	Air	109	59.9	168
7		Air	131	55.8	174
10		Steam	87.5	55.4	162

4.2 Thermal Expansion

The coefficient of linear thermal expansion was calculated by using thermal strain measured in the tests. Thermal strain was measured using the linear part of the strain-time curve while heating up the test environment to the elevated test temperature. The following equation gives us the relation between thermal strain and the coefficient of linear thermal expansion

$$\varepsilon_t = \alpha_t \cdot \Delta T$$

where ε_t is the thermal strain (m/m), α_t is the coefficient of linear thermal expansion and ΔT is the change in temperature (K) that was the difference between the elevated temperature and the room temperature. The room temperature was defined as 23 °C for all tests performed in this effort. Thermal properties are summarized in Table 6.

Table 6. Summary of thermal properties for the N720/AM composite obtained from all tests.

Specimen (#)	Environment	Temperature (°C)	Thermal Strain (%)	Coefficient of Linear Thermal Expansion (10^{-6}K^{-1})
1	Air	900	0.56	6.39
2	Air	1000	0.69	7.07
4	Air	1100	0.71	6.56
6	Air	1100	0.69	6.38
7	Air	1100	0.70	6.49
8	Steam	1100	0.74	6.86
9	Steam	1100	0.72	6.67
10	Steam	1100	0.71	6.58
11	Steam	1000	0.66	6.78
12	Steam	1000	0.63	6.45
13	Steam	1100	0.73	6.76
14	Steam	1100	0.70	6.49
15	Steam	1100	0.76	7.06
16	Steam	1100	0.74	6.88

The average values of ε_t at 900, 1000 and 1100 °C were 56%, 0.66% and 0.72% and the average of calculated α_t values were 6.39, 6.76 and $6.67 \cdot 10^{-6} \text{ K}^{-1}$, respectively.

Average thermal measurements for the N720/A and N720/AM ceramic matrix composites are summarized in Table 7.

Table 7. Average thermal properties measured for the N720/A and N720/AM composites due to temperature rise from 23°C to 900, 1000 and 1100 °C. Data for N720/A from Braun[18]

Material	Temperature	Average Thermal Strain (%)	Coefficient of Linear Thermal Expansion (10^{-6}K^{-1})
N720/A	1000	0.58	7.57
	1100	0.68	8.2
N720/AM	900	0.56	6.39
	1000	0.66	6.76
	1100	0.72	6.67

The average α_t for the N720/AM composite due to temperature rise from 23 to 1000 °C is close to that for the N720/A composite. The average α_t value for the N720/AM composite due to temperature rise from 23 to 1100 °C is slightly lower than that for the N720/A composite.

4.3 Monotonic Tension

To understand the tensile properties of N720/AM ceramic matrix composite, three specimens were subjected to tensile tests at 900, 1000 and 1100 °C. All tests were performed in laboratory air. Displacement control method at the constant rate of 0.05 mm/s was used. Tensile stress-strain curves for the N720/AM ceramic matrix composite at 900, 1000, and 1100 °C in air are illustrated in Figure 26.

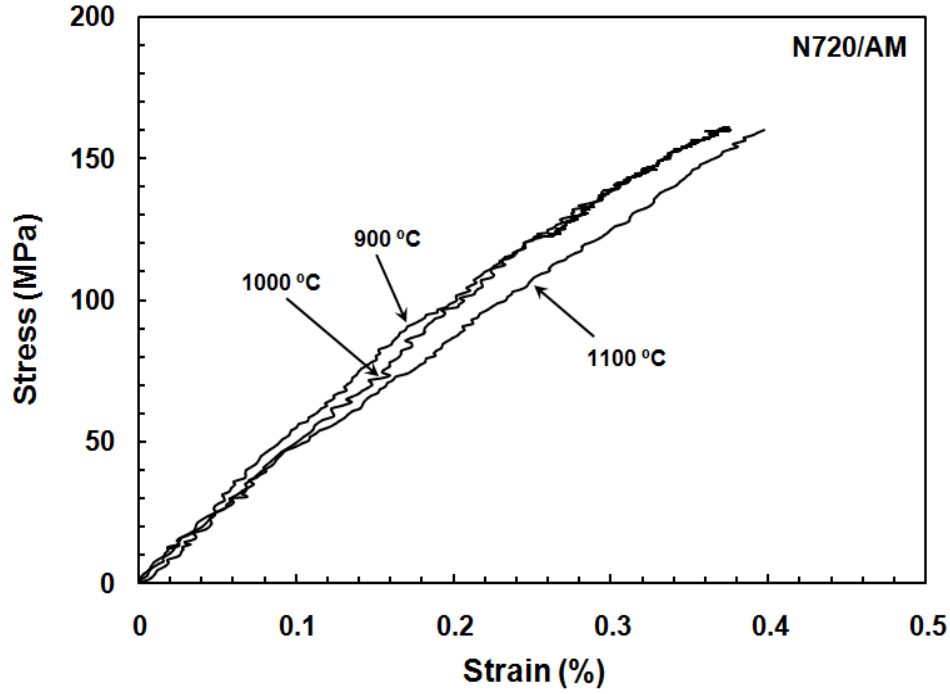


Figure 26. Tensile stress-strain curves for N720/AM composite obtained at 0.05mm/s in the 900-1200 °C range.

For the specimens having 0°/90° fiber orientation, the fiber orientation is in the same direction of the load and dominates the mechanism in failure to tension. As a result, fiber volume fraction, V_f , must be considered as a critical parameter to facilitate comparison of the experimental results obtained from different composites. Previous work [18] for the N720/A ceramic matrix composite had a fiber volume fraction of 44%, but in this research the fiber volume fraction of the N720/AM ceramic matrix composite was 38.5%. After normalizing the UTS values to 44% V_f by using the relationship:

$$UTS_{adj} = \left(\frac{44}{38.5}\right) * UTS, \text{ the adjusted UTS values for the N720/AM composite at 900,}$$

1000 and 1100 °C become 167.3, 184 and 183 MPa, respectively.

The results of average tensile properties for N720/A and N720/AM ceramic matrix composites are represented in Table 8.

Table 8. The average tensile properties for the N720/A and N720/AM composites at various temperatures. Data for N720/A from Braun[18,19]

Material	Elastic Modulus (GPa)	UTS (MPa)	Failure Strain (%)
<i>Tests at 900 °C</i>			
N720/A	70.1	190	0.33
N720/AM	77.1 ^a	167.3 ^a	0.32
<i>Tests at 1000 °C</i>			
N720/A	73.5	187.5	0.32
N720/AM	72.5 ^a	184 ^a	0.37
<i>Tests at 1100 °C</i>			
N720/A	69.6	186	0.33
N720/AM	72.5 ^a	183 ^a	0.4

^a Adjusted for $V_f=0.44$

As it is seen in Table 8, as the temperature increases the failure strain specimen increases for the N720/AM and it is noteworthy that the N720/A specimens have bigger UTS values at all temperature levels.

To identify the effects of loading rate on tensile properties of the N720/AM composite, four specimens were subjected to tension to failure at 1100 °C in steam. Tests were conducted with constant loading rates of 25 and 0.0025 MPa/s. The effect of loading rate on stress-strain curves of the N720/AM at 1100 °C in steam is shown in Figure 27.

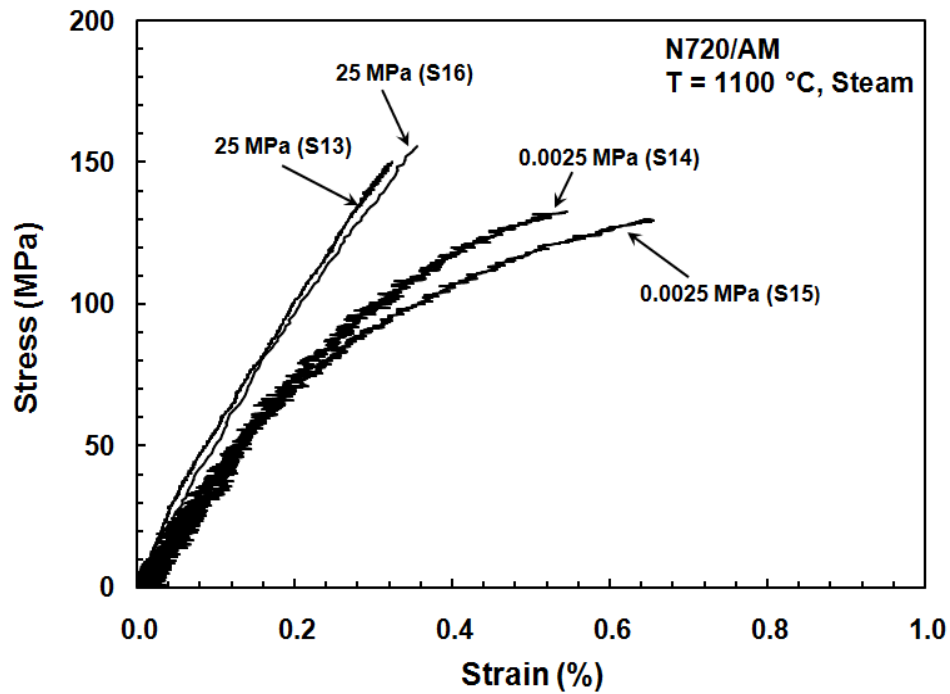


Figure 27. Tensile stress vs. strain curves for the N720/AM with constant loading rates of 25 and 0.0025 MPa/s at 1100 °C in steam. Effect of loading rate on stress-strain behavior and strength properties is evident.

At the constant loading rate of 25 MPa/s, the tensile stress-strain curves seem nearly linear from beginning to failure. The average UTS obtained from two tests is 153 MPa (equivalent to 174.9 MPa for $V_f = 0.44$), the average elastic modulus was 63.8 GPa (equivalent to 72.9 GPa for $V_f = 0.44$), the average failure strain, 0.34%, is 0.06% lower than that measured in tensile test with displacement control in air. The UTS value is decreased by 4.5% and the modulus of elasticity is increased by 0.55% compare to those measured with displacement control at 0.05mm/s at 1100 °C in air.

At the constant loading rate of 0.0025MPa/s which is a change in loading rate by four orders, there is a significant change in the tensile stress-strain behavior of N720/AM composite at 1100 °C in steam. It can be seen in Figure 27 that the stress-strain curves

obtained at the constant loading rate of 0.0025 MPa are nonlinear to failure. The linearity of the both curves for 0.0025 MPa/s loading rate tests only remains until approximately 40 MPa stress level, then, a considerable deviation from linearity begins. The average UTS obtained from two tests at 1100 °C is 131 MPa. The average UTS value is much lower than that at the constant loading rate of 25 MPa/s. The average elastic modulus, 44.1 GPa, is 21% lower than that at 25 MPa/s. The failure strain values are ranging from 0.55 to 0.64% where the average is 0.6% which is 174%, of that obtained at 25 MPa/s. The average results for the N720/A and N720/AM ceramic matrix composites at 1100 and 1200 °C are presented in Table 9.

Table 9. The average tensile properties for N720/AM composite with constant loading rates at 25 and 0.0025MPa/s in steam. Data at 1200 °C from Genelin [16]

Temperature (°C)	Elastic Modulus (GPa)	UTS (MPa)	Failure Strain (%)	Time to Failure (h)
<i>Loading rate at 25MPa/s</i>				
1100	72.9 ^a	174.2 ^a	0.34	0.0017
1200	50.1 ^a	149.6 ^a	0.6	14.57
<i>Loading rate at 00.25MPa/s</i>				
1100	66.44 ^a	165.4 ^a	0.55	0.0016
1200	27.64 ^a	103 ^a	1.26	10.38

^a Adjusted for $V_f=0.44$

As it was reported for N720/A ceramic matrix composite at 1100 °C by Braun [18] and as it is seen in Table 9 for N720/AM ceramic matrix composite at 1100 and 1200 °C, a strong dependence of tensile behavior on loading rate was observed in this effort like in the previous researches.

4.4 Creep-Rupture

Creep tests were performed at 1100 °C in both air and steam and at 1000° C only in steam. Creep run-out time was defined as 100 hours in all tests. Results of creep-rupture tests for N720/AM ceramic matrix composite are given in Table 10.

Table 10. Results of Creep-Rupture tests for N720/AM.

Specimen (#)	Environment	Temperature (°C)	Creep Stress (MPa)	Creep Strain (%)	Creep Life (h)	Secondary Creep Rate (s ⁻¹)
6*	Air	1100	109	0.2	>100	2.29E-07
7*	Air	1100	131	0.23	>100	3.32E-07
8	Steam	1100	131	0.42	4.12	1.93E-05
9	Steam	1100	109	0.87	35.2	5.81E-06
10*	Steam	1100	87.5	0.69	>100	9.87E07
11*	Steam	1000	131	0.20	>100	6.51E-08
12*	Steam	1000	140	0.21	>100	2.17E07

*Run-out

Creep-rupture tests for N720/A ceramic matrix composite with 0°/90° fiber orientation were performed at 1100 °C in previous research by Braun [18]. He studied with N720/A specimens having fiber volume fraction of 44%. In contrast, in this effort fiber volume fraction was 38.5%. To facilitate the comparison of creep behavior of composites, equivalent creep stress levels must be used. Therefore; the creep stress values

have to be adjusted to values for $V_f=0.44$ by using the relation: $\sigma_{adj} = \left(\frac{44}{38.5}\right) * \sigma$.

Consequently, instead of the creep stress levels 87.5, 109, 131 and 140 MPa, especially in the comparison charts, the equivalent creep stress levels of 100, 125, 150 and 160 MPa are used , respectively.

4.4.1 Creep-Rupture Tests at 1100°C

Two creep-rupture tests were performed at 1100 °C in air. At 109 MPa (equivalent to 125 MPa for $V_f = 0.44$), creep run out was achieved with a creep strain accumulation of 0.2%. Creep run-out was also achieved at 131 MPa (equivalent to 150 MPa for $V_f = 0.44$) in air. Accumulated creep strain was 0.23%.

As a result of increasing creep stress, creep strain accumulation increases as it was expected. It is worth to note that creep strain accumulations remain below $< 0.25\%$ at both stress levels. Although the creep strain accumulation is low for each stress levels, in previous effort [18] for the N720/A, creep strain accumulation was only 0.13% at 150MPa for $V_f = 0.44$. This is nearly 50% of that accumulated for the N720/AM in this effort. Note that, the N720/A specimen also achieved run-out at 150 MPa for $V_f = 0.44$ in air.

Notice that creep curves obtained at both 109 and 131 MPa stress levels show primary and secondary creep regimes. Figure 28 shows the creep strain vs. time curves at 1100 °C in air with the curves obtained in steam.

Three creep tests were performed at 1100 °C in steam at the creep stress levels of 131, 109 and 87.5MPa (equivalent to 100, 125 and 150 MPa for $V_f = 0.44$, respectively). Creep run-out stress was 87.5MPa. Results of the creep tests conducted at 1100 °C both for the N720/AM and N720/A composites are summarized in Table 11. Results for the N720/A composite from Braun [18] are included for comparison.

Table 11. Results of Creep-Rupture tests for the N720/A and N720/AM composites with 0°/90° fiber orientation at 1100 °C. Data for N720/A from Braun[18]

Material	Creep Stress (MPa)	Creep Strain (%)	Creep Life (h)
<i>Tests in laboratory air</i>			
N720/A	150	0.13	>100
N720/AM	125 ^a	0.2	>100
	150 ^a	0.23	>100
<i>Tests in steam</i>			
N720/A	100	0.50	>100
	125	0.49	53.7
	150	0.46	12.2
N720/AM	100 ^a	0.69	>100
	125 ^a	0.87	35.2
	150 ^a	0.42	4.12

^a Adjusted for $V_f=0.44$

Notice that the creep run-out stress level of 87.5MPa (equivalent to 100 MPa for $V_f=0.44$) is same for both the N720/AM and N720/A tested in steam. Creep life times for the stresses of 109 MPa (equivalent to 125 MPa for $V_f=0.44$) and 131 MPa (equivalent to 150 MPa for $V_f=0.44$) for N720/AM are lower than those for N720/A. Figure 28 and 29 illustrate the creep strain vs. time curves for the N720/AM and N720/A composites at 1100 °C, respectively. It is noteworthy that curves for the same stress levels of the N720/AM and N720/A exhibit similar trends at the same stress levels.

It can be seen in Figure 28 that the accelerated creep behavior in steam is apparent compared to the creep behavior in air at the same temperature. Furthermore; the acceleration rate increased with the applied creep stress. However, an increase in creep strain accumulation occurs as the stress level increases from 87.5 to 109 MPa and then a significant decrease occurs in the creep strain from 0.87% to 0.42% as the stress level

increase to 131 MPa. Similar behavior for the N720/AM ceramic matrix composite at 1200 °C was also reported by Genelin [16]. Creep strain-time curves at 1100 °C in steam also show primary and secondary creep regimes for all creep stresses in this research. Creep strain vs. time curves for 109 and 131 MPa creep stresses exhibit little tertiary regimes after showing primary and secondary regimes.

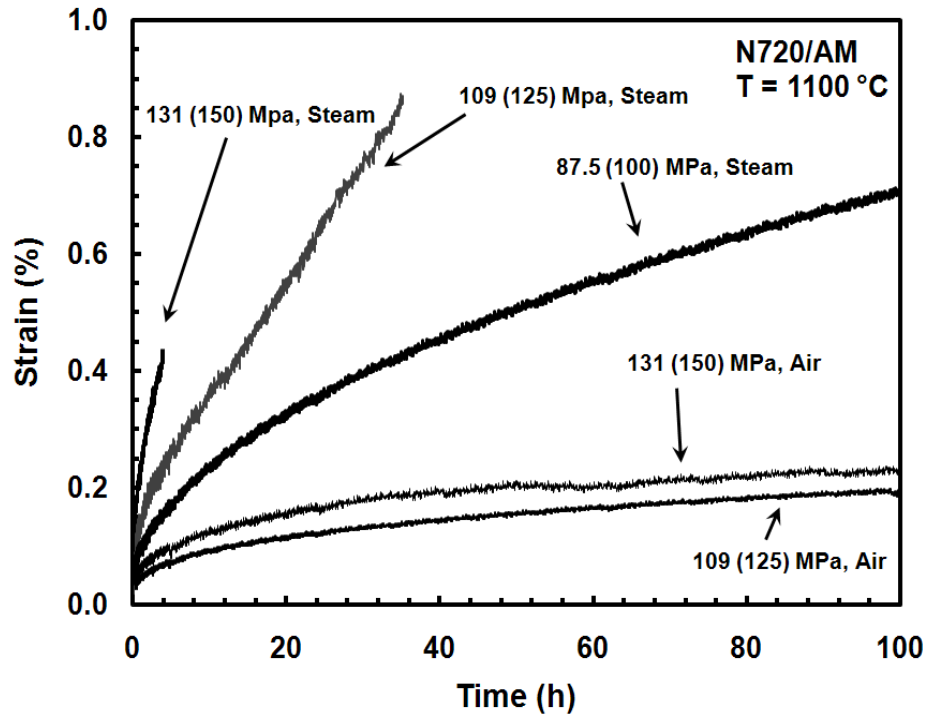


Figure 28. Creep strain vs. time curves for N720/AM composite at 1100 °C in air and steam. Stress levels adjusted for $V_f = 0.44$ are shown in parentheses.

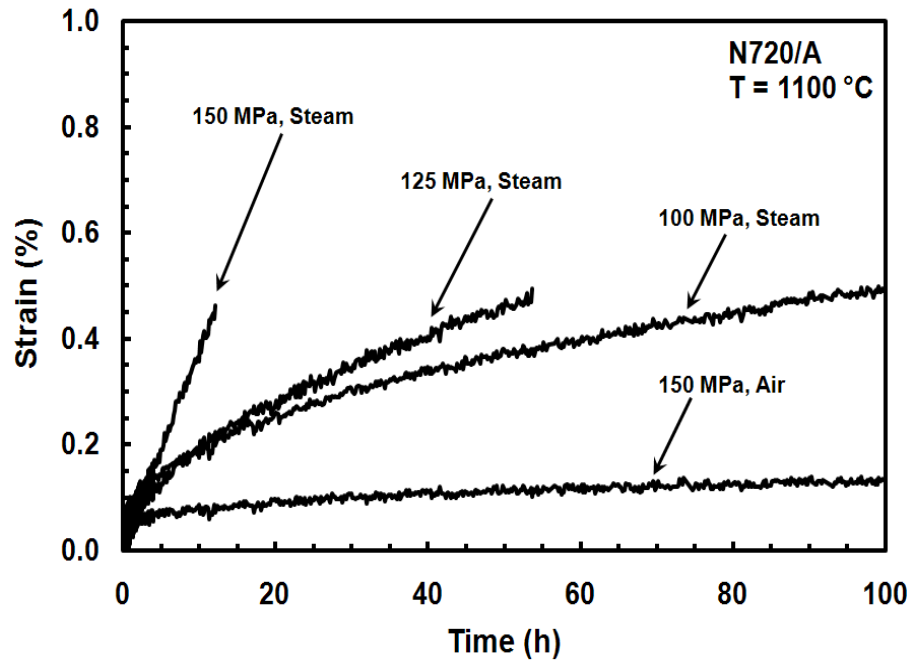


Figure 29. Creep strain vs. time curves for N720/A composite at 1100 °C in air and steam. Data from reference [18].

4.4.2 Creep-Rupture Tests at 1000 °C

Two creep-rupture tests were performed at 1000 °C only in steam. Creep stress levels were 131MPa and 140MPa. At 131 MPa (equivalent to 150 MPa for $V_f = 0.44$), creep run out was achieved with a creep strain accumulation of 0.2%. Creep run-out was also achieved at 140 MPa (equivalent to 160 MPa for $V_f = 0.44$) in steam. Accumulated creep strain, 0.21%, is only 0.01% larger than that accumulated at 131MPa. Similar behavior for the N720/A ceramic matrix composite at 1000 °C was also reported by Braun [19]. Results of the creep tests conducted at 1000 °C both for the N720/AM and N720/A composites are summarized in Table 12. Results for the N720/A composite from reference [18] are included for comparison.

Table 12 Results of Creep-Rupture tests for the N720/A and N720/AM composites at 1000 °C. Data for N720/A from Braun [18].

Material	Creep Stress (MPa)	Creep Strain (%)	Creep Life (h)
<i>Tests in laboratory air</i>			
N720/A	150	0.08	>100
<i>Tests in steam</i>			
N720/A	135	0.13	>100
	150	0.14	>100
	160	0.18	>100
N720/AM	150 ^a	0.2	>100
	160 ^a	0.21	>100

^a Adjusted for $V_f=0.44$

Creep strain accumulation increases as the applied creep stress increases, as it was expected. It is worth to note that creep strain accumulations remained very low at all stress levels. Although the creep strains produced for the N720/AM were < 0.22%, they are higher compare to the same stress levels for the N720/A composite. Figure 30 and 31 illustrates the creep strain vs. time curves for the N720/AM and N720/A composites at 1000 °C. Creep curves for the N720/A from Braun [18] are shown in Figure 31 for comparison.

Primary creep and secondary creep regimes are observed both for the N720/AM and the N720/A curves at all stress levels. Secondary creep until run-out is apparent for all stress levels conducted at 1000 °C. As it is seen in the Figure 30 and 31, the creep strain vs. time curves at the same stress levels of the N720/AM and N720/A exhibit similar trends at 1000 °C.

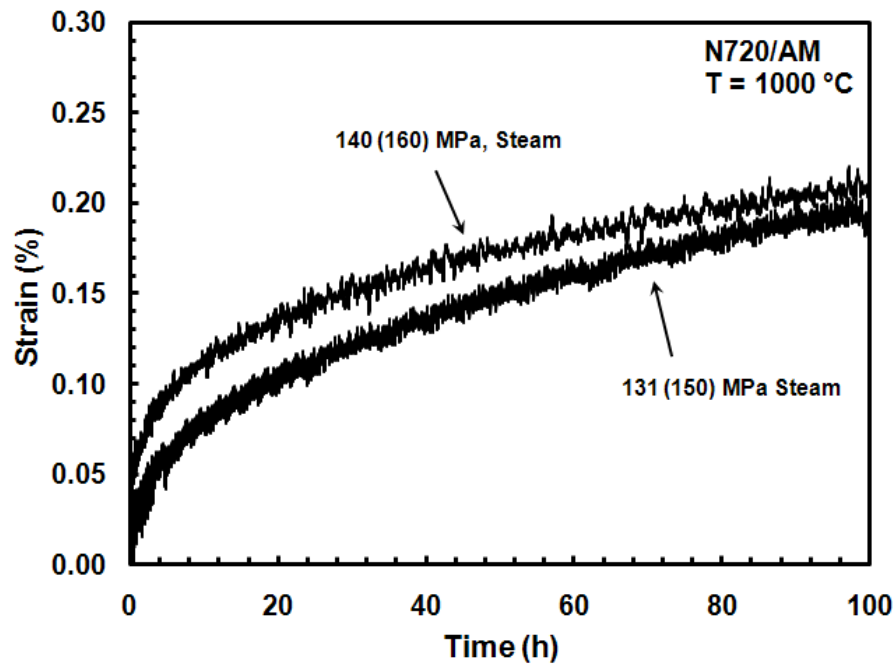


Figure 30. Creep strain vs. time curves for the N720/AM ceramic matrix composite at 1000 °C. Stress levels adjusted for $V_f = 0.44$ are shown in parentheses.

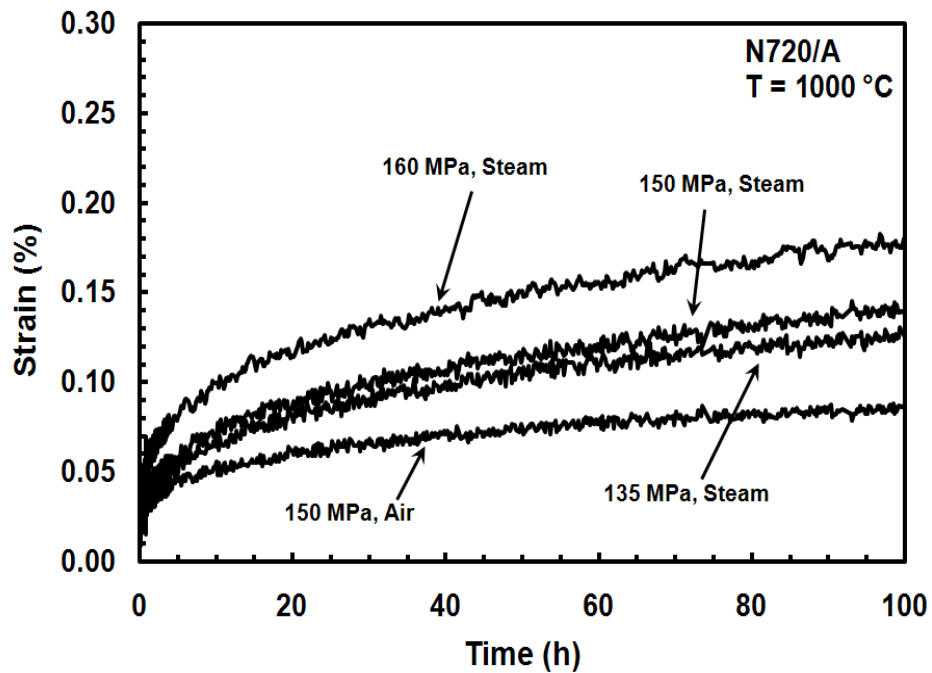


Figure 31. Creep strain vs. time curves for the N720/A ceramic matrix composite at 1000 °C. Data from reference [18]

4.5 Effects of Temperature and Steam on Creep Rupture Behavior

The effect of temperature on creep behavior for the N720/AM ceramic matrix composite in air at 1100 and 1200 °C can be seen in Figure 32. Creep curves at 1200 °C from Genelin's research [16] are included for comparison. At the adjusted stress levels of 125 and 150 MPa for $V_f = 0.44$ in air, creep strain accumulation increased significantly with the increase of temperature from 1100 to 1200 °C. Creep run-out was achieved at each stress level at 1000 °C, but in the case of 1200 °C creep life time decreased at each stress dramatically for the N720/AM composite.

As it is seen clearly in Figure 32b, the creep life time at the adjusted stress level of 150 MPa for $V_f = 0.44$ is only 0.6 hours. All of the creep strain vs. time curves exhibit primary and secondary creep regimes at each stress level. Secondary creep until run-out trend is apparent for all stress levels conducted at 1100 and 1200 °C in air.

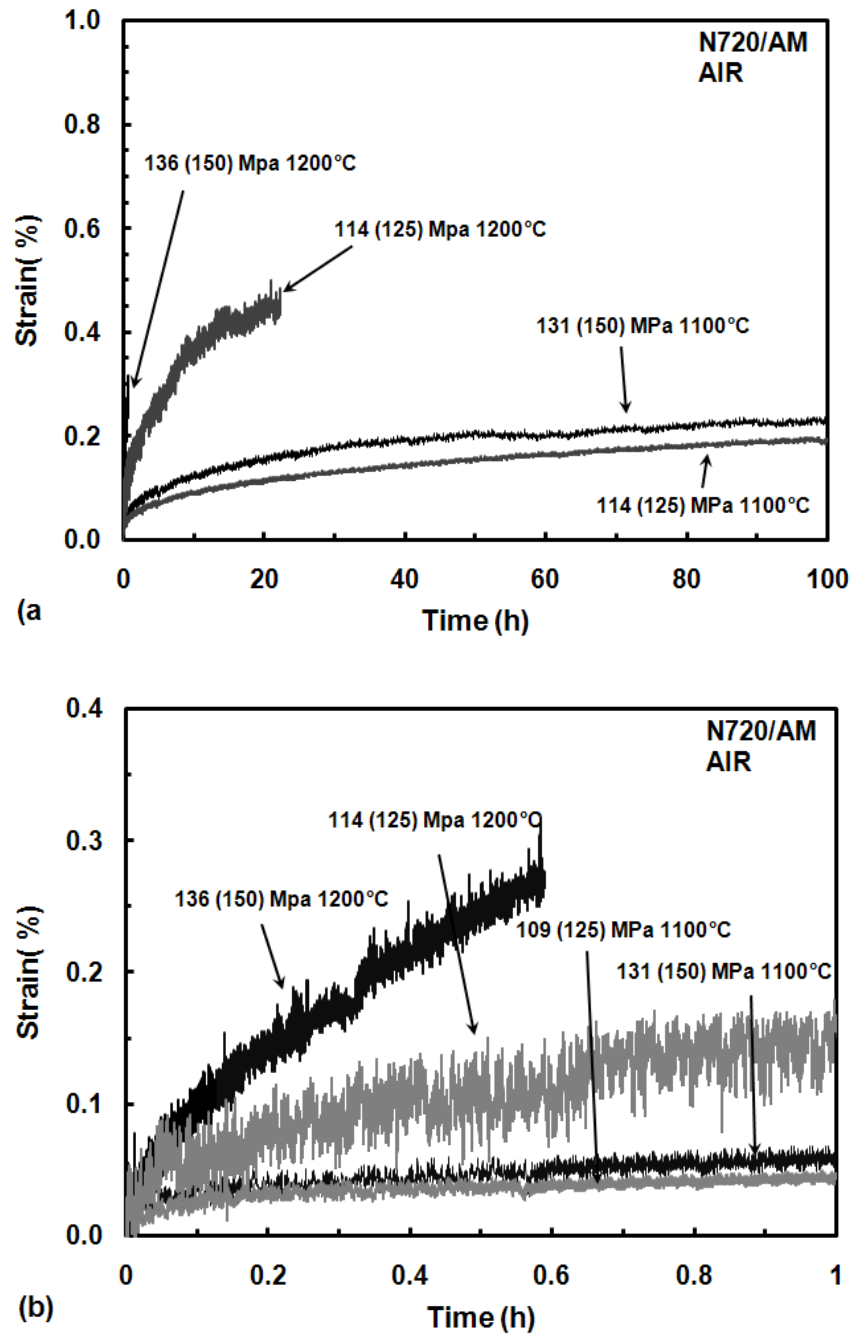


Figure 32. Creep strain vs. time curves for N720/AM ceramic matrix composite at 1100 and 1200 °C in laboratory air. Time scale is reduced to clearly show the creep curve at 150MPa. Data at 1200 °C from Genelin [16]. Stress levels adjusted for $V_f = 0.44$ are shown in parentheses.

Figure 33 shows the effect of temperature on creep behavior for the N720/AM ceramic matrix composite in steam at 1100 and 1200 °C. Creep curves at 1200 °C from Genelin [16] are also shown for comparison. At the adjusted stress level of 100 MPa for $V_f = 0.44$ in steam, increase in the amount of creep strain accumulation is obvious as the temperature increases from 1100 to 1200 °C, but the creep life time decreased significantly as it was expected. In contrast, accumulated strain decreases with the increase of temperature in the case of the adjusted creep stress of 125 MPa for $V_f = 0.44$. Consequently, increasing accumulated creep strain with the increasing temperature behavior is only possible until certain creep stress level.

As it was seen Figure 28, the effect of steam on creep behavior for N720/AM is apparent. The trend of curves reveals that the presence of steam has a significant effect on increasing the creep rates. Since presence of steam accelerates the creep rates, we have larger creep strains. This behavior was also reported by Braun [18], Mehrman [13] and Ruggles-Wrenn et al [24] for the N720/A composite at elevated temperatures. For the N720/AM composite creep strain accumulated at 131 MPa in steam is nearly two times the creep strain accumulated at the same stress level in air at 1100 °C. Furthermore; dramatically longer lifetimes were observed in air than in steam during creep tests at 1100 °C.

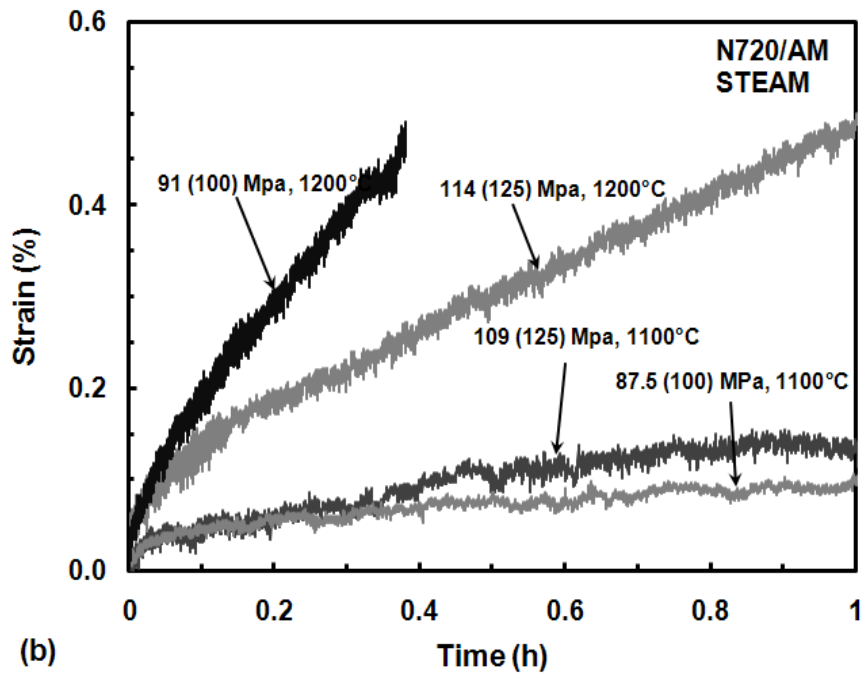
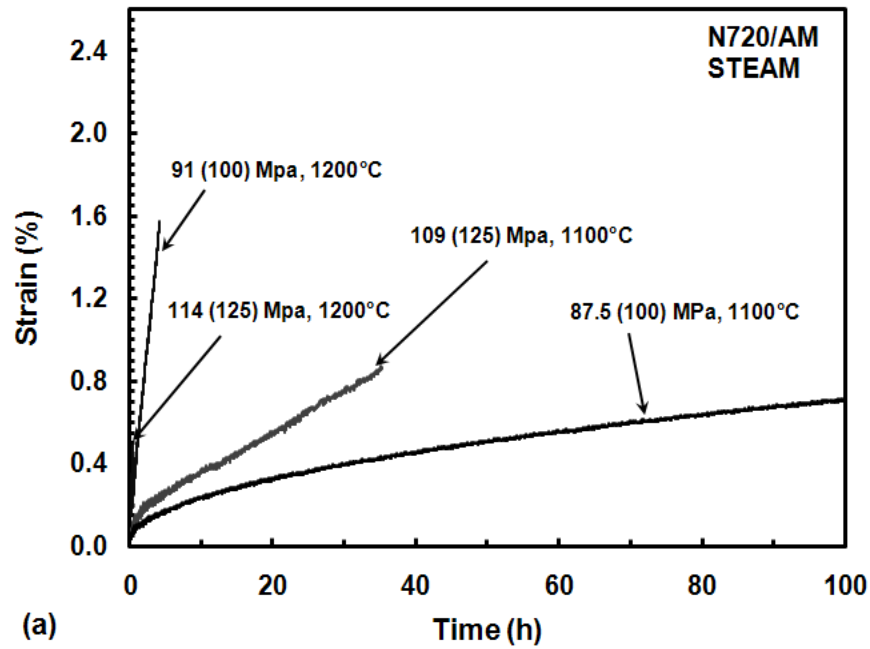


Figure 33. Creep strain vs. time curves for N720/AM ceramic matrix composite at 1000, 1100 and 1200 °C in steam. Data at 1200 °C from Genelin [16]. Stress levels adjusted for $V_f = 0.44$ are shown in parentheses.

Figure 34 illustrates the creep curves produced at a given applied stress level in air and steam to gain a further understanding of the effect of the environment on creep behavior for N720/AM at 1100 °C. Note that creep curves for N720/AM composite obtained in steam differ significantly from that obtained in air at 1100 °C for the creep stress level of 131 MPa (equivalent to 150 MPa for $V_f = 0.44$). Recall that creep run-out was achieved only at the equivalent stress of 100 MPa for $V_f = 0.44$ in steam at 1100 °C for N720/AM. Creep curves for N720/A at the creep stress levels of 150 MPa in both steam and air at 1100 °C from Braun [18] are also shown for comparison in Figure 34b.

It can be clearly seen that the behavior of the curves in Figure 34a and b are similar. In addition, larger creep strain was accumulated by the N720/AM than by the N720/A for the creep stress level equivalent to 150 MPa for $V_f = 0.44$ in air. In contrast, N720/A produced larger creep strain than N720/AM did in steam.

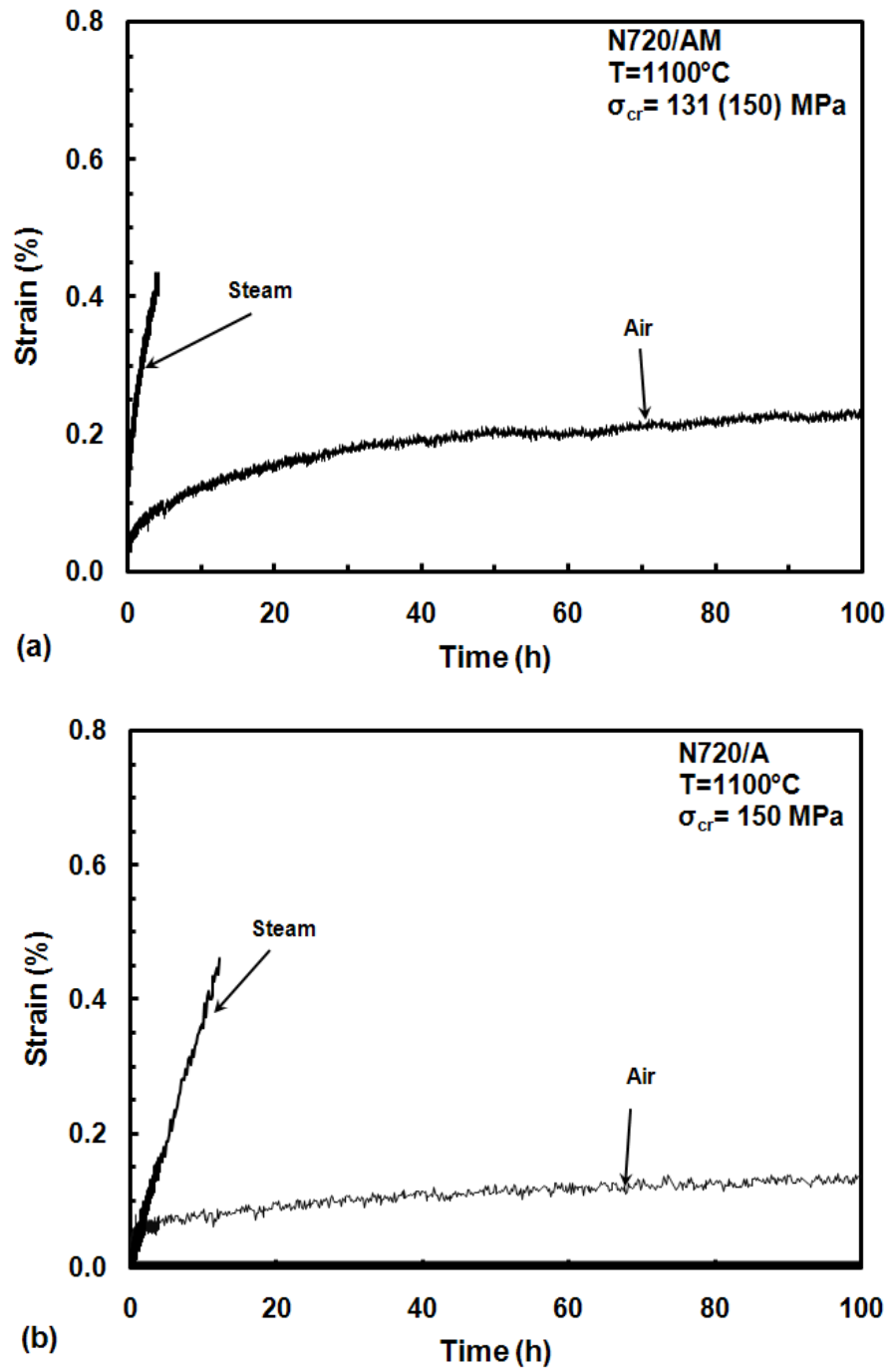


Figure 34. Creep strain vs. time curves for N720/A and N720/AM ceramic matrix composites at 150 MPa creep stress level at 1100 °C. Stress level adjusted for $V_f = 0.44$ is shown in parentheses. Data for N720/A from reference [18].

Minimum creep strain rate was reached in all tests. Creep rate as a function of applied stress for N720/AM and N720/A composites with 0°/90° fiber orientation in air and steam are illustrated in Figure 35 and 36. Notice that the secondary creep rates for the N720/AM are bigger than those for the N720A.

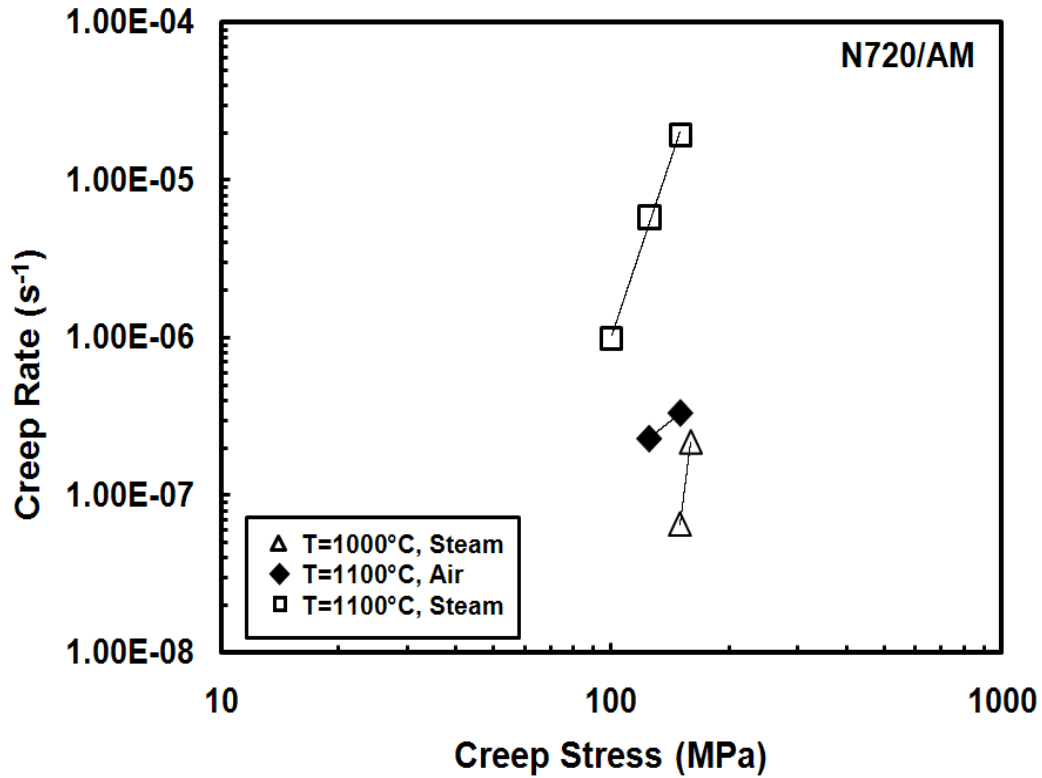


Figure 35. Minimum creep rate as a function of applied stress for N720/AM ceramic matrix composite at 1100 °C. Creep stress levels are adjusted to $V_f = 0.44$.

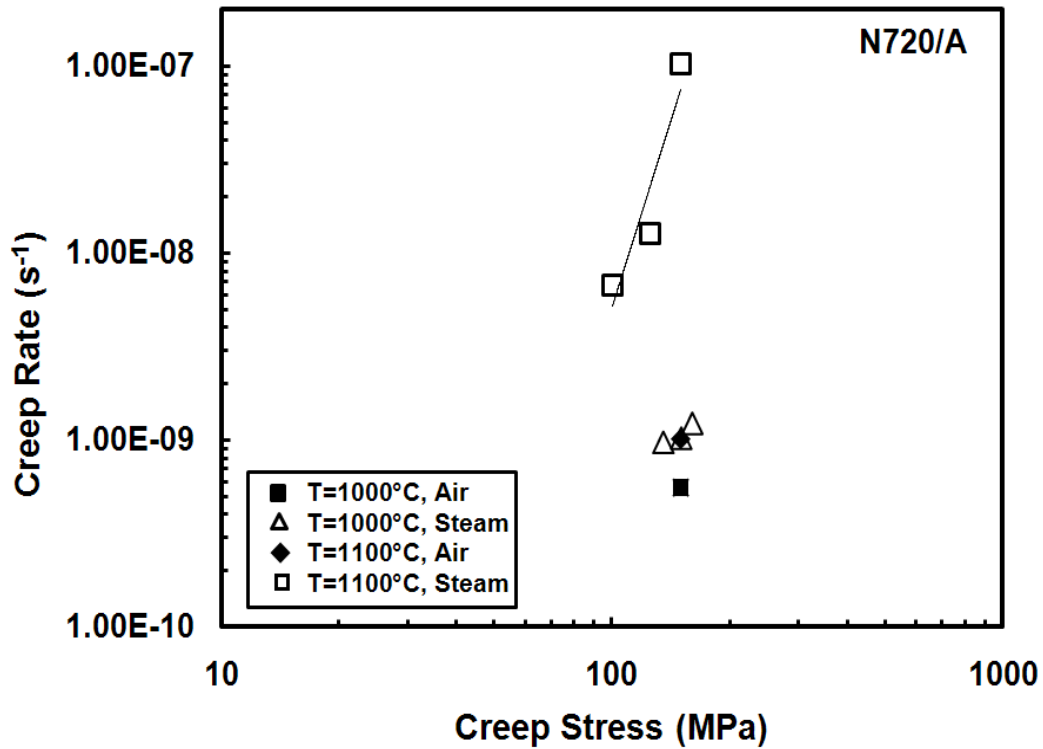


Figure 36. Minimum creep rate as a function of applied stress for N720/A ceramic matrix composite at 1100 °C. Data from reference [18].

Figure 37 summarizes the stress-rupture behavior of both the N720/A and N720/AM ceramic matrix composites where the results for the N720/A obtained from prior effort [18]. Notice that creep tests conducted at the equivalent stress levels of 150 and 160 MPa for $V_f = 0.44$ at 1000 °C in steam achieved run-out in this effort. Furthermore, the creep-rupture tests were performed in prior work [18] also achieved run-out at 150 MPa in air and 150 and 160 MPa in steam. As a result, increase in temperature from 1000 to 1100 °C has no effect on creep lifetime up to 100h, run-out time, for both N720/A and N720AM in steam and air. This behavior for N720/A was also reported by Braun [18]. Creep run-out stress for the N720/AM composite at 1100 °C

was 150 MPa for $V_f=0.44$ in air. At 1200 °C, the effect of temperature was dramatically apparent in Genelin's work [16] where the creep lifetime was only 0.59h for N720/AM at the stress level of 150 MPa for $V_f=0.44$ and the creep run-out stress was 100 MPa for $V_f=0.44$ in air. In steam at 1100° C the effect of temperature was also obvious. Run-out achieved at 100 MPa for $V_f=0.44$ and the creep lifetime was only 4.12h at 150 MPa for $V_f=0.44$ for N720/AM. In Braun's work [18] the creep-run out stress was also 100 MPa and the creep lifetime was 12.2h at 150 MPa.

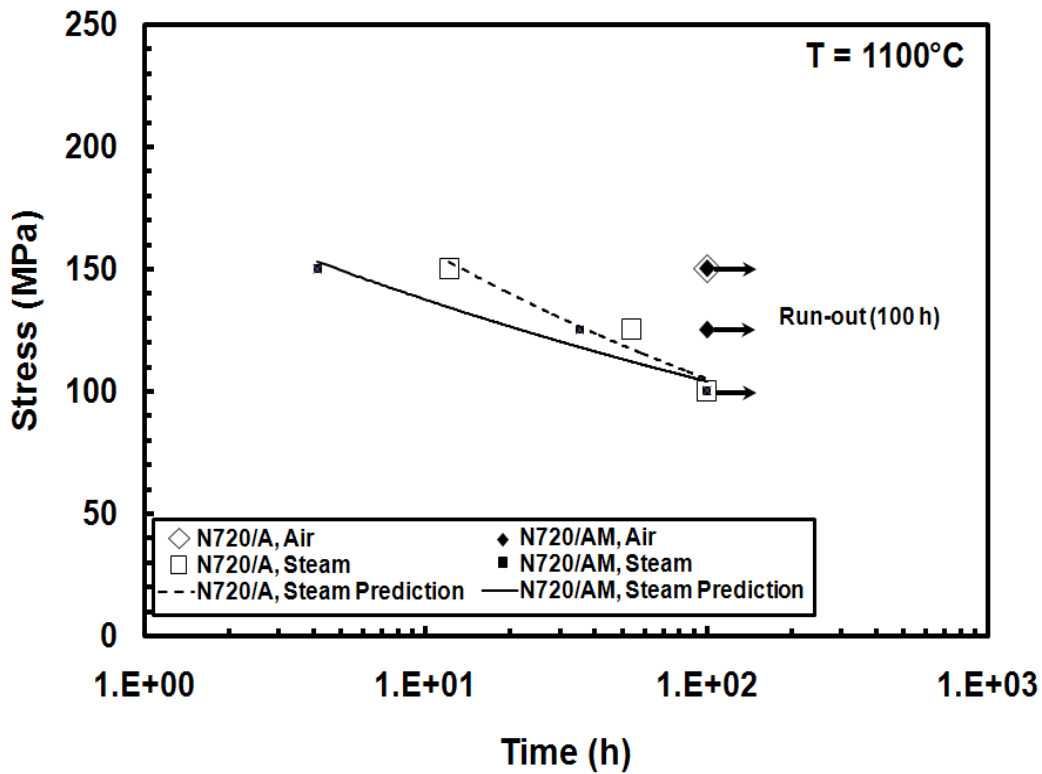


Figure 37. Creep stress vs. time to rupture for N720/AM ceramic matrix composite at 1100 °C in air and steam. Data for N720/A from reference [18]. Stress levels of N720/AM are adjusted for $V_f=0.44$.

4.6 Retained Tensile Properties

Retained strength and modulus of the specimens subjected to prior creep are presented in Table 13. The tensile stress-strain curves for the specimens subjected to prior creep at 1000 and 1100 °C are illustrated in Figure 38a and 38b, respectively. Stress-strain curves for the as processed material are also presented in figures for comparison.

Table 13. Retained properties for the N720/AM specimen subjected to prior creep

Environment	Creep Stress (MPa)	Retained Modulus (GPa)	Retained Strength (MPa)	Failure Strain (%)	Modulus Retention (%)	Strength Retention (%)
<i>Tests at 1000 °C</i>						
Steam	131	58.6	166.2	0.20	89.6	103.2
	140	60.6	173.2	0.21	92.8	107.6
<i>Tests at 1100 °C</i>						
Air	109	59.8	168	0.2	91.7	104.9
	131	55.8	174.4	0.23	86.2	108.9
Steam	87.5	55.4	162.8	0.69	86	101.6

Prior creep in both air and steam had effect on tensile strength at 1000 and 1100 °C. For the specimens subjected to prior creep stress levels of 131 and 140 in steam at 1000 °C, tensile strength retentions were 103.7% and 107.6%, modulus losses were 10.4% and 7.2%, respectively. For the specimens subjected to prior creep stress levels of 109 and 131 in air at 1100 °C, the tensile strength increased by 4.9% and 8.9%, respectively. The minimum strength retention was observed for the specimen subjected to prior creep stress level of 87.5 in steam as 101.6%. However, the loss in modulus was 14%.

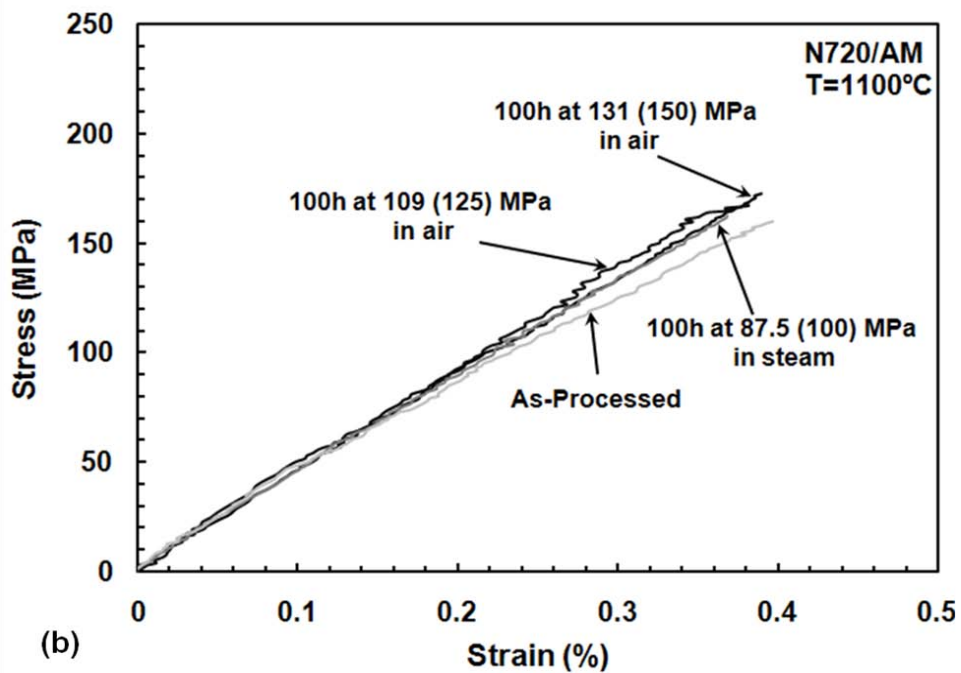
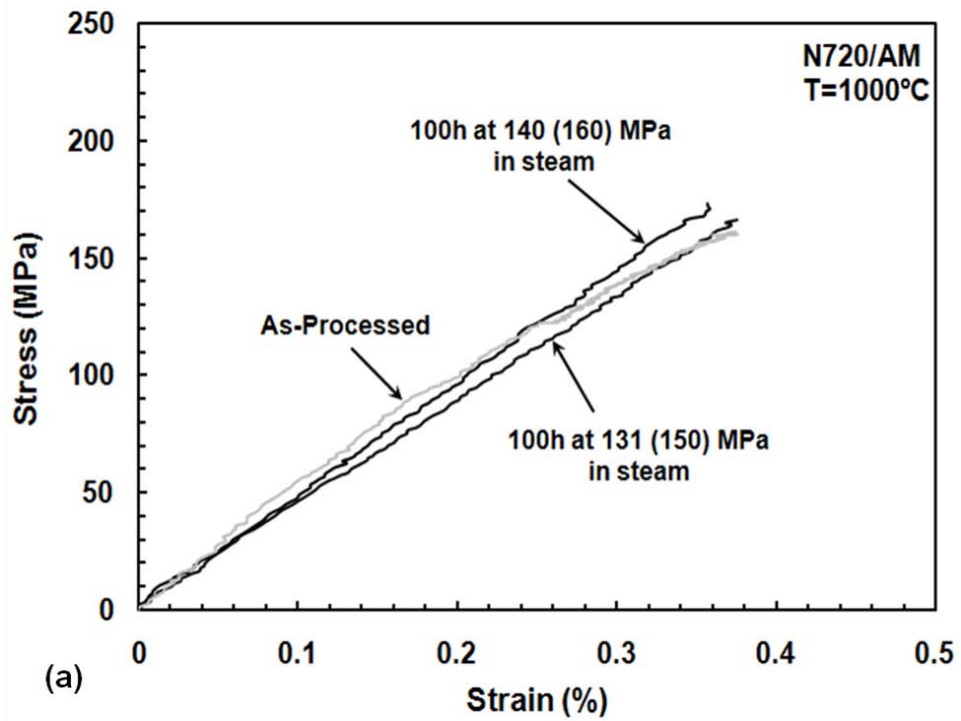


Figure 38. Effect of prior creep on tensile stress-strain behavior of the N720/AM composite at (a) 1000 °C (b) 1100 °C. Stress levels adjusted for $V_f = 0.44$ are shown in parentheses.

4.7 Microstructural Analysis

In this part of the chapter, the fracture surfaces of the N720/AM specimens are characterized. As it was mentioned in chapter 4, after the mechanical testing process, the specimens were examined using both an optical and a scanning electron microscope (SEM).

4.7.1 Optical Microscopy Analysis

Optical micrographs of the N720/AM specimens are presented in Figure 39 through 43. Possible effects of temperature, environment, creep stress level and lifetime are investigated.

The fracture surfaces obtained from the specimens subjected to tensile to failure at 900, 1000, 1100 and 1200 °C in air are presented in Figure 39. Specimen for 1200 °C obtained from prior work [16]. The similar damage zones can be seen for all temperature levels. The fibers in the 0° direction exhibit random fiber pull-out characterization. However, the damage zone appears relatively short at 900 °C and the specimens tested at 1000 and 1200 °C exhibit relatively longer damage zones. Consequently, a clear correlation between the fracture surface and the increasing temperature is not apparent.

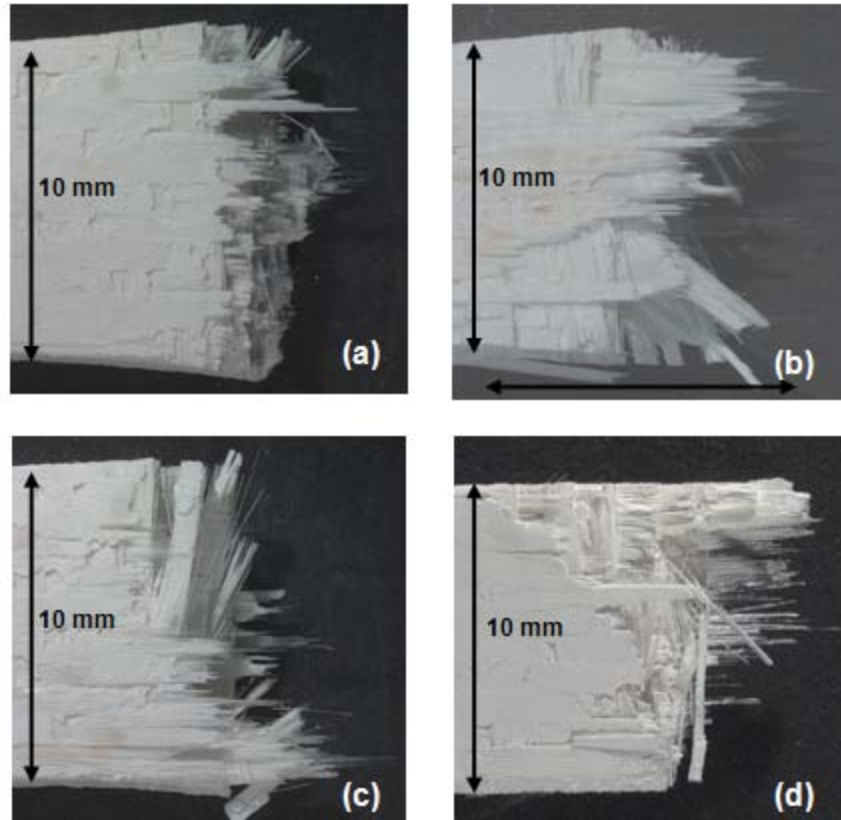


Figure 39. Fracture surfaces of the N720/AM specimens tested in tension to failure in air at: (a) 900 (b) 1000 and (c) 1100 °C and (d) 1200 °C. Micrograph at 1200 °C was obtained from Genelin [22].

Figure 40 shows the fracture surfaces of the N720/AM specimens obtained in creep tests at 109 and 131 MPa in air at 1100 °C. Note that, the specimens achieved run-out and then subjected to tension to failure. It can be seen that the size of the damage zone is large for each. The fiber pull-out lengths are clearly seen especially from the side views of micrographs.

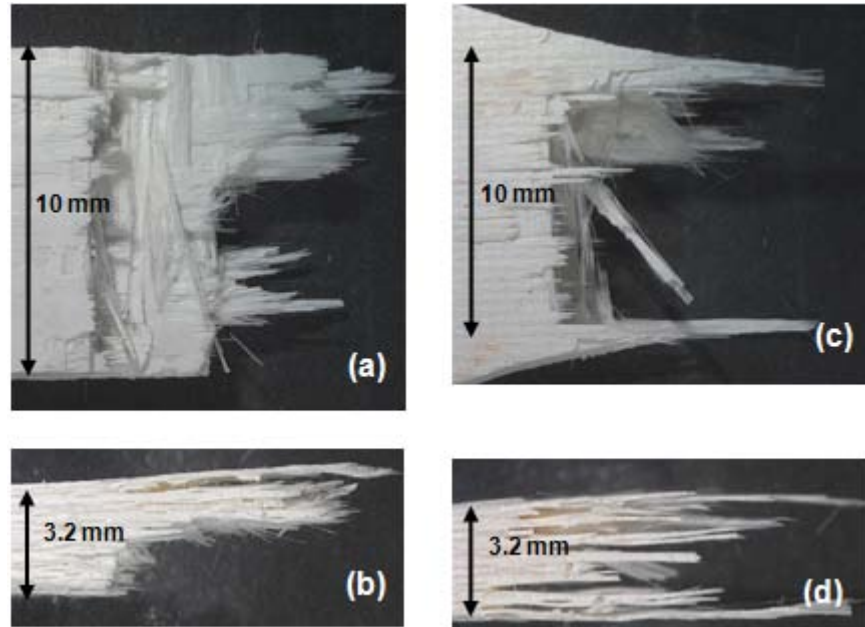


Figure 40. Fracture surfaces of the N720/AM specimens obtained in creep tests at 1100 °C in air at: (a-b) 131MPa (equivalent to 150 MPa for $V_f = 0.44$), $t_f = > 100$ h and (c-d) 109 MPa (equivalent to 125 MPa for $V_f = 0.44$), $t_f = > 100$ h.

Figure 41 illustrates the fracture surfaces of specimens obtained in the 87.5, 109 and 131 MPa creep tests in steam. The noticeable difference in the length of the damage zones is apparent. The damage zone for the specimens tested at 109 MPa is the longest among all. Since the specimen tested at 131MPa has the shortest damage zone, there is no correlation between creep stress level and damage zone length. Similar observation was reported by Genelin [16] for the N720/AM specimens at 1200 °C.

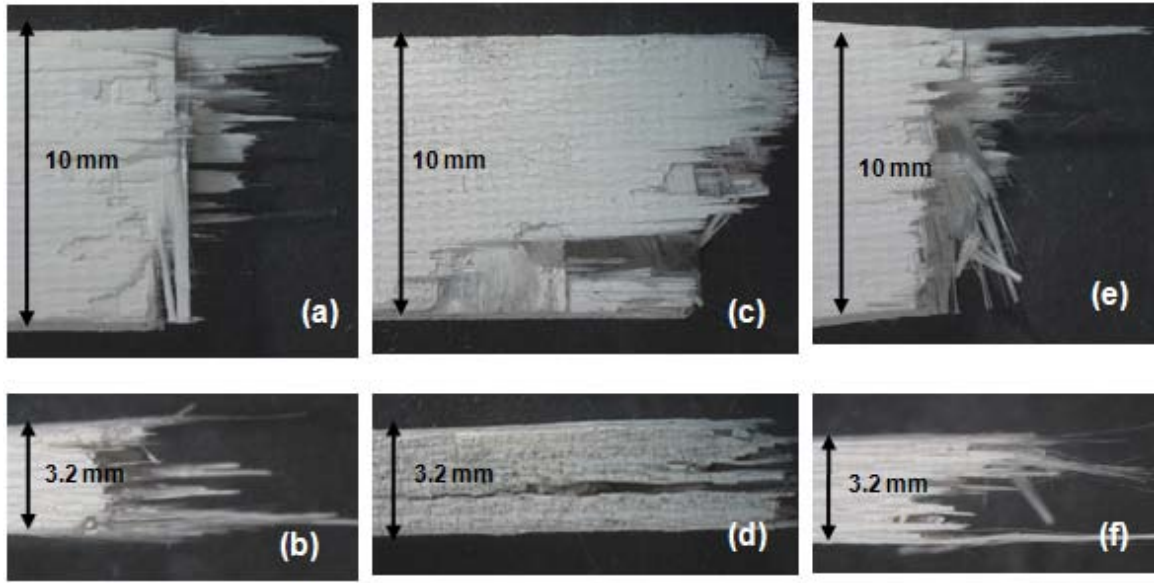


Figure 41. Fracture surfaces of the N720/AM specimens obtained in creep tests at 1100 °C in steam at: (a-b) 87.5MPa (equivalent to 100 MPa for $V_f=0.44$), $t_f = >100$ h and (c-d) 109 MPa (equivalent to 125 MPa for $V_f=0.44$), $t_f= 35.2$ h (e-f) 131 MPa (equivalent to 150 MPa for $V_f=0.44$), $t_f= 4.12$.

Fracture surfaces of the N720/AM specimens tested in creep at the equivalent stress level of 150 MPa for $V_f=0.44$ at 1000, 1100 and 1200 °C are presented in Figure 42. Correlation between the damage zone length and the increasing temperature is apparent for this case. Specimen for 1200 °C (obtained from Genelin [16] shows relatively short damage zone. As the temperature decreases from 1200°C to 1100 and 1000°C, the length of the damage zone increases significantly. The difference can be seen clearly from the side views of the specimens presented. (see Figure 42b, d and f) Note that the specimen tested at 1000 °C achieved run-out and subsequently subjected to tensile test to failure.

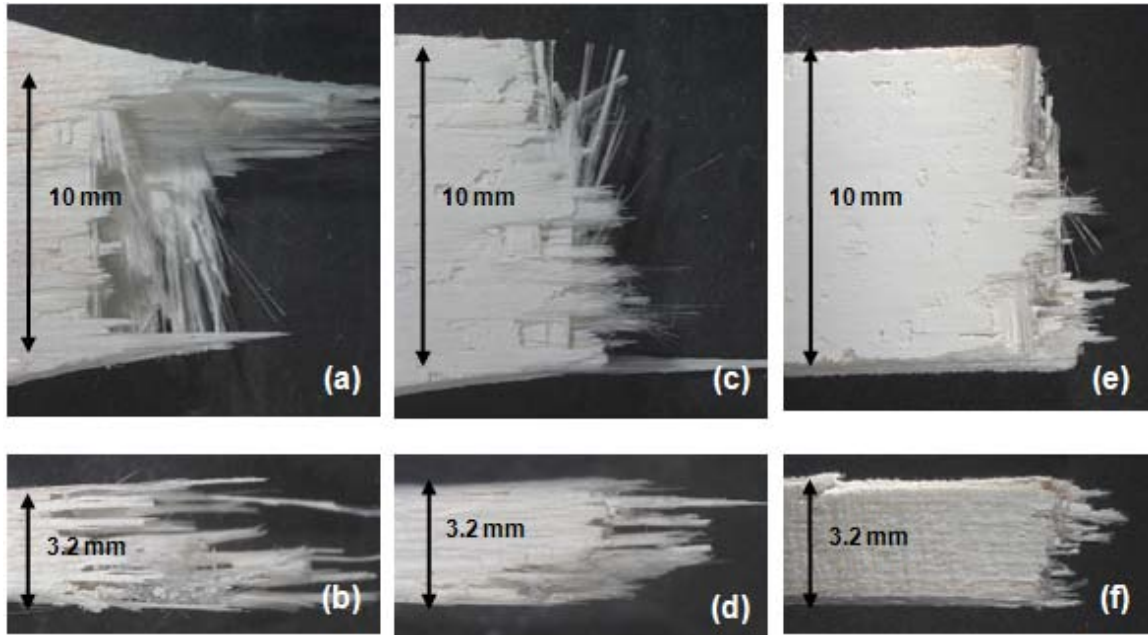


Figure 42. Fracture surfaces of the N720/AM specimens obtained in creep tests in steam at (a-b) 131 MPa (equivalent to 150 MPa for $V_f = 0.44$), $t_f = > 100$ h at 1000 °C and (c-d) 131 MPa (equivalent to 150 MPa for $V_f = 0.44$), $t_f = 4.12$ h at 1100°C (e-f) 136 MPa (equivalent to 150 MPa for $V_f = 0.44$), $t_f = 0.012$ h at 1200°C in steam. Micrographs of the specimen tested in 1200°C from Genelin [16].

To investigate the effect of loading rate on the fracture surface, optical micrographs of the N720/AM specimens subjected to tension to failure with constant loading rates of 25 and 0.0025 MPa are shown in Figure 43. From prior work at 1200° C, Genelin observed that the N720/AM specimen subjected to tensile to failure with the loading rate of 25 MPa has a relatively short damage zone and small amount of fiber pull-out [16]. In these figures below, there is a small difference between the damage zones, but the different is not so apparent compare to the figures of the same tests at 1200 °C obtained by Genelin [16]. The fracture surface of the specimen tested with the

constant load rate of 0.0025 MPa exhibit more brushier surface than that tested with the constant loading rate of 25 MPa/s.

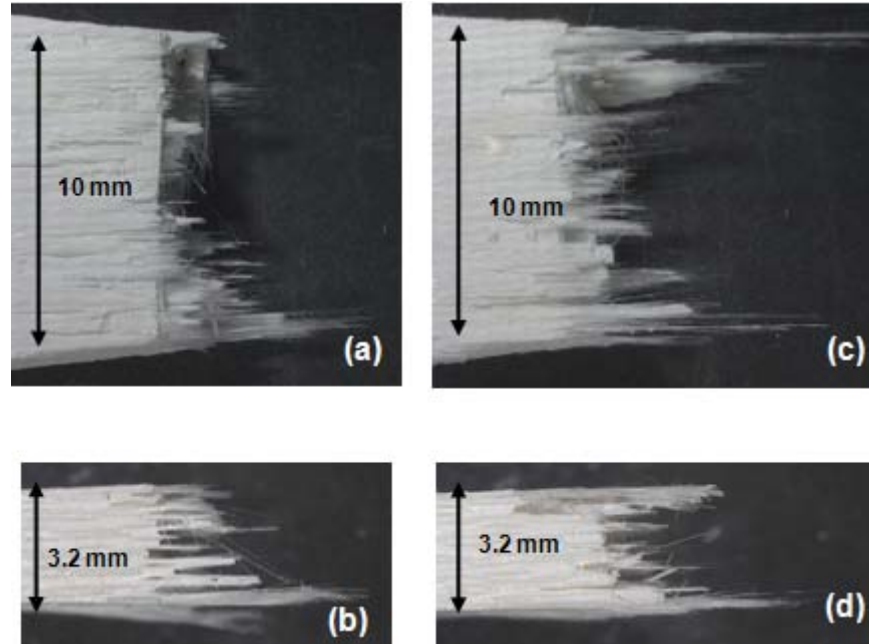


Figure 43. Fracture surfaces of the N720/AM specimens subjected to tensile test to failure in steam at 1100 °C with the constant loading rates of: (a-b) 25 MPa/s, $t_f = 0.0017$ h and (c-d) 0.0025 MPa/s, $t_f = 10.38$ h.

4.7.2 Scanning Electron Microscopy Analysis

Optical micrographs presented in the previous section helped us to understand the general characteristic of the fracture surface. To obtain detailed information about the fracture surface, the SEM micrographs are inspected in this part of the chapter. Notice that scanning electron microscope allows us to get micrographs of the fracture surface of the specimens at higher magnifications.

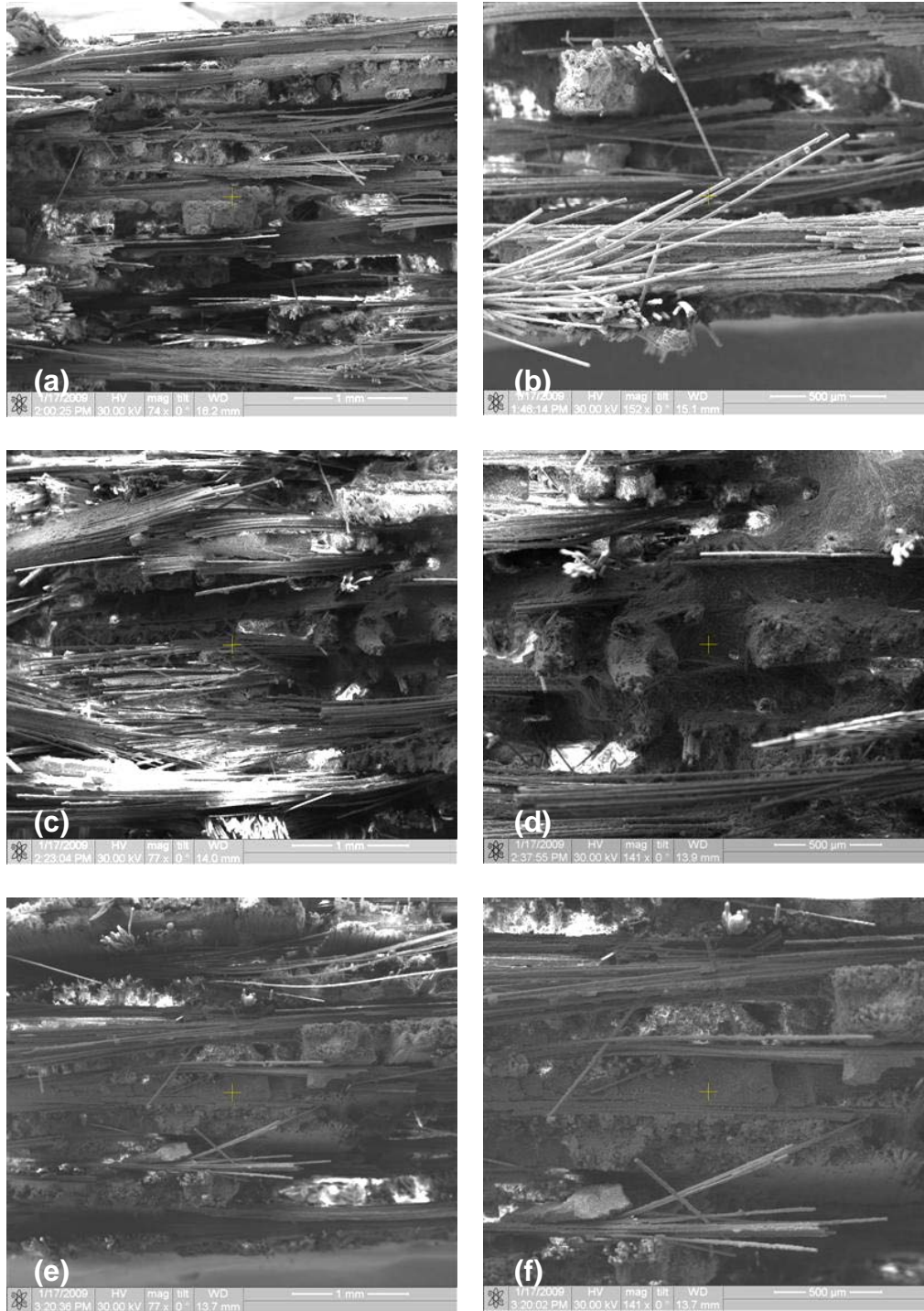


Figure 44. Fracture surface of the N720/AM specimens tested in tension to failure in air at: (a-b) 900 °C (c-d) 1000 °C and (e-f) 1100 °C

The fracture surfaces of the specimens tested in tensile to failure at various temperatures to understand the temperature effect on the fracture surface and to find a correlation between temperature and topography in Figure 44. The fracture surfaces contain large amounts of uncoordinated brushy 0° fibers especially at 900 and 1000 °C tests. The fracture surface at 1100 °C is dominated by planar failure. Although there are some differences in the brushiness and fibrousness, the three fracture surfaces have basically the same topography.

Figure 45 shows additional micrographs of the surface fracture for the N720/AM specimens tested in tensile to failure at various temperatures. Minimal 0° fiber pull-out which is typical for the specimens subjected to tensile can be seen in Figure 45a and b. Furthermore Figure 45c shows also 0° and 90° orientation after the failure and short fiber pull out also seen. Individual fiber with small amount matrix adhering on is shown in Figure 45d.

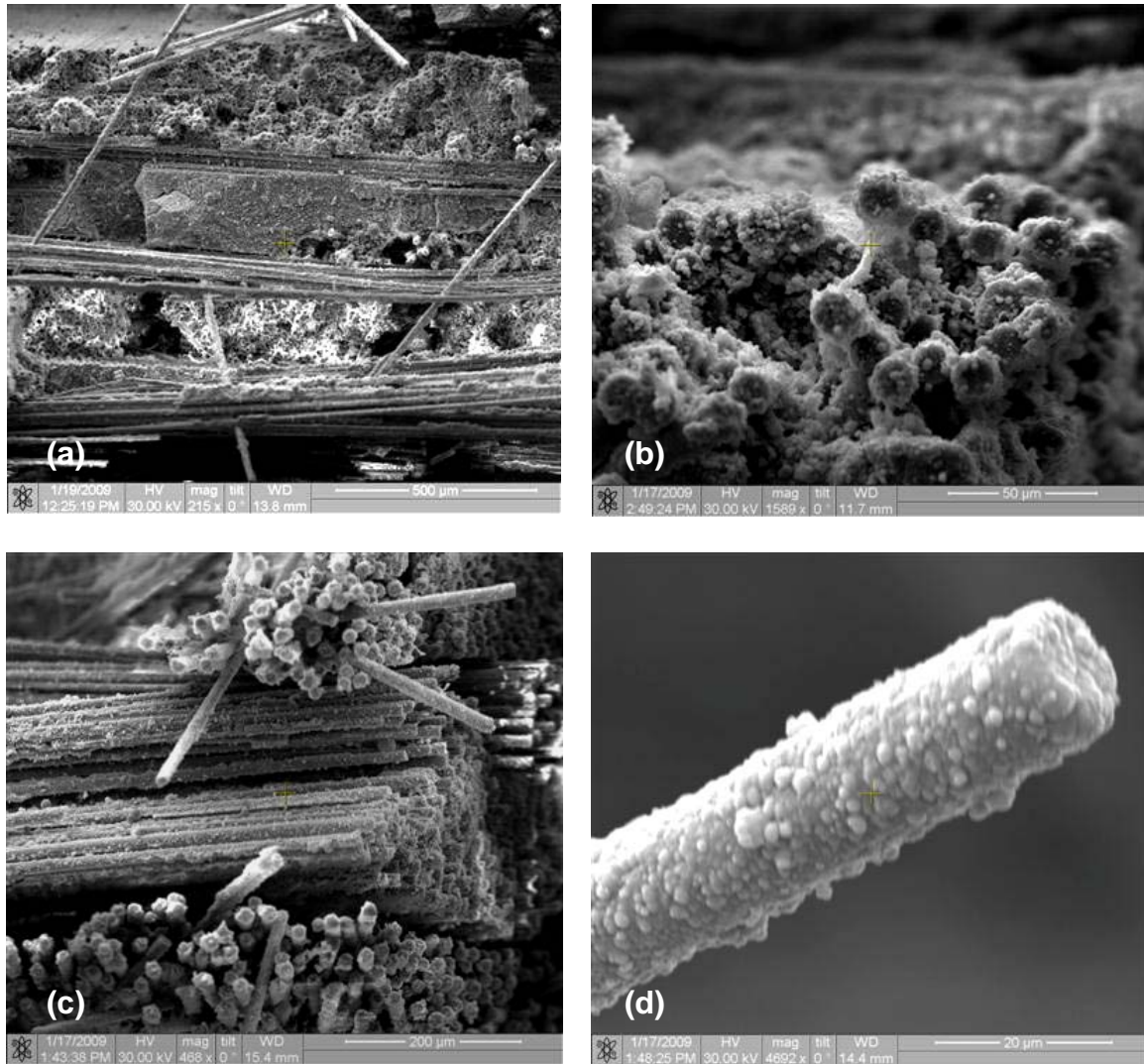


Figure 45. Fracture surfaces of specimens tested in tension to failure with displacement control at various magnifications in air at a) 1100 °C b) 1000 °C and (c-d) 900 °C

The fracture surface of two N720/AM specimens tested in creep at 109 and 131 MPa in steam at 1100 °C are showed in Figure 46. For the case of the specimen tested at 109 MPa, the fracture surface predominantly brushy with long fiber pull-out. Notice that the specimen at 109 MPa achieved run-out and subsequently subjected to tensile to

failure. In contrast, the fracture surface of the specimen at 131 MPa is dominated by planar areas with coordinated fiber failure.

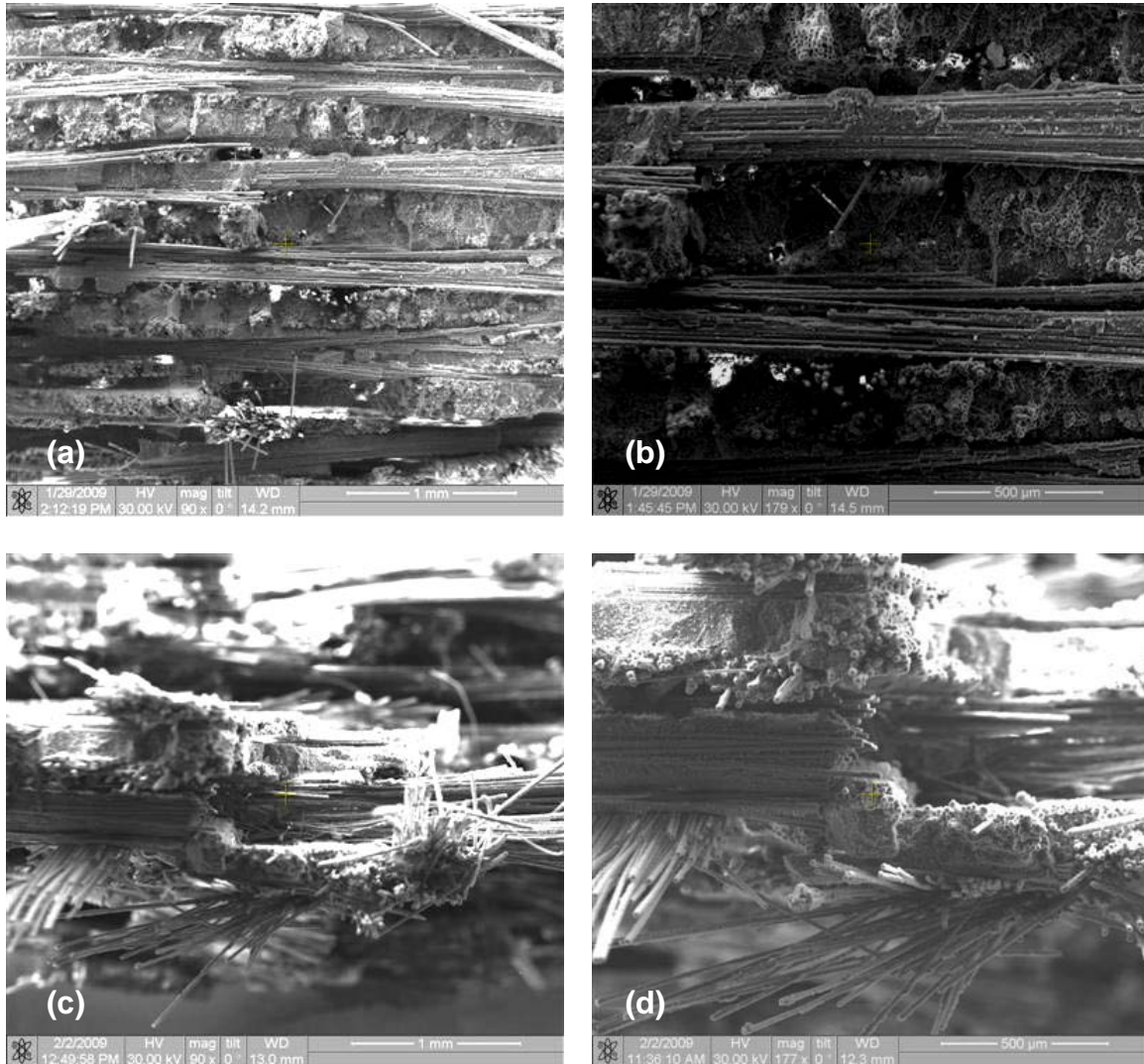


Figure 46. Fracture surfaces of the N720/AM specimens obtained in creep tests at 1100 °C in steam at: (a-b) 131MPa (c-d) 109 MPa

Figure 47 shows the detailed fracture surfaces of the N720/AM specimens tested in creep at 131 and 109 MPa in air and in steam at 1100 °C. The effect of environment on the fracture surfaces is apparent. Figure 47b shows a greater amount of matrix adhering

to the fibers.. Likewise, steam effect is also evident for the fibers of the N720/AM specimens at 109 MPa. Recall that the creep lifetime of the specimen at 109 MPa in steam at 1100 °C was 35.2 hours.

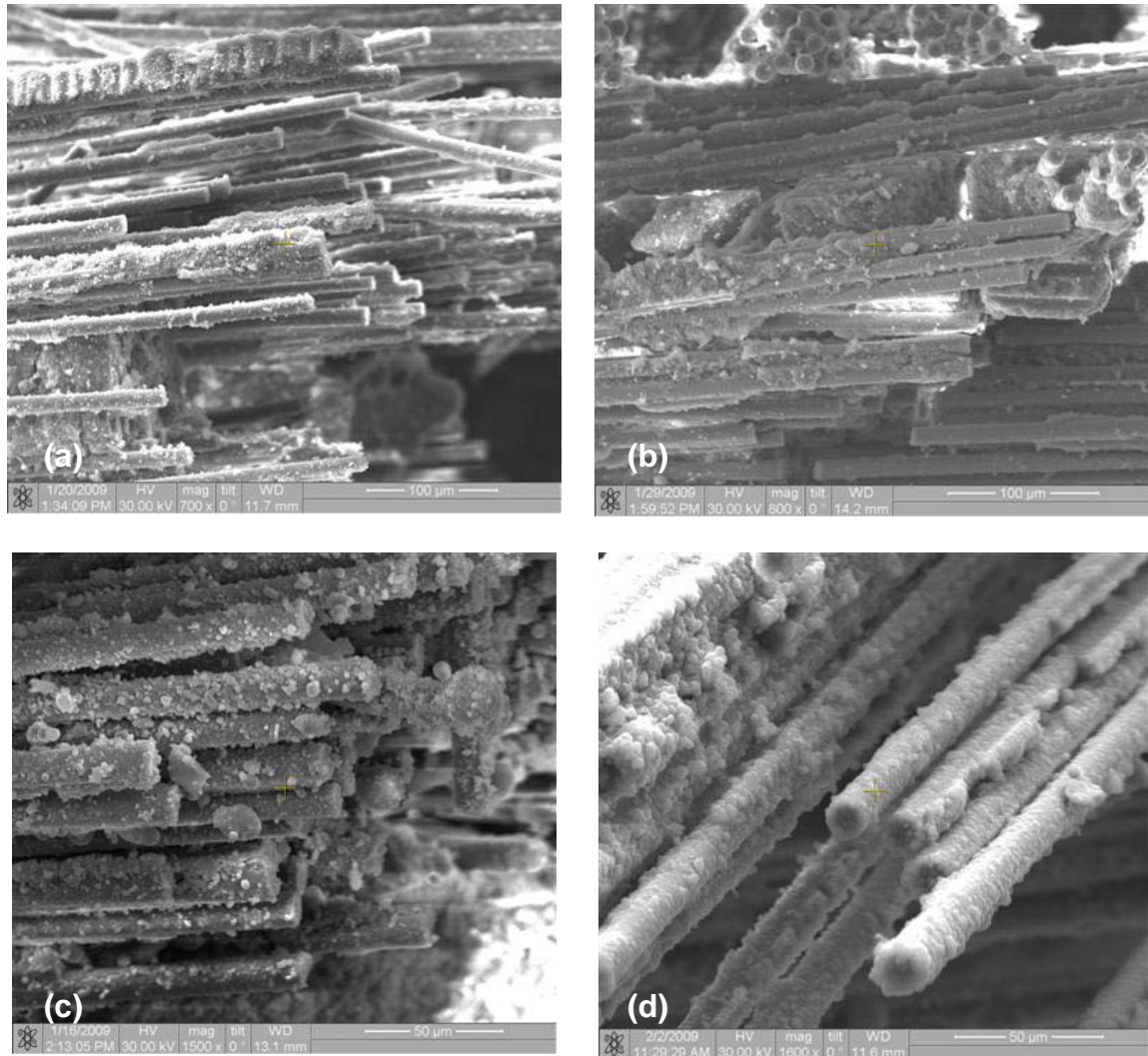


Figure 47. Detailed fracture surfaces of N720/AM specimens subjected to creep at 131 MPa at (a) 1100 °C in air (b) 1100 °C in steam and at 109 MPa at (a) 1100 °C in air and (b) 1100 °C in steam

Figure 48 shows the micrographs of the N720/AM specimens obtained at 131 MPa at 1000 and 1100 °C in steam. Matrix material remaining bonded to the fibers in the

specimen at 1000 and 1100 °C in steam is apparent in Figure 48b and d, respectively. Notice that the amount of matrix bonded to the fibers at 1000 °C is greater than that at 1100 °C in steam. Although the temperature level was higher, the creep life of the specimen at 1100 °C is only 4.12 hours that has the critical effect on the amount of matrix bonded to the fibers. Notice that the N720/AM specimen tested at 131 MPa at 1000 °C in steam achieved run-out of 100 hours.

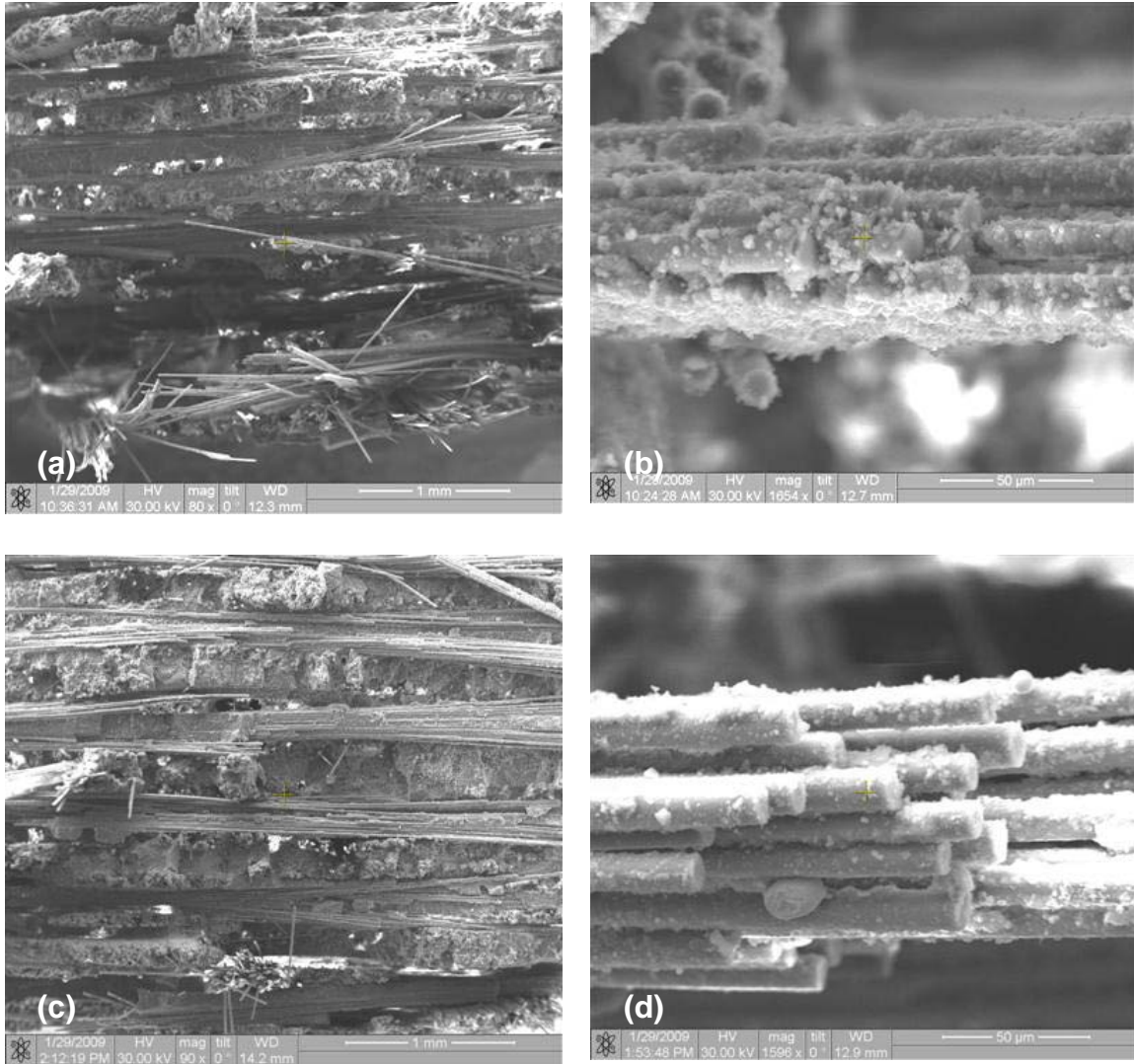


Figure 48. Fracture surfaces of the N720/AM specimens subjected to creep at 131 MPa in steam at (a-b) 1000 °C and (c-d) 1100 °C.

Figure 49 shows the loading rate effect on the fracture surface of the N720/AM specimens with the micrographs at various magnifications. The fracture surface of the specimen tested at 0.0025 Mpa/s in Figure 49a and b exhibit more brushy uncoordinated fiber failure than that tested at 25 MPa/s in Figure 49d and f. The specimen tested in tensile to failure at the loading rate of 25 MPa/s also has a similar topography like the

specimens tested in tensile to failure at displacement control shown in Figure 44. The effect of steam exposure time is also apparent in Figure 49c and f. As it was expected, larger amount of matrix bonded to the fibers at 0.0025 MPa test where time to failure is 14.5 hours.

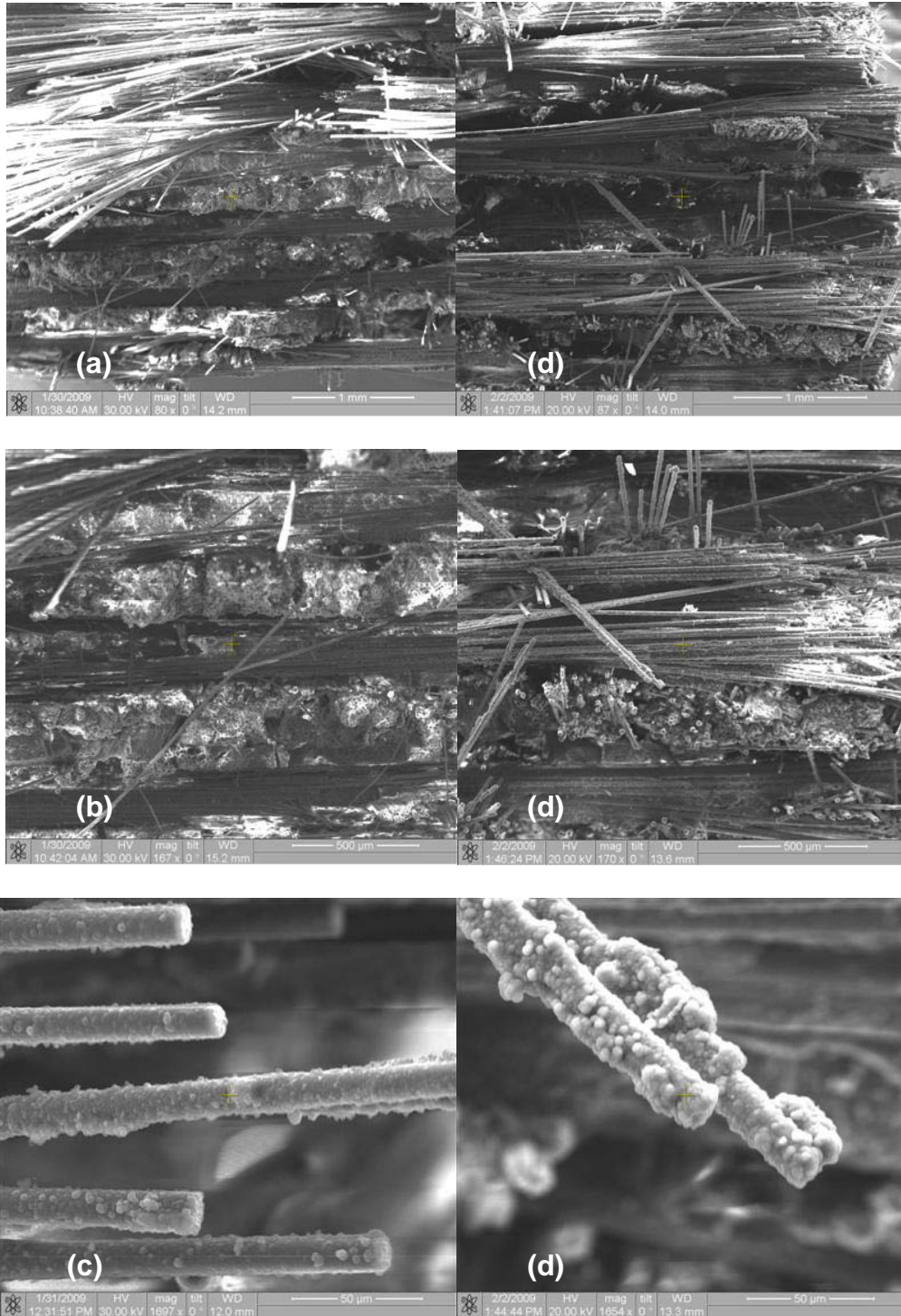


Figure 49. Fracture surface of N720/A specimen subjected tensile to failure at 1100 °C in steam with the constant loading rates of: (a-b-c) 25MPa/s and (d-e-f) 0.0025 MPa/s

V. Conclusions

Tensile-strain behavior was investigated and tensile properties measured at 900, 1000 and 1100 °C. The UTS values for N720/AM are below the corresponding values for N720/A at 900, 1000, and 1100 [18,19]. The average elastic modulus, 65.5GPa for N720/AM (equivalent to 74,9GPa for $V_f = 0.44$), was higher than for N720/A [18,19]. Similar tensile comparison results were reported for the N720/AM and the N720/A composites at 1200 °C [16,22].

The influence of loading rate on tensile behavior also investigated with constant loading rates of 25 and 0.0025 MPa at 1100 °C in steam. At the constant loading rate of 0.0025 MPa/s, which is a change in loading rate by four orders, a significant decrease in the tensile stress-strain behavior of the N720/AM was observed. The failure strain values ranges from 0.55 to 0.64% where the average is 174% of that obtained at 25 MPa/s. The average tensile modulus and strength were 21% and 15% lower than those at 25 MPa/s, respectively. As it was reported for N720/A composite at 1100 °C by Braun [18] and for N720/AM composite at 1100 and 1200°C [ref. 16], a strong dependence of tensile behavior on loading rate was observed in this effort.

Creep tests were conducted at 1000 and 1100 °C in air and steam. At 1000 °C, tests were conducted at 131 and 140 MPa in steam. Tests at both 131 and 140 MPa achieved run-out. Creep strain accumulations were 0.2 and 0.21%, respectively. Creep run-out stress was 140 Mpa in steam at 1000 °C

At 1100 °C in air creep run out achieved at 109 and 131 MPa. Accumulated creep accumulations were 0.2 and 0.23%, respectively. Creep stresses were 87.5, 109 and 131

MPa in steam. Creep run-out stress was 87.5 MPa in steam at 1100 °C. Strain accumulations in steam at 1100°C were larger than those at 1000 °C. Largest creep strain 0.87% was observed at 109 MPa in steam at 1100 °C. In air at 1100 °C, the largest creep strain accumulated was 0.23%.

140 MPa, creep run-out stress in steam at 1000 °C, was 87% of UTS and 87.5 MPa, creep run-out stress in steam at 1100 °C, was only 54.7% of UTS. At all creep stresses, the strain accumulation of the N720/AM was higher than that of the N720/A [18] except at 131 MPa (equivalent to 150 MPa for $V_f = 0.44$) in steam at 1100 °C.

In creep-rupture tests, creep strain accumulation increased with the applied creep stress and/or temperature as it was expected. It is worth to note that creep strain accumulations remained very low especially at 1000 °C in steam and 1100 °C in air. Although the creep strains produced for the N720/AM were very low, they are higher compared to the same stress levels for the N720/A composite [18]

At 1000 °C in steam and 1100 °C in air the creep run out stresses of the N720/AM composite were same as those of the N720/A composite, but on the other hand the creep lifetimes of the failed N720/AM specimens were lower than those of the N720/A specimens.

Minimum creep rate reached in all tests. At 1100 °C, creep strain rates ranged from 2.2×10^{-7} to 3.3×10^{-7} in air and from 9.8×10^{-7} to 1.9×10^{-5} in steam. At 1000 °C, strain rates were 6.5×10^{-8} at 131 MPa and 2.17×10^{-7} at 140 MPa in steam.

Specimens achieved run-out were subjected to tensile tests to failure in order to find the retained properties. All specimens retained at least 100% of their tensile strength.

At 1000 °C, tensile strength retentions were 103.7 and 107.6, modulus losses were 10.4% and 7.2% at 131 and 140 MPa, respectively. At 1100 °C, the tensile strength increased by 4.9% and 8.9% in air at 109 and 131 MPa, respectively. The minimum strength retention was observed for the specimen subjected to prior creep stress level of 87.5 in steam as 101.6%. However, the loss in modulus was 14%.

Appendix. Additional Micrographs

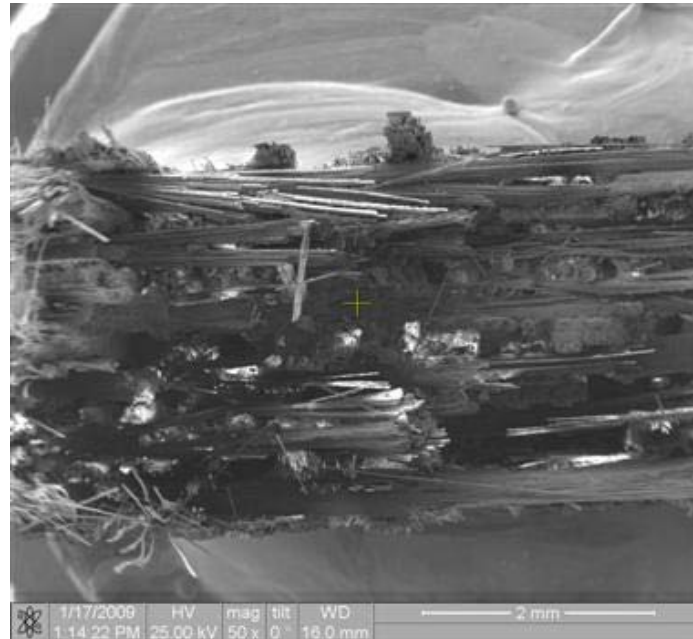


Figure 50. Fracture surface of the N720/AM specimen tested in tension to failure at 900°C in laboratory air

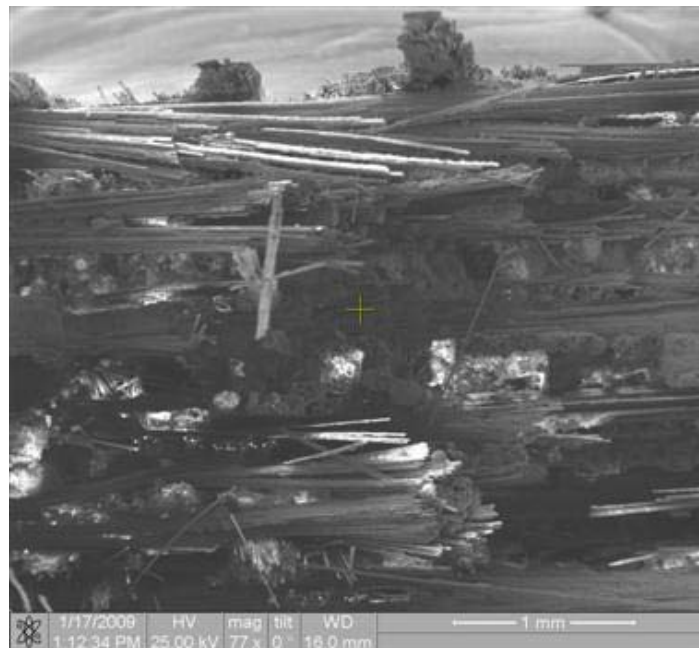


Figure 51. Fracture surface of the N720/AM specimen tested in tension to failure at 900°C in laboratory air



Figure 52. Fracture surface of the N720/AM specimen tested in tension to failure at 900°C in laboratory air

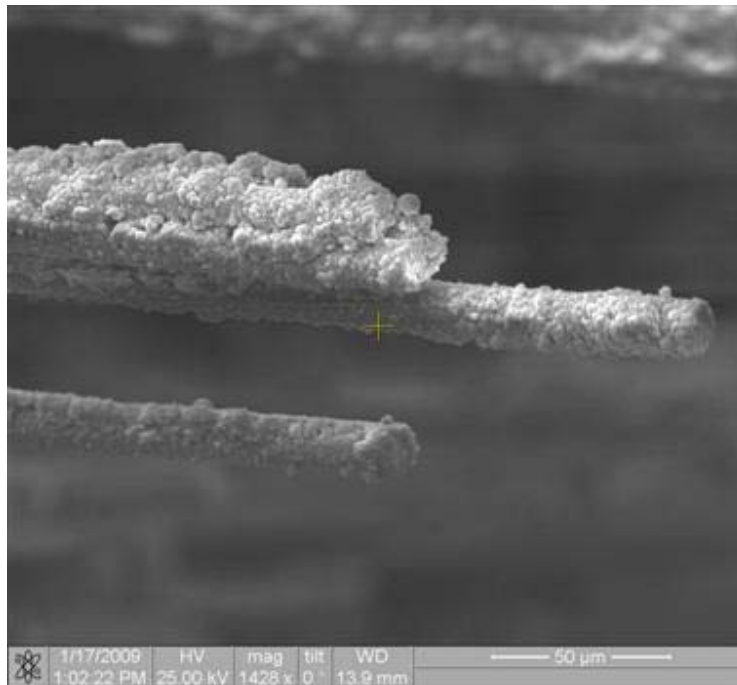


Figure 53. Fracture surface of the N720/AM specimen tested in tension to failure at 900°C in laboratory air



Figure 54. Fracture surface of the N720/AM specimen tested in tension to failure at 900°C in laboratory air

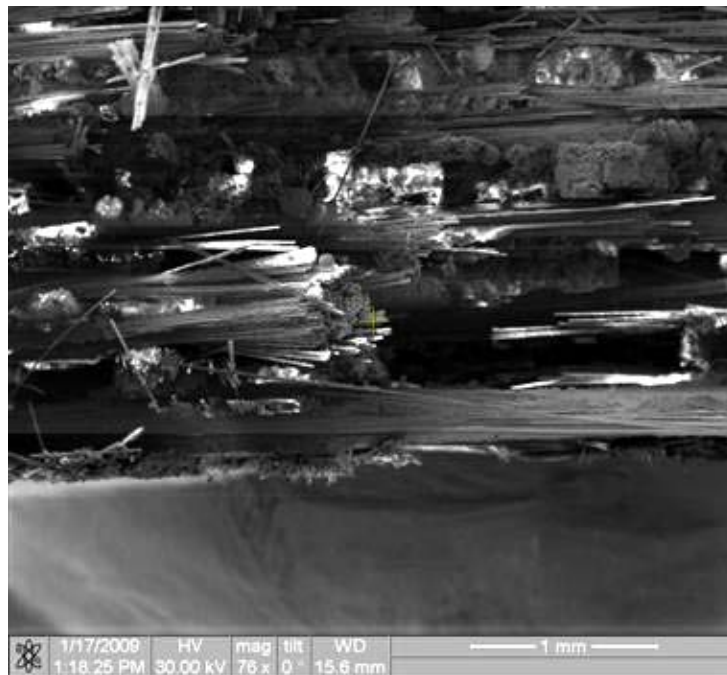


Figure 55. Fracture surface of the N720/AM specimen tested in tension to failure at 900°C in laboratory air

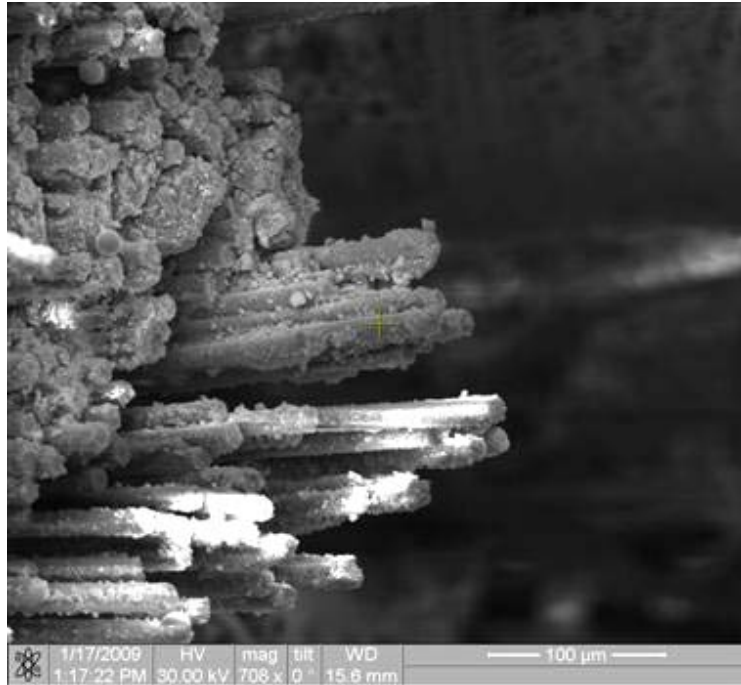


Figure 56. Fracture surface of the N720/AM specimen tested in tension to failure at 900°C in laboratory air

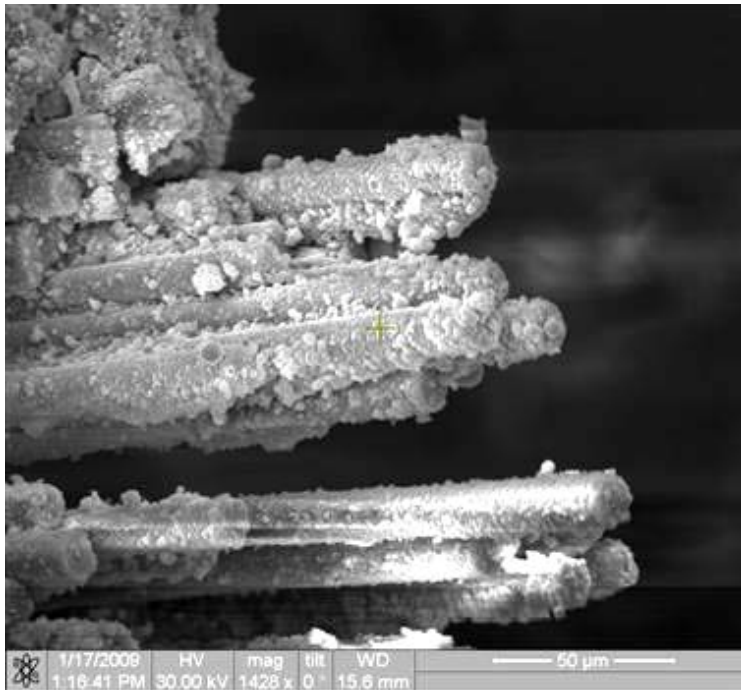


Figure 57. Fracture surface of the N720/AM specimen tested in tension to failure at 900°C in laboratory air

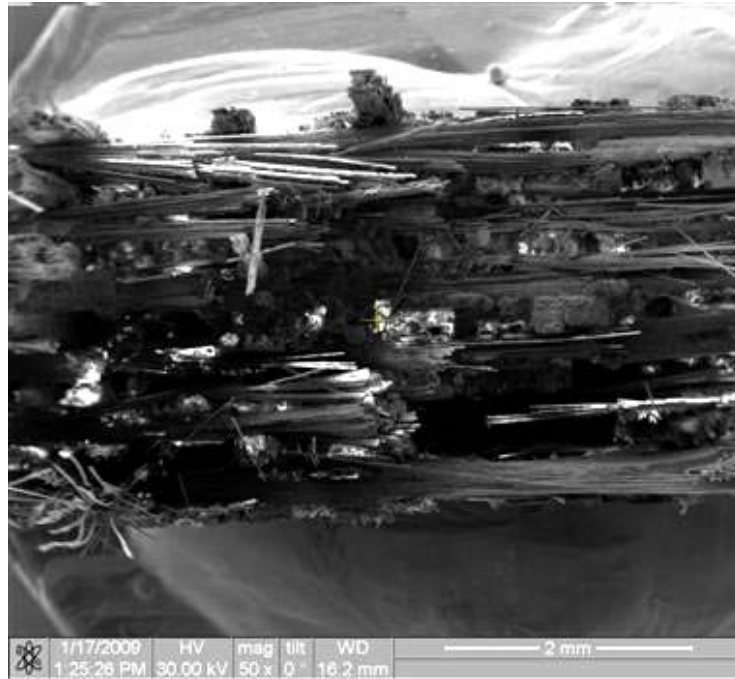


Figure 58. . Fracture surface of the N720/AM specimen tested in tension to failure at 900°C in laboratory air

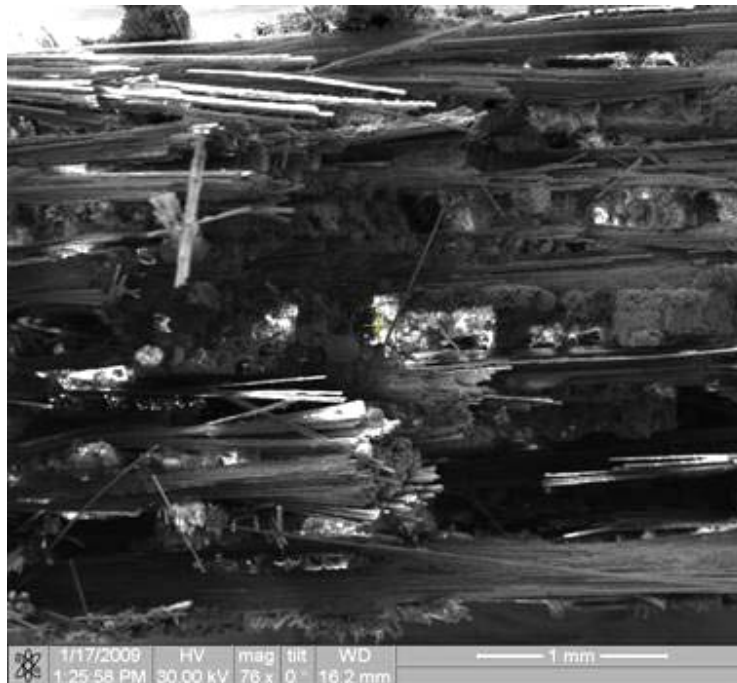


Figure 59. Fracture surface of the N720/AM specimen tested in tension to failure at 900°C in laboratory air

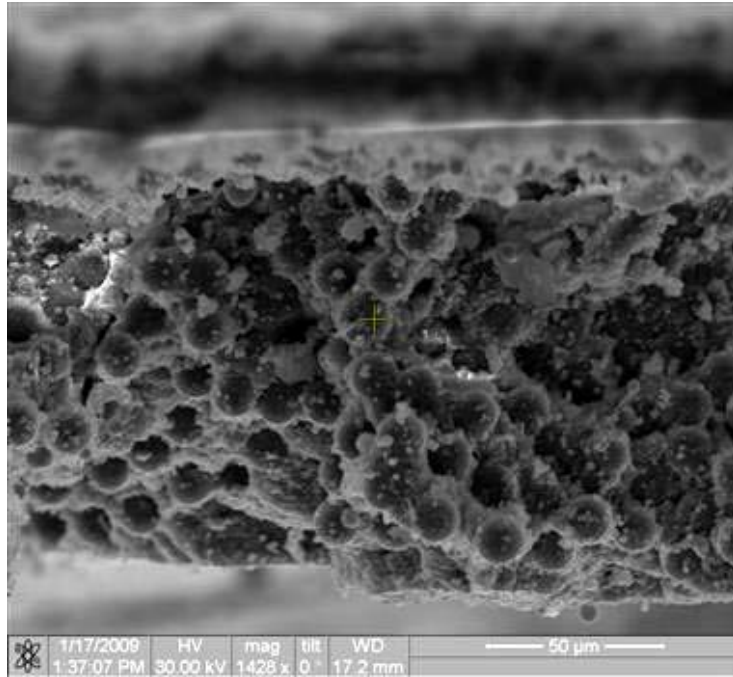


Figure 60. Fracture surface of the N720/AM specimen tested in tension to failure at 900°C in laboratory air

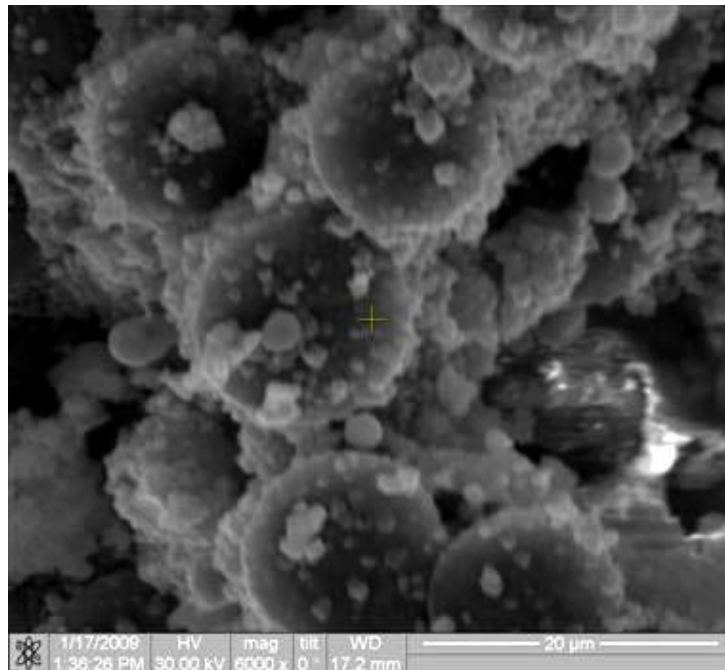


Figure 61. Fracture surface of the N720/AM specimen tested in tension to failure at 900°C in laboratory air

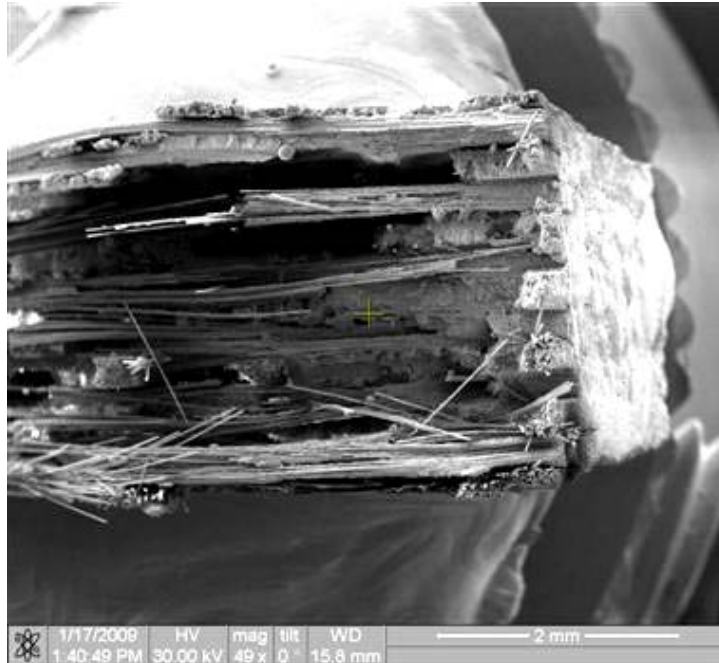


Figure 62. Fracture surface of the N720/AM specimen tested in tension to failure at 900°C in laboratory air

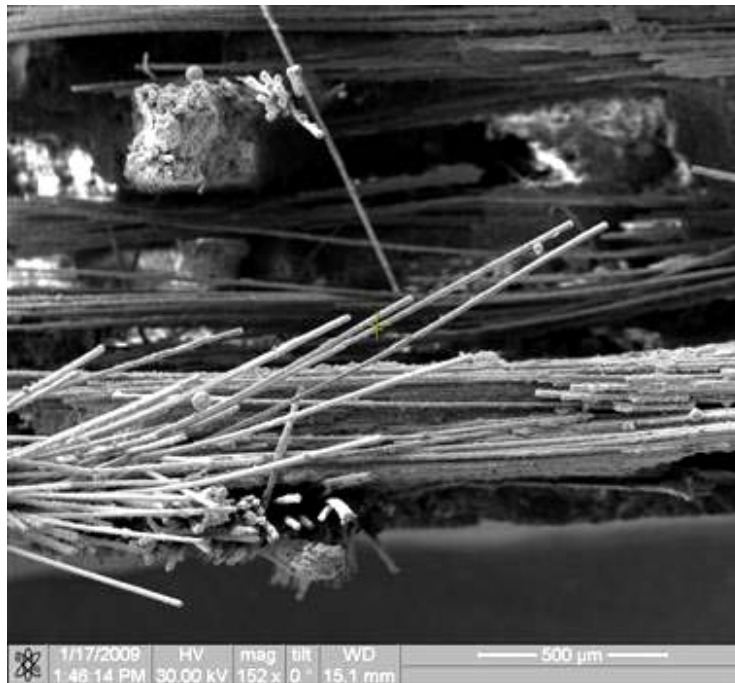


Figure 63. Fracture surface of the N720/AM specimen tested in tension to failure at 900°C in laboratory air



Figure 64. Fracture surface of the N720/AM specimen tested in tension to failure at 900°C in laboratory air

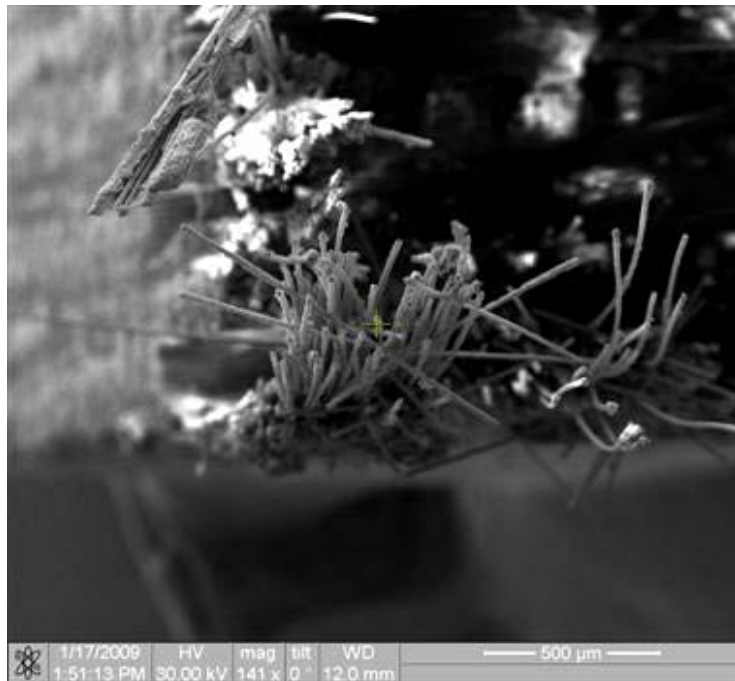


Figure 65. Fracture surface of the N720/AM specimen tested in tension to failure at 900°C in laboratory air

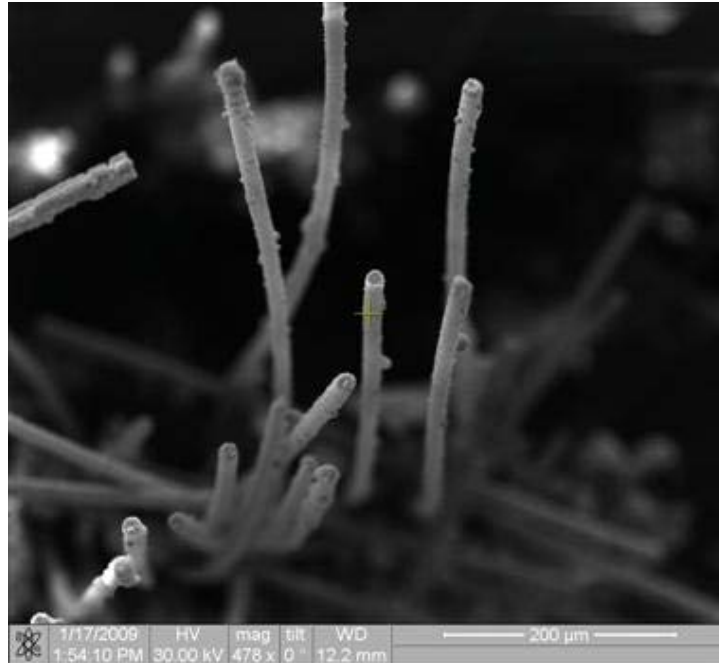


Figure 66. Fracture surface of the N720/AM specimen tested in tension to failure at 900°C in laboratory air

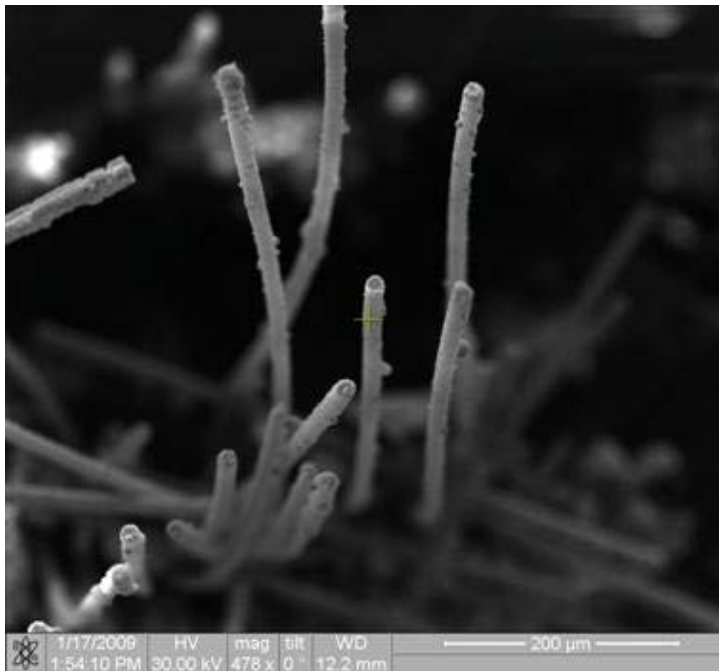


Figure 67. Fracture surface of the N720/AM specimen tested in tension to failure at 900°C in laboratory air

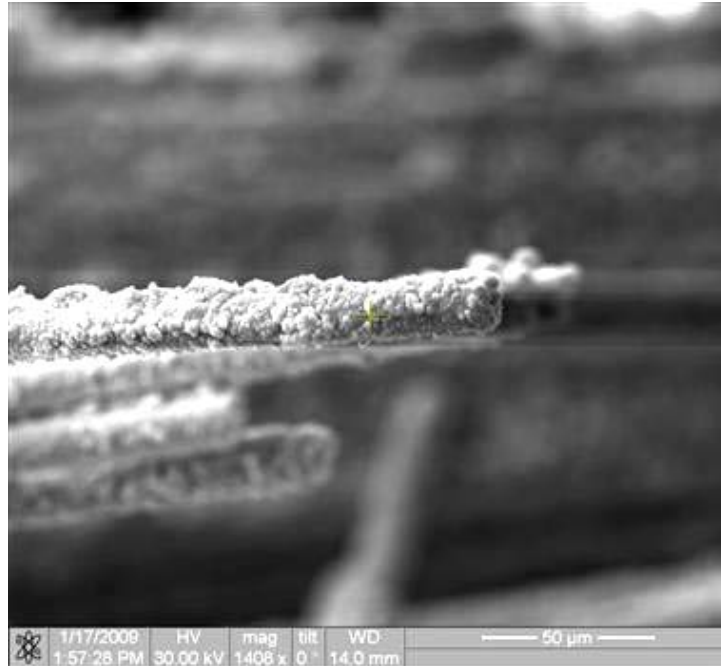


Figure 68. Fracture surface of the N720/AM specimen tested in tension to failure at 900°C in laboratory air



Figure 69. Fracture surface of the N720/AM specimen tested in tension to failure at 900°C in laboratory air

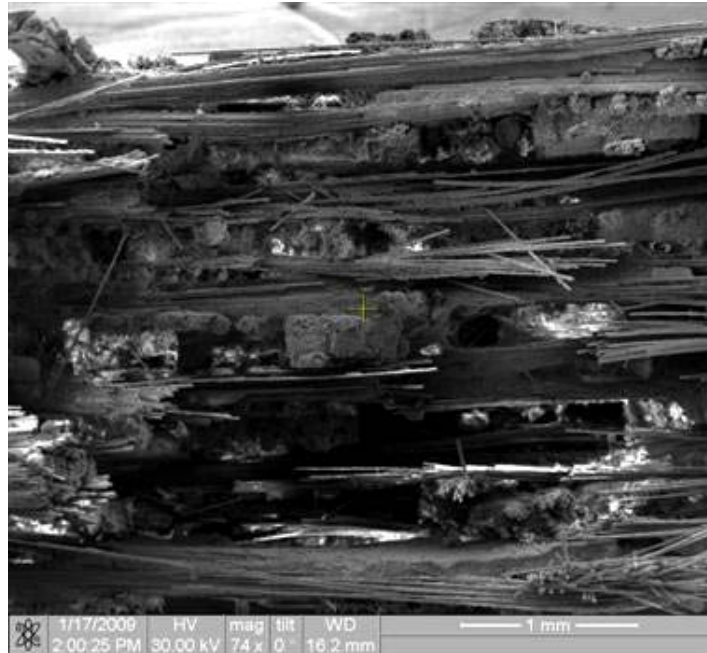


Figure 70. Fracture surface of the N720/AM specimen tested in tension to failure at 900°C in laboratory air

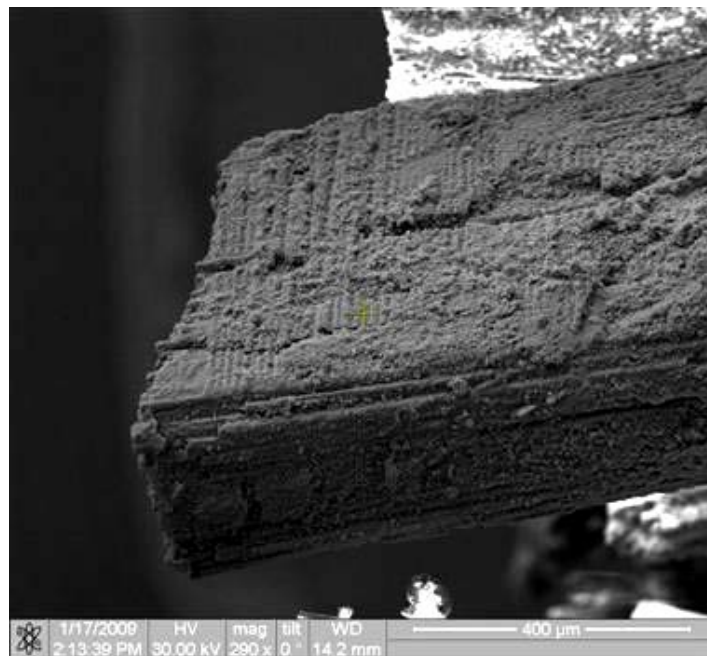


Figure 71. Fracture surface of the N720/AM specimen tested in tension to failure at 1000°C in laboratory air

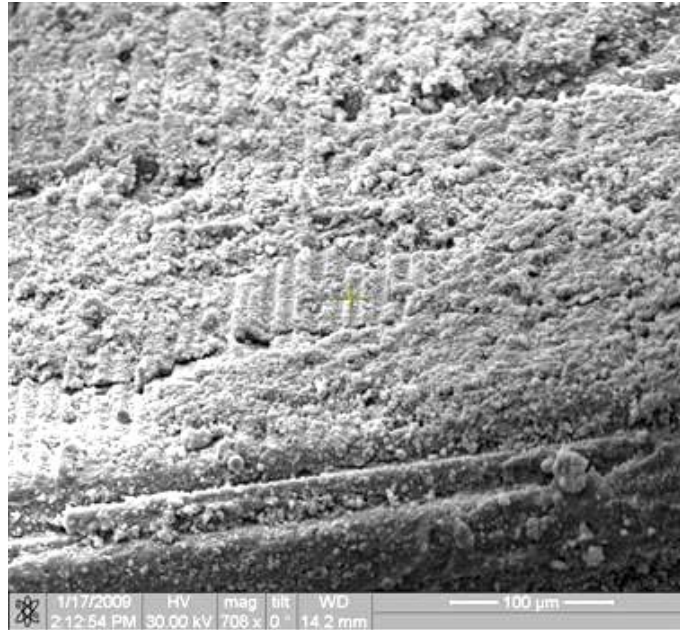


Figure 72. Fracture surface of the N720/AM specimen tested in tension to failure at 1000°C in laboratory air

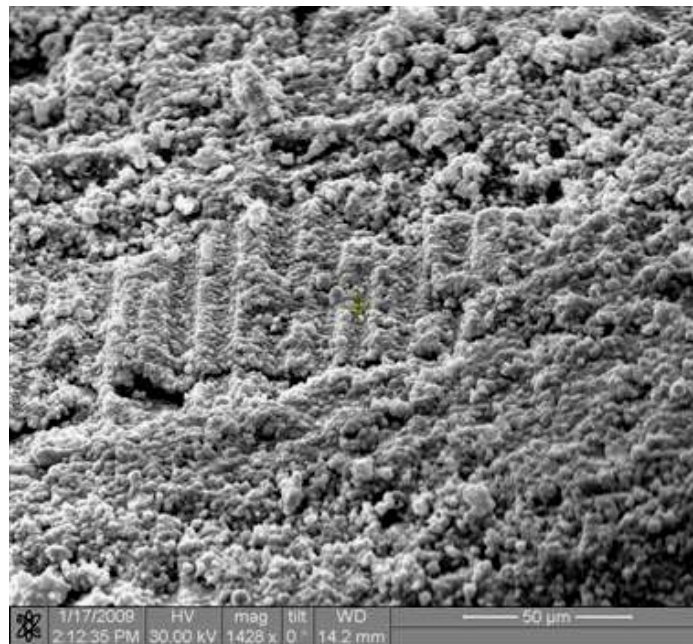


Figure 73. Fracture surface of the N720/AM specimen tested in tension to failure at 1000°C in laboratory air.

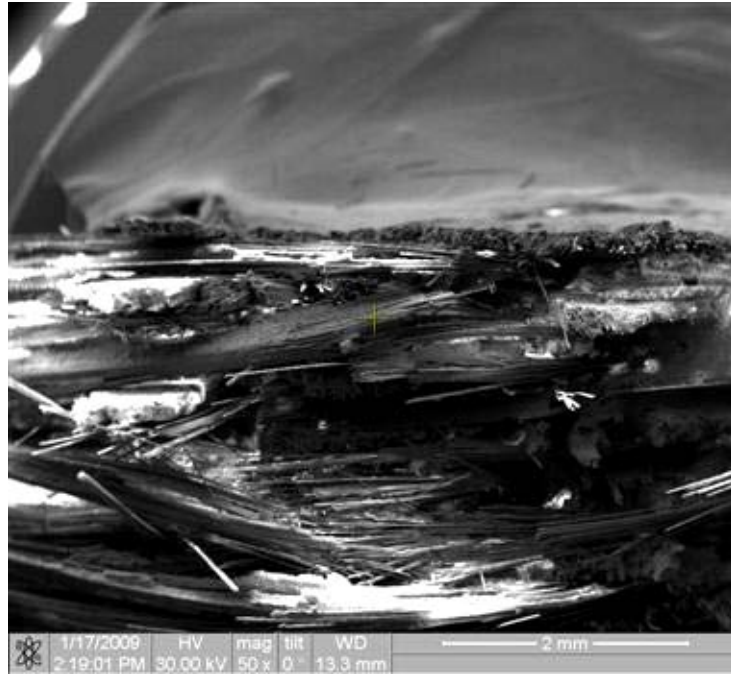


Figure 74. Fracture surface of the N720/AM specimen tested in tension to failure at 1000°C in laboratory air



Figure 75. Fracture surface of the N720/AM specimen tested in tension to failure at 1000°C in laboratory air



Figure 76. Fracture surface of the N720/AM specimen tested in tension to failure at 1000°C in laboratory air

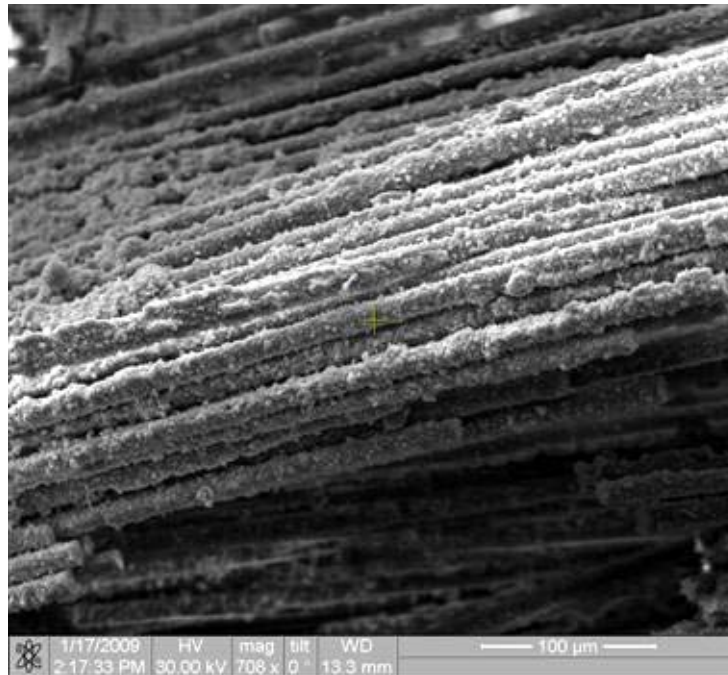


Figure 77. Fracture surface of the N720/AM specimen tested in tension to failure at 1000°C in laboratory air

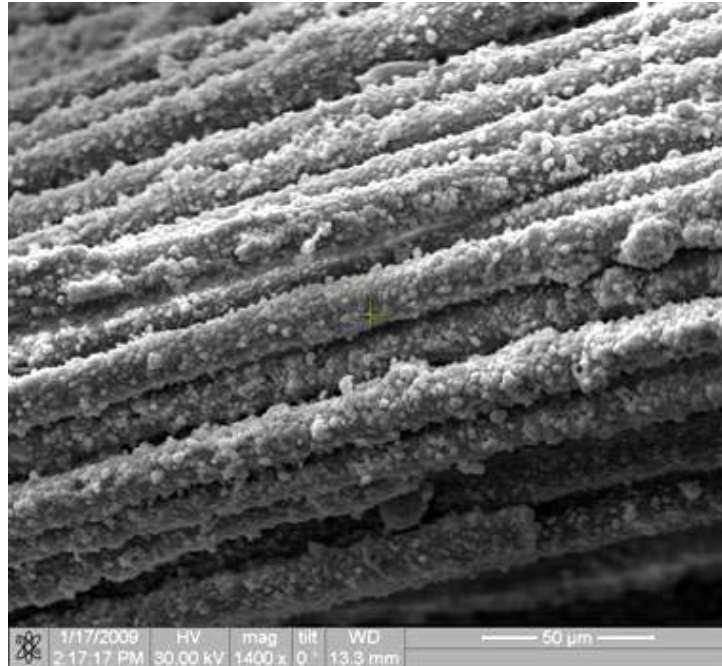


Figure 78. Fracture surface of the N720/AM specimen tested in tension to failure at 1000°C in laboratory air

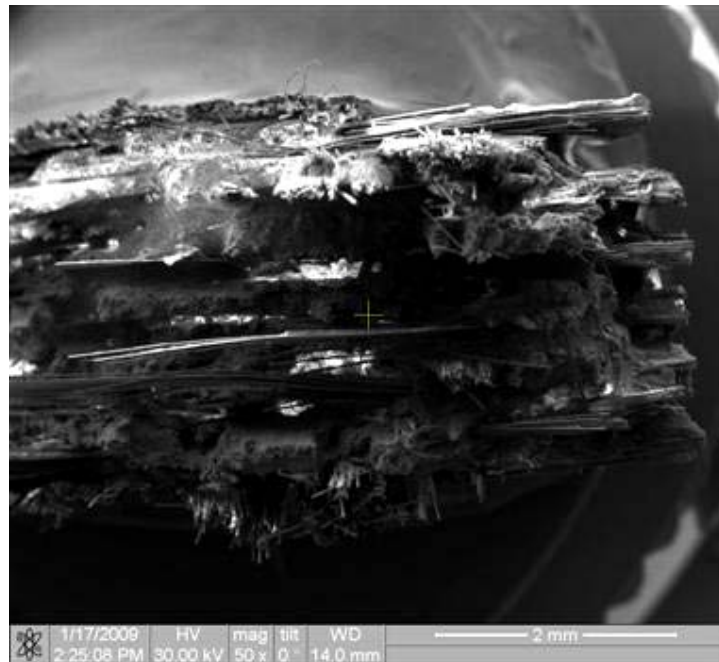


Figure 79. Fracture surface of the N720/AM specimen tested in tension to failure at 1000°C in laboratory air

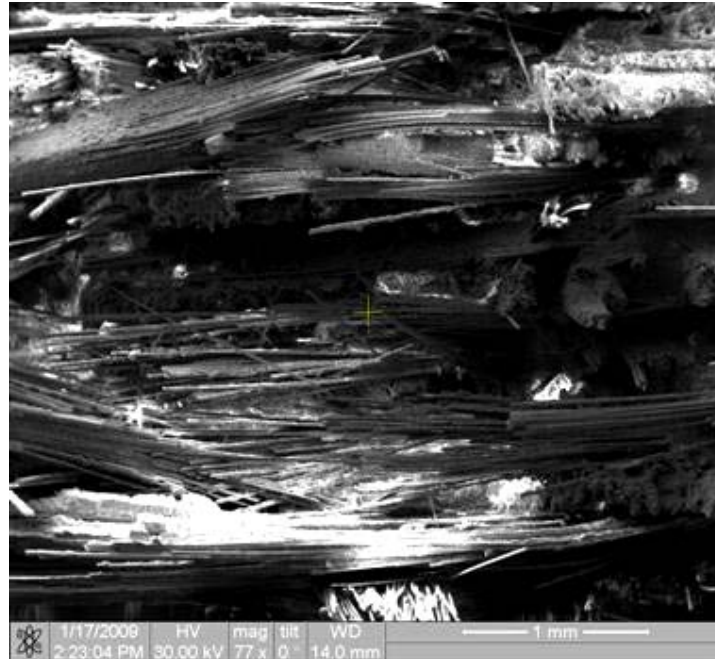


Figure 80. Fracture surface of the N720/AM specimen tested in tension to failure at 1000°C in laboratory air

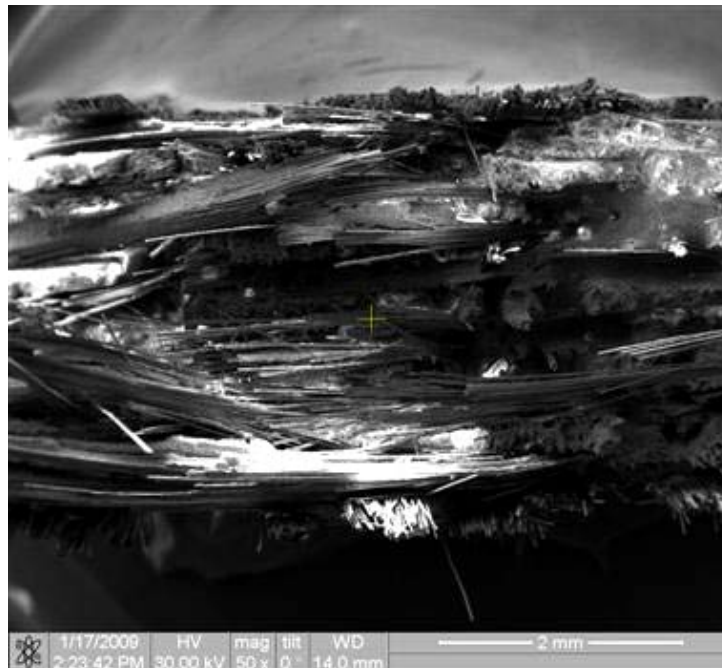


Figure 81. Fracture surface of the N720/AM specimen tested in tension to failure at 1000°C in laboratory air

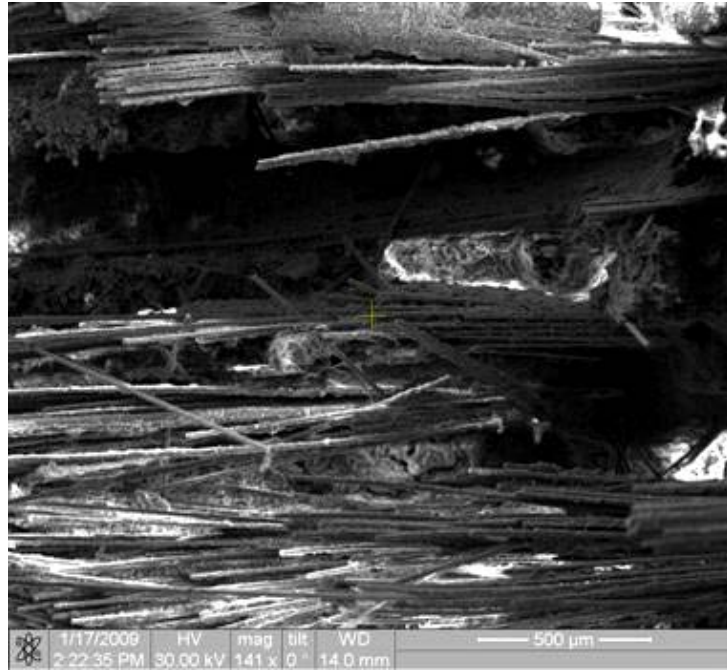


Figure 82. Fracture surface of the N720/AM specimen tested in tension to failure at 1000°C in laboratory air

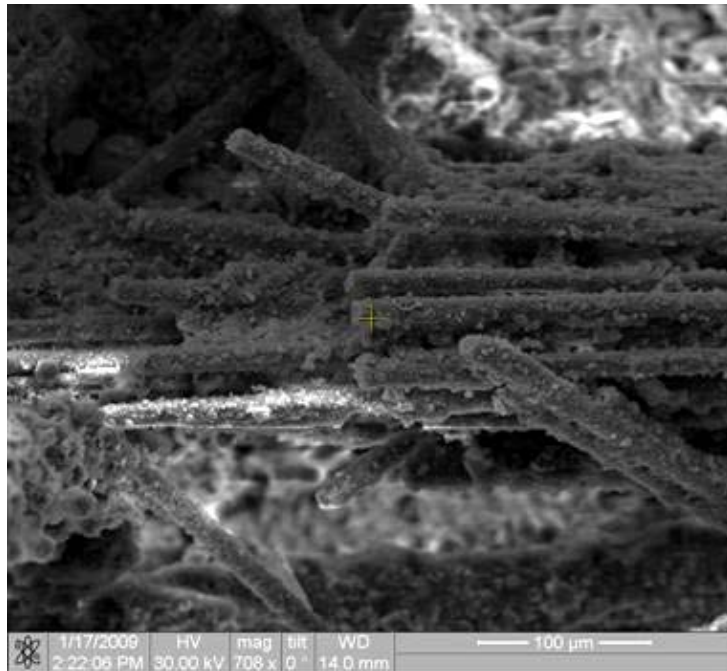


Figure 83. Fracture surface of the N720/AM specimen tested in tension to failure at 1000°C in laboratory air



Figure 84. Fracture surface of the N720/AM specimen tested in tension to failure at 1000°C in laboratory air



Figure 85. Fracture surface of the N720/AM specimen tested in tension to failure at 1000°C in laboratory air



Figure 86. Fracture surface of the N720/AM specimen tested in tension to failure at 1000°C in laboratory air

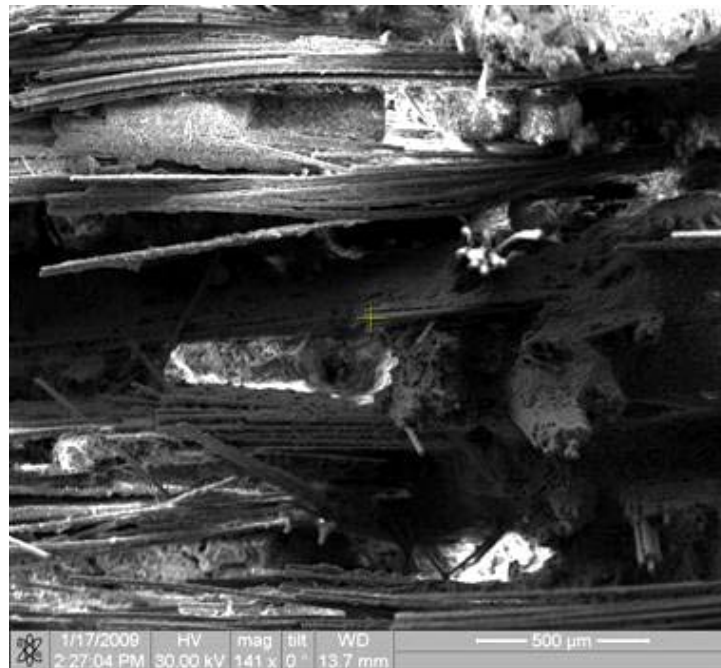


Figure 87. Fracture surface of the N720/AM specimen tested in tension to failure at 1000°C in laboratory air

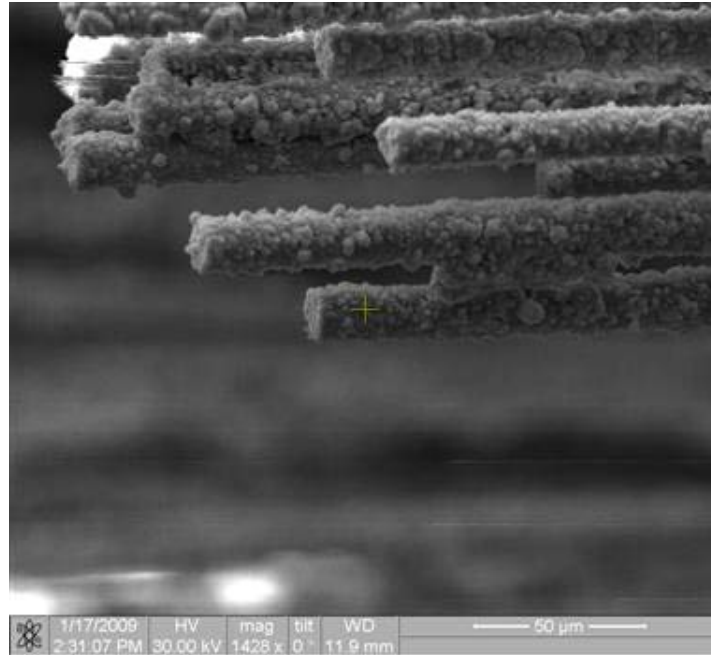


Figure 88. Fracture surface of the N720/AM specimen tested in tension to failure at 1000°C in laboratory air

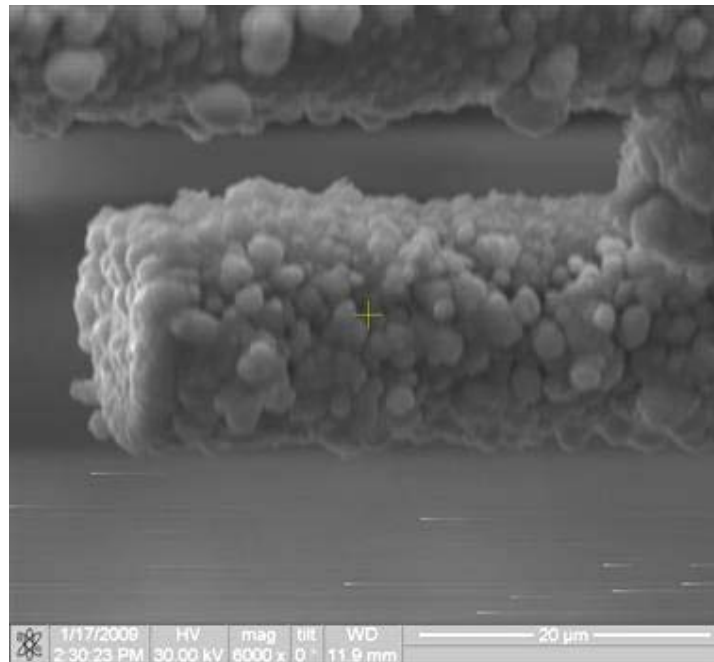


Figure 89. Fracture surface of the N720/AM specimen tested in tension to failure at 1000°C in laboratory air

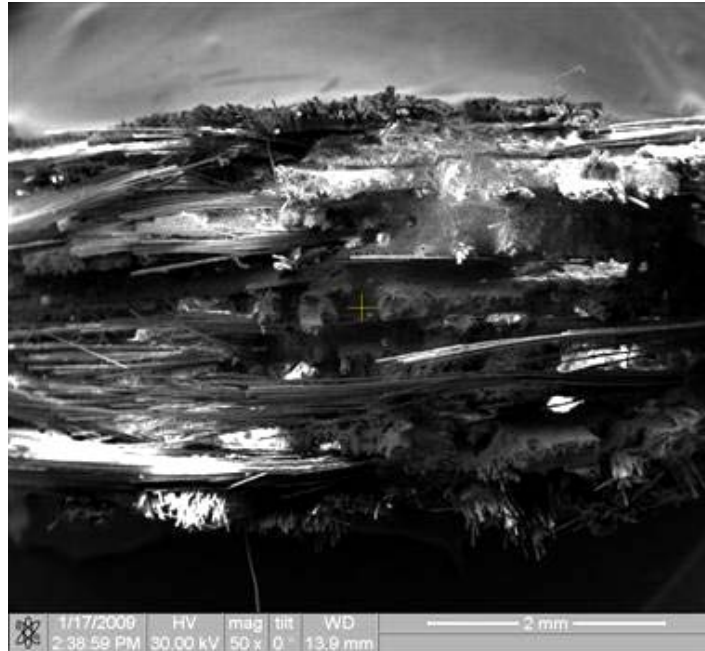


Figure 90. Fracture surface of the N720/AM specimen tested in tension to failure at 1000°C in laboratory air

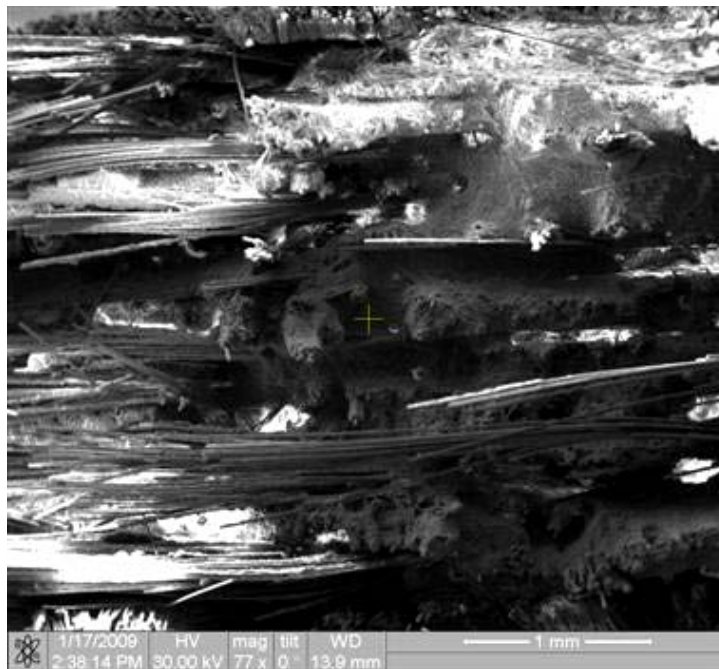


Figure 91. Fracture surface of the N720/AM specimen tested in tension to failure at 1000°C in laboratory air



Figure 92. Fracture surface of the N720/AM specimen tested in tension to failure at 1000°C in laboratory air

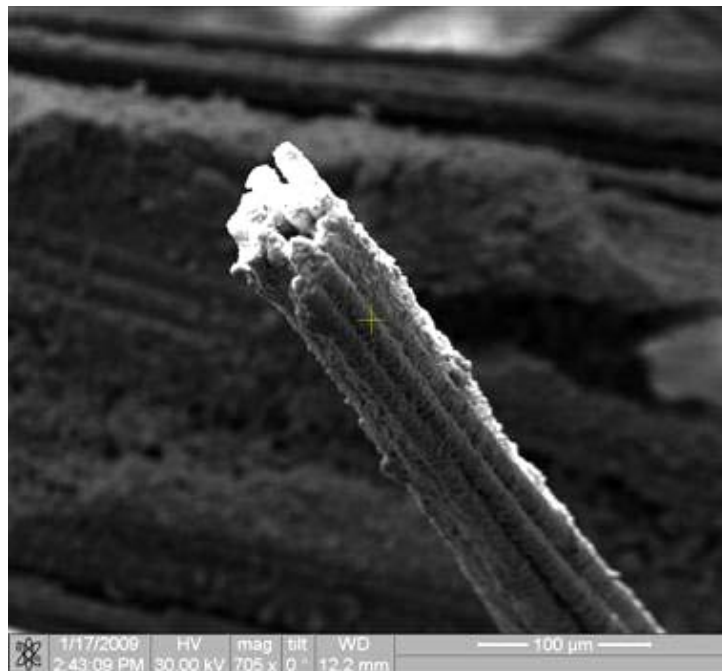


Figure 93. Fracture surface of the N720/AM specimen tested in tension to failure at 1000°C in laboratory air

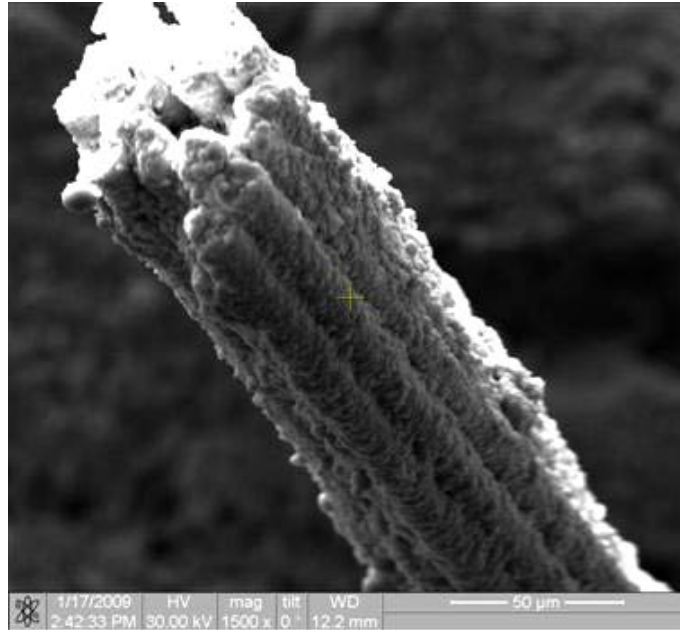


Figure 94. Fracture surface of the N720/AM specimen tested in tension to failure at 1000°C in laboratory air

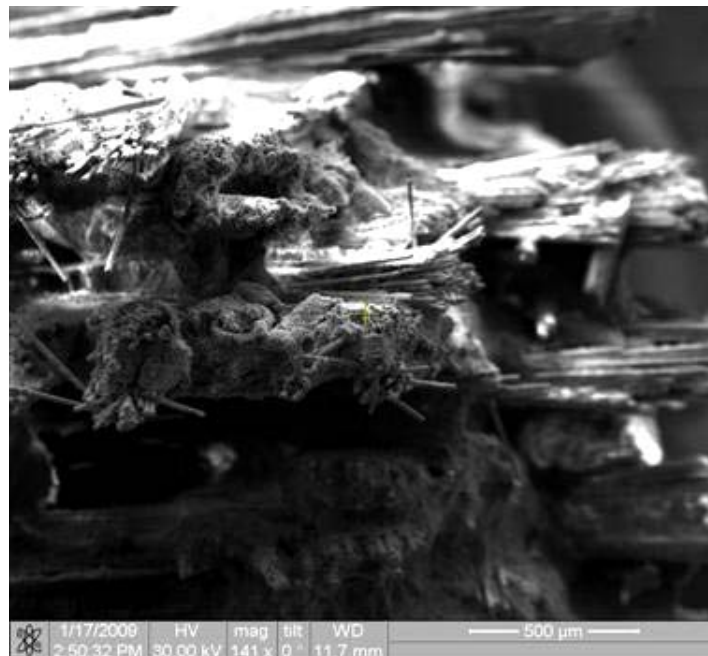


Figure 95. Fracture surface of the N720/AM specimen tested in tension to failure at 1000°C in laboratory air

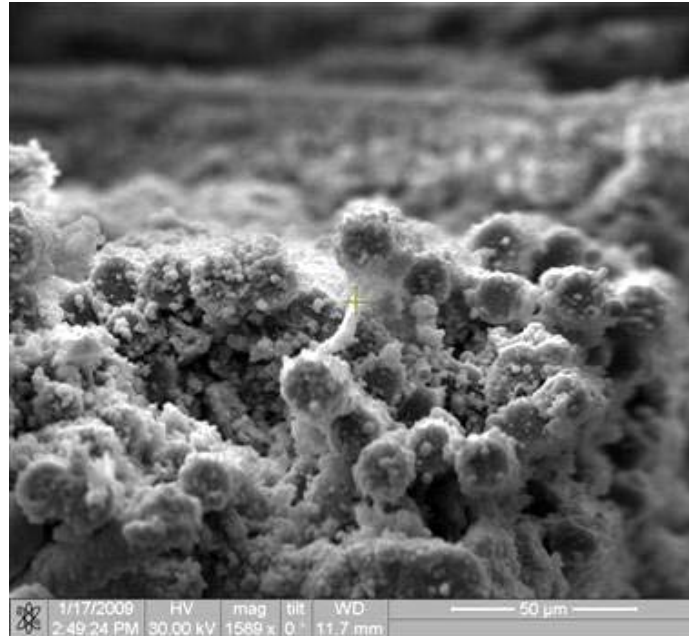


Figure 96. Fracture surface of the N720/AM specimen tested in tension to failure at 1000°C in laboratory air

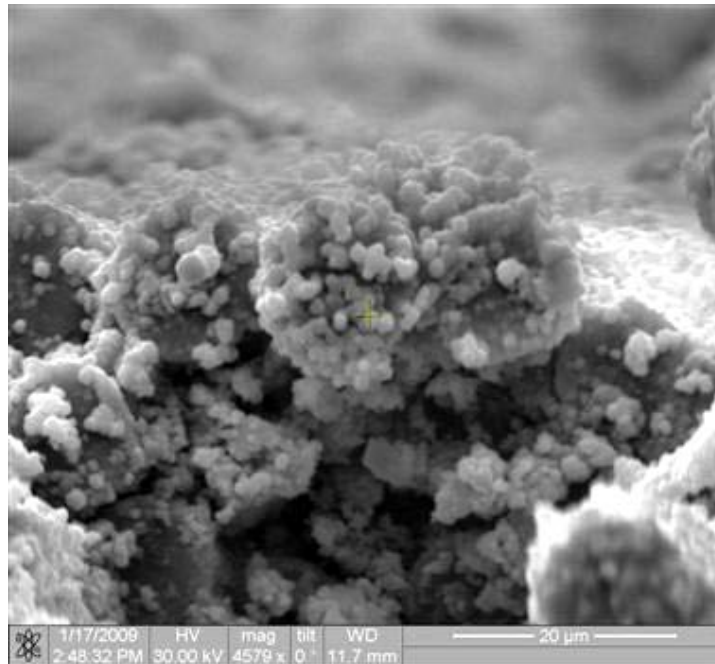


Figure 97. Fracture surface of the N720/AM specimen tested in tension to failure at 1000°C in laboratory air

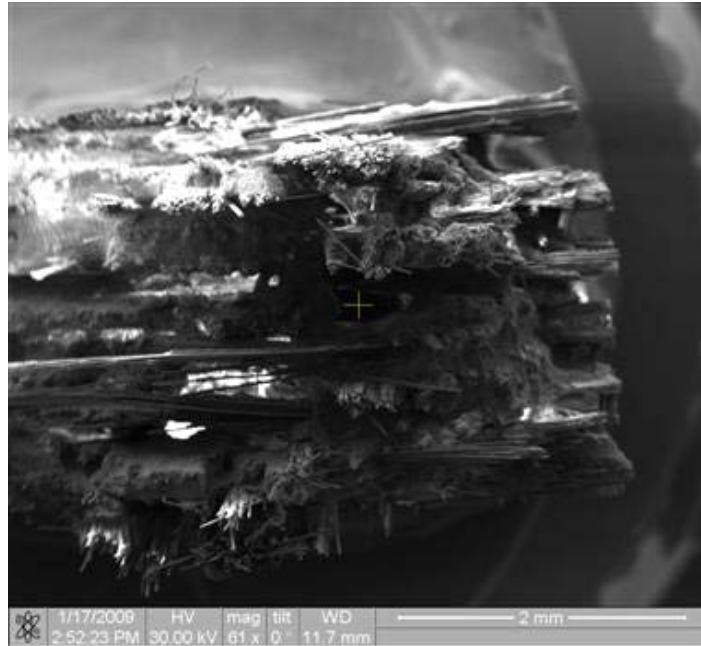


Figure 98. Fracture surface of the N720/AM specimen tested in tension to failure at 1000°C in laboratory air



Figure 99. Fracture surface of the N720/AM specimen tested in tension to failure at 1000°C in laboratory air

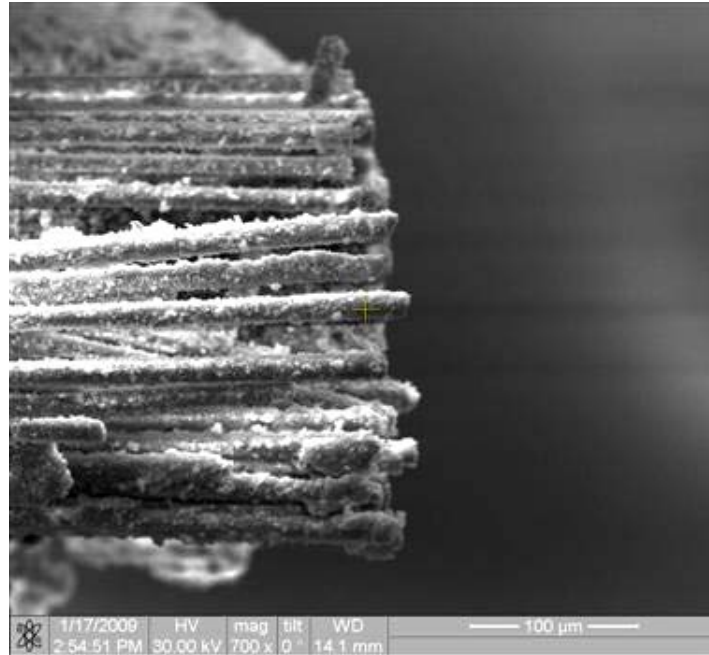


Figure 100. Fracture surface of the N720/AM specimen tested in tension to failure at 1000°C in laboratory air

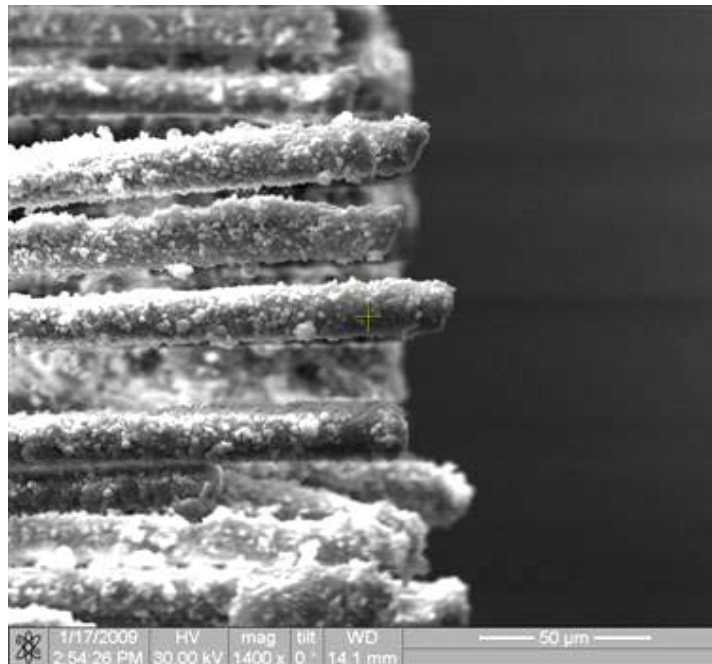


Figure 101. Fracture surface of the N720/AM specimen tested in tension to failure at 1000°C in laboratory air

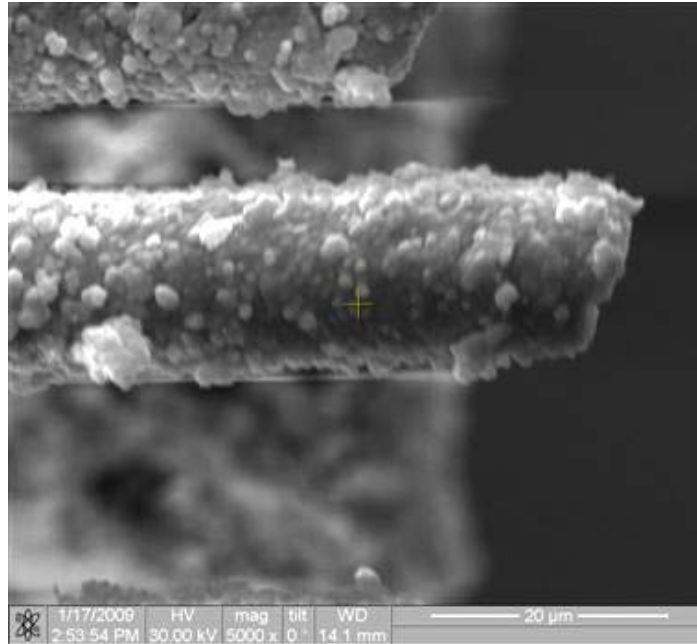


Figure 102. Fracture surface of the N720/AM specimen tested in tension to failure at 1000°C in laboratory air

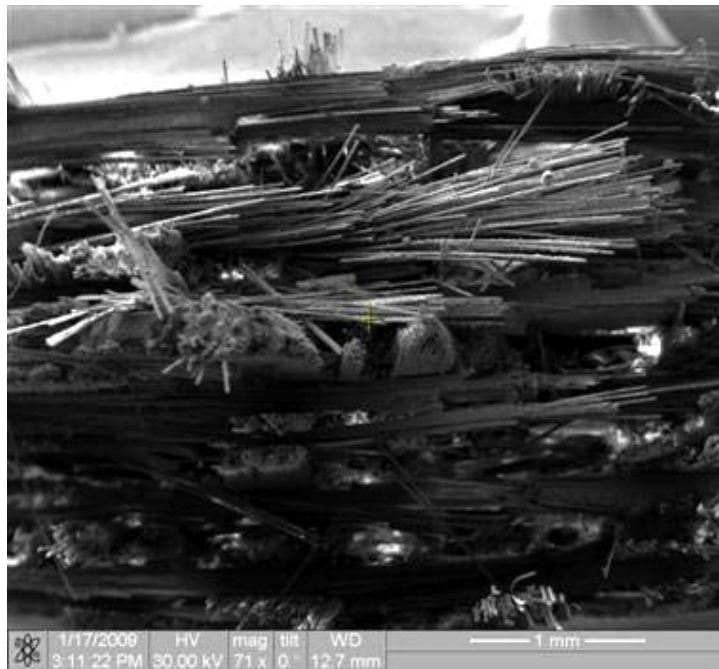


Figure 103. Fracture surface of the N720/AM specimen tested in tension to failure at 1100°C in laboratory air

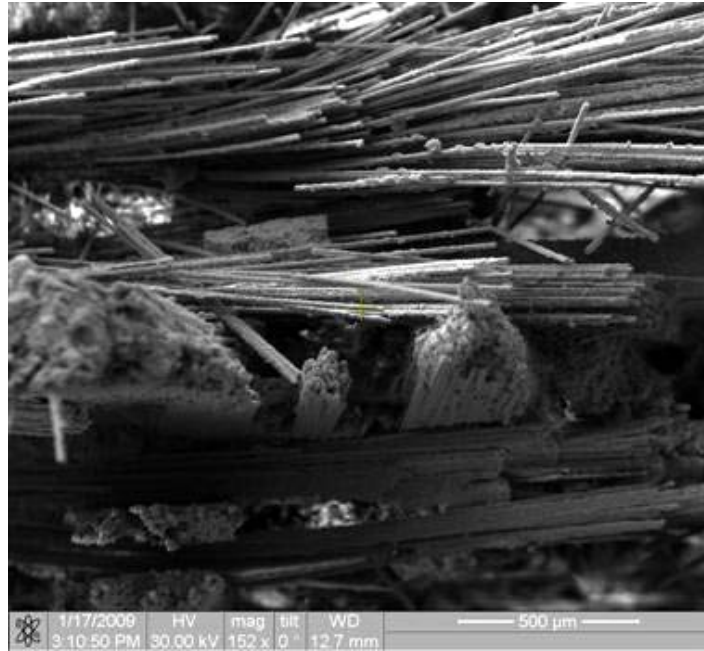


Figure 104. Fracture surface of the N720/AM specimen tested in tension to failure at 1100°C in laboratory air



Figure 105. Fracture surface of the N720/AM specimen tested in tension to failure at 1000°C in laboratory air

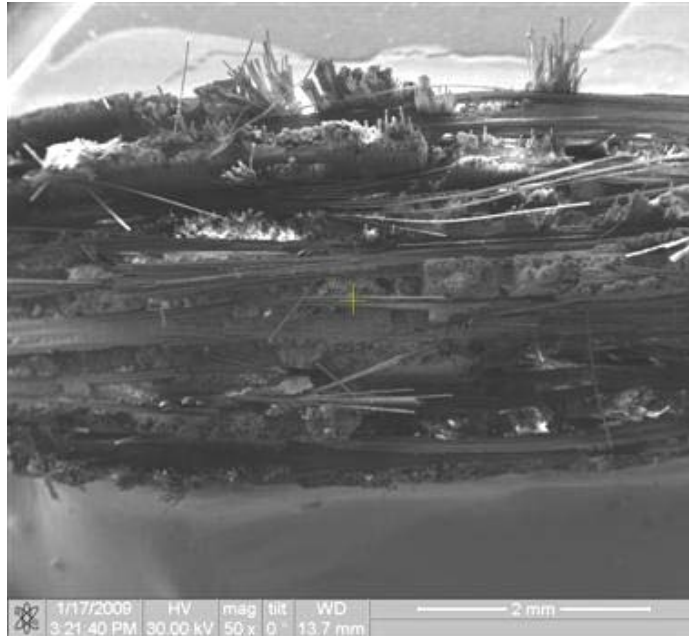


Figure 106. Fracture surface of the N720/AM specimen tested in tension to failure at 1000°C in laboratory air

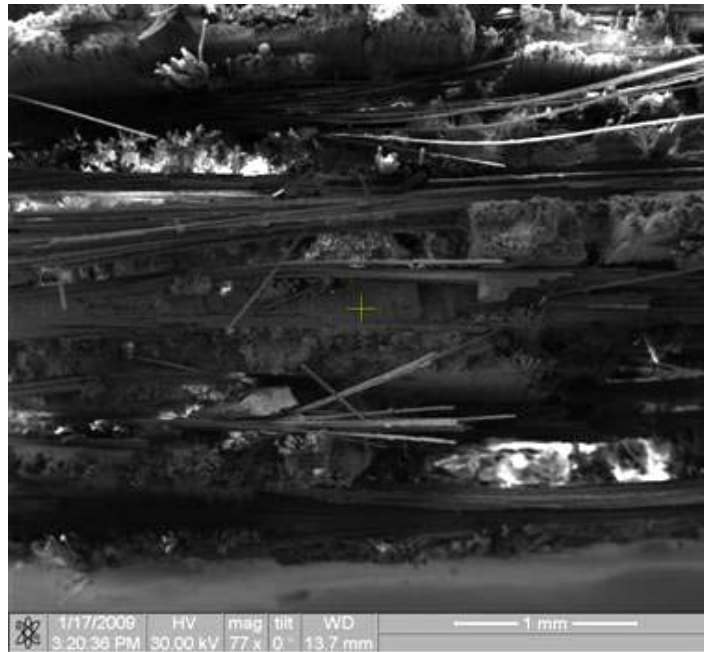


Figure 107. Fracture surface of the N720/AM specimen tested in tension to failure at 1000°C in laboratory air

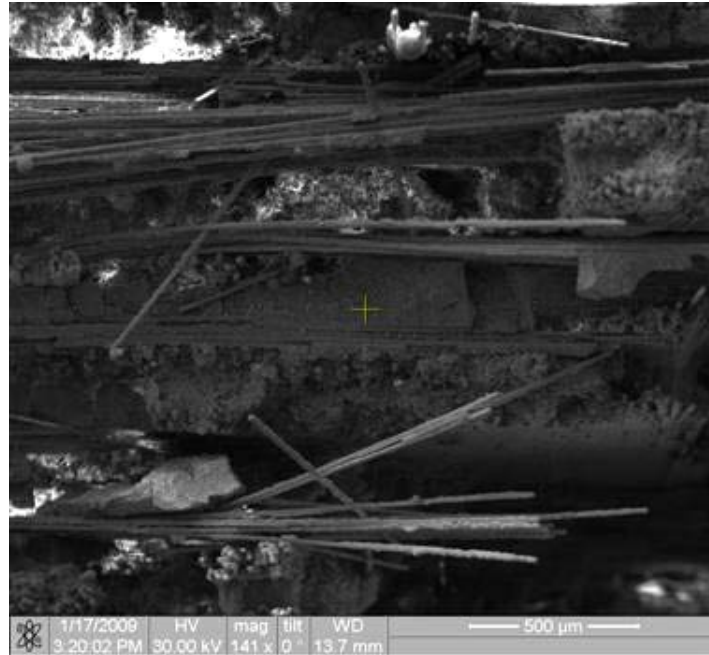


Figure 108. . Fracture surface of the N720/AM specimen tested in tension to failure at 1000°C in laboratory air

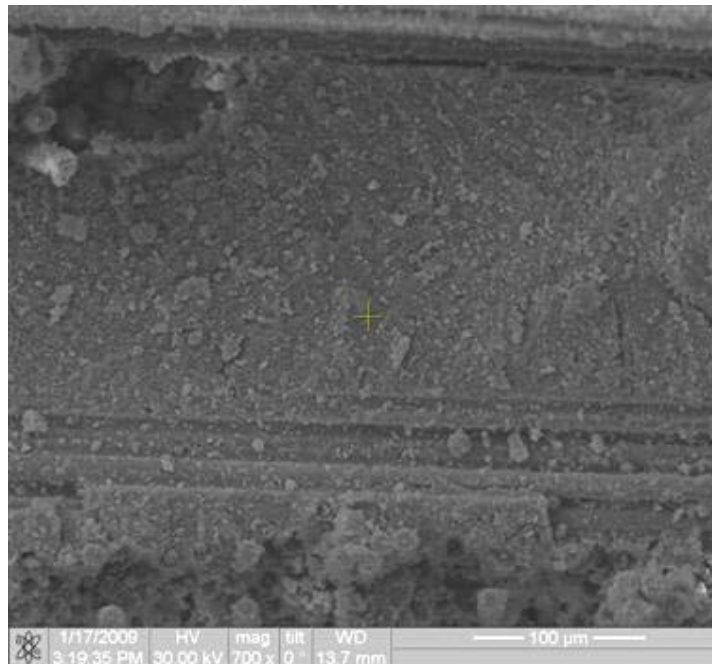


Figure 109. Fracture surface of the N720/AM specimen tested in tension to failure at 1100°C in laboratory air

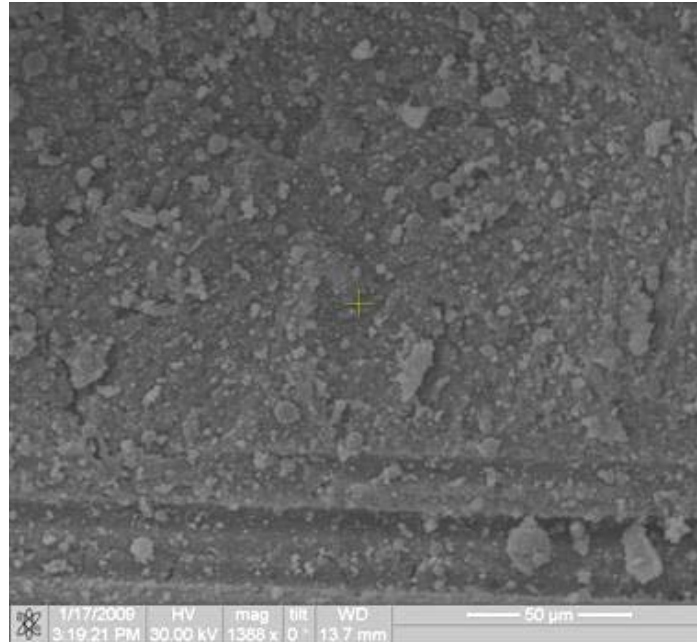


Figure 110. Fracture surface of the N720/AM specimen tested in tension to failure at 1100°C in laboratory air



Figure 111. Fracture surface of the N720/AM specimen tested in tension to failure at 1100°C in laboratory air



Figure 112. Fracture surface of the N720/AM specimen tested in tension to failure at 1100°C in laboratory air

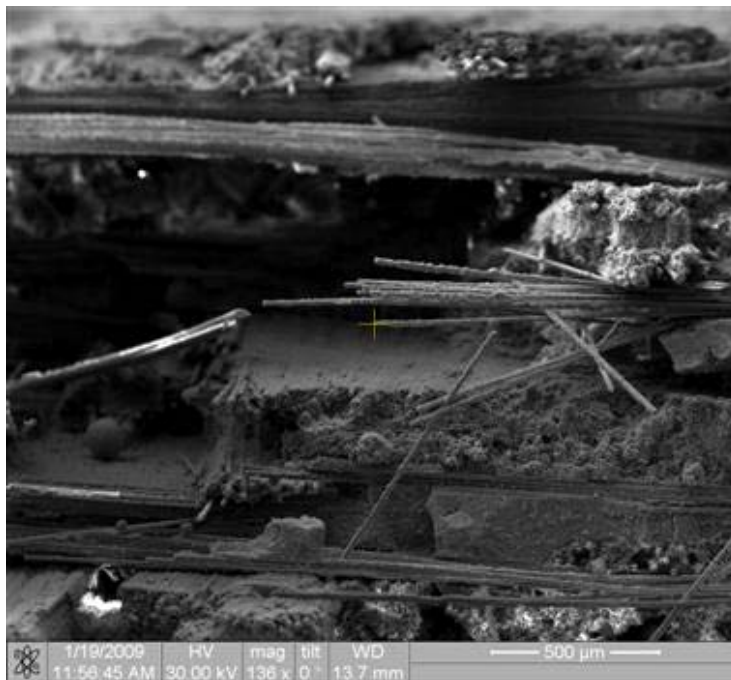


Figure 113. Fracture surface of the N720/AM specimen tested in tension to failure at 1100°C in laboratory air

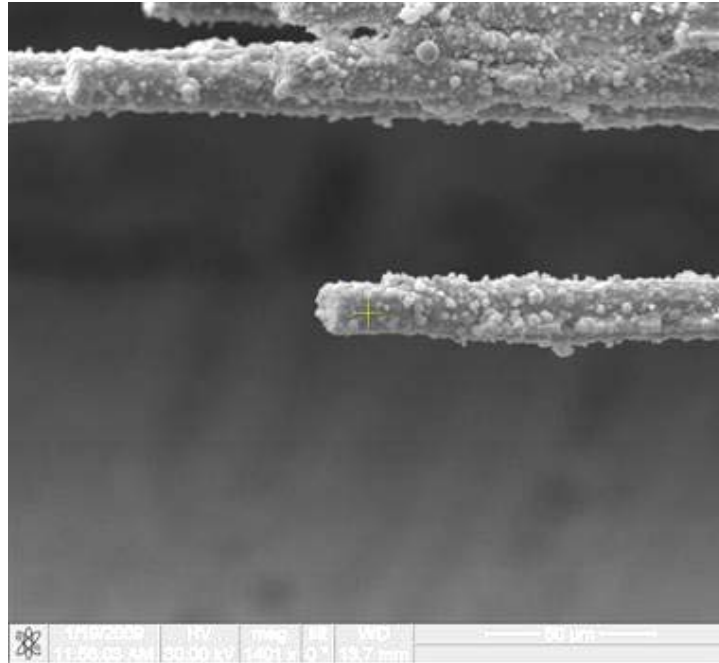


Figure 114. Fracture surface of the N720/AM specimen tested in tension to failure at 1100°C in laboratory air

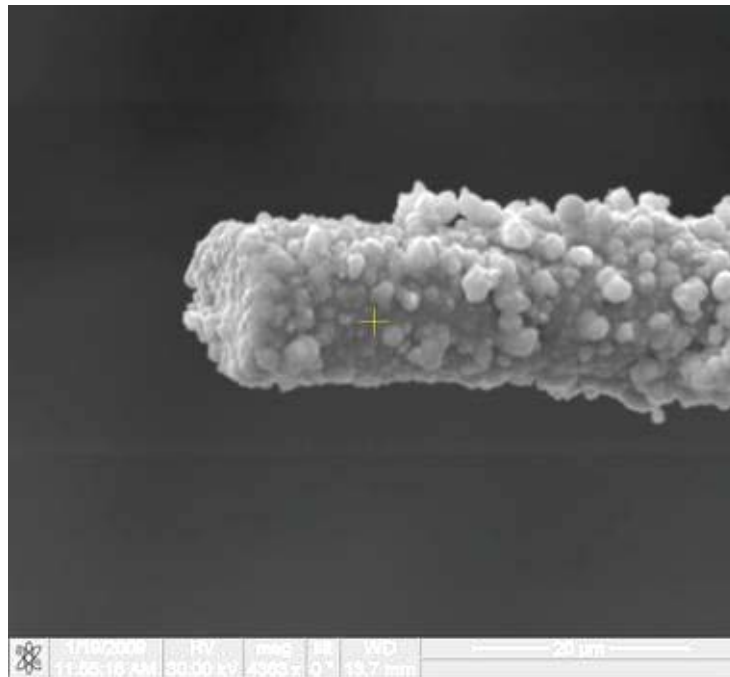


Figure 115. Fracture surface of the N720/AM specimen tested in tension to failure at 1100°C in laboratory air

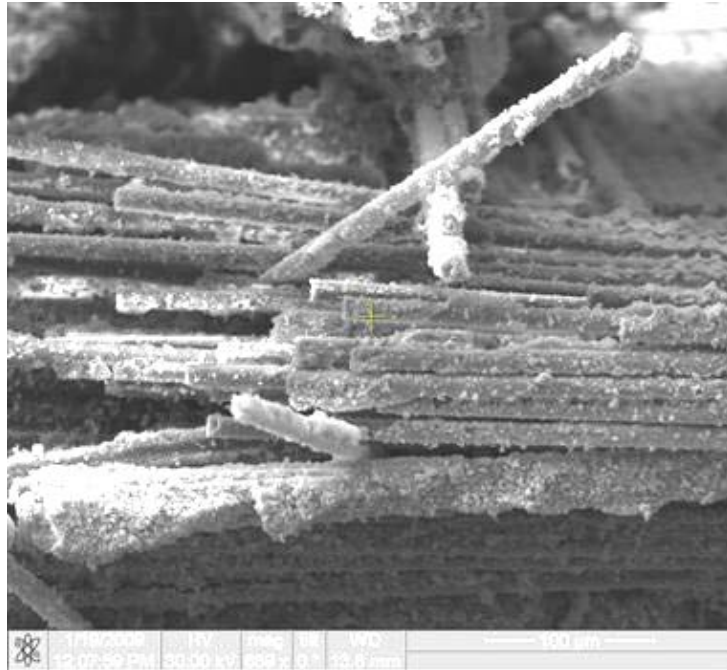


Figure 116. Fracture surface of the N720/AM specimen tested in tension to failure at 1100°C in laboratory air

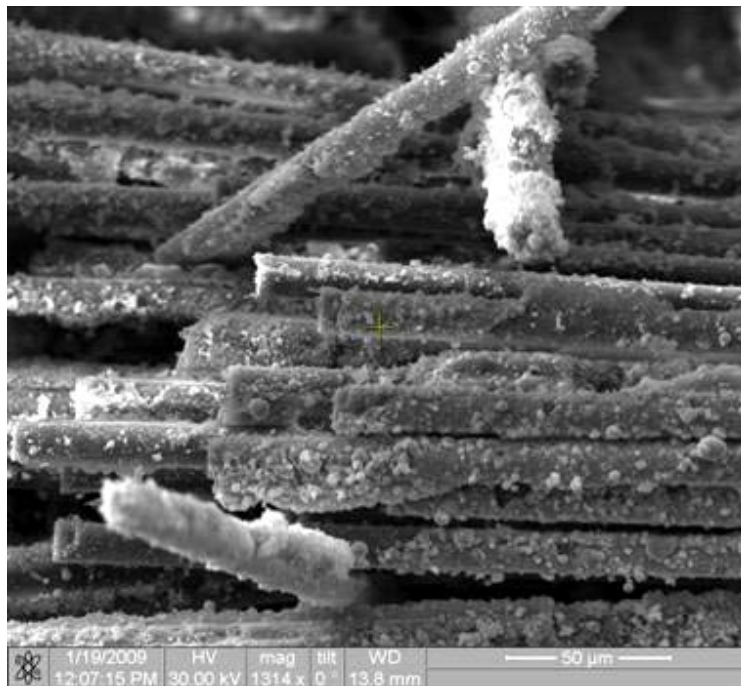


Figure 117. Fracture surface of the N720/AM specimen tested in tension to failure at 1100°C in laboratory air

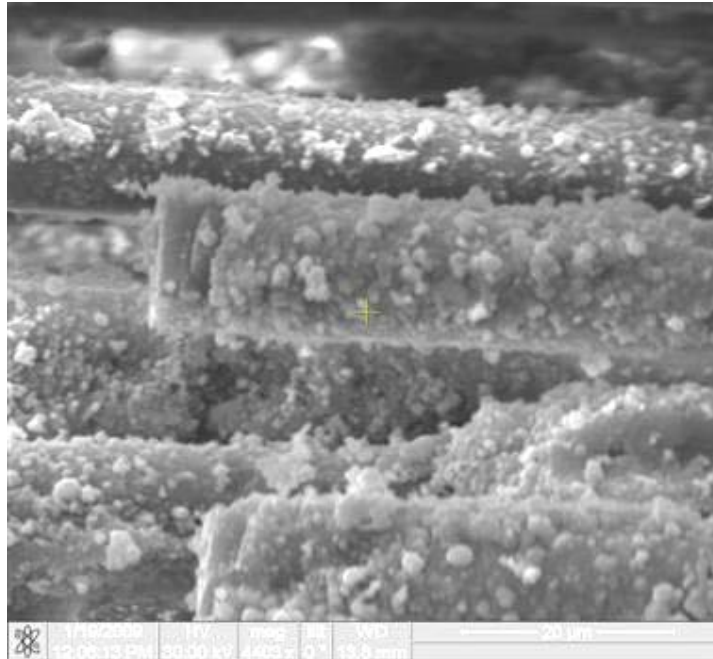


Figure 118. Fracture surface of the N720/AM specimen tested in tension to failure at 1100°C in laboratory air

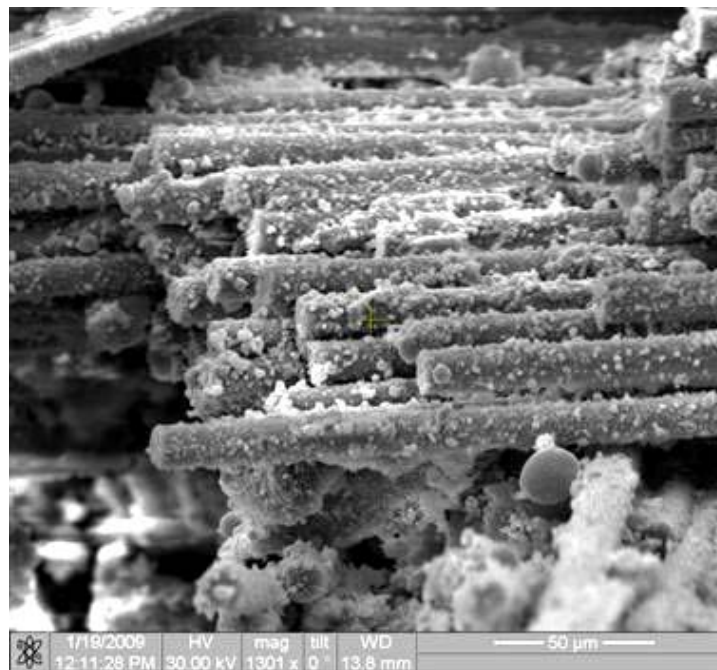


Figure 119. Fracture surface of the N720/AM specimen tested in tension to failure at 1100°C in laboratory air

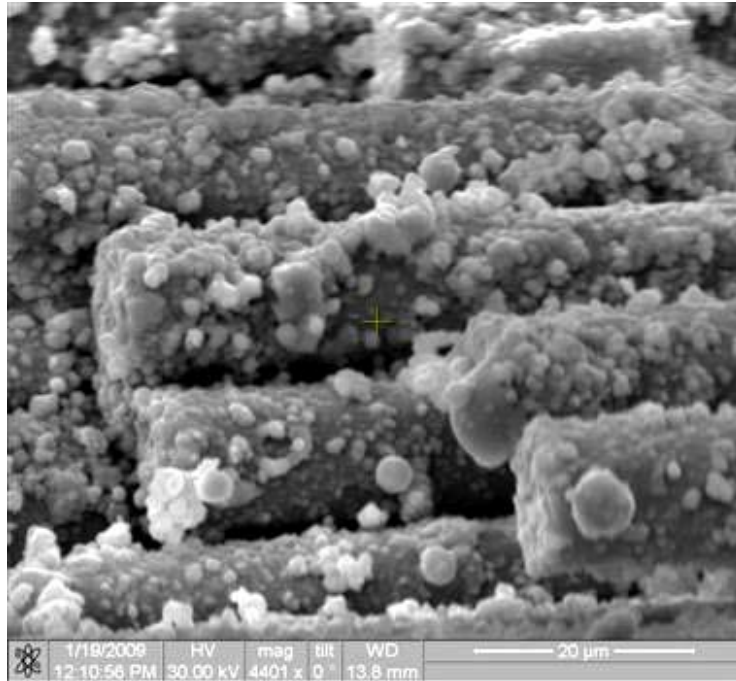


Figure 120. Fracture surface of the N720/AM specimen tested in tension to failure at 1100°C in laboratory air.

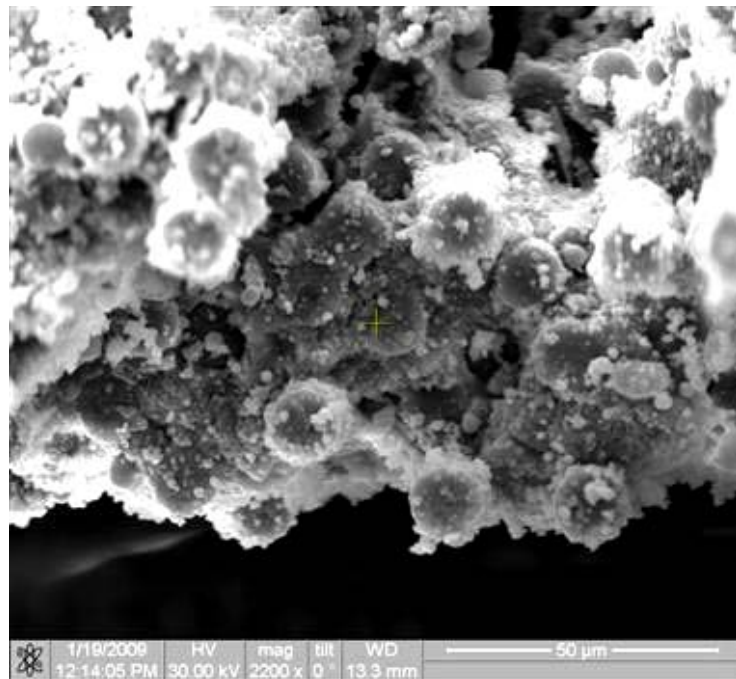


Figure 121. Fracture surface of the N720/AM specimen tested in tension to failure at 1100°C in laboratory air.

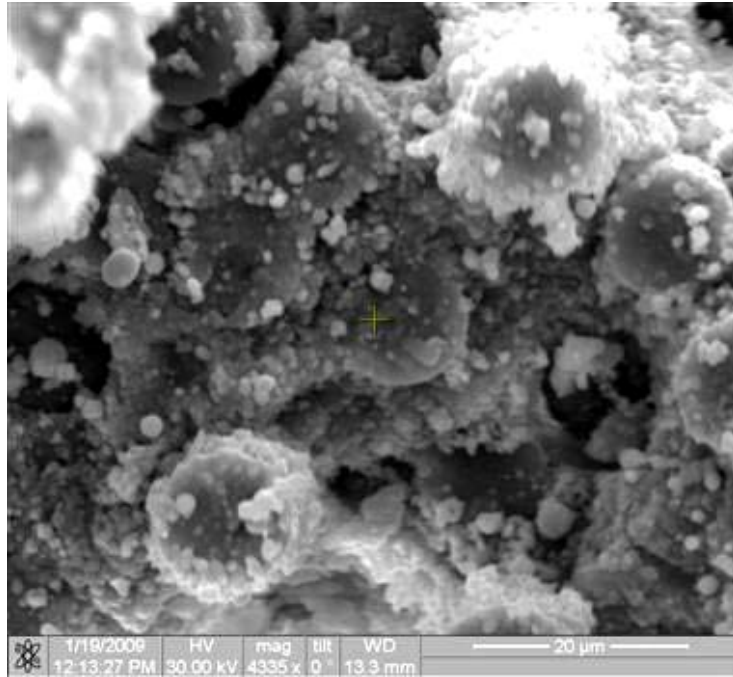


Figure 122. Fracture surface of the N720/AM specimen tested in tension to failure at 1100°C in laboratory air.

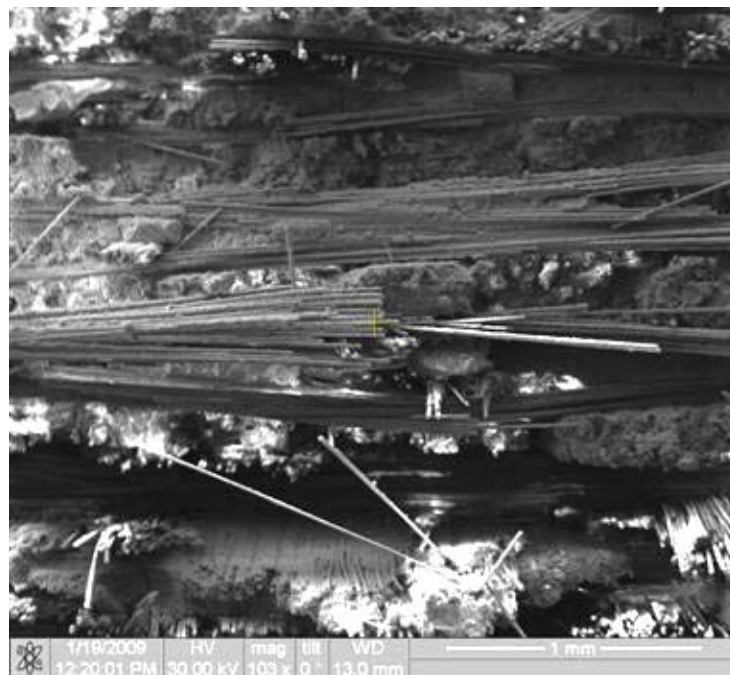


Figure 123. Fracture surface of the N720/AM specimen tested in tension to failure at 1100°C in laboratory air.

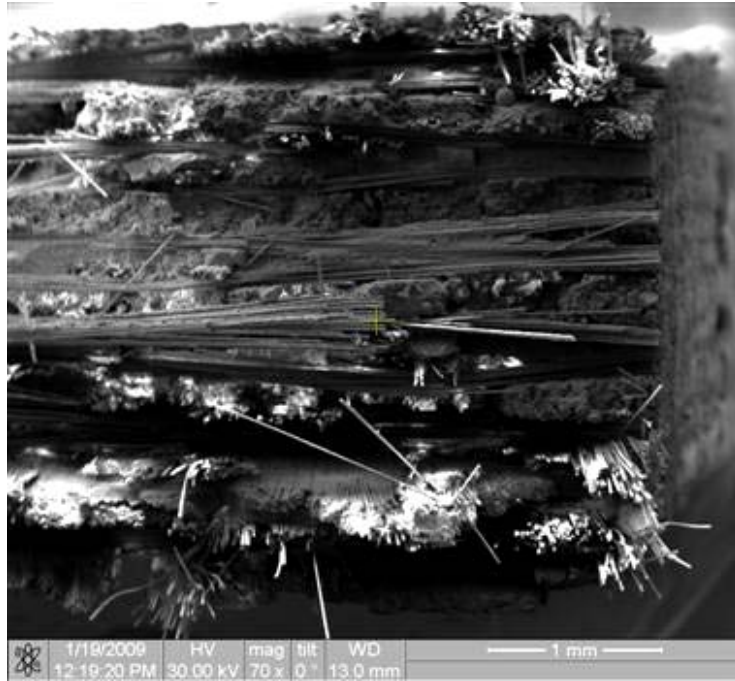


Figure 124. Fracture surface of the N720/AM specimen tested in tension to failure at 1100°C in laboratory air.

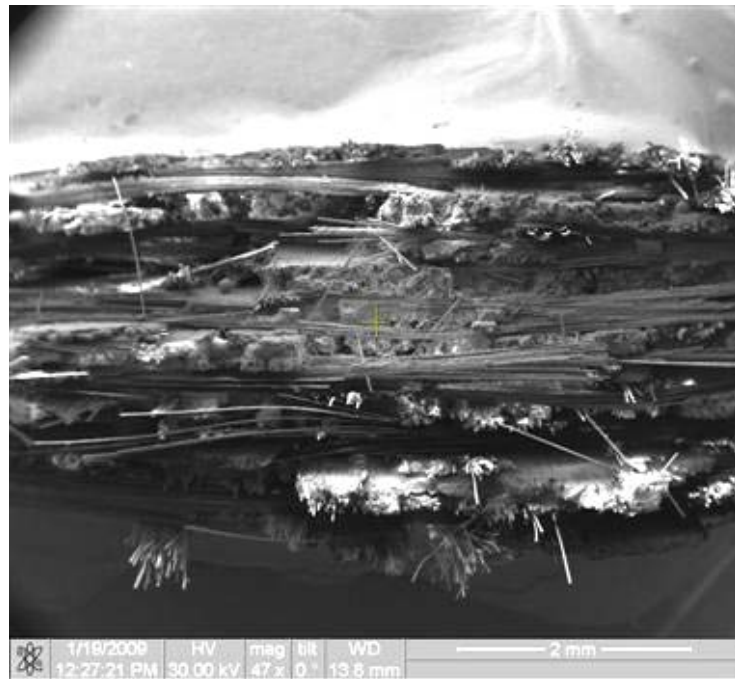


Figure 125. Fracture surface of the N720/AM specimen tested in tension to failure at 1100°C in laboratory air.

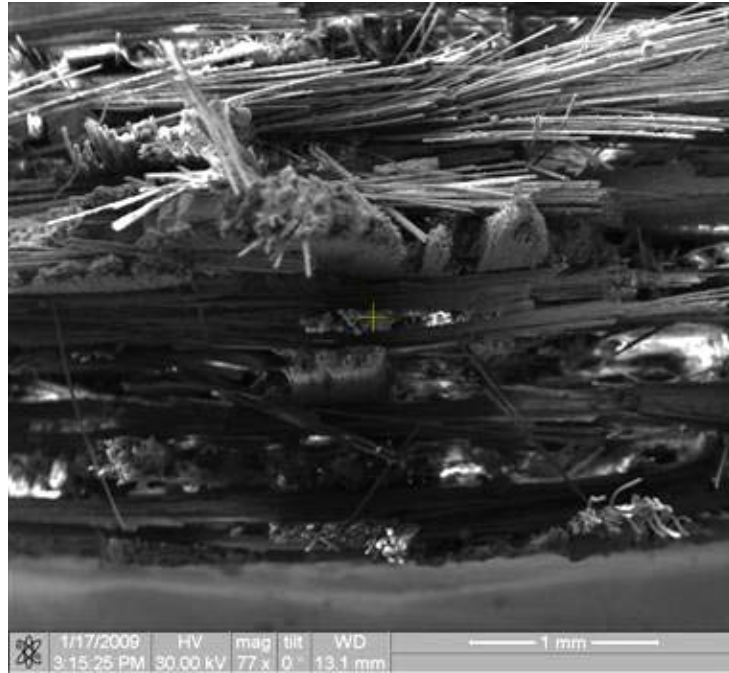


Figure 126. Fracture surface of the N720/AM specimen tested in tension to failure at 1000°C in laboratory air

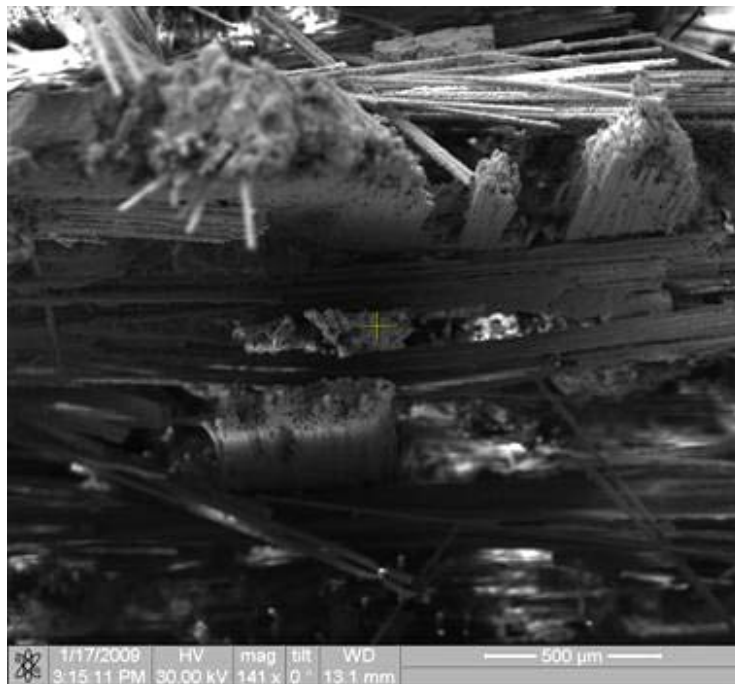


Figure 127. Fracture surface of the N720/AM specimen tested in tension to failure at 1000°C in laboratory air

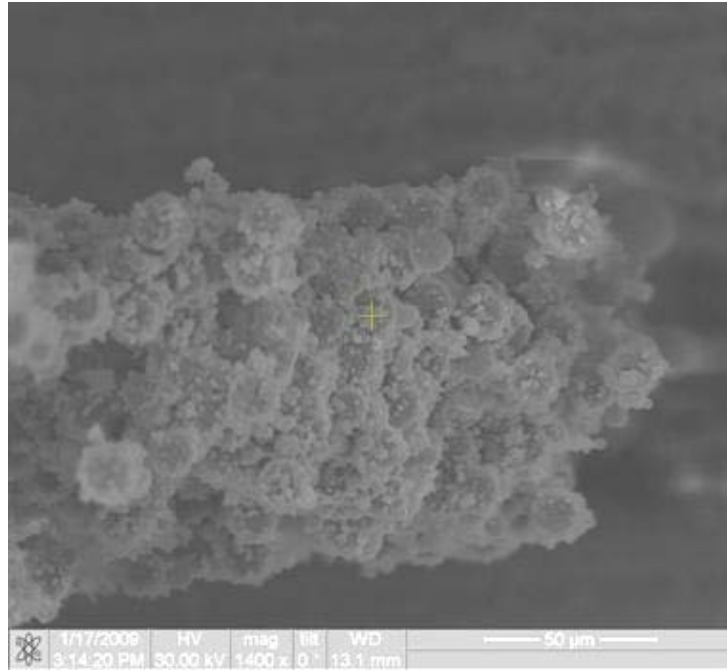


Figure 128. Fracture surface of the N720/AM specimen tested in tension to failure at 1000°C in laboratory air



Figure 129. Fracture surface of the N720/AM specimen tested in tension to failure at 1000°C in laboratory air



Figure 130. Fracture surface of the N720/AM specimen tested in tension to failure at 1000°C in laboratory air

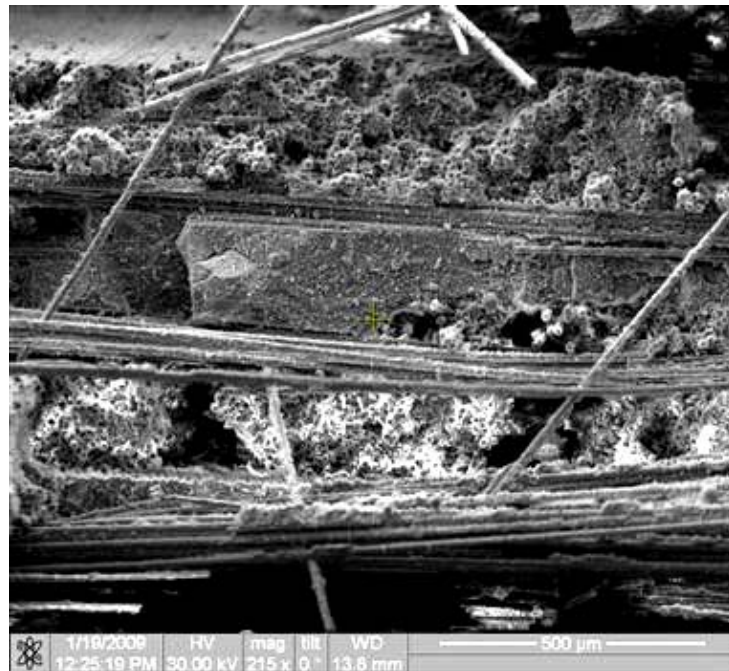


Figure 131. Fracture surface of the N720/AM specimen tested in tension to failure at 1000°C in laboratory air

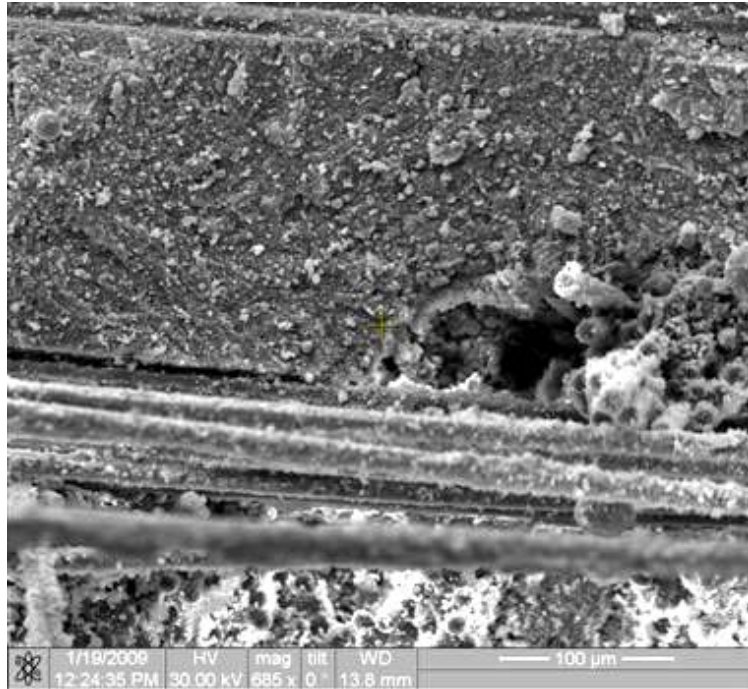


Figure 132. Fracture surface of the N720/AM specimen tested in tension to failure at 1000°C in laboratory air

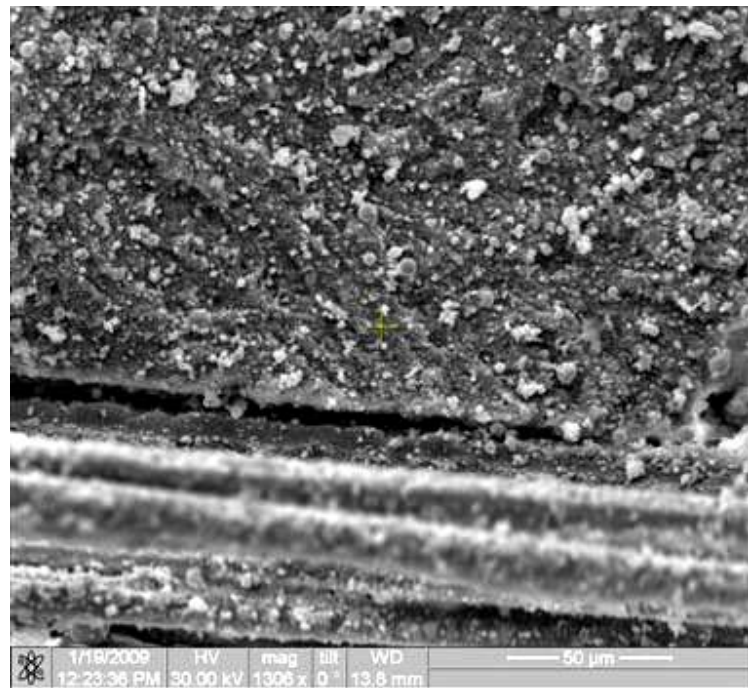


Figure 133. Fracture surface of the N720/AM specimen tested in tension to failure at 1000°C in laboratory air



Figure 134. Fracture surface of the N720/AM specimen tested in tension to failure at 1100°C in laboratory air



Figure 135. Fracture surface of the N720/AM specimen tested in tension to failure with constant loading rate of 25MPa at 1100°C in steam.



Figure 136. Fracture surface of the N720/AM specimen tested in tension to failure with constant loading rate of 25MPa at 1100°C in steam.



Figure 137. Fracture surface of the N720/AM specimen tested in tension to failure with constant loading rate of 25MPa at 1100°C in steam.

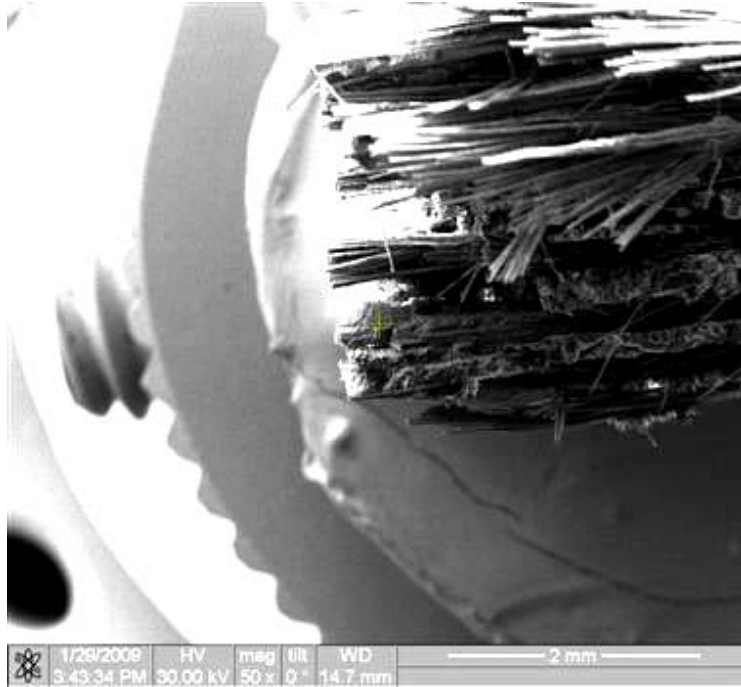


Figure 138. Fracture surface of the N720/AM specimen tested in tension to failure with constant loading rate of 25MPa at 1100°C in steam.

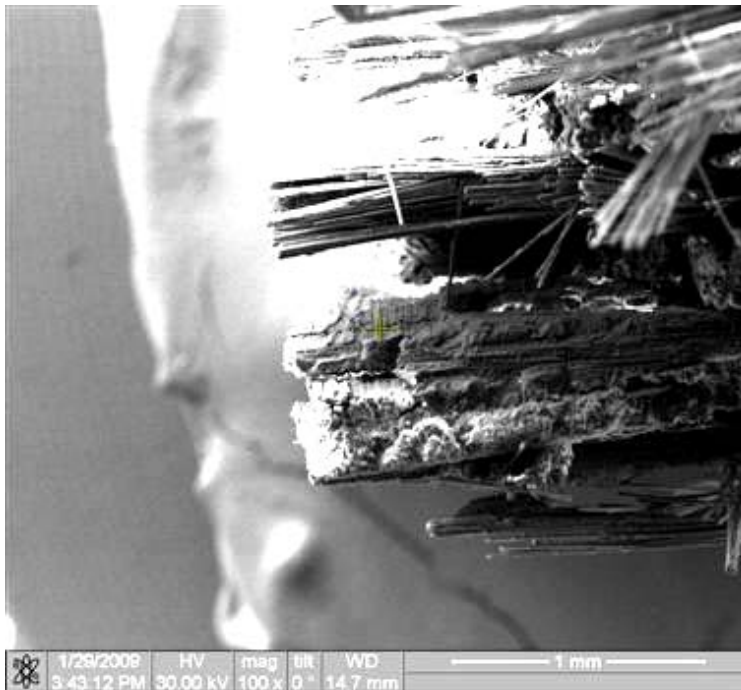


Figure 139. Fracture surface of the N720/AM specimen tested in tension to failure with constant loading rate of 25MPa at 1100°C in steam.

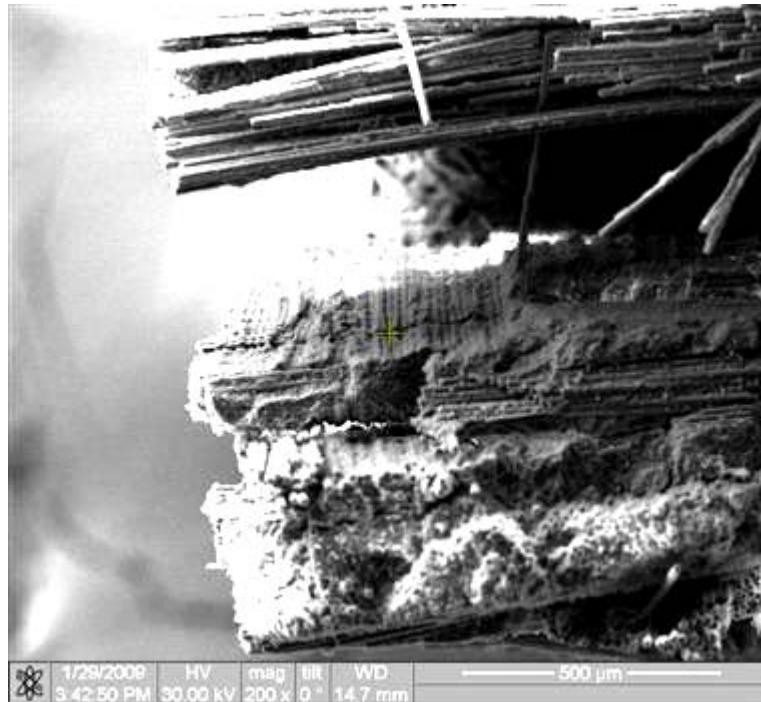


Figure 140. Fracture surface of the N720/AM specimen tested in tension to failure with constant loading rate of 25MPa at 1100°C in steam.

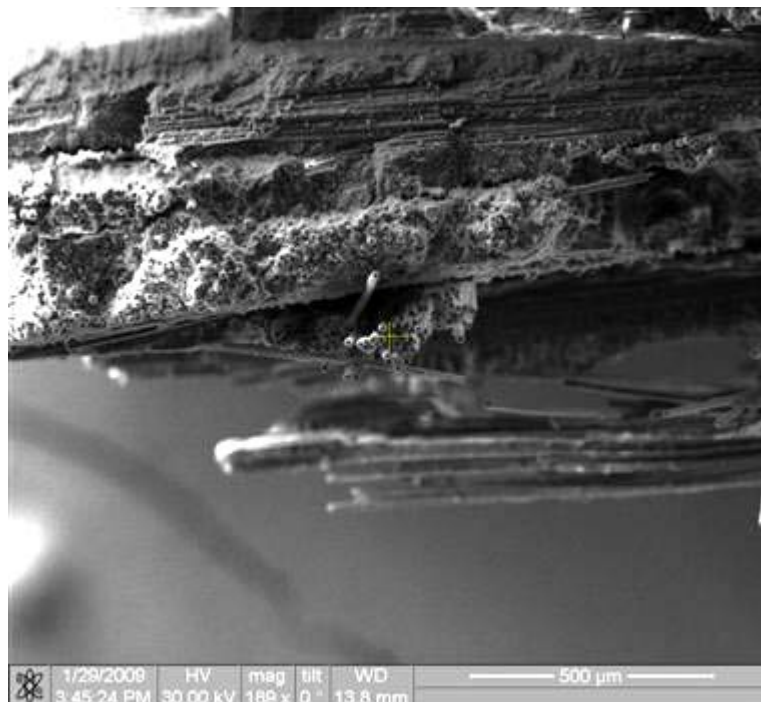


Figure 141. Fracture surface of the N720/AM specimen tested in tension to failure with constant loading rate of 25MPa at 1100°C in steam.



Figure 142. Fracture surface of the N720/AM specimen tested in tension to failure with constant loading rate of 25MPa at 1100°C in steam.



Figure 143. Fracture surface of the N720/AM specimen tested in tension to failure with constant loading rate of 25MPa at 1100°C in steam.

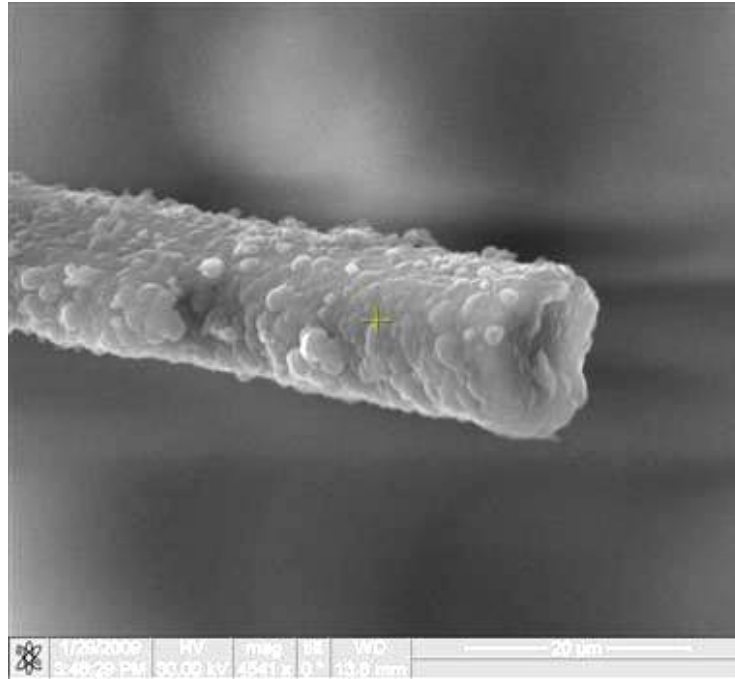


Figure 144. Fracture surface of the N720/AM specimen tested in tension to failure with constant loading rate of 25MPa at 1100°C in steam.

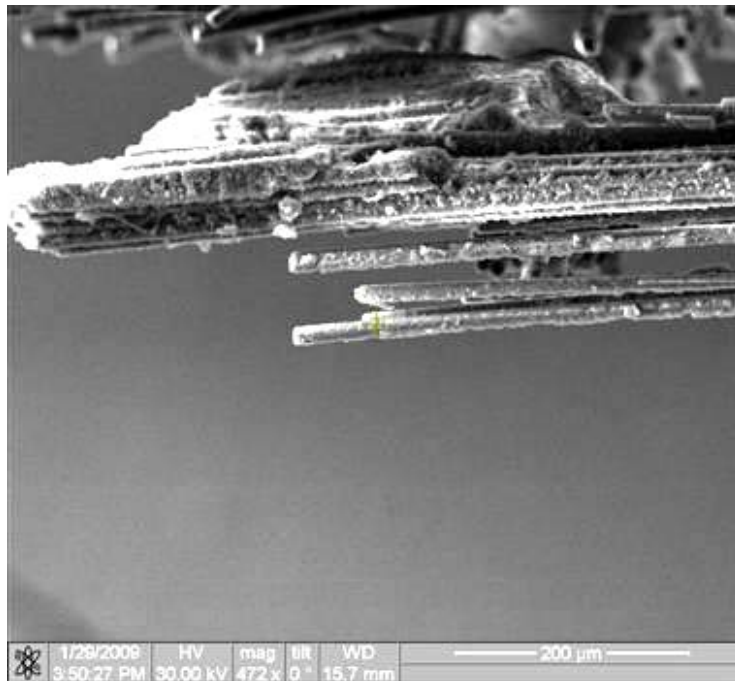


Figure 145. Fracture surface of the N720/AM specimen tested in tension to failure with constant loading rate of 25MPa at 1100°C in steam.

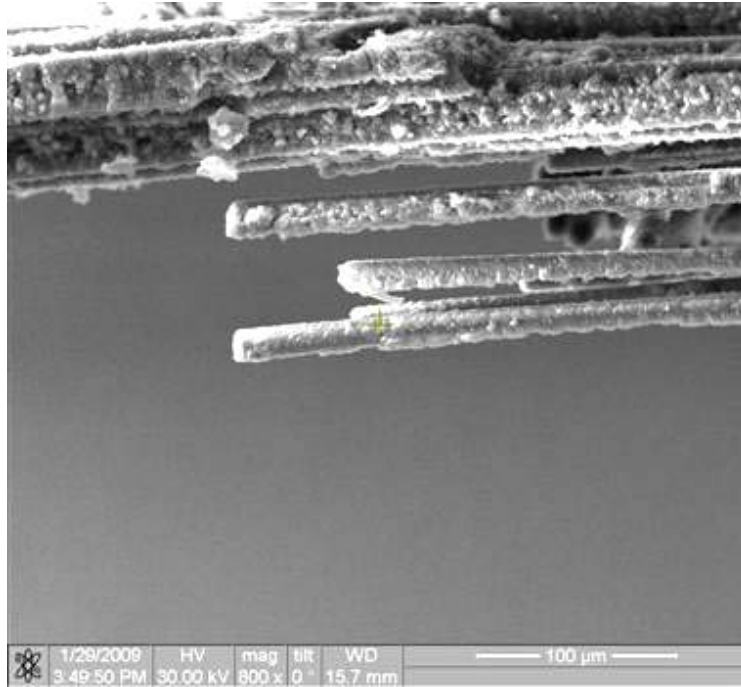


Figure 146. Fracture surface of the N720/AM specimen tested in tension to failure with constant loading rate of 25MPa at 1100°C in steam.

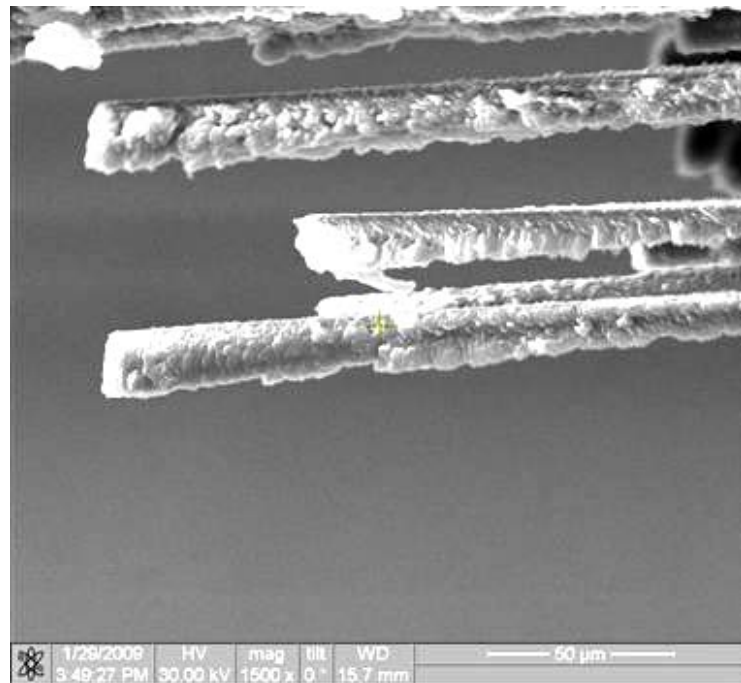


Figure 147. Fracture surface of the N720/AM specimen tested in tension to failure with constant loading rate of 25MPa at 1100°C in steam.

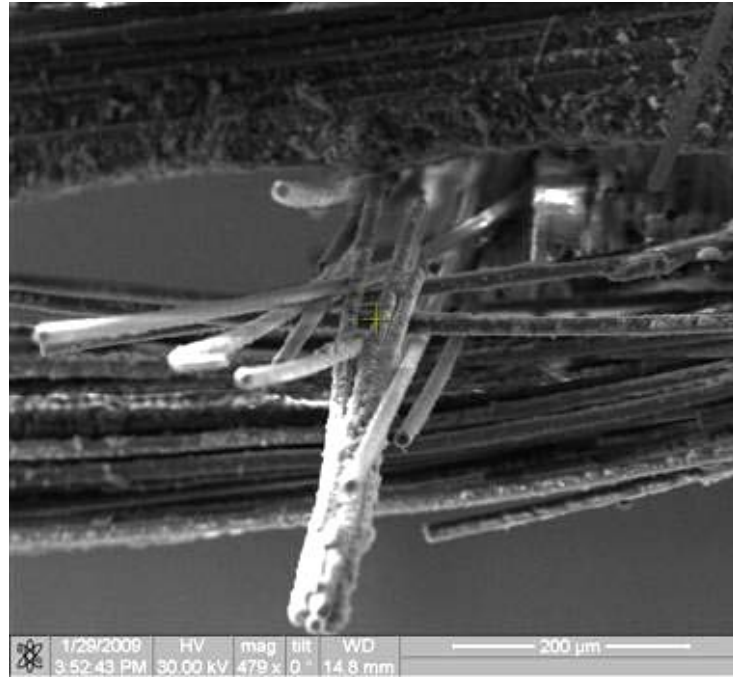


Figure 148. Fracture surface of the N720/AM specimen tested in tension to failure with constant loading rate of 25MPa at 1100°C in steam.

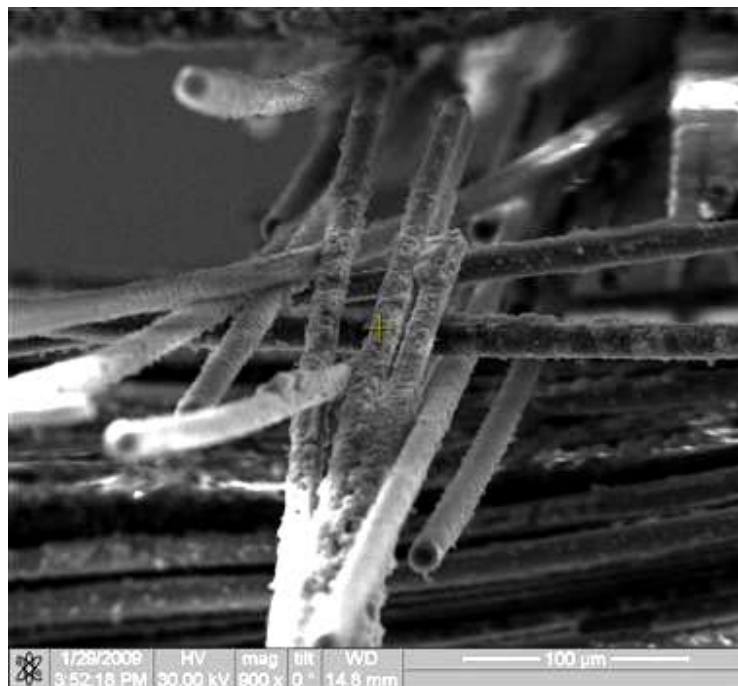


Figure 149. Fracture surface of the N720/AM specimen tested in tension to failure with constant loading rate of 25MPa at 1100°C in steam.

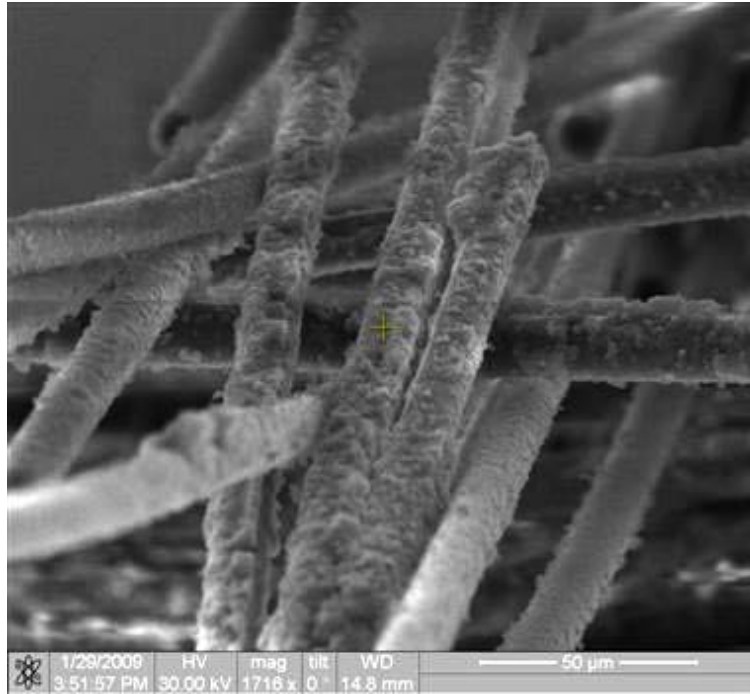


Figure 150. Fracture surface of the N720/AM specimen tested in tension to failure with constant loading rate of 25MPa at 1100°C in steam.

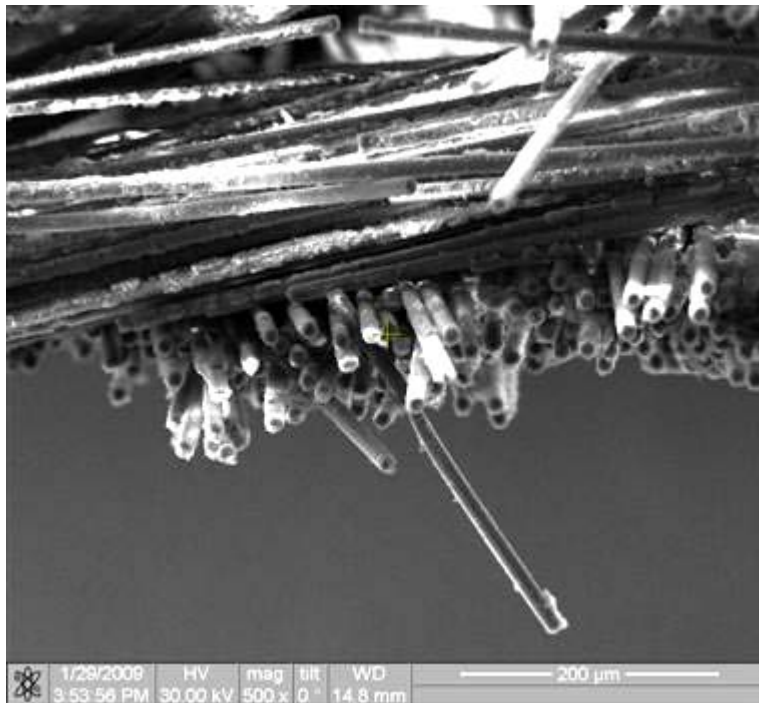


Figure 151. Fracture surface of the N720/AM specimen tested in tension to failure with constant loading rate of 25MPa at 1100°C in steam.

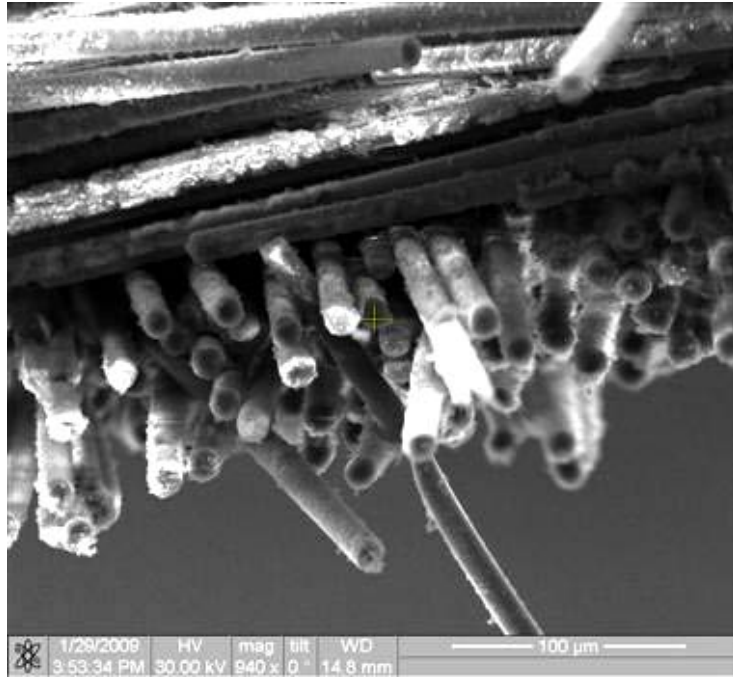


Figure 152. Fracture surface of the N720/AM specimen tested in tension to failure with constant loading rate of 25MPa at 1100°C in steam.

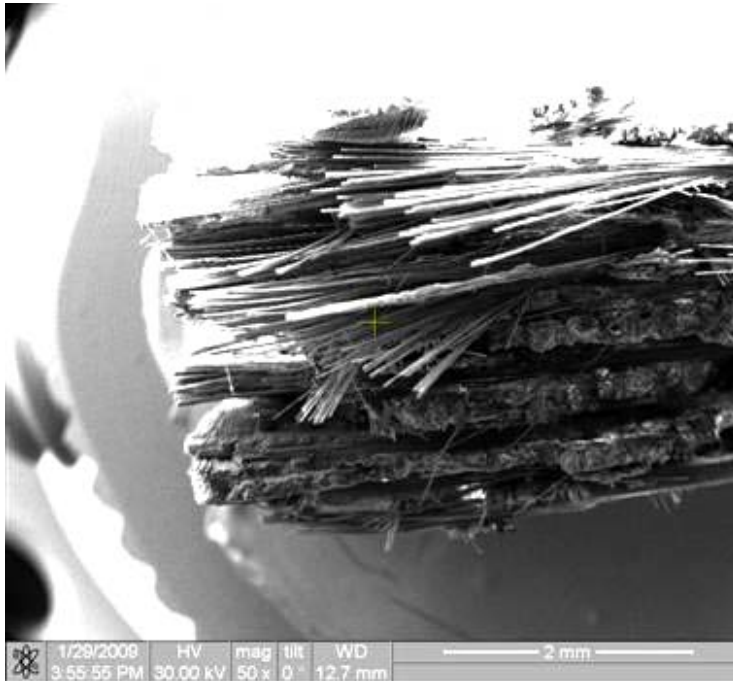


Figure 153. Fracture surface of the N720/AM specimen tested in tension to failure with constant loading rate of 25MPa at 1100°C in steam.



Figure 154. Fracture surface of the N720/AM specimen tested in tension to failure with constant loading rate of 25MPa at 1100°C in steam.

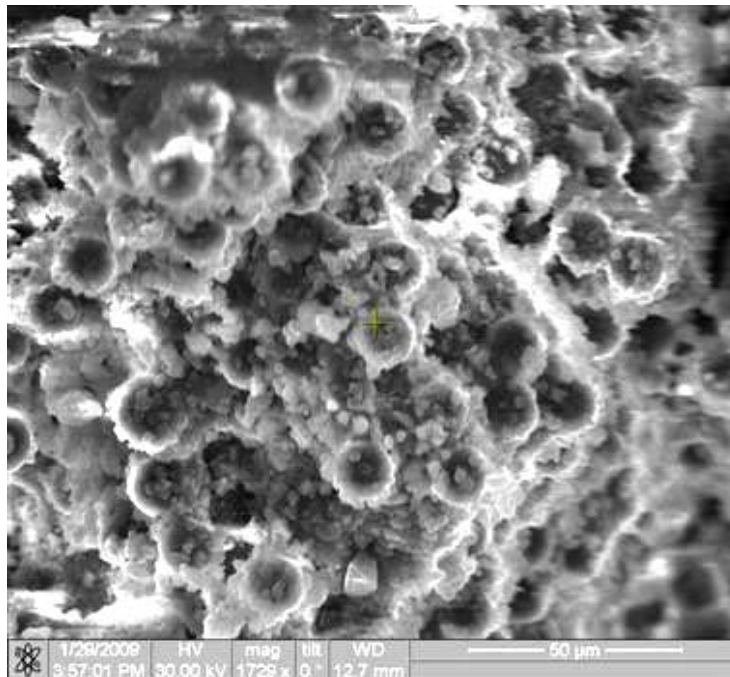


Figure 155. Fracture surface of the N720/AM specimen tested in tension to failure with constant loading rate of 25MPa at 1100°C in steam.

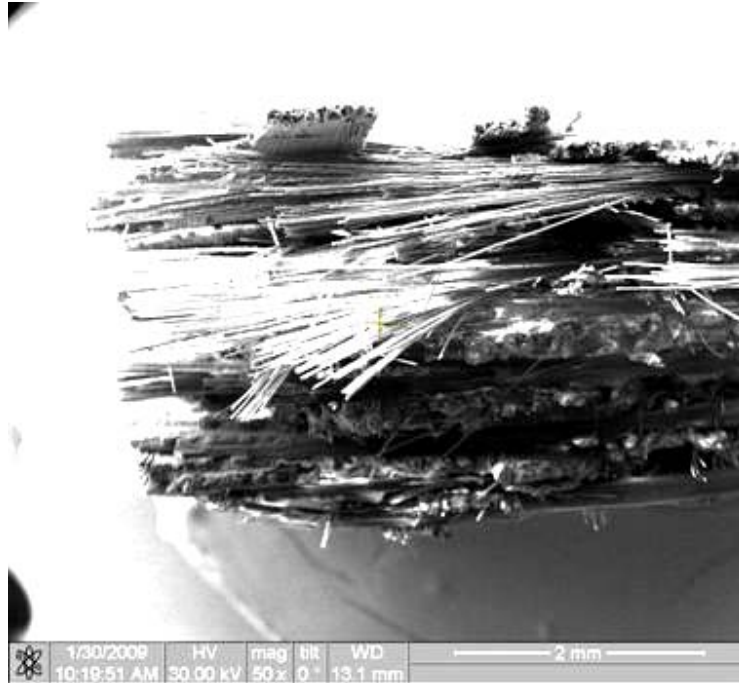


Figure 156. Fracture surface of the N720/AM specimen tested in tension to failure with constant loading rate of 25MPa at 1100°C in steam.

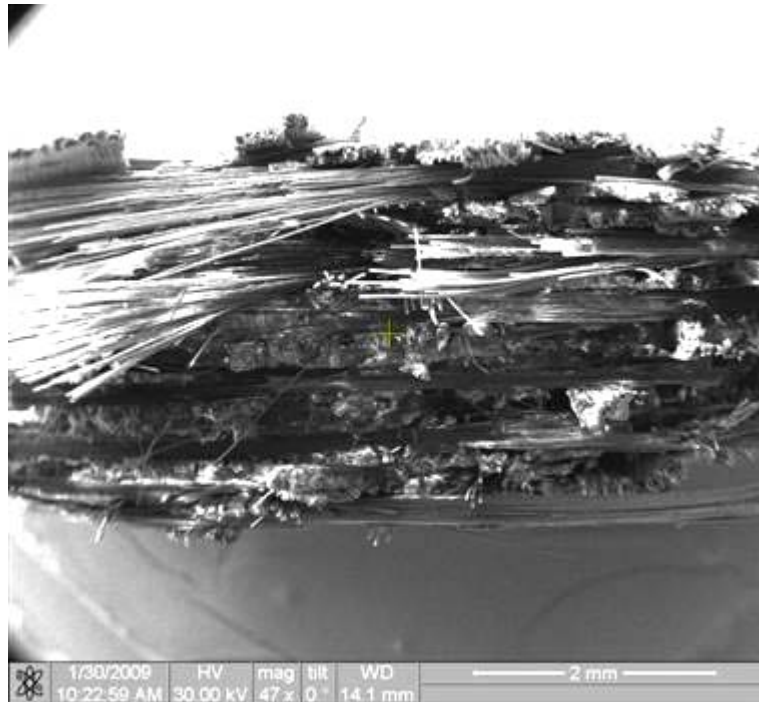


Figure 157. Fracture surface of the N720/AM specimen tested in tension to failure with constant loading rate of 25MPa at 1100°C in steam.



Figure 158. Fracture surface of the N720/AM specimen tested in tension to failure with constant loading rate of 25MPa at 1100°C in steam.

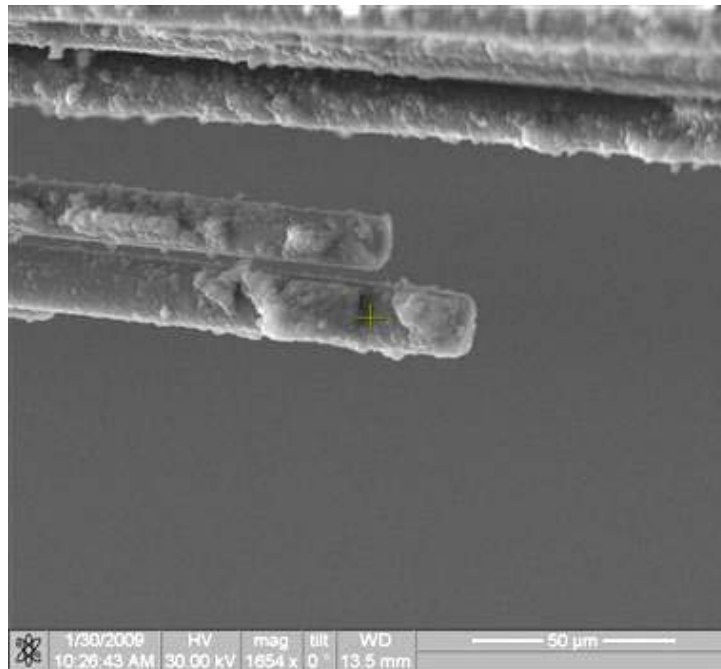


Figure 159. Fracture surface of the N720/AM specimen tested in tension to failure with constant loading rate of 25MPa at 1100°C in steam.

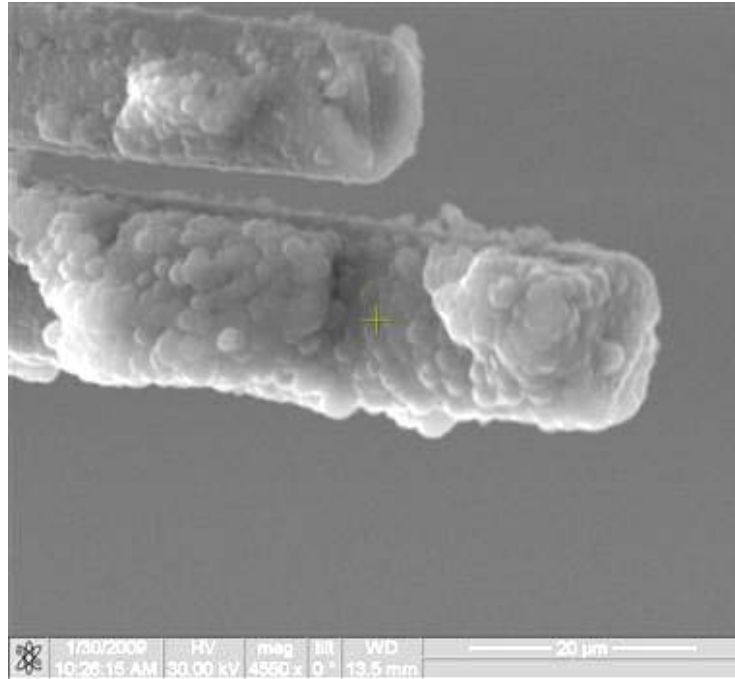


Figure 160. Fracture surface of the N720/AM specimen tested in tension to failure with constant loading rate of 25MPa at 1100°C in steam.

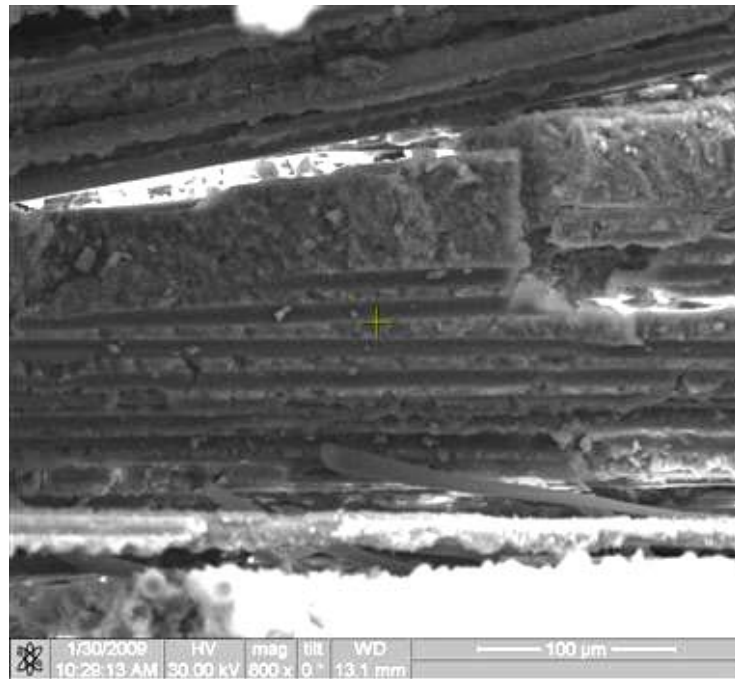


Figure 161. Fracture surface of the N720/AM specimen tested in tension to failure with constant loading rate of 25MPa at 1100°C in steam.



Figure 162. Fracture surface of the N720/AM specimen tested in tension to failure with constant loading rate of 25MPa at 1100°C in steam.

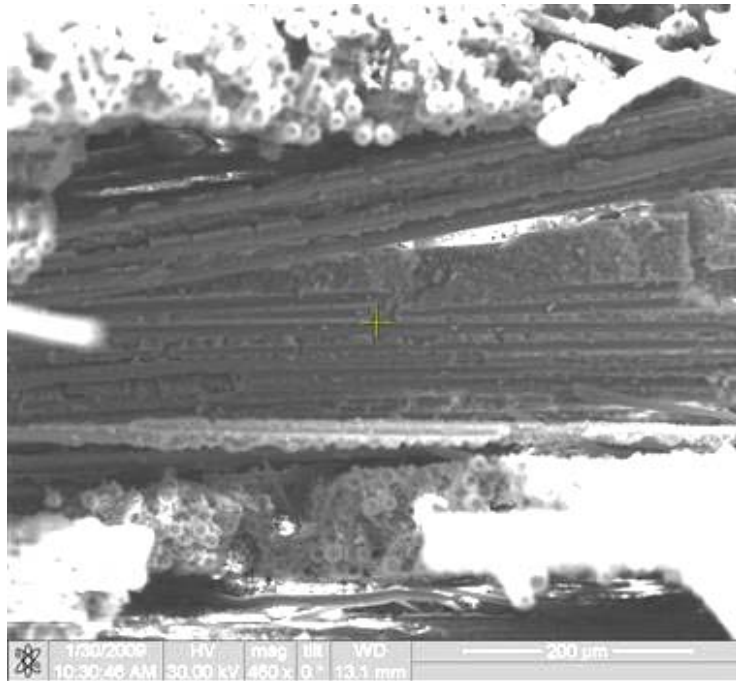


Figure 163. Fracture surface of the N720/AM specimen tested in tension to failure with constant loading rate of 25MPa at 1100°C in steam.

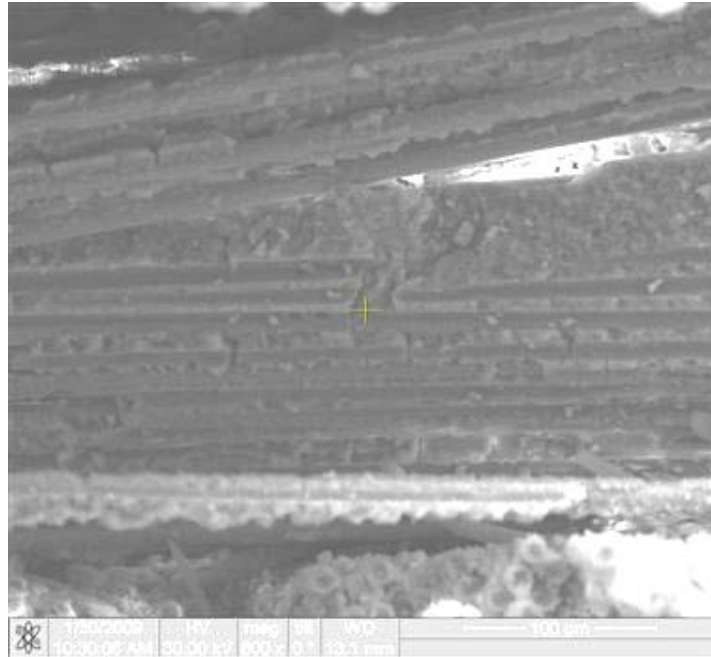


Figure 164. Fracture surface of the N720/AM specimen tested in tension to failure with constant loading rate of 25MPa at 1100°C in steam.

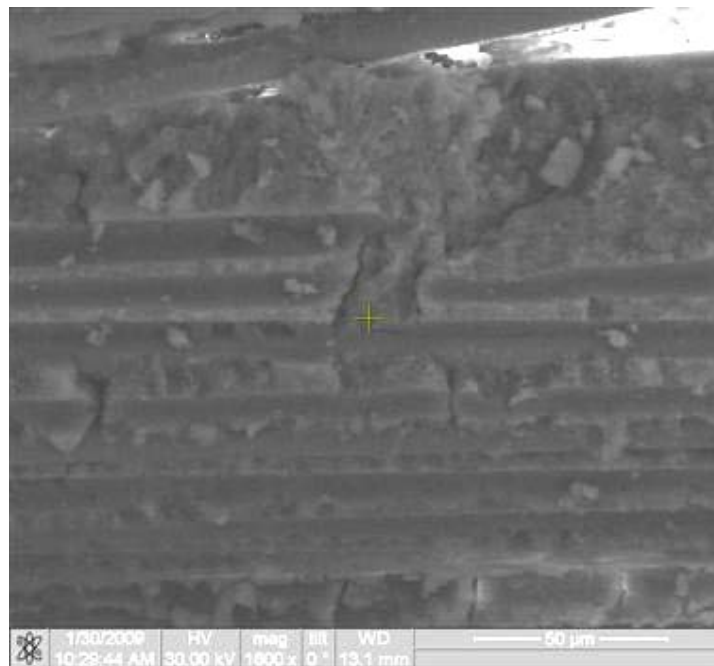


Figure 165. Fracture surface of the N720/AM specimen tested in tension to failure with constant loading rate of 25MPa at 1100°C in steam.

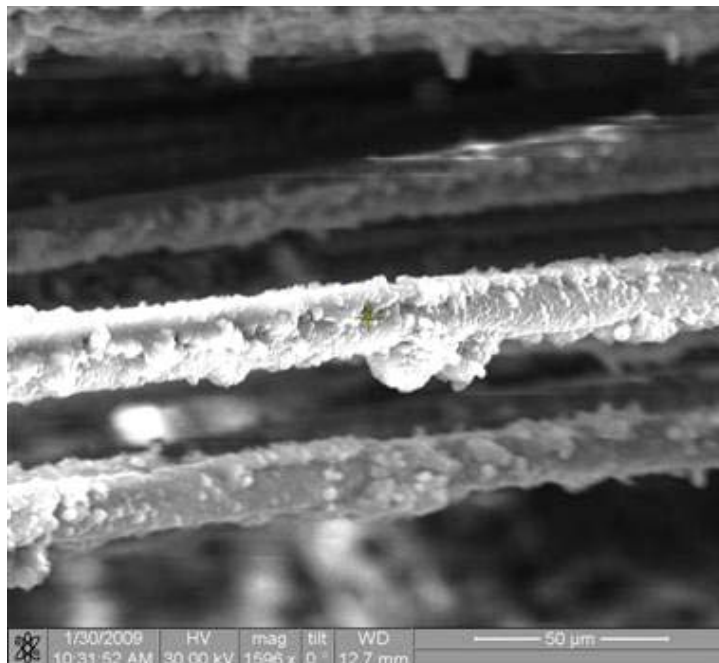


Figure 166. Fracture surface of the N720/AM specimen tested in tension to failure with constant loading rate of 25MPa at 1100°C in steam.

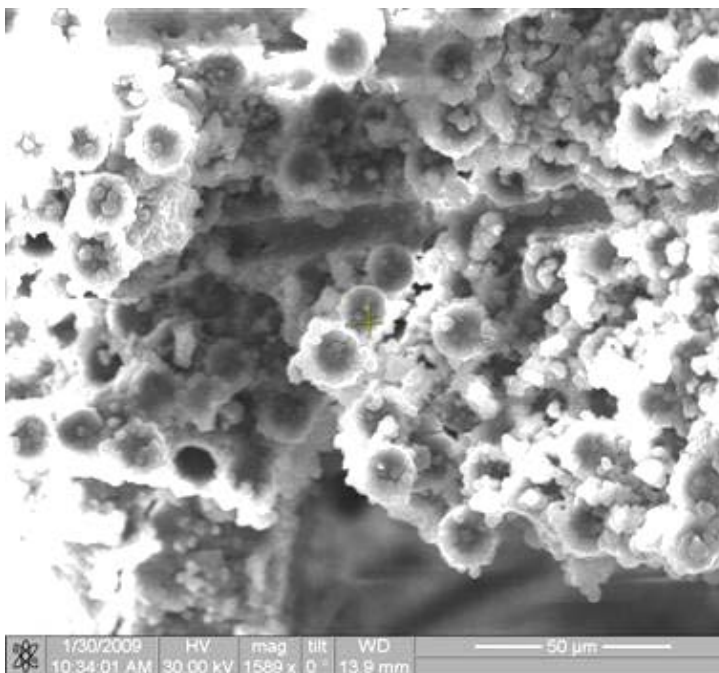


Figure 167. Fracture surface of the N720/AM specimen tested in tension to failure with constant loading rate of 25MPa at 1100°C in steam.

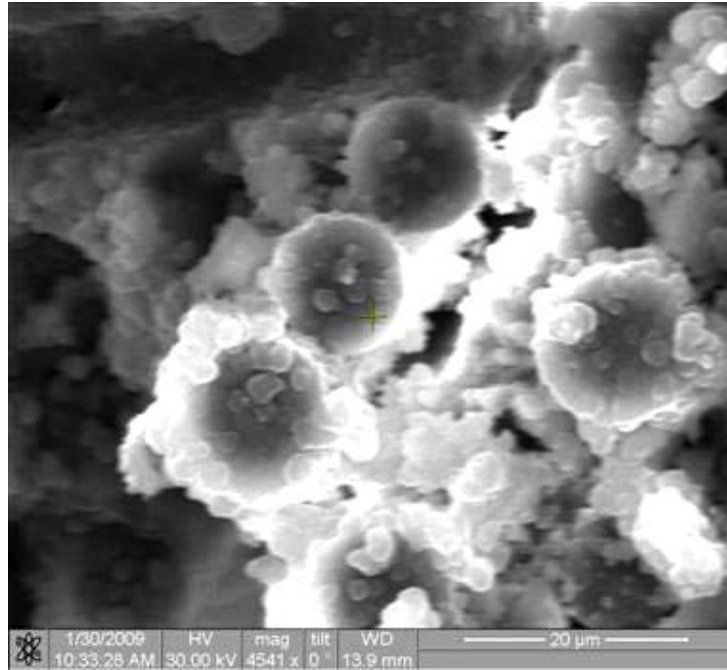


Figure 168. Fracture surface of the N720/AM specimen tested in tension to failure with constant loading rate of 25MPa at 1100°C in steam.

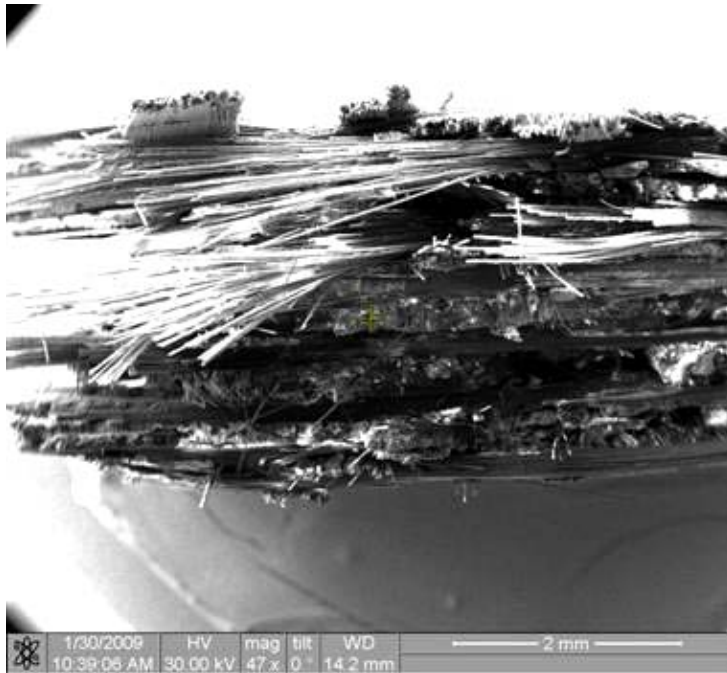


Figure 169. Fracture surface of the N720/AM specimen tested in tension to failure with constant loading rate of 25MPa at 1100°C in steam.

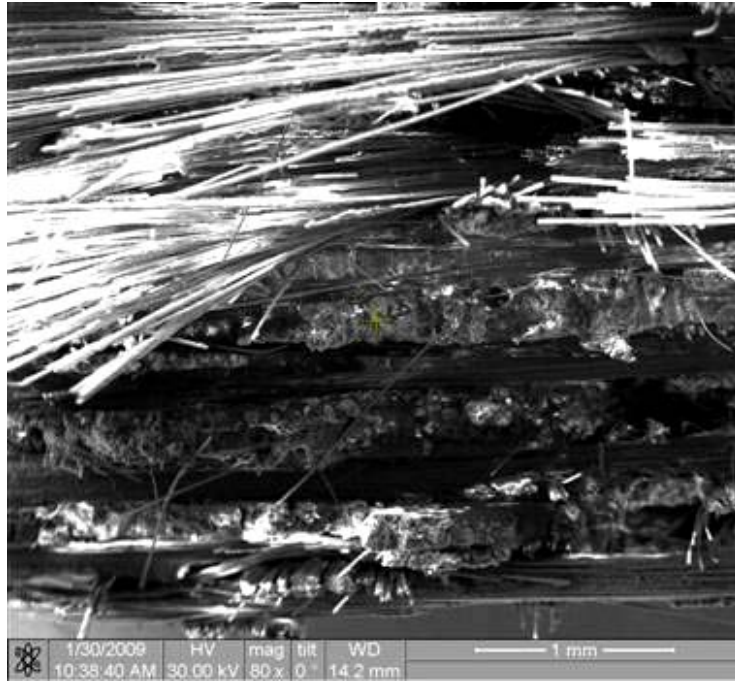


Figure 170. Fracture surface of the N720/AM specimen tested in tension to failure with constant loading rate of 25MPa at 1100°C in steam.

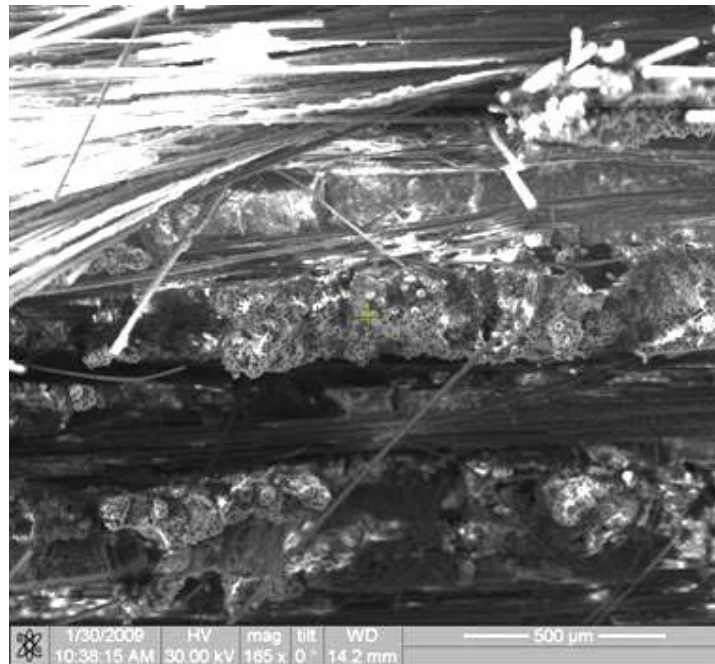


Figure 171. Fracture surface of the N720/AM specimen tested in tension to failure with constant loading rate of 25MPa at 1100°C in steam.

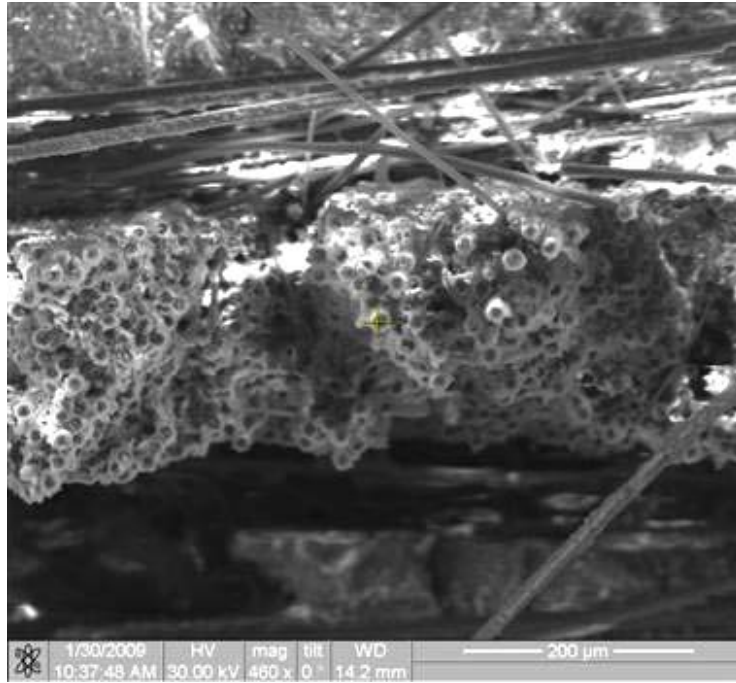


Figure 172. Fracture surface of the N720/AM specimen tested in tension to failure with constant loading rate of 25MPa at 1100°C in steam.

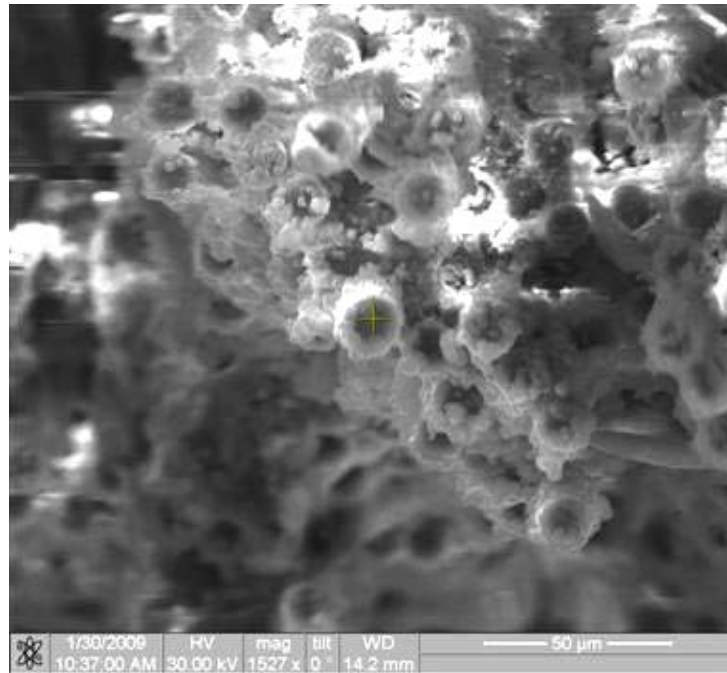


Figure 173. Fracture surface of the N720/AM specimen tested in tension to failure with constant loading rate of 25MPa at 1100°C in steam.

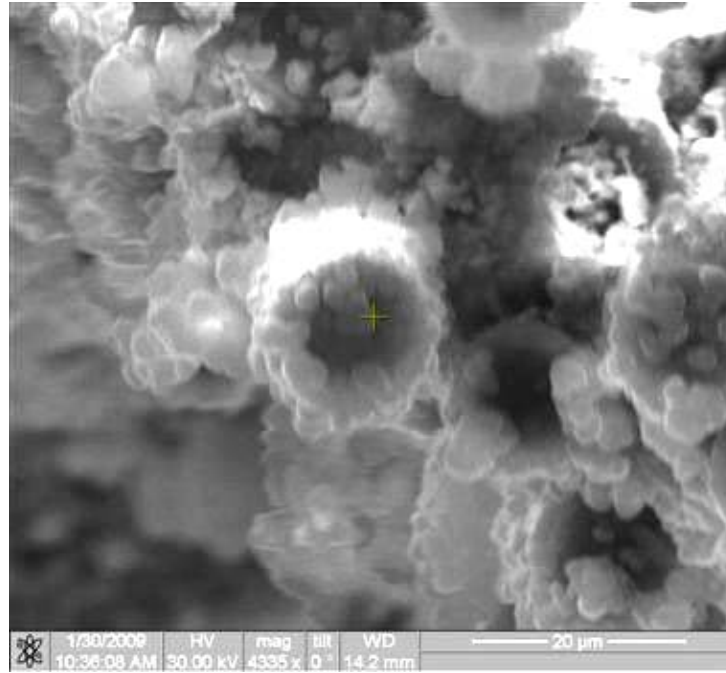


Figure 174. Fracture surface of the N720/AM specimen tested in tension to failure with constant loading rate of 25MPa at 1100°C in steam.

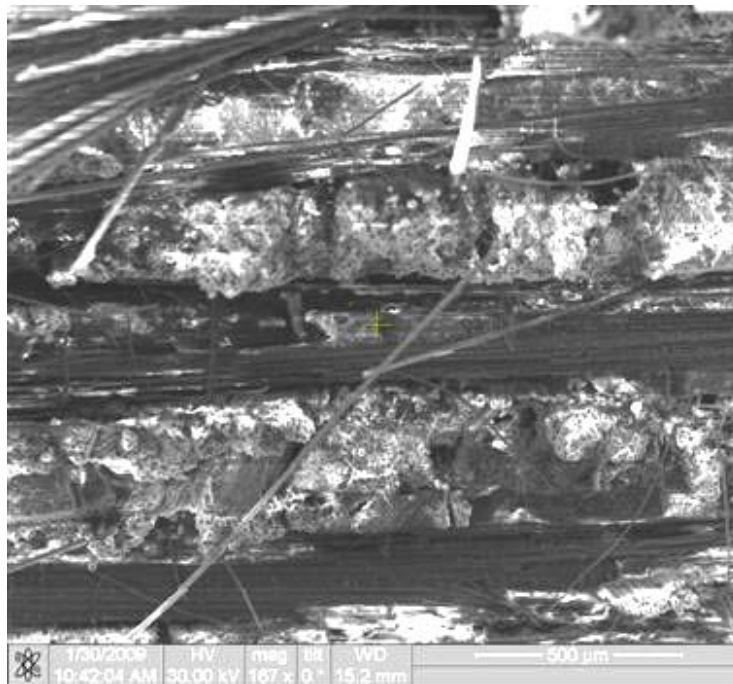


Figure 175. Fracture surface of the N720/AM specimen tested in tension to failure with constant loading rate of 25MPa at 1100°C in steam.

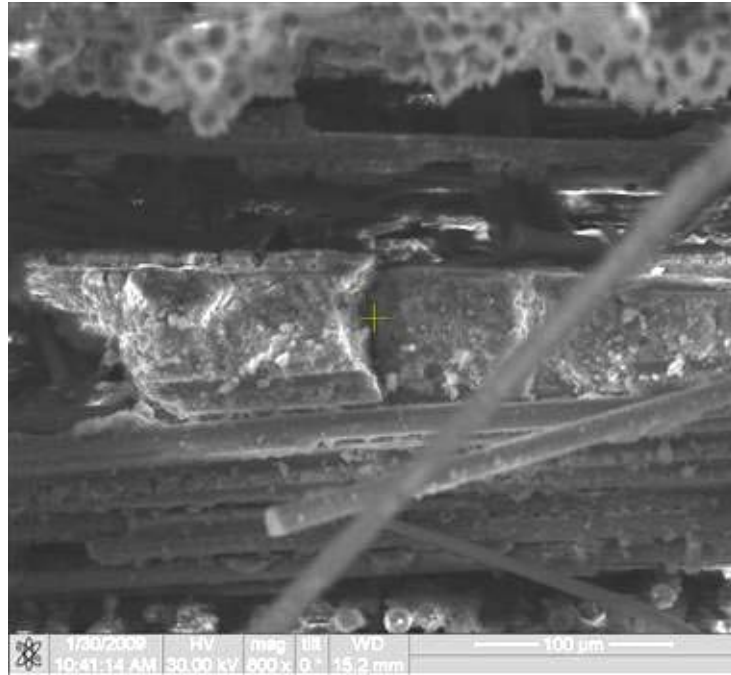


Figure 176. Fracture surface of the N720/AM specimen tested in tension to failure with constant loading rate of 25MPa at 1100°C in steam.

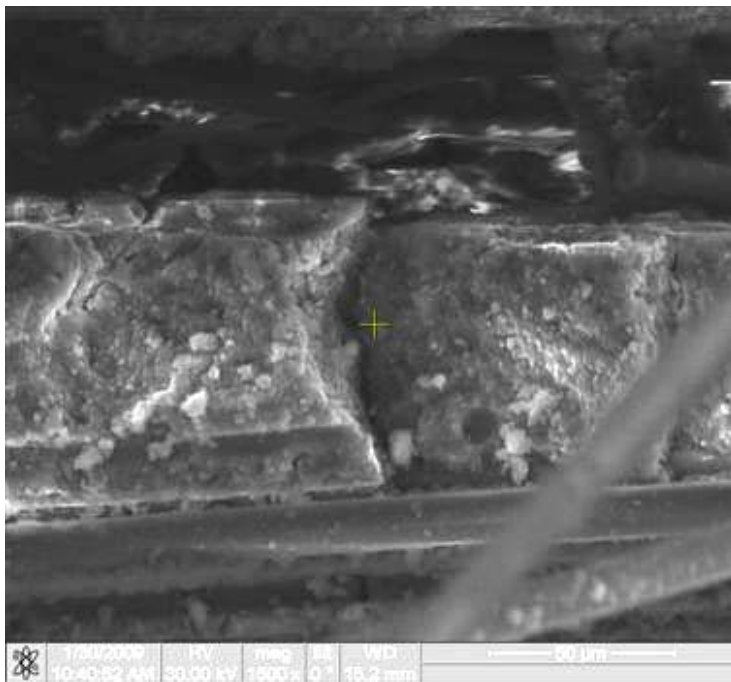


Figure 177. Fracture surface of the N720/AM specimen tested in tension to failure with constant loading rate of 25MPa at 1100°C in steam.

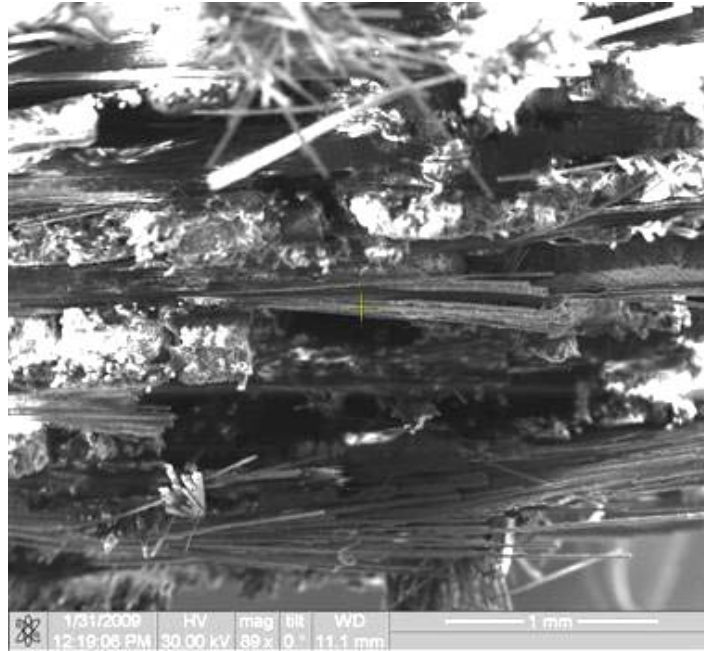


Figure 178. Fracture surface of the N720/AM specimen tested in tension to failure with constant loading rate of 25MPa at 1100°C in steam.

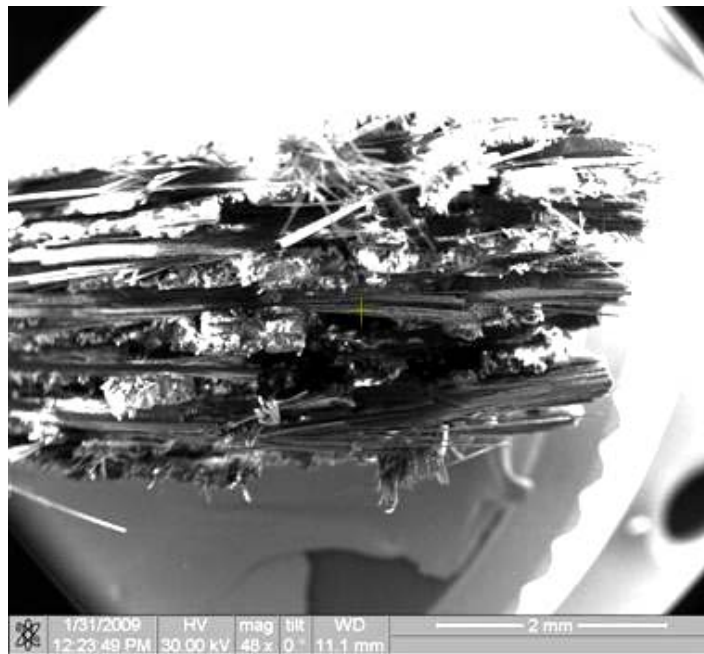


Figure 179. Fracture surface of the N720/AM specimen tested in tension to failure with constant loading rate of 25MPa at 1100°C in steam.

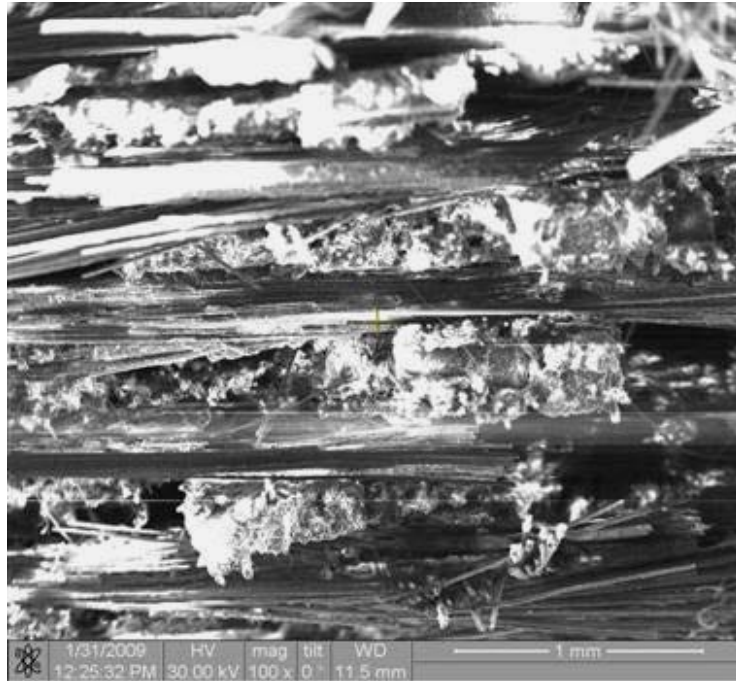


Figure 180. Fracture surface of the N720/AM specimen tested in tension to failure with constant loading rate of 25MPa at 1100°C in steam.

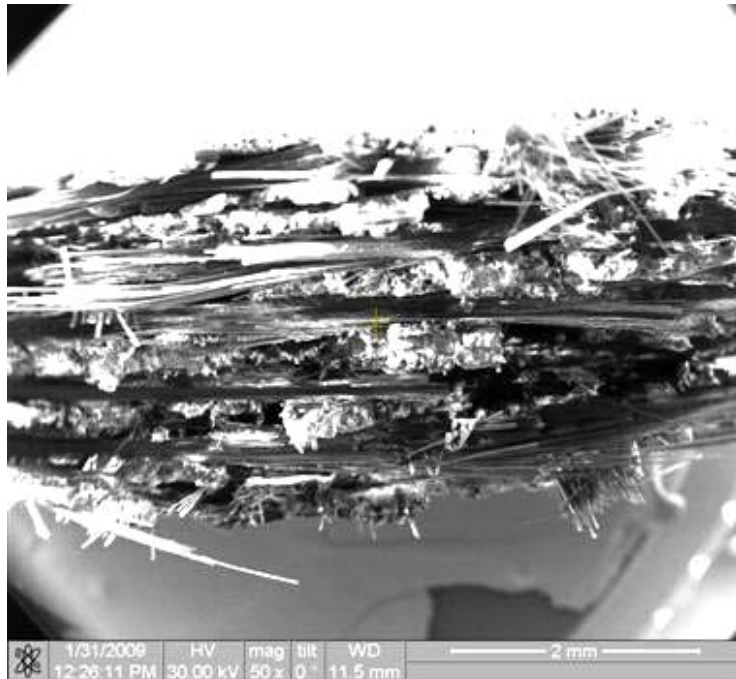


Figure 181. Fracture surface of the N720/AM specimen tested in tension to failure with constant loading rate of 25MPa at 1100°C in steam.

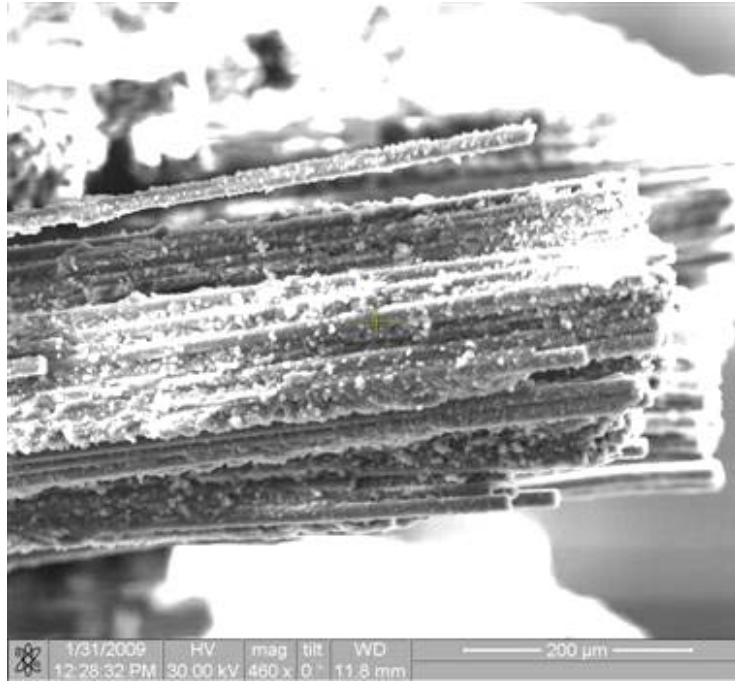


Figure 182. Fracture surface of the N720/AM specimen tested in tension to failure with constant loading rate of 25MPa at 1100°C in steam.

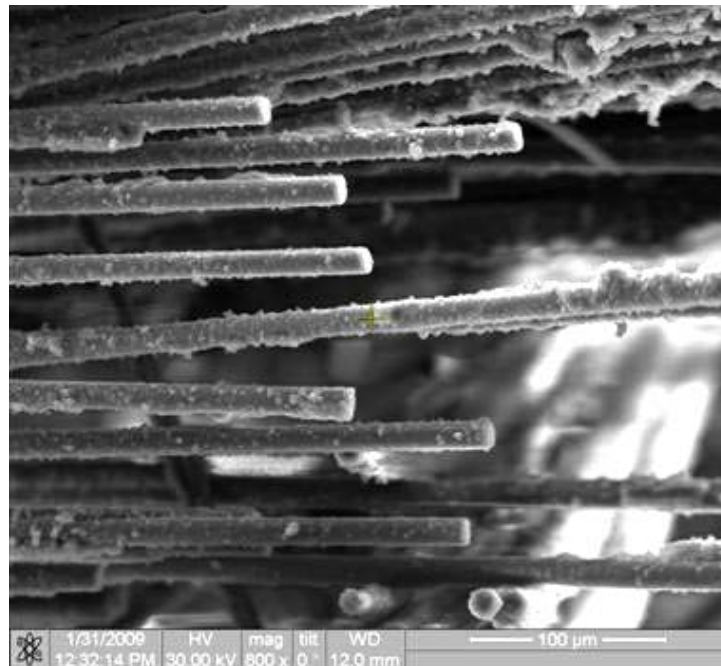


Figure 183. Fracture surface of the N720/AM specimen tested in tension to failure with constant loading rate of 25MPa at 1100°C in steam.

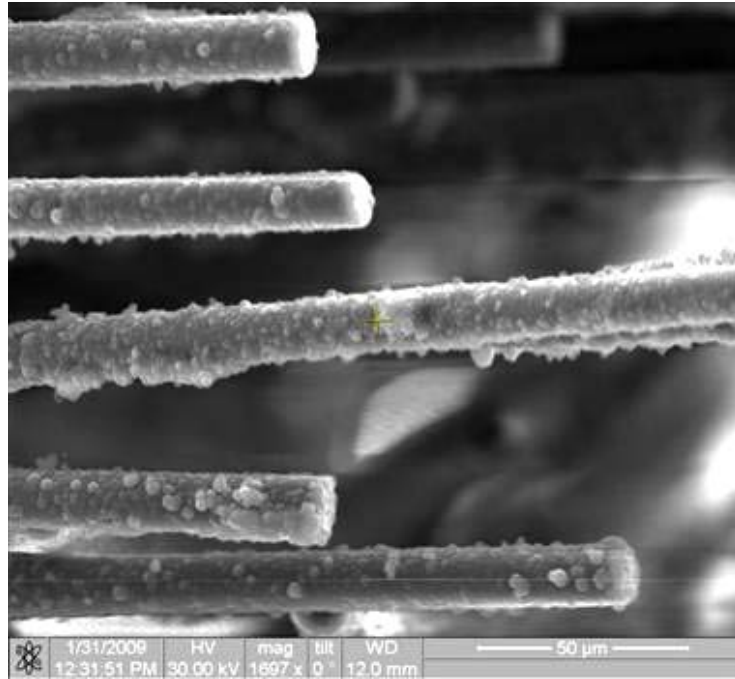


Figure 184. Fracture surface of the N720/AM specimen tested in tension to failure with constant loading rate of 25MPa at 1100°C in steam.

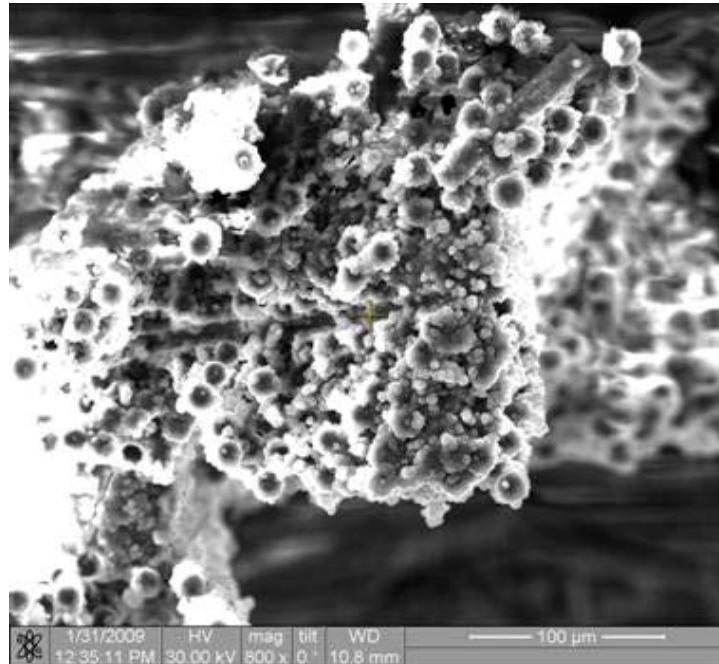


Figure 185. Fracture surface of the N720/AM specimen tested in tension to failure with constant loading rate of 25MPa at 1100°C in steam.

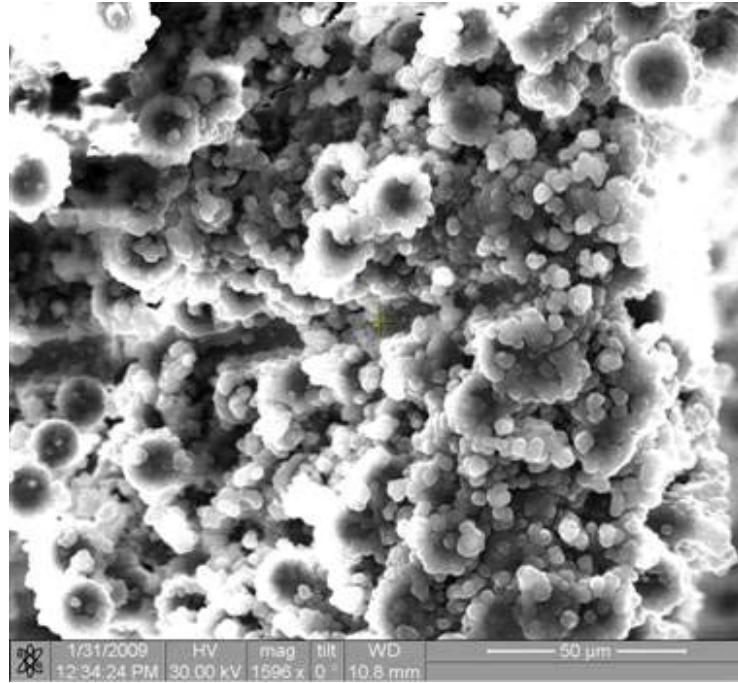


Figure 186. Fracture surface of the N720/AM specimen tested in tension to failure with constant loading rate of 25MPa at 1100°C in steam.

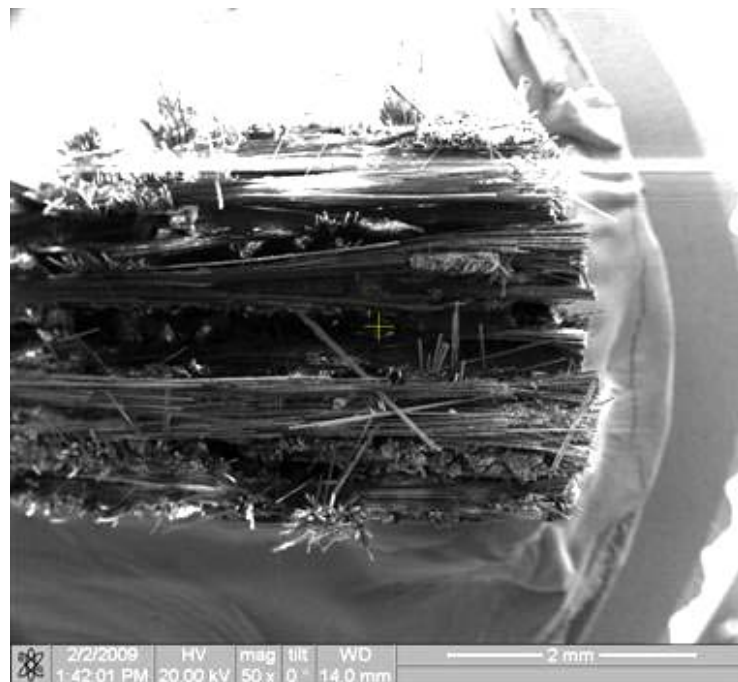


Figure 187. Fracture surface of the N720/AM specimen tested in tension to failure with constant loading rate of 0.0025MPa at 1100°C in steam.

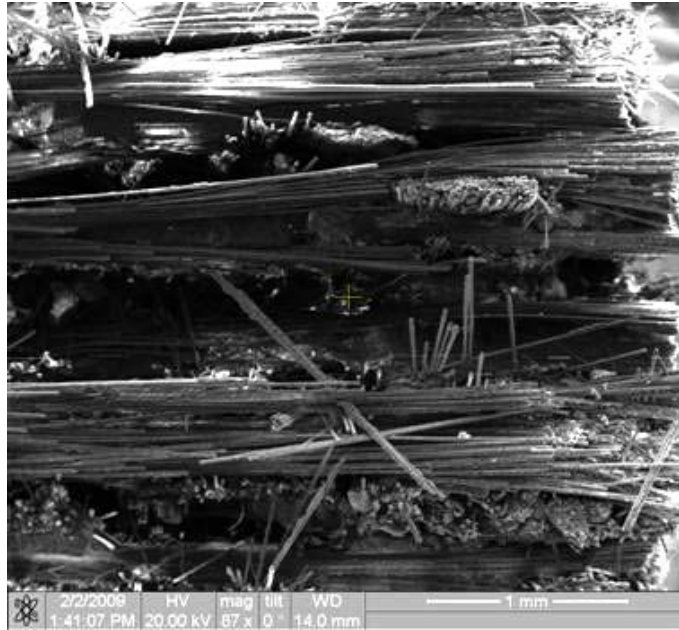


Figure 188. Fracture surface of the N720/AM specimen tested in tension to failure with constant loading rate of 0.0025MPa at 1100°C in steam.

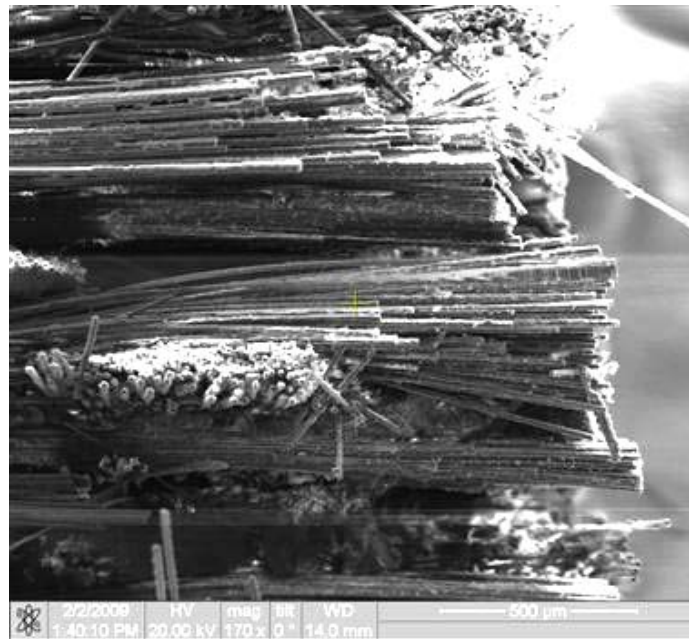


Figure 189 Fracture surface of the N720/AM specimen tested in tension to failure with constant loading rate of 0.0025MPa at 1100°C in steam.

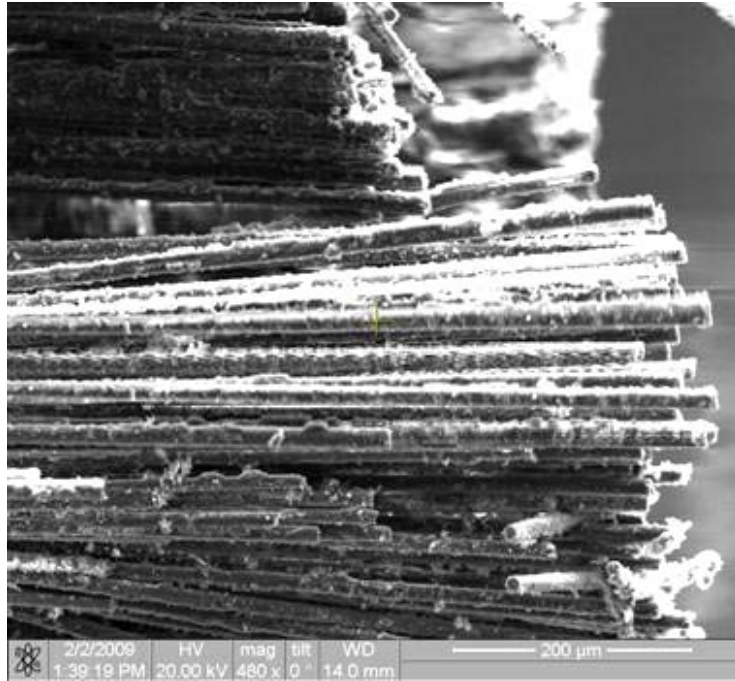


Figure 190 Fracture surface of the N720/AM specimen tested in tension to failure with constant loading rate of 0.0025MPa at 1100°C in steam.

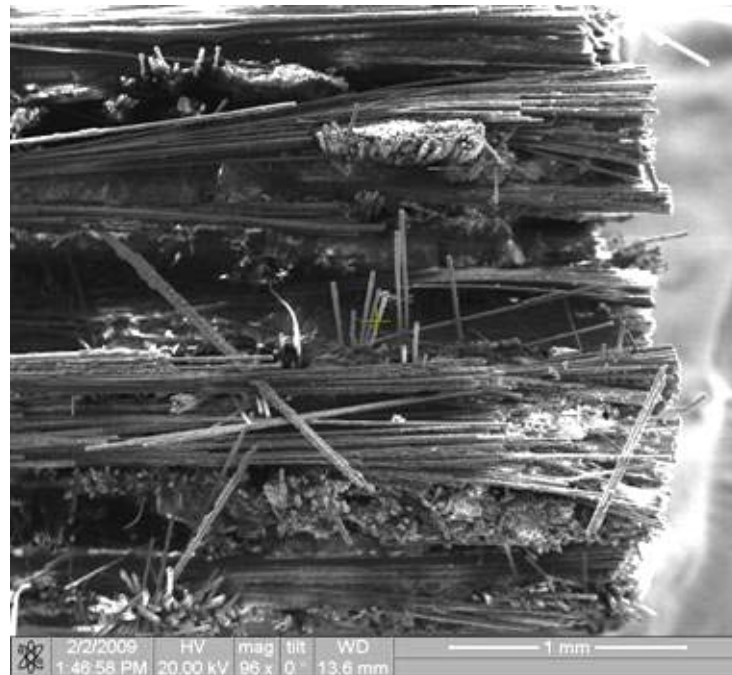


Figure 191 Fracture surface of the N720/AM specimen tested in tension to failure with constant loading rate of 0.0025MPa at 1100°C in steam.

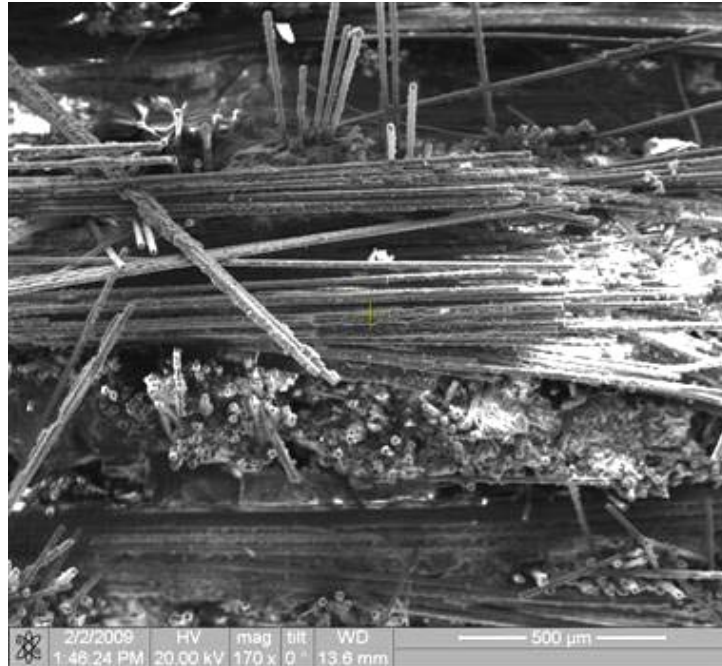


Figure 192 Fracture surface of the N720/AM specimen tested in tension to failure with constant loading rate of 0.0025MPa at 1100°C in steam.

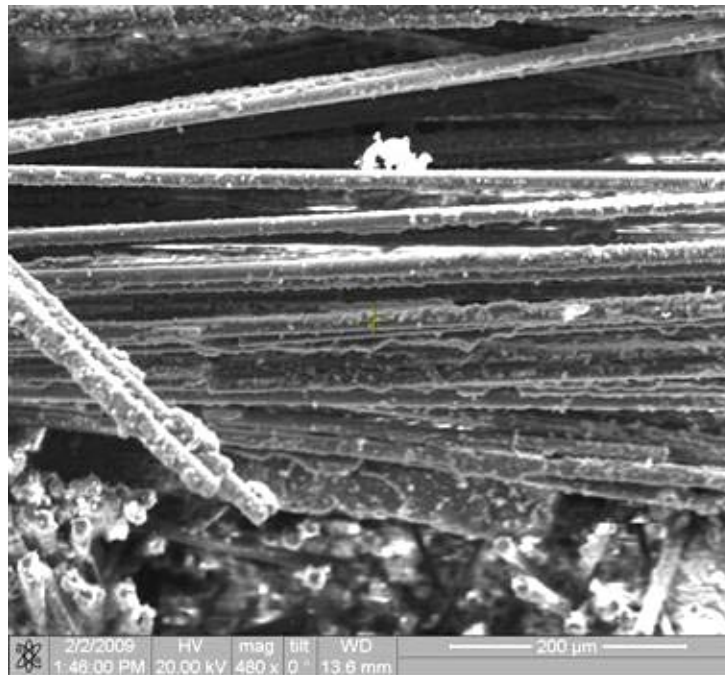


Figure 193 Fracture surface of the N720/AM specimen tested in tension to failure with constant loading rate of 0.0025MPa at 1100°C in steam.

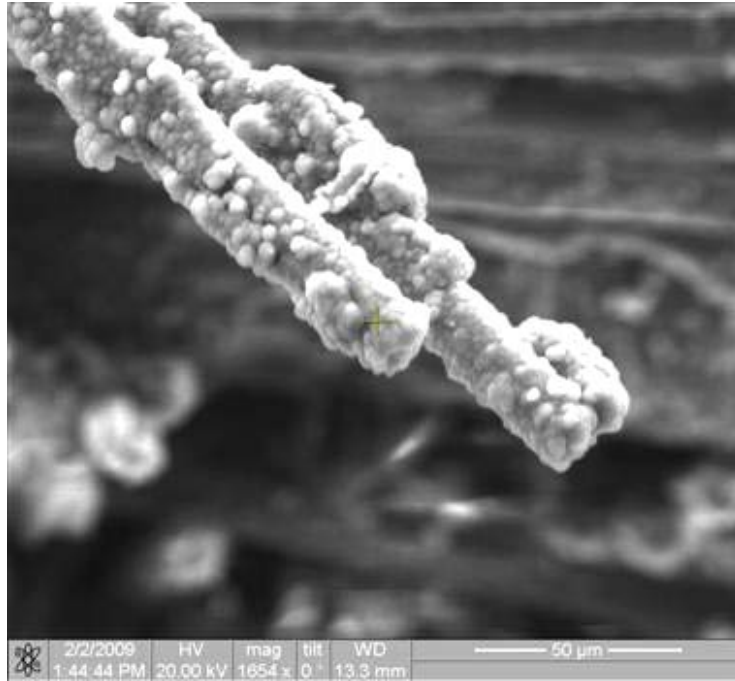


Figure 194 Fracture surface of the N720/AM specimen tested in tension to failure with constant loading rate of 0.0025MPa at 1100°C in steam.

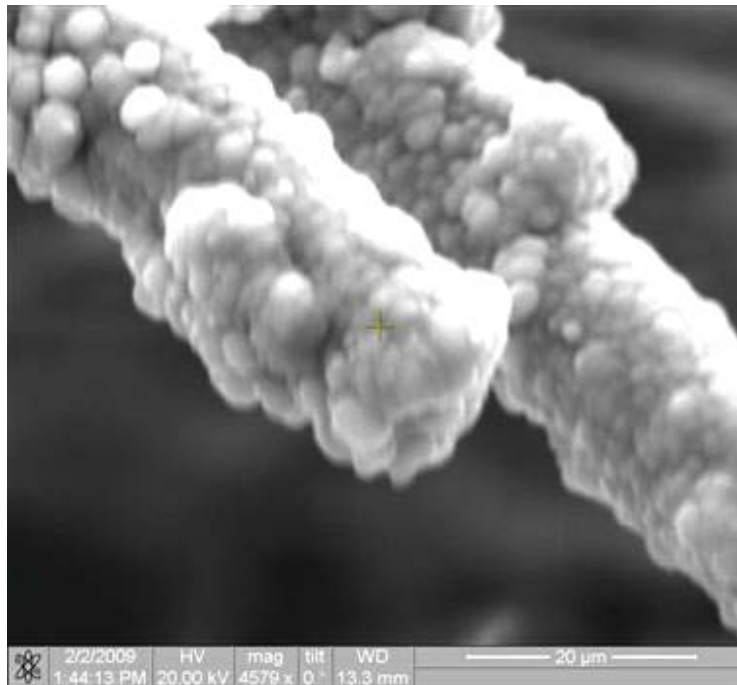


Figure 195 Fracture surface of the N720/AM specimen tested in tension to failure with constant loading rate of 0.0025MPa at 1100°C in steam.

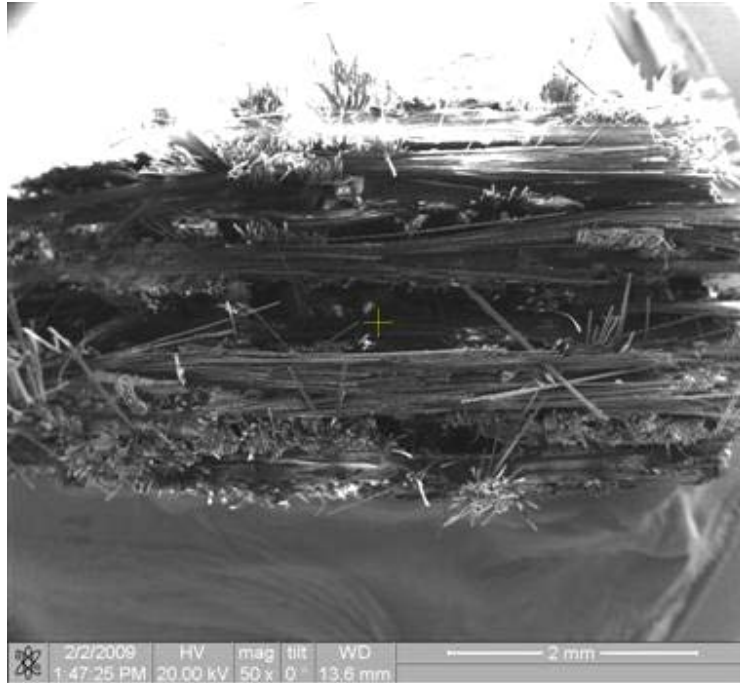


Figure 203. Fracture surface of the N720/AM specimen tested in tension to failure with constant loading rate of 0.0025MPa at 1100°C in steam.

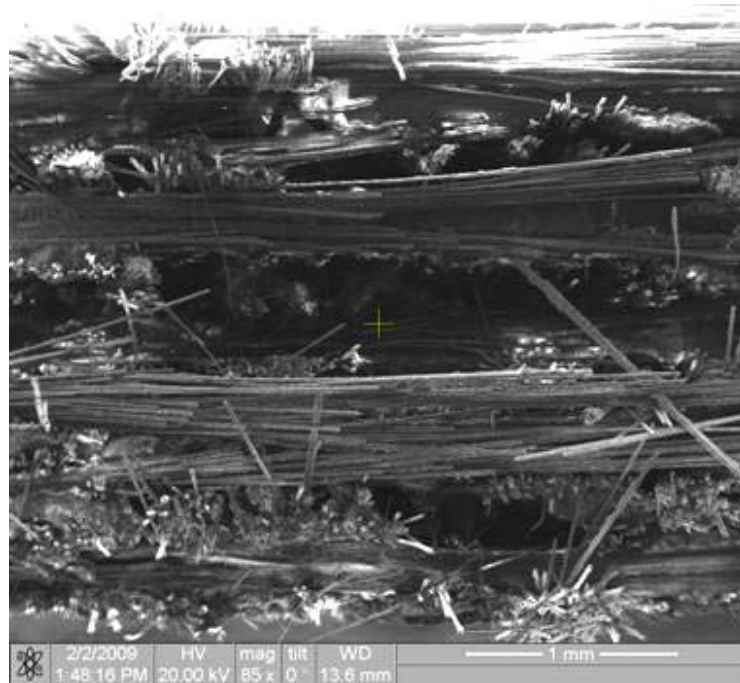


Figure 196. Fracture surface of the N720/AM specimen tested in tension to failure with constant loading rate of 0.0025MPa at 1100°C in steam.

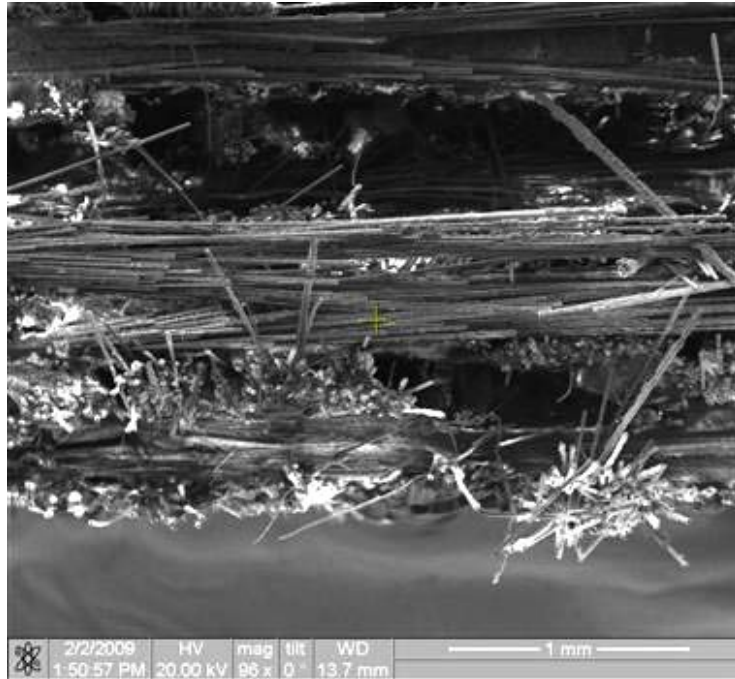


Figure 197. Fracture surface of the N720/AM specimen tested in tension to failure with constant loading rate of 0.0025MPa at 1100°C in steam.

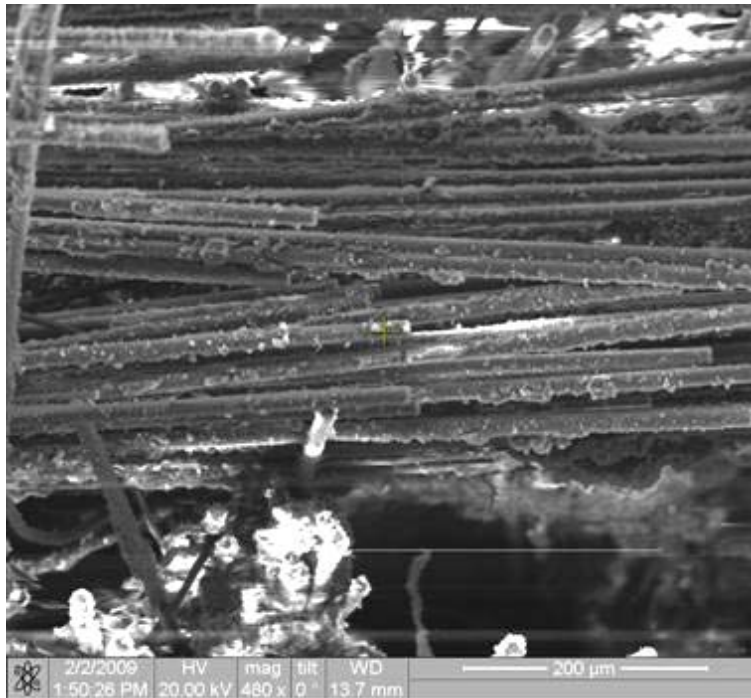


Figure 198. Fracture surface of the N720/AM specimen tested in tension to failure with constant loading rate of 0.0025MPa at 1100°C in steam.

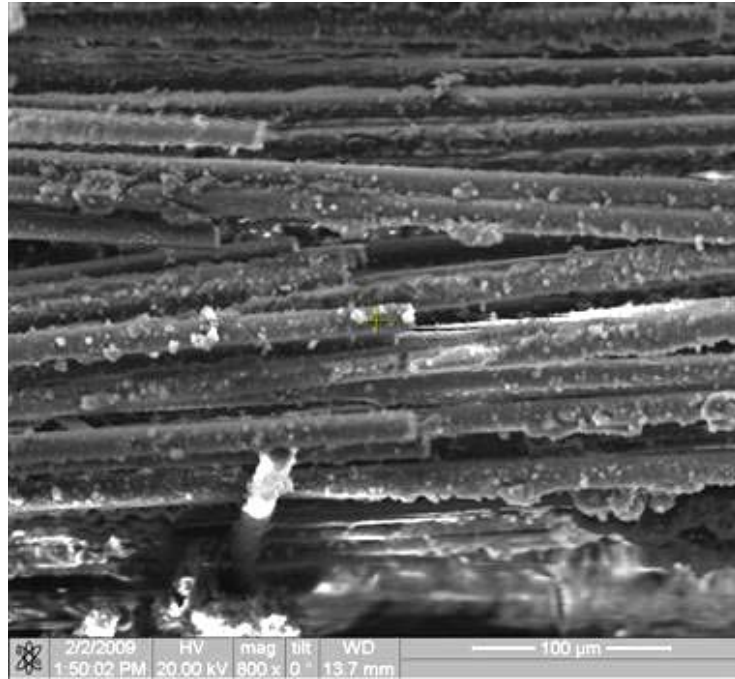


Figure 199. Fracture surface of the N720/AM specimen tested in tension to failure with constant loading rate of 0.0025MPa at 1100°C in steam.

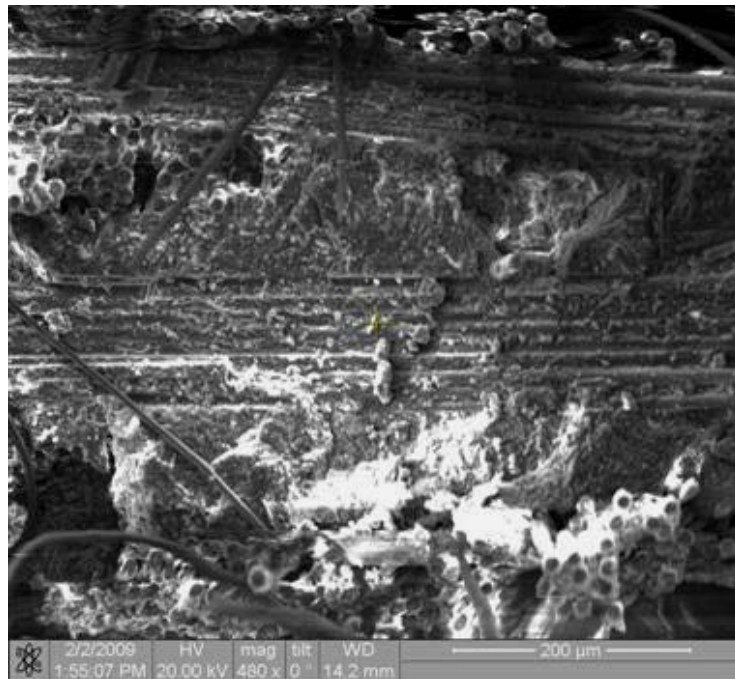


Figure 200. Fracture surface of the N720/AM specimen tested in tension to failure with constant loading rate of 0.0025MPa at 1100°C in steam.

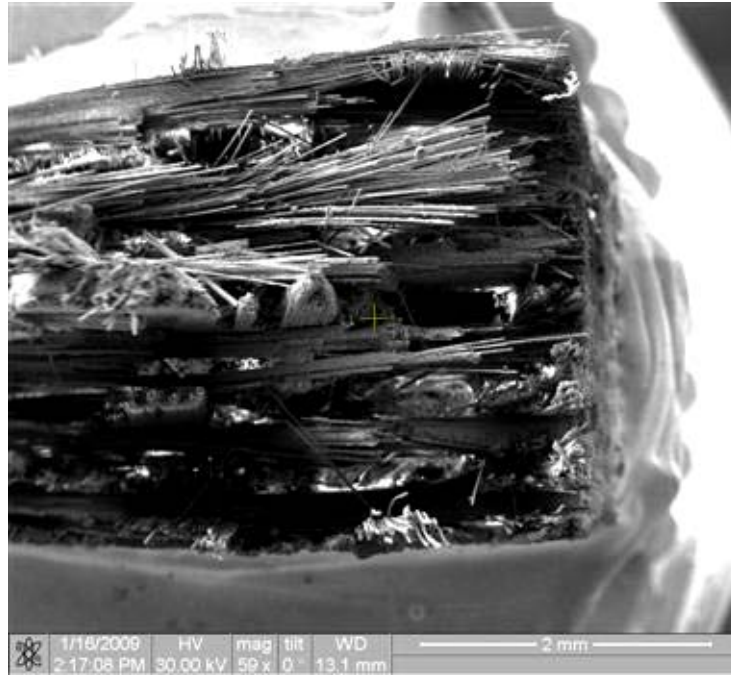


Figure 201. Fracture surface of the N720/AM specimen tested in creep at 109 MPa in laboratory air at 1100°C.

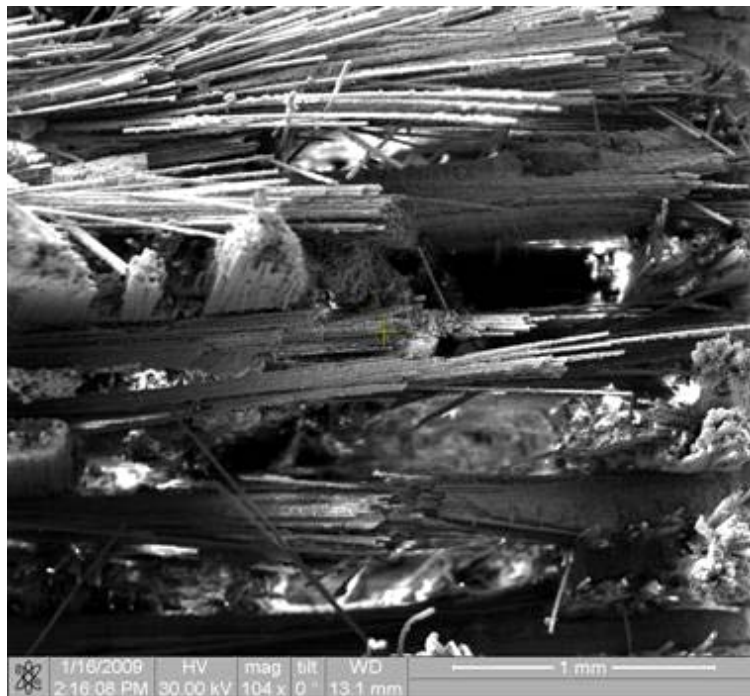


Figure 202. Fracture surface of the N720/AM specimen tested in creep at 109 MPa in laboratory air at 1100°C.

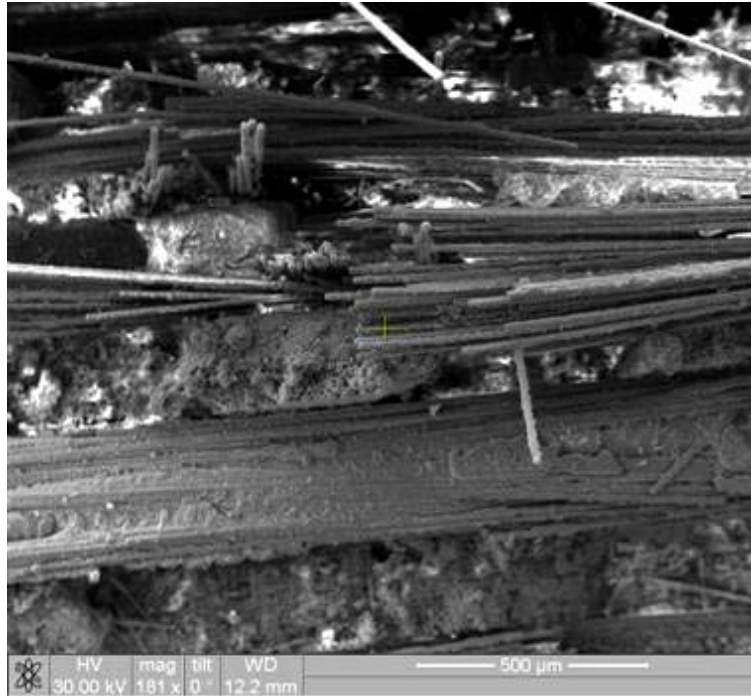


Figure 203. Fracture surface of the N720/AM specimen tested in creep at 109 MPa in laboratory air at 1100°C.

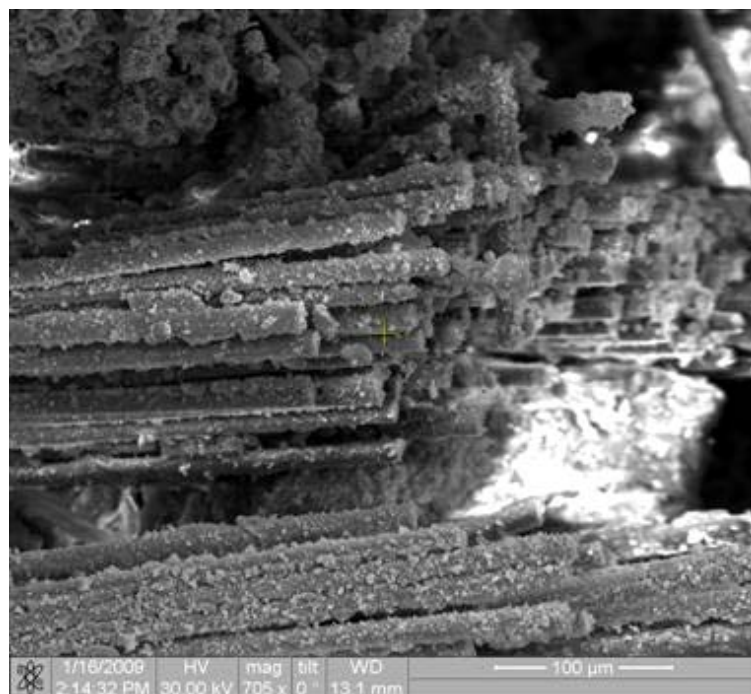


Figure 204. Fracture surface of the N720/AM specimen tested in creep at 109 MPa in laboratory air at 1100°C.

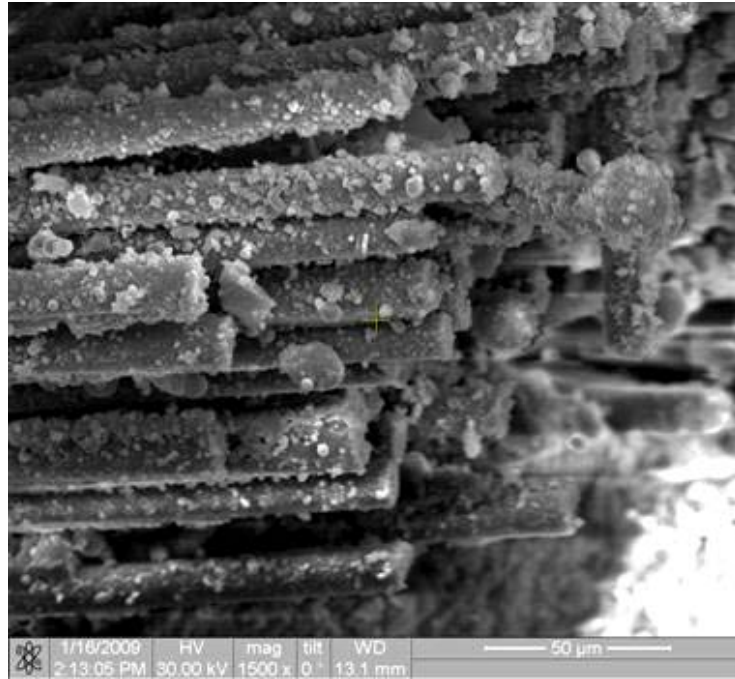


Figure 205. Fracture surface of the N720/AM specimen tested in creep at 109 MPa in laboratory air at 1100°C.

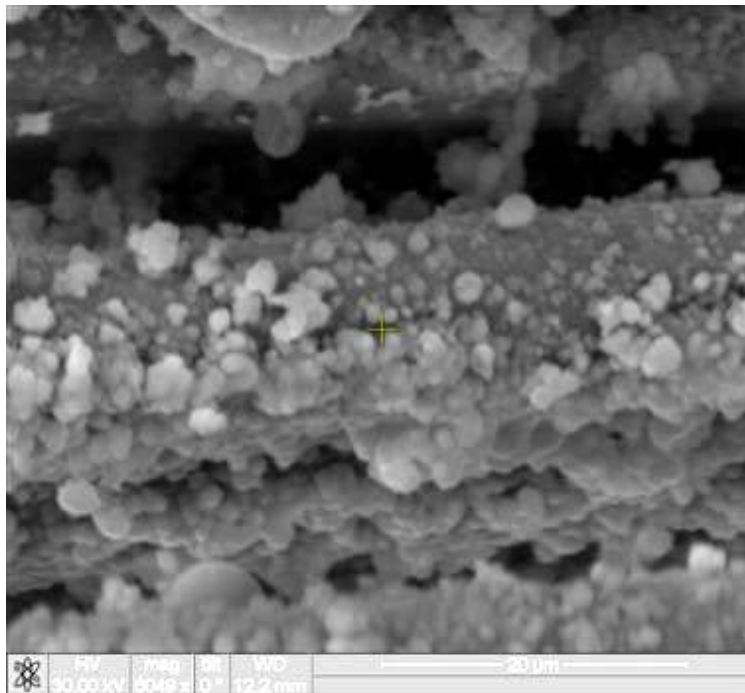


Figure 206. Fracture surface of the N720/AM specimen tested in creep at 109 MPa in laboratory air at 1100°C.

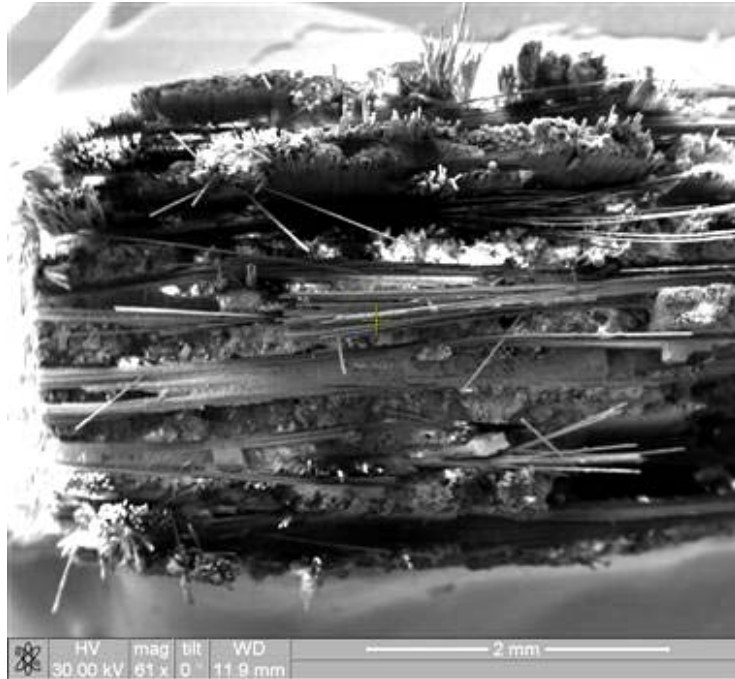


Figure 207. Fracture surface of the N720/AM specimen tested in creep at 109 MPa in laboratory air at 1100°C.

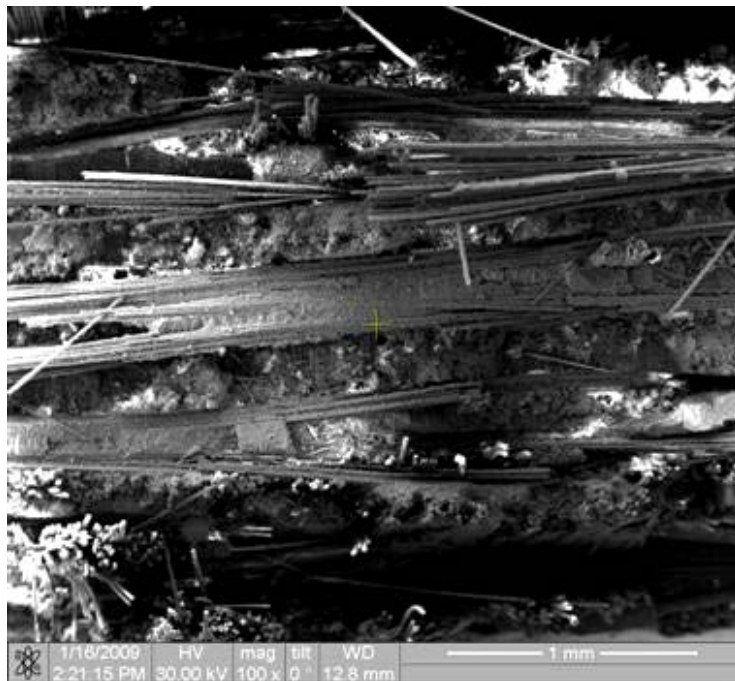


Figure 208. Fracture surface of the N720/AM specimen tested in creep at 109 MPa in laboratory air at 1100°C.

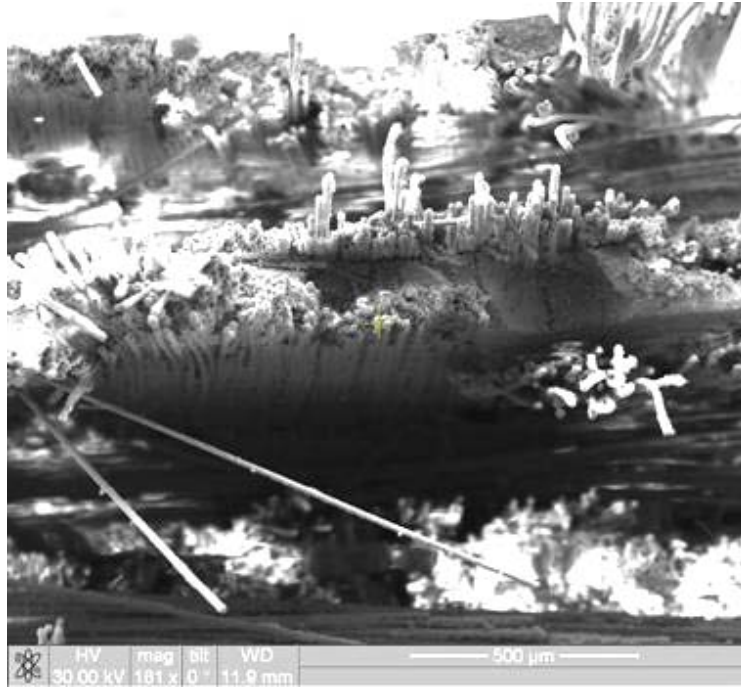


Figure 209. Fracture surface of the N720/AM specimen tested in creep at 109 MPa in laboratory air at 1100°C.

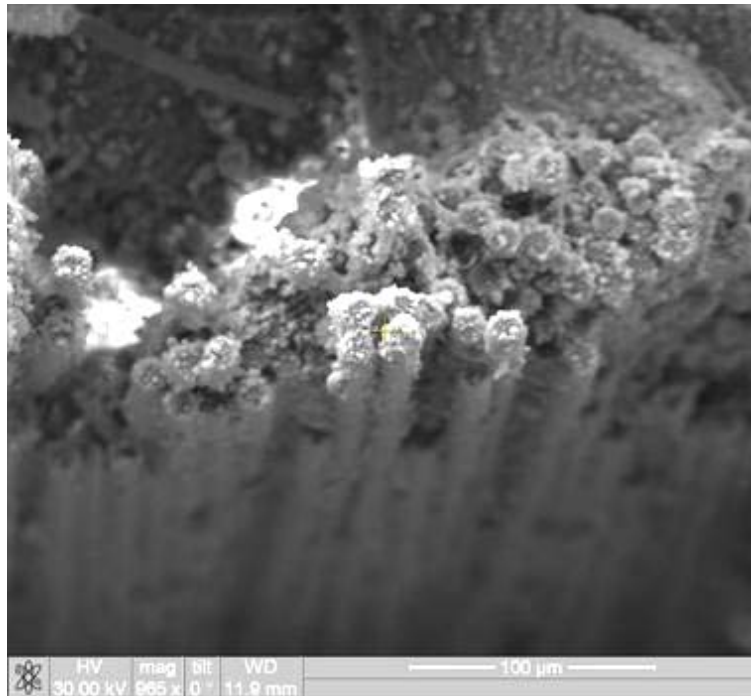


Figure 210. Fracture surface of the N720/AM specimen tested in creep at 109 MPa in laboratory air at 1100°C.

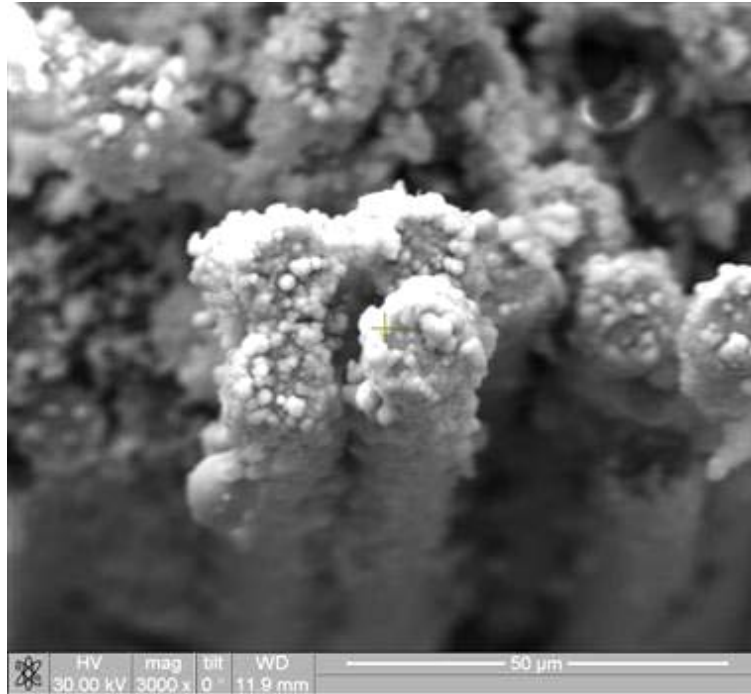


Figure 211. Fracture surface of the N720/AM specimen tested in creep at 109 MPa in laboratory air at 1100°C.

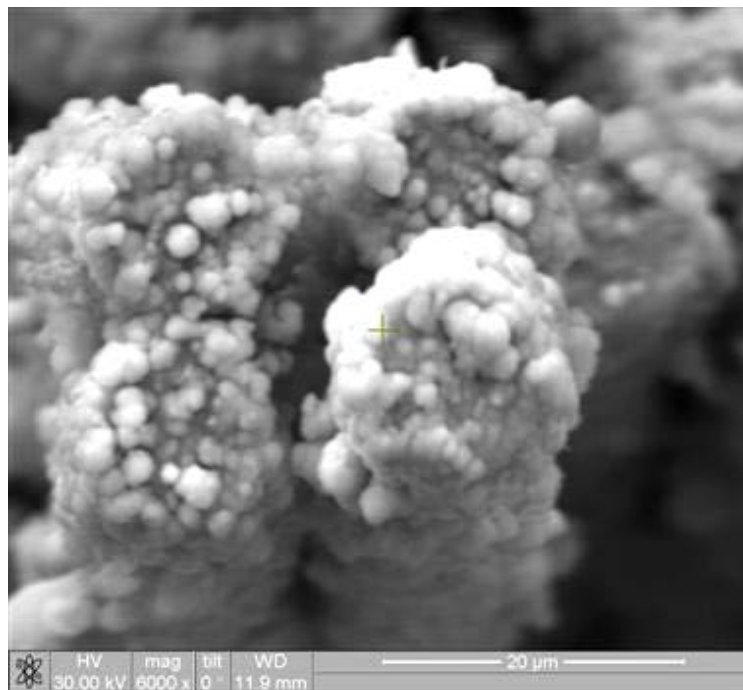


Figure 212. Fracture surface of the N720/AM specimen tested in creep at 109 MPa in laboratory air at 1100°C.

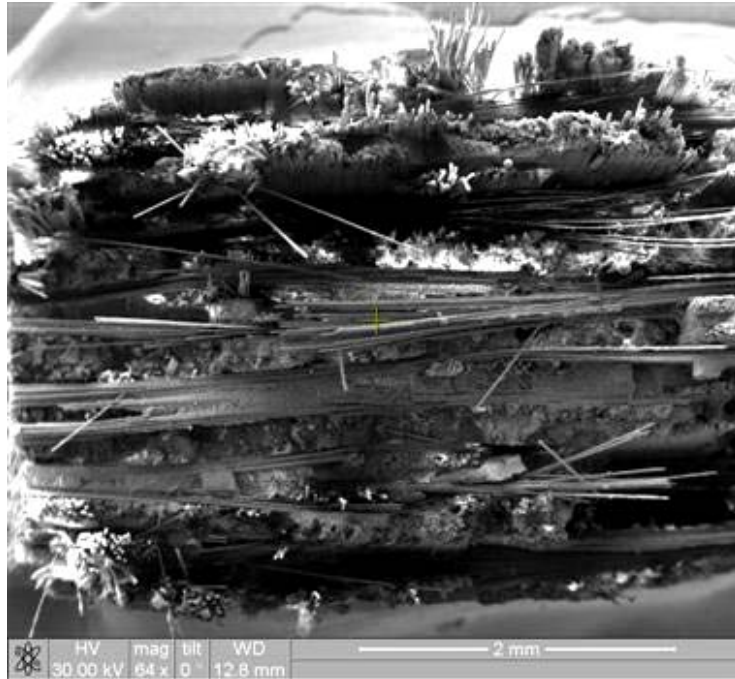


Figure 213. Fracture surface of the N720/AM specimen tested in creep at 109 MPa in laboratory air at 1100°C.



Figure 214. Fracture surface of the N720/AM specimen tested in creep at 109 MPa in laboratory air at 1100°C.



Figure 215. Fracture surface of the N720/AM specimen tested in creep at 109 MPa in laboratory air at 1100°C.

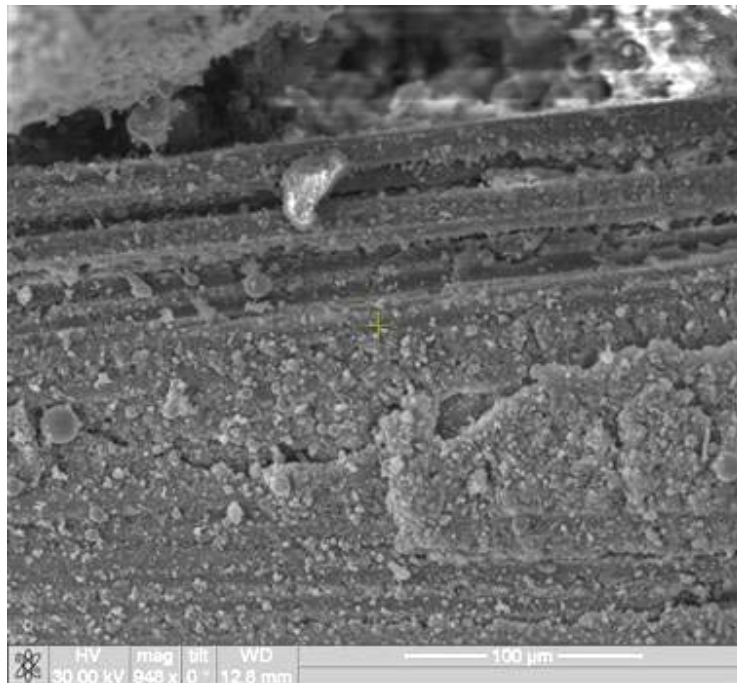


Figure 216. Fracture surface of the N720/AM specimen tested in creep at 109 MPa in laboratory air at 1100°C.

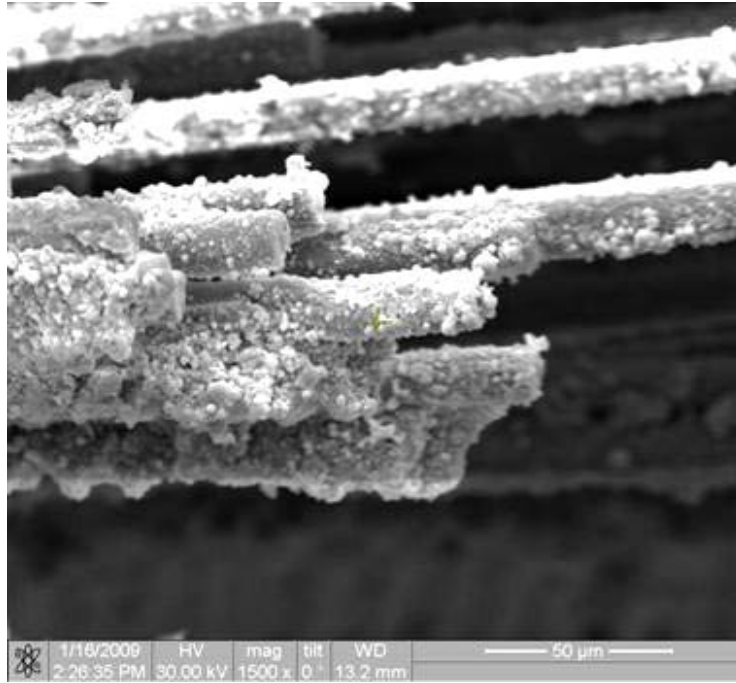


Figure 217. Fracture surface of the N720/AM specimen tested in creep at 109 MPa in laboratory air at 1100°C.



Figure 218. Fracture surface of the N720/AM specimen tested in creep at 109 MPa in laboratory air at 1100°C.



Figure 219. Fracture surface of the N720/AM specimen tested in creep at 109 MPa in laboratory air at 1100°C.

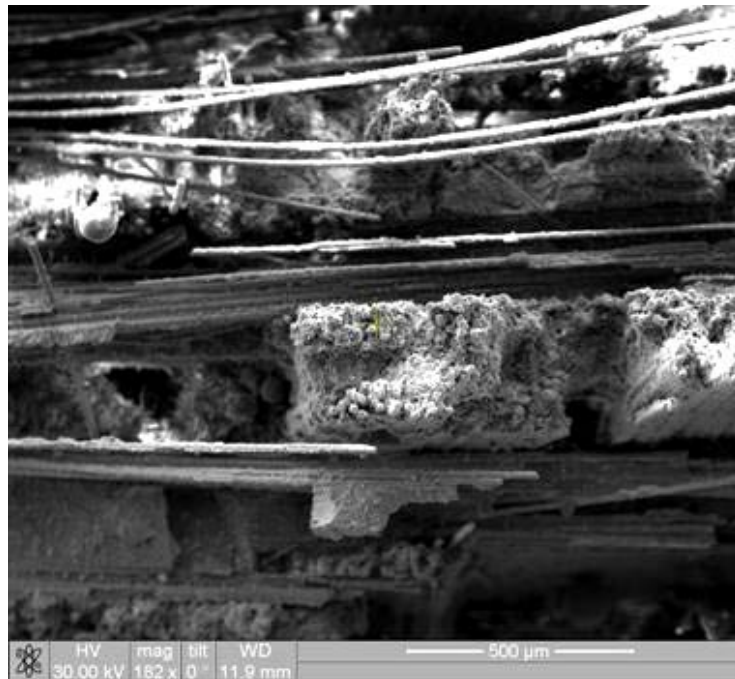


Figure 220. Fracture surface of the N720/AM specimen tested in creep at 109 MPa in laboratory air at 1100°C.

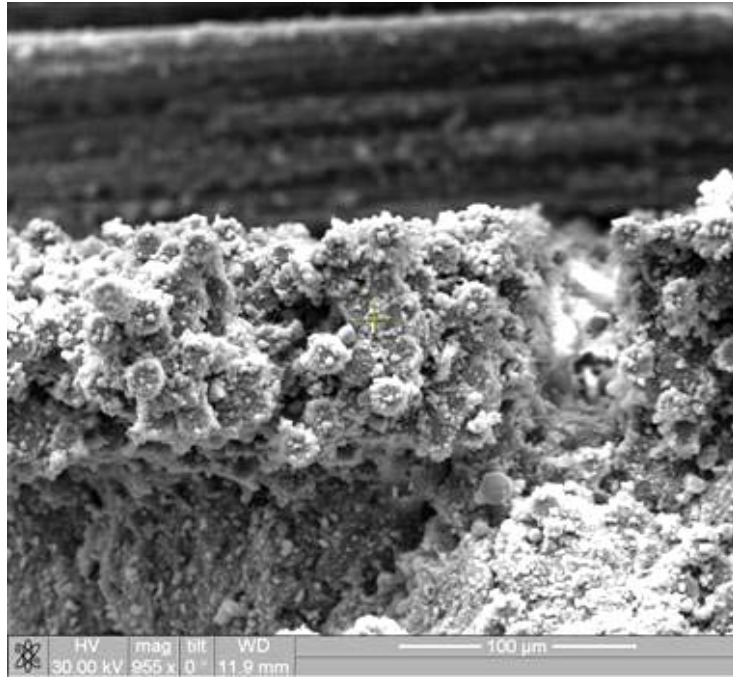


Figure 221. Fracture surface of the N720/AM specimen tested in creep at 109 MPa in laboratory air at 1100°C.

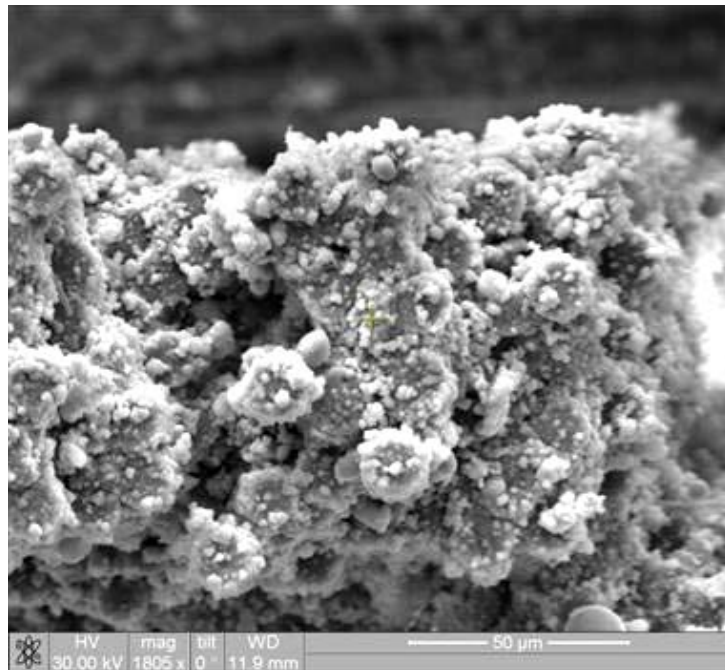


Figure 222. Fracture surface of the N720/AM specimen tested in creep at 109 MPa in laboratory air at 1100°C.



Figure 223. Fracture surface of the N720/AM specimen tested in creep at 109 MPa in laboratory air at 1100°C.

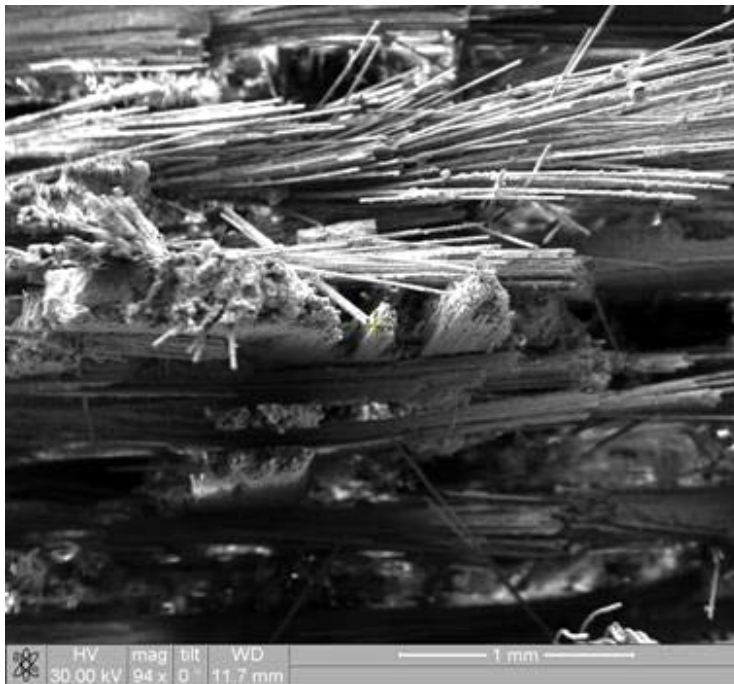


Figure 224. Fracture surface of the N720/AM specimen tested in creep at 109 MPa in laboratory air at 1100°C.

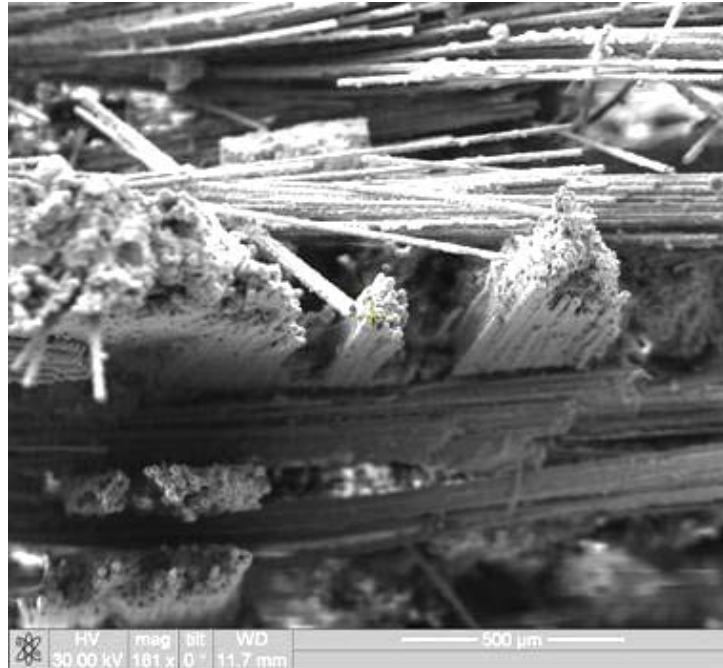


Figure 225. Fracture surface of the N720/AM specimen tested in creep at 109 MPa in laboratory air at 1100°C.

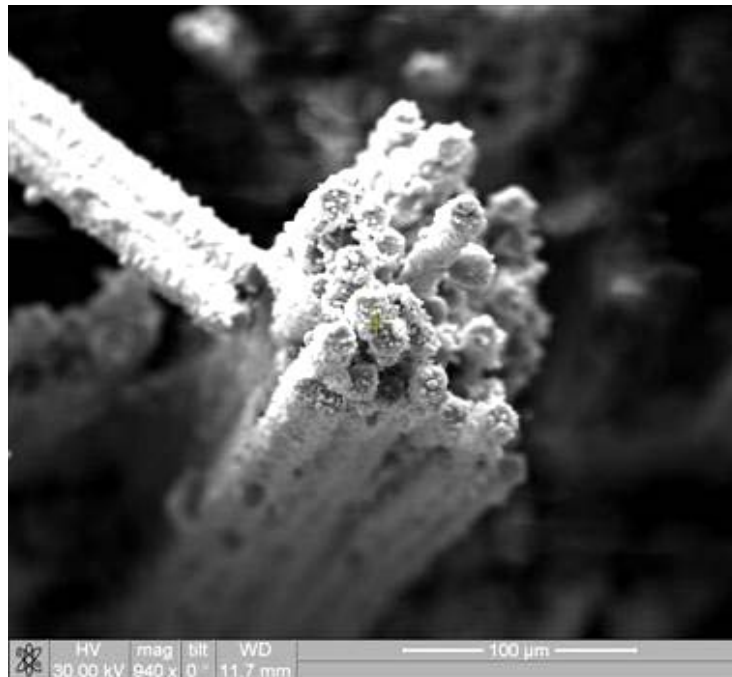


Figure 226. Fracture surface of the N720/AM specimen tested in creep at 109 MPa in laboratory air at 1100°C.

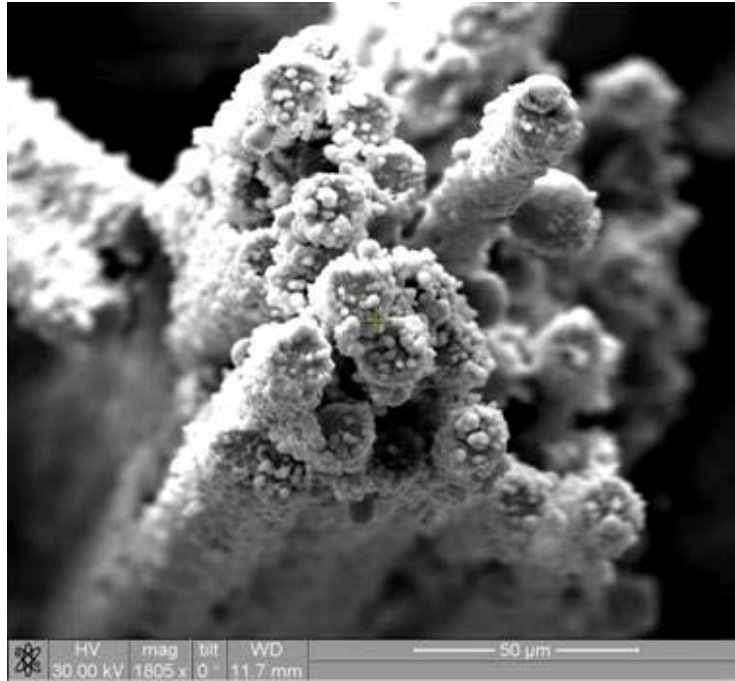


Figure 227. Fracture surface of the N720/AM specimen tested in creep at 109 MPa in laboratory air at 1100°C.



Figure 228. Fracture surface of the N720/AM specimen tested in creep at 109 MPa in laboratory air at 1100°C.

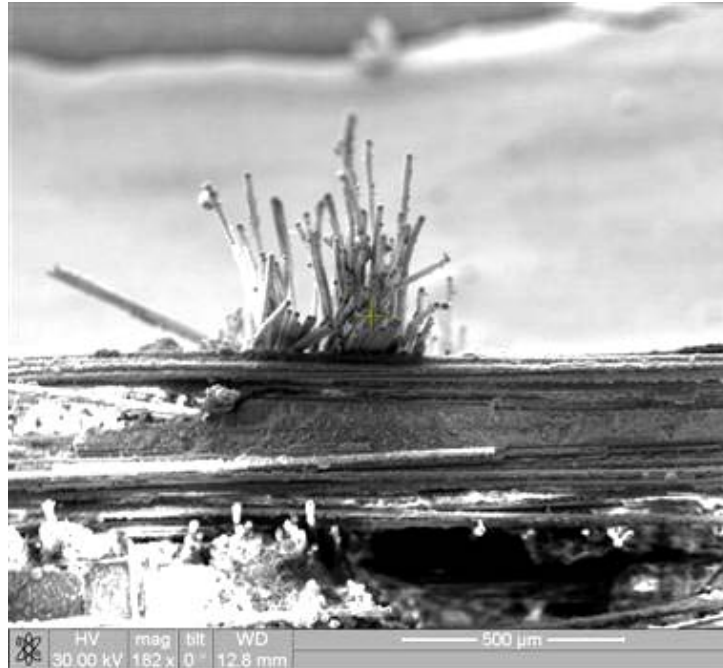


Figure 229. Fracture surface of the N720/AM specimen tested in creep at 109 MPa in laboratory air at 1100°C.



Figure 230. Fracture surface of the N720/AM specimen tested in creep at 109 MPa in laboratory air at 1100°C.



Figure 231. Fracture surface of the N720/AM specimen tested in creep at 109 MPa in laboratory air at 1100°C.

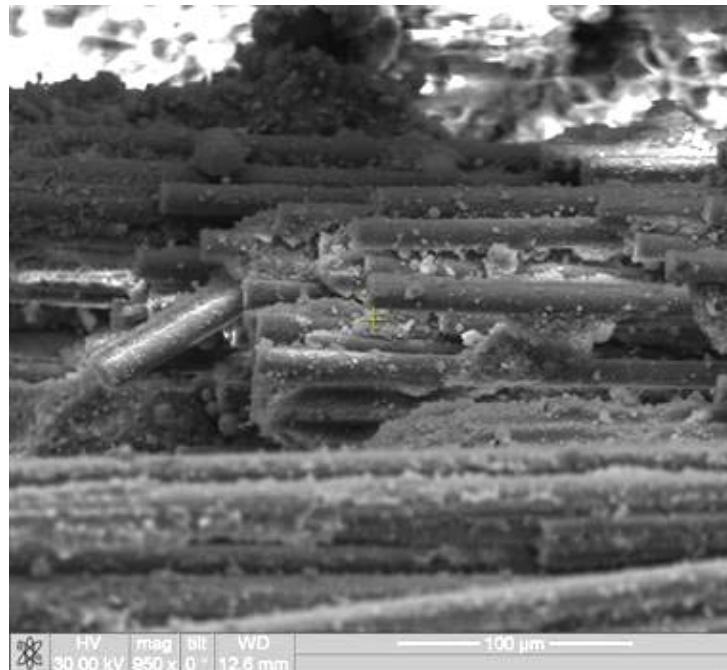


Figure 232. Fracture surface of the N720/AM specimen tested in creep at 109 MPa in laboratory air at 1100°C.

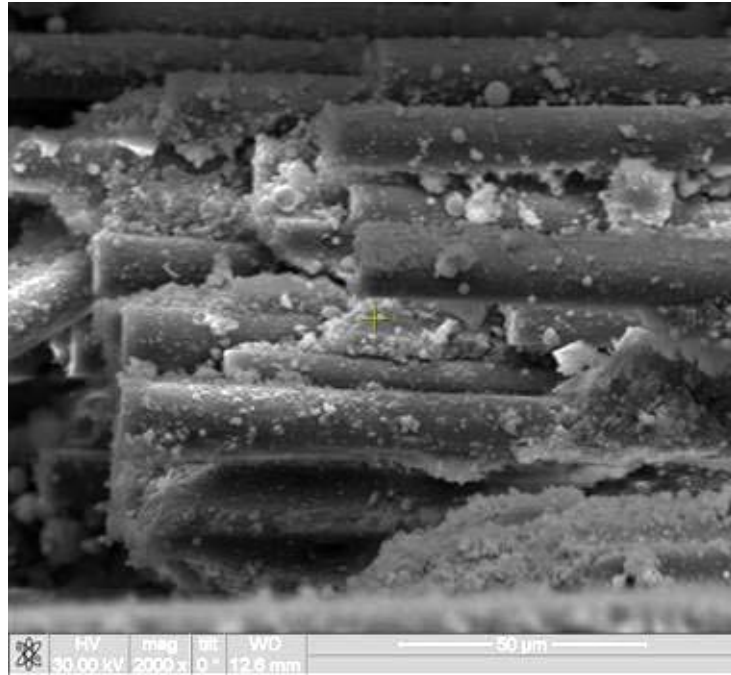


Figure 233. Fracture surface of the N720/AM specimen tested in creep at 109 MPa in laboratory air at 1100°C.

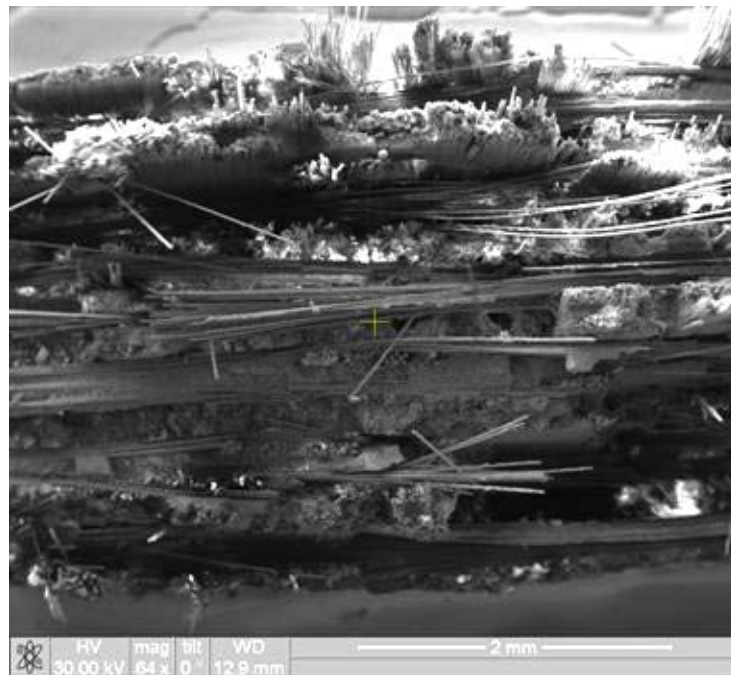


Figure 234. Fracture surface of the N720/AM specimen tested in creep at 109 MPa in laboratory air at 1100°C.



Figure 235. Fracture surface of the N720/AM specimen tested in creep at 109 MPa in laboratory air at 1100°C.

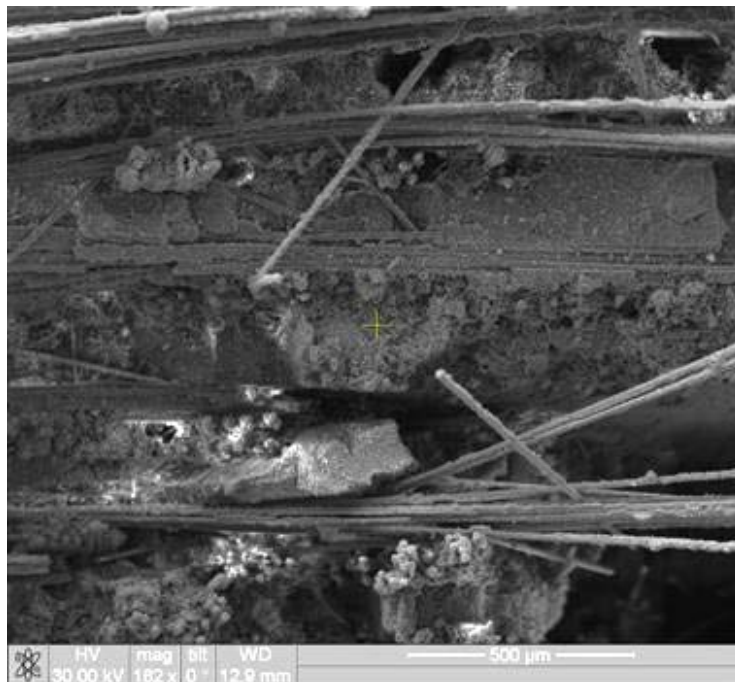


Figure 236. Fracture surface of the N720/AM specimen tested in creep at 109 MPa in laboratory air at 1100°C.

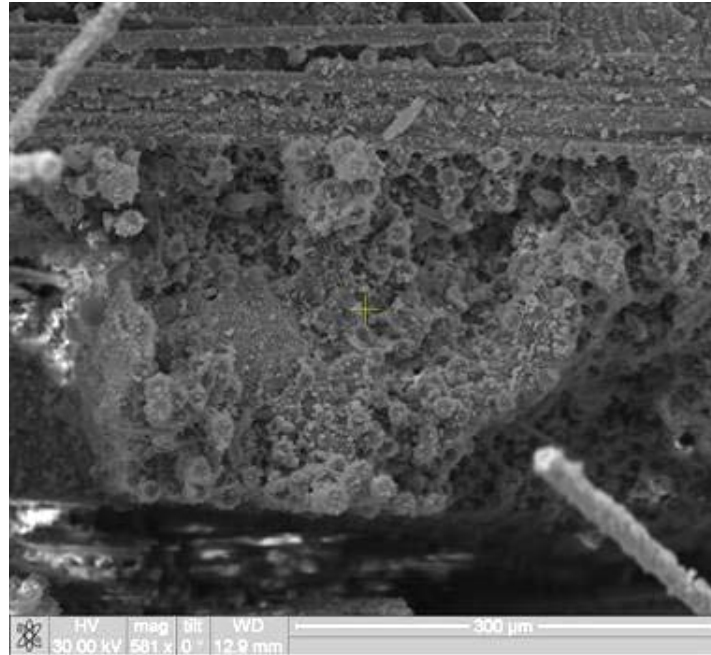


Figure 237. Fracture surface of the N720/AM specimen tested in creep at 109 MPa in laboratory air at 1100°C.

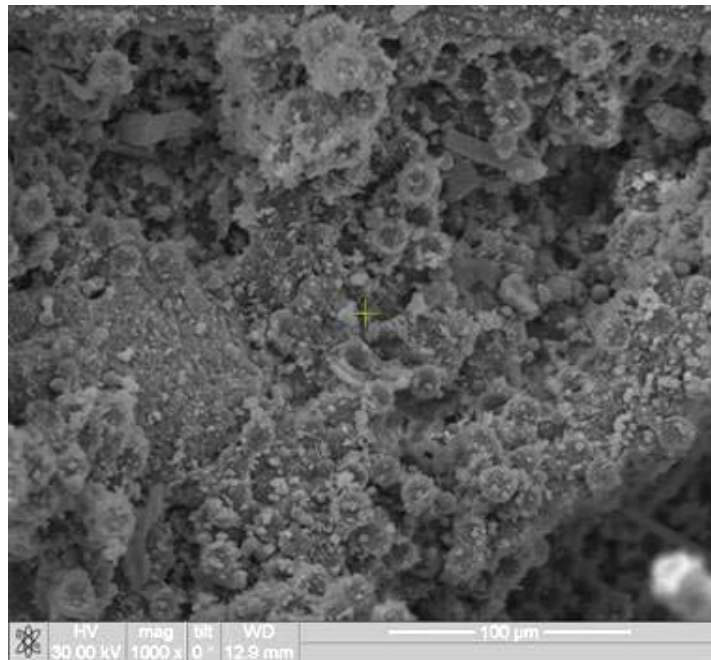


Figure 238. Fracture surface of the N720/AM specimen tested in creep at 109 MPa in laboratory air at 1100°C.



Figure 239. Fracture surface of the N720/AM specimen tested in creep at 131 MPa in laboratory air at 1100°C.

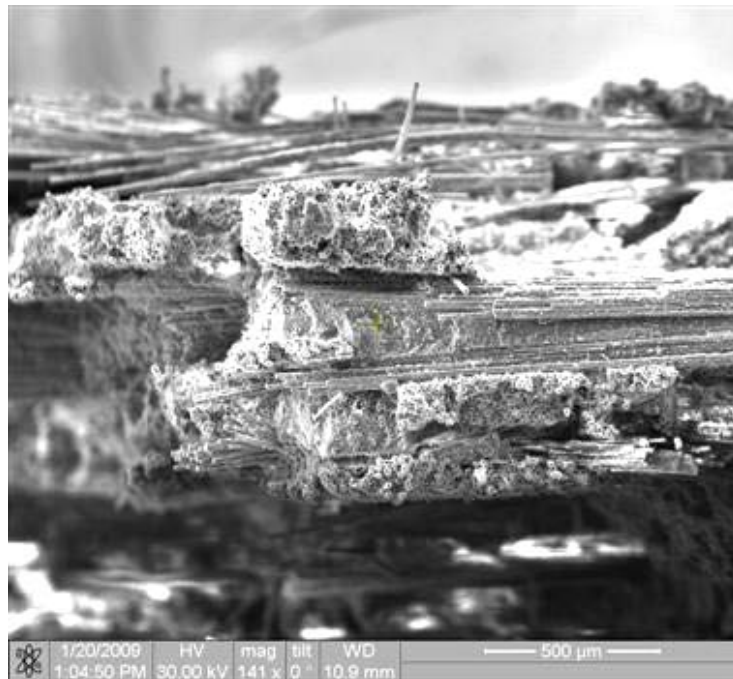


Figure 240. Fracture surface of the N720/AM specimen tested in creep at 131 MPa in laboratory air at 1100°C.

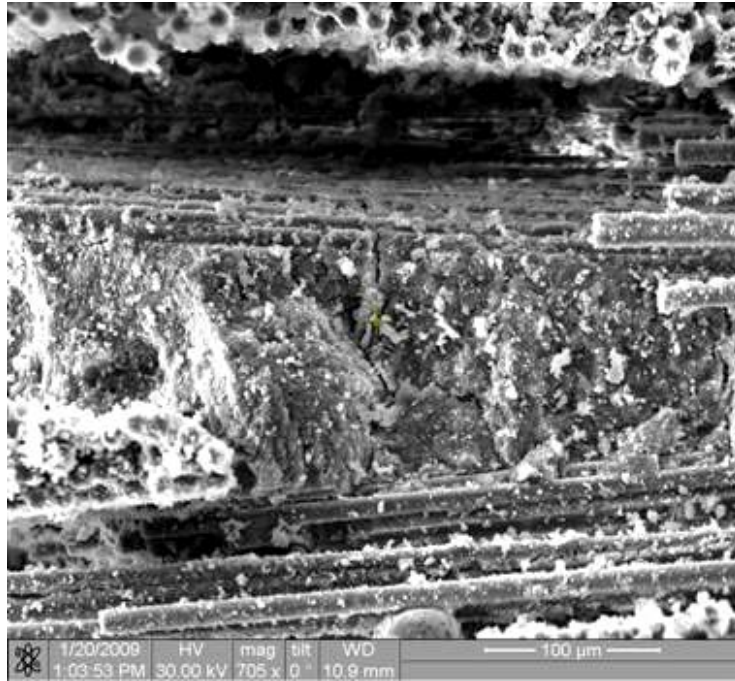


Figure 241. Fracture surface of the N720/AM specimen tested in creep at 131 MPa in laboratory air at 1100°C.

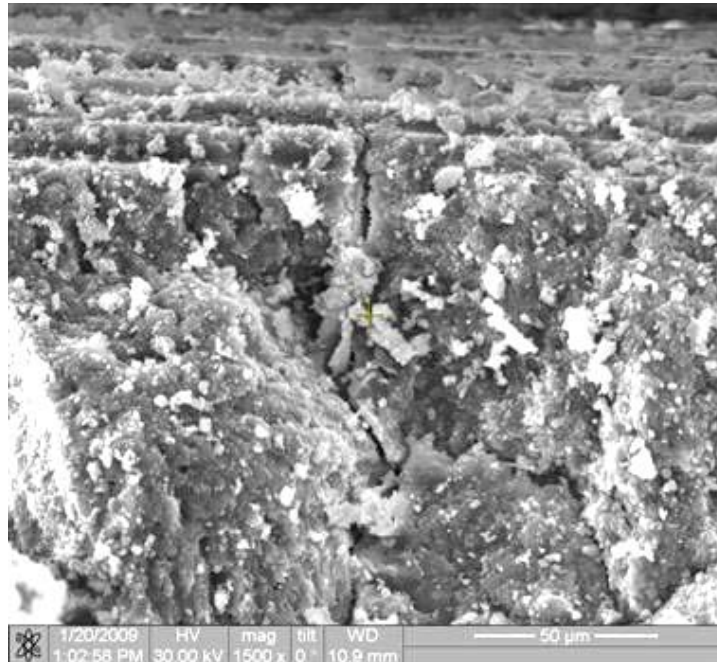


Figure 242. Fracture surface of the N720/AM specimen tested in creep at 131 MPa in laboratory air at 1100°C.

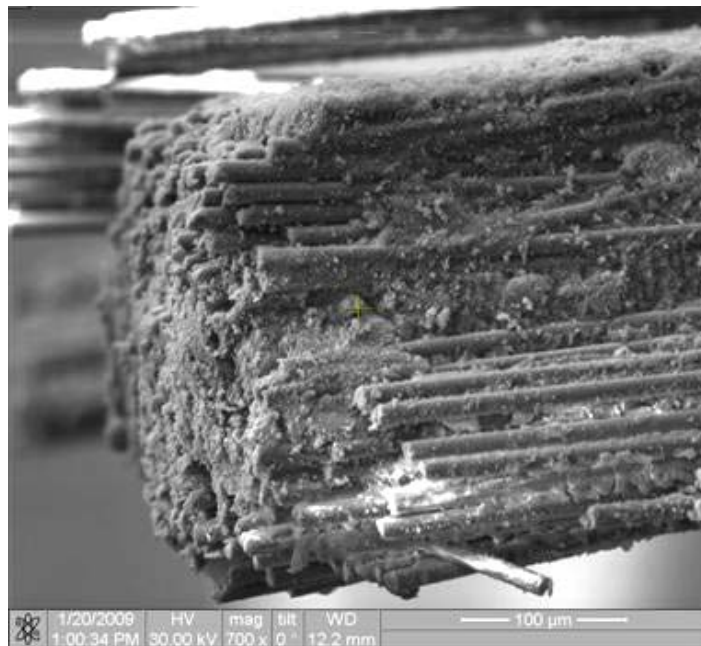


Figure 243. Fracture surface of the N720/AM specimen tested in creep at 131 MPa in laboratory air at 1100°C.

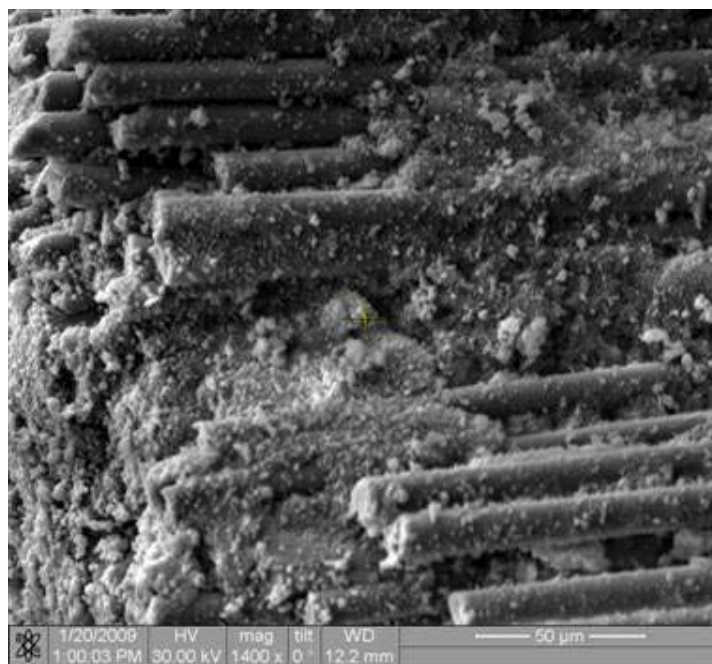


Figure 244. Fracture surface of the N720/AM specimen tested in creep at 131 MPa in laboratory air at 1100°C.



Figure 245. Fracture surface of the N720/AM specimen tested in creep at 131 MPa in laboratory air at 1100°C.

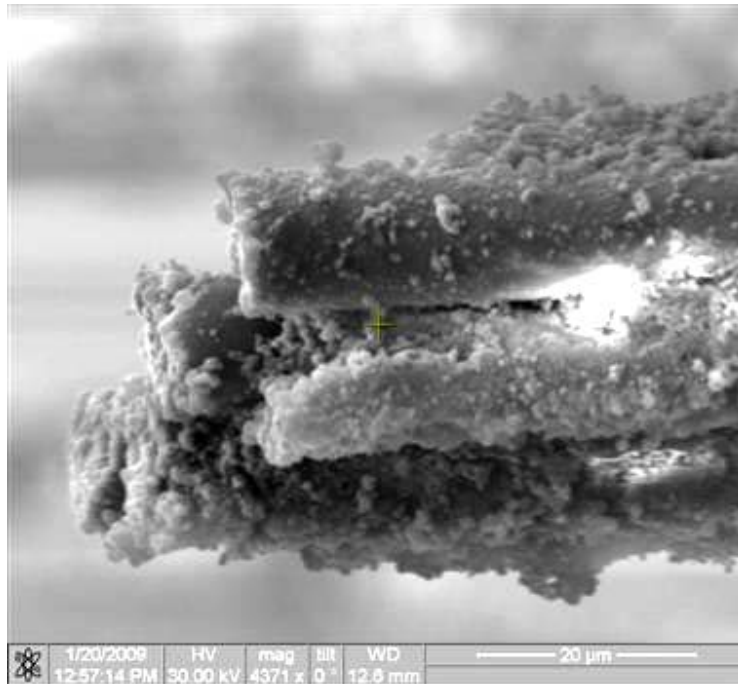


Figure 246. Fracture surface of the N720/AM specimen tested in creep at 131 MPa in laboratory air at 1100°C.



Figure 247. Fracture surface of the N720/AM specimen tested in creep at 131 MPa in laboratory air at 1100°C.



Figure 248. Fracture surface of the N720/AM specimen tested in creep at 131 MPa in laboratory air at 1100°C.



Figure 249. Fracture surface of the N720/AM specimen tested in creep at 131 MPa in laboratory air at 1100°C.

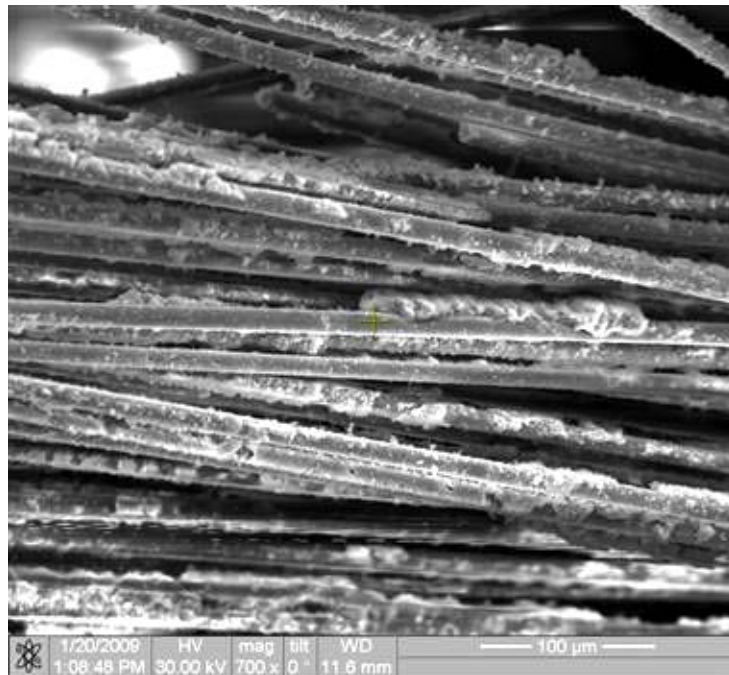


Figure 250. Fracture surface of the N720/AM specimen tested in creep at 131 MPa in laboratory air at 1100°C.

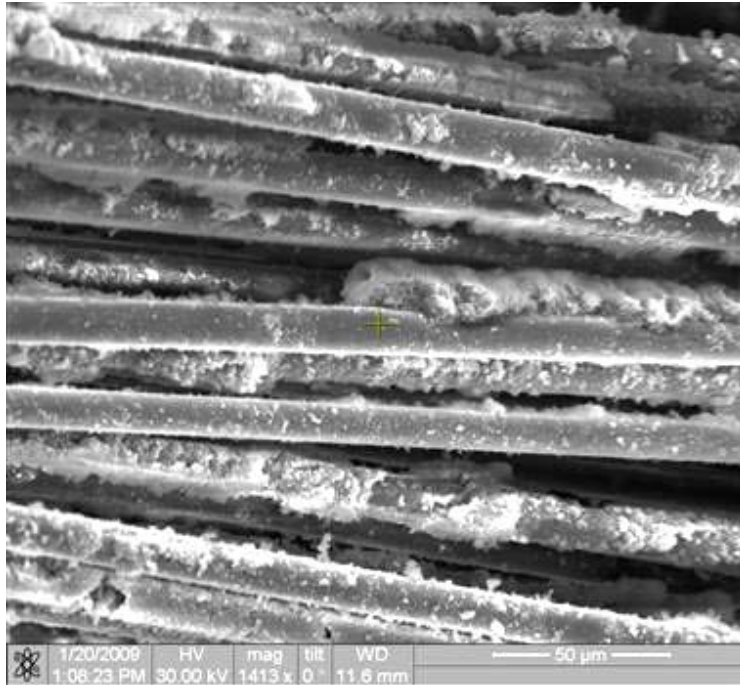


Figure 251. Fracture surface of the N720/AM specimen tested in creep at 131 MPa in laboratory air at 1100°C.

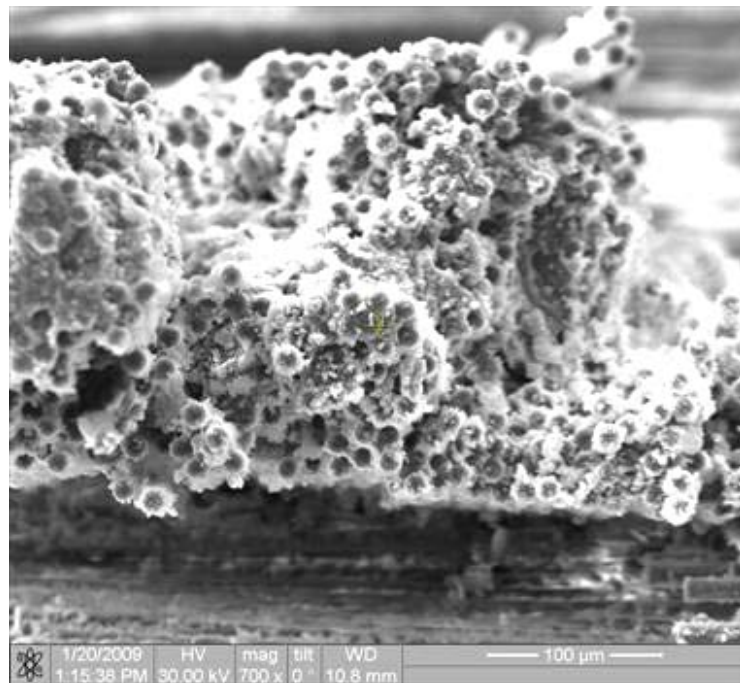


Figure 252. Fracture surface of the N720/AM specimen tested in creep at 131 MPa in laboratory air at 1100°C.

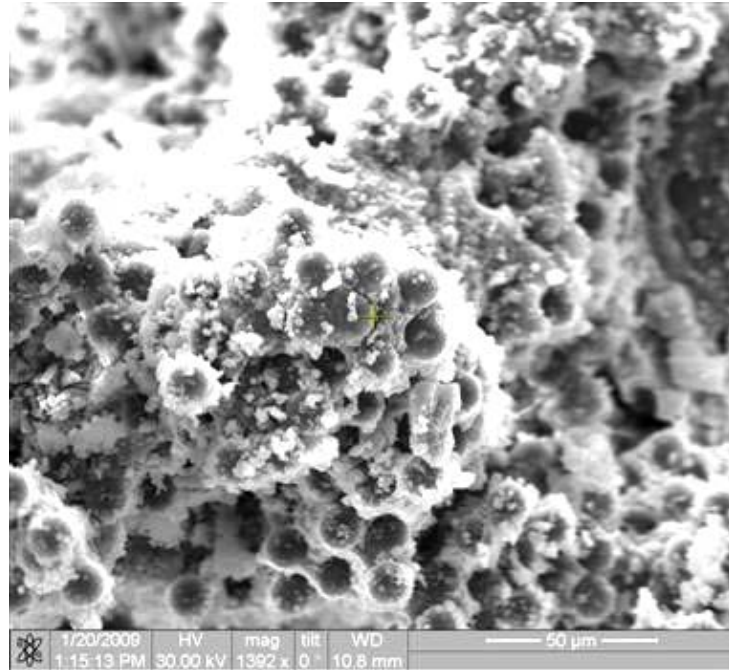


Figure 262. Fracture surface of the N720/AM specimen tested in creep at 131 MPa in laboratory air at 1100°C

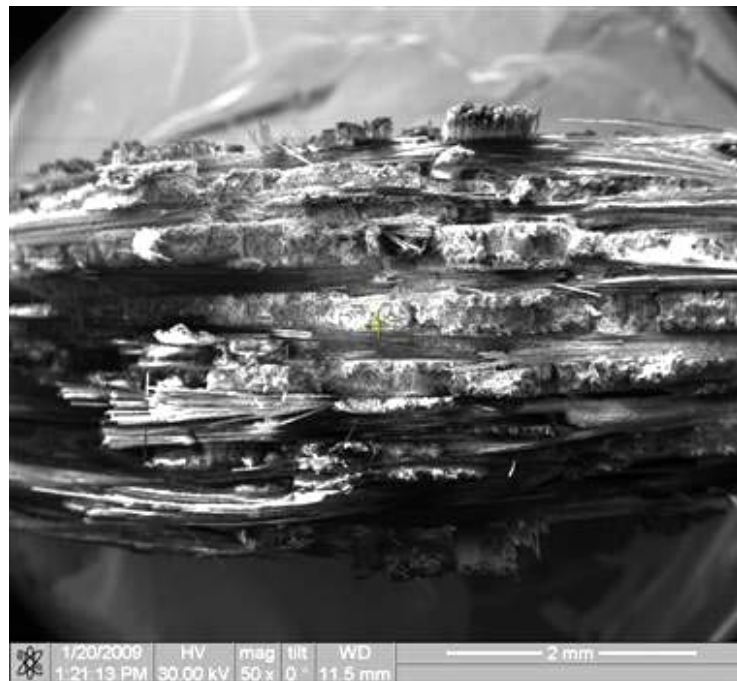


Figure 253. Fracture surface of the N720/AM specimen tested in creep at 131 MPa in laboratory air at 1100°C.



Figure 254. Fracture surface of the N720/AM specimen tested in creep at 131 MPa in laboratory air at 1100°C.



Figure 255. Fracture surface of the N720/AM specimen tested in creep at 131 MPa in laboratory air at 1100°C.

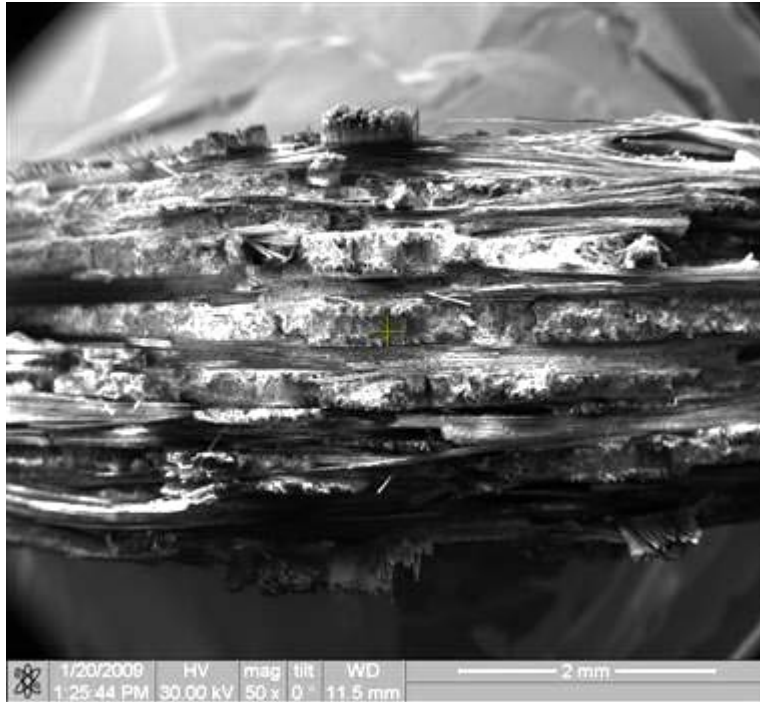


Figure 256. Fracture surface of the N720/AM specimen tested in creep at 131 MPa in laboratory air at 1100°C.

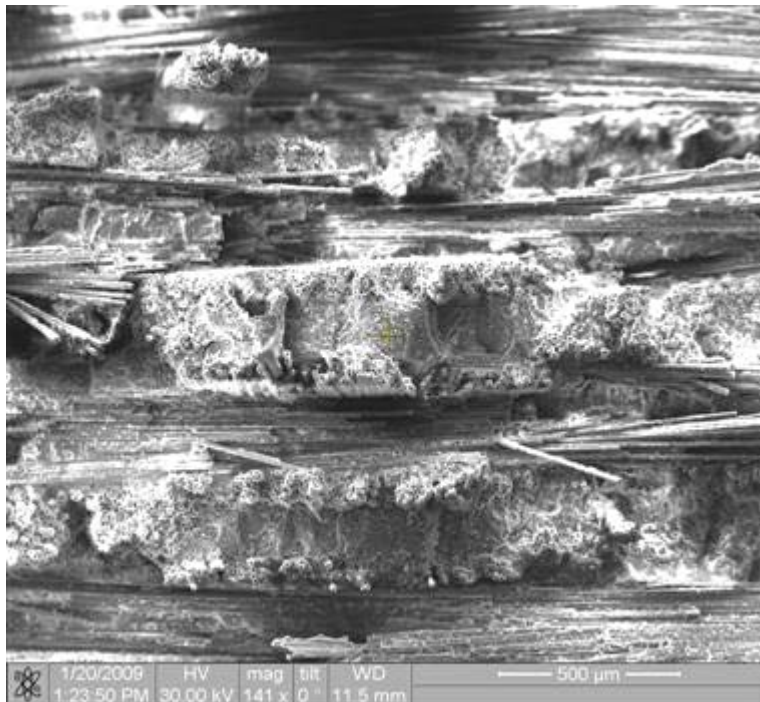


Figure 257. Fracture surface of the N720/AM specimen tested in creep at 131 MPa in laboratory air at 1100°C.



Figure 258. Fracture surface of the N720/AM specimen tested in creep at 131 MPa in laboratory air at 1100°C.

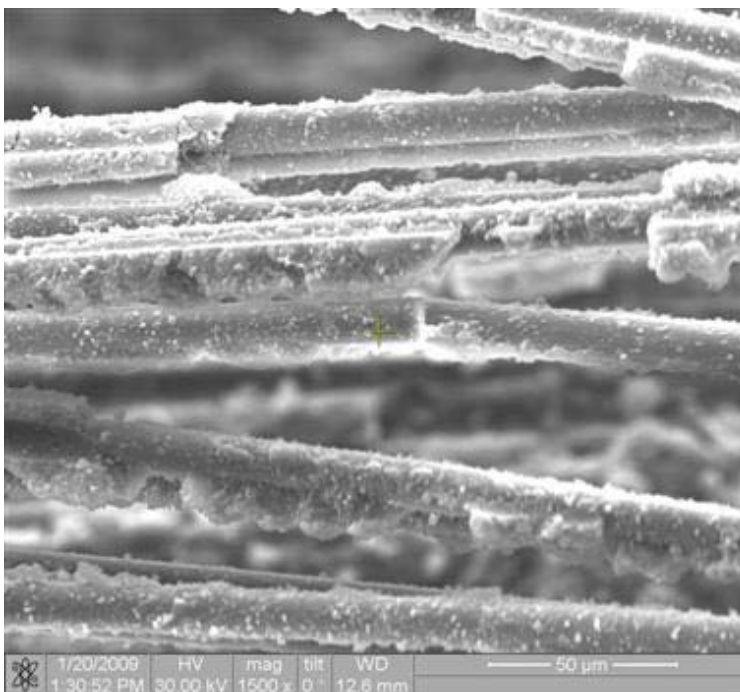


Figure 259. Fracture surface of the N720/AM specimen tested in creep at 131 MPa in laboratory air at 1100°C.

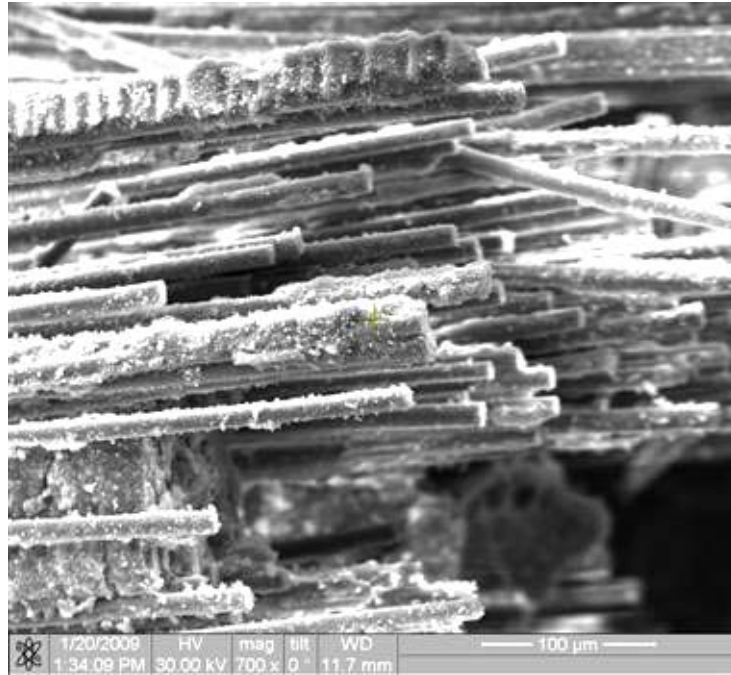


Figure 260. Fracture surface of the N720/AM specimen tested in creep at 131 MPa in laboratory air at 1100°C.

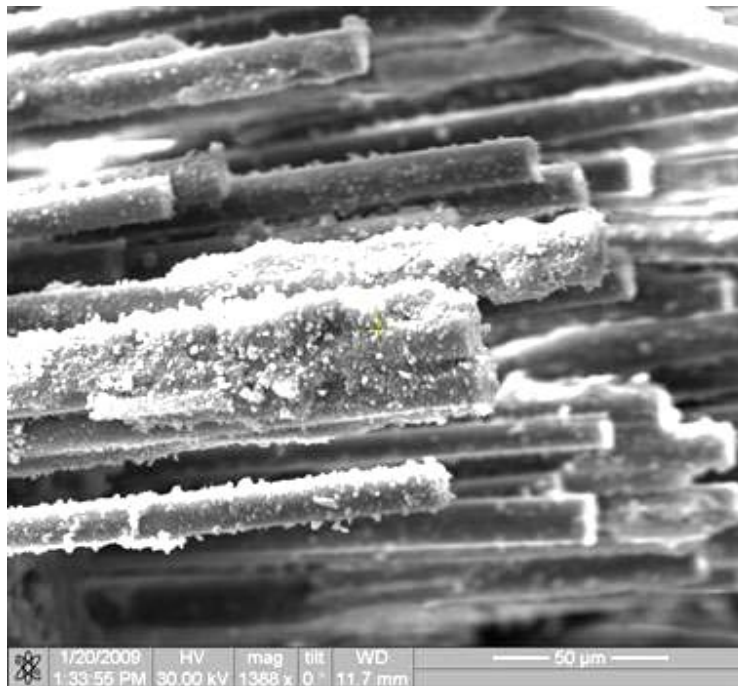


Figure 261. Fracture surface of the N720/AM specimen tested in creep at 131 MPa in laboratory air at 1100°C.

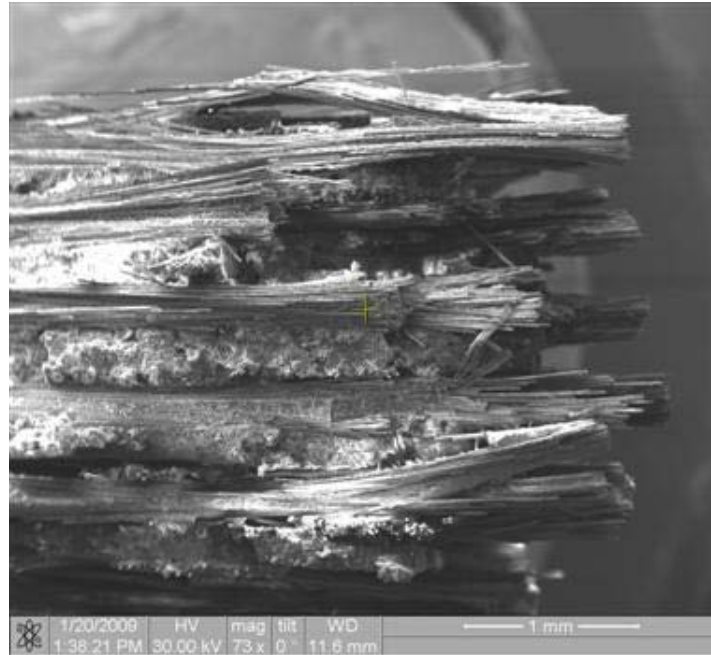


Figure 262. Fracture surface of the N720/AM specimen tested in creep at 131 MPa in laboratory air at 1100°C.

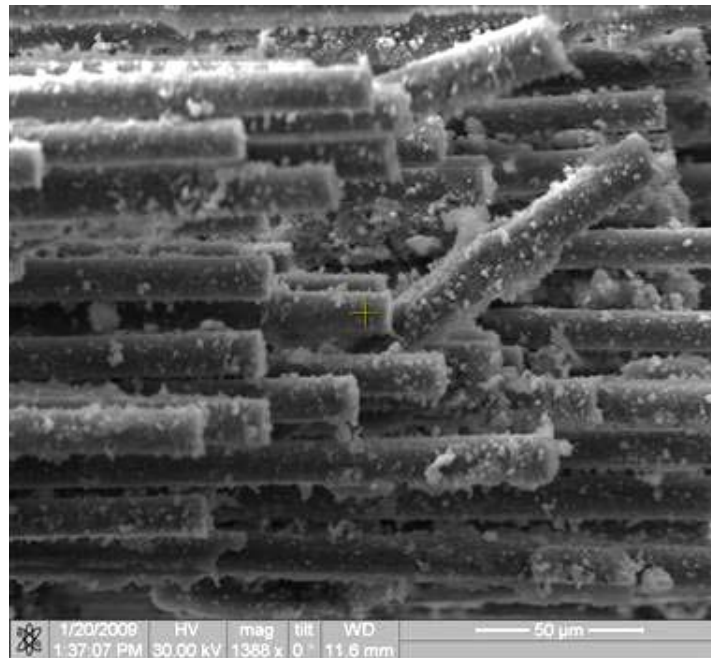


Figure 263. Fracture surface of the N720/AM specimen tested in creep at 131 MPa in laboratory air at 1100°C.

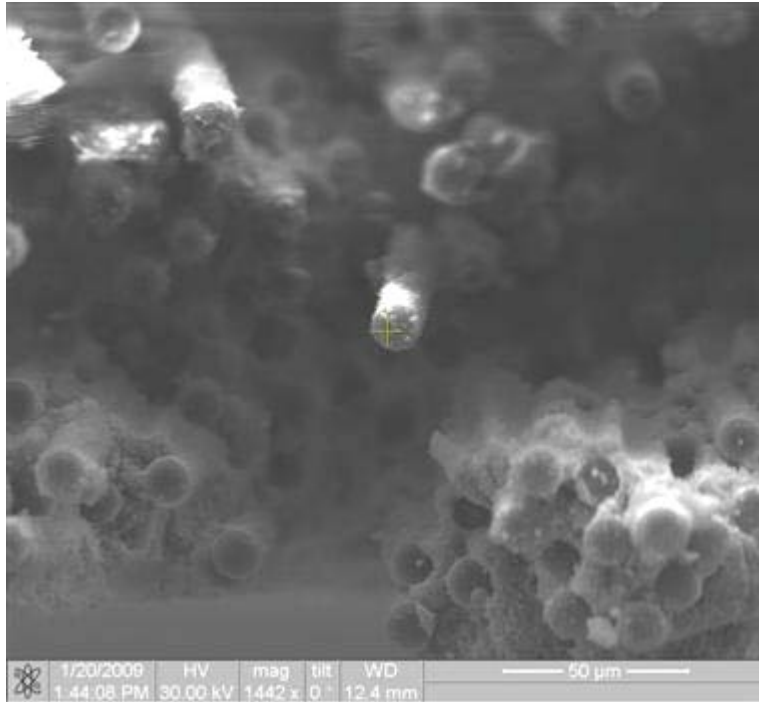


Figure 264. Fracture surface of the N720/AM specimen tested in creep at 131 MPa in laboratory air at 1100°C.

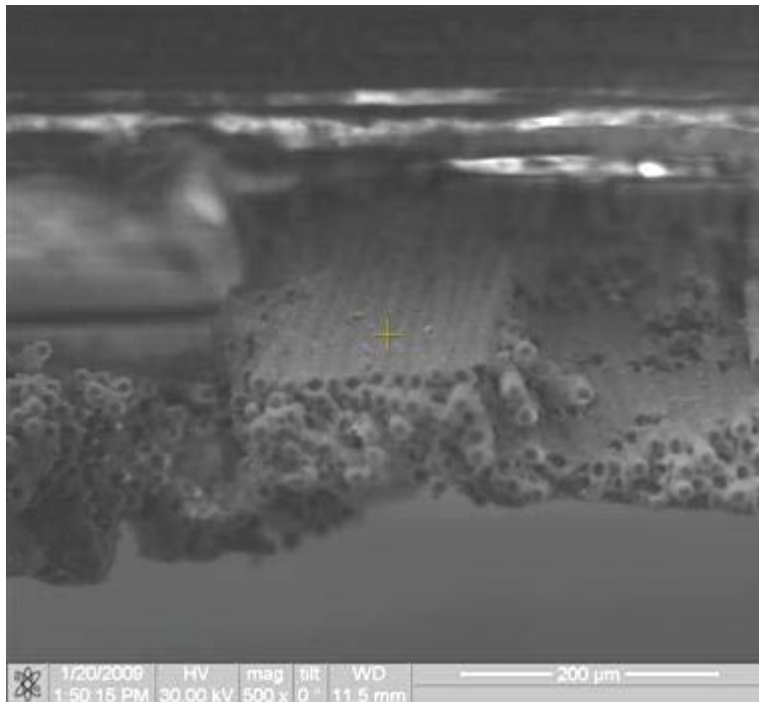


Figure 265. Fracture surface of the N720/AM specimen tested in creep at 131 MPa in laboratory air at 1100°C.

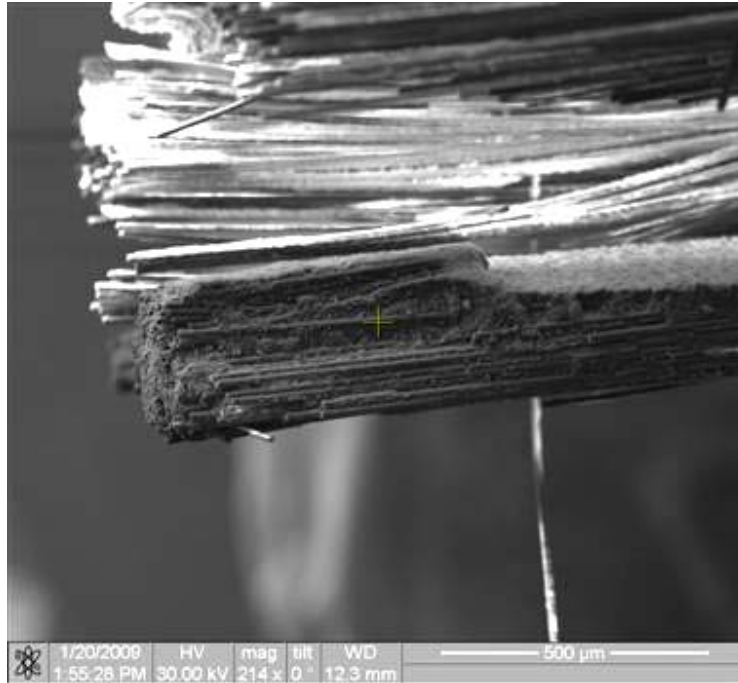


Figure 266. Fracture surface of the N720/AM specimen tested in creep at 131 MPa in laboratory air at 1100°C.

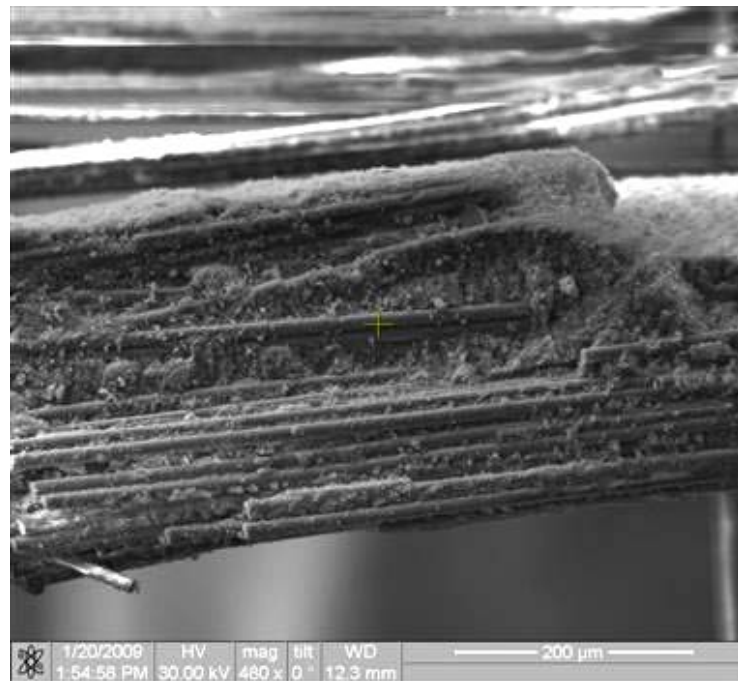


Figure 267. Fracture surface of the N720/AM specimen tested in creep at 131 MPa in laboratory air at 1100°C.

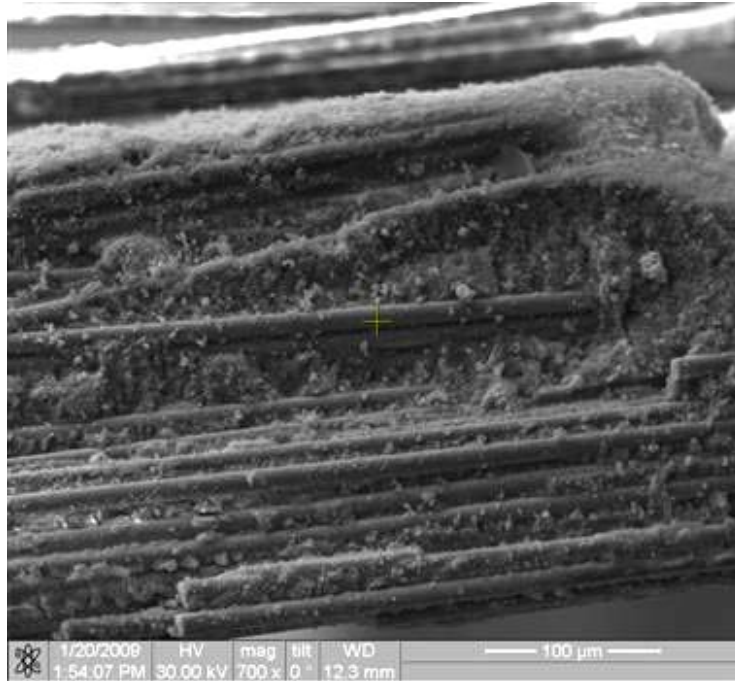


Figure 268. Fracture surface of the N720/AM specimen tested in creep at 131 MPa in laboratory air at 1100°C.

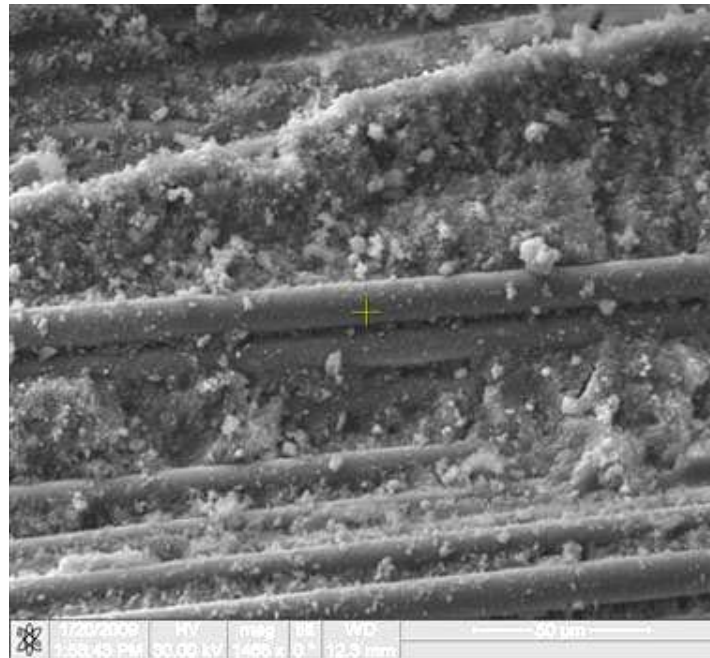


Figure 269. Fracture surface of the N720/AM specimen tested in creep at 131 MPa in laboratory air at 1100°C.

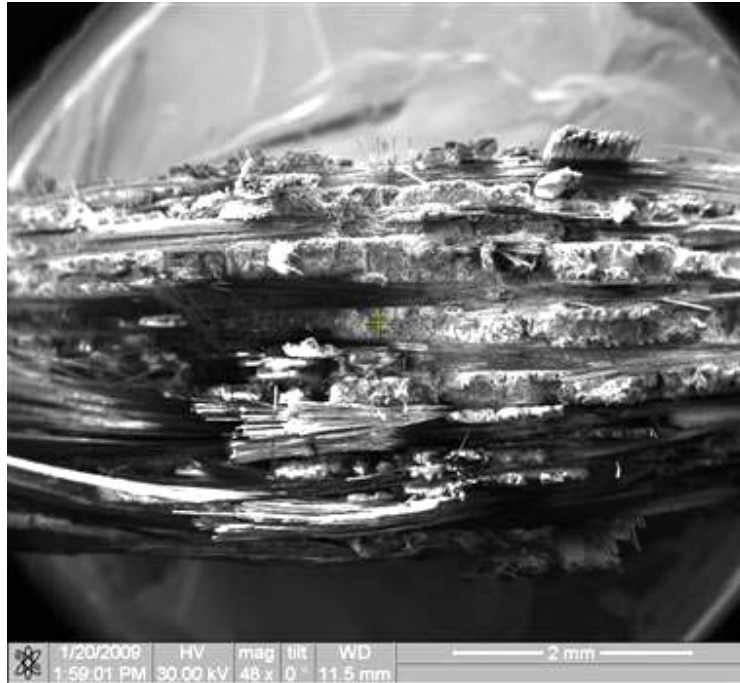


Figure 270. Fracture surface of the N720/AM specimen tested in creep at 131 MPa in laboratory air at 1100°C.



Figure 271. Fracture surface of the N720/AM specimen tested in creep at 131 MPa in laboratory air at 1100°C.

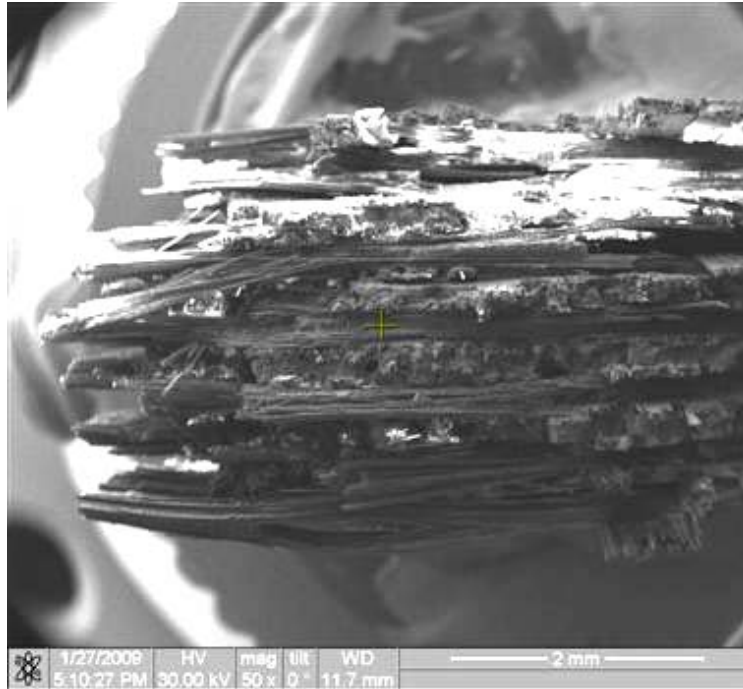


Figure 272. Fracture surface of the N720/AM specimen tested in creep at 131 MPa in laboratory air at 1100°C.

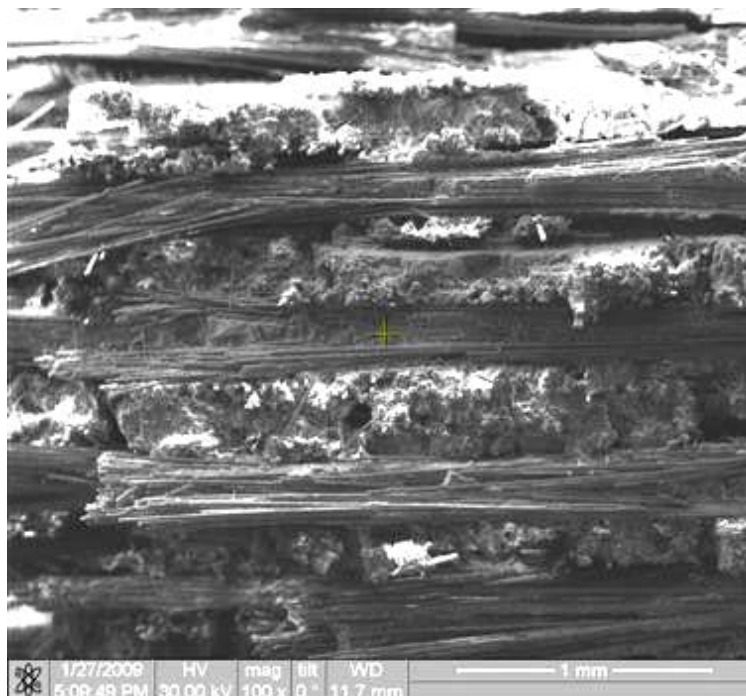


Figure 273. Fracture surface of the N720/AM specimen tested in creep at 131 MPa in laboratory air at 1100°C.

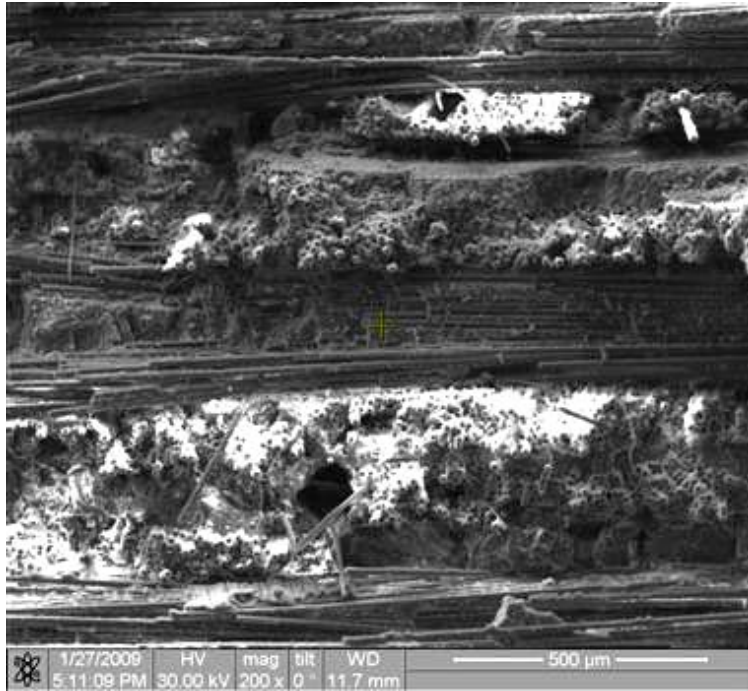


Figure 274. Fracture surface of the N720/AM specimen tested in creep at 131 MPa in laboratory air at 1100°C.

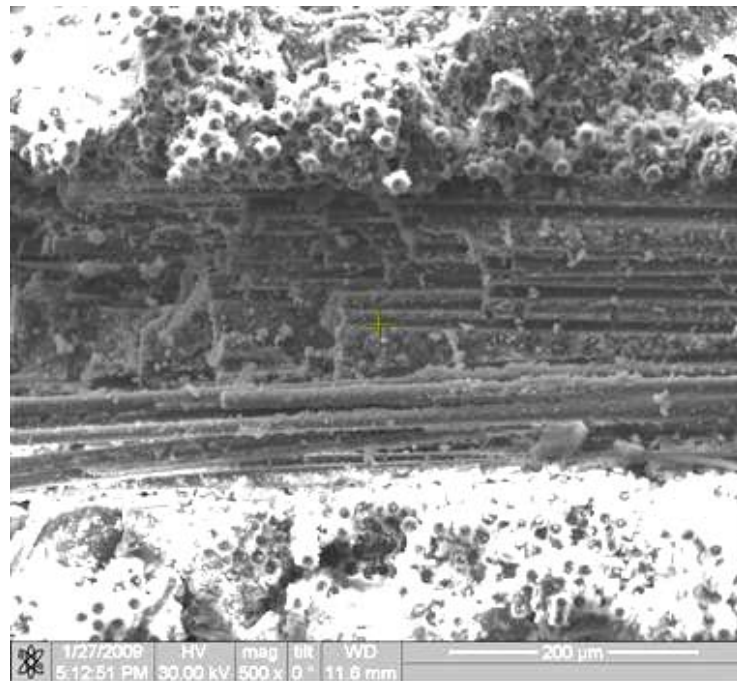


Figure 275. Fracture surface of the N720/AM specimen tested in creep at 131 MPa in laboratory air at 1100°C.

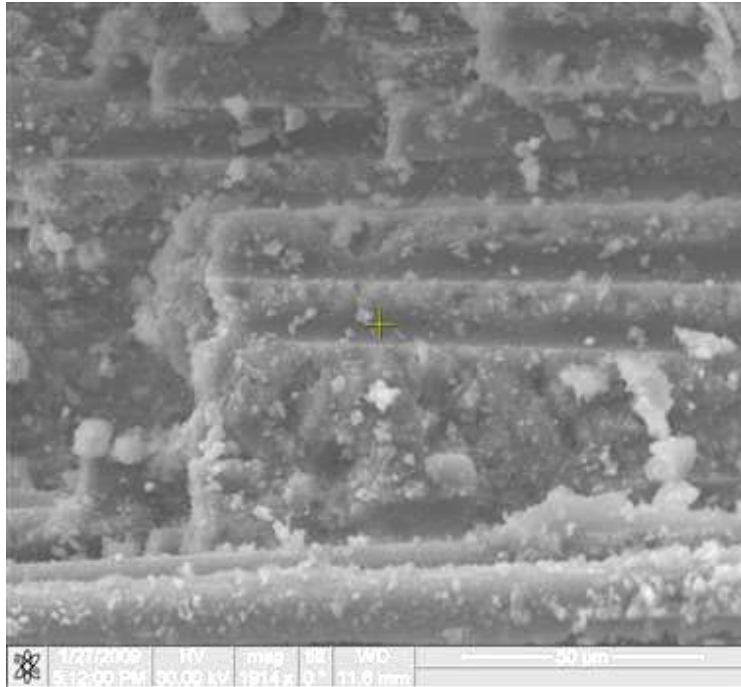


Figure 276. Fracture surface of the N720/AM specimen tested in creep at 131 MPa in laboratory air at 1100°C.

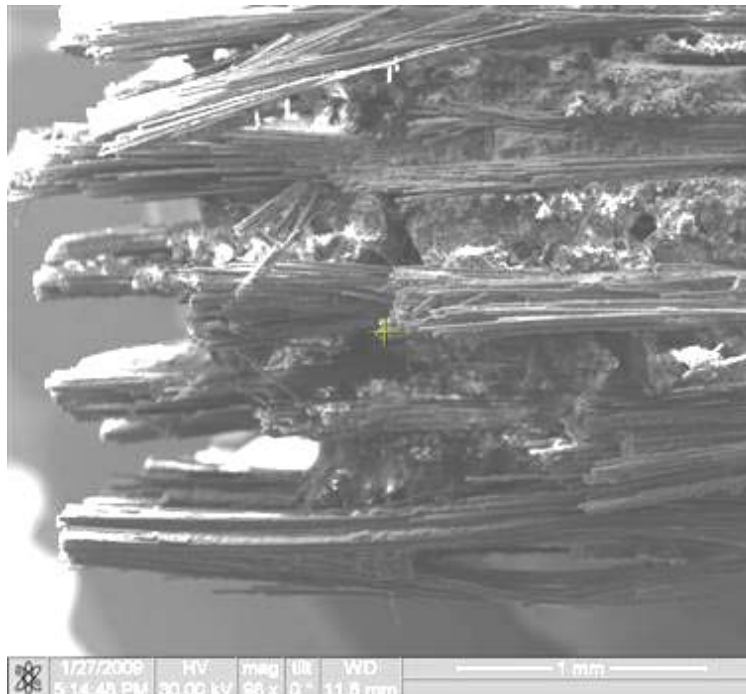


Figure 277. Fracture surface of the N720/AM specimen tested in creep at 131 MPa in laboratory air at 1100°C.

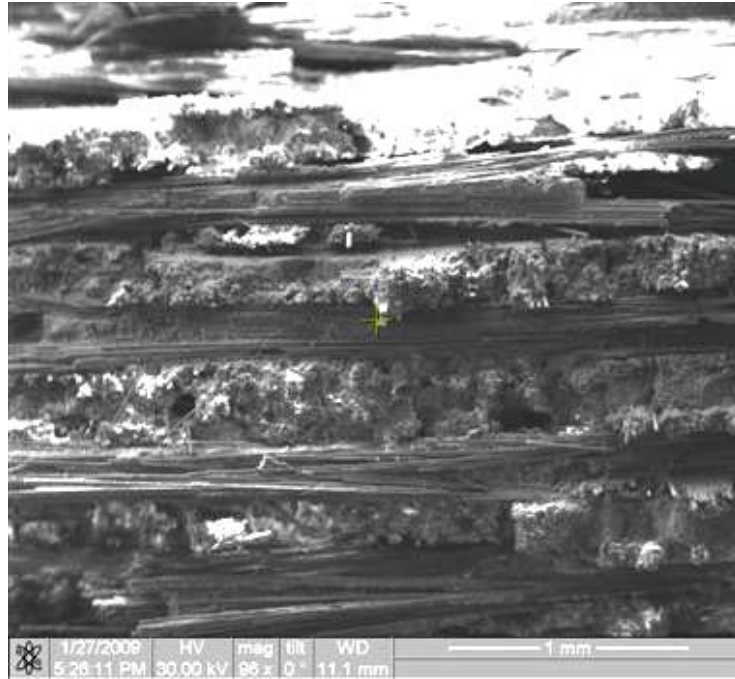


Figure 278. Fracture surface of the N720/AM specimen tested in creep at 131 MPa in laboratory air at 1100°C.

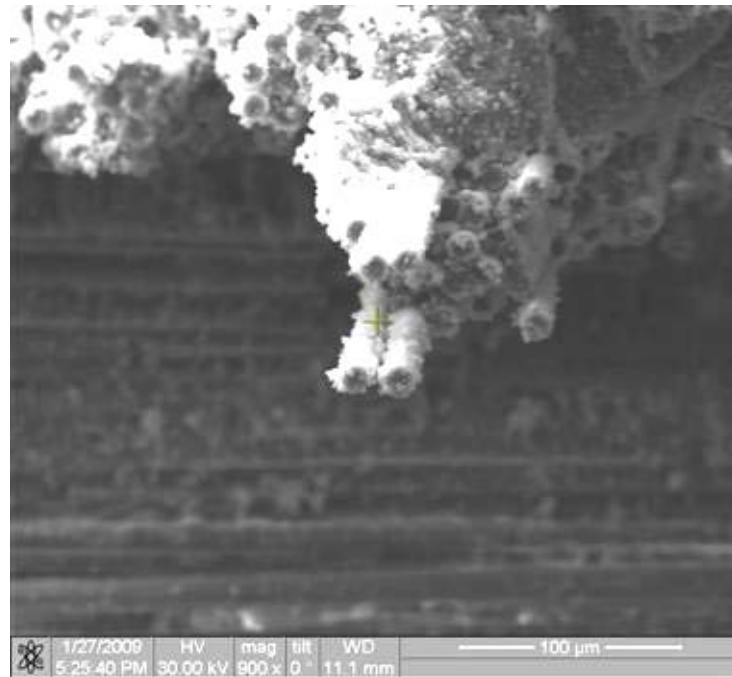


Figure 279. Fracture surface of the N720/AM specimen tested in creep at 131 MPa in laboratory air at 1100°C.

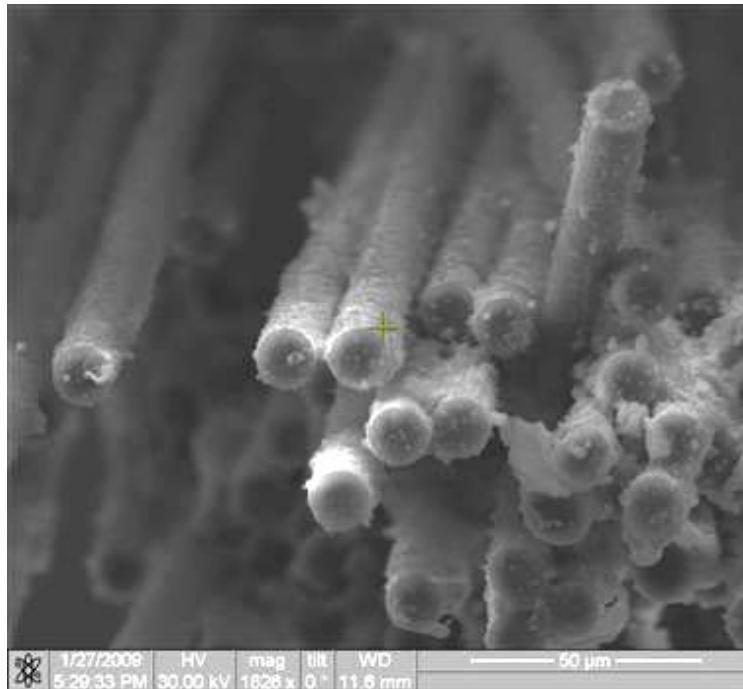


Figure 280. Fracture surface of the N720/AM specimen tested in creep at 131 MPa in laboratory air at 1100°C.

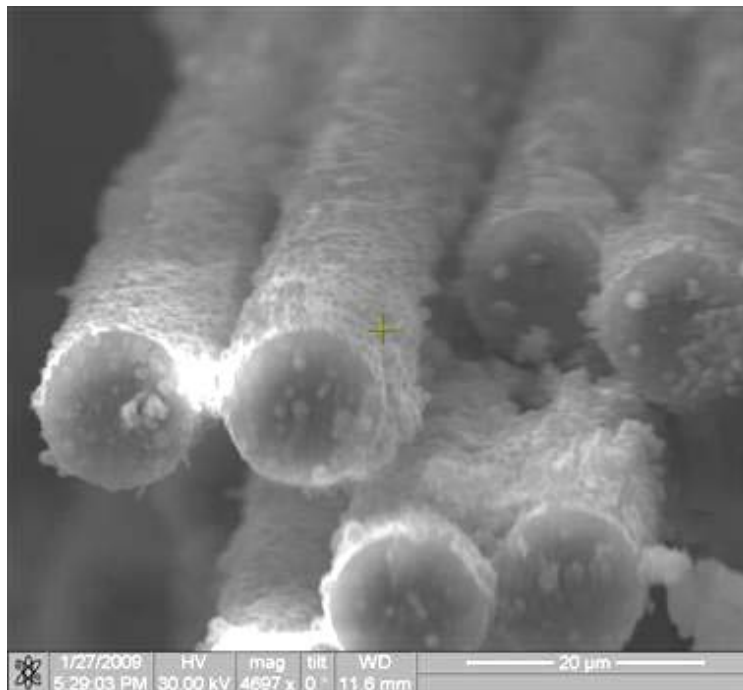


Figure 281. Fracture surface of the N720/AM specimen tested in creep at 131 MPa in laboratory air at 1100°C.

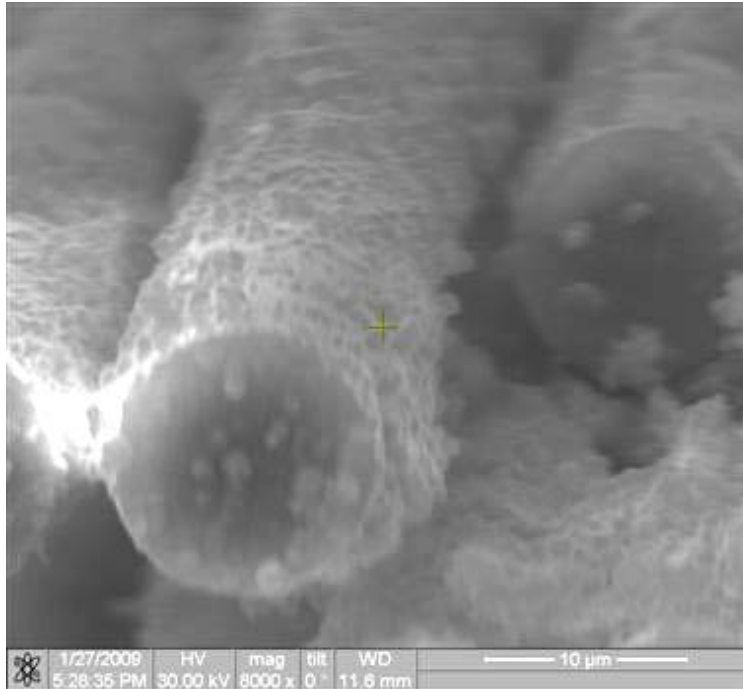


Figure 282. Fracture surface of the N720/AM specimen tested in creep at 131 MPa in laboratory air at 1100°C.

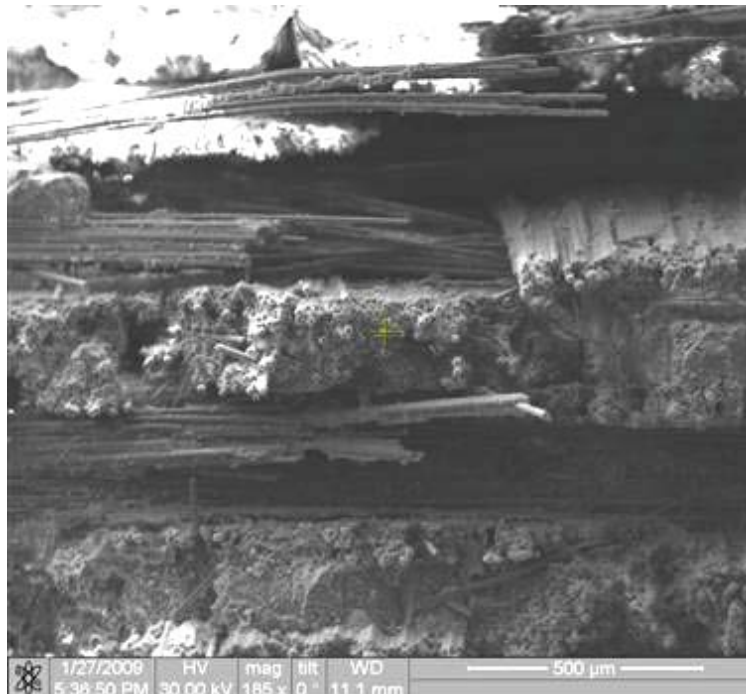


Figure 283. Fracture surface of the N720/AM specimen tested in creep at 131 MPa in laboratory air at 1100°C.

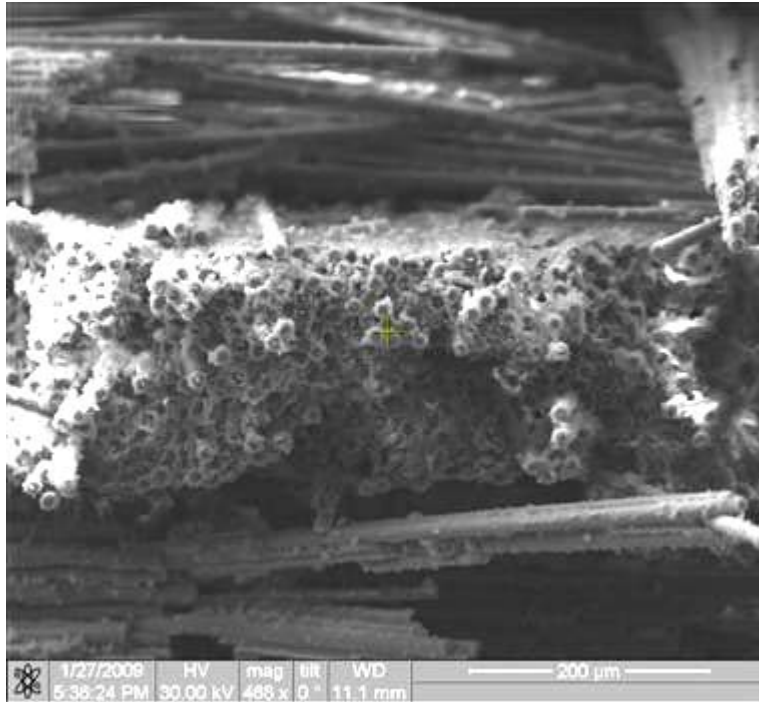


Figure 284. Fracture surface of the N720/AM specimen tested in creep at 131 MPa in laboratory air at 1100°C.

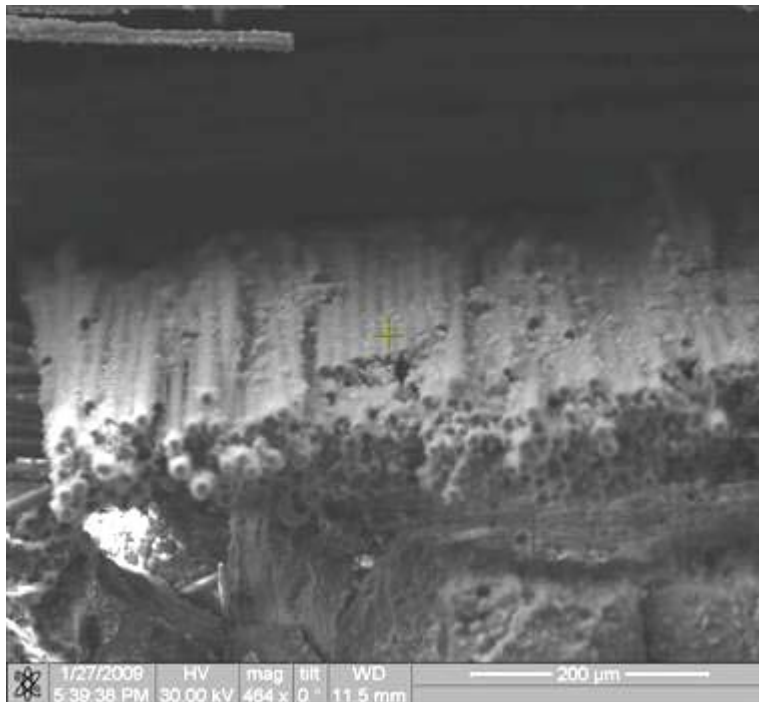


Figure 285. Fracture surface of the N720/AM specimen tested in creep at 131 MPa in laboratory air at 1100°C.

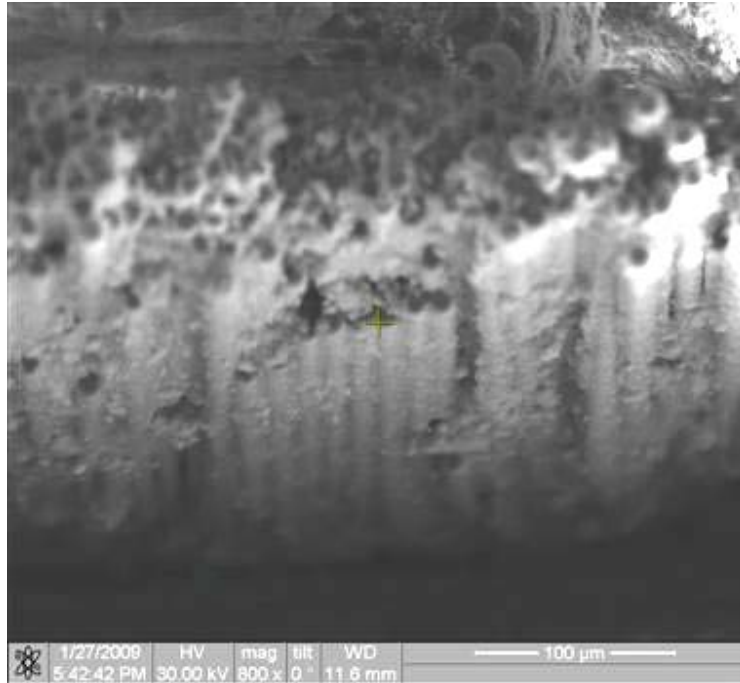


Figure 286. Fracture surface of the N720/AM specimen tested in creep at 131 MPa in laboratory air at 1100°C.

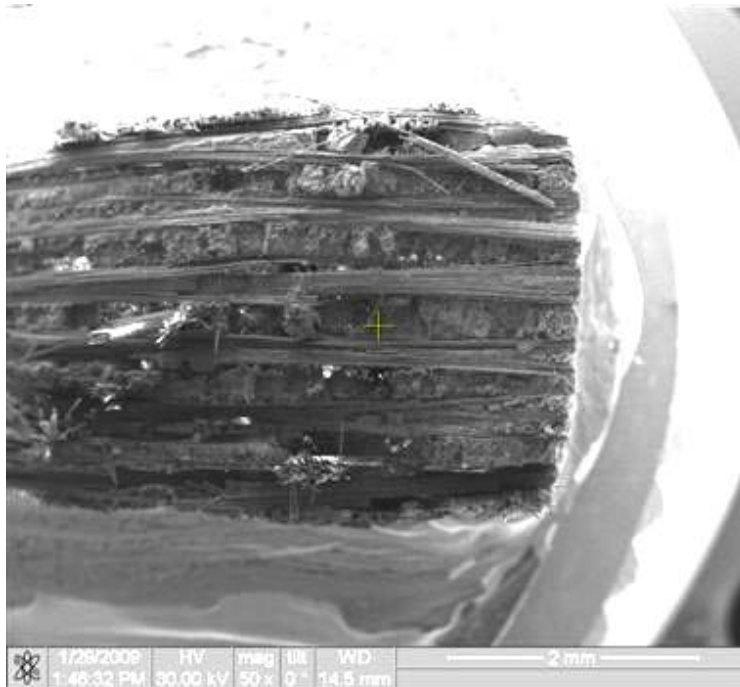


Figure 287. Fracture surface of the N720/AM specimen tested in creep at 131 MPa in laboratory air at 1100°C.

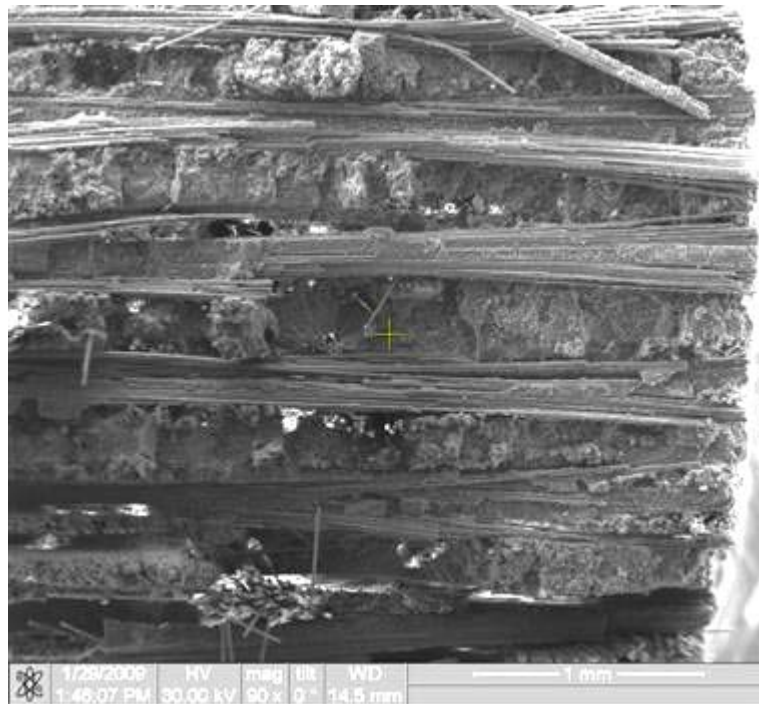


Figure 288. Fracture surface of the N720/AM specimen tested in creep at 131 MPa in steam at 1100°C.

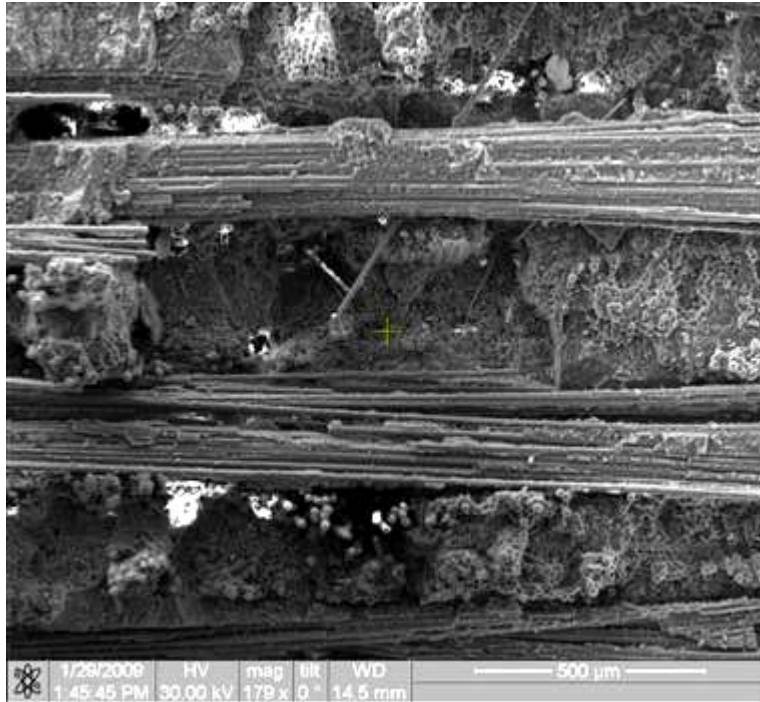


Figure 289. Fracture surface of the N720/AM specimen tested in creep at 131 MPa in steam at 1100°C.

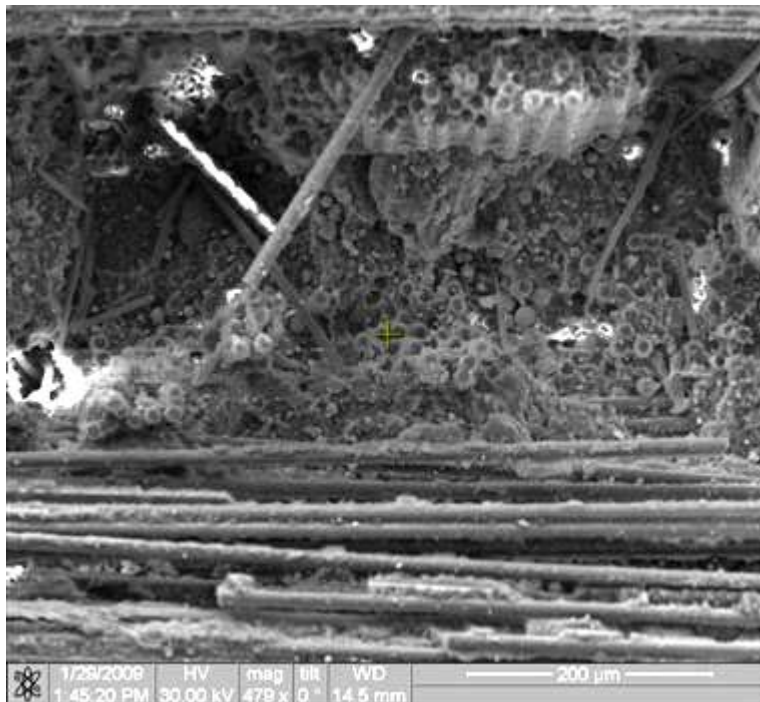


Figure 290. Fracture surface of the N720/AM specimen tested in creep at 131 MPa in steam at 1100°C.

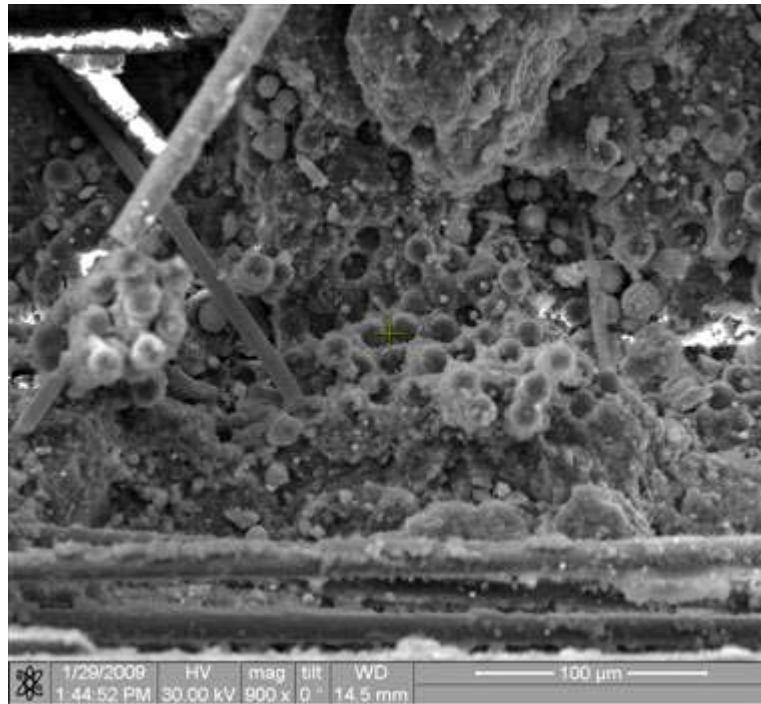


Figure 291. Fracture surface of the N720/AM specimen tested in creep at 131 MPa in steam at 1100°C.

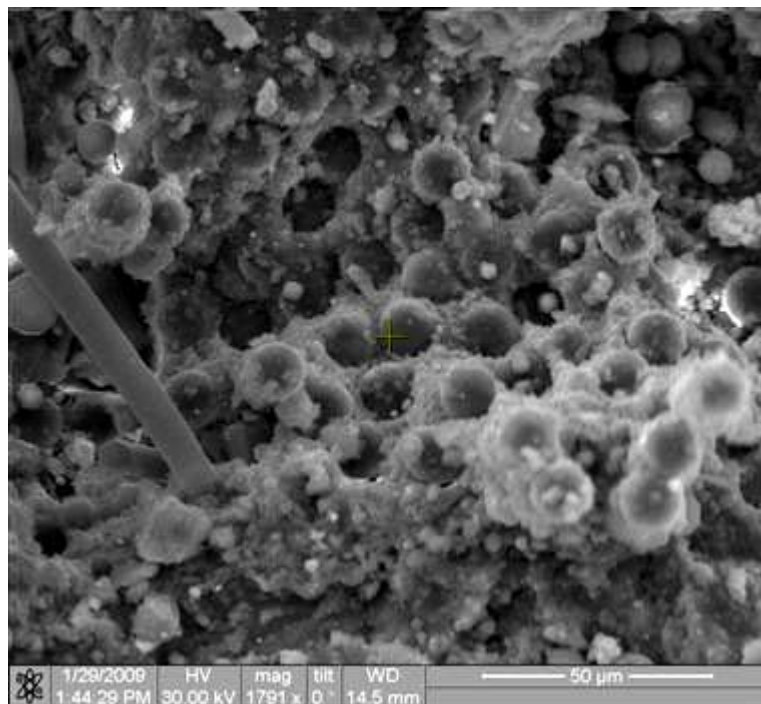


Figure 292. Fracture surface of the N720/AM specimen tested in creep at 131 MPa in steam at 1100°C.

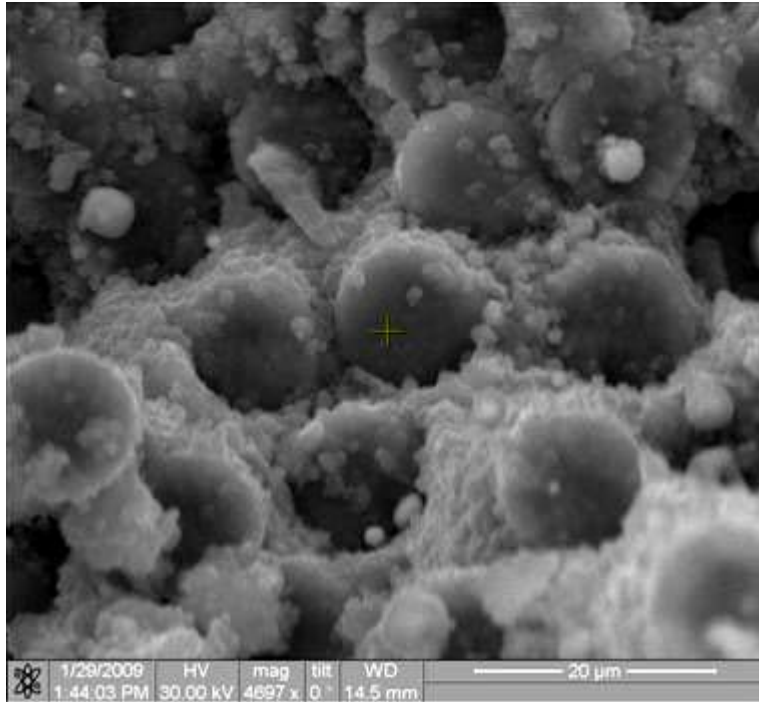


Figure 293. Fracture surface of the N720/AM specimen tested in creep at 131 MPa in steam at 1100°C.

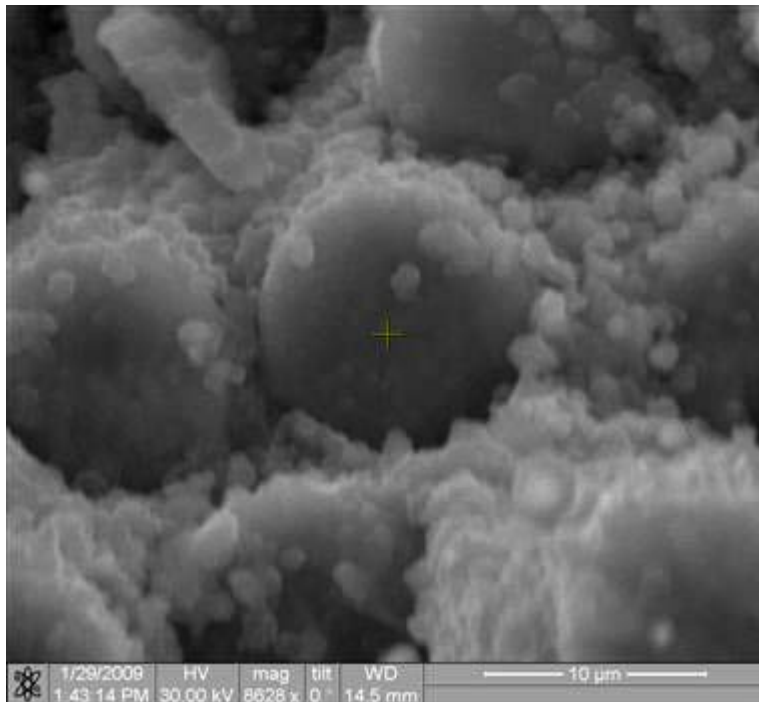


Figure 294. Fracture surface of the N720/AM specimen tested in creep at 131 MPa in steam at 1100°C.

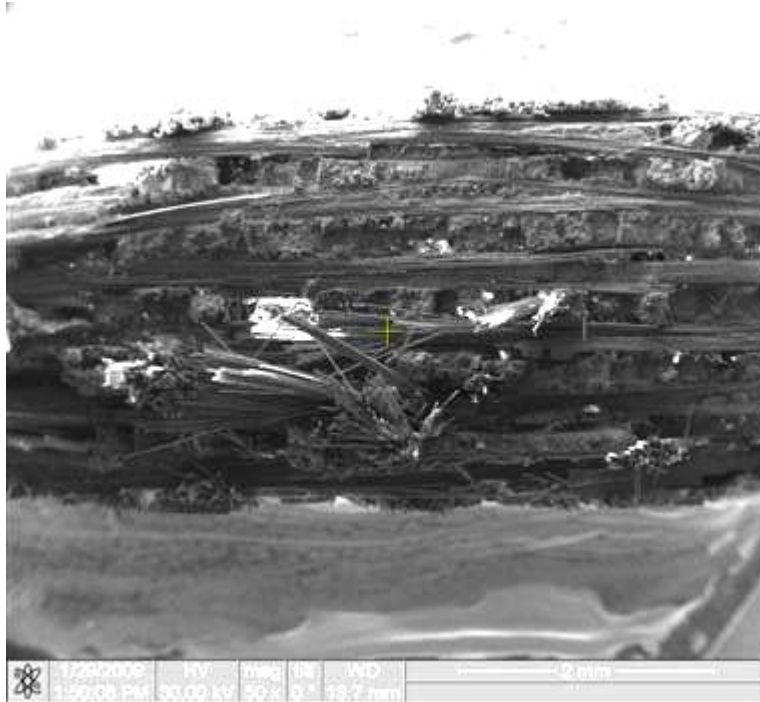


Figure 295. Fracture surface of the N720/AM specimen tested in creep at 131 MPa in steam at 1100°C.

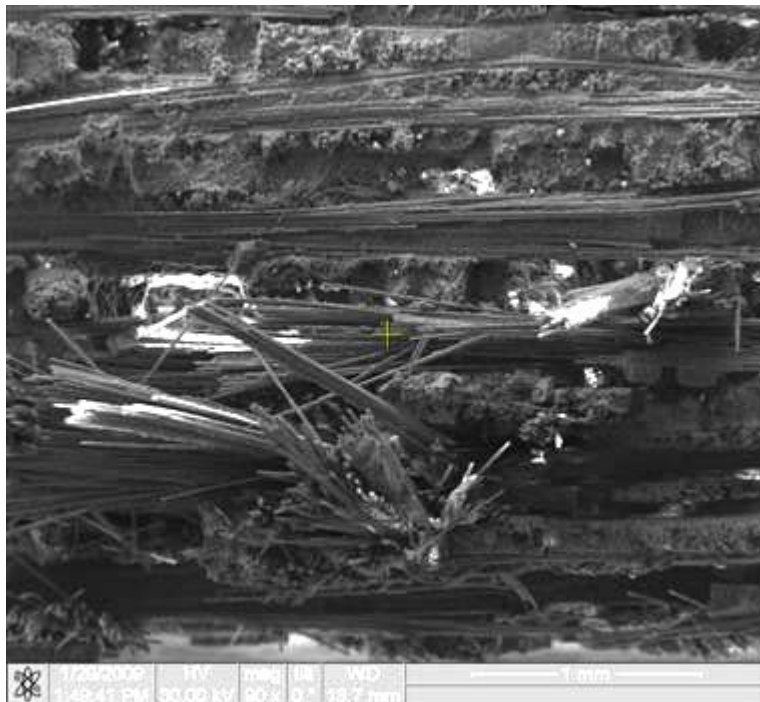


Figure 296. Fracture surface of the N720/AM specimen tested in creep at 131 MPa in steam at 1100°C.



Figure 297. Fracture surface of the N720/AM specimen tested in creep at 131 MPa in steam at 1100°C.

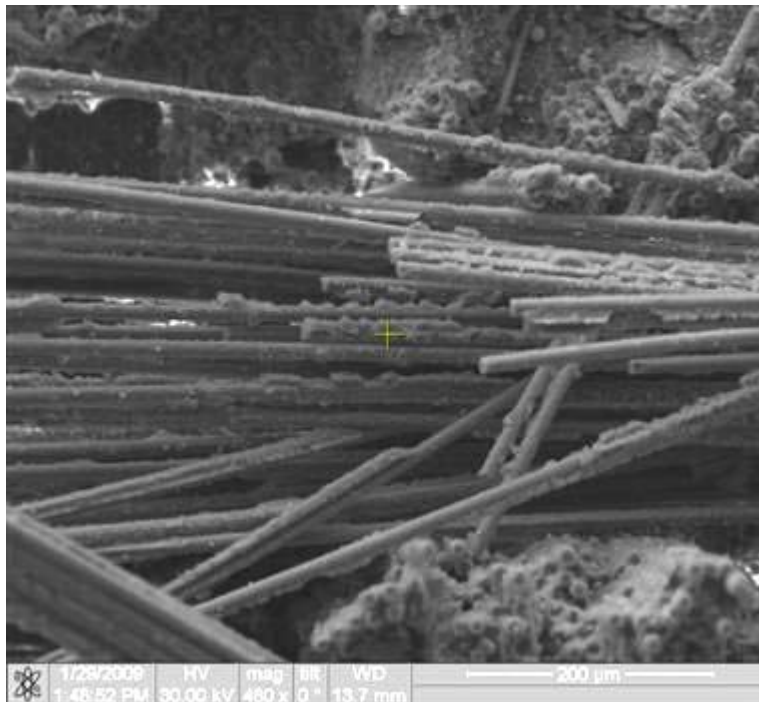


Figure 298. Fracture surface of the N720/AM specimen tested in creep at 131 MPa in steam at 1100°C.

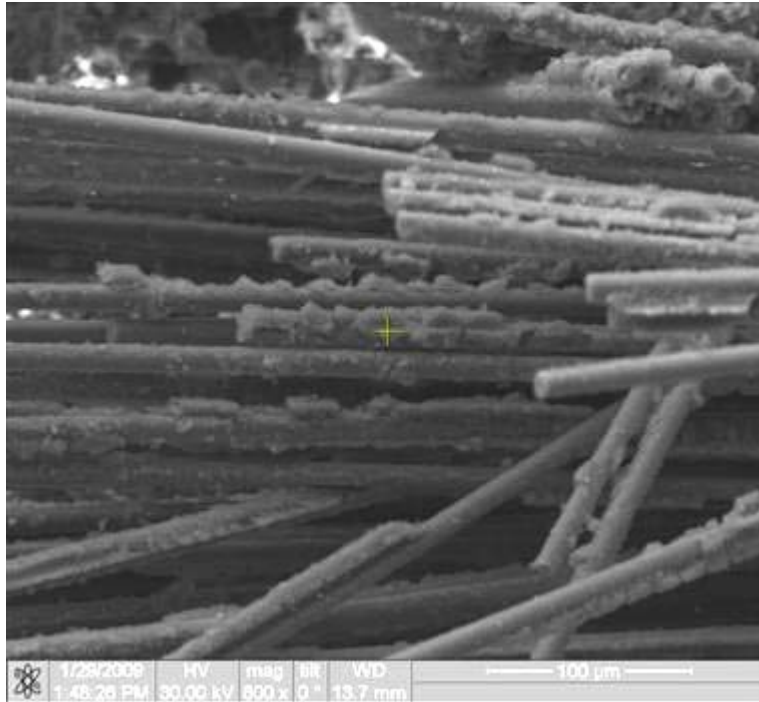


Figure 299. Fracture surface of the N720/AM specimen tested in creep at 131 MPa in steam at 1100°C.

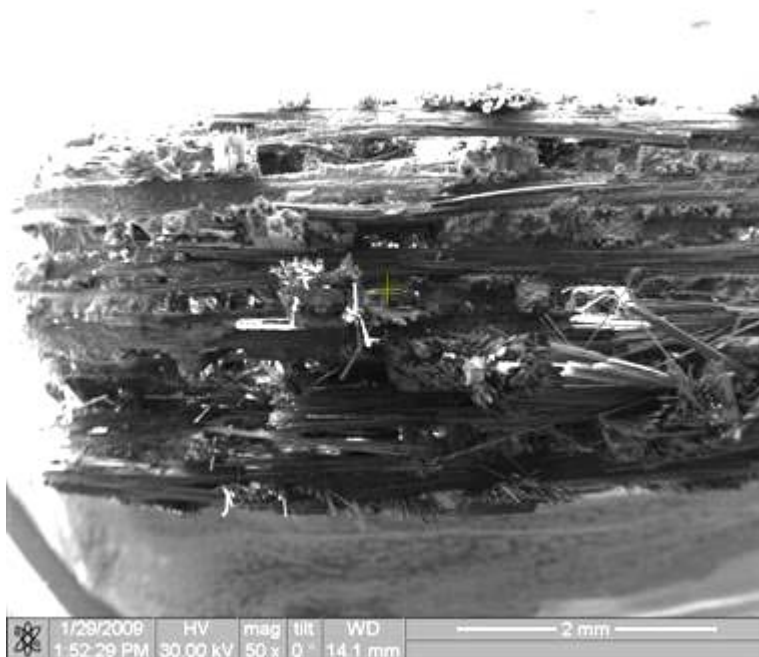


Figure 300. Fracture surface of the N720/AM specimen tested in creep at 131 MPa in steam at 1100°C.

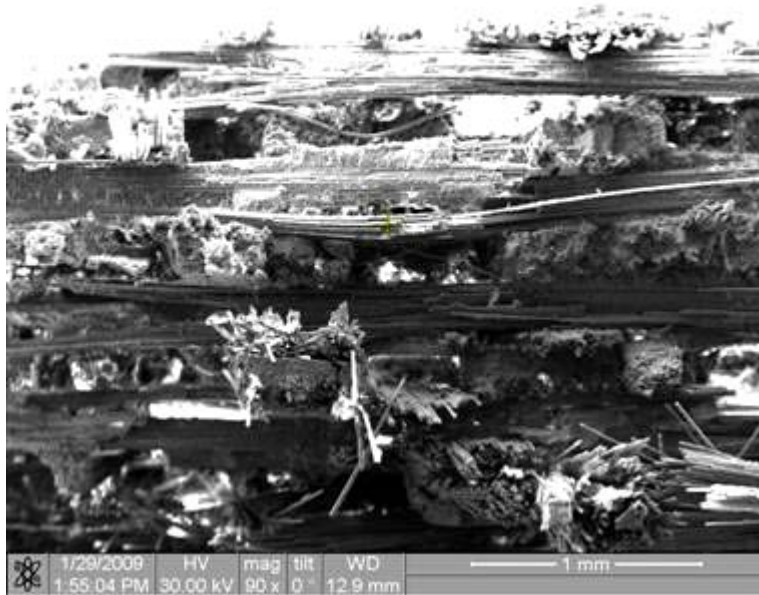


Figure 301. Fracture surface of the N720/AM specimen tested in creep at 131 MPa in steam at 1100°C.

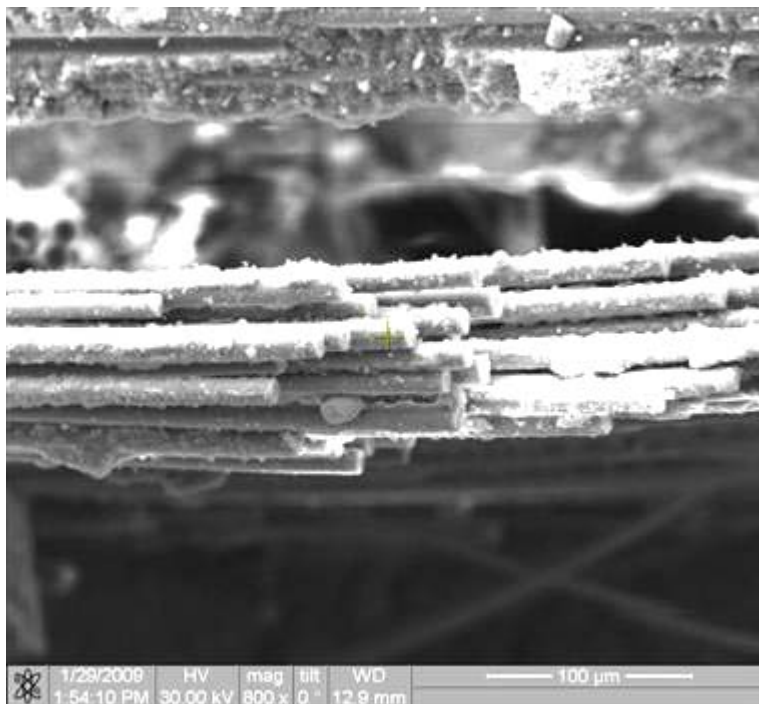


Figure 302. Fracture surface of the N720/AM specimen tested in creep at 131 MPa in steam at 1100°C.

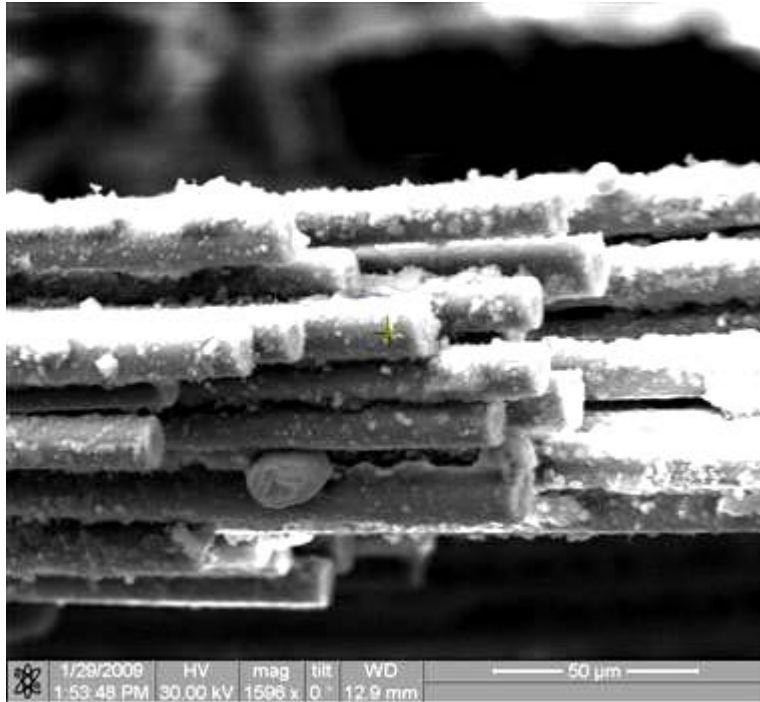


Figure 303. Fracture surface of the N720/AM specimen tested in creep at 131 MPa in steam at 1100°C.

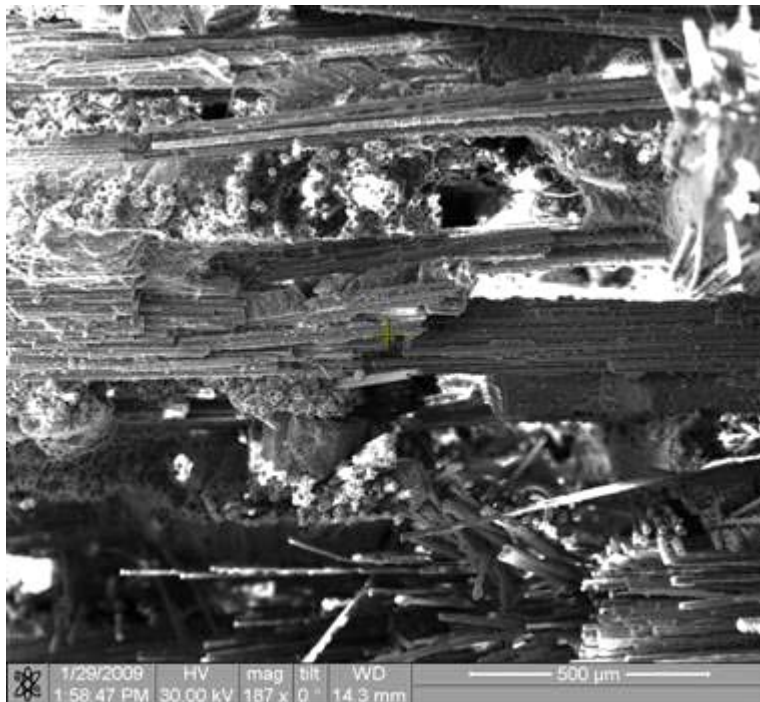


Figure 304. Fracture surface of the N720/AM specimen tested in creep at 131 MPa in steam at 1100°C.

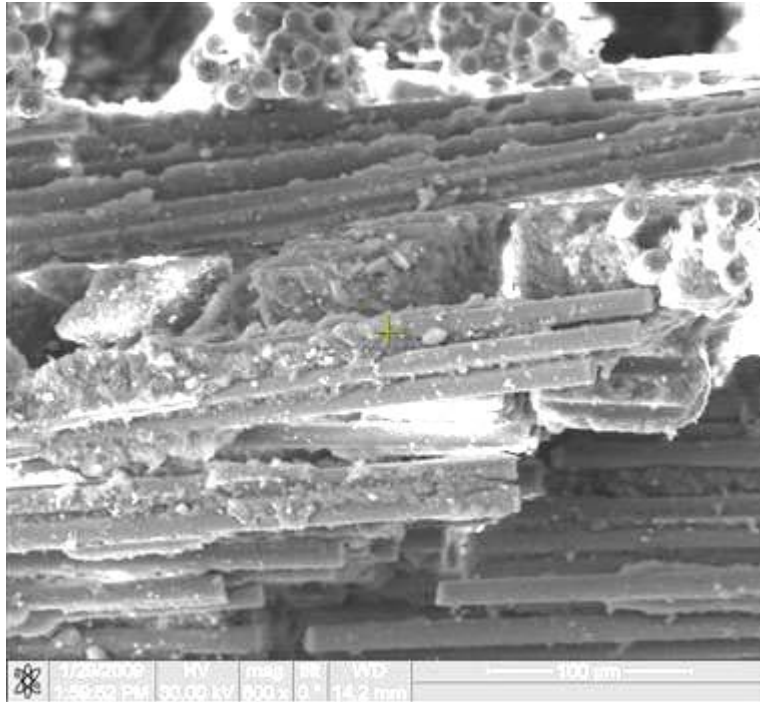


Figure 305. Fracture surface of the N720/AM specimen tested in creep at 131 MPa in steam at 1100°C.

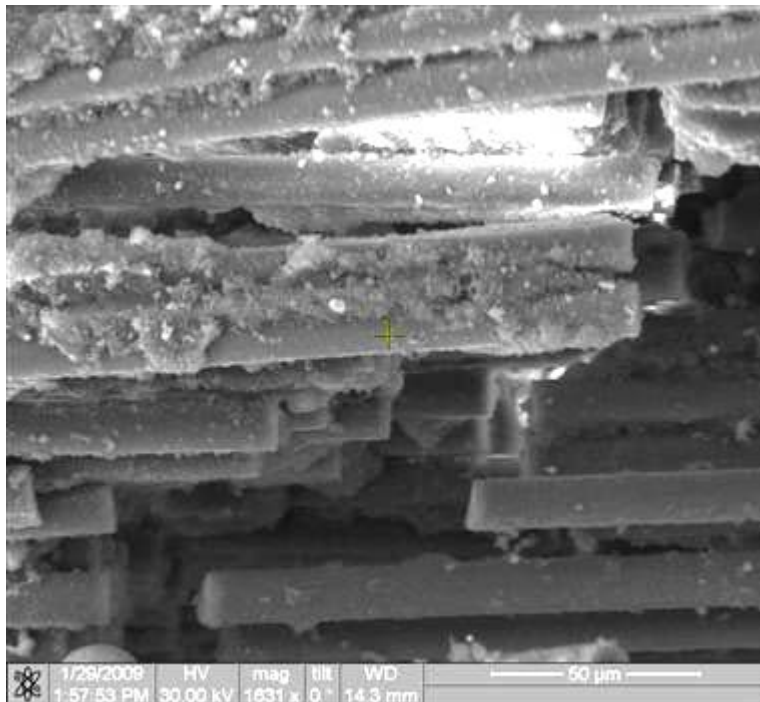


Figure 306. Fracture surface of the N720/AM specimen tested in creep at 131 MPa in steam at 1100°C.

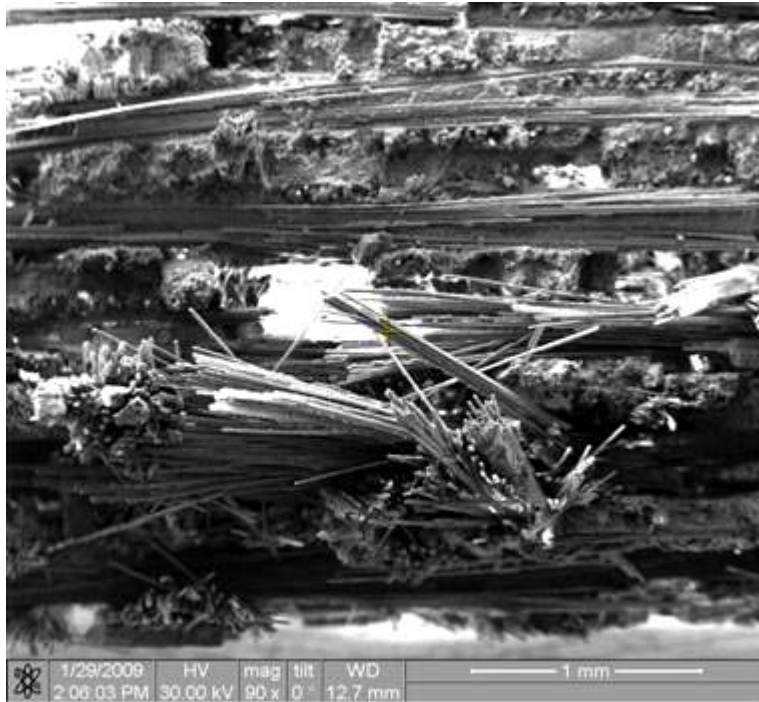


Figure 307. Fracture surface of the N720/AM specimen tested in creep at 131 MPa in steam at 1100°C.

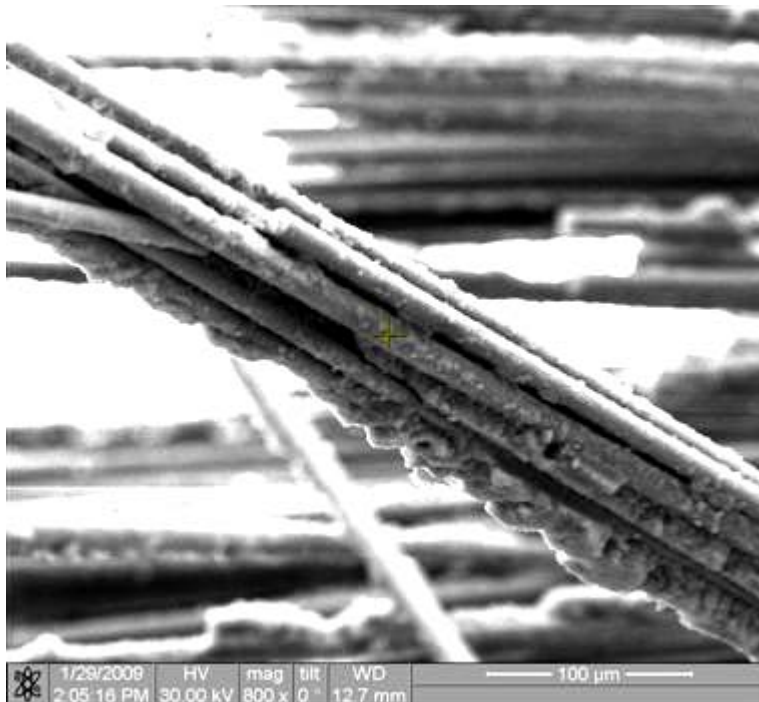


Figure 308. Fracture surface of the N720/AM specimen tested in creep at 131 MPa in steam at 1100°C.

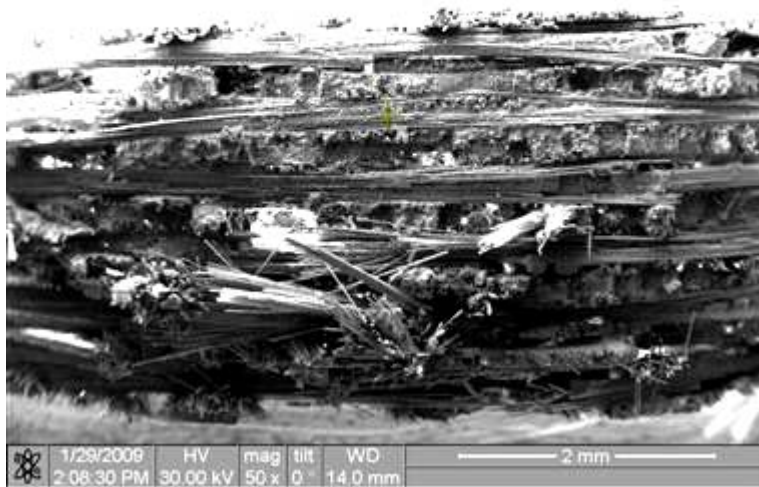


Figure 309. Fracture surface of the N720/AM specimen tested in creep at 131 MPa in steam at 1100°C.



Figure 310. Fracture surface of the N720/AM specimen tested in creep at 131 MPa in steam at 1100°C.

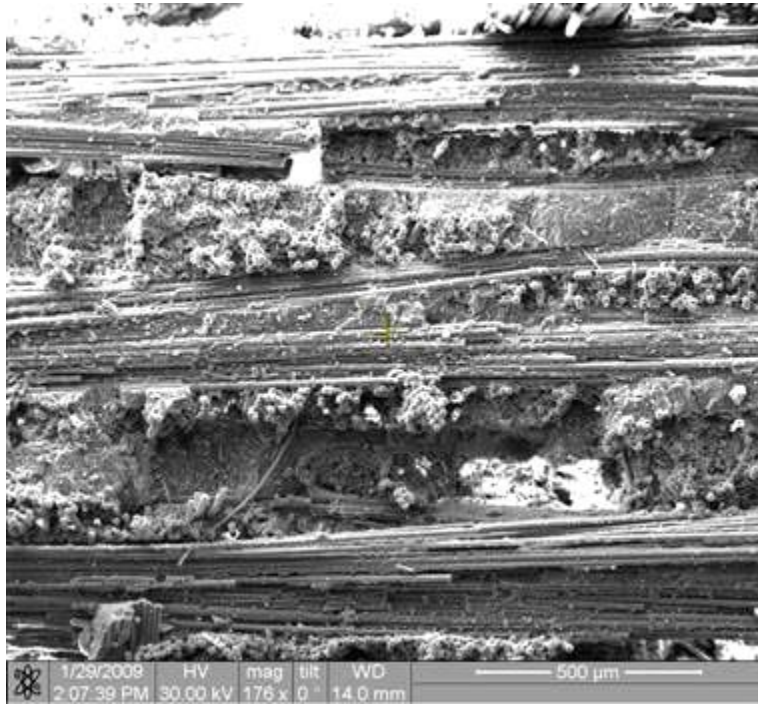


Figure 311. Fracture surface of the N720/AM specimen tested in creep at 131 MPa in steam at 1100°C.

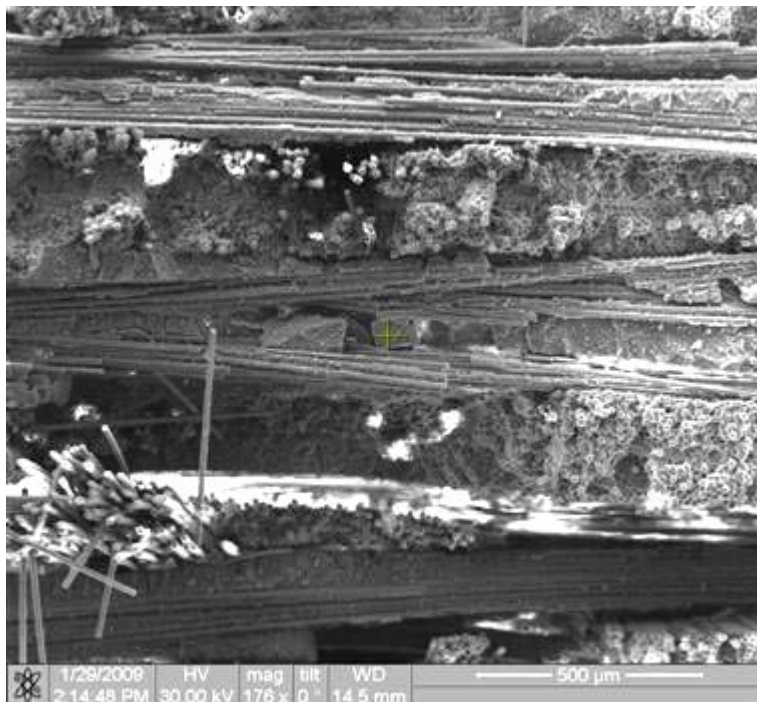


Figure 312. Fracture surface of the N720/AM specimen tested in creep at 131 MPa in steam at 1100°C.



Figure 313. Fracture surface of the N720/AM specimen tested in creep at 131 MPa in steam at 1100°C.

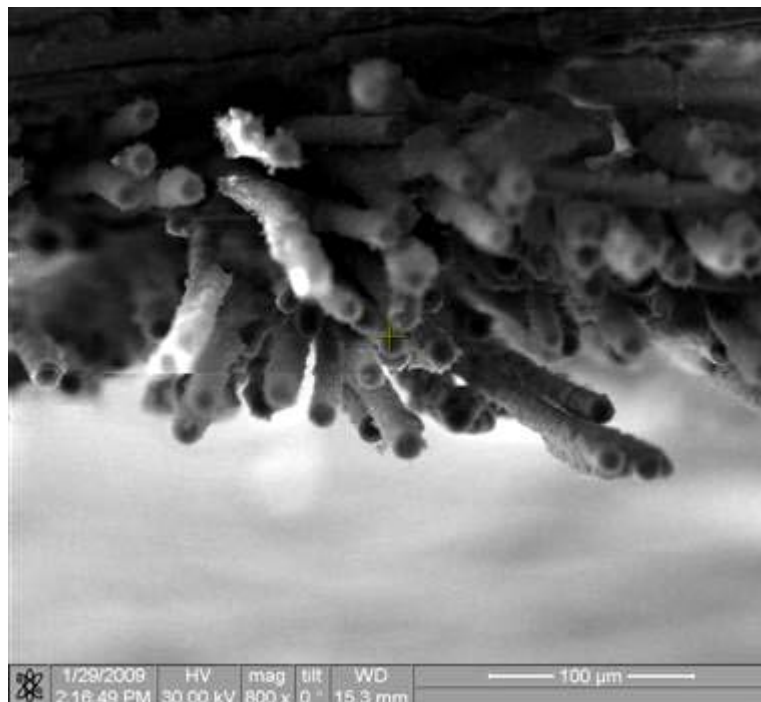


Figure 314. Fracture surface of the N720/AM specimen tested in creep at 131 MPa in steam at 1100°C.

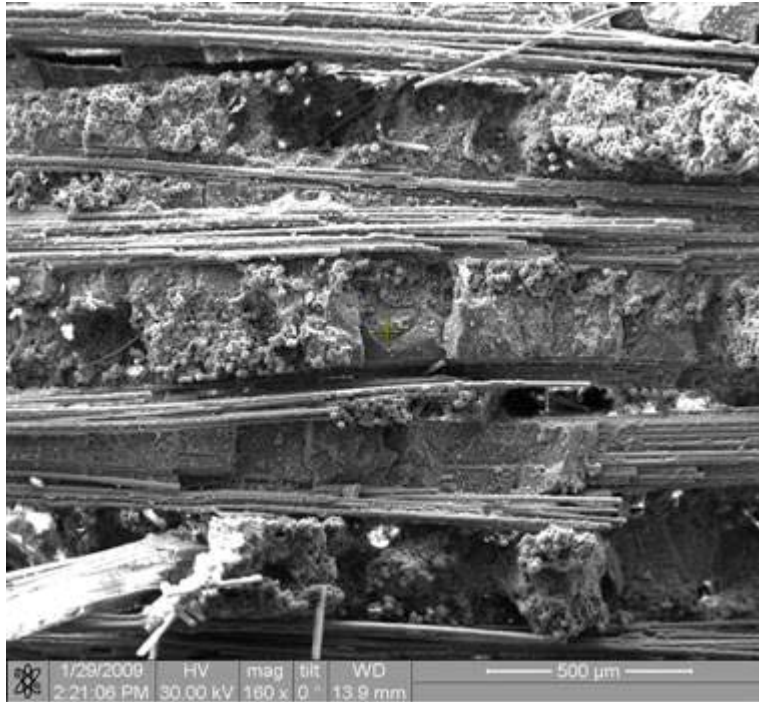


Figure 315. Fracture surface of the N720/AM specimen tested in creep at 131 MPa in steam at 1100°C.

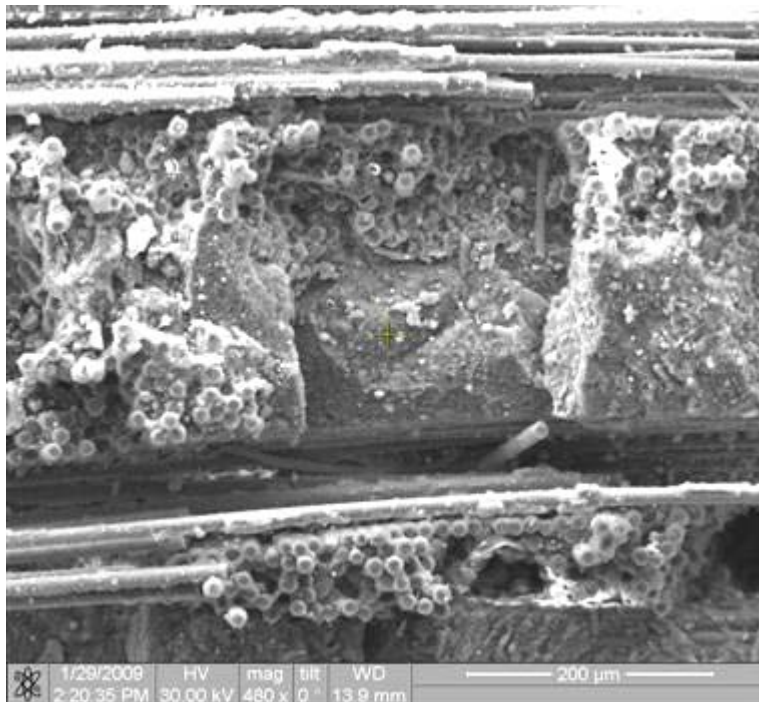


Figure 316. Fracture surface of the N720/AM specimen tested in creep at 131 MPa in steam at 1100°C.

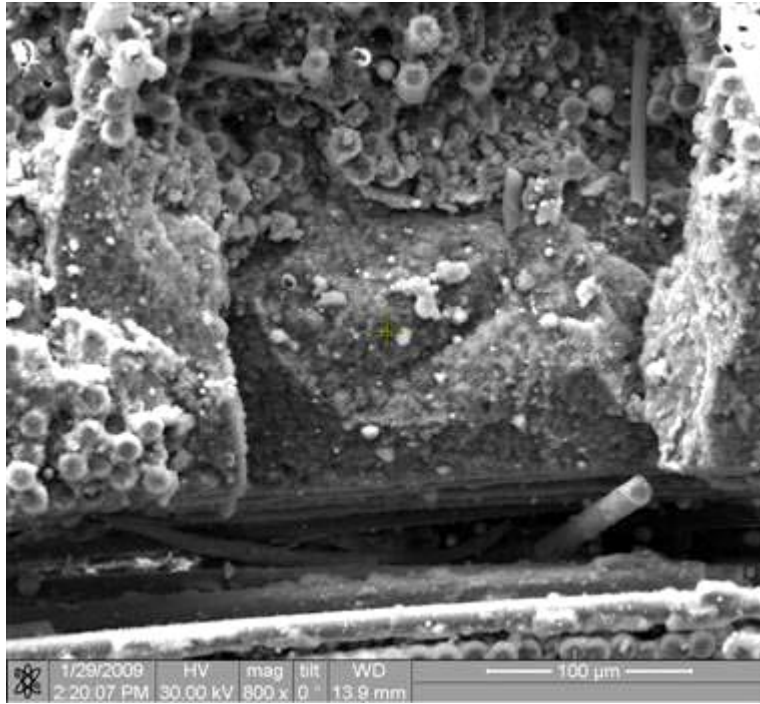


Figure 317. Fracture surface of the N720/AM specimen tested in creep at 131 MPa in steam at 1100°C.

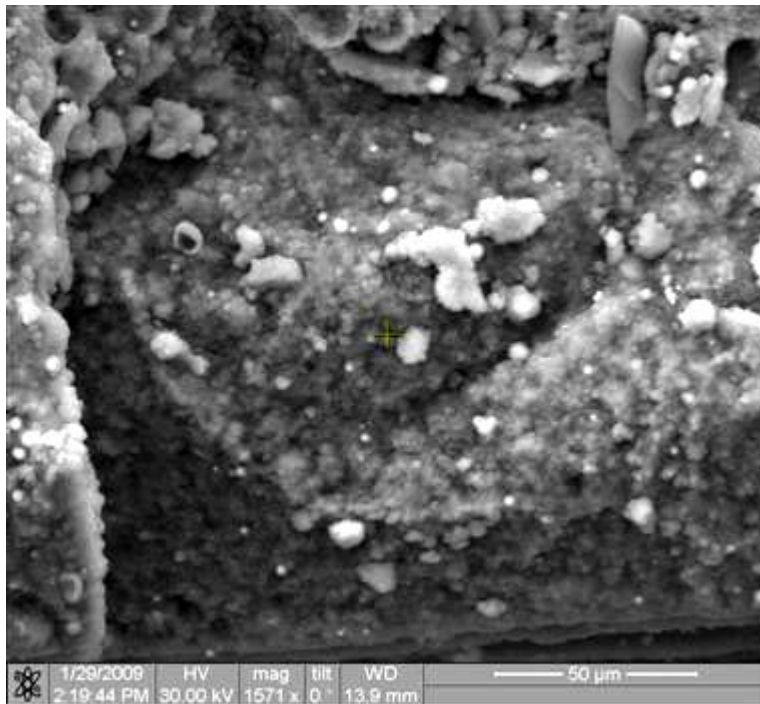


Figure 318. Fracture surface of the N720/AM specimen tested in creep at 131 MPa in steam at 1100°C.

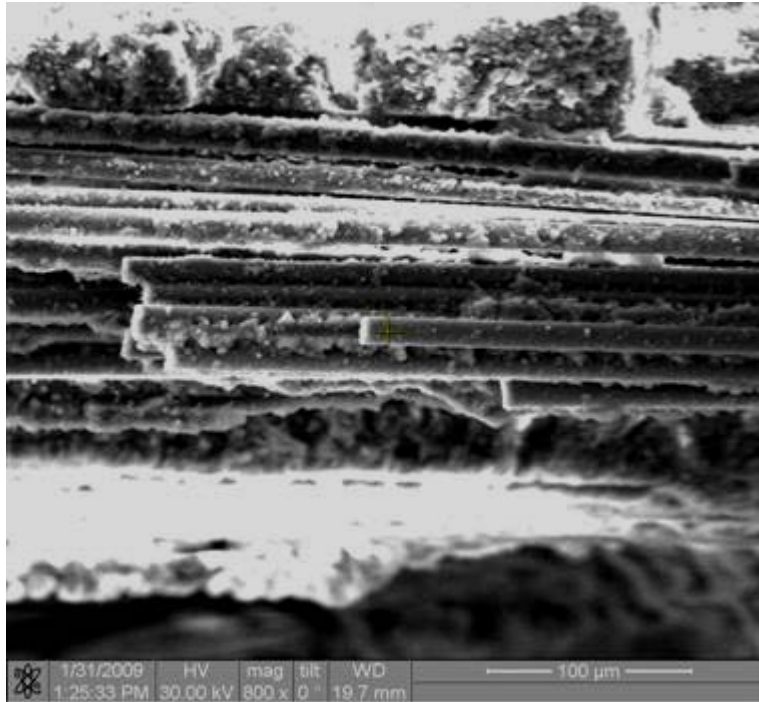


Figure 319. Fracture surface of the N720/AM specimen tested in creep at 131 MPa in steam at 1100°C.

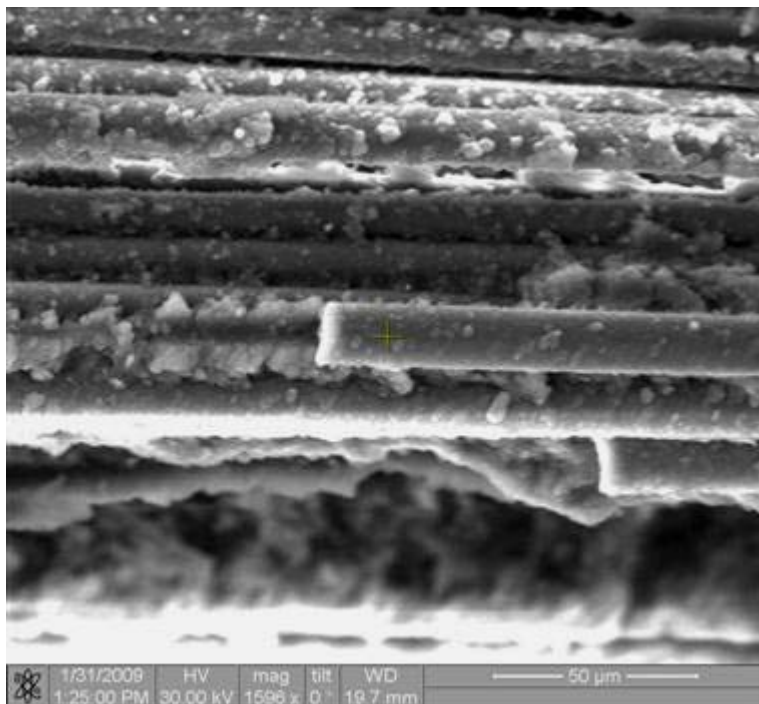


Figure 320. Fracture surface of the N720/AM specimen tested in creep at 109 MPa in steam at 1100°C.

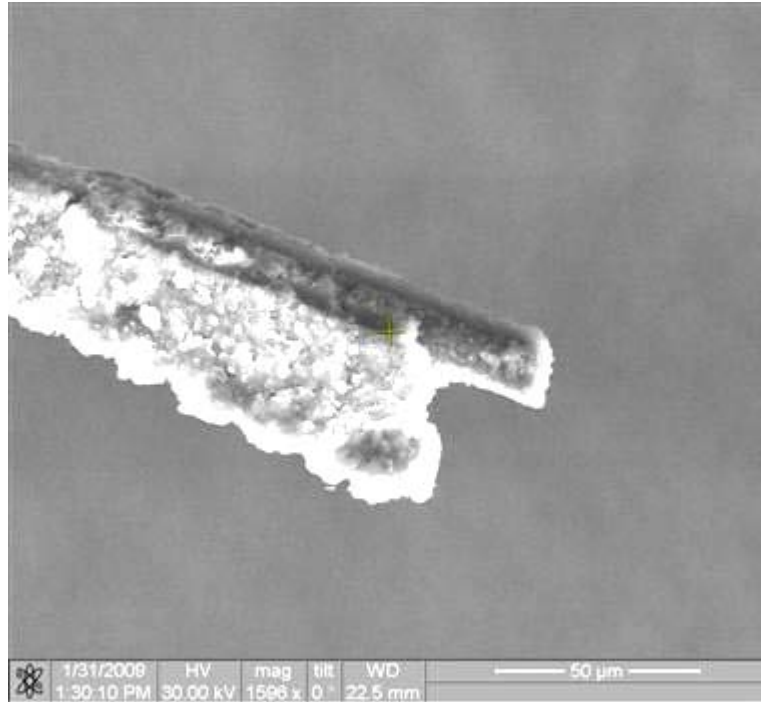


Figure 321. Fracture surface of the N720/AM specimen tested in creep at 109 MPa in steam at 1100°C.

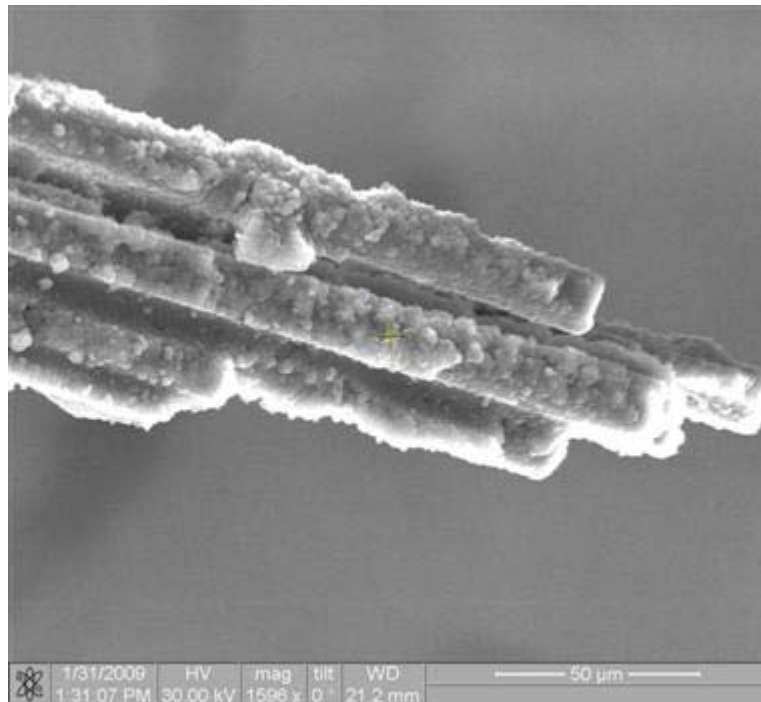


Figure 322. Fracture surface of the N720/AM specimen tested in creep at 109 MPa in steam at 1100°C.

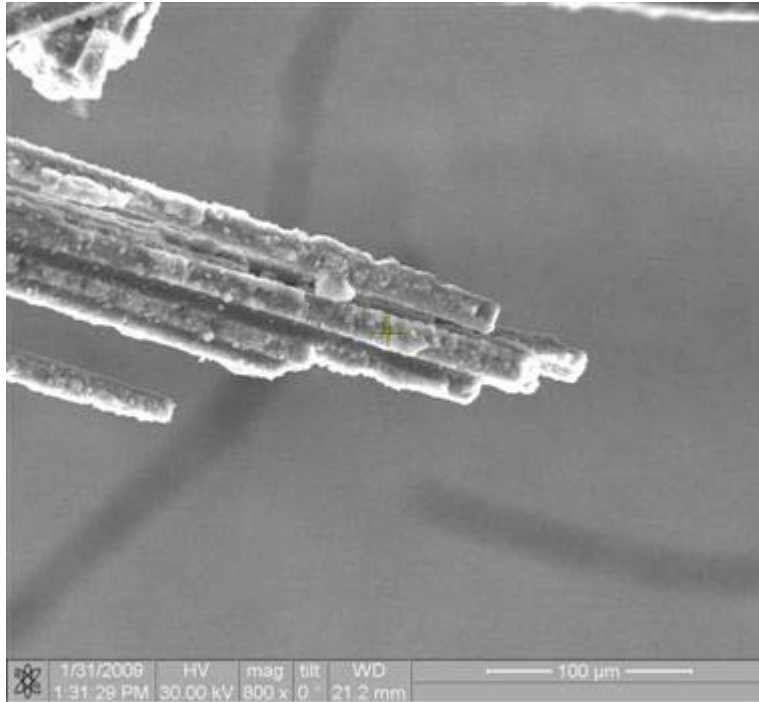


Figure 323. Fracture surface of the N720/AM specimen tested in creep at 109 MPa in steam at 1100°C.

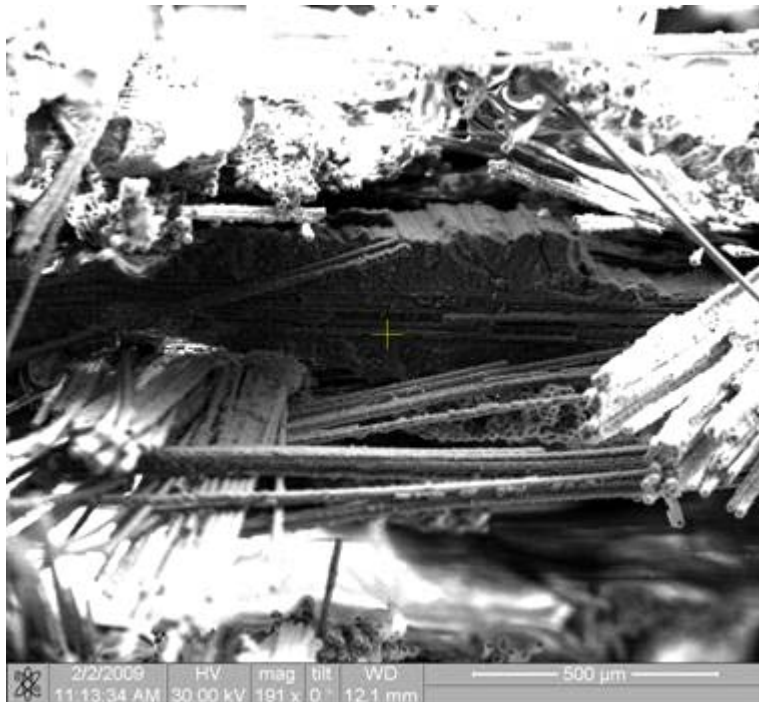


Figure 324. Fracture surface of the N720/AM specimen tested in creep at 109 MPa in steam at 1100°C..



Figure 325. Fracture surface of the N720/AM specimen tested in creep at 109 MPa in steam at 1100°C.

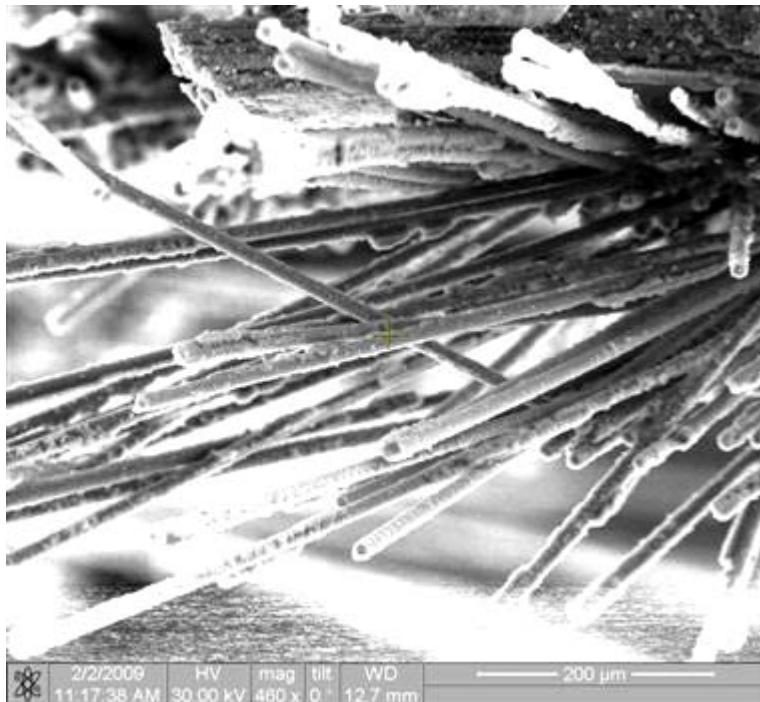


Figure 326. Fracture surface of the N720/AM specimen tested in creep at 109 MPa in steam at 1100°C.

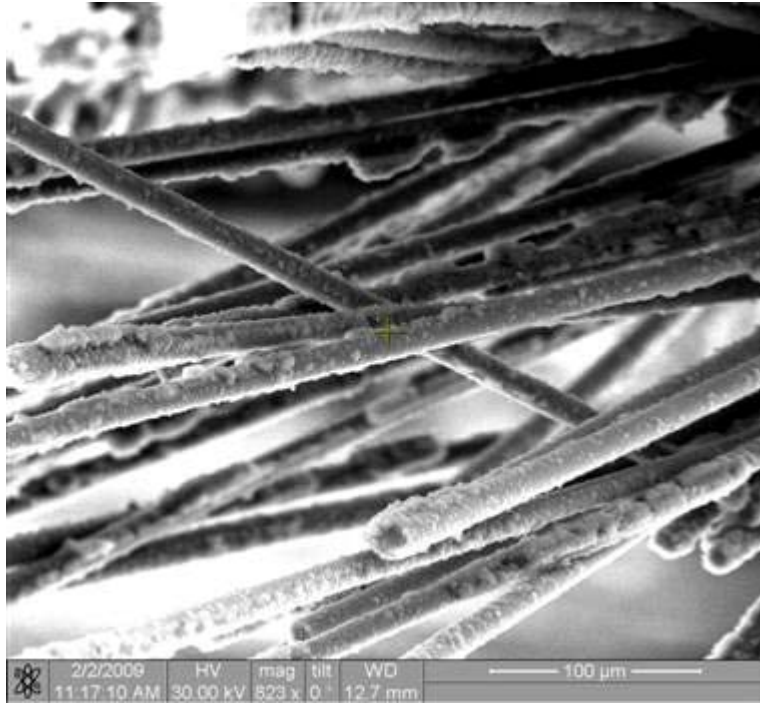


Figure 327. Fracture surface of the N720/AM specimen tested in creep at 109 MPa in steam at 1100°C.

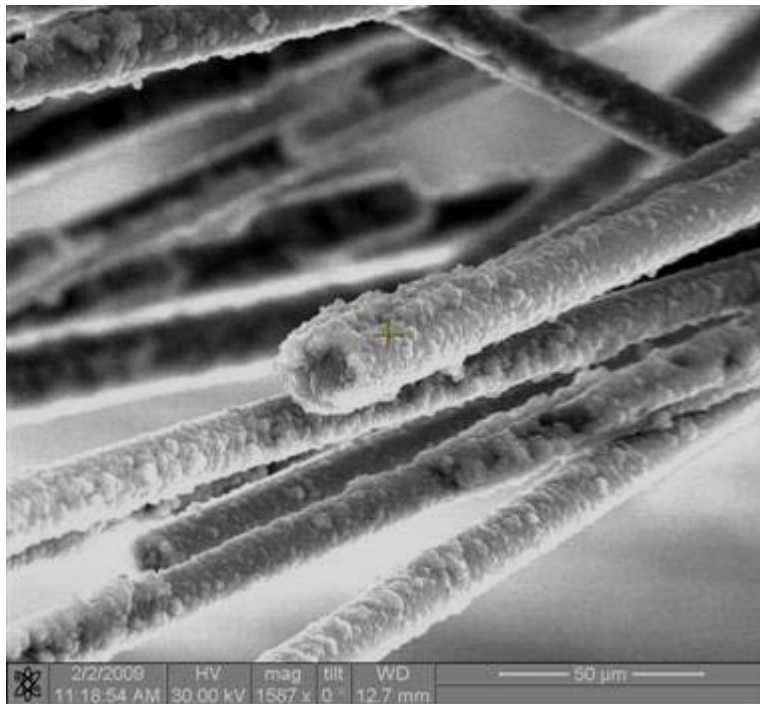


Figure 328. Fracture surface of the N720/AM specimen tested in creep at 109 MPa in steam at 1100°C.

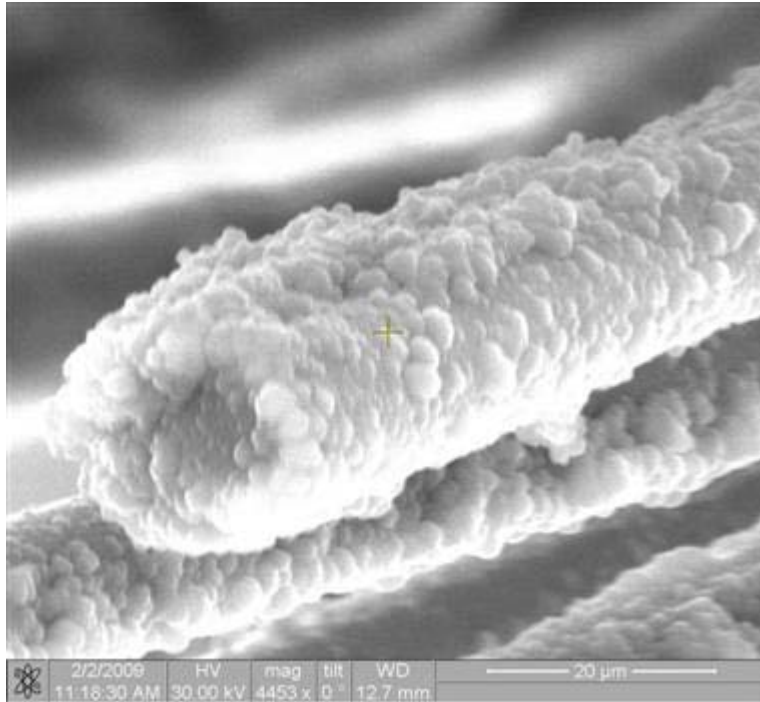


Figure 329. Fracture surface of the N720/AM specimen tested in creep at 109 MPa in steam at 1100°C.

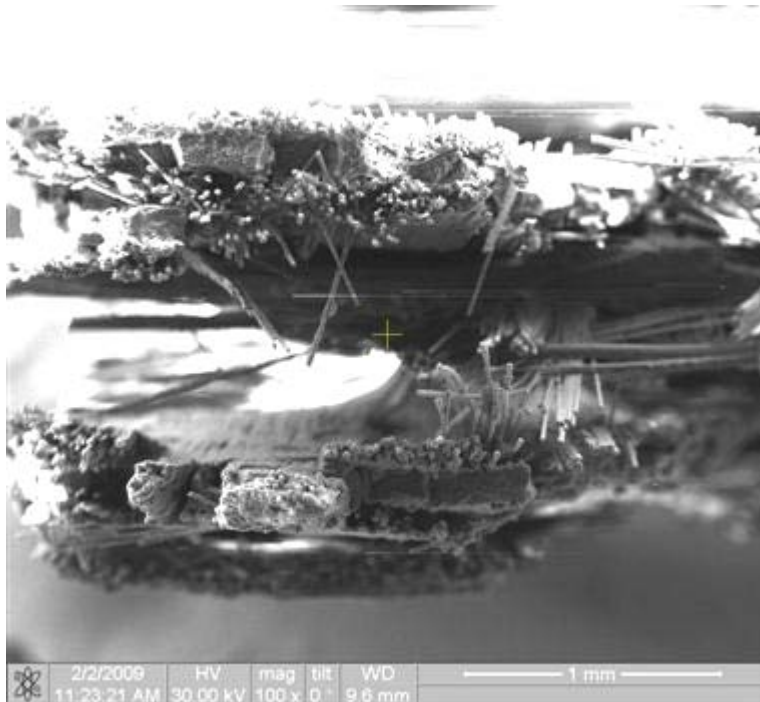


Figure 330. Fracture surface of the N720/AM specimen tested in creep at 109 MPa in steam at 1100°C.

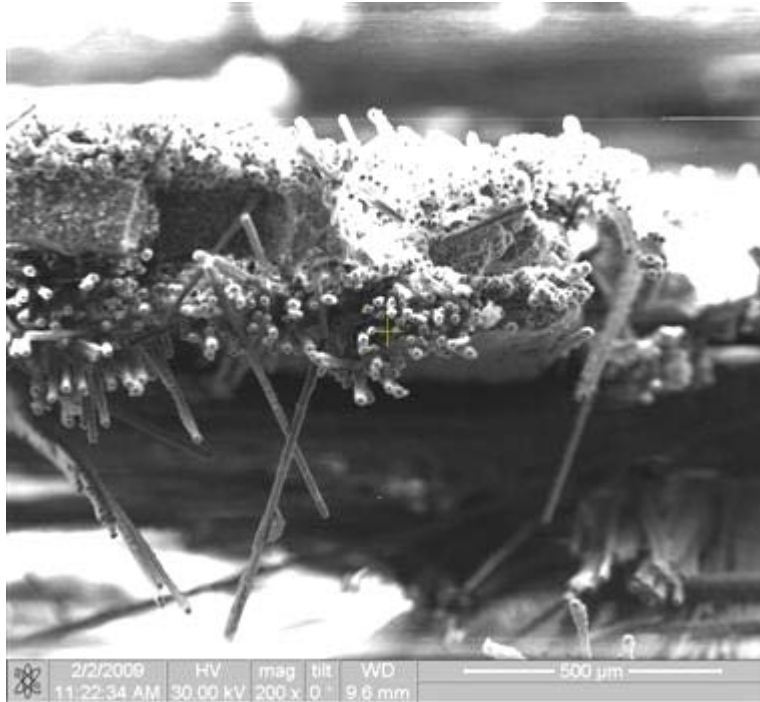


Figure 331. Fracture surface of the N720/AM specimen tested in creep at 109 MPa in steam at 1100°C.

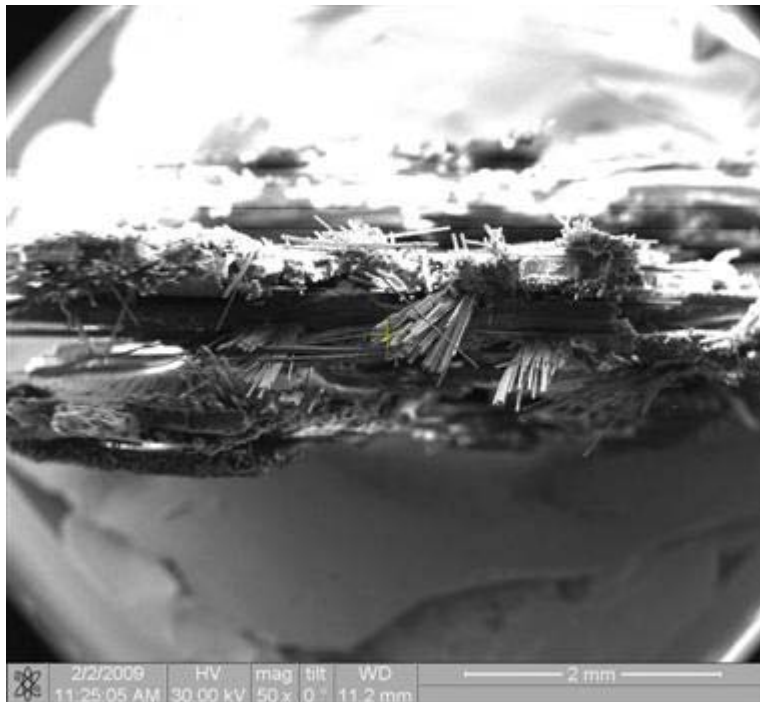


Figure 332. Fracture surface of the N720/AM specimen tested in creep at 109 MPa in steam at 1100°C.

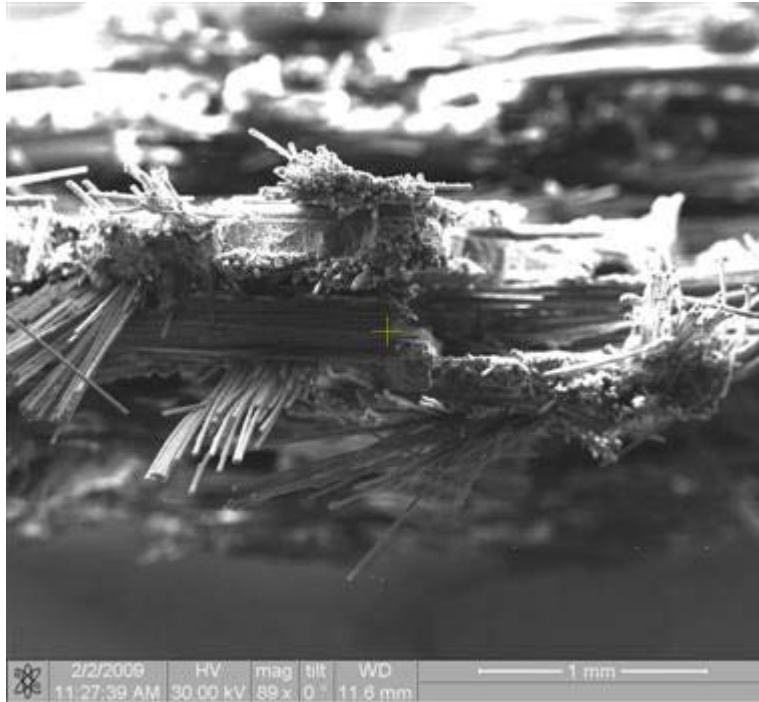


Figure 333. Fracture surface of the N720/AM specimen tested in creep at 109 MPa in steam at 1100°C.

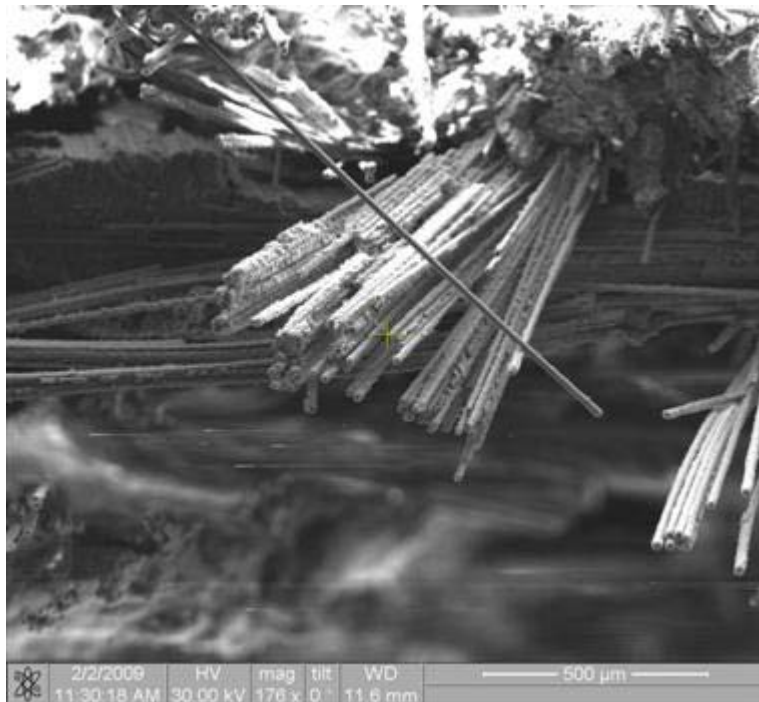


Figure 334. Fracture surface of the N720/AM specimen tested in creep at 109 MPa in steam at 1100°C.

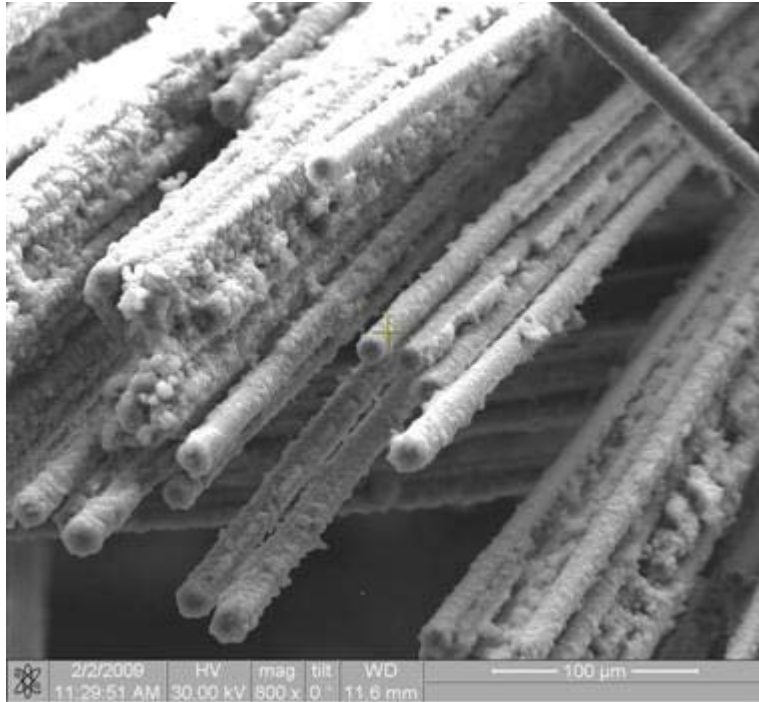


Figure 335. Fracture surface of the N720/AM specimen tested in creep at 109 MPa in steam at 1100°C.

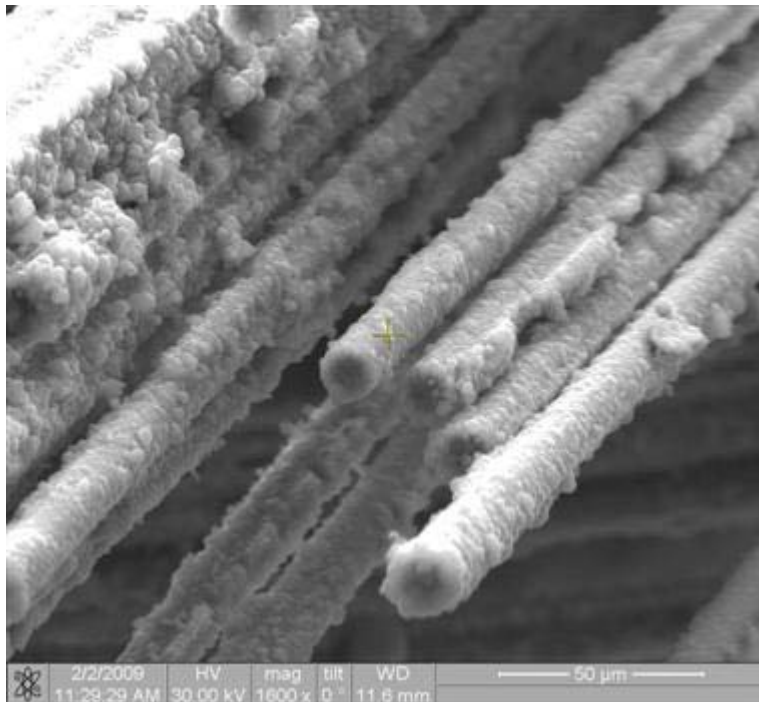


Figure 336. Fracture surface of the N720/AM specimen tested in creep at 109 MPa in steam at 1100°C..

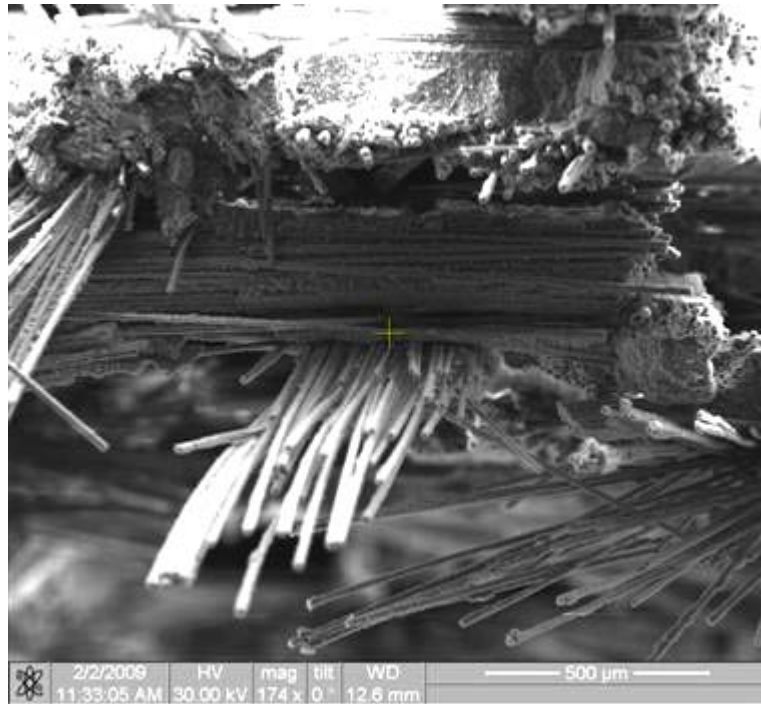


Figure 337. Fracture surface of the N720/AM specimen tested in creep at 109 MPa in steam at 1100°C.

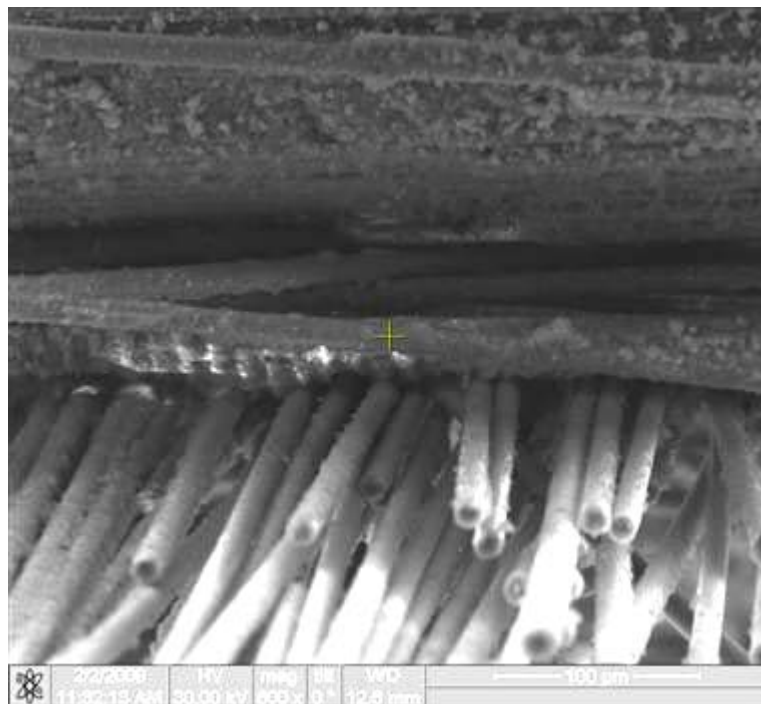


Figure 338. Fracture surface of the N720/AM specimen tested in creep at 109 MPa in steam at 1100°C.

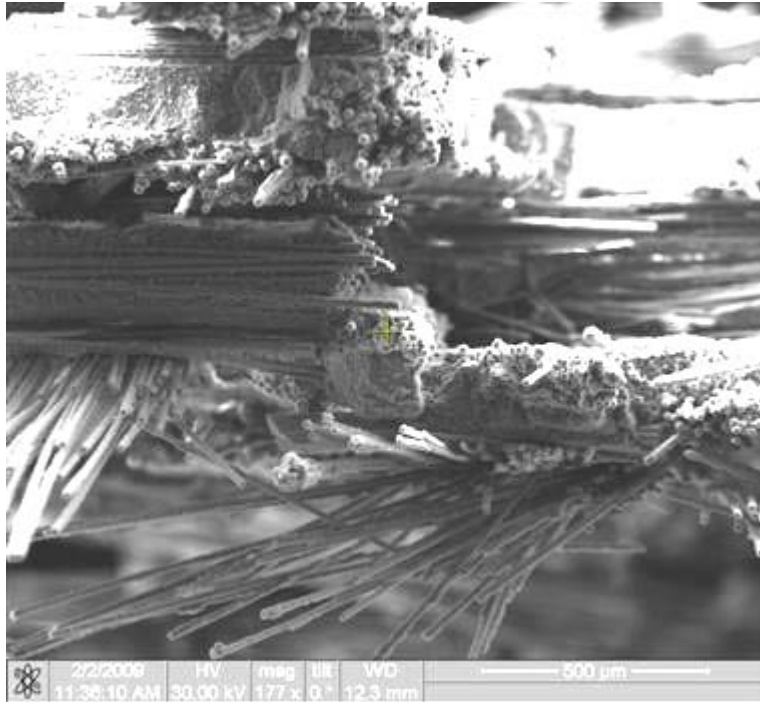


Figure 339. Fracture surface of the N720/AM specimen tested in creep at 109 MPa in steam at 1100°C.

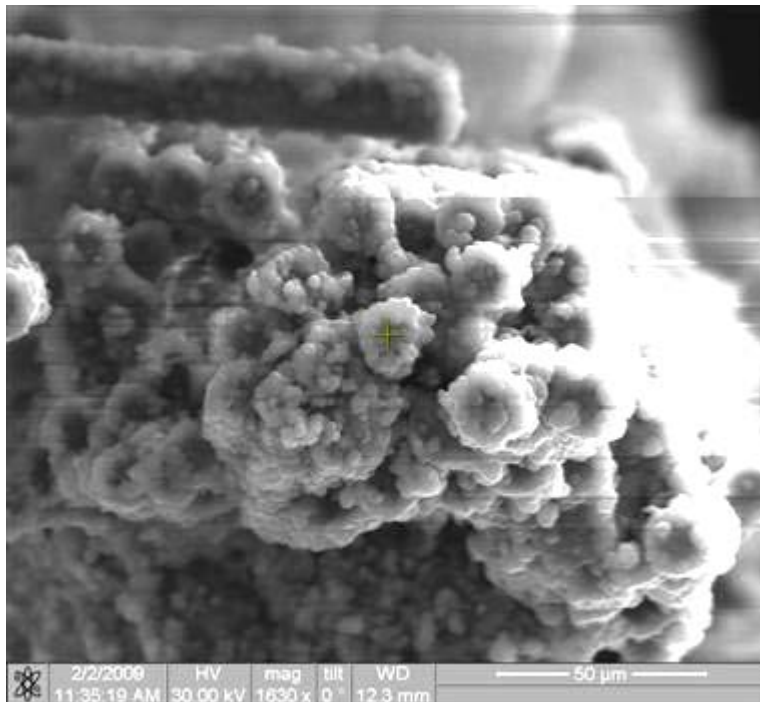


Figure 340. Fracture surface of the N720/AM specimen tested in creep at 109 MPa in steam at 1100°C.

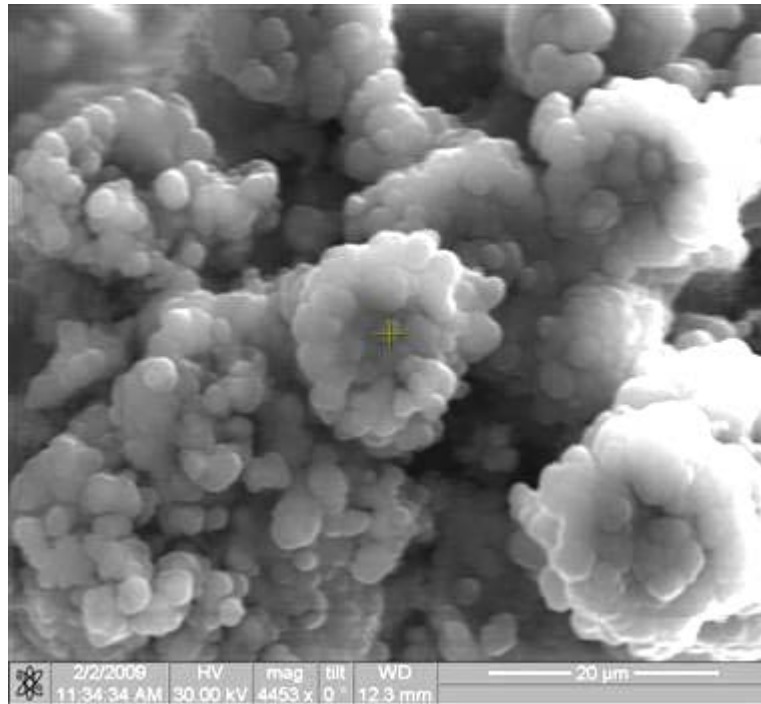


Figure 341. Fracture surface of the N720/AM specimen tested in creep at 109 MPa in steam at 1100°C.

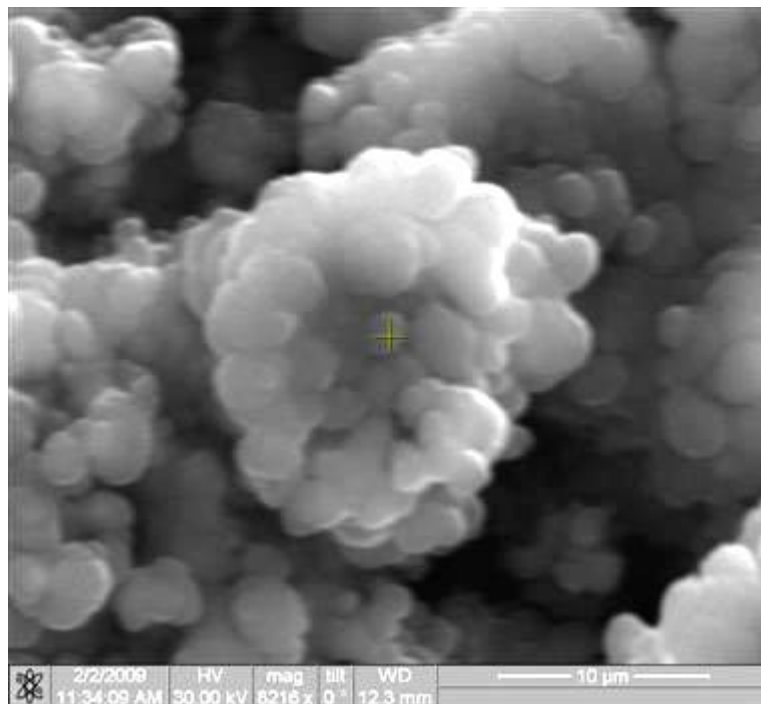


Figure 342. Fracture surface of the N720/AM specimen tested in creep at 109 MPa in steam at 1100°C.

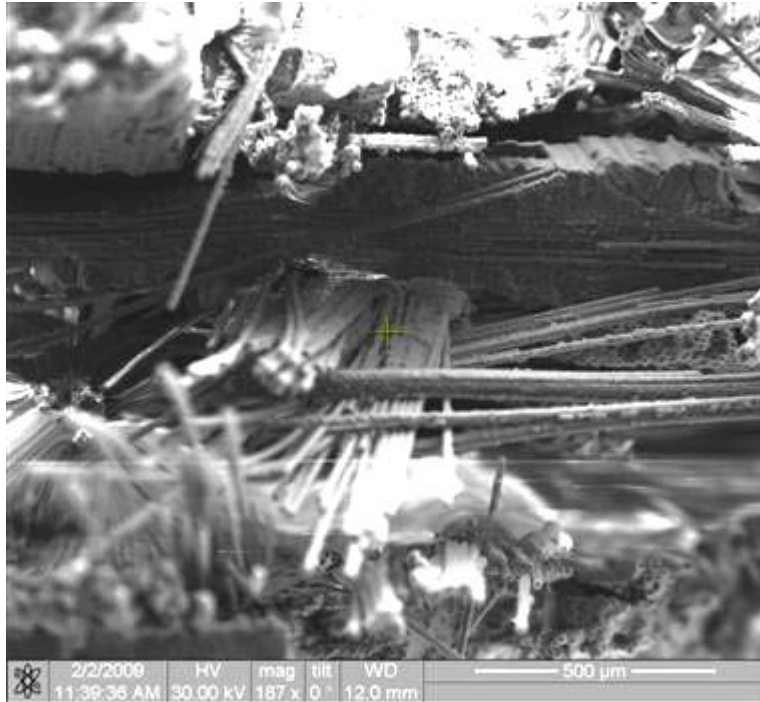


Figure 343. Fracture surface of the N720/AM specimen tested in creep at 109 MPa in steam at 1100°C.

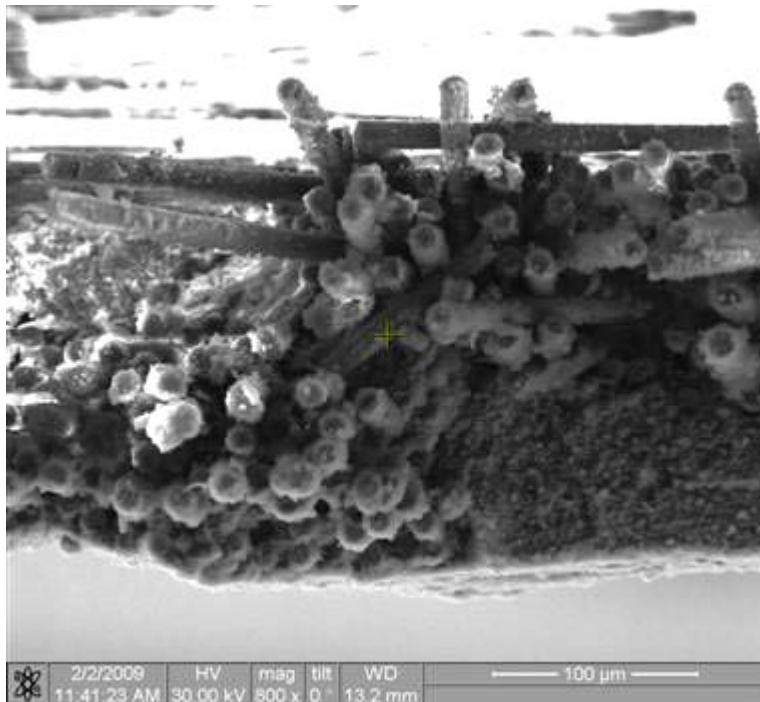


Figure 344. Fracture surface of the N720/AM specimen tested in creep at 109 MPa in steam at 1100°C.

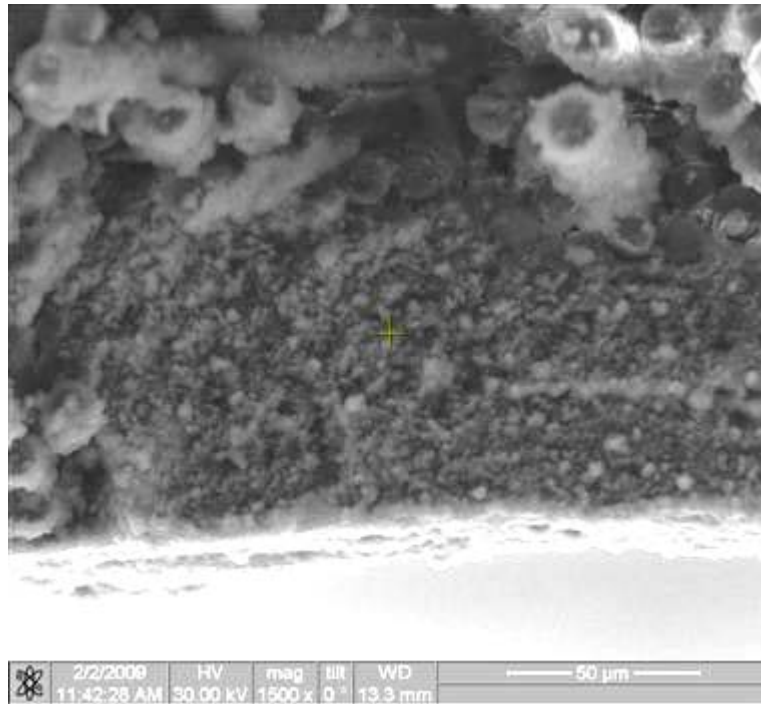


Figure 345. Fracture surface of the N720/AM specimen tested in creep at 109 MPa in steam at 1100°C.

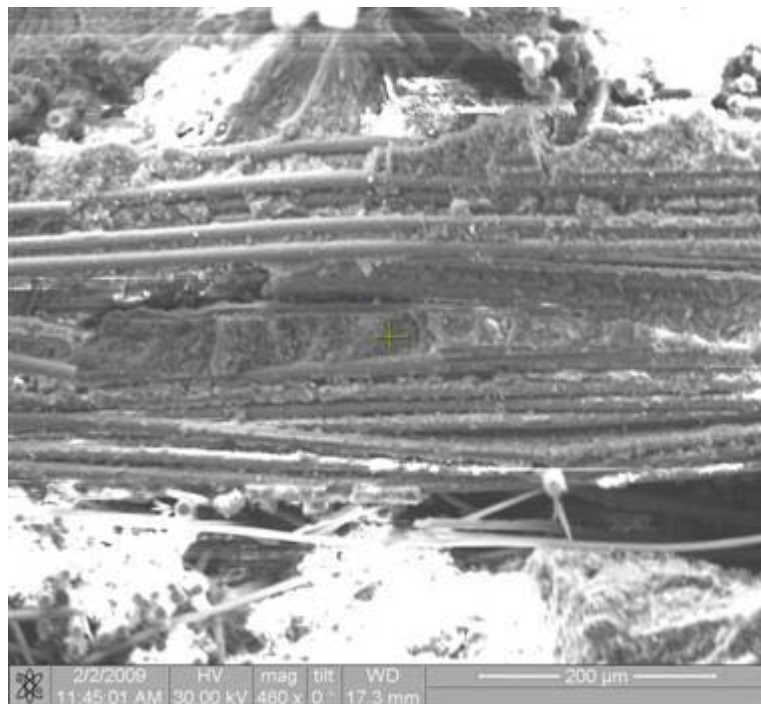


Figure 346. Fracture surface of the N720/AM specimen tested in creep at 109 MPa in steam at 1100°C.

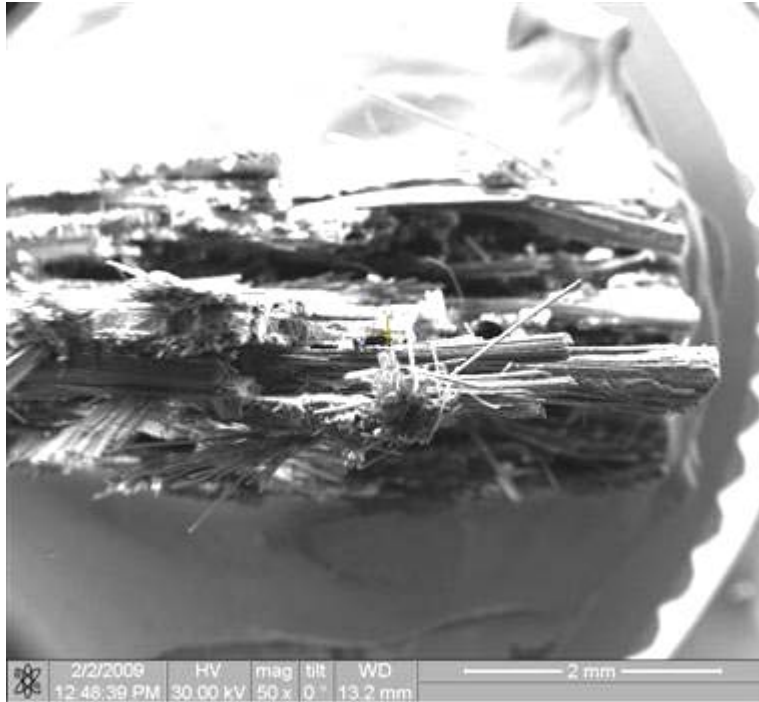


Figure 347. Fracture surface of the N720/AM specimen tested in creep at 109 MPa in steam at 1100°C.

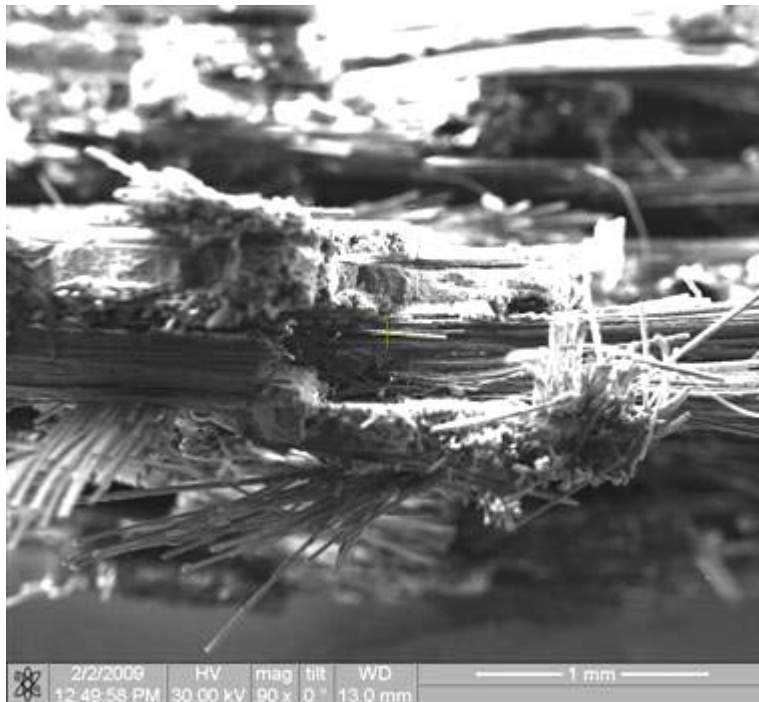


Figure 348. Fracture surface of the N720/AM specimen tested in creep at 109 MPa in steam at 1100°C.

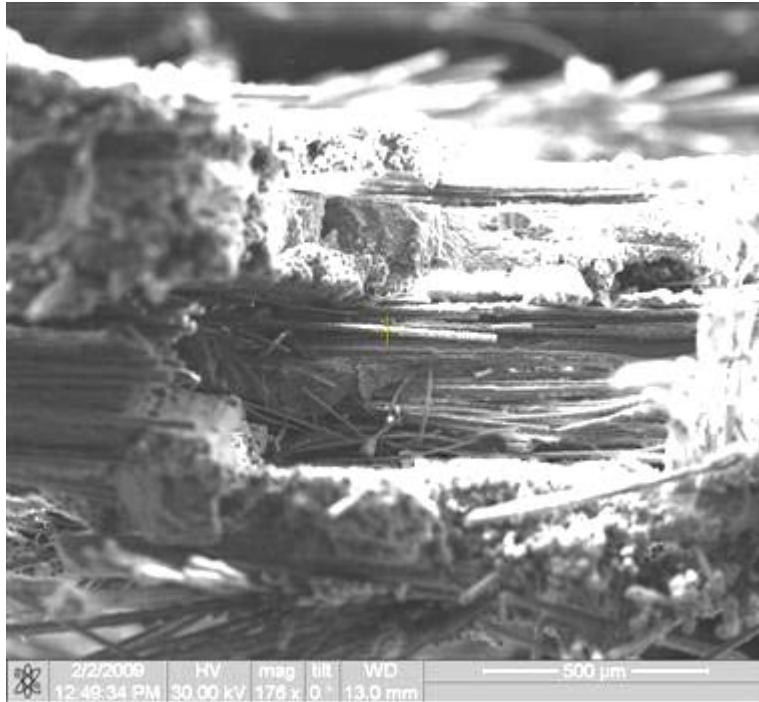


Figure 349. Fracture surface of the N720/AM specimen tested in creep at 109 MPa in steam at 1100°C.

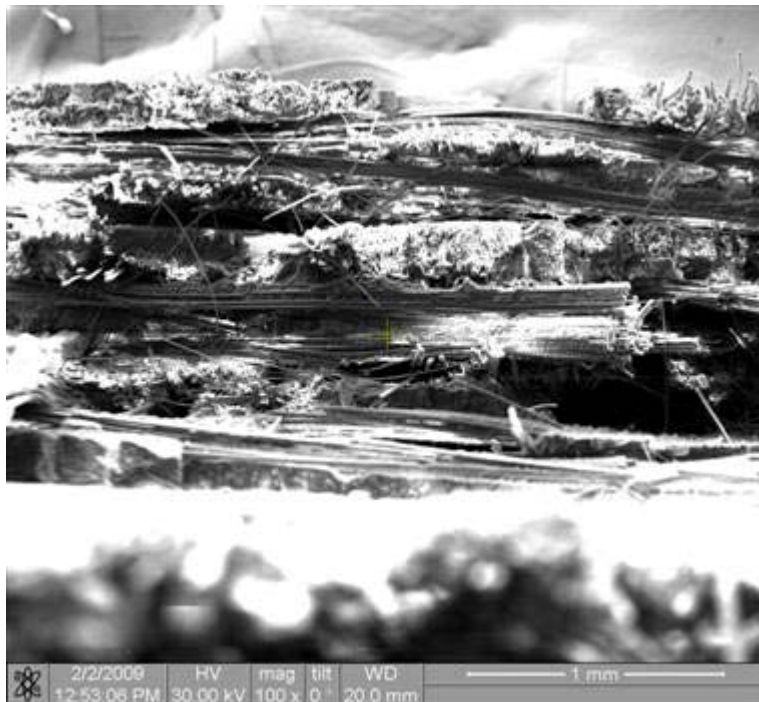


Figure 350. Fracture surface of the N720/AM specimen tested in creep at 109 MPa in steam at 1100°C.

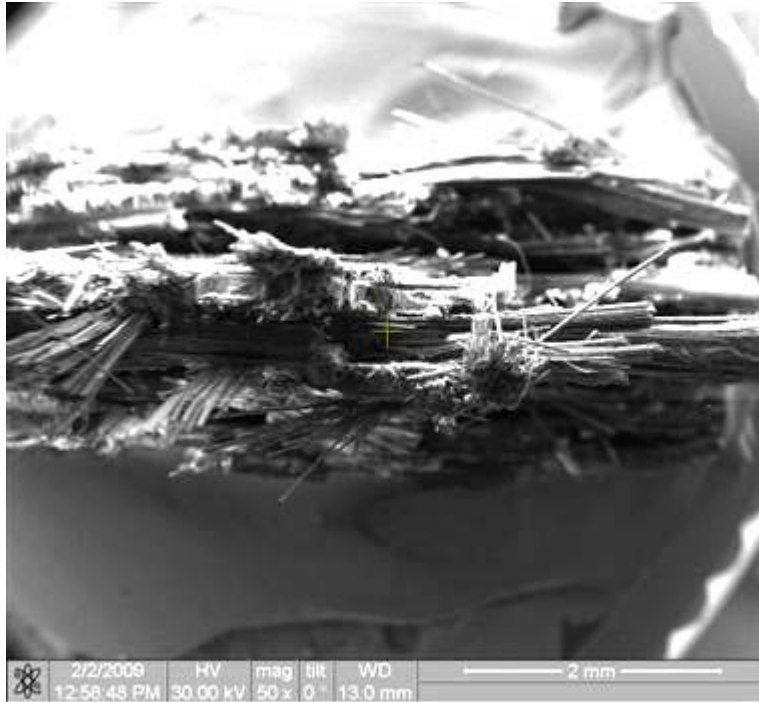


Figure 351. Fracture surface of the N720/AM specimen tested in creep at 109 MPa in steam at 1100°C.

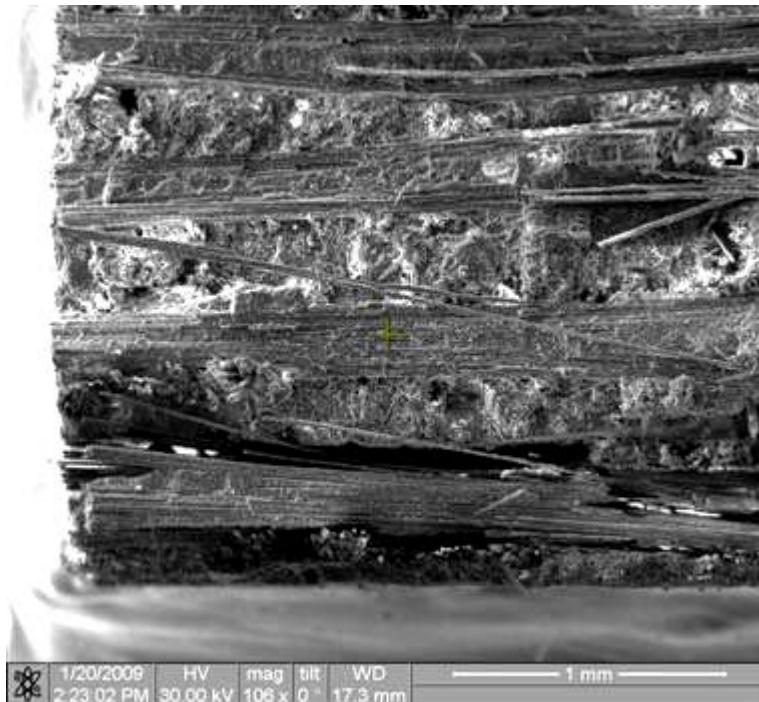


Figure 352. Fracture surface of the N720/AM specimen tested in creep at 87.5 MPa in steam at 1100°C.

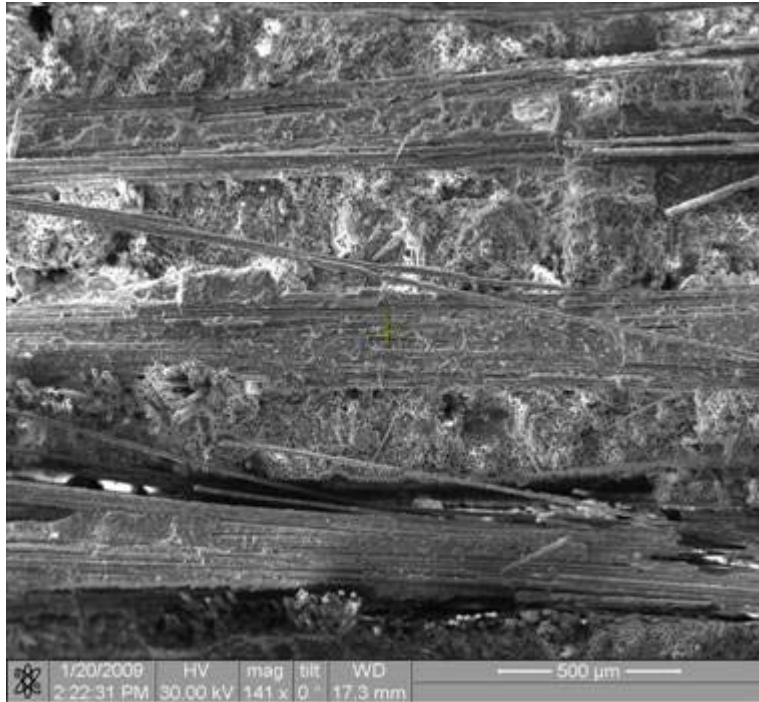


Figure 353. Fracture surface of the N720/AM specimen tested in creep at 87.5 MPa in steam at 1100°C.

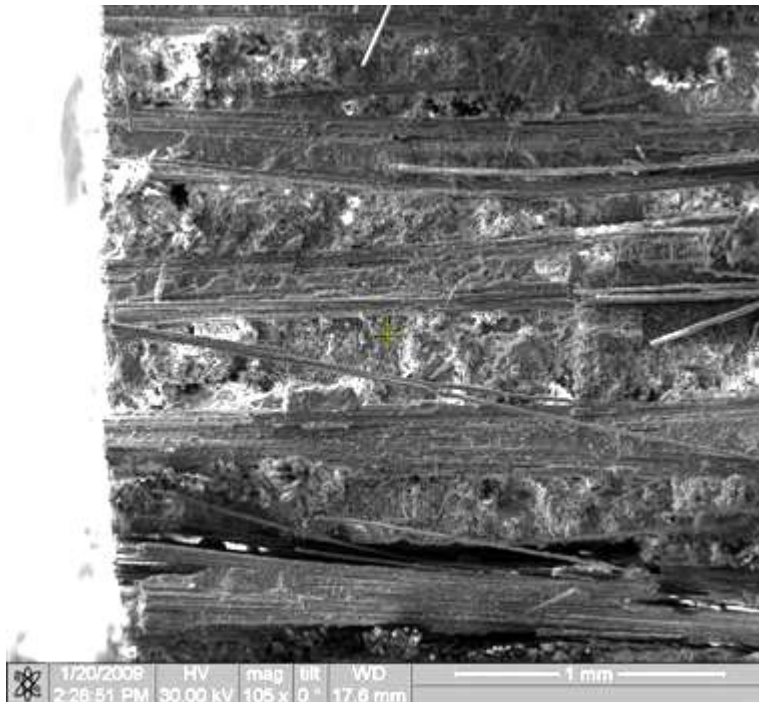


Figure 354. Fracture surface of the N720/AM specimen tested in creep at 87.5 MPa in steam at 1100°C.

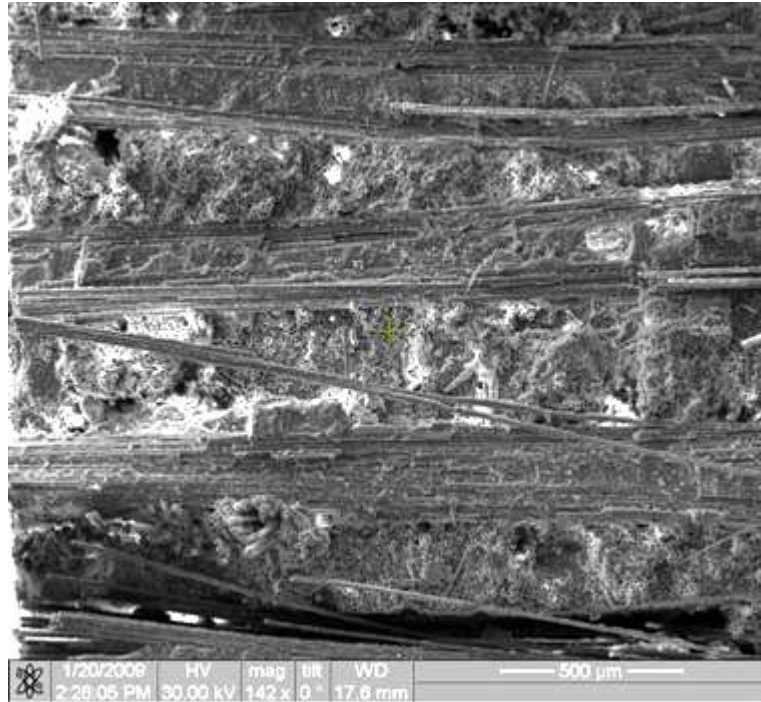


Figure 355. Fracture surface of the N720/AM specimen tested in creep at 87.5 MPa in steam at 1100°C.

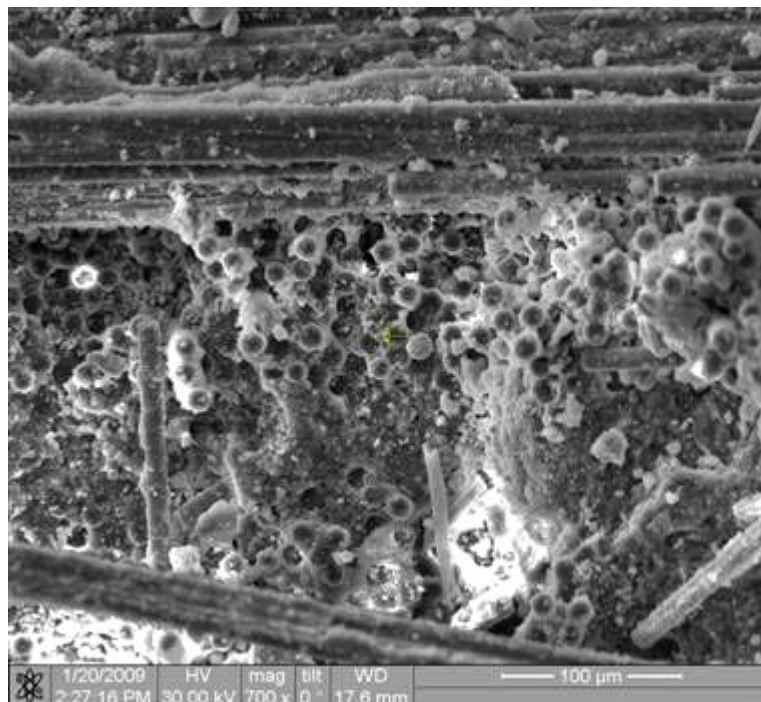


Figure 356. Fracture surface of the N720/AM specimen tested in creep at 87.5 MPa in steam at 1100°C.

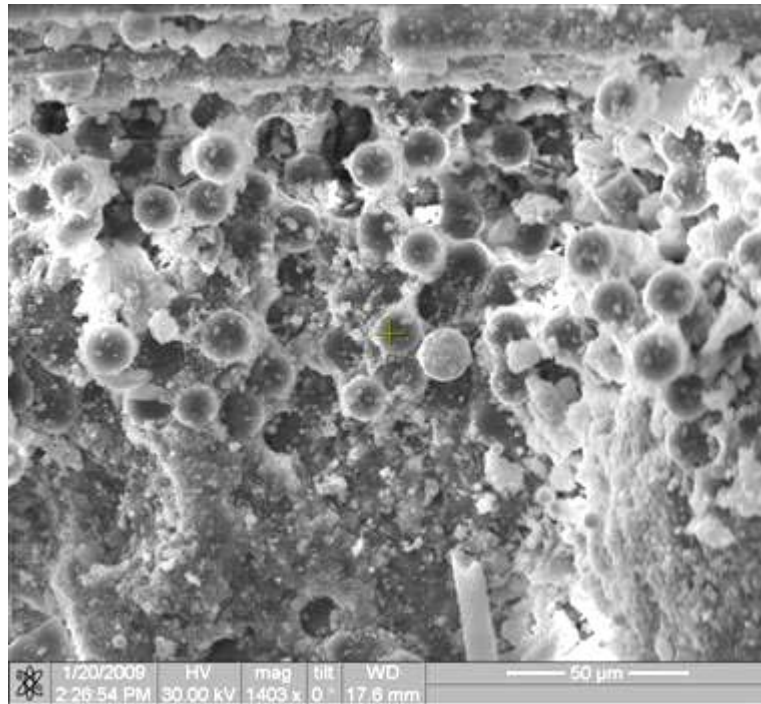


Figure 357. Fracture surface of the N720/AM specimen tested in creep at 87.5 MPa in steam at 1100°C.

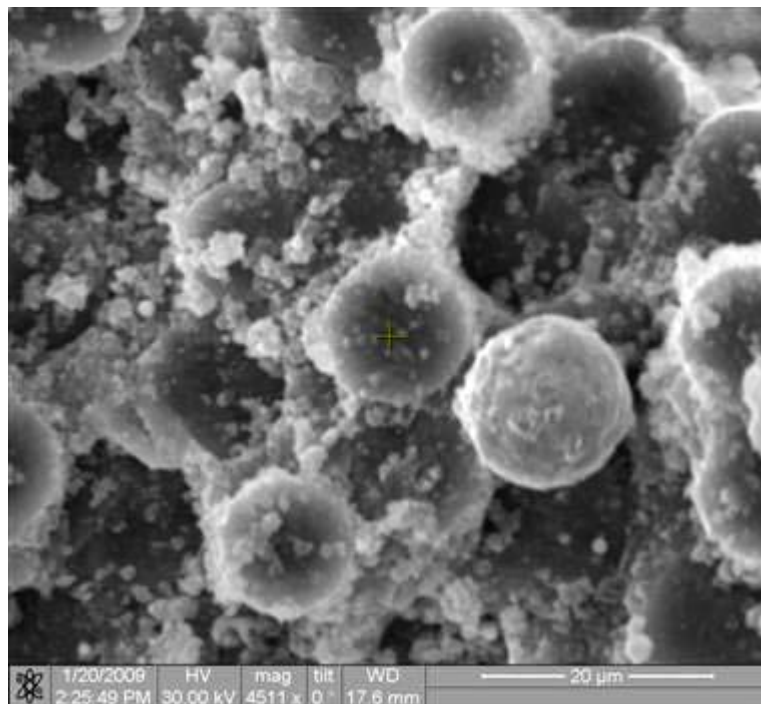


Figure 358. Fracture surface of the N720/AM specimen tested in creep at 87.5 MPa in steam at 1100°C.

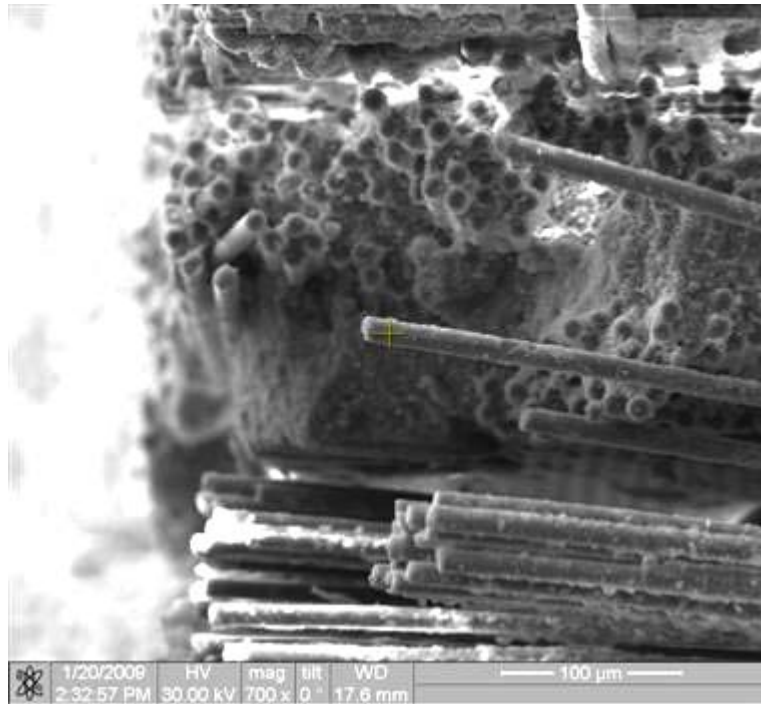


Figure 359. Fracture surface of the N720/AM specimen tested in creep at 87.5 MPa in steam at 1100°C.

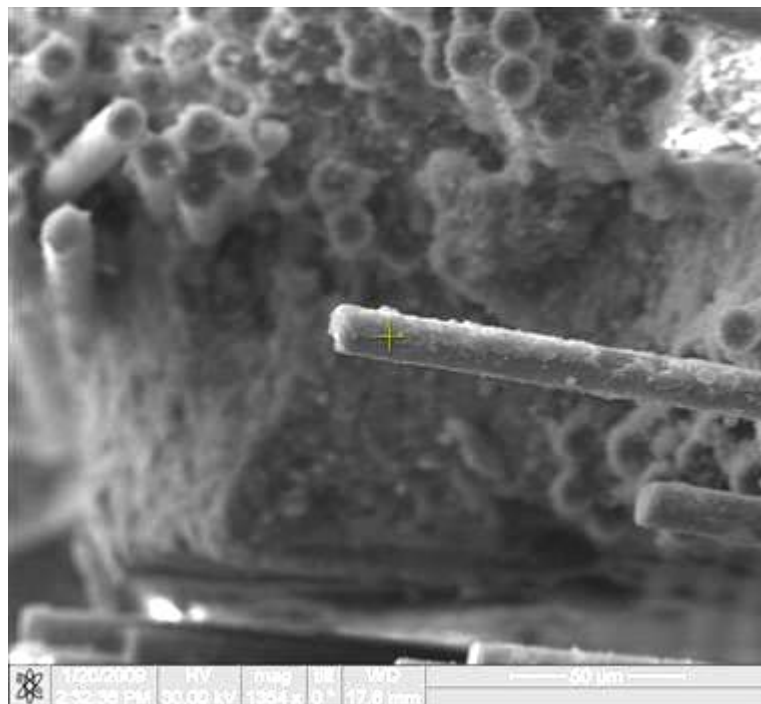


Figure 360. Fracture surface of the N720/AM specimen tested in creep at 87.5 MPa in steam at 1100°C.



Figure 361. Fracture surface of the N720/AM specimen tested in creep at 87.5 MPa in steam at 1100°C.

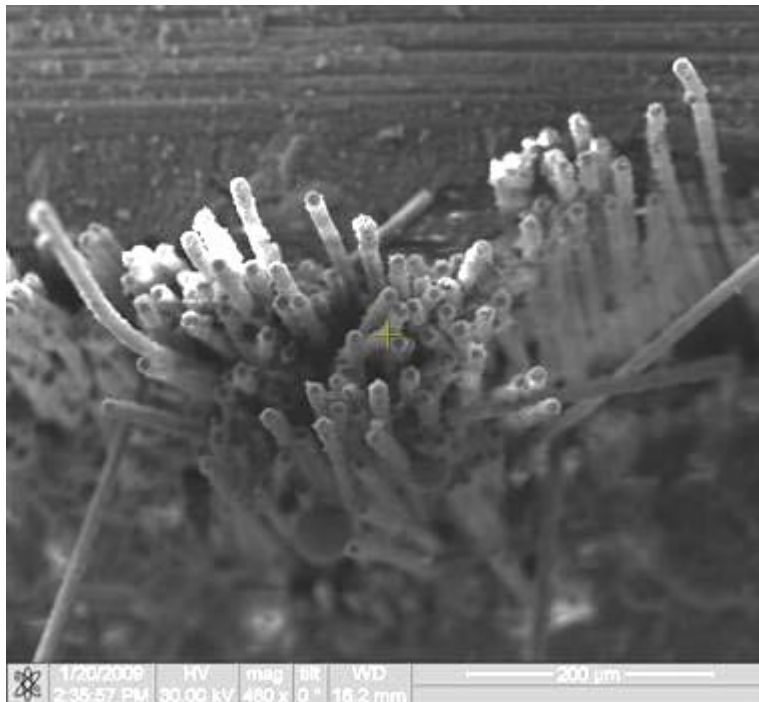


Figure 362. Fracture surface of the N720/AM specimen tested in creep at 87.5 MPa in steam at 1100°C.

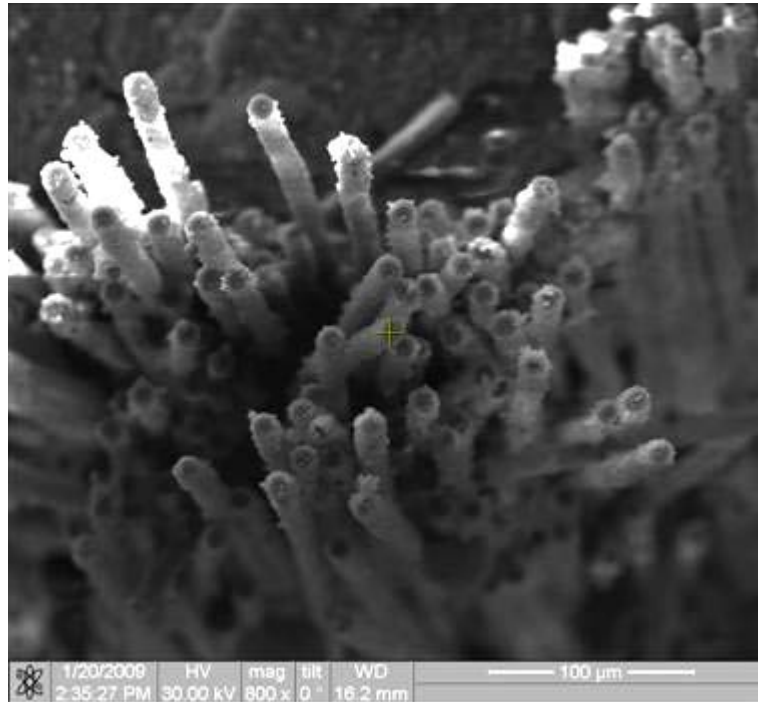


Figure 363. Fracture surface of the N720/AM specimen tested in creep at 87.5 MPa in steam at 1100°C.

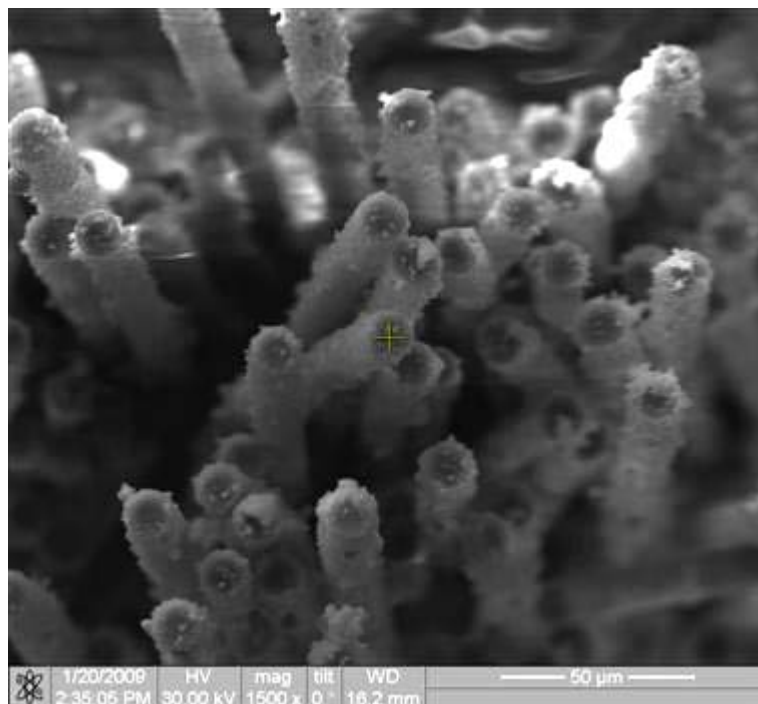


Figure 364. Fracture surface of the N720/AM specimen tested in creep at 87.5 MPa in steam at 1100°C.

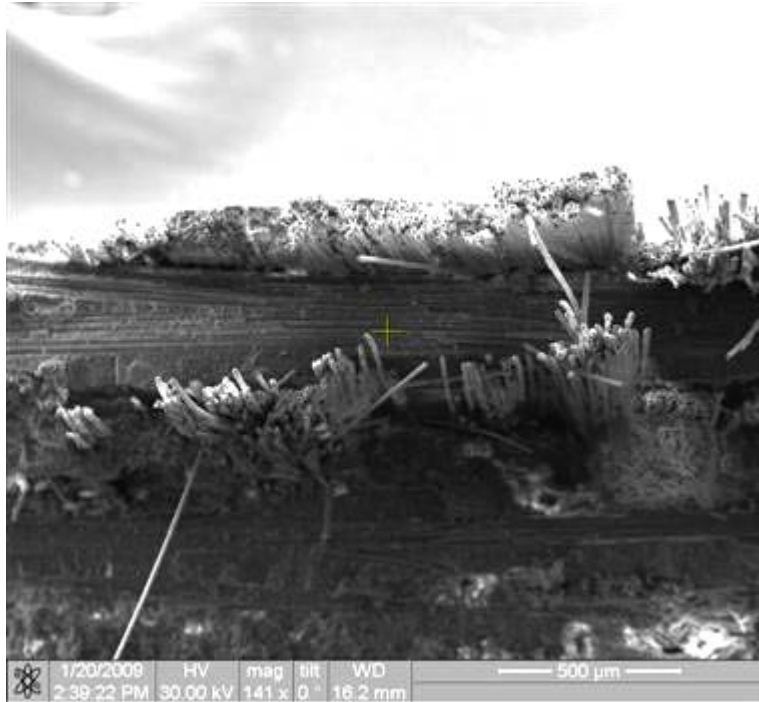


Figure 365. Fracture surface of the N720/AM specimen tested in creep at 87.5 MPa in steam at 1100°C.



. Figure 366. Fracture surface of the N720/AM specimen tested in creep at 87.5 MPa in steam at 1100°C.

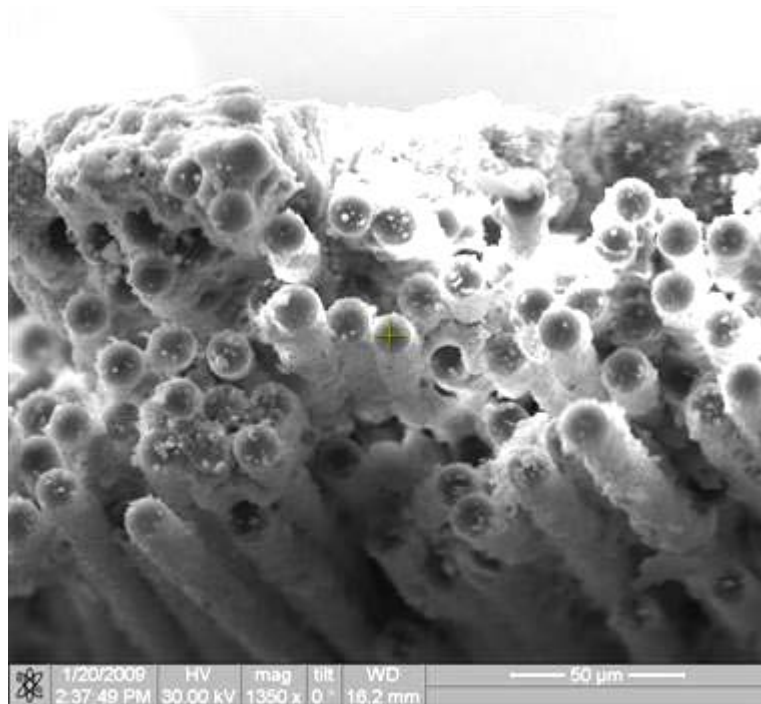


Figure 367. Fracture surface of the N720/AM specimen tested in creep at 87.5 MPa in steam at 1100°C.

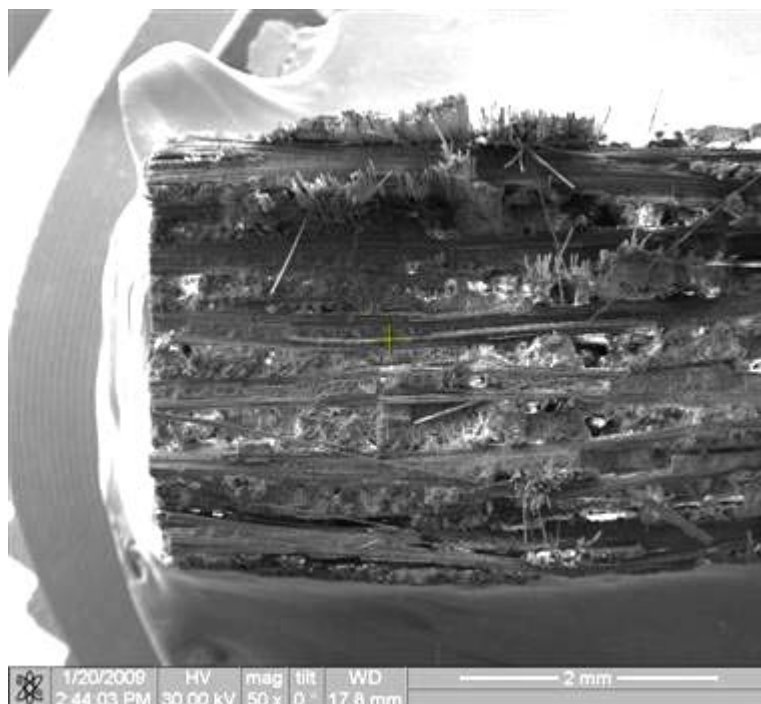


Figure 368. Fracture surface of the N720/AM specimen tested in creep at 87.5 MPa in steam at 1100°C.

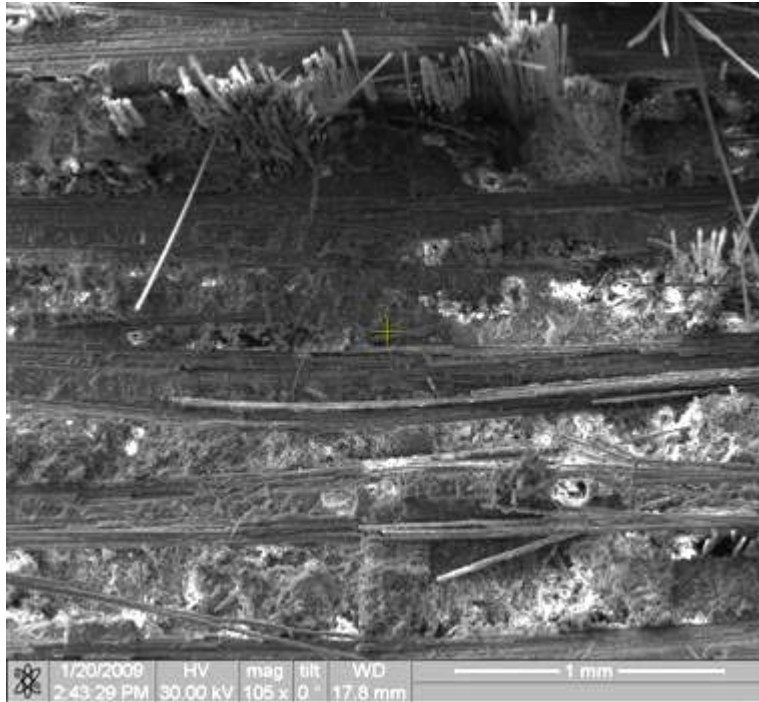


Figure 369. Fracture surface of the N720/AM specimen tested in creep at 87.5 MPa in steam at 1100°C.



Figure 370. Fracture surface of the N720/AM specimen tested in creep at 87.5 MPa in steam at 1100°C.

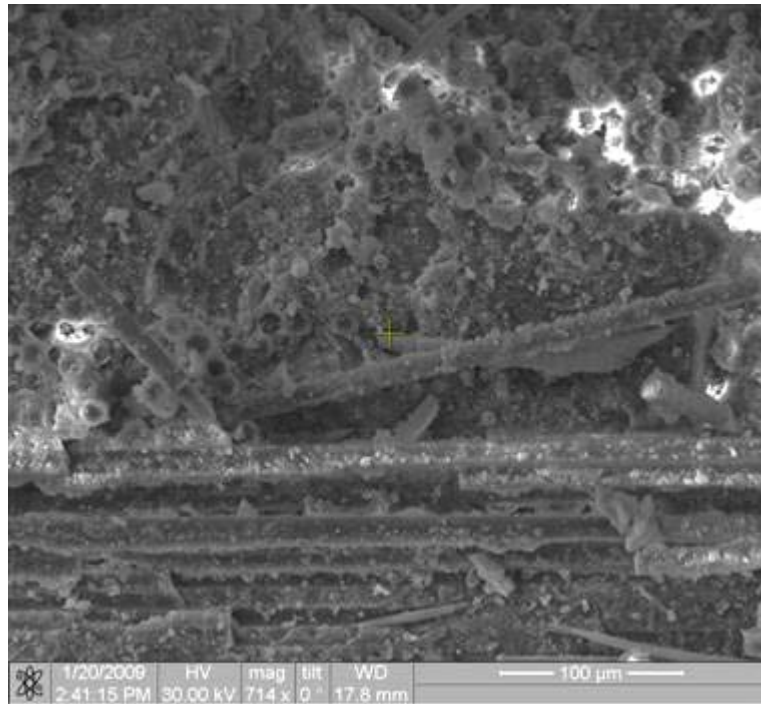


Figure 371. Fracture surface of the N720/AM specimen tested in creep at 87.5 MPa in steam at 1100°C.



Figure 372. Fracture surface of the N720/AM specimen tested in creep at 87.5 MPa in steam at 1100°C.

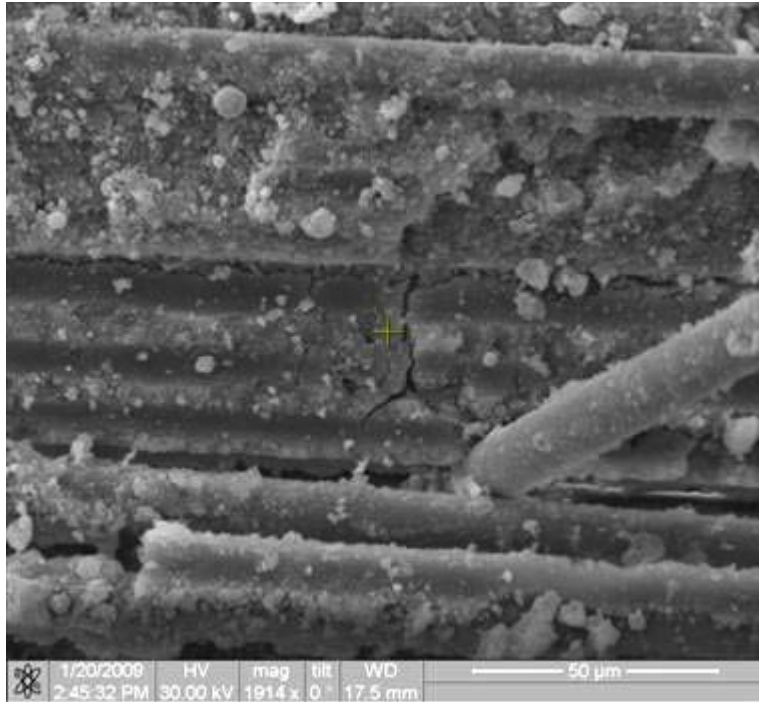


Figure 373. Fracture surface of the N720/AM specimen tested in creep at 87.5 MPa in steam at 1100°C.

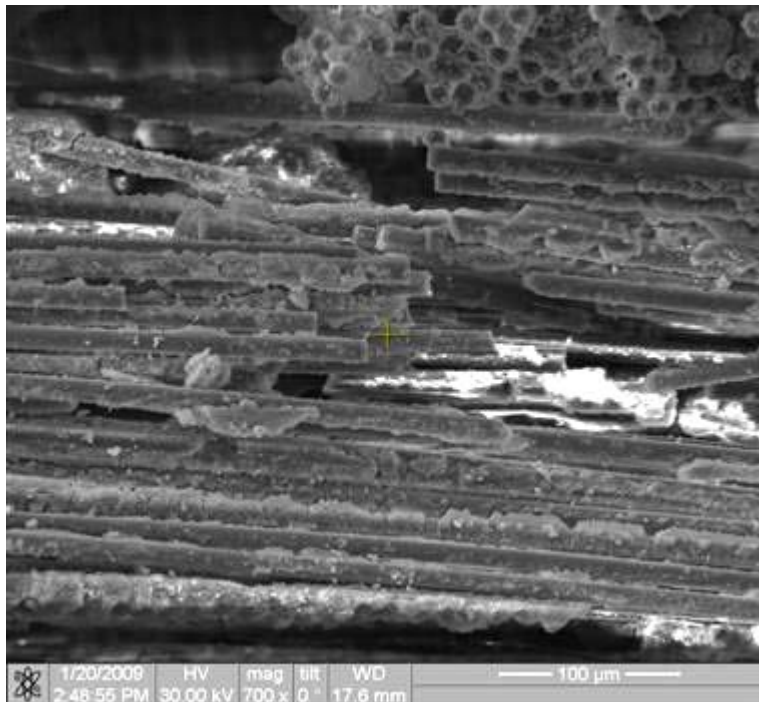


Figure 374. Fracture surface of the N720/AM specimen tested in creep at 87.5 MPa in steam at 1100°C.

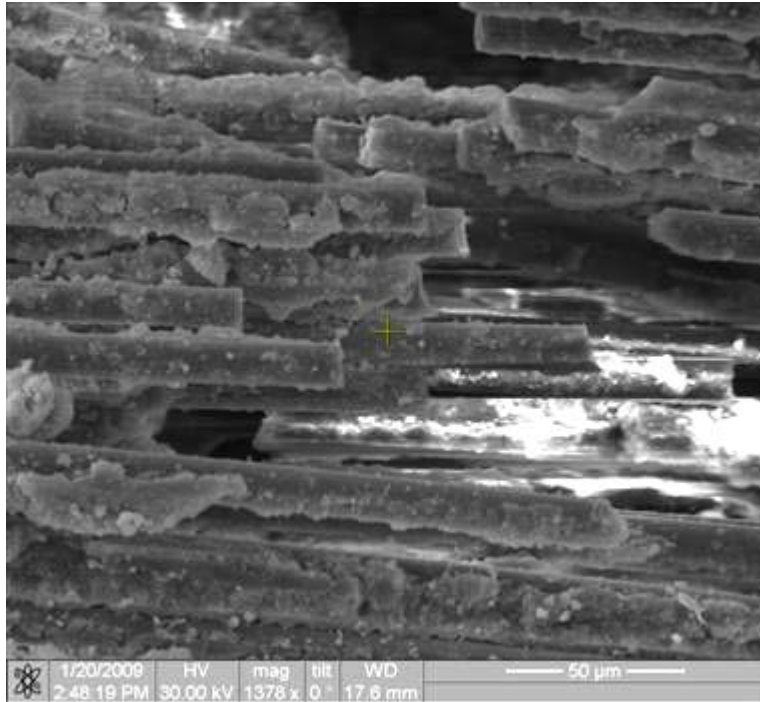


Figure 375. Fracture surface of the N720/AM specimen tested in creep at 87.5 MPa in steam at 1100°C.



Figure 376. Fracture surface of the N720/AM specimen tested in creep at 87.5 MPa in steam at 1100°C.

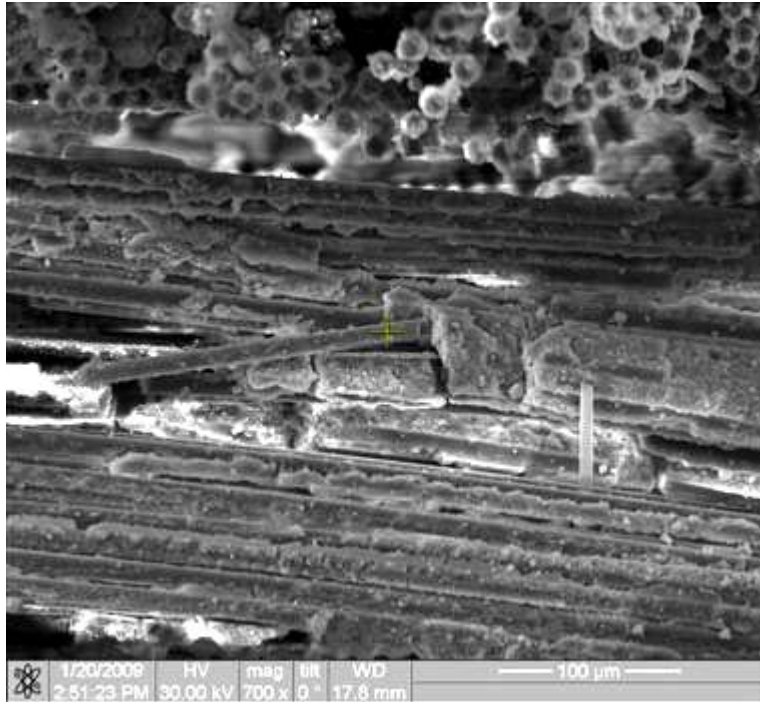


Figure 377. Fracture surface of the N720/AM specimen tested in creep at 87.5 MPa in steam at 1100°C.

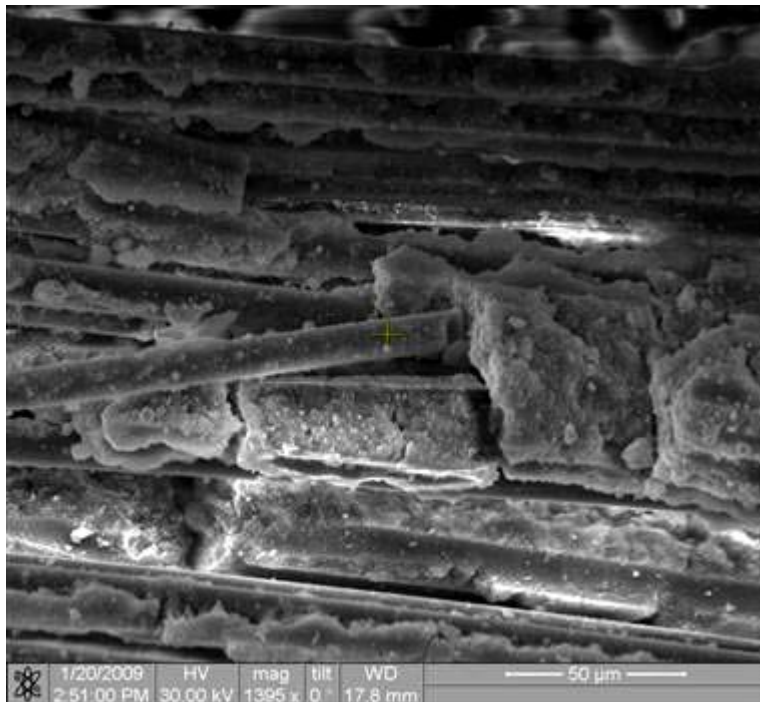


Figure 378. Fracture surface of the N720/AM specimen tested in creep at 87.5 MPa in steam at 1100°C.

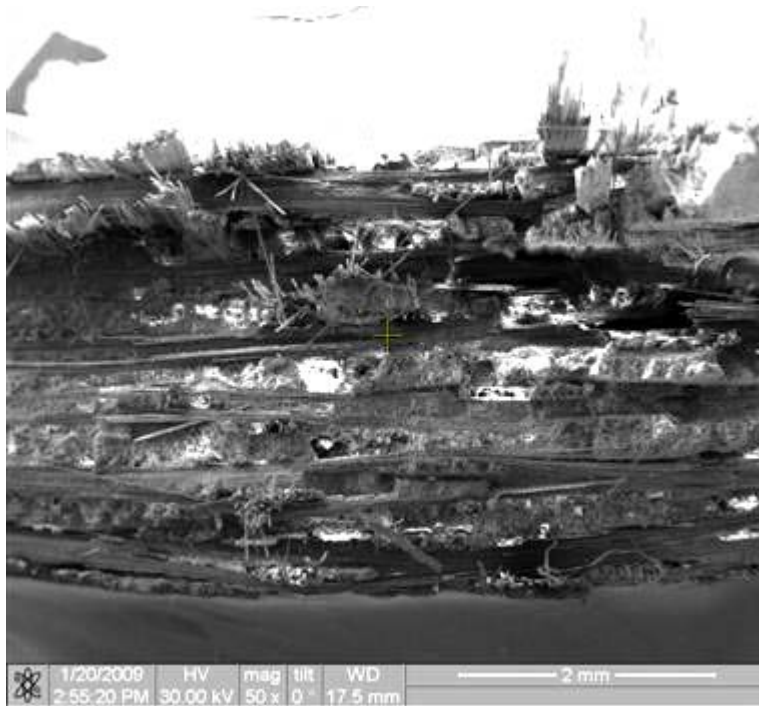


Figure 379. Fracture surface of the N720/AM specimen tested in creep at 87.5 MPa in steam at 1100°C.

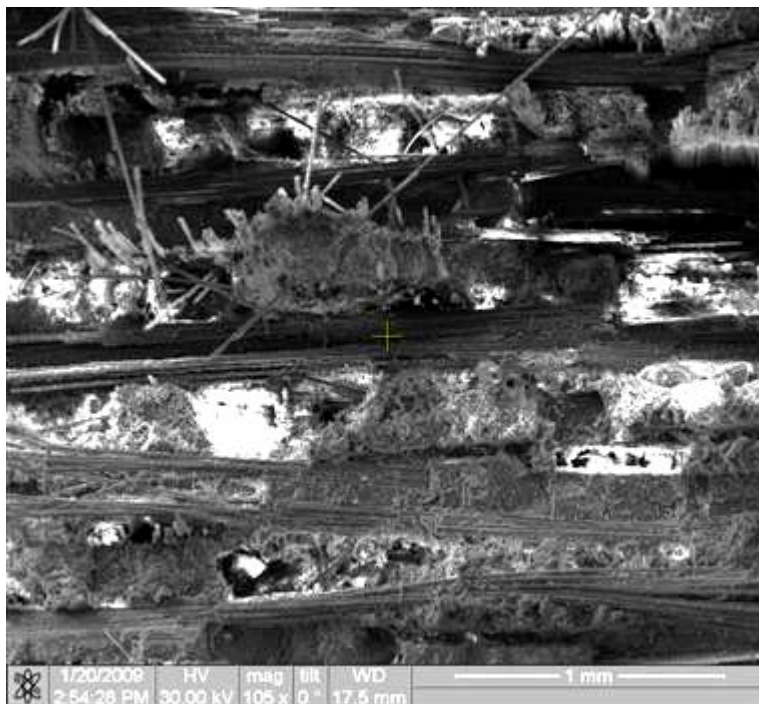


Figure 380. Fracture surface of the N720/AM specimen tested in creep at 87.5 MPa in steam at 1100°C.



Figure 381. Fracture surface of the N720/AM specimen tested in creep at 87.5 MPa in steam at 1100°C.

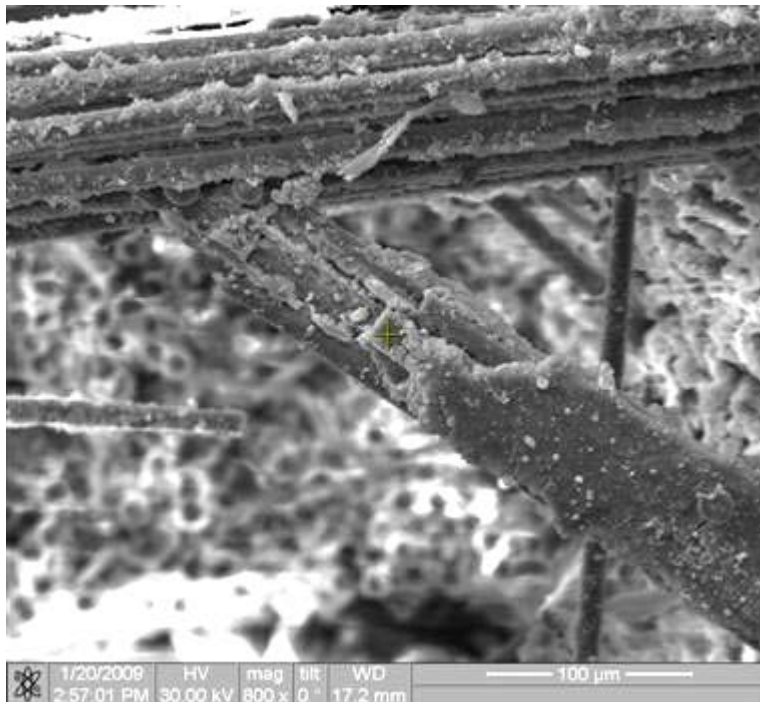


Figure 382. Fracture surface of the N720/AM specimen tested in creep at 87.5 MPa in steam at 1100°C.

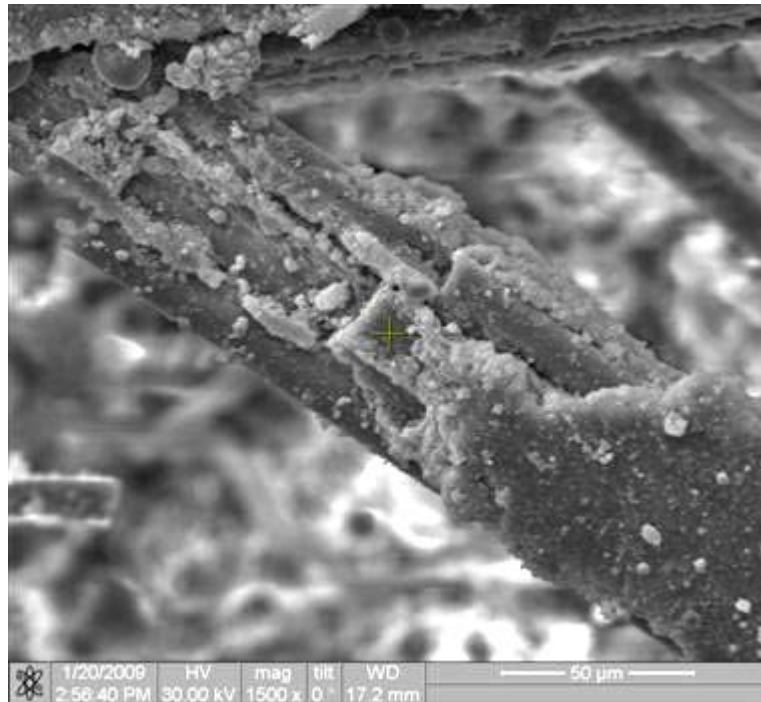


Figure 383. Fracture surface of the N720/AM specimen tested in creep at 87.5 MPa in steam at 1100°C.

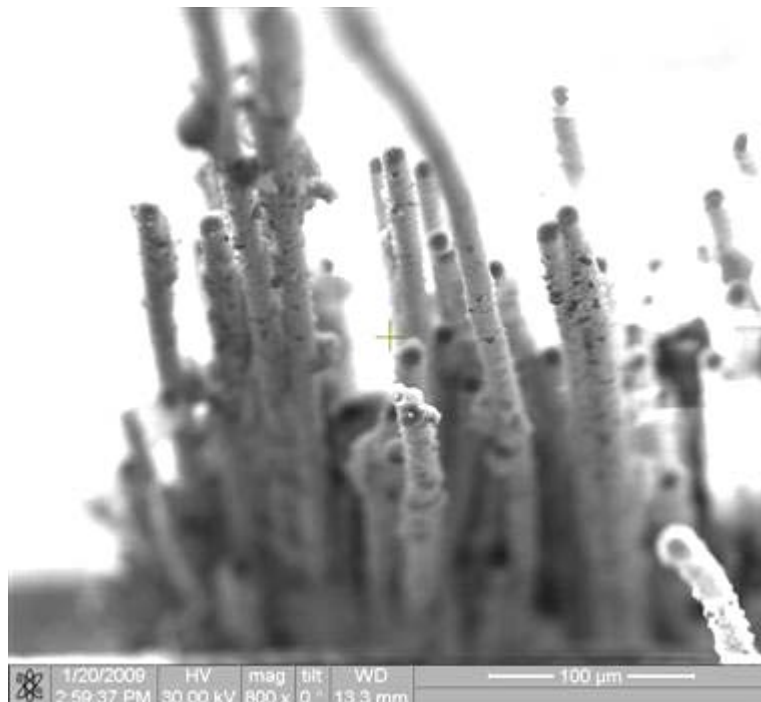


Figure 384. Fracture surface of the N720/AM specimen tested in creep at 87.5 MPa in steam at 1100°C.

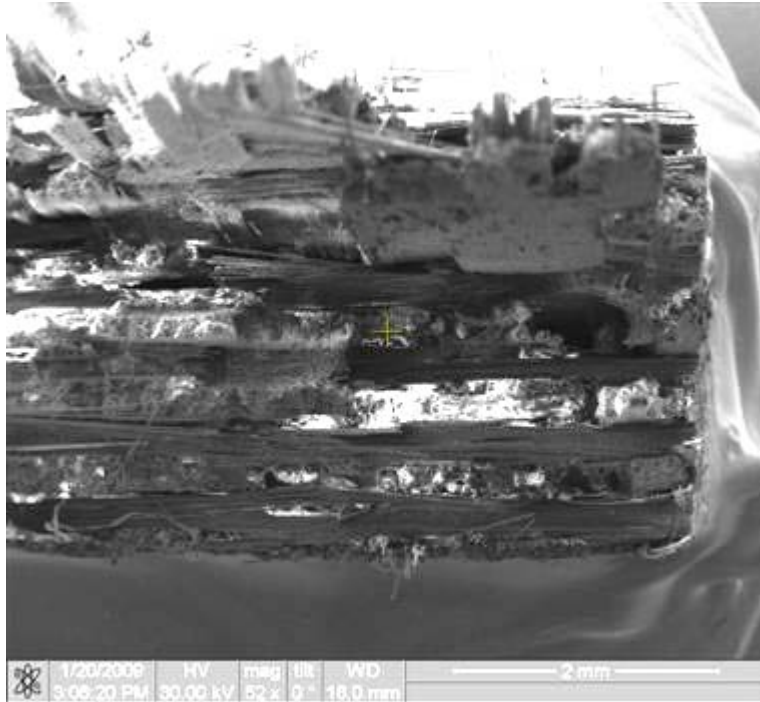


Figure 385. Fracture surface of the N720/AM specimen tested in creep at 87.5 MPa in steam at 1100°C.

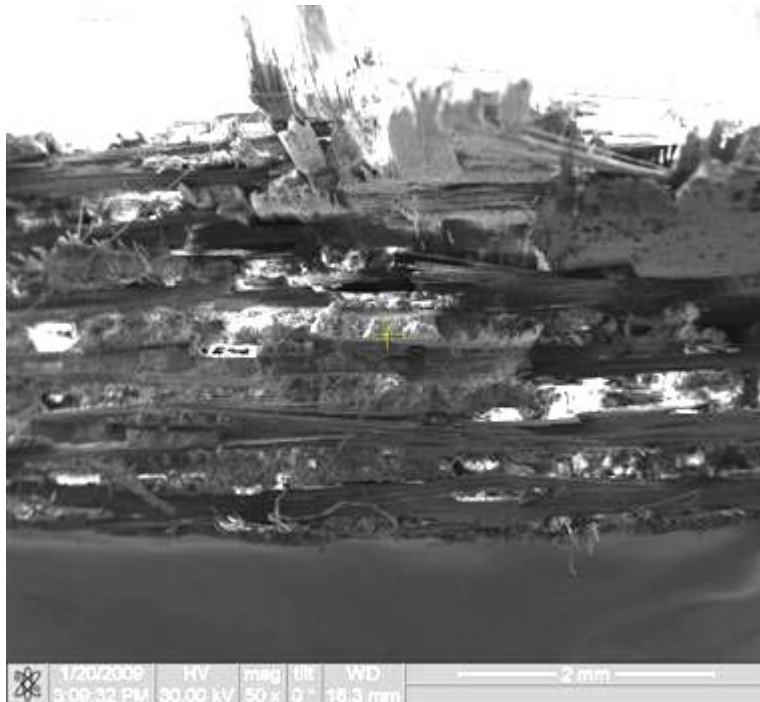


Figure 386. Fracture surface of the N720/AM specimen tested in creep at 87.5 MPa in steam at 1100°C.

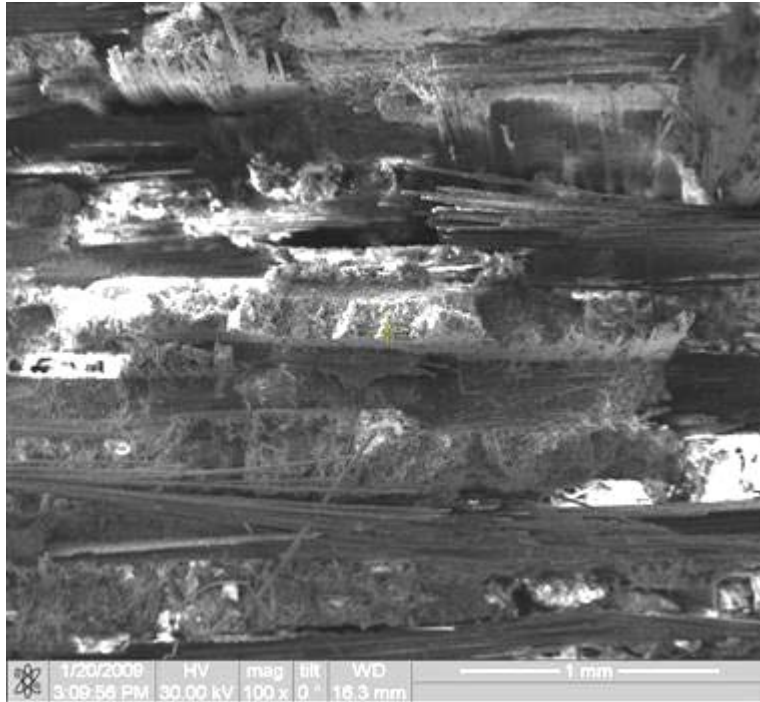


Figure 387. Fracture surface of the N720/AM specimen tested in creep at 87.5 MPa in steam at 1100°C.

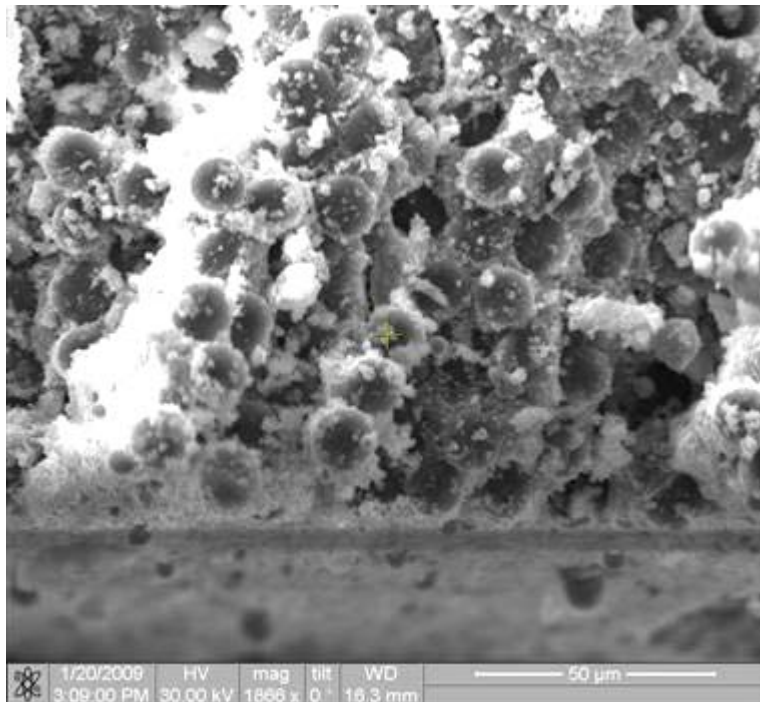


Figure 388. Fracture surface of the N720/AM specimen tested in creep at 87.5 MPa in steam at 1100°C.

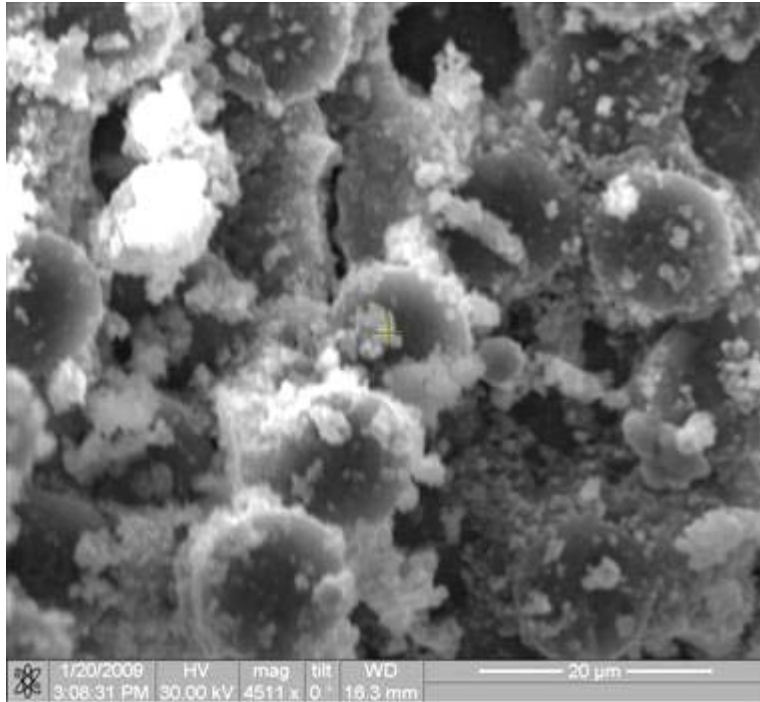


Figure 389. Fracture surface of the N720/AM specimen tested in creep at 87.5 MPa in steam at 1100°C.

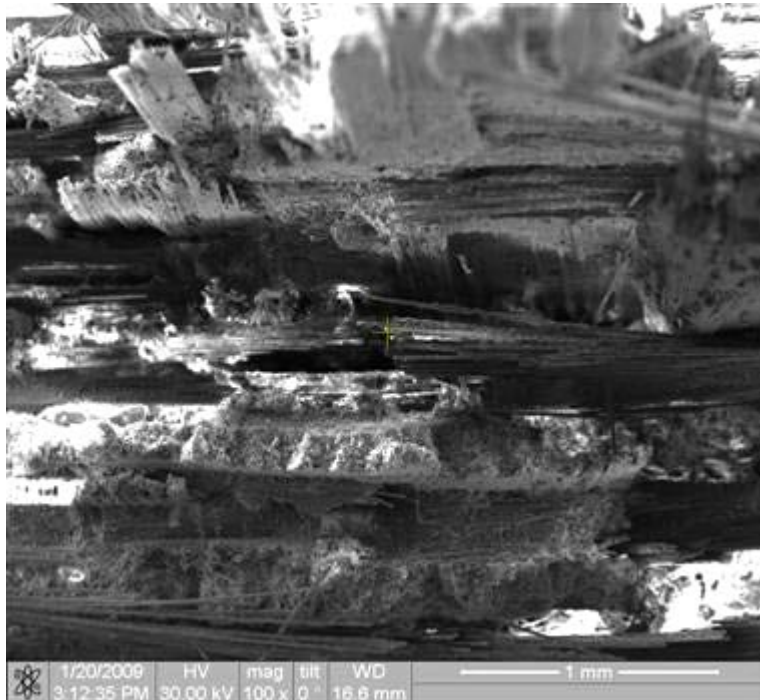


Figure 390. Fracture surface of the N720/AM specimen tested in creep at 87.5 MPa in steam at 1100°C.

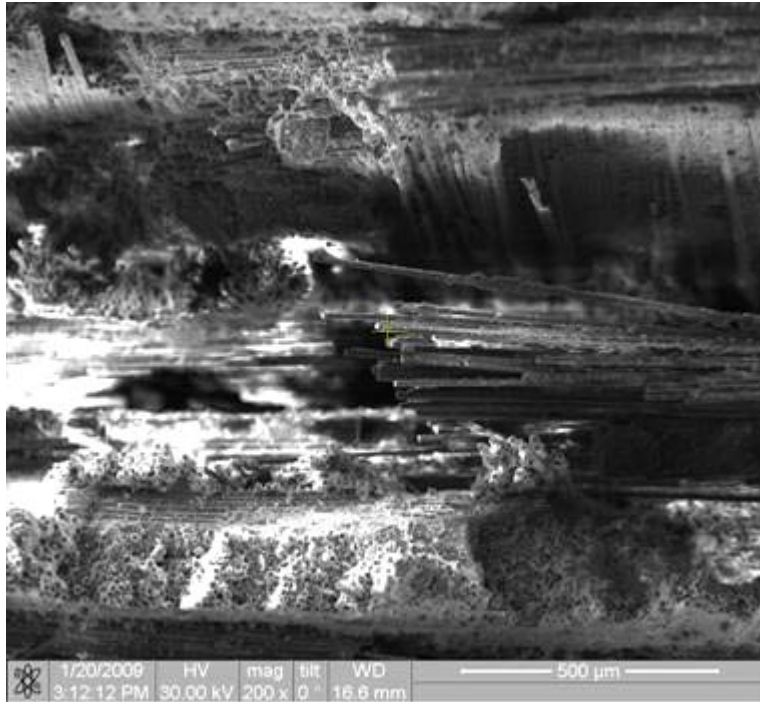


Figure 391. Fracture surface of the N720/AM specimen tested in creep at 87.5 MPa in steam at 1100°C.

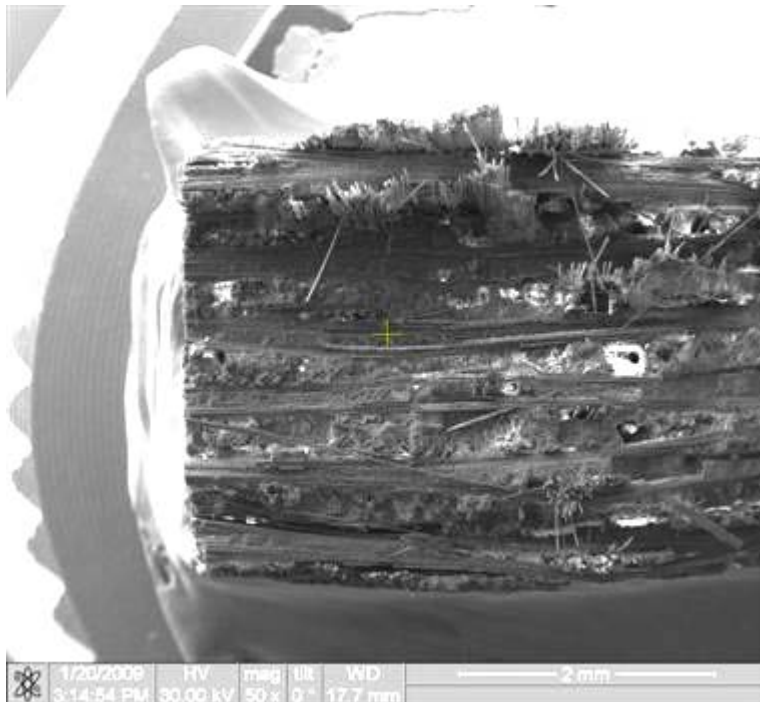


Figure 392. Fracture surface of the N720/AM specimen tested in creep at 87.5 MPa in steam at 1100°C.



Figure 393. Fracture surface of the N720/AM specimen tested in creep at 87.5 MPa in steam at 1100°C.



Figure 394. Fracture surface of the N720/AM specimen tested in creep at 87.5 MPa in steam at 1100°C.

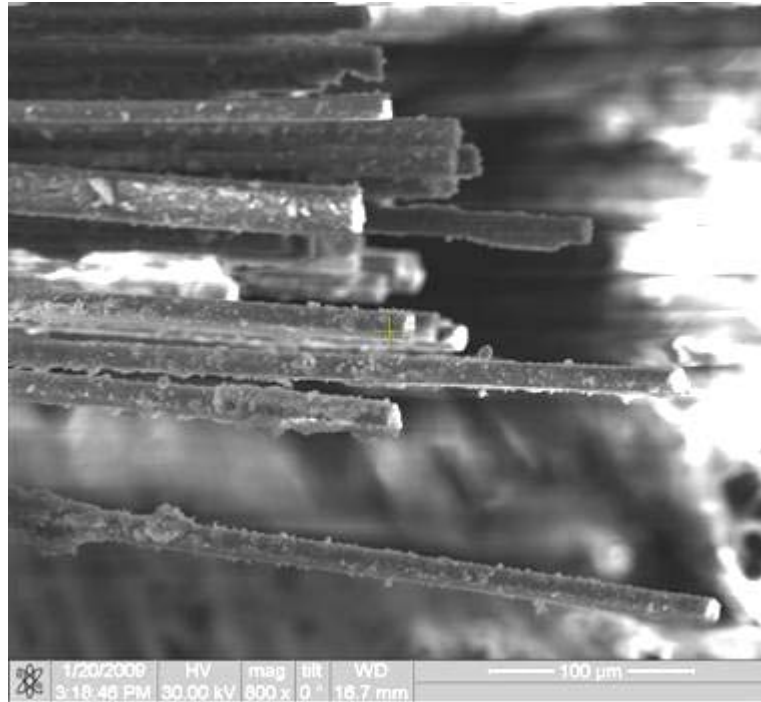


Figure 395. Fracture surface of the N720/AM specimen tested in creep at 87.5 MPa in steam at 1100°C.

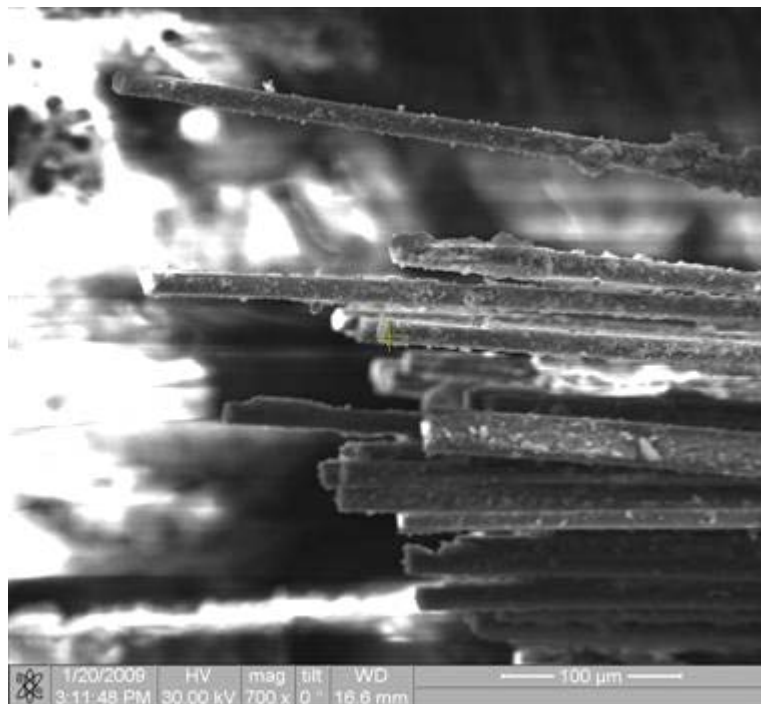


Figure 396. Fracture surface of the N720/AM specimen tested in creep at 87.5 MPa in steam at 1100°C.



Figure 397. Fracture surface of the N720/AM specimen tested in creep at 131 MPa in steam at 1000°C.

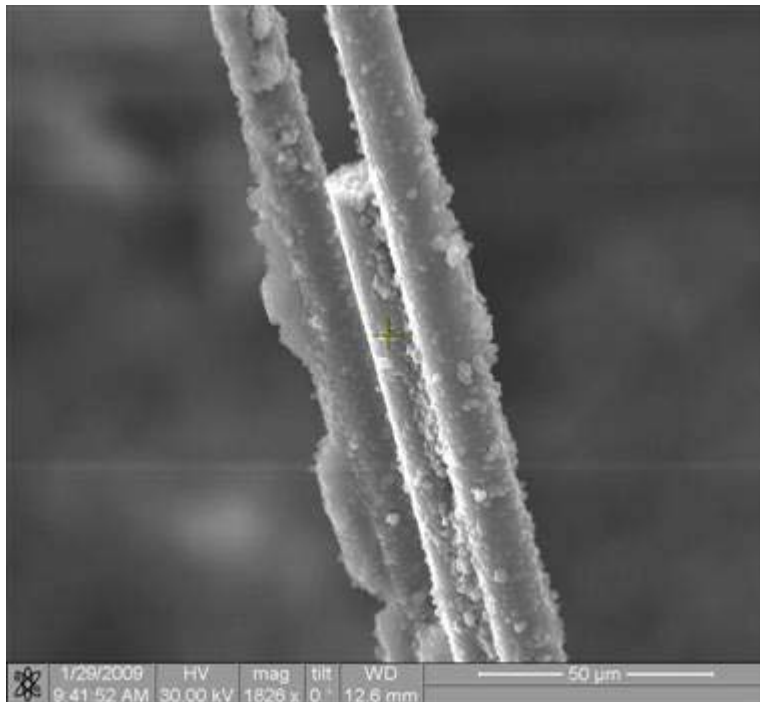


Figure 398. Fracture surface of the N720/AM specimen tested in creep at 131 MPa in steam at 1000°C.

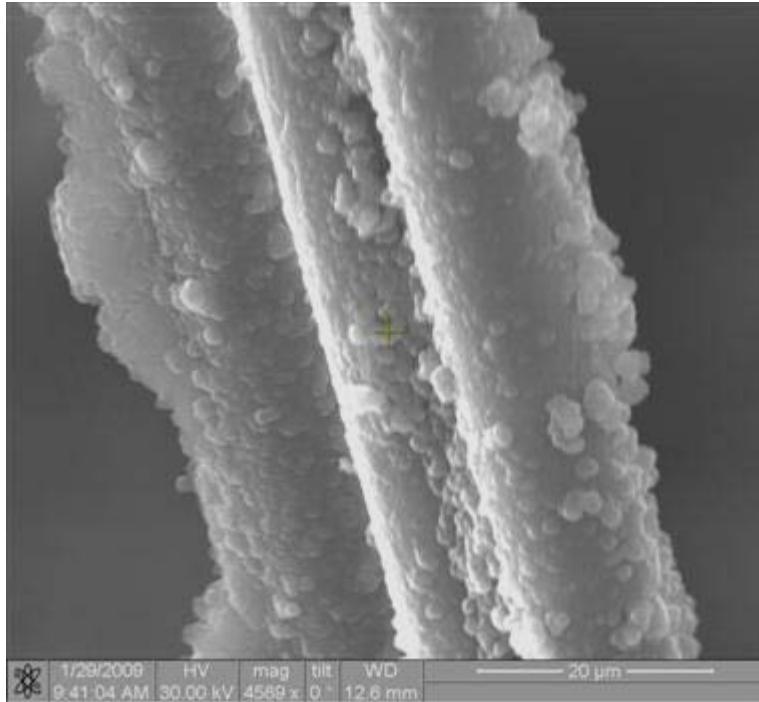


Figure 399. Fracture surface of the N720/AM specimen tested in creep at 131 MPa in steam at 1000°C.

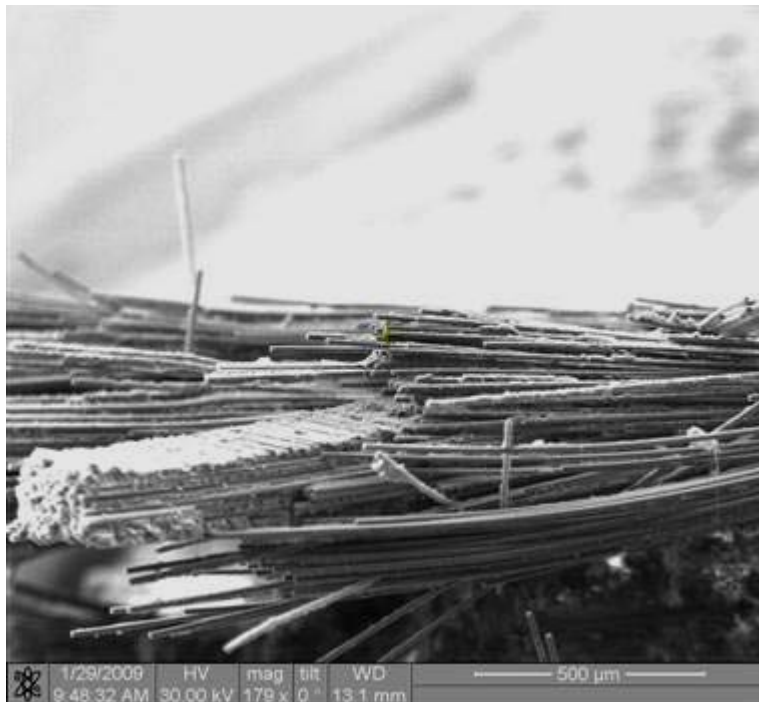


Figure 400. Fracture surface of the N720/AM specimen tested in creep at 131 MPa in steam at 1000°C.

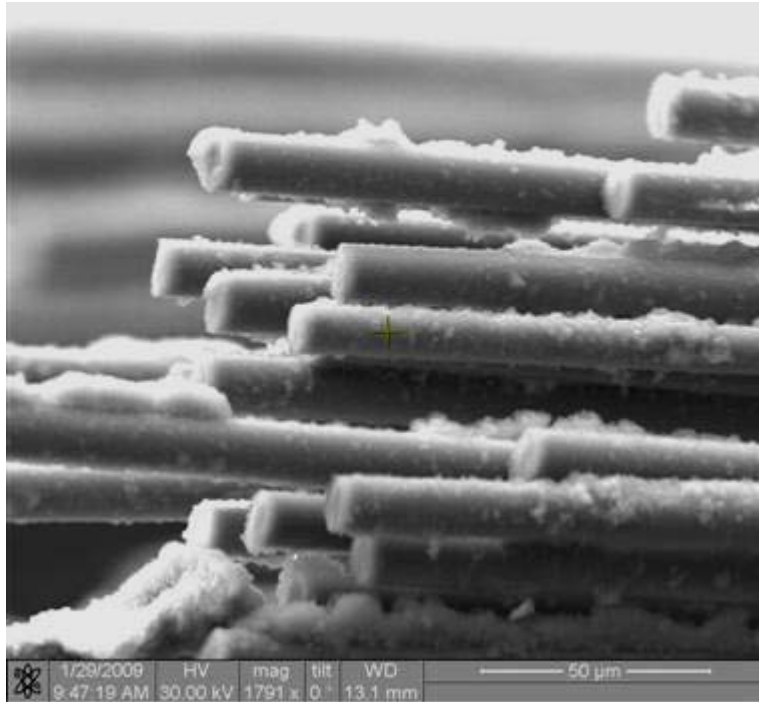


Figure 401. Fracture surface of the N720/AM specimen tested in creep at 131 MPa in steam at 1000°C.

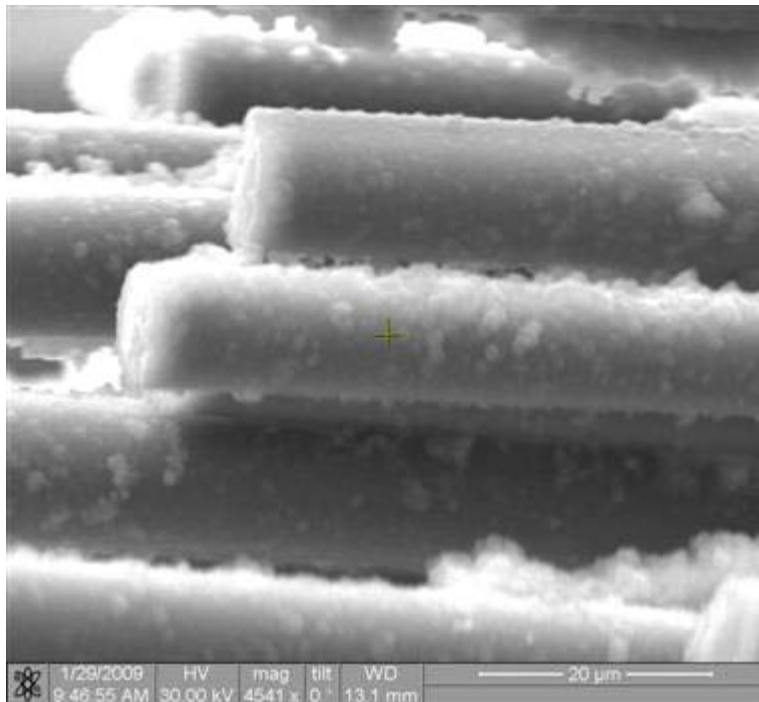


Figure 402. Fracture surface of the N720/AM specimen tested in creep at 131 MPa in steam at 1000°C.



Figure 403. Fracture surface of the N720/AM specimen tested in creep at 131 MPa in steam at 1000°C.

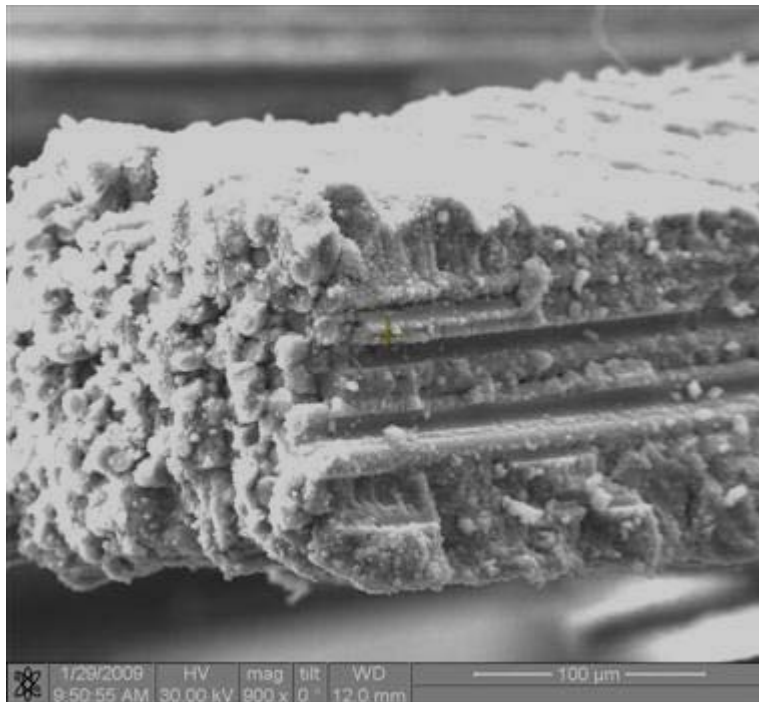


Figure 404. Fracture surface of the N720/AM specimen tested in creep at 131 MPa in steam at 1000°C.

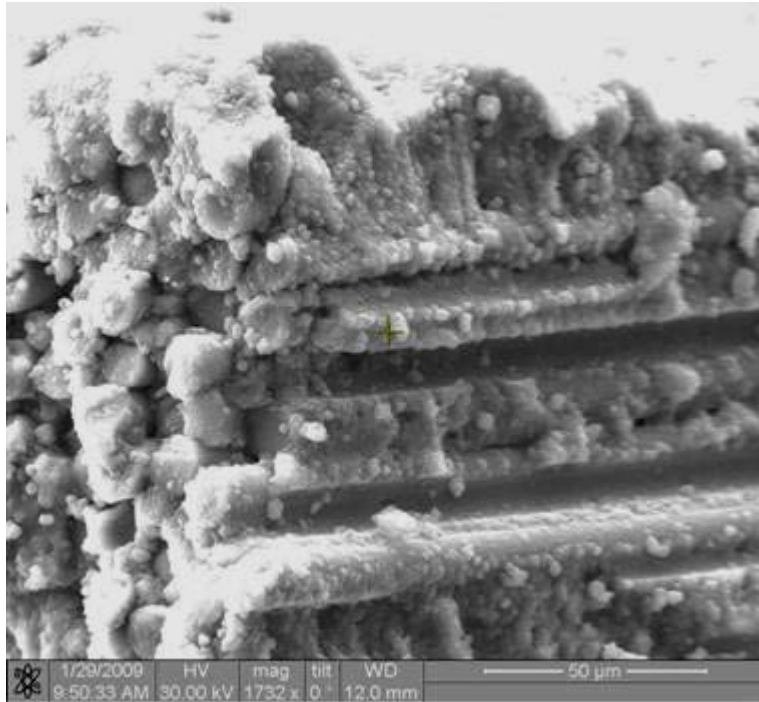


Figure 405. Fracture surface of the N720/AM specimen tested in creep at 131 MPa in steam at 1000°C.

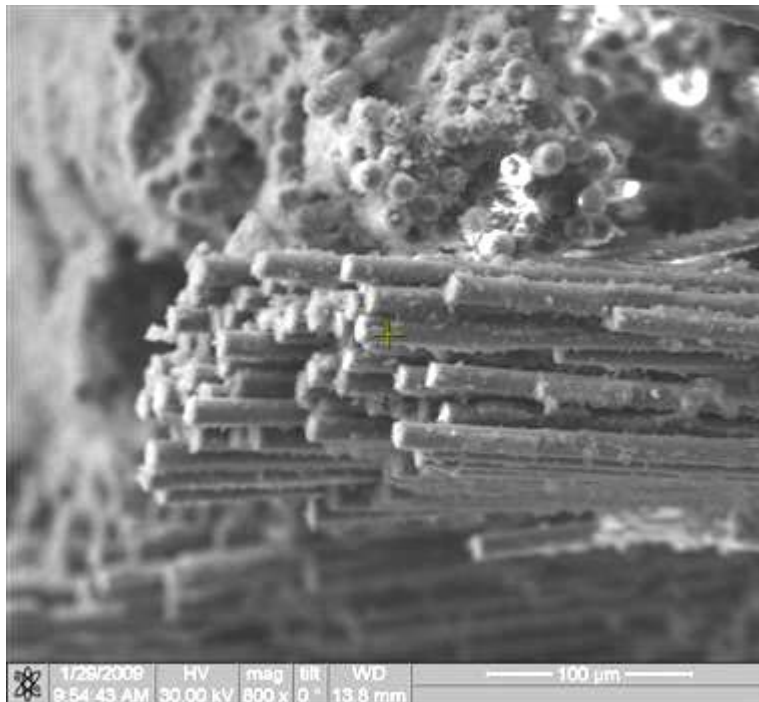


Figure 406. Fracture surface of the N720/AM specimen tested in creep at 131 MPa in steam at 1000°C.

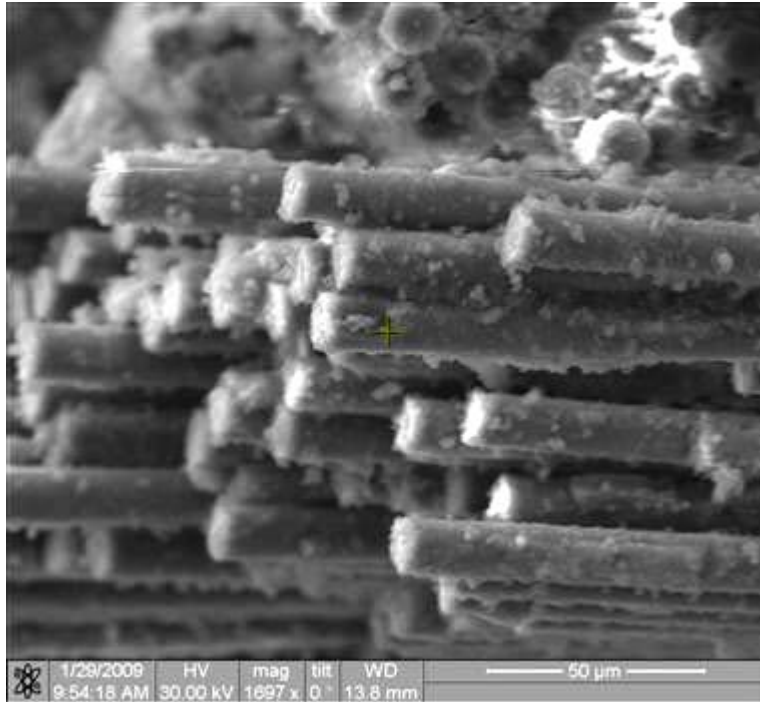


Figure 407. Fracture surface of the N720/AM specimen tested in creep at 131 MPa in steam at 1000°C.

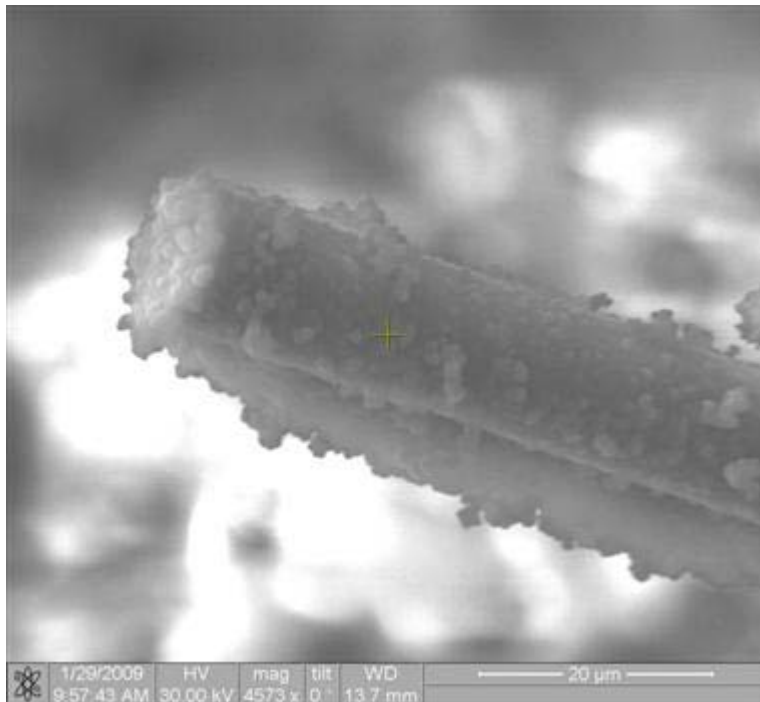


Figure 408. Fracture surface of the N720/AM specimen tested in creep at 131 MPa in steam at 1000°C.

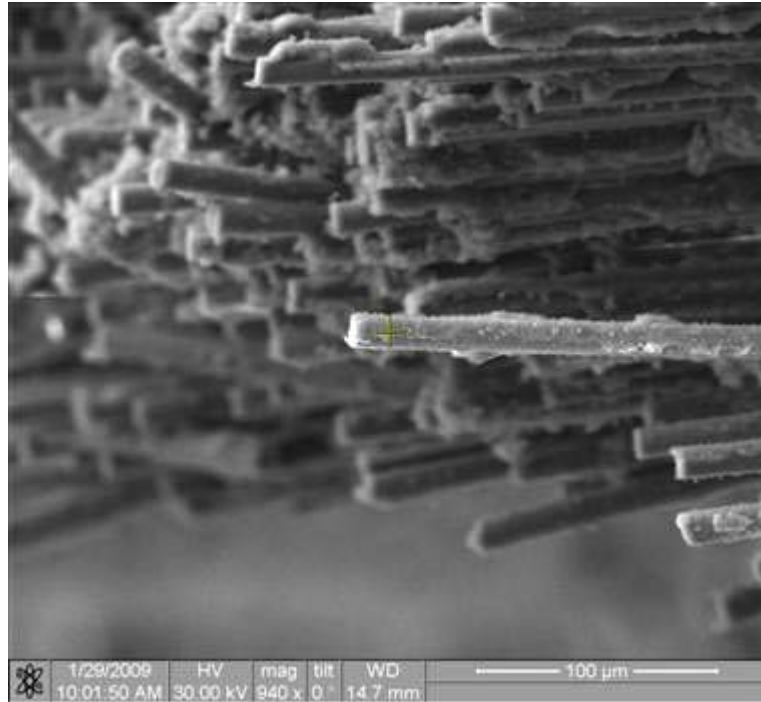


Figure 409. Fracture surface of the N720/AM specimen tested in creep at 131 MPa in steam at 1000°C.

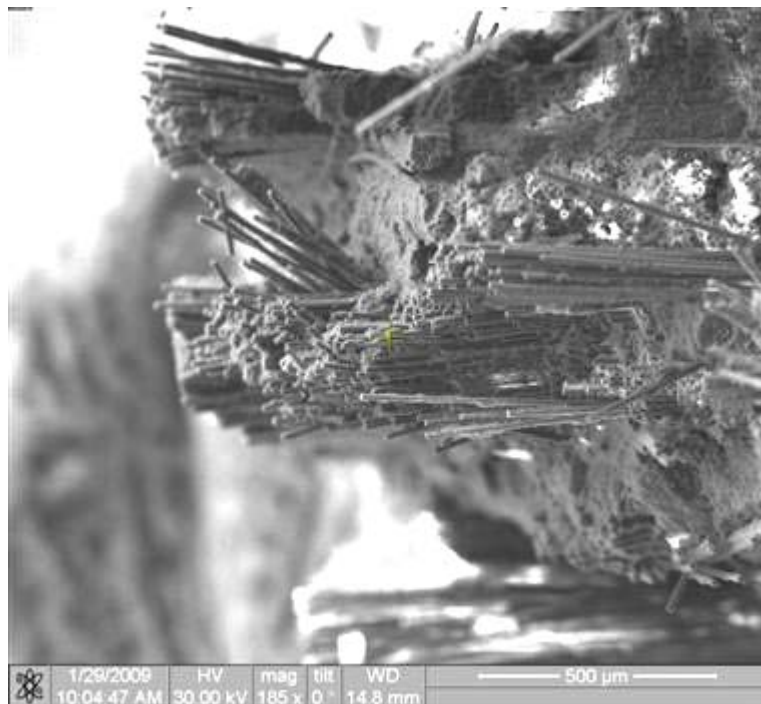


Figure 410. Fracture surface of the N720/AM specimen tested in creep at 131 MPa in steam at 1000°C.

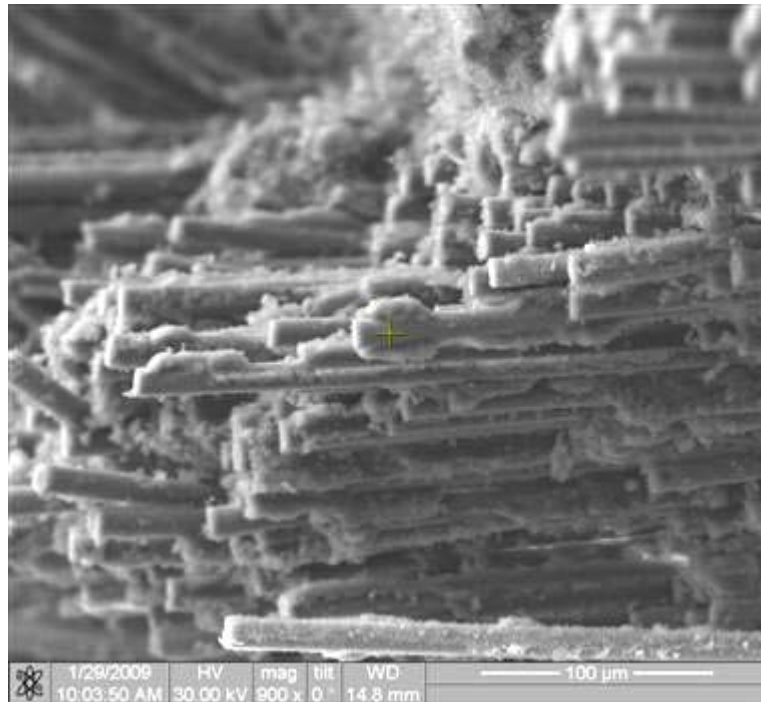


Figure 411. Fracture surface of the N720/AM specimen tested in creep at 131 MPa in steam at 1000°C.

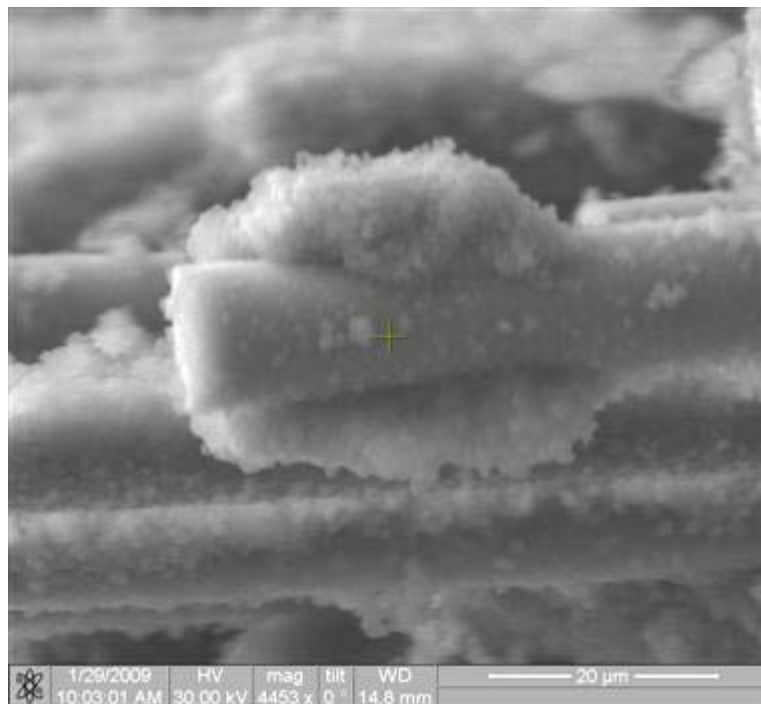


Figure 412. Fracture surface of the N720/AM specimen tested in creep at 131 MPa in steam at 1000°C.

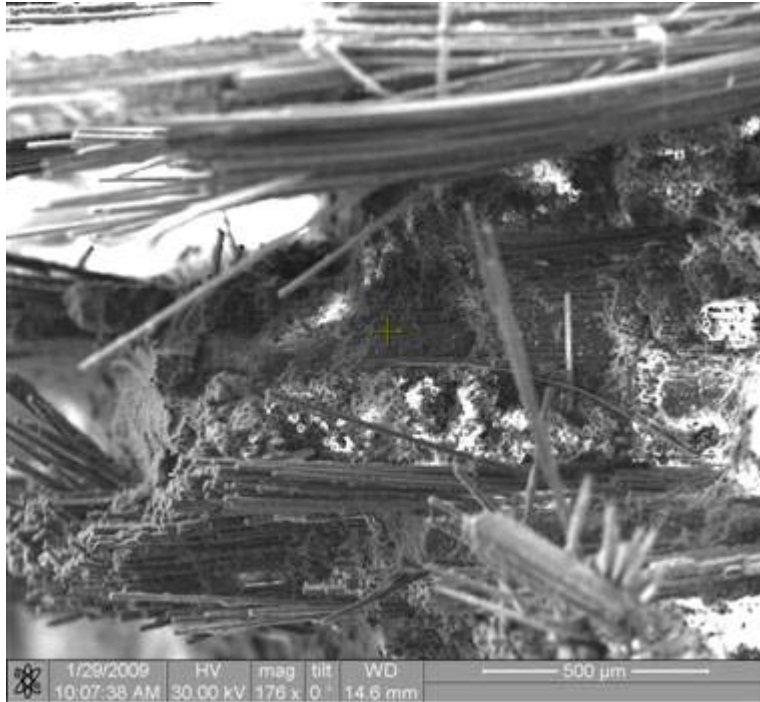


Figure 413. Fracture surface of the N720/AM specimen tested in creep at 131 MPa in steam at 1000°C.



Figure 414. Fracture surface of the N720/AM specimen tested in creep at 131 MPa in steam at 1000°C.



Figure 415. Fracture surface of the N720/AM specimen tested in creep at 131 MPa in steam at 1000°C.



Figure 416. Fracture surface of the N720/AM specimen tested in creep at 131 MPa in steam at 1000°C.

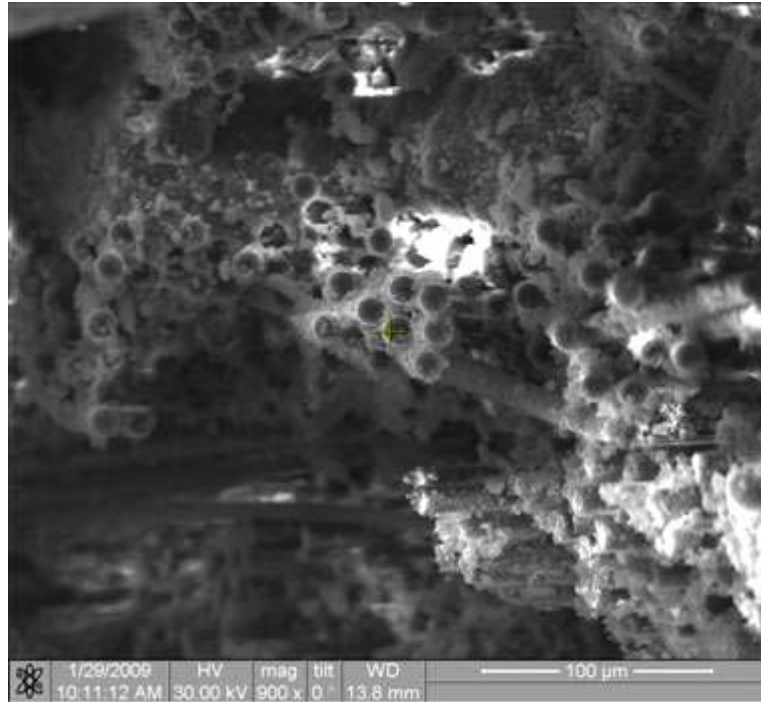


Figure 417. Fracture surface of the N720/AM specimen tested in creep at 131 MPa in steam at 1000°C.

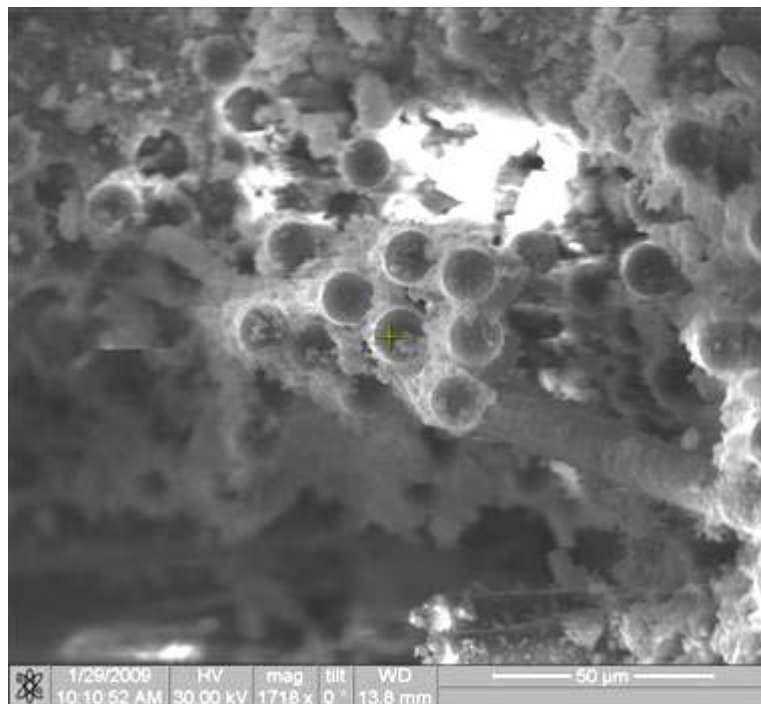


Figure 418. Fracture surface of the N720/AM specimen tested in creep at 131 MPa in steam at 1000°C.

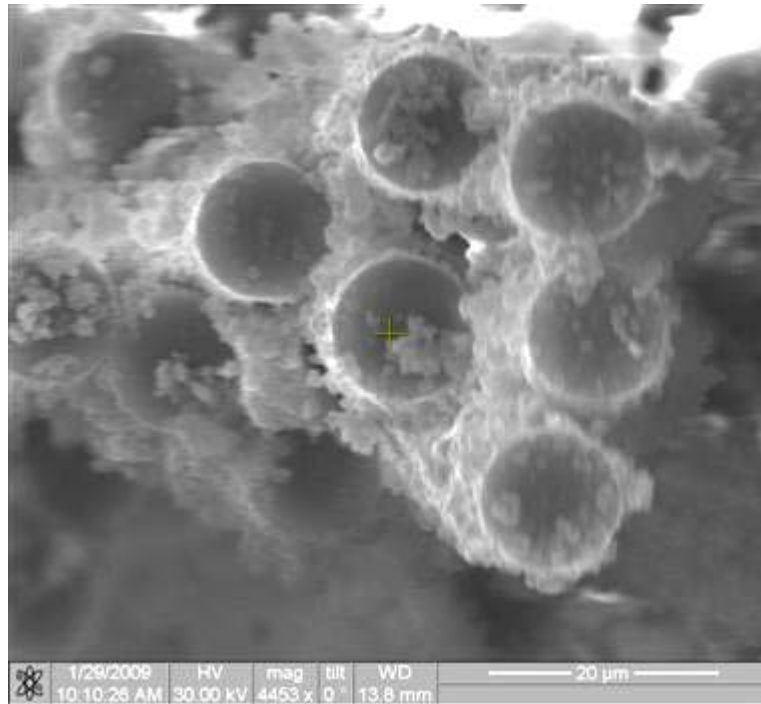


Figure 419. Fracture surface of the N720/AM specimen tested in creep at 131 MPa in steam at 1000°C.

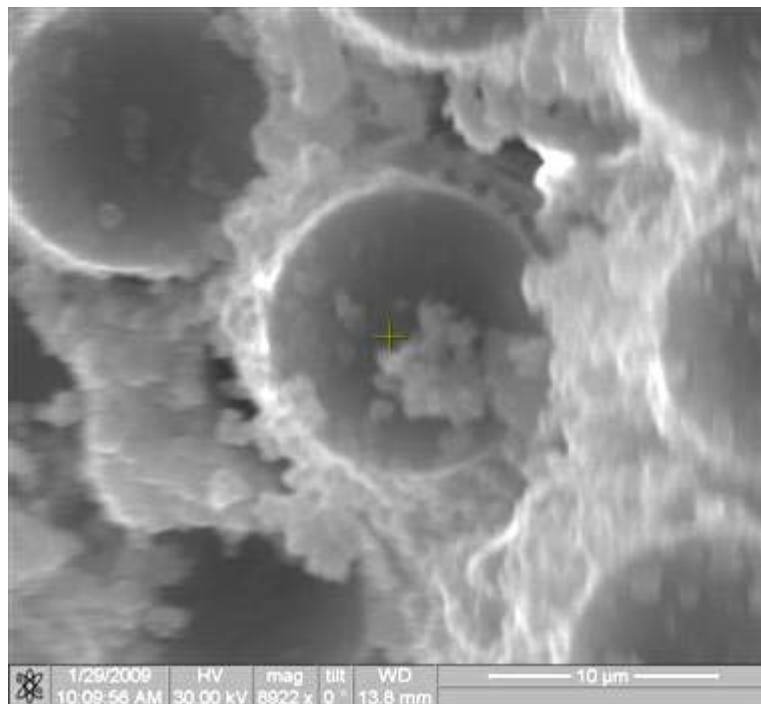


Figure 420. Fracture surface of the N720/AM specimen tested in creep at 131 MPa in steam at 1000°C.

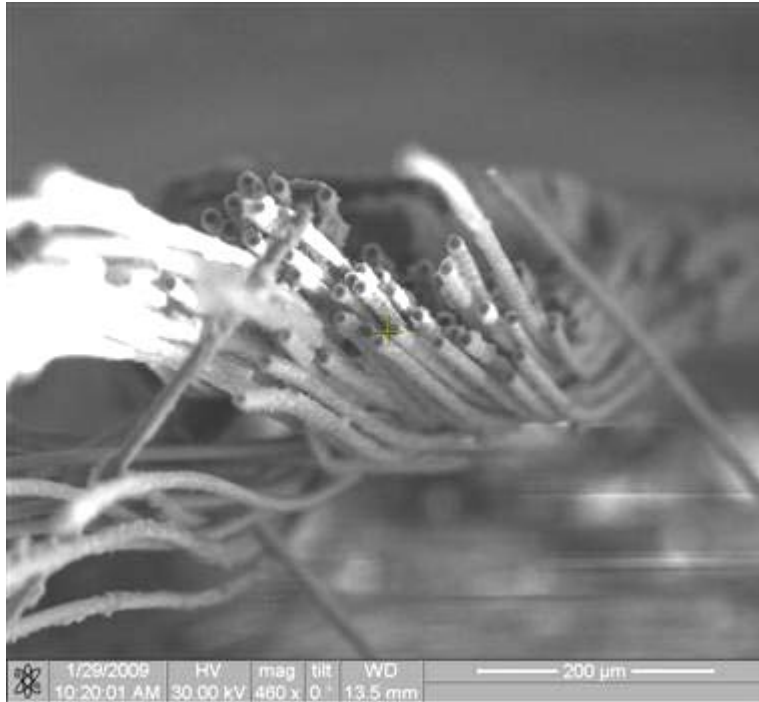


Figure 421. Fracture surface of the N720/AM specimen tested in creep at 131 MPa in steam at 1000°C.

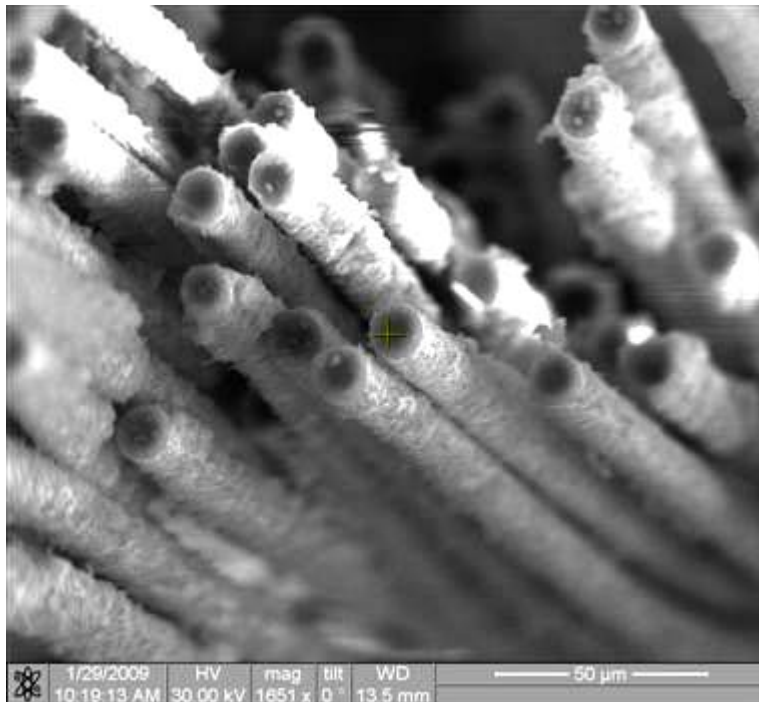


Figure 422. Fracture surface of the N720/AM specimen tested in creep at 131 MPa in steam at 1000°C.



Figure 423. Fracture surface of the N720/AM specimen tested in creep at 131 MPa in steam at 1000°C.

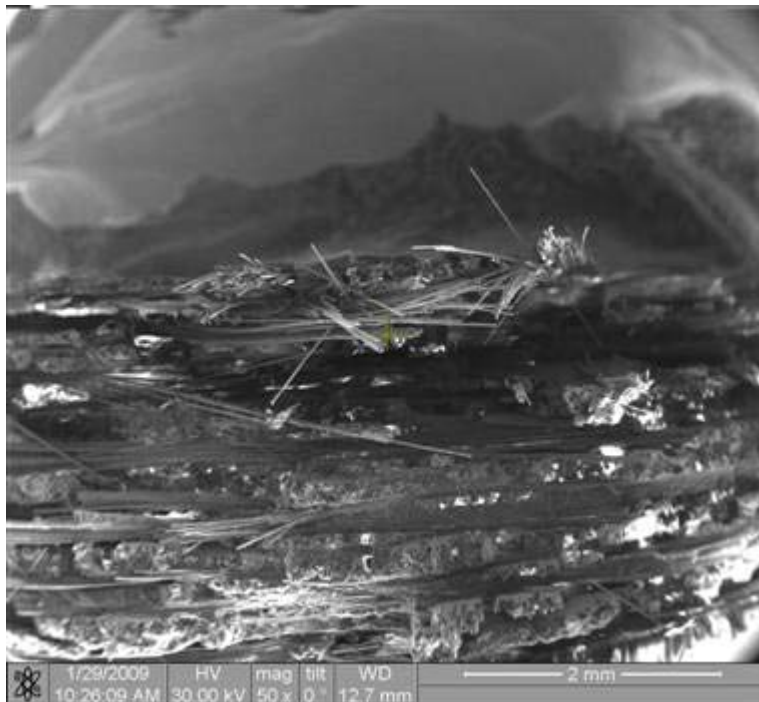


Figure 424. Fracture surface of the N720/AM specimen tested in creep at 131 MPa in steam at 1000°C.



Figure 425. Fracture surface of the N720/AM specimen tested in creep at 131 MPa in steam at 1000°C.



Figure 426. Fracture surface of the N720/AM specimen tested in creep at 131 MPa in steam at 1000°C.

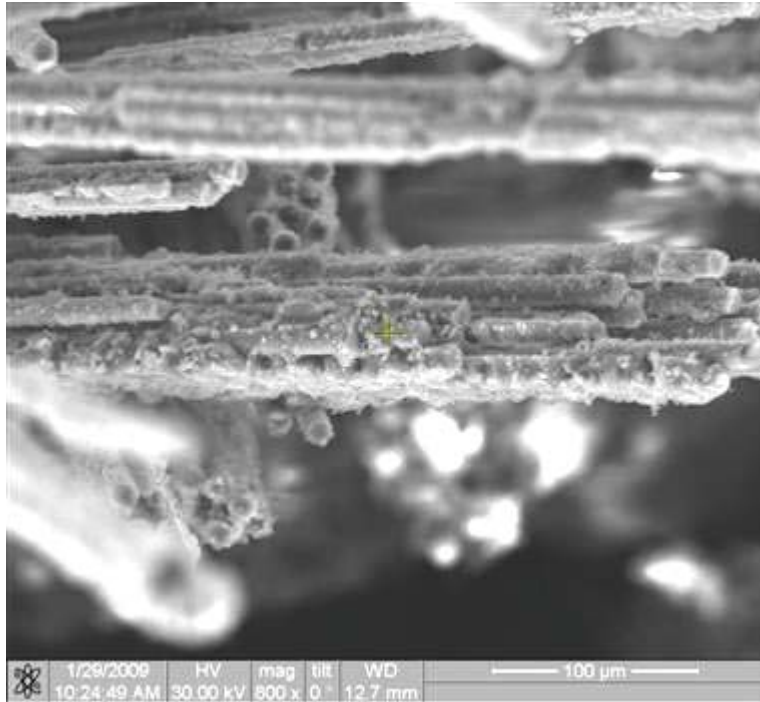


Figure 427. Fracture surface of the N720/AM specimen tested in creep at 131 MPa in steam at 1000°C.

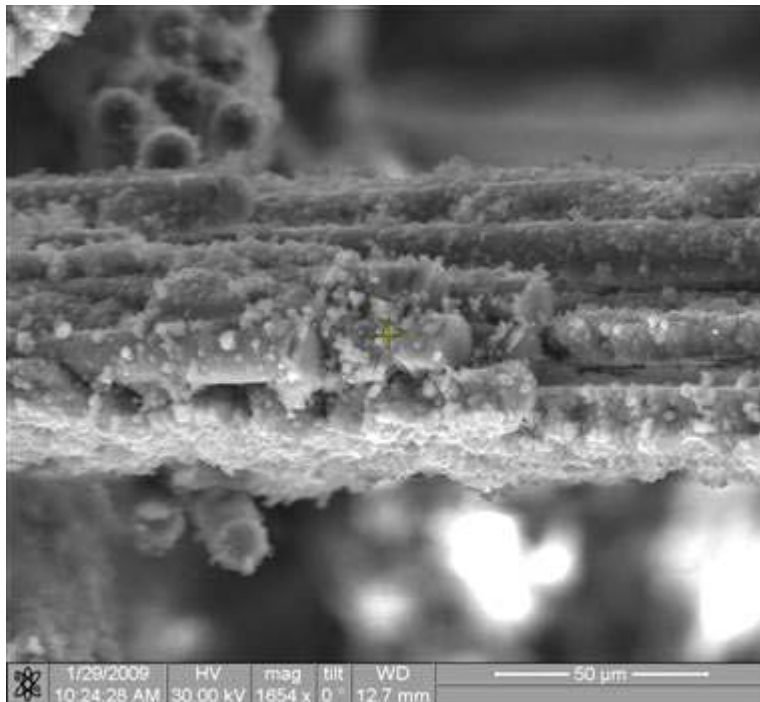


Figure 428. Fracture surface of the N720/AM specimen tested in creep at 131 MPa in steam at 1000°C.

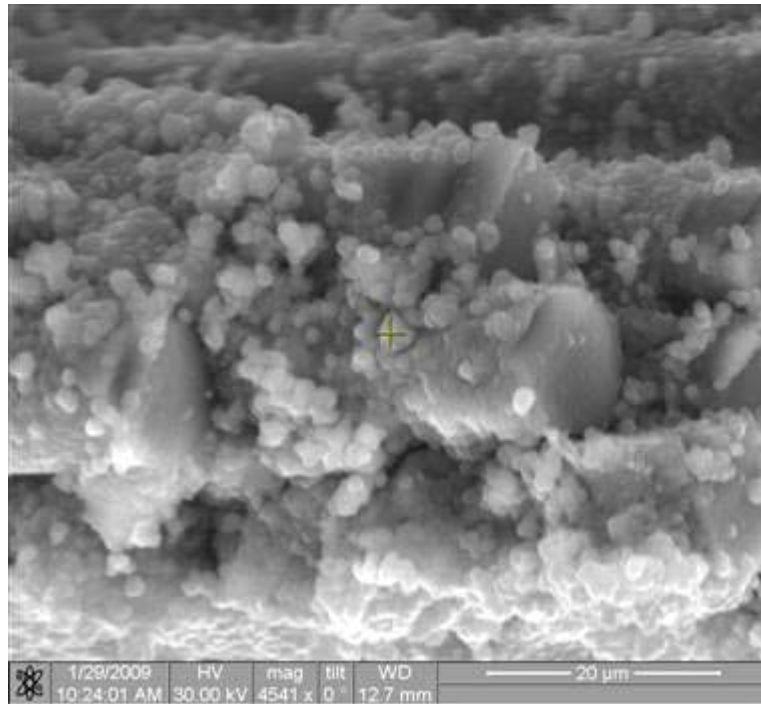


Figure 429. Fracture surface of the N720/AM specimen tested in creep at 131 MPa in steam at 1000°C.

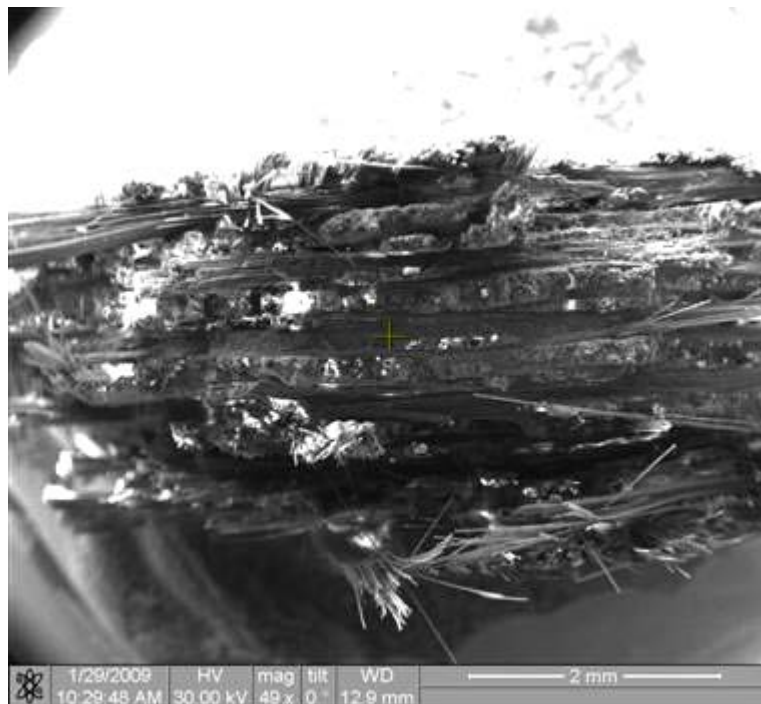


Figure 430. Fracture surface of the N720/AM specimen tested in creep at 131 MPa in steam at 1000°C.

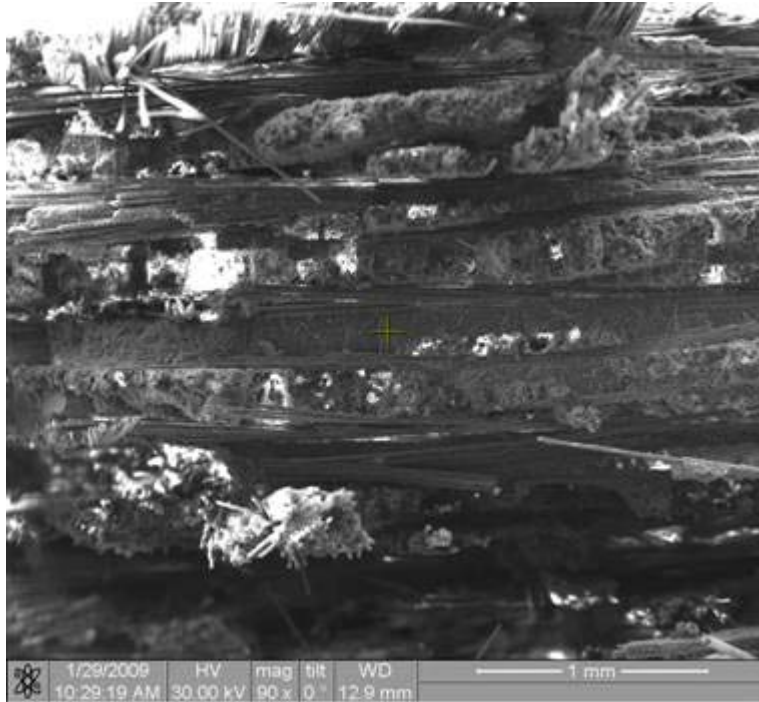


Figure 431. Fracture surface of the N720/AM specimen tested in creep at 131 MPa in steam at 1000°C.

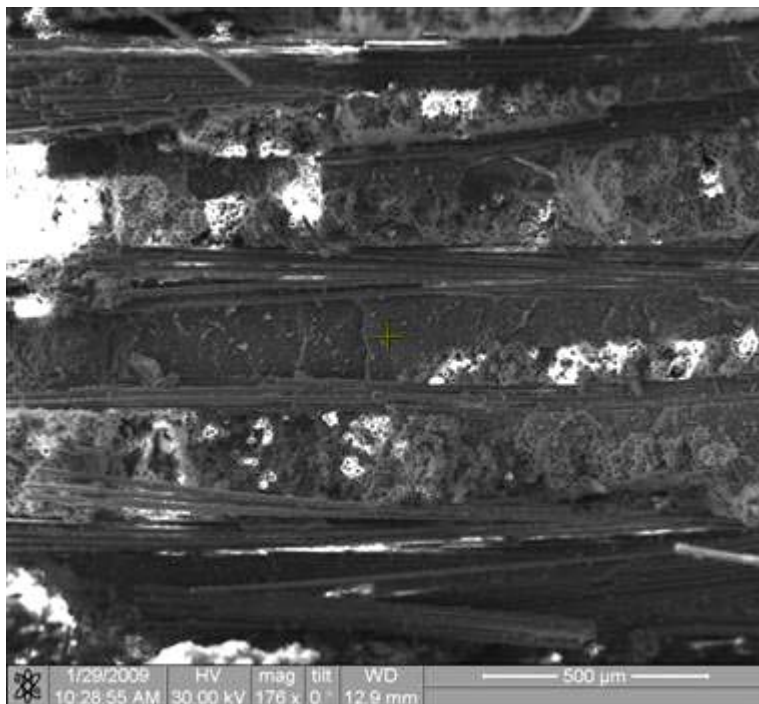


Figure 432. Fracture surface of the N720/AM specimen tested in creep at 131 MPa in steam at 1000°C.

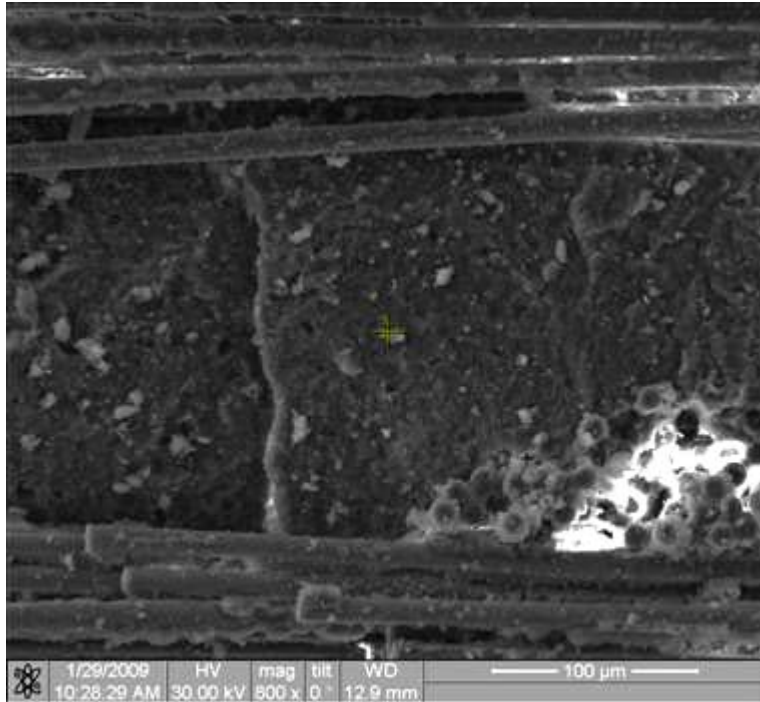


Figure 433. Fracture surface of the N720/AM specimen tested in creep at 131 MPa in steam at 1000°C.

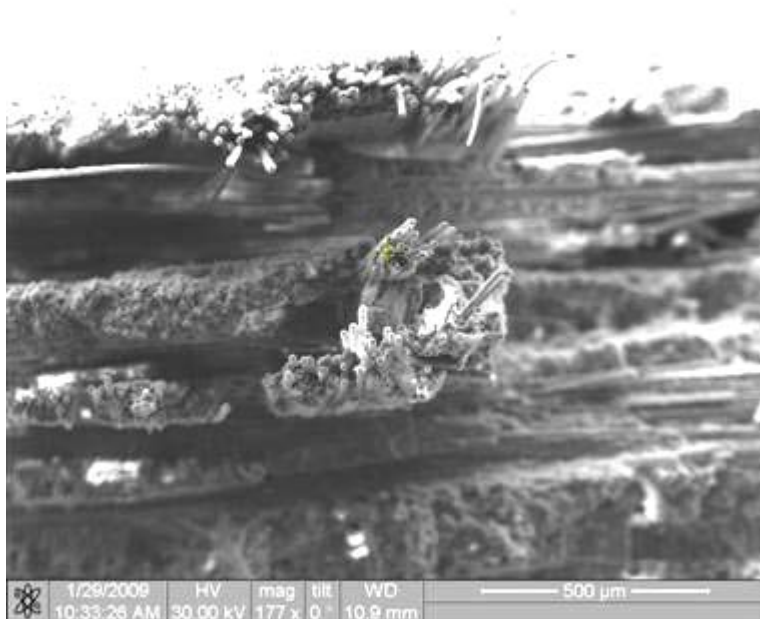


Figure 434. Fracture surface of the N720/AM specimen tested in creep at 131 MPa in steam at 1000°C.

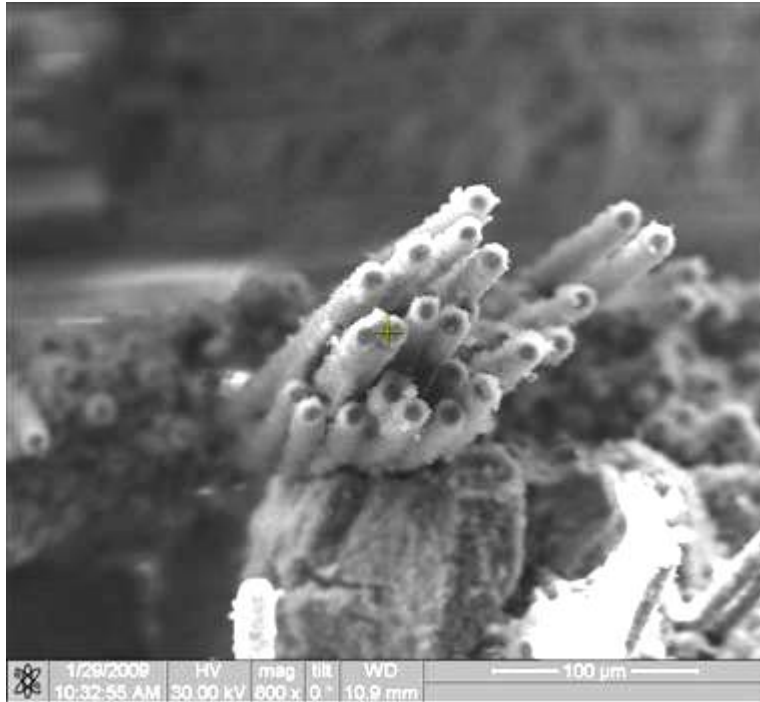


Figure 435. Fracture surface of the N720/AM specimen tested in creep at 131 MPa in steam at 1000°C.



Figure 436. Fracture surface of the N720/AM specimen tested in creep at 131 MPa in steam at 1000°C.

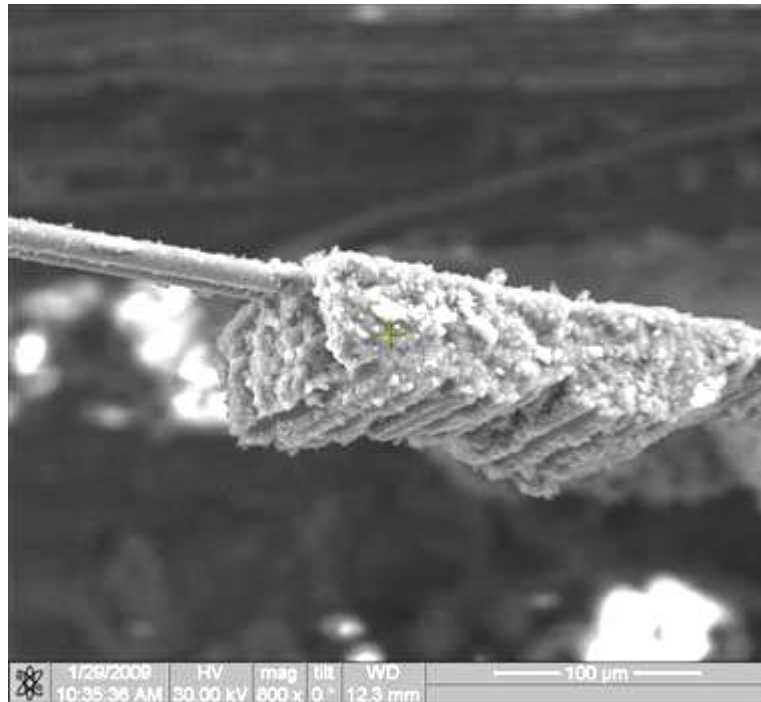


Figure 437. Fracture surface of the N720/AM specimen tested in creep at 131 MPa in steam at 1000°C.

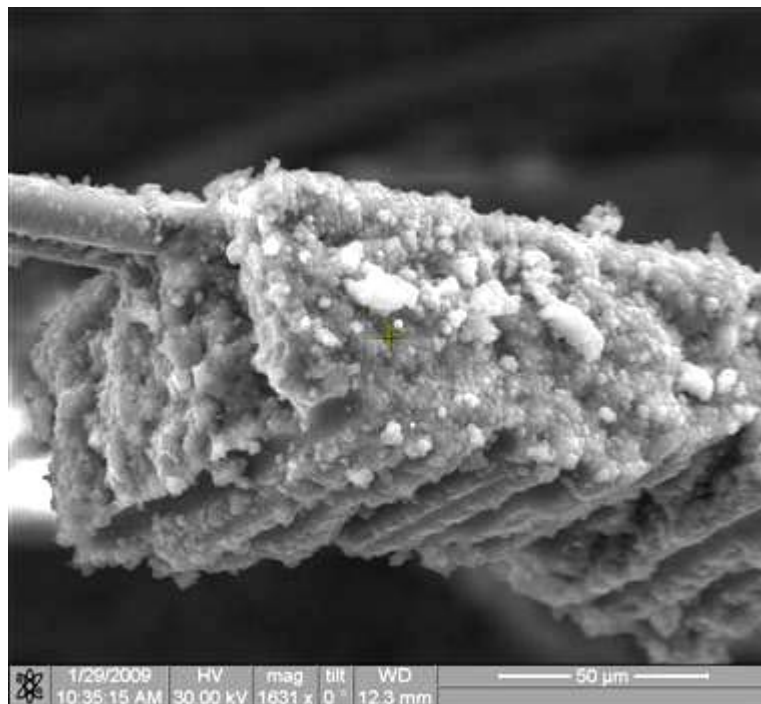


Figure 438. Fracture surface of the N720/AM specimen tested in creep at 131 MPa in steam at 1000°C.

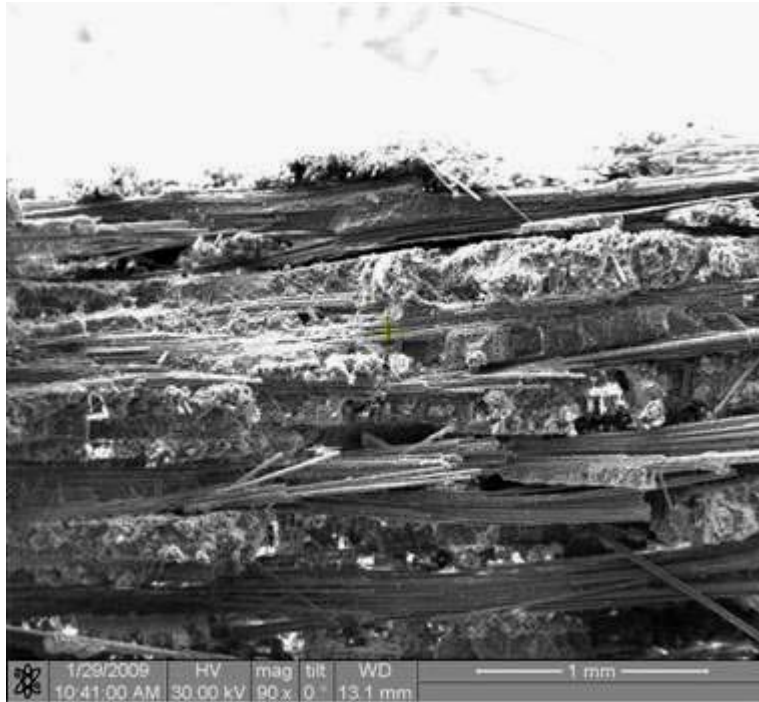


Figure 439. Fracture surface of the N720/AM specimen tested in creep at 131 MPa in steam at 1000°C.

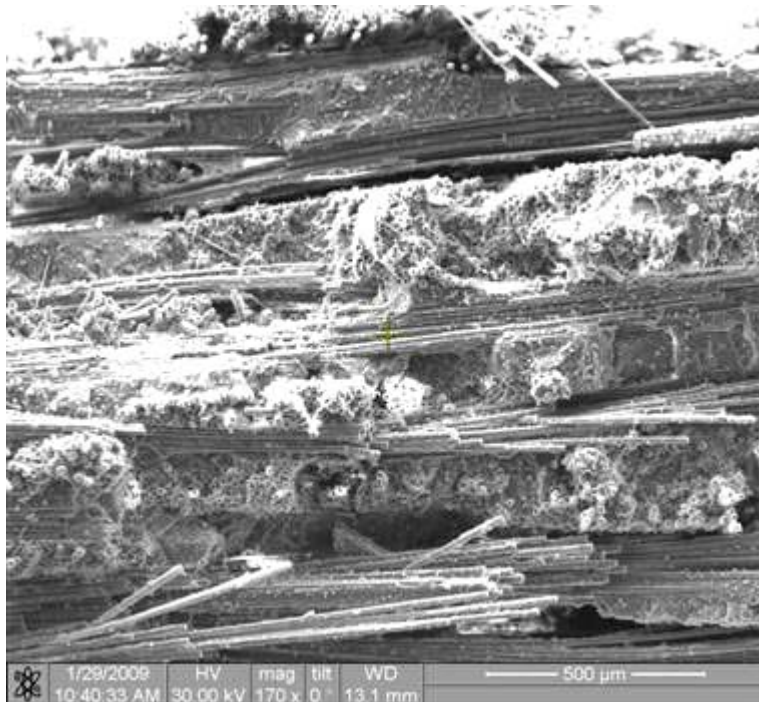


Figure 440. Fracture surface of the N720/AM specimen tested in creep at 131 MPa in steam at 1000°C.

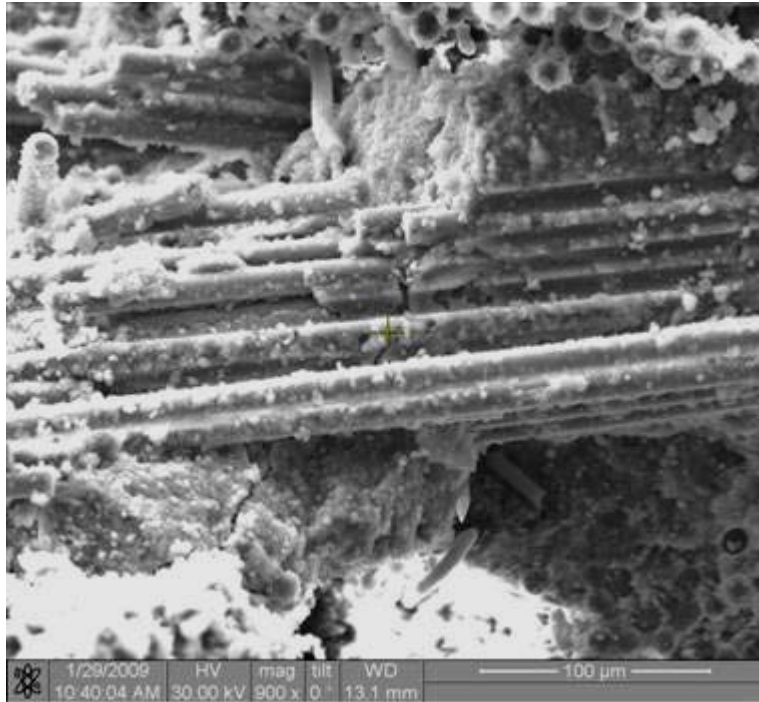


Figure 441. Fracture surface of the N720/AM specimen tested in creep at 131 MPa in steam at 1000°C.

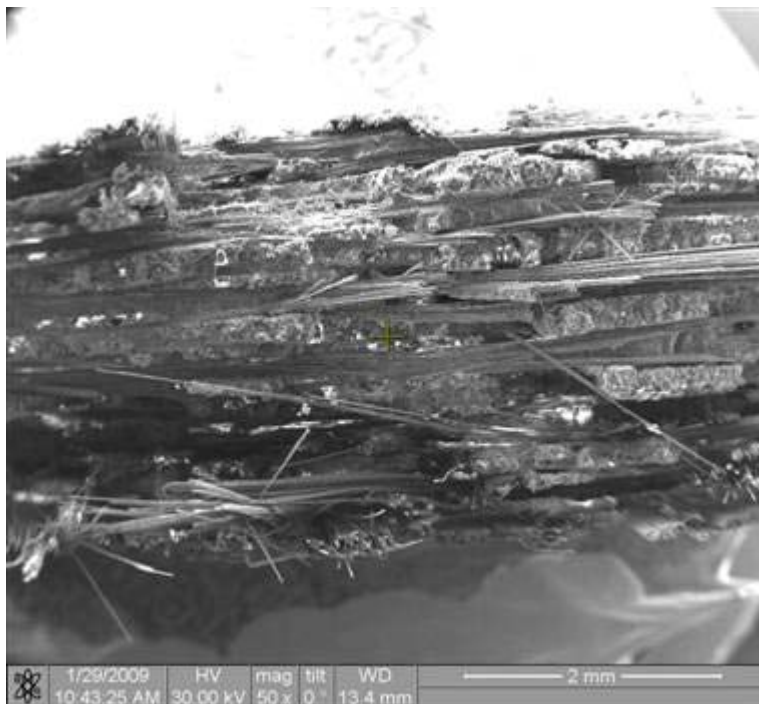


Figure 442. Fracture surface of the N720/AM specimen tested in creep at 131 MPa in steam at 1000°C.

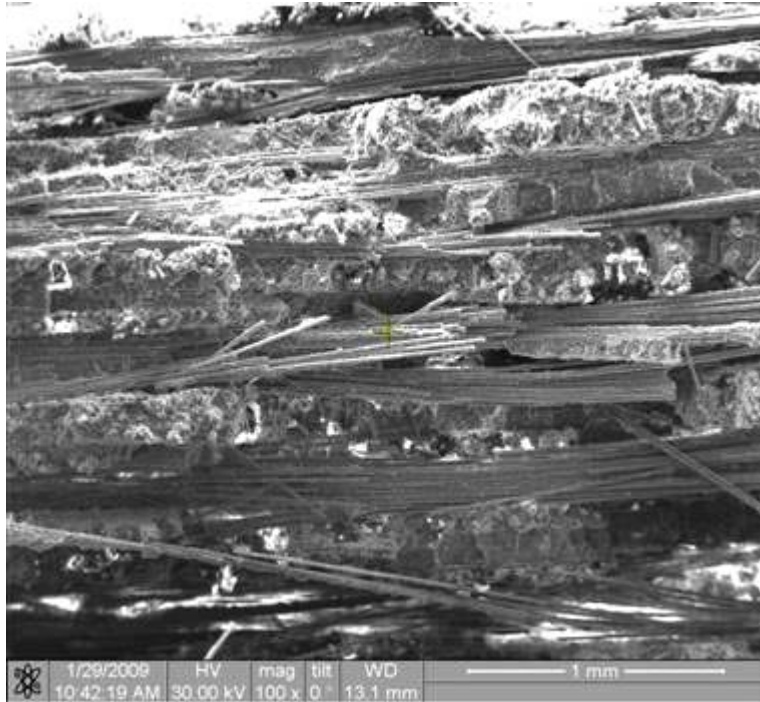


Figure 443. Fracture surface of the N720/AM specimen tested in creep at 131 MPa in steam at 1000°C.

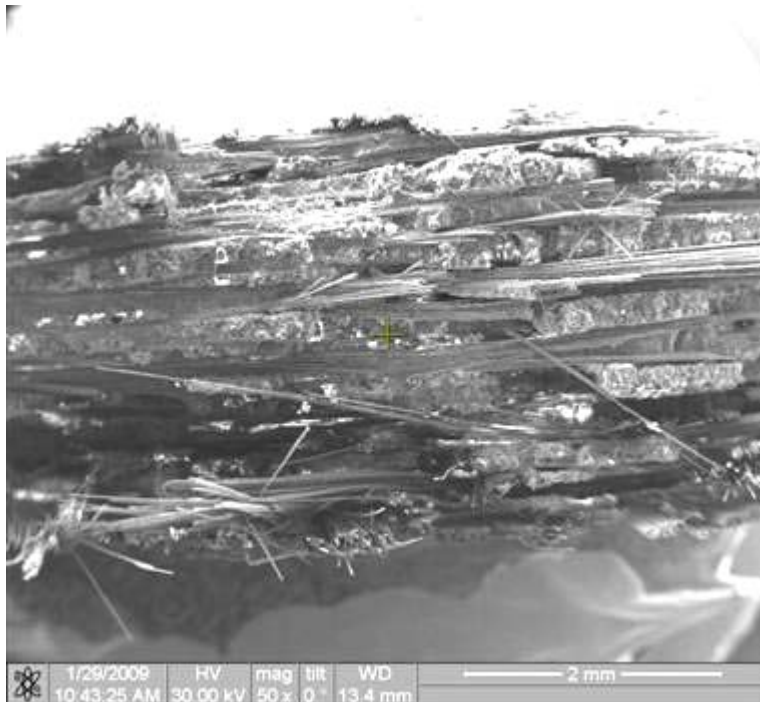


Figure 444. Fracture surface of the N720/AM specimen tested in creep at 131 MPa in steam at 1000°C.

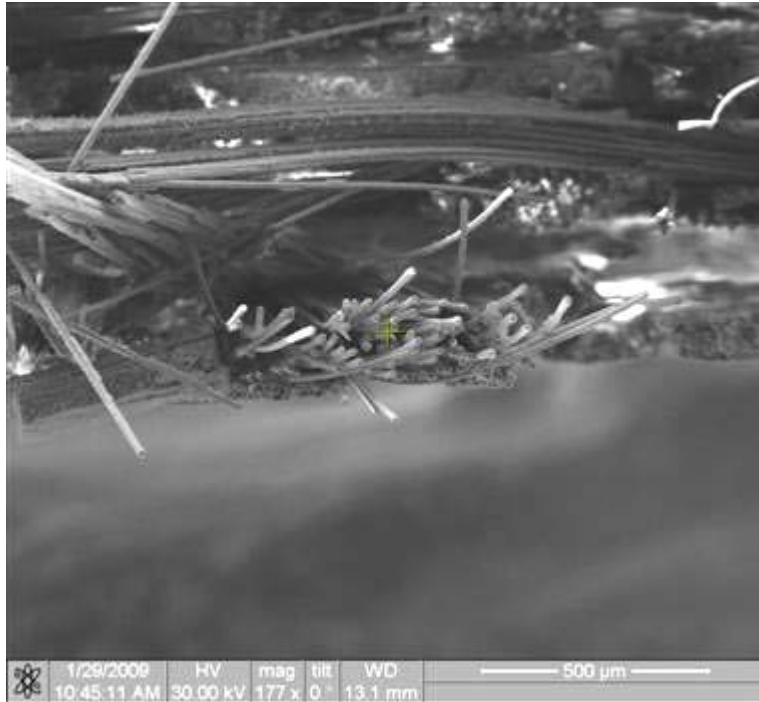


Figure 445. Fracture surface of the N720/AM specimen tested in creep at 131 MPa in steam at 1000°C.

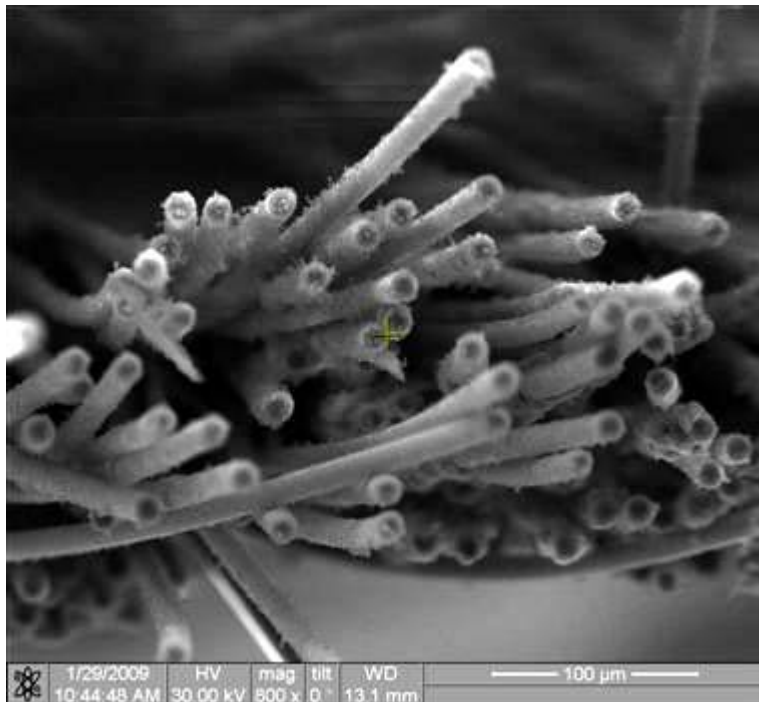


Figure 446. Fracture surface of the N720/AM specimen tested in creep at 131 MPa in steam at 1000°C.

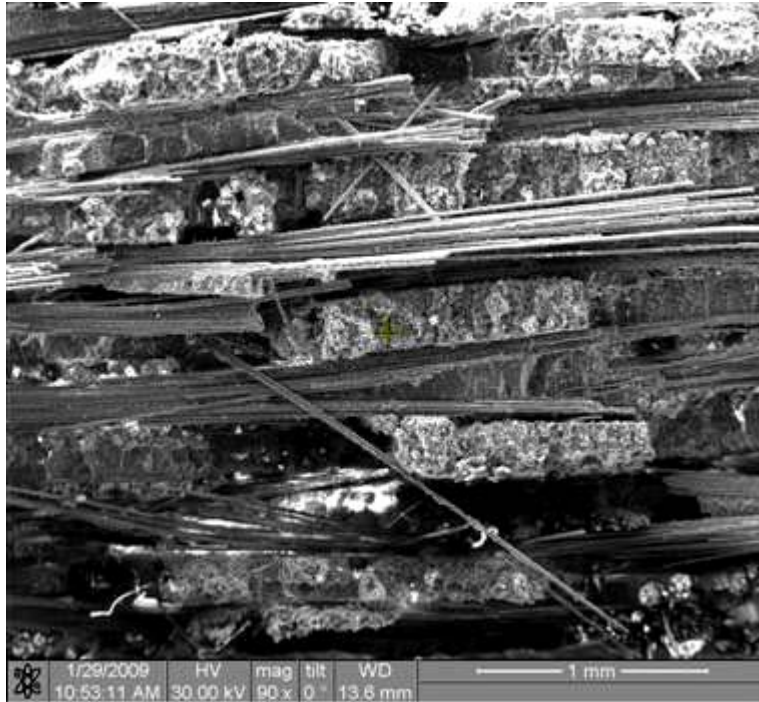


Figure 447. Fracture surface of the N720/AM specimen tested in creep at 131 MPa in steam at 1000°C.

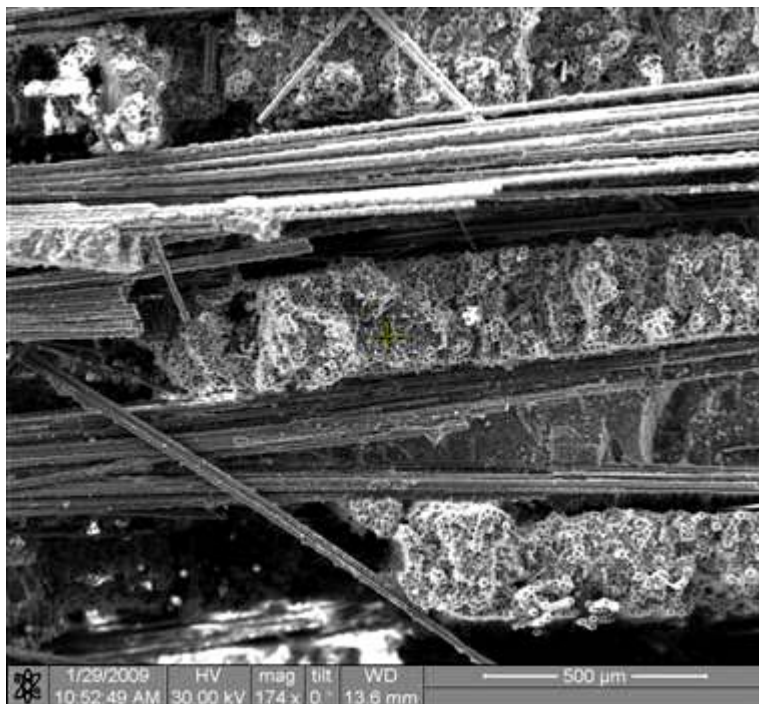


Figure 448. Fracture surface of the N720/AM specimen tested in creep at 131 MPa in steam at 1000°C.

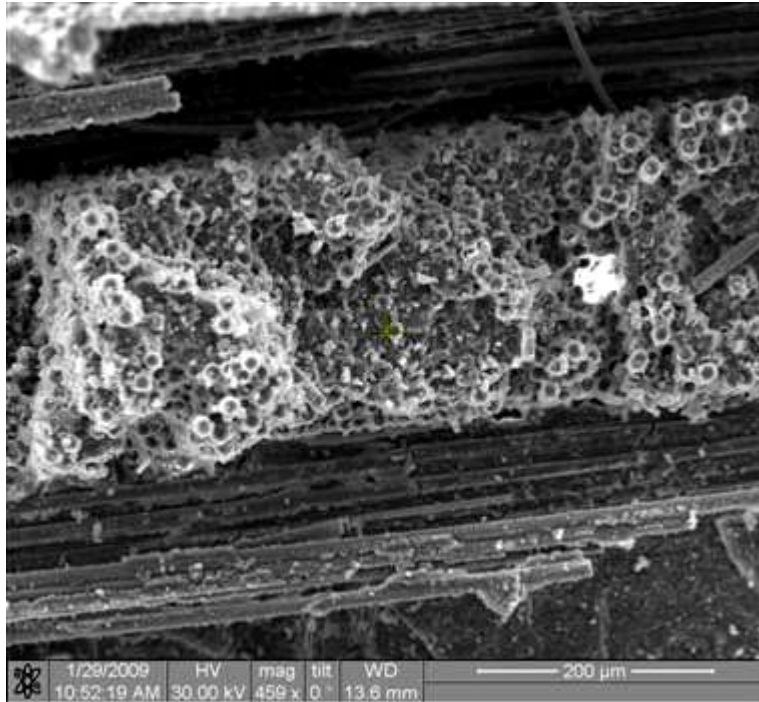


Figure 449. Fracture surface of the N720/AM specimen tested in creep at 131 MPa in steam at 1000°C.

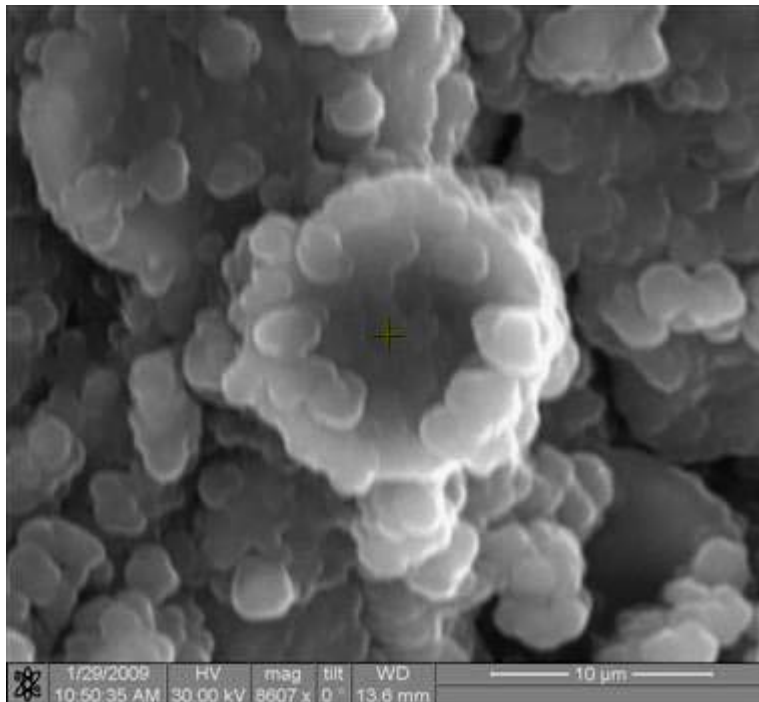


Figure 450. Fracture surface of the N720/AM specimen tested in creep at 131 MPa in steam at 1000°C.

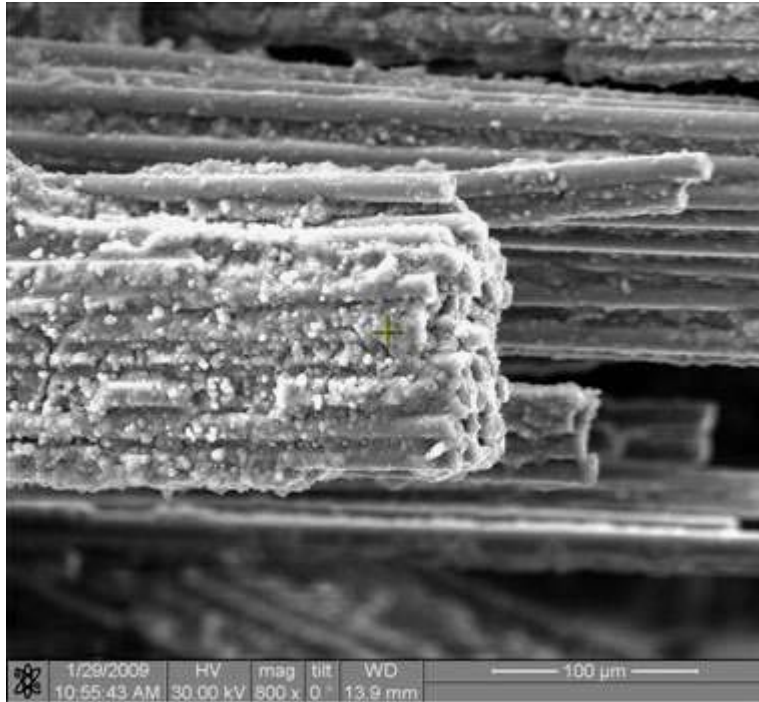


Figure 451. Fracture surface of the N720/AM specimen tested in creep at 131 MPa in steam at 1000°C.

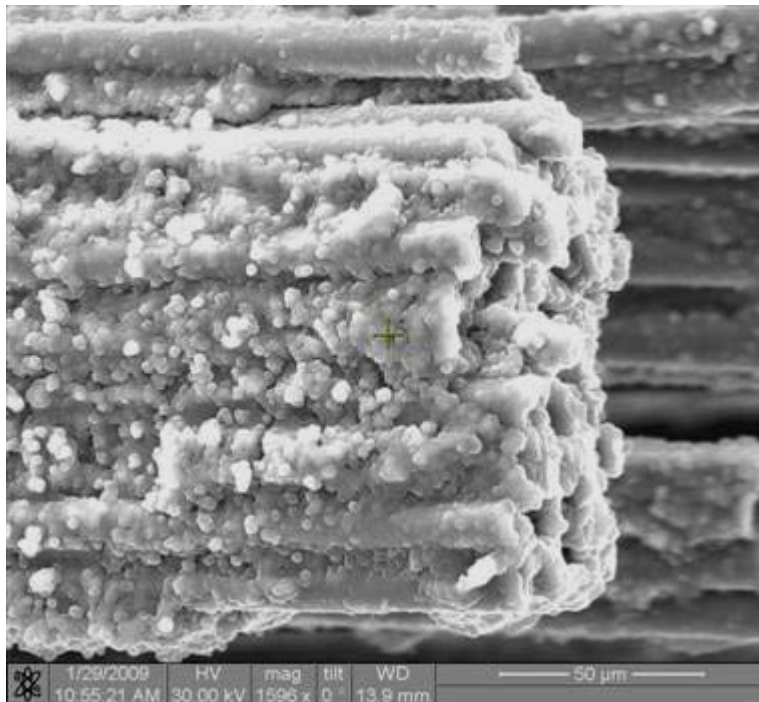


Figure 452. Fracture surface of the N720/AM specimen tested in creep at 131 MPa in steam at 1000°C.



Figure 453. Fracture surface of the N720/AM specimen tested in creep at 131 MPa in steam at 1000°C.

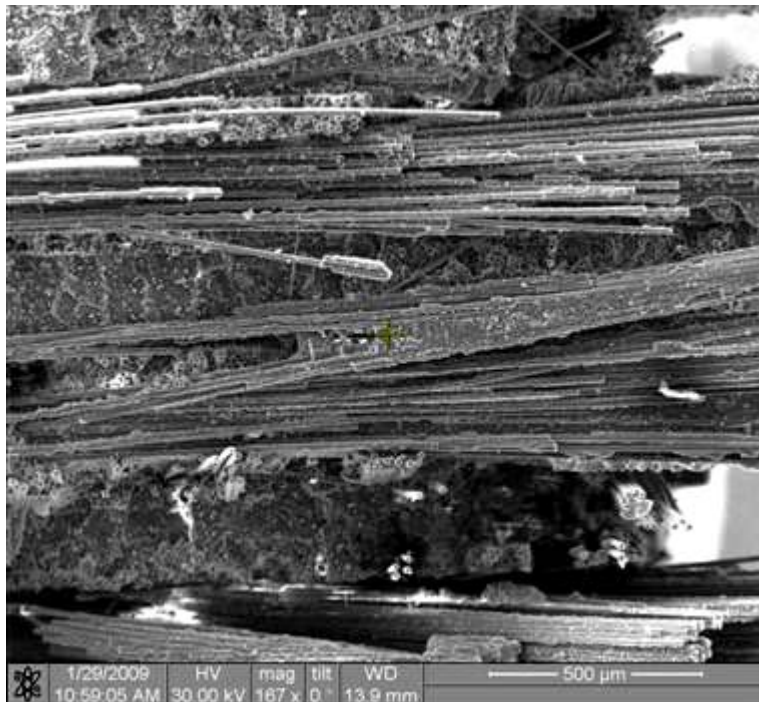


Figure 454. Fracture surface of the N720/AM specimen tested in creep at 131 MPa in steam at 1000°C.

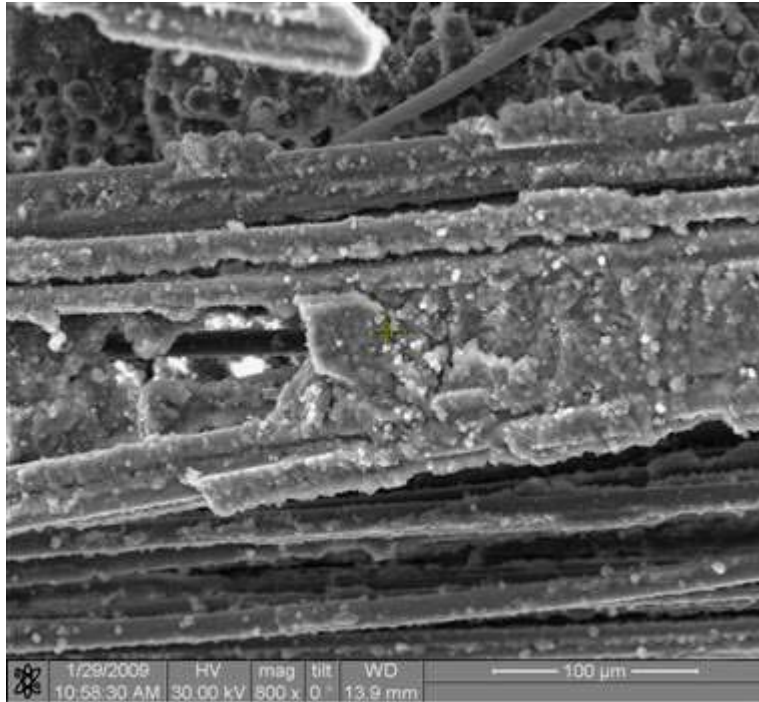


Figure 455. Fracture surface of the N720/AM specimen tested in creep at 131 MPa in steam at 1000°C.

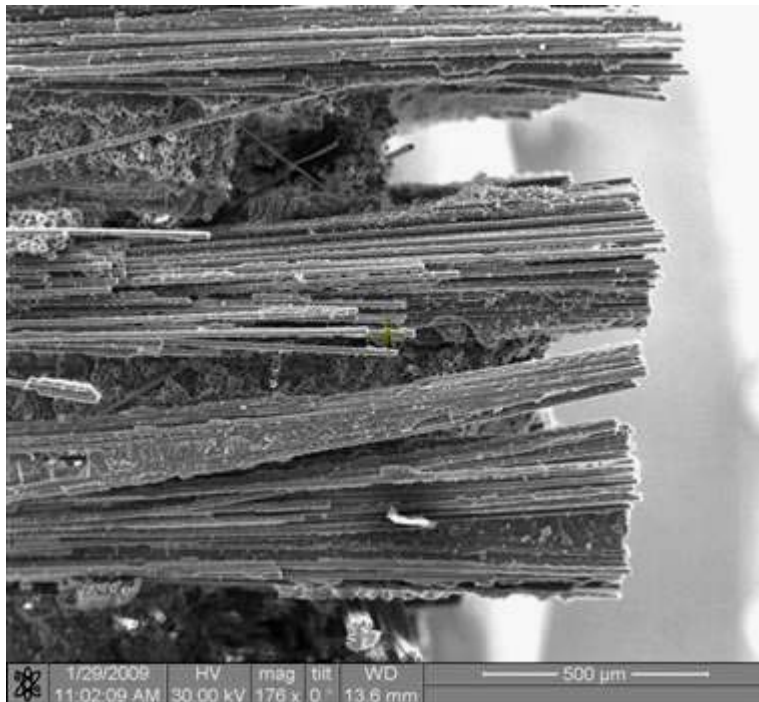


Figure 456. Fracture surface of the N720/AM specimen tested in creep at 131 MPa in steam at 1000°C.



Figure 457. Fracture surface of the N720/AM specimen tested in creep at 131 MPa in steam at 1000°C.

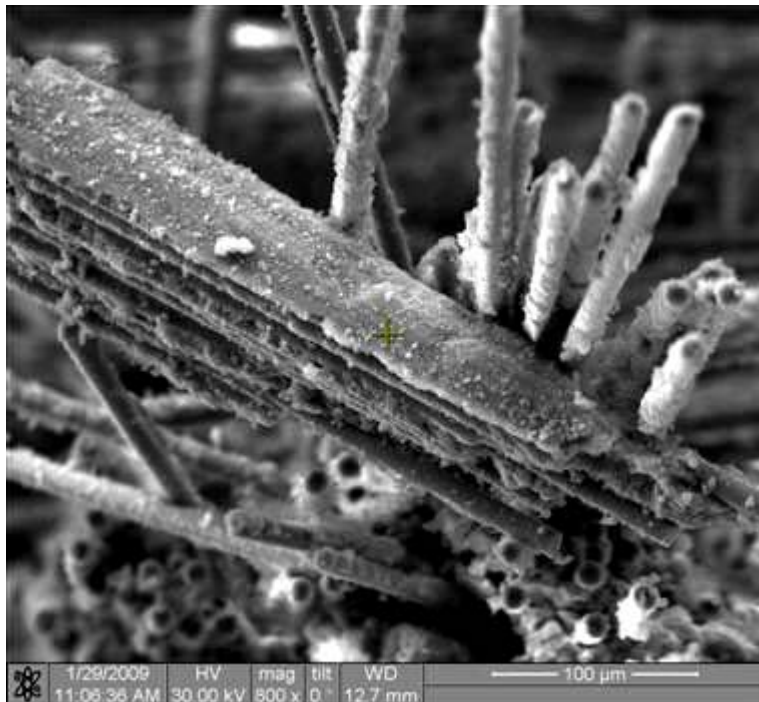


Figure 458. Fracture surface of the N720/AM specimen tested in creep at 131 MPa in steam at 1000°C.

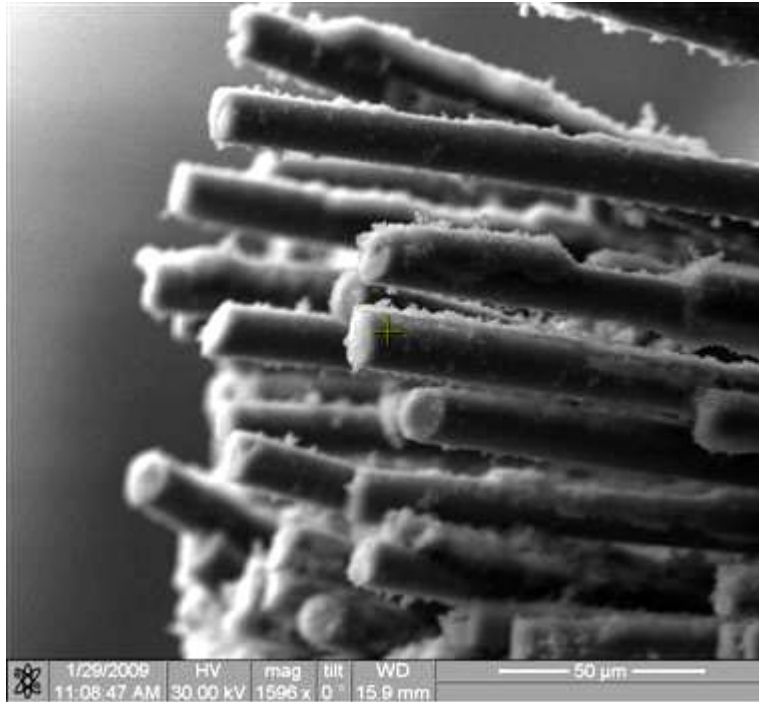


Figure 459. Fracture surface of the N720/AM specimen tested in creep at 131 MPa in steam at 1000°C.

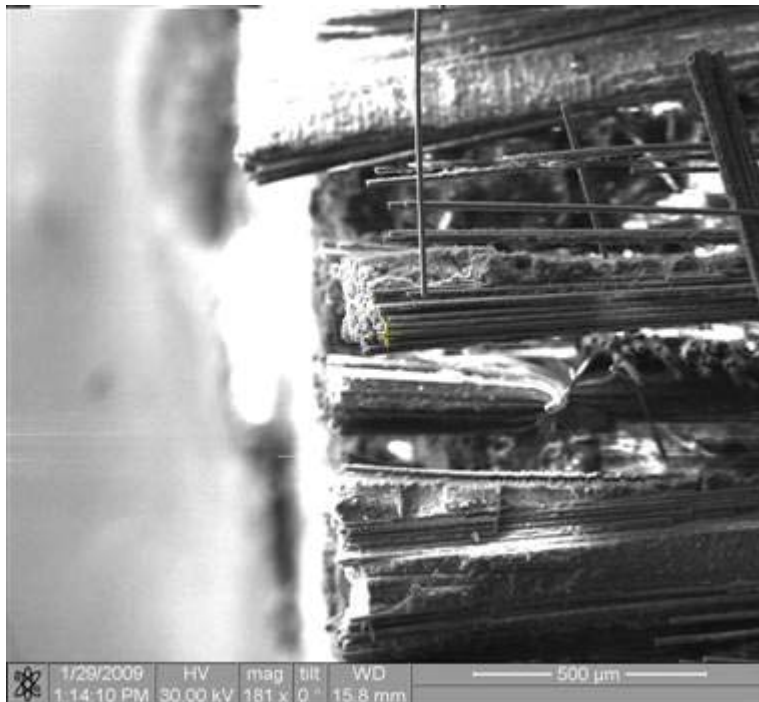


Figure 460. Fracture surface of the N720/AM specimen tested in creep at 140 MPa in steam at 1000°C.

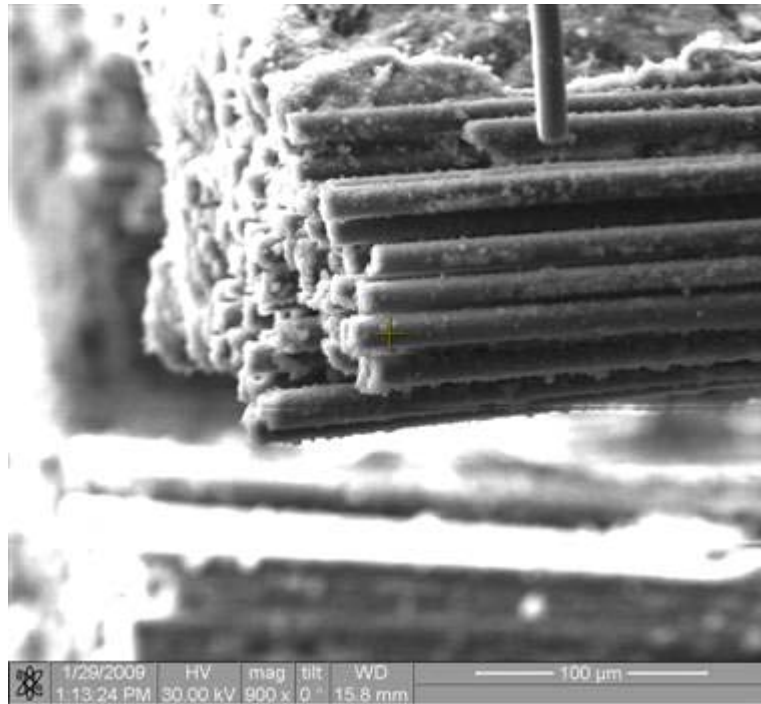


Figure 461. Fracture surface of the N720/AM specimen tested in creep at 140 MPa in steam at 1000°C.

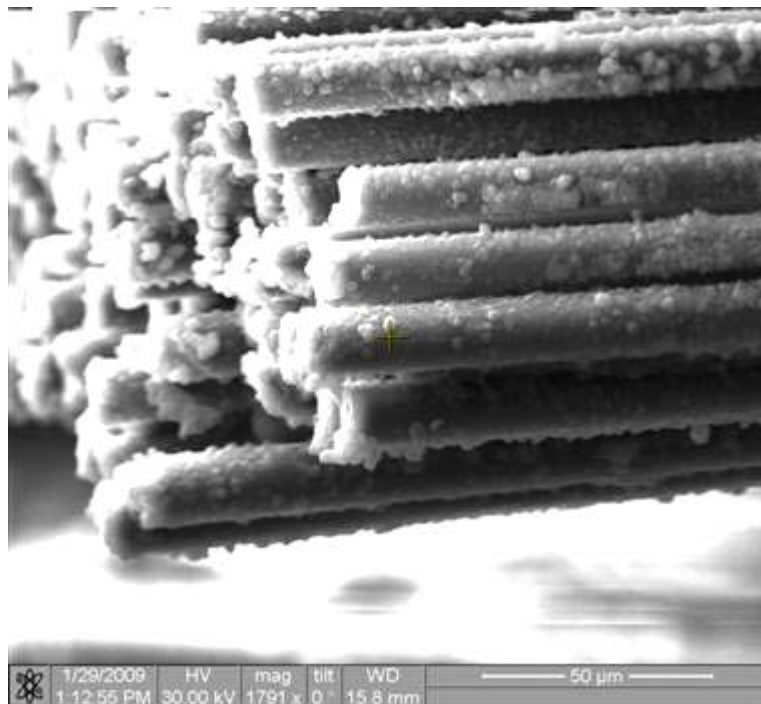


Figure 462. Fracture surface of the N720/AM specimen tested in creep at 140 MPa in steam at 1000°C.

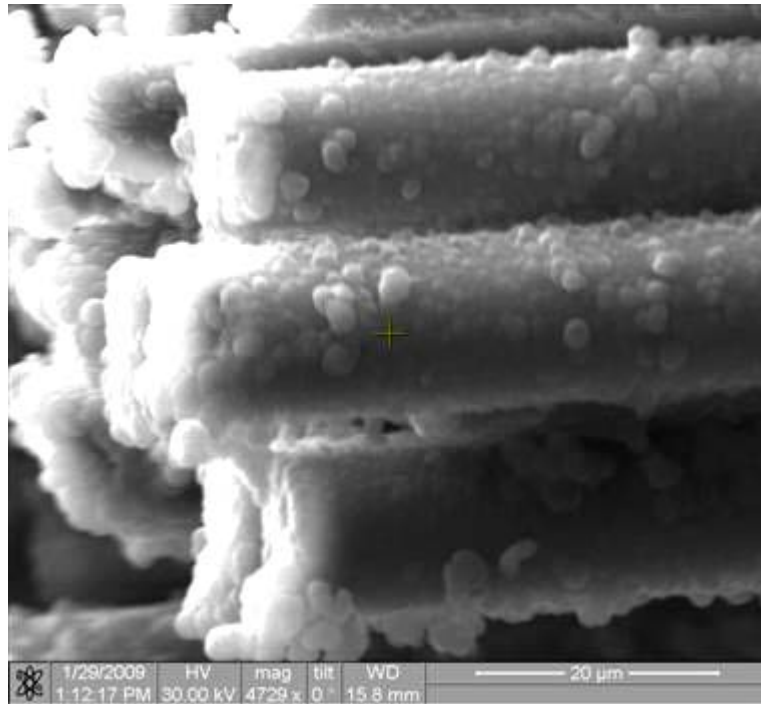


Figure 463. Fracture surface of the N720/AM specimen tested in creep at 140 MPa in steam at 1000°C.

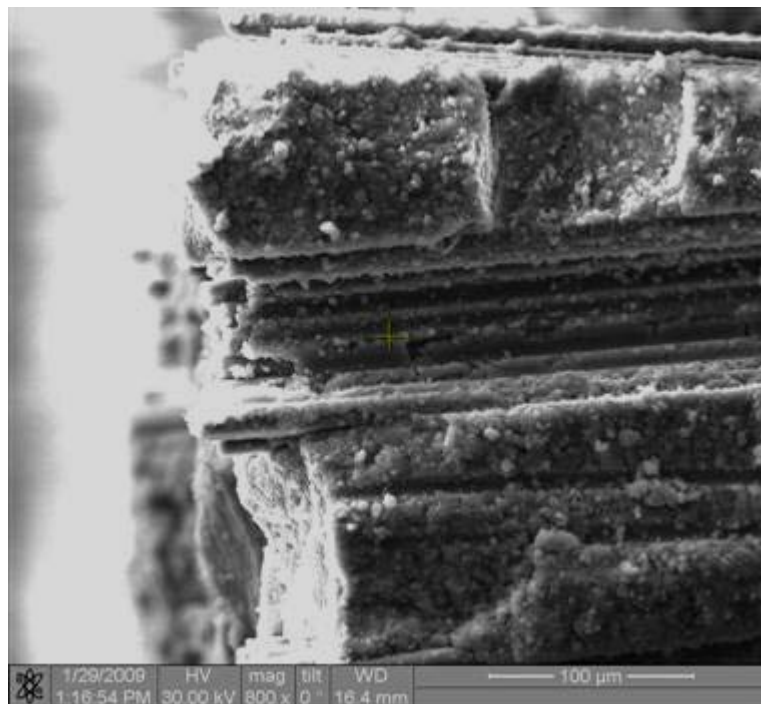


Figure 464. Fracture surface of the N720/AM specimen tested in creep at 140 MPa in steam at 1000°C.

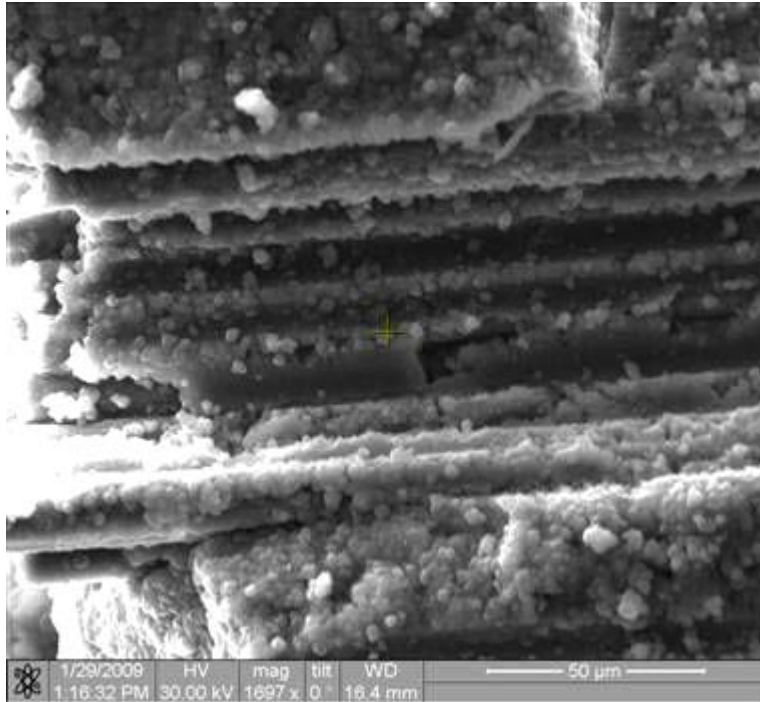


Figure 465. Fracture surface of the N720/AM specimen tested in creep at 140 MPa in steam at 1000°C.

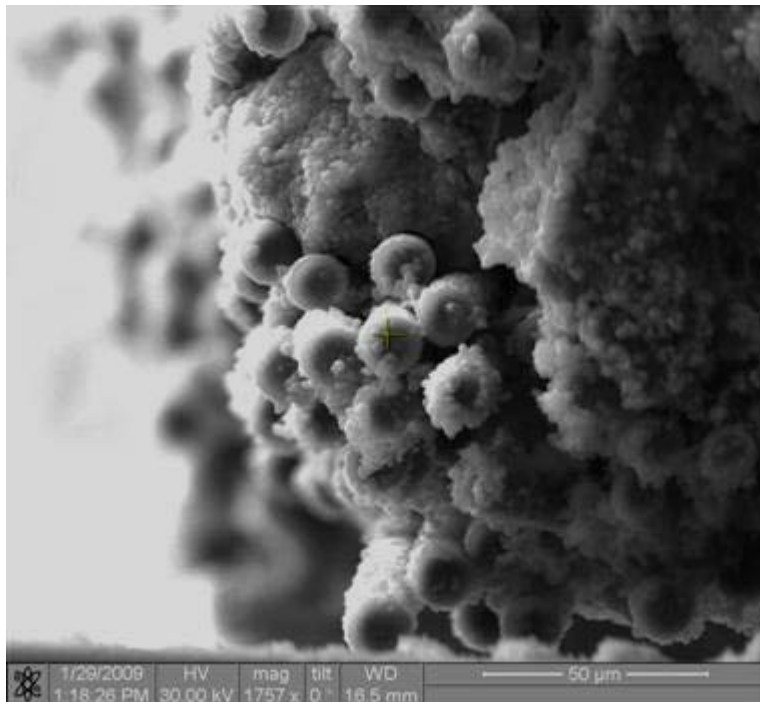


Figure 466. Fracture surface of the N720/AM specimen tested in creep at 140 MPa in steam at 1000°C.

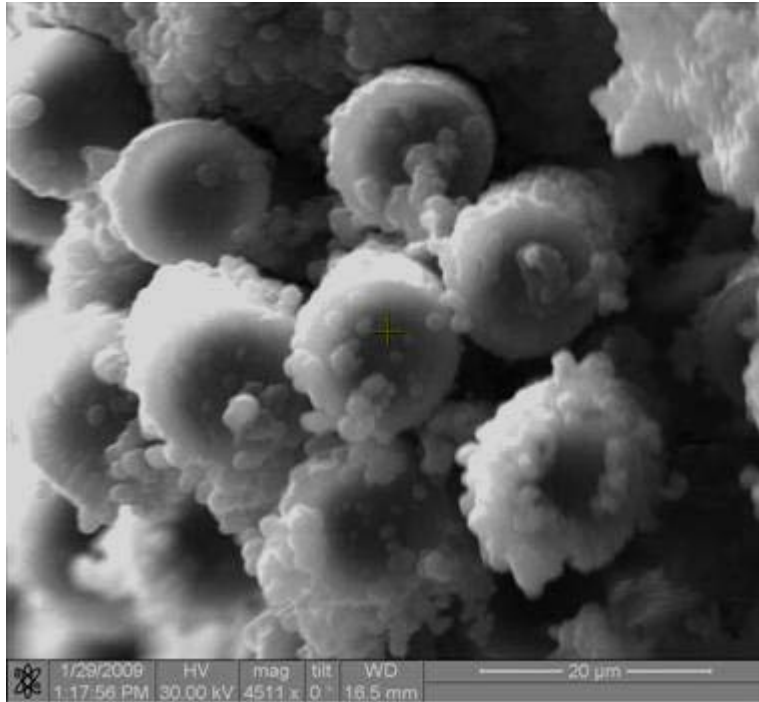


Figure 467. Fracture surface of the N720/AM specimen tested in creep at 140 MPa in steam at 1000°C.



Figure 468. Fracture surface of the N720/AM specimen tested in creep at 140 MPa in steam at 1000°C.

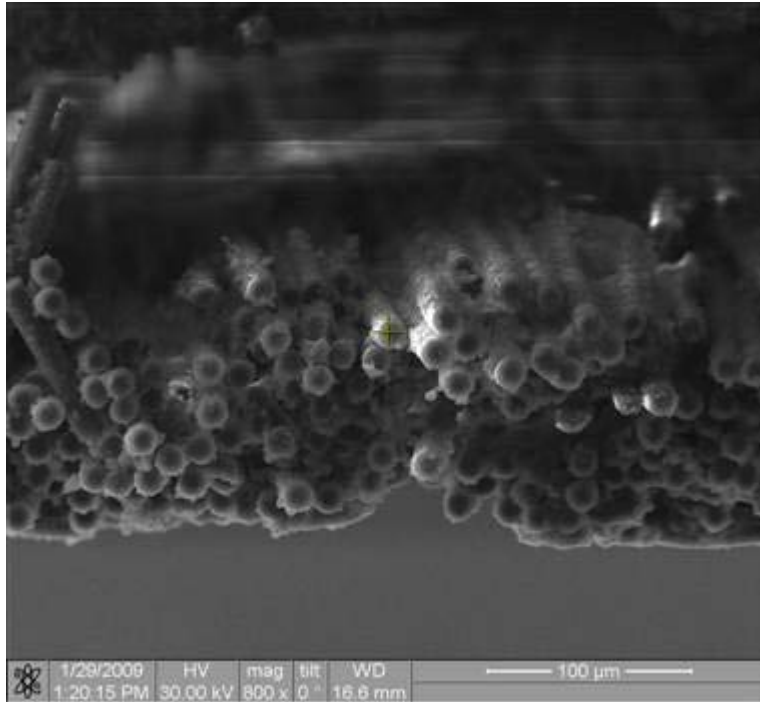


Figure 469. Fracture surface of the N720/AM specimen tested in creep at 140 MPa in steam at 1000°C.

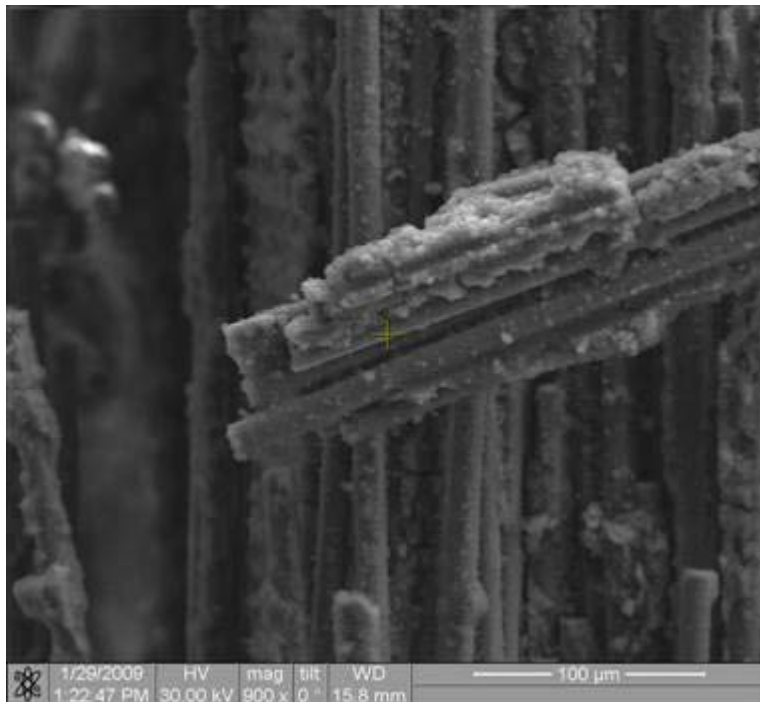


Figure 470. Fracture surface of the N720/AM specimen tested in creep at 140 MPa in steam at 1000°C.

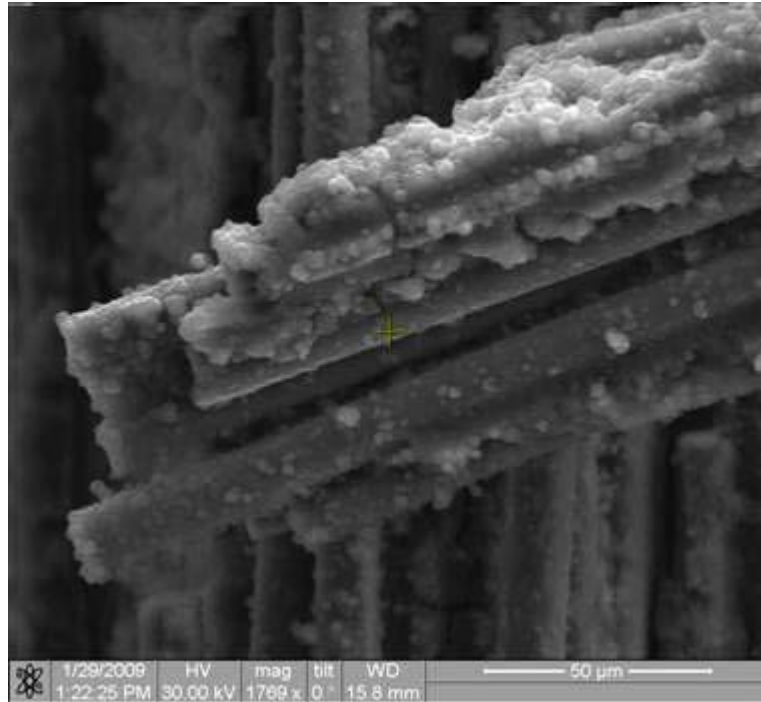


Figure 471. Fracture surface of the N720/AM specimen tested in creep at 140 MPa in steam at 1000°C.



Figure 472. Fracture surface of the N720/AM specimen tested in creep at 140 MPa in steam at 1000°C.



Figure 473. Fracture surface of the N720/AM specimen tested in creep at 140 MPa in steam at 1000°C.

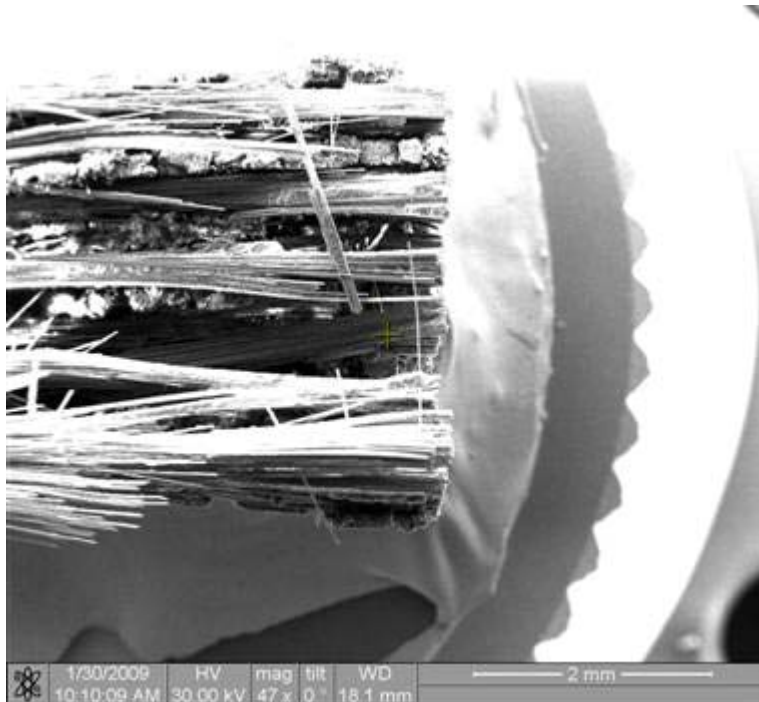


Figure 474. Fracture surface of the N720/AM specimen tested in creep at 140 MPa in steam at 1000°C.

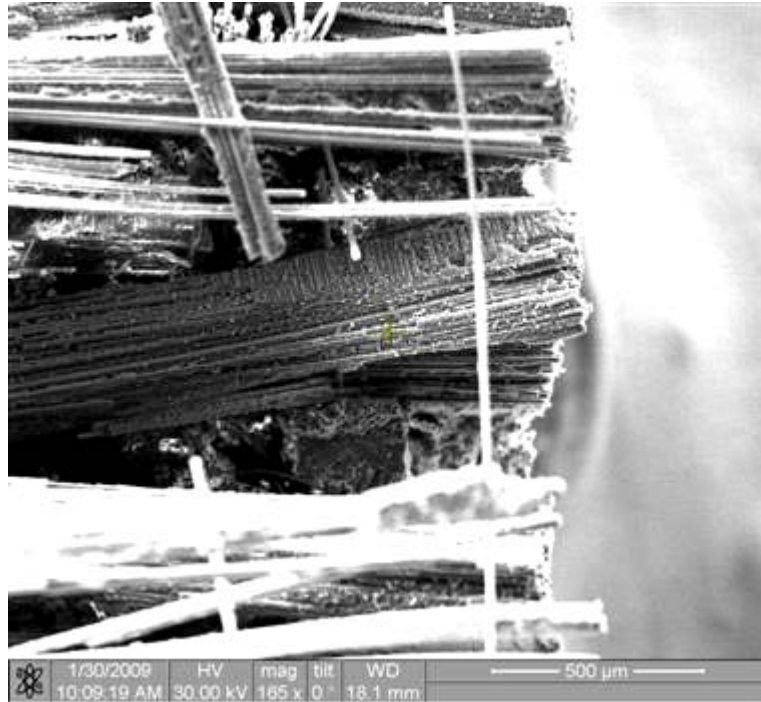


Figure 475. Fracture surface of the N720/AM specimen tested in creep at 140 MPa in steam at 1000°C.



Figure 476. Fracture surface of the N720/AM specimen tested in creep at 140 MPa in steam at 1000°C.

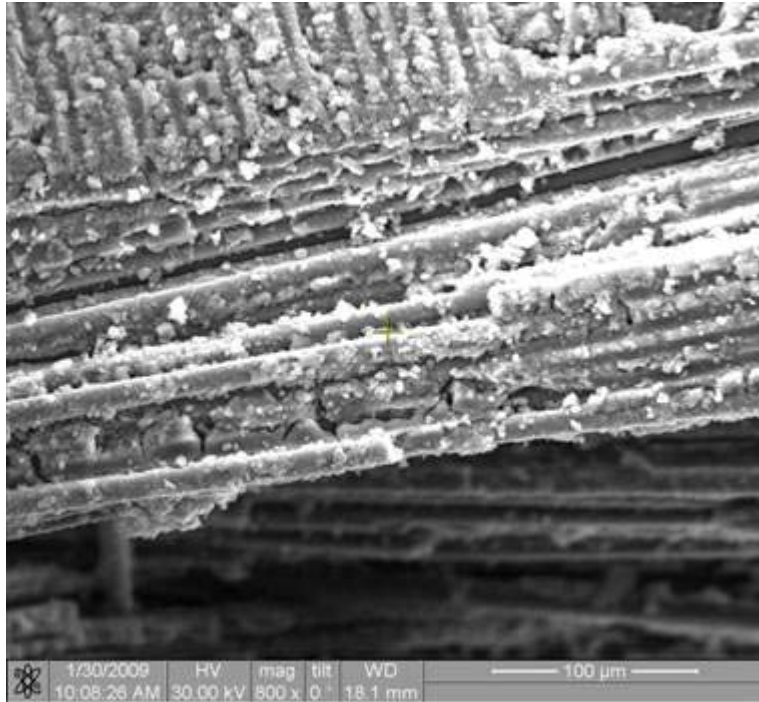


Figure 477. Fracture surface of the N720/AM specimen tested in creep at 140 MPa in steam at 1000°C.

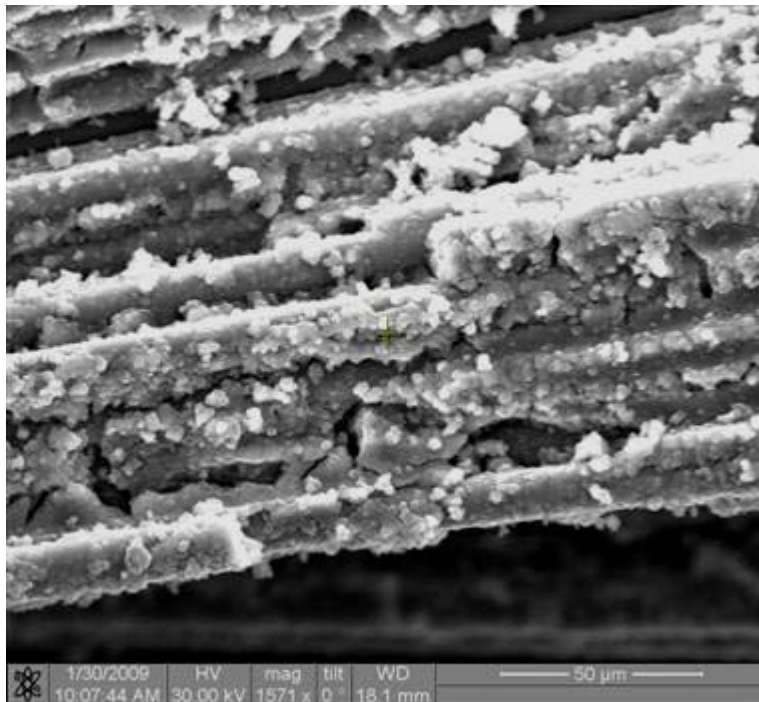


Figure 478. Fracture surface of the N720/AM specimen tested in creep at 140 MPa in steam at 1000°C.



Figure 479. Fracture surface of the N720/AM specimen tested in creep at 140 MPa in steam at 1000°C.

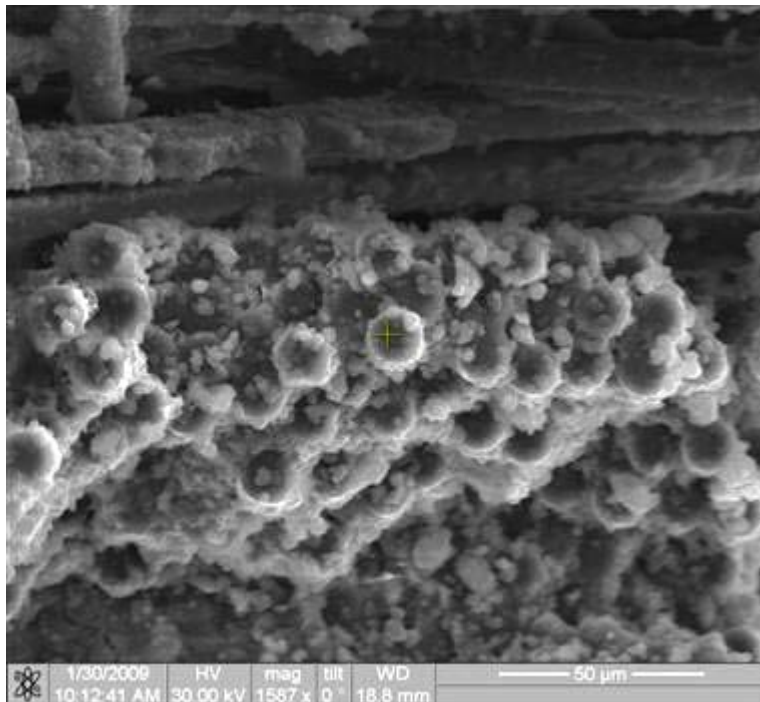


Figure 480. Fracture surface of the N720/AM specimen tested in creep at 140 MPa in steam at 1000°C.

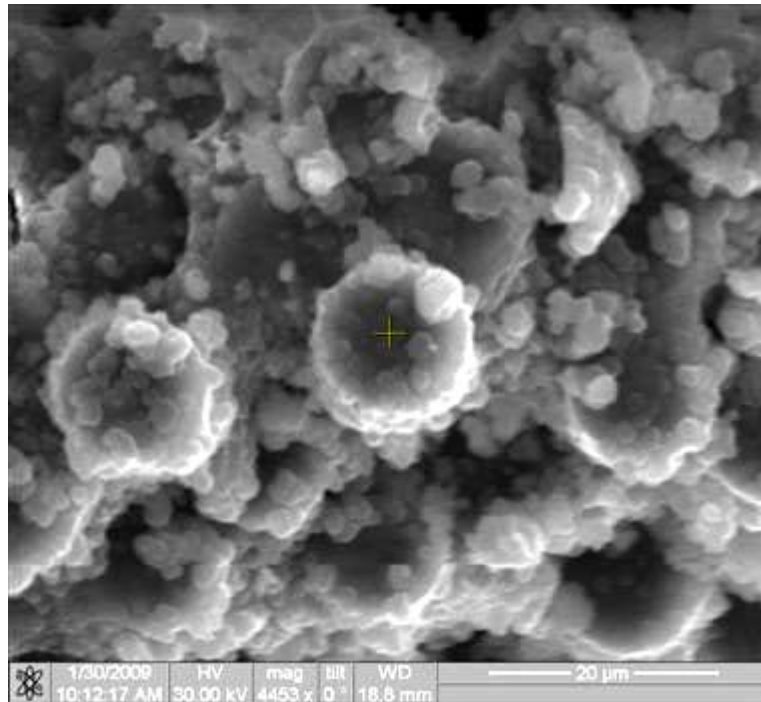


Figure 481. Fracture surface of the N720/AM specimen tested in creep at 140 MPa in steam at 1000°C.



Figure 482. Fracture surface of the N720/AM specimen tested in creep at 140 MPa in steam at 1000°C.

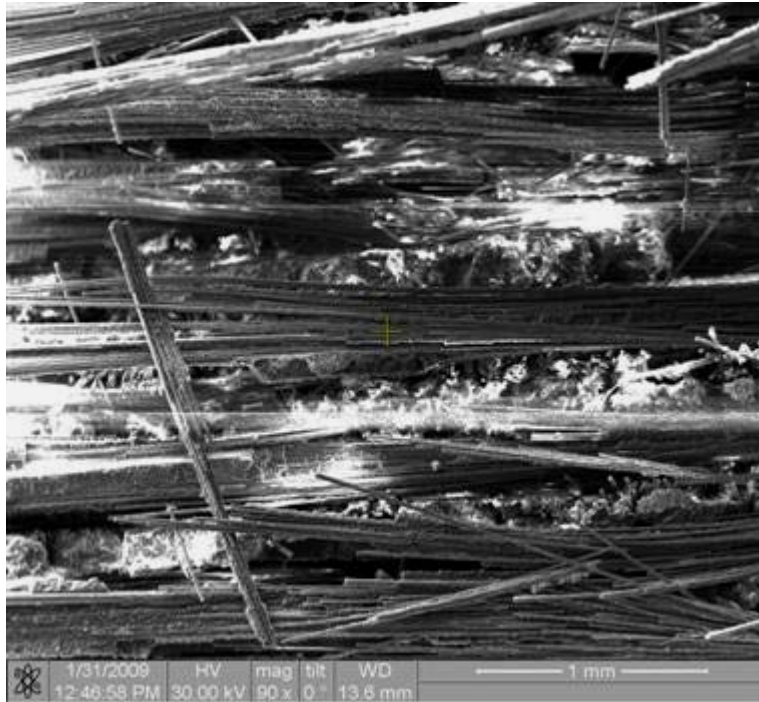


Figure 483. Fracture surface of the N720/AM specimen tested in creep at 140 MPa in steam at 1000°C.

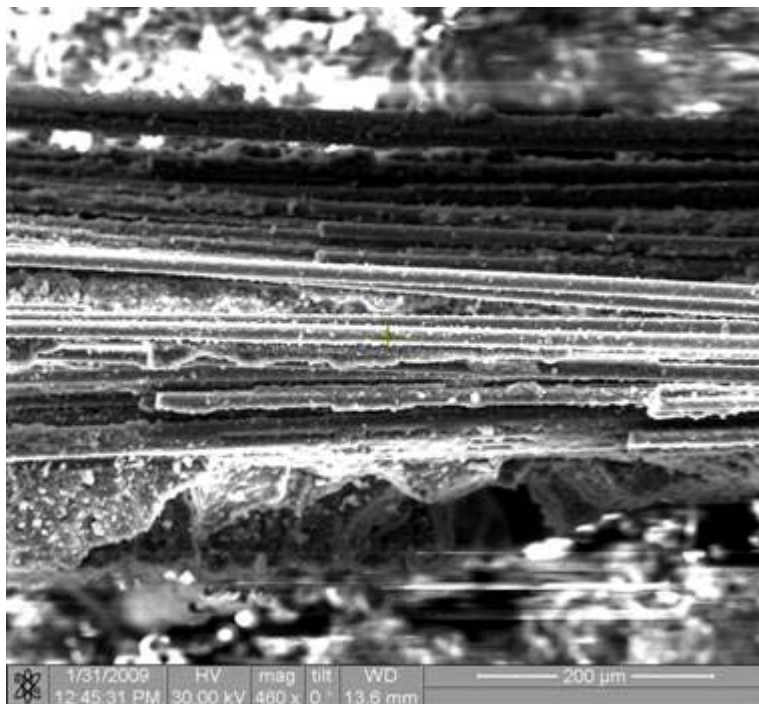


Figure 484. Fracture surface of the N720/AM specimen tested in creep at 140 MPa in steam at 1000°C.

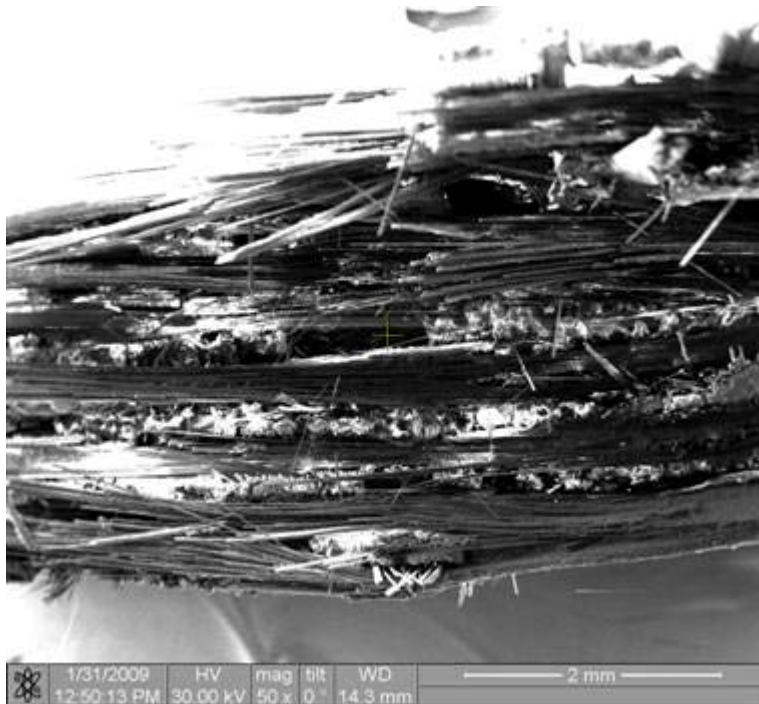


Figure 485. Fracture surface of the N720/AM specimen tested in creep at 140 MPa in steam at 1000°C.

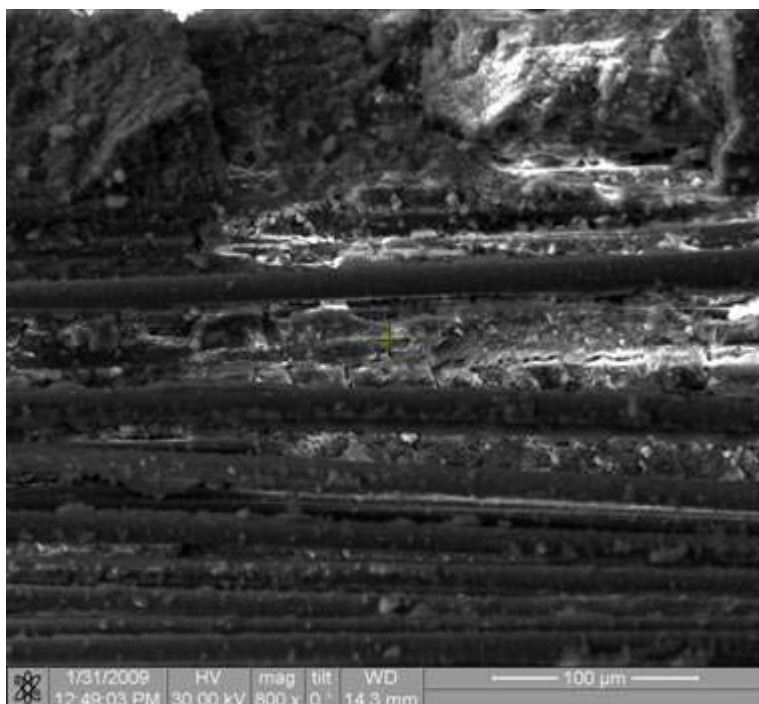


Figure 486. Fracture surface of the N720/AM specimen tested in creep at 140 MPa in steam at 1000°C.

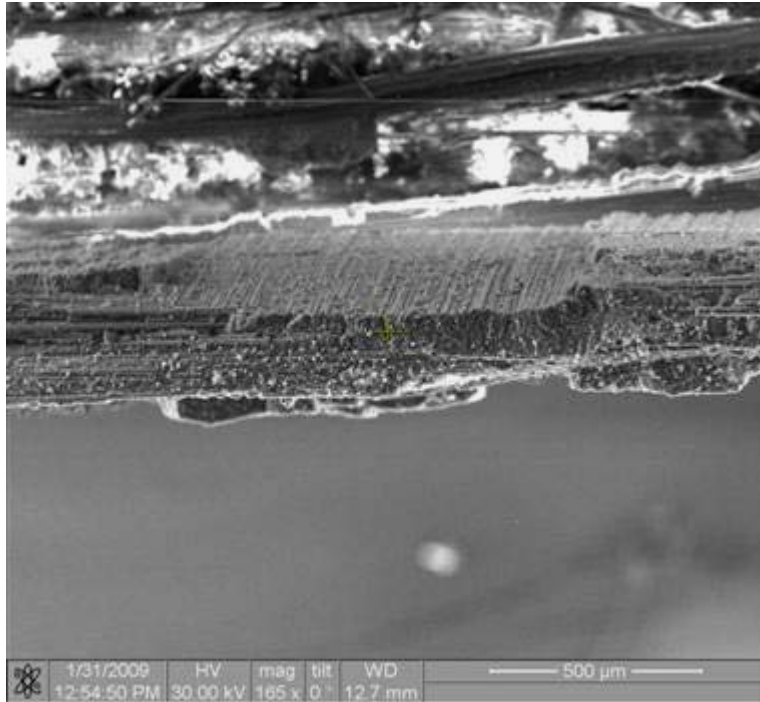


Figure 487. Fracture surface of the N720/AM specimen tested in creep at 140 MPa in steam at 1000°C.

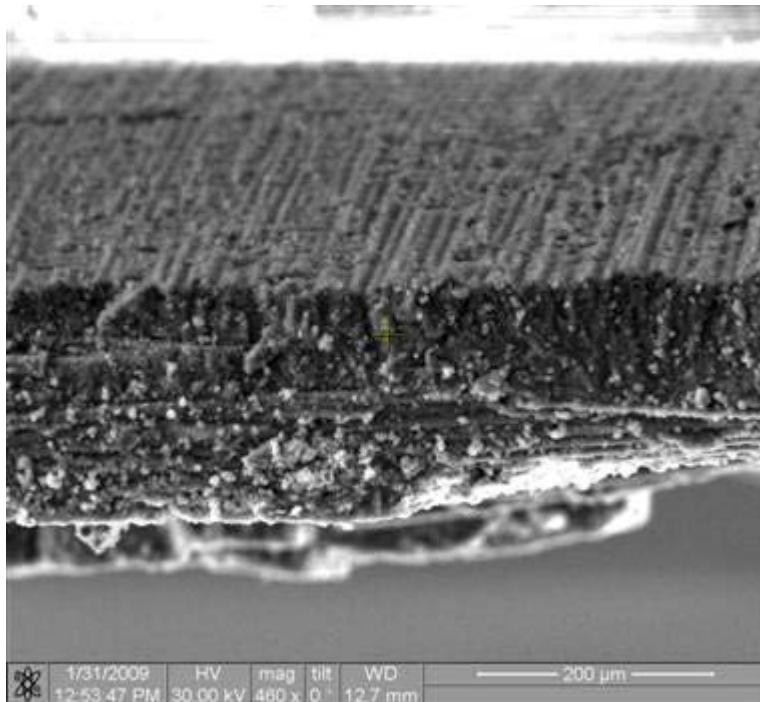


Figure 488. Fracture surface of the N720/AM specimen tested in creep at 140 MPa in steam at 1000°C.



Figure 489. Fracture surface of the N720/AM specimen tested in creep at 140 MPa in steam at 1000°C.

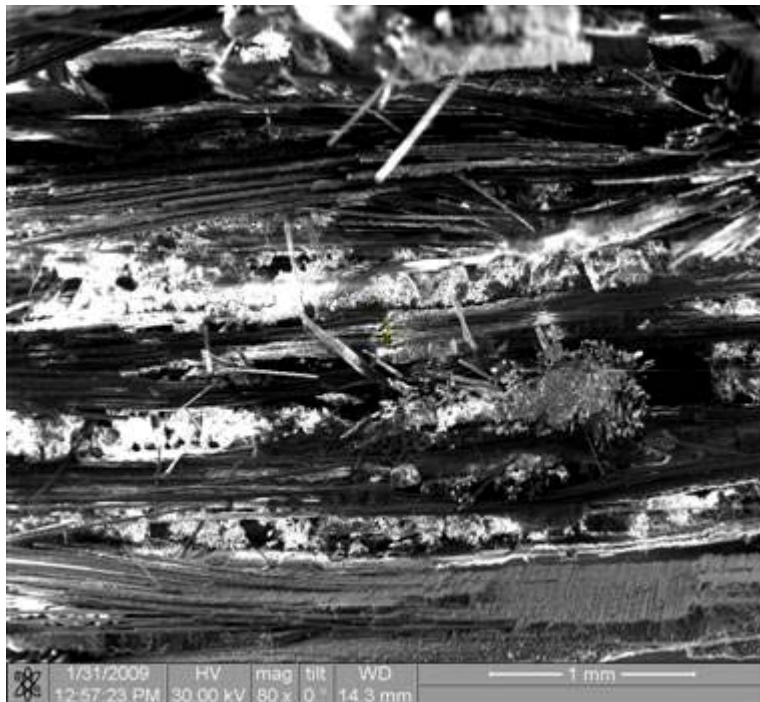


Figure 490. Fracture surface of the N720/AM specimen tested in creep at 140 MPa in steam at 1000°C.

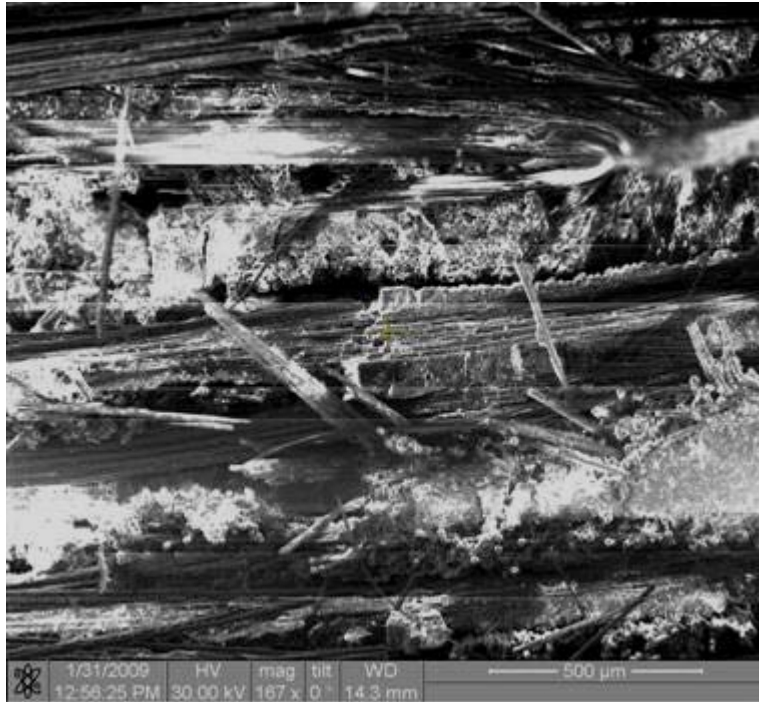


Figure 491. Fracture surface of the N720/AM specimen tested in creep at 140 MPa in steam at 1000°C.



Figure 492. Fracture surface of the N720/AM specimen tested in creep at 140 MPa in steam at 1000°C.

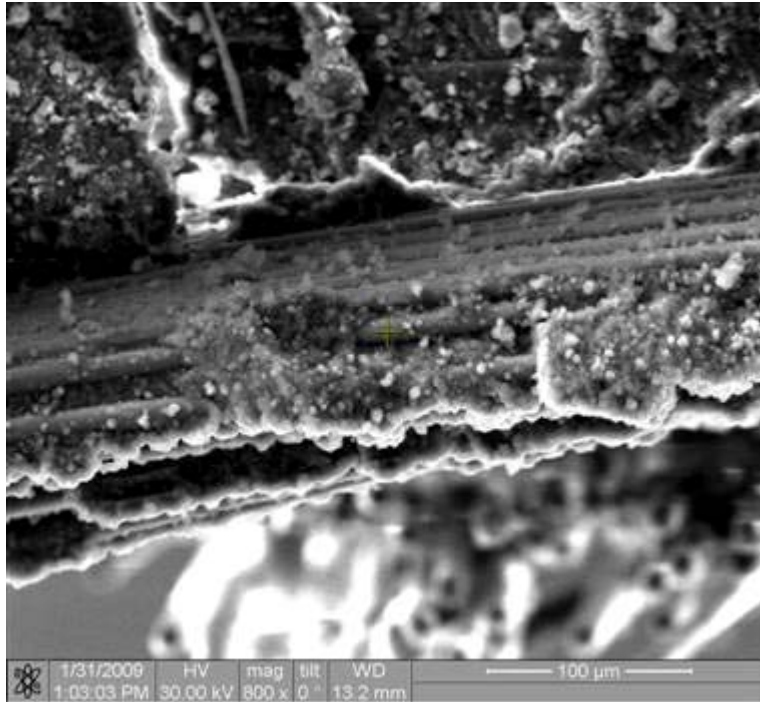


Figure 493. Fracture surface of the N720/AM specimen tested in creep at 140 MPa in steam at 1000°C.

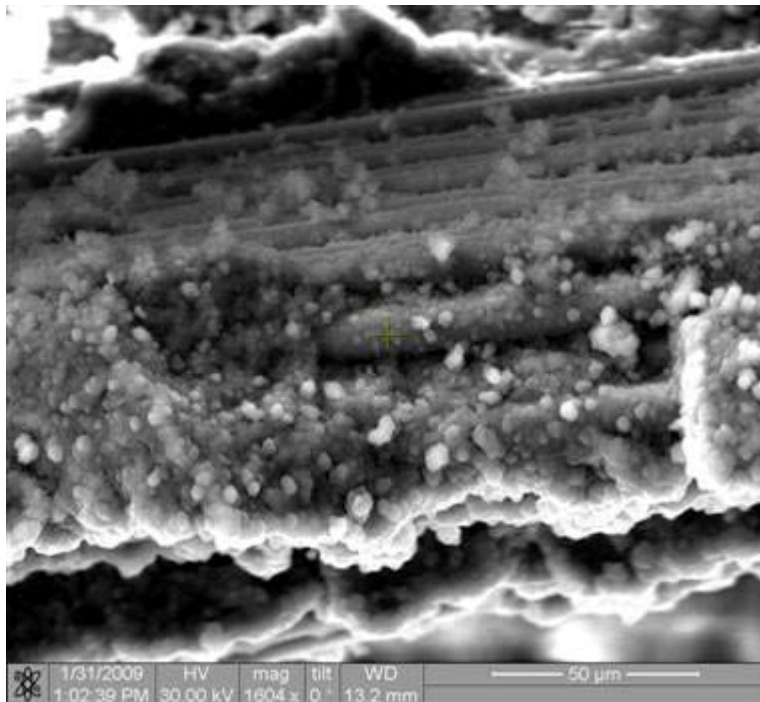


Figure 494. Fracture surface of the N720/AM specimen tested in creep at 140 MPa in steam at 1000°C.



Figure 495. Fracture surface of the N720/AM specimen tested in creep at 140 MPa in steam at 1000°C.

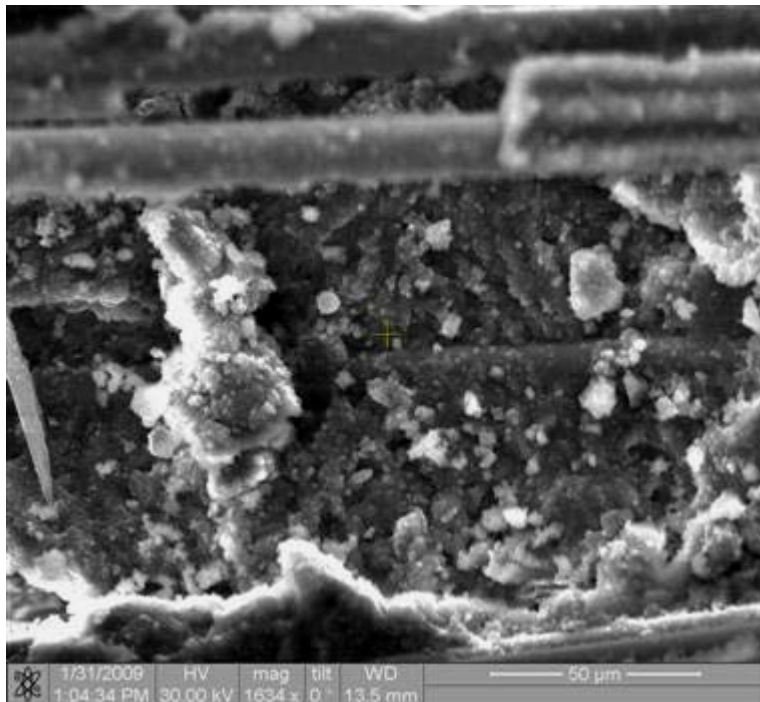


Figure 496. Fracture surface of the N720/AM specimen tested in creep at 140 MPa in steam at 1000°C.

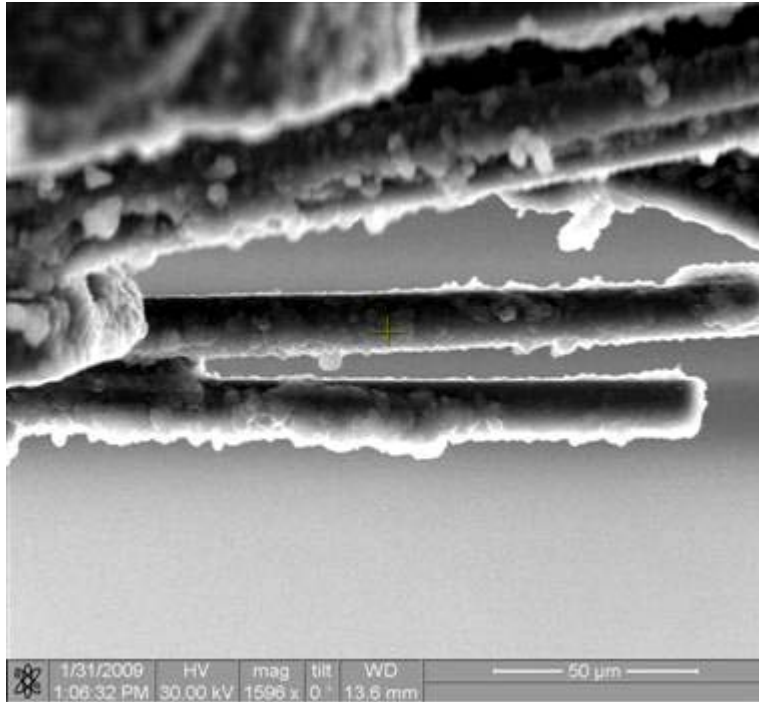


Figure 497. Fracture surface of the N720/AM specimen tested in creep at 140 MPa in steam at 1000°C.



Figure 498. Fracture surface of the N720/AM specimen tested in creep at 140 MPa in steam at 1000°C.

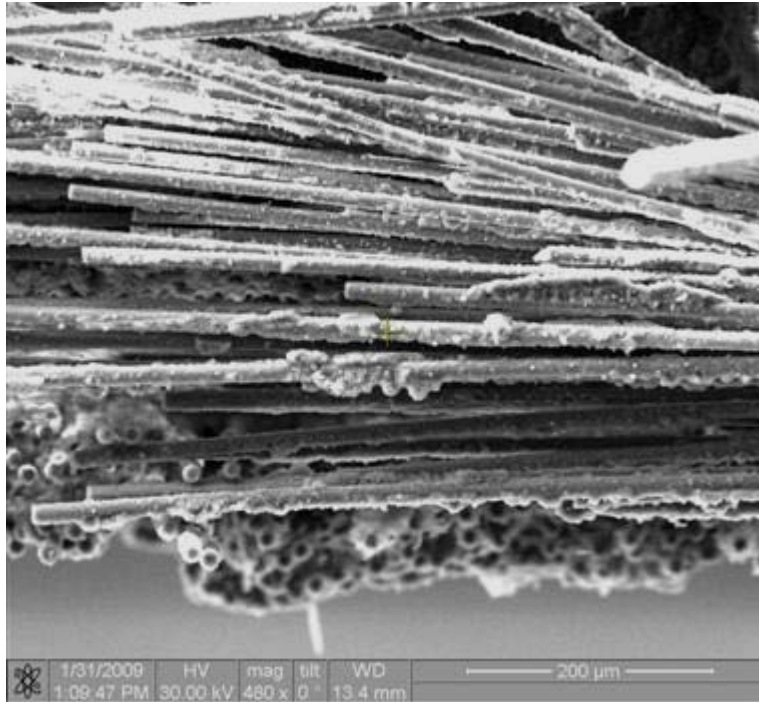


Figure 499. Fracture surface of the N720/AM specimen tested in creep at 140 MPa in steam at 1000°C.

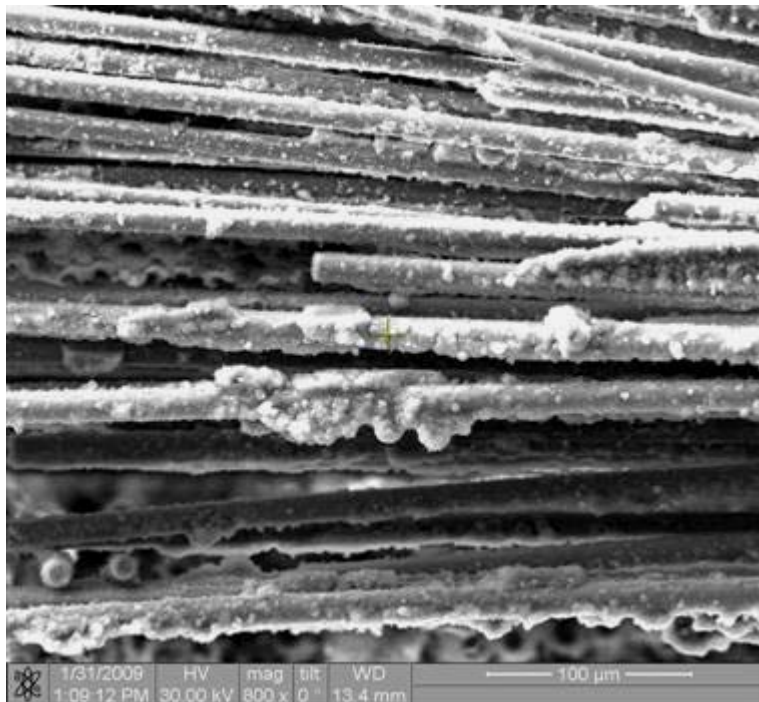


Figure 500. Fracture surface of the N720/AM specimen tested in creep at 140 MPa in steam at 1000°C.

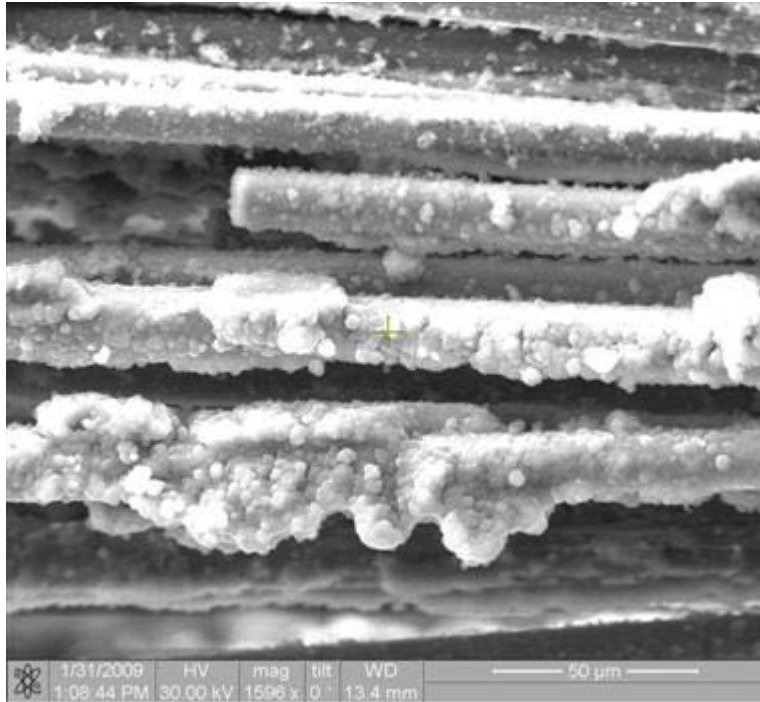


Figure 501. Fracture surface of the N720/AM specimen tested in creep at 140 MPa in steam at 1000°C.

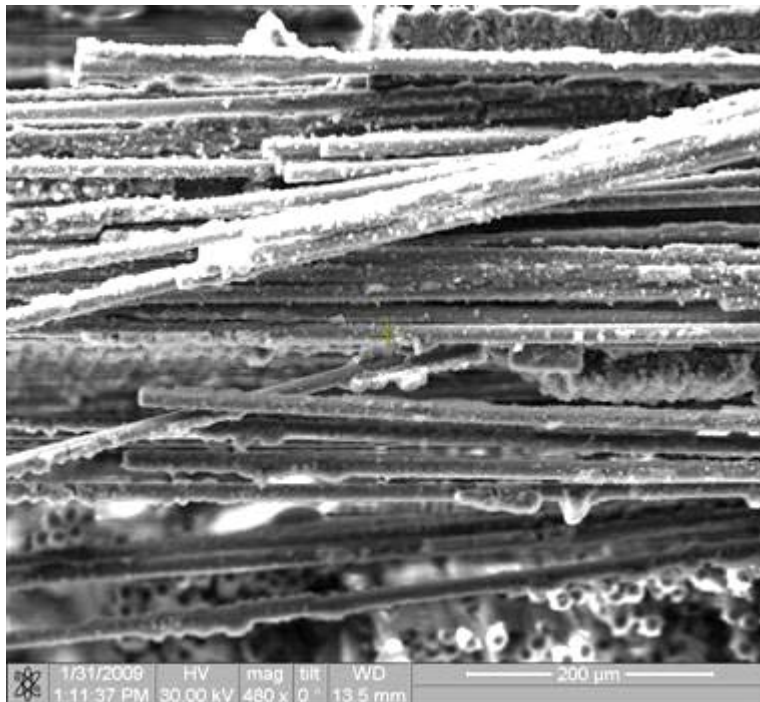


Figure 502. Fracture surface of the N720/AM specimen tested in creep at 140 MPa in steam at 1000°C.

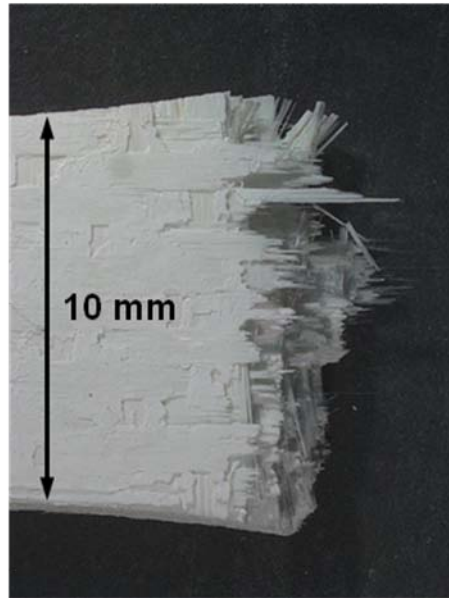


Figure 503. Fracture surface of the N720/AM specimen tested in tension to failure at 900°C in laboratory air.

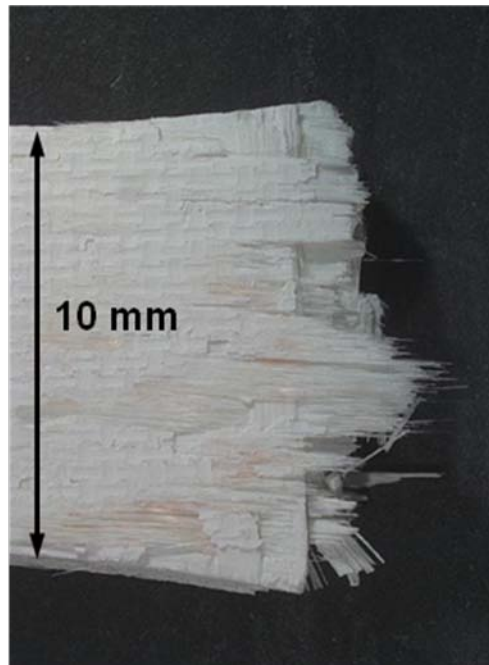


Figure 504. Fracture surface of the N720/AM specimen tested in tension to failure at 900°C in laboratory air.

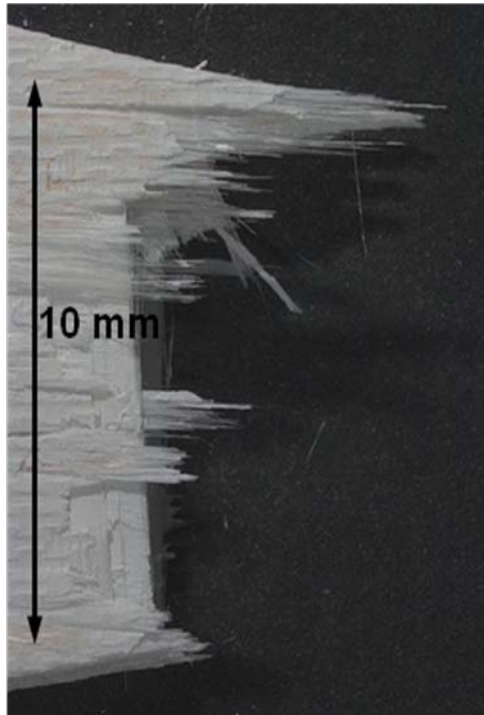


Figure 505 Fracture surface of the N720/AM specimen tested in tension to failure at 900°C in laboratory air.

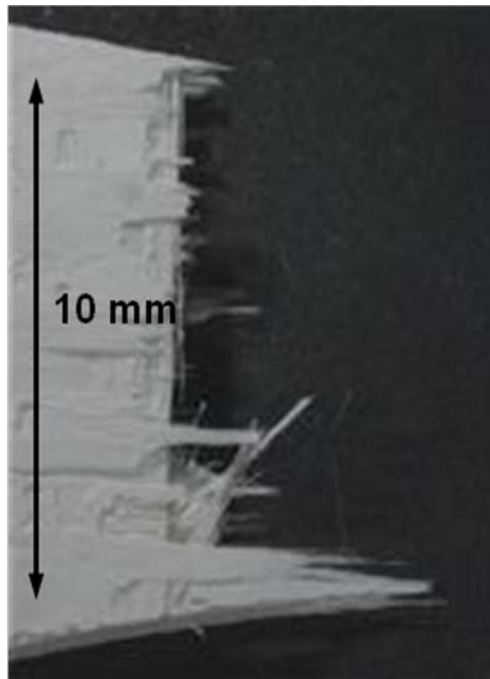


Figure 506. Fracture surface of the N720/AM specimen tested in tension to failure at 900°C in laboratory air.

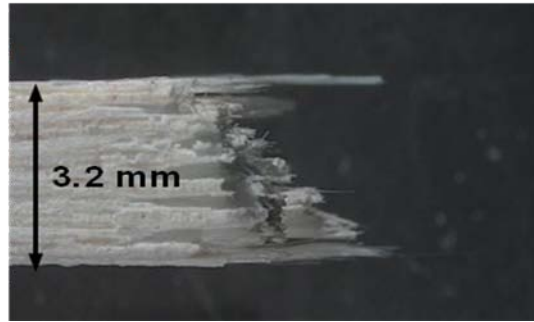


Figure 507. Fracture surface of the N720/AM specimen tested in tension to failure at 900°C in laboratory air (side view).



Figure 508. Fracture surface of the N720/AM specimen tested in tension to failure at 900°C in laboratory air (side view).



Figure 509. Fracture surface of the N720/AM specimen tested in tension to failure at 900°C in laboratory air (side view).

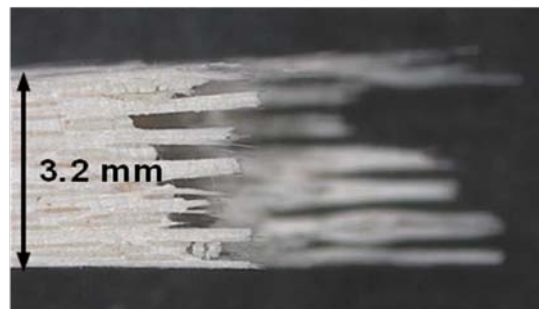


Figure 510. Fracture surface of the N720/AM specimen tested in tension to failure at 900°C in laboratory air (side view).

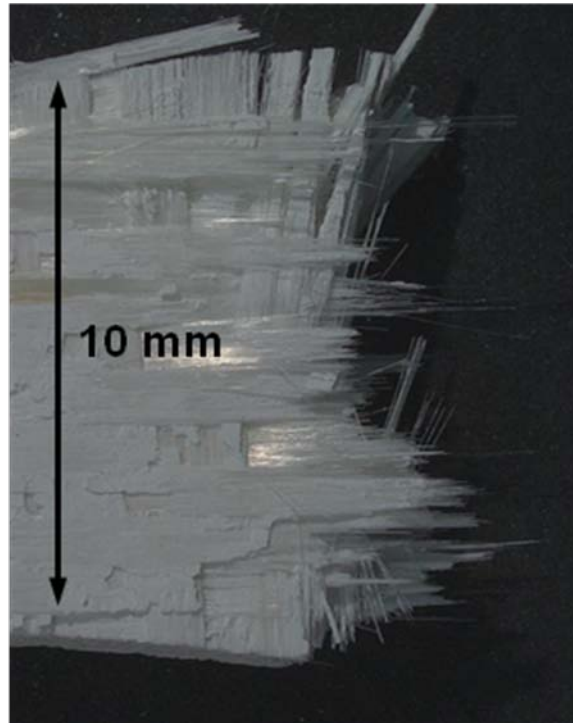


Figure 511. Fracture surface of the N720/AM specimen tested in tension to failure at 1000°C in laboratory air.

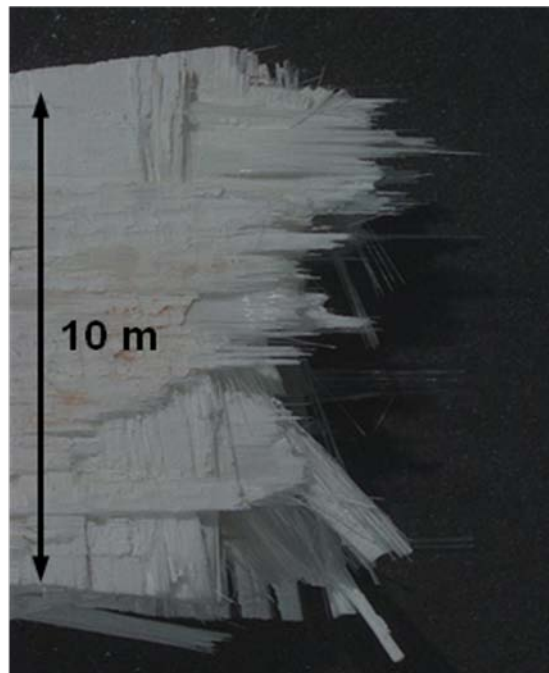


Figure 512. Fracture surface of the N720/AM specimen tested in tension to failure at 1000°C in laboratory air.

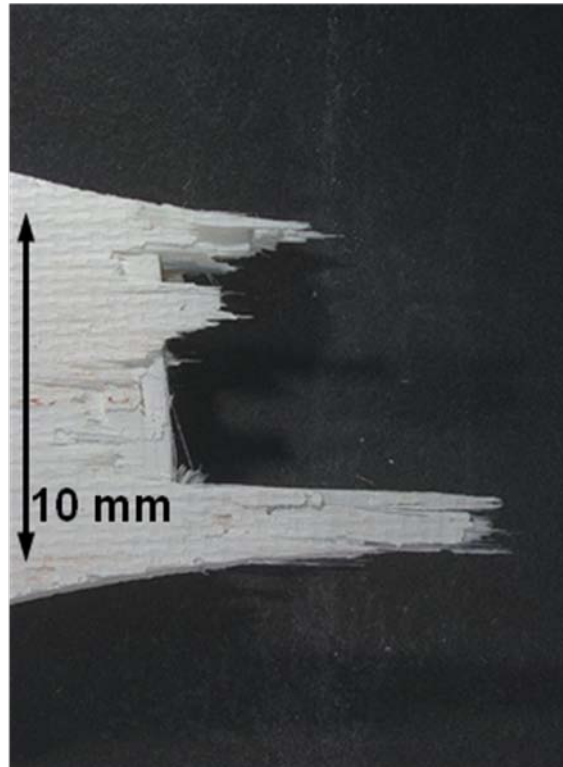


Figure 513. Fracture surface of the N720/AM specimen tested in tension to failure at 1000°C in laboratory air.

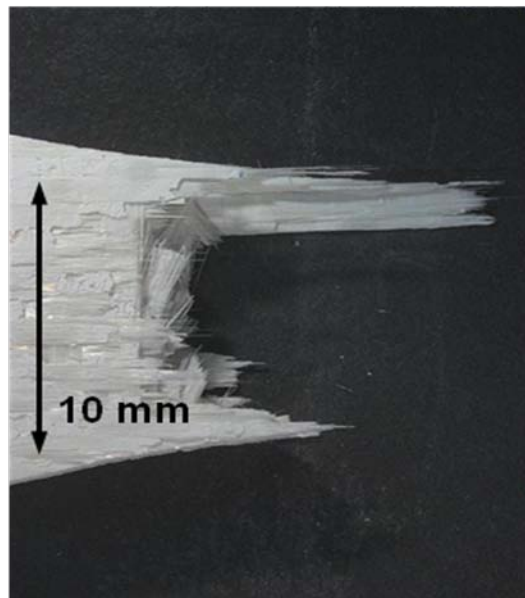


Figure 514. Fracture surface of the N720/AM specimen tested in tension to failure at 1000°C in laboratory air.

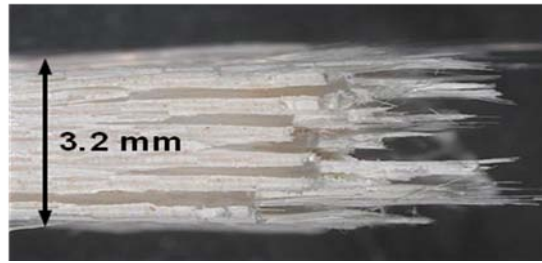


Figure 515. Fracture surface of the N720/AM specimen tested in tension to failure at 1000°C in laboratory air (side view).

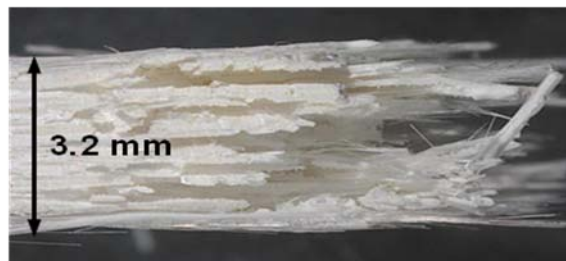


Figure 516. Fracture surface of the N720/AM specimen tested in tension to failure at 1000°C in laboratory air (side view).



Figure 517. Fracture surface of the N720/AM specimen tested in tension to failure at 1000°C in laboratory air (side view).

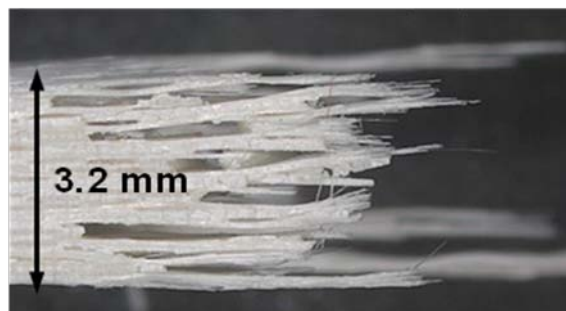


Figure 518. Fracture surface of the N720/AM specimen tested in tension to failure at 1000°C in laboratory air (side view).

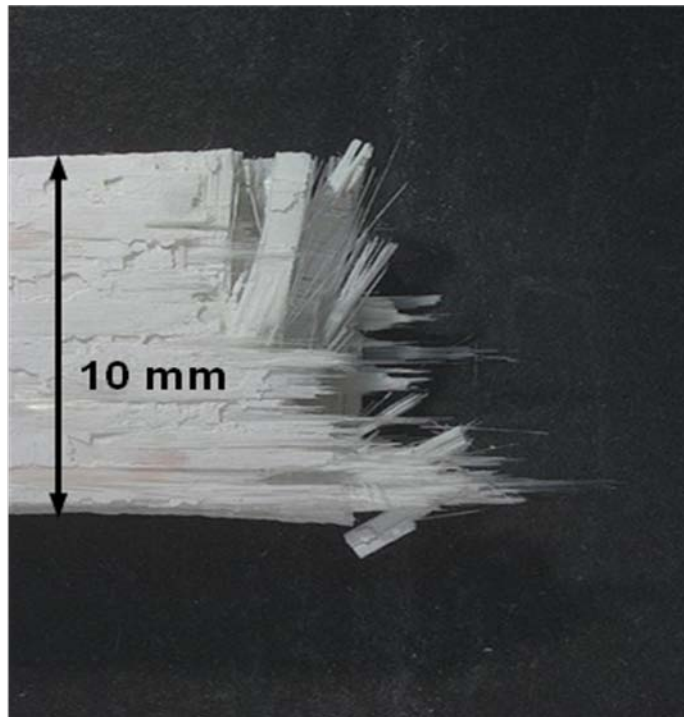


Figure 519. Fracture surface of the N720/AM specimen tested in tension to failure at 1100°C in laboratory air.

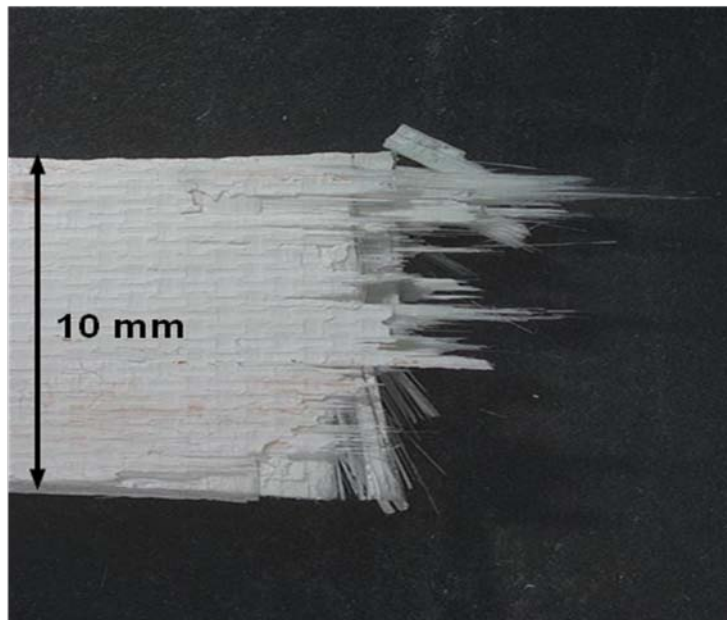


Figure 520. Fracture surface of the N720/AM specimen tested in tension to failure at 1100°C in laboratory air.

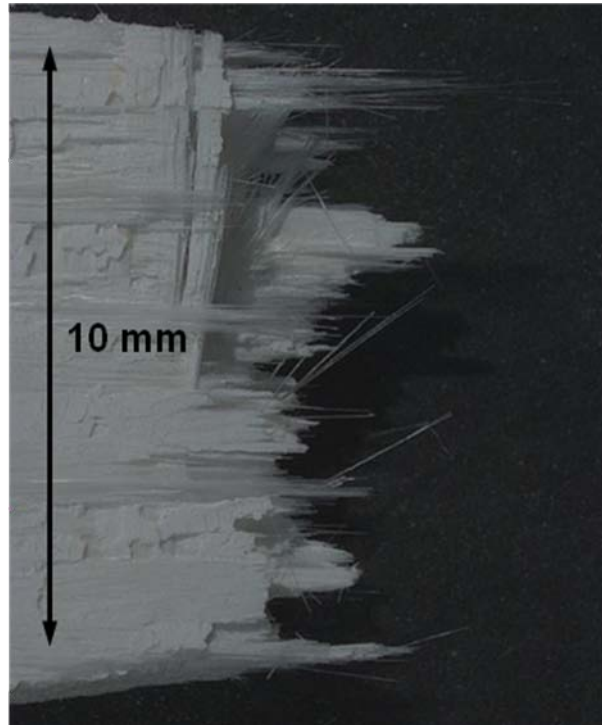


Figure 521. Fracture surface of the N720/AM specimen tested in tension to failure at 1100°C in laboratory air.

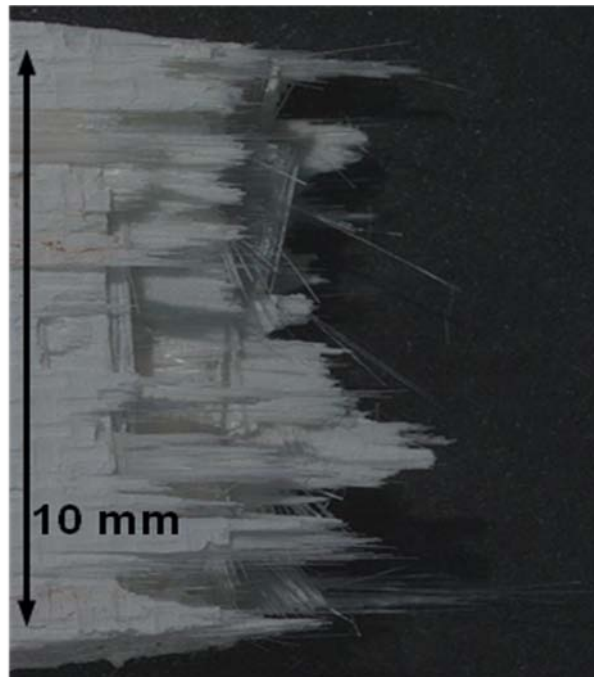


Figure 522. Fracture surface of the N720/AM specimen tested in tension to failure at 1100°C in laboratory air.



Figure 523. Fracture surface of the N720/AM specimen tested in tension to failure at 1100°C in laboratory air (side view).

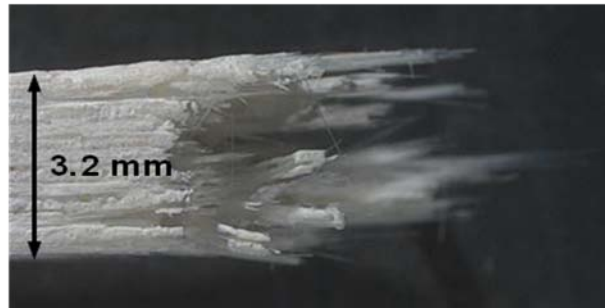


Figure 524. Fracture surface of the N720/AM specimen tested in tension to failure at 1100°C in laboratory air (side view).

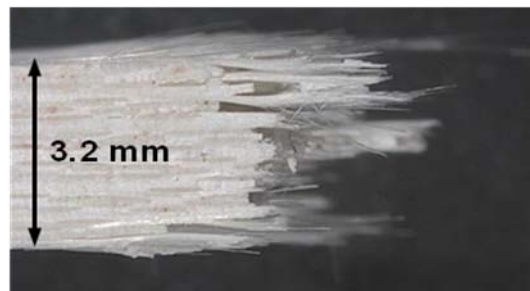


Figure 525. Fracture surface of the N720/AM specimen tested in tension to failure at 1100°C in laboratory air (side view).

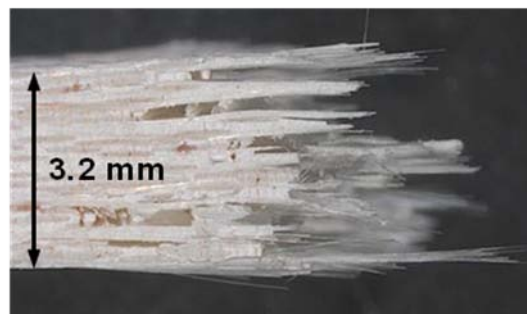


Figure 526. Fracture surface of the N720/AM specimen tested in tension to failure at 1100°C in laboratory air (side view).

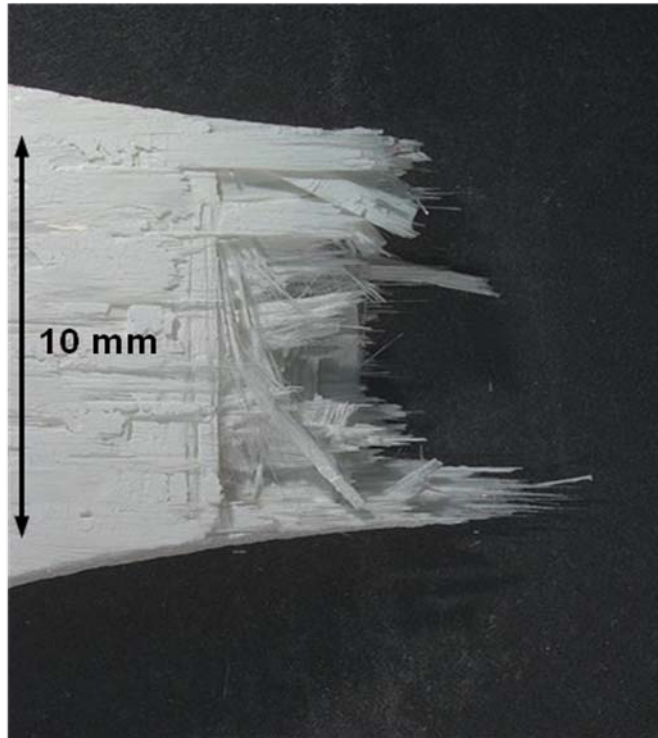


Figure 527. Fracture surface of the N720/AM specimen tested in tension to failure with constant loading rate of 25MPa at 1100°C in steam.

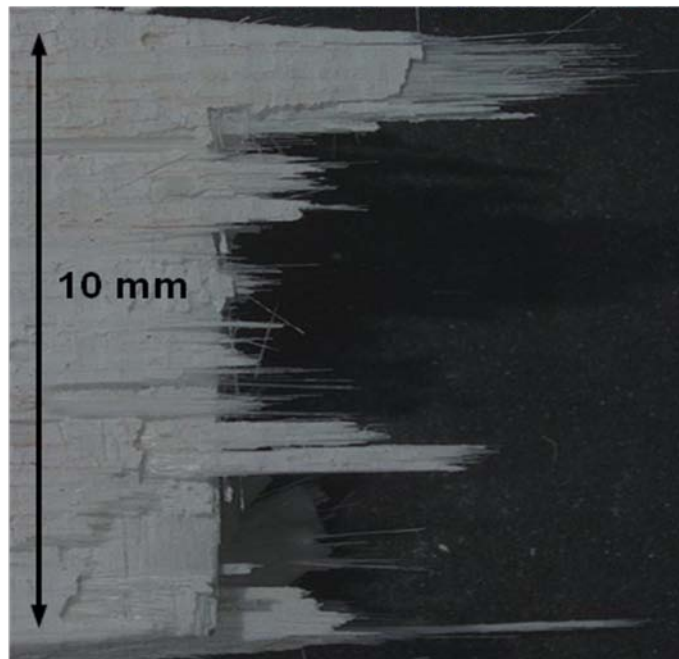


Figure 528. Fracture surface of the N720/AM specimen tested in tension to failure with constant loading rate of 25MPa at 1100°C in steam.

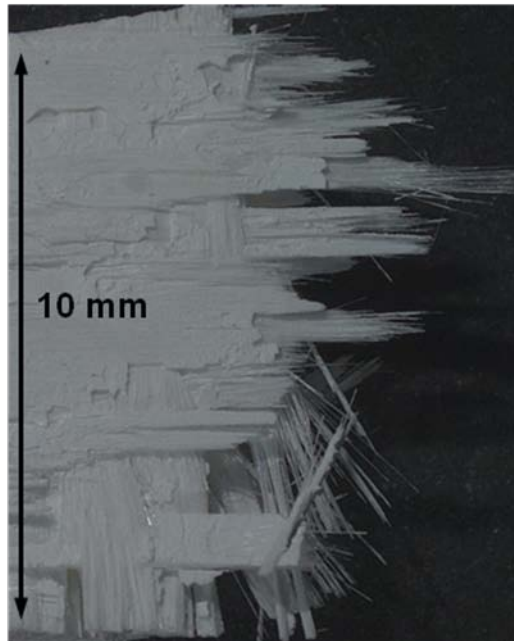


Figure 529. Fracture surface of the N720/AM specimen tested in tension to failure with constant loading rate of 25MPa at 1100°C in steam.

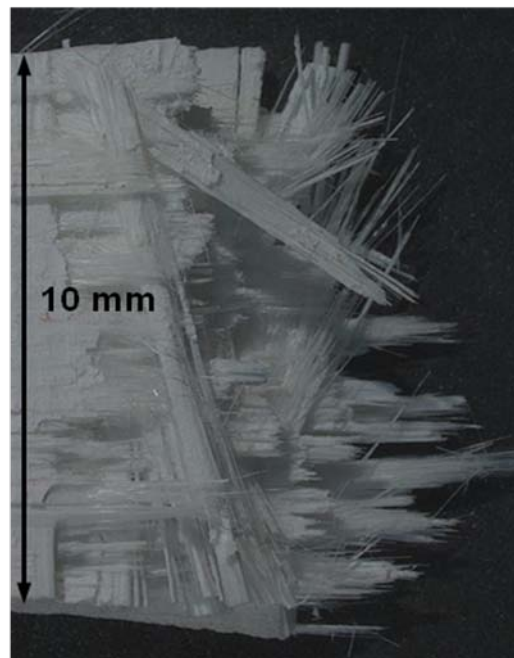


Figure 530. Fracture surface of the N720/AM specimen tested in tension to failure with constant loading rate of 25MPa at 1100°C in steam.



Figure 531. Fracture surface of the N720/AM specimen tested in tension to failure with constant loading rate of 25MPa at 1100°C in steam (side view).

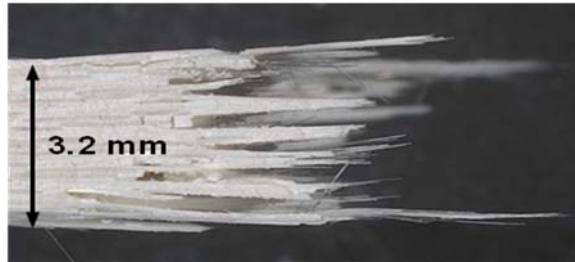


Figure 532. Fracture surface of the N720/AM specimen tested in tension to failure with constant loading rate of 25MPa at 1100°C in steam (side view).

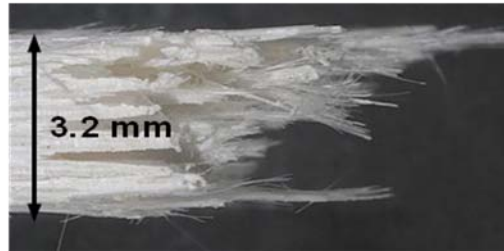


Figure 533. Fracture surface of the N720/AM specimen tested in tension to failure with constant loading rate of 25MPa at 1100°C in steam (side view).

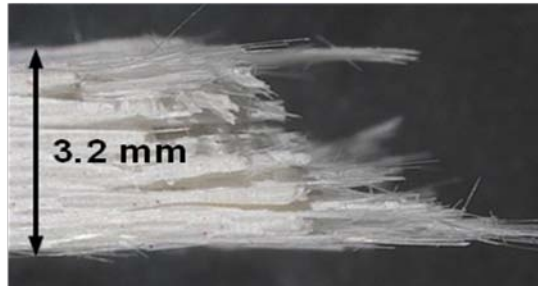


Figure 534. Fracture surface of the N720/AM specimen tested in tension to failure with constant loading rate of 25MPa at 1100°C in steam (side view).

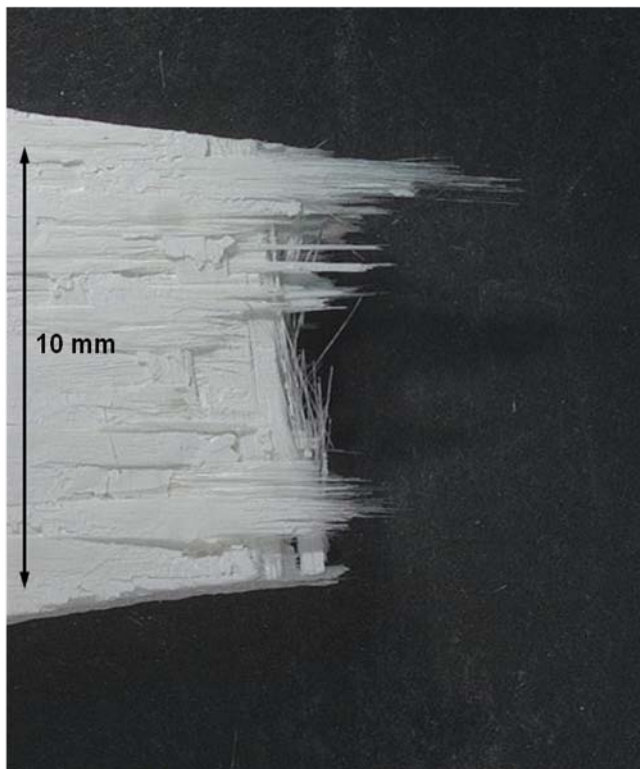


Figure 535. Fracture surface of the N720/AM specimen(2) tested in tension to failure with constant loading rate of 25MPa at 1100°C in steam.

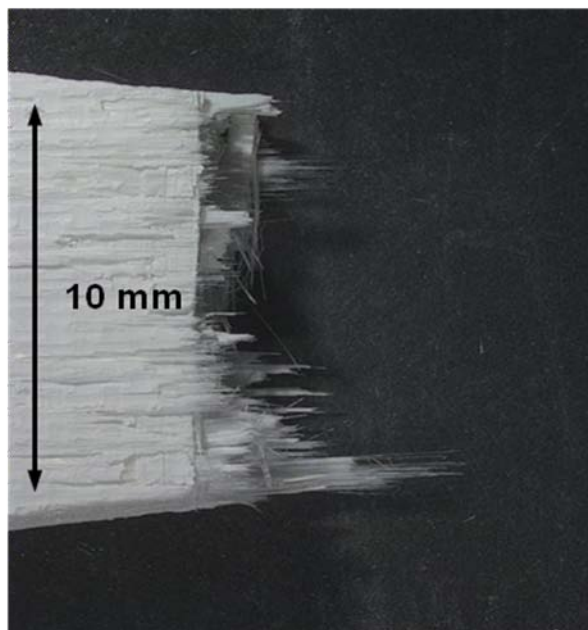


Figure 536. Fracture surface of the N720/AM specimen(2) tested in tension to failure with constant loading rate of 25MPa at 1100°C in steam.

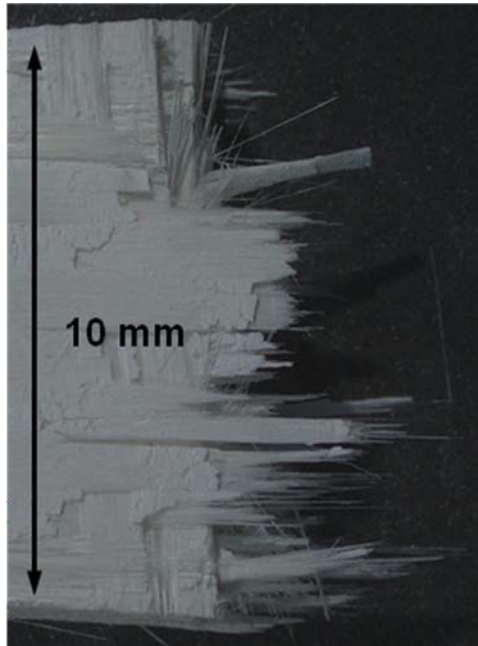


Figure 537. Fracture surface of the N720/AM specimen(2) tested in tension to failure with constant loading rate of 25MPa at 1100°C in steam.

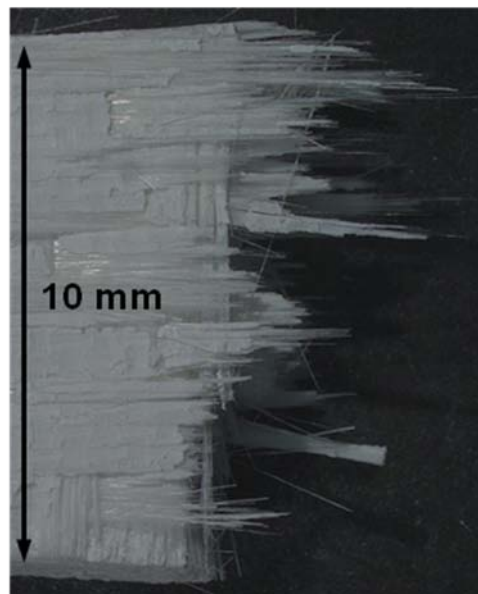


Figure 538. Fracture surface of the N720/AM specimen(2) tested in tension to failure with constant loading rate of 25MPa at 1100°C in steam.

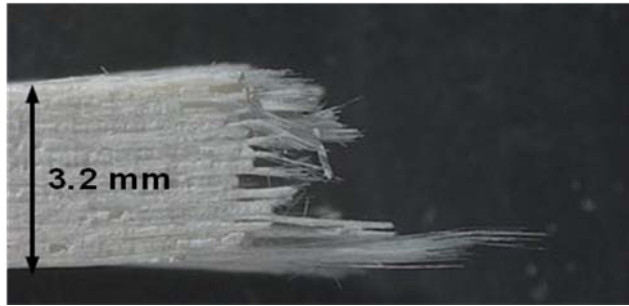


Figure 539. Fracture surface of the N720/AM specimen(2) tested in tension to failure with constant loading rate of 25MPa at 1100°C in steam (side view).

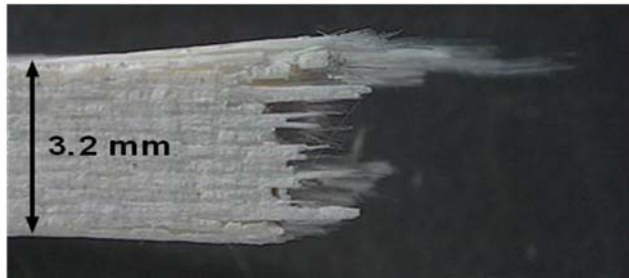


Figure 540. Fracture surface of the N720/AM specimen(2) tested in tension to failure with constant loading rate of 25MPa at 1100°C in steam (side view).

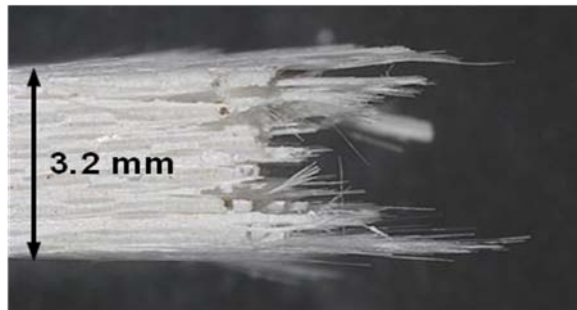


Figure 541. Fracture surface of the N720/AM specimen(2) tested in tension to failure with constant loading rate of 25MPa at 1100°C in steam (side view).

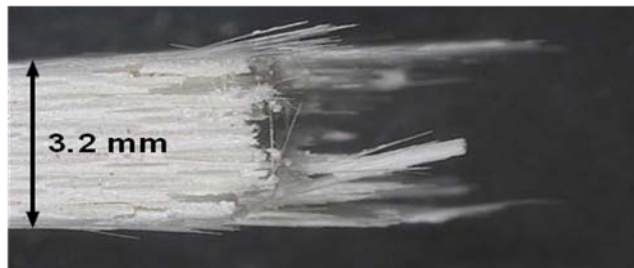


Figure 542. Fracture surface of the N720/AM specimen(2) tested in tension to failure with constant loading rate of 25MPa at 1100°C in steam (side view).

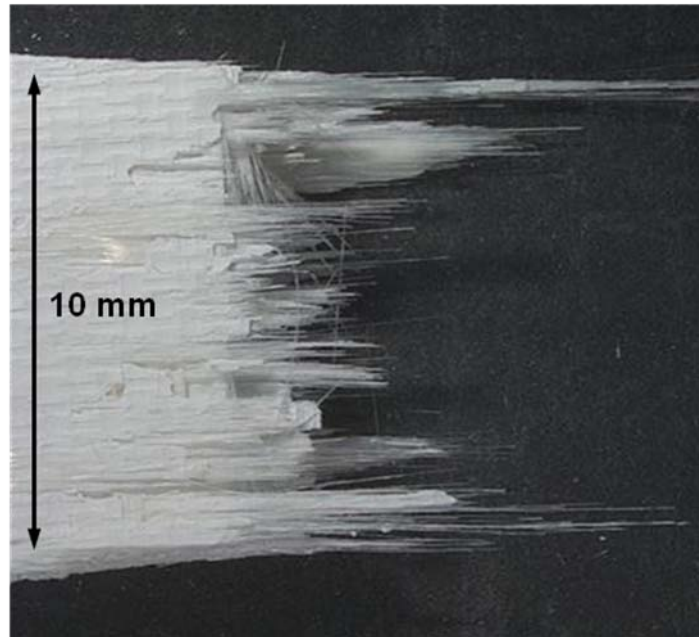


Figure 543. Fracture surface of the N720/AM specimen(2) tested in tension to failure with constant loading rate of 25MPa at 1100°C in steam (side view).

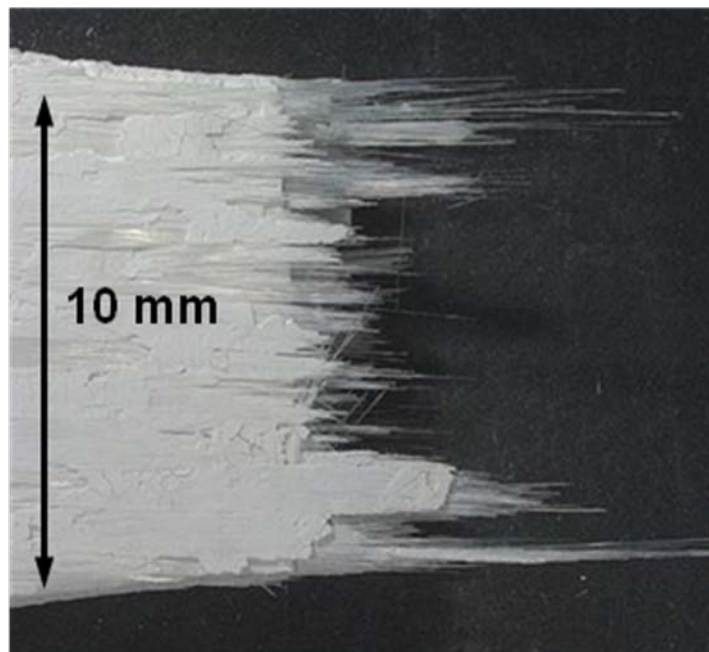


Figure 544. Fracture surface of the N720/AM specimen(2) tested in tension to failure with constant loading rate of 25MPa at 1100°C in steam (side view).

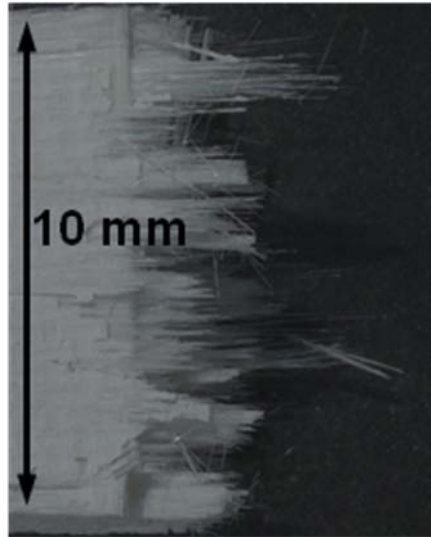


Figure 545. Fracture surface of the N720/AM specimen tested in tension to failure with constant loading rate of 0.0025MPa at 1100°C in steam.

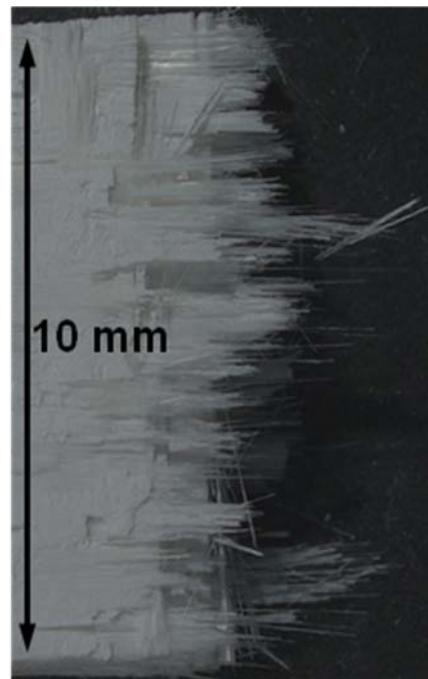


Figure 546. Fracture surface of the N720/AM specimen tested in tension to failure with constant loading rate of 0.0025MPa at 1100°C in steam.

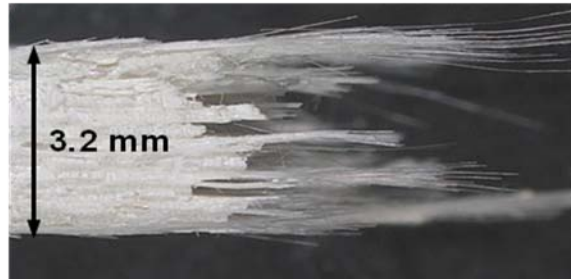


Figure 547. Fracture surface of the N720/AM specimen tested in tension to failure with constant loading rate of 0.0025MPa at 1100°C in steam (side view).

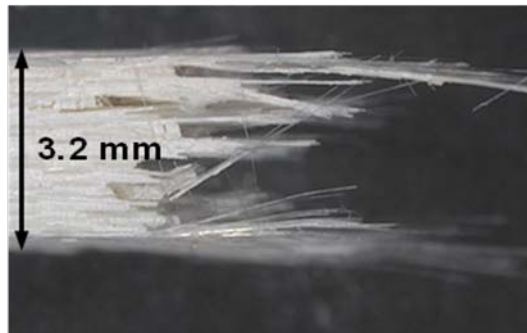


Figure 548. Fracture surface of the N720/AM specimen tested in tension to failure with constant loading rate of 0.0025MPa at 1100°C in steam (side view).



Figure 549. Fracture surface of the N720/AM specimen tested in tension to failure with constant loading rate of 0.0025MPa at 1100°C in steam (side view).

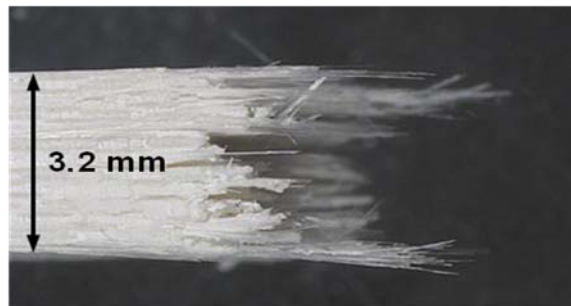


Figure 550. Fracture surface of the N720/AM specimen tested in tension to failure with constant loading rate of 0.0025MPa at 1100°C in steam (side view).

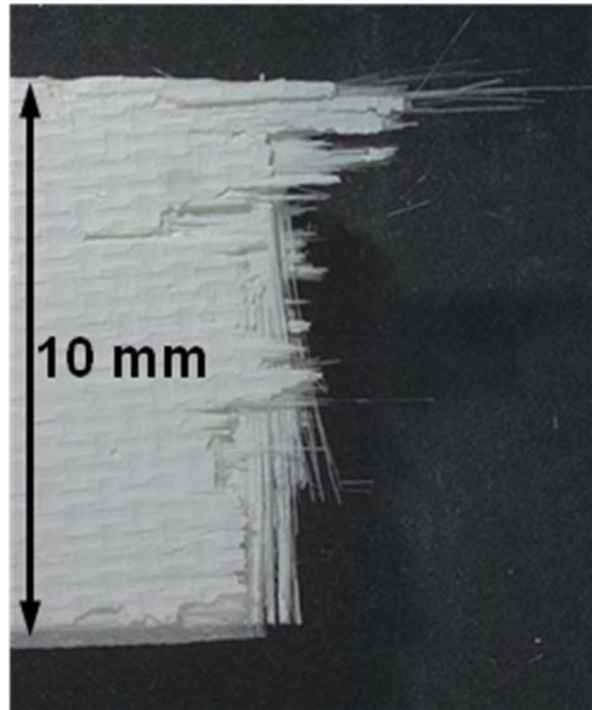


Figure 551. Fracture surface of the N720/AM specimen(2) tested in tension to failure with constant loading rate of 0.0025MPa at 1100°C in steam.

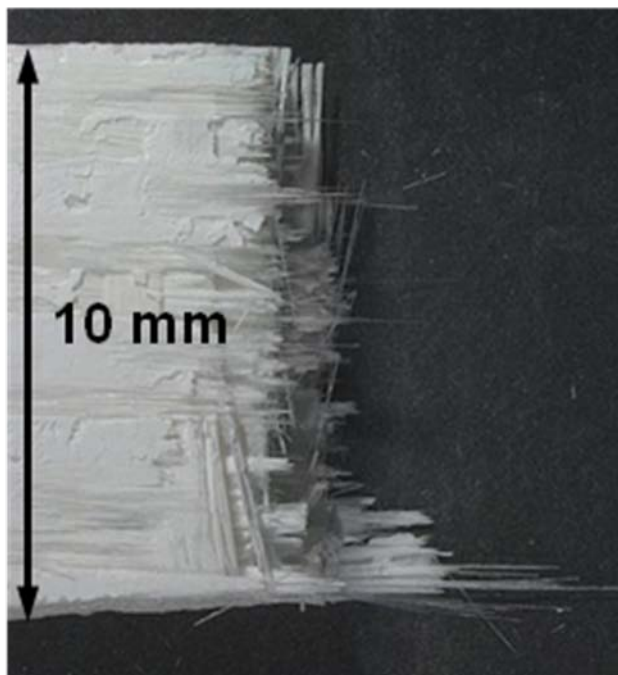


Figure 552. Fracture surface of the N720/AM specimen(2) tested in tension to failure with constant loading rate of 0.0025MPa at 1100°C in steam.

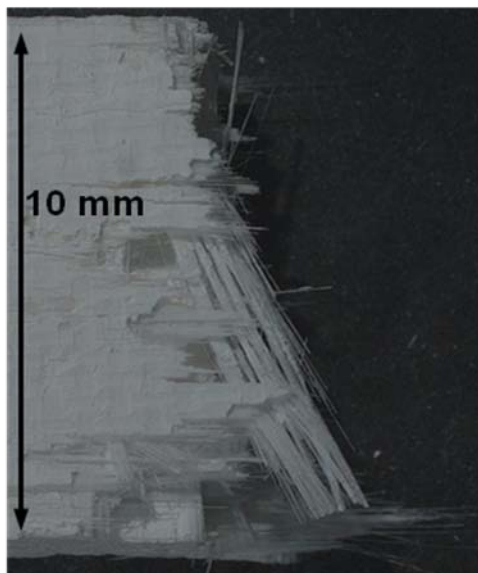


Figure 553. Fracture surface of the N720/AM specimen(2) tested in tension to failure with constant loading rate of 0.0025MPa at 1100°C in steam.

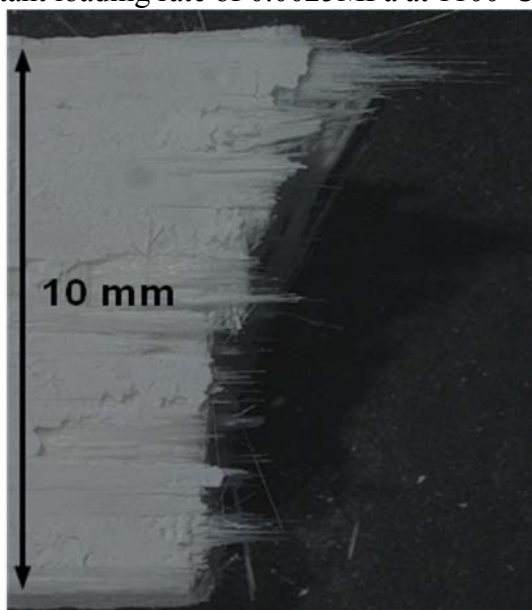


Figure 554. Fracture surface of the N720/AM specimen(2) tested in tension to failure with constant loading rate of 0.0025MPa at 1100°C in steam.

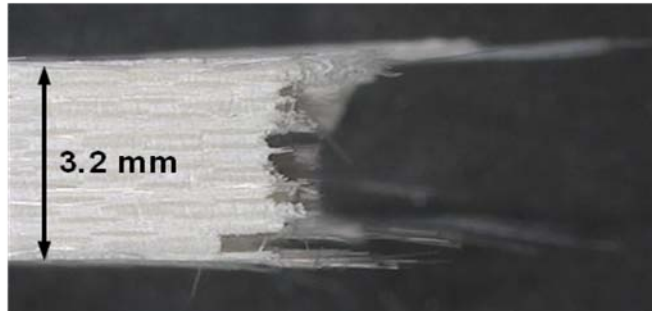


Figure 555. Fracture surface of the N720/AM specimen(2) tested in tension to failure with constant loading rate of 0.0025MPa at 1100°C in steam (side view).

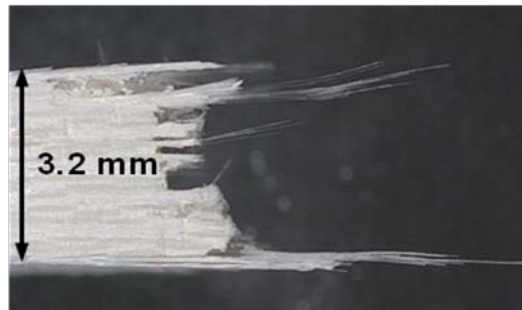


Figure 556. Fracture surface of the N720/AM specimen(2) tested in tension to failure with constant loading rate of 0.0025MPa at 1100°C in steam (side view).

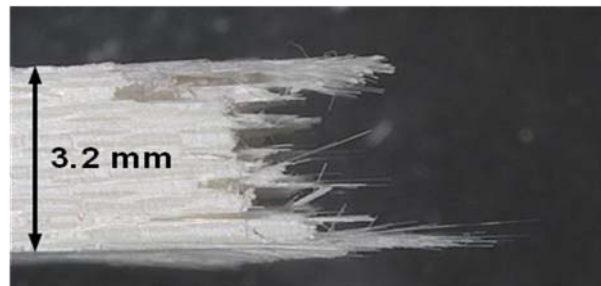


Figure 557. Fracture surface of the N720/AM specimen(2) tested in tension to failure with constant loading rate of 0.0025MPa at 1100°C in steam (side view).



Figure 558. Fracture surface of the N720/AM specimen(2) tested in tension to failure with constant loading rate of 0.0025MPa at 1100°C in steam (side view).

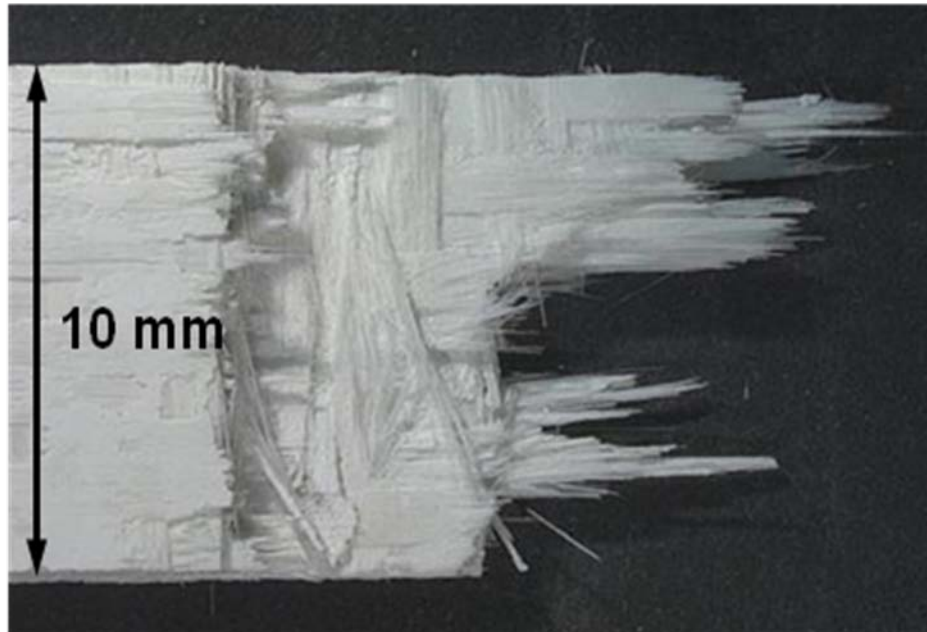


Figure 559. Fracture surface of the N720/AM specimen tested in creep at 109 MPa in laboratory air at 1100°C.

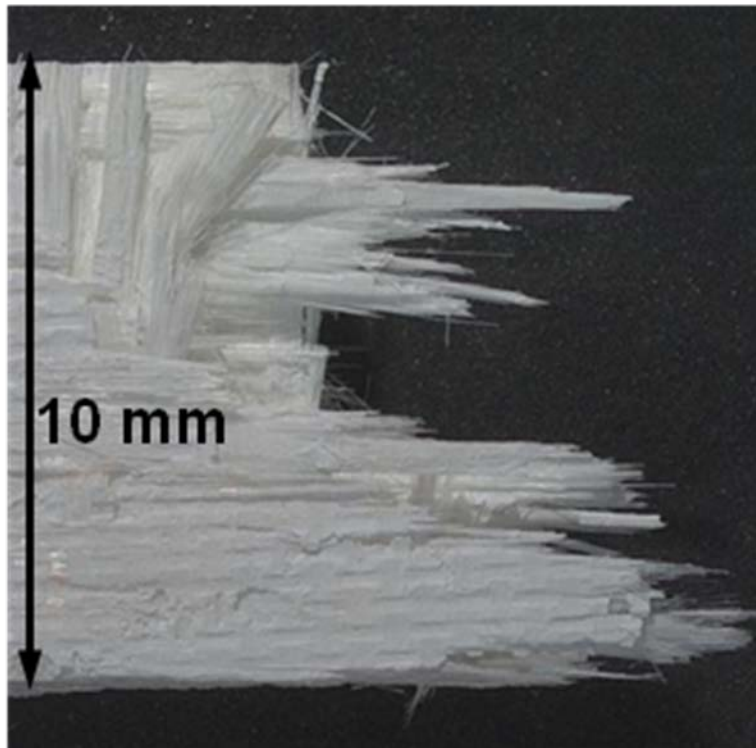


Figure 560. Fracture surface of the N720/AM specimen tested in creep at 109 MPa in laboratory air at 1100°C.

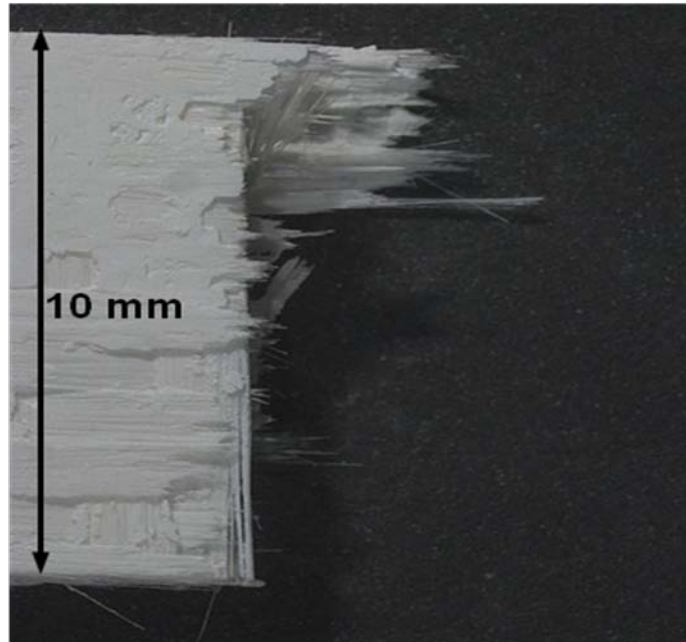


Figure 561. Fracture surface of the N720/AM specimen tested in creep at 109 MPa in laboratory air at 1100°C.

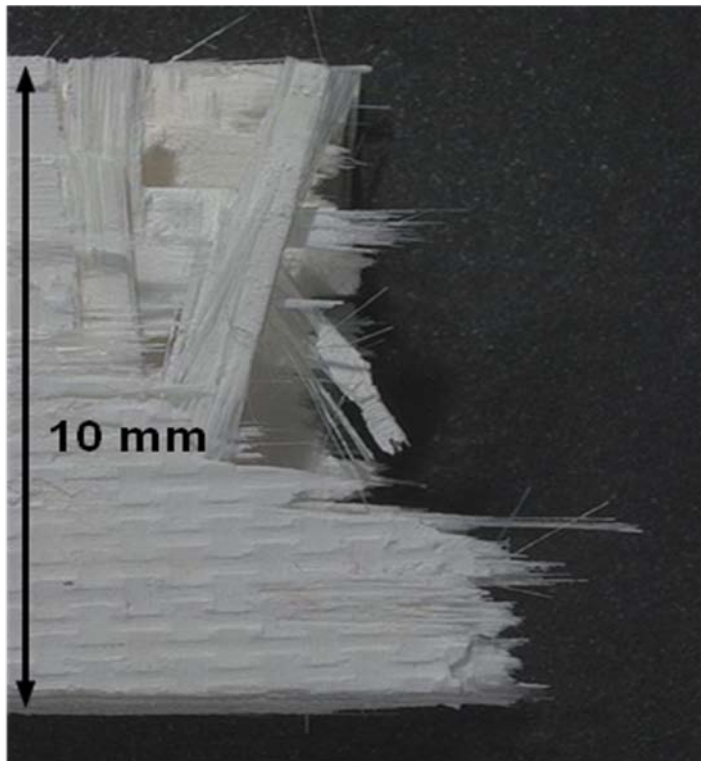


Figure 562. Fracture surface of the N720/AM specimen tested in creep at 109 MPa in laboratory air at 1100°C.



Figure 563. Fracture surface of the N720/AM specimen tested in creep at 109 MPa in laboratory air at 1100°C (side view).



Figure 564. Fracture surface of the N720/AM specimen tested in creep at 109 MPa in laboratory air at 1100°C (side view).



Figure 565. Fracture surface of the N720/AM specimen tested in creep at 109 MPa in laboratory air at 1100°C (side view).

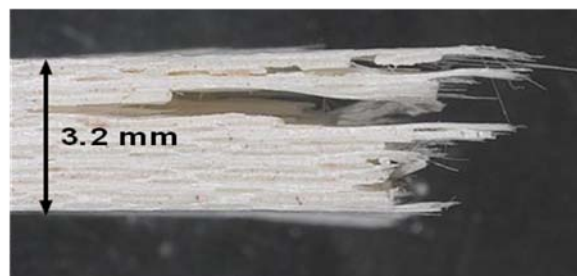


Figure 566. Fracture surface of the N720/AM specimen tested in creep at 109 MPa in laboratory air at 1100°C (side view).

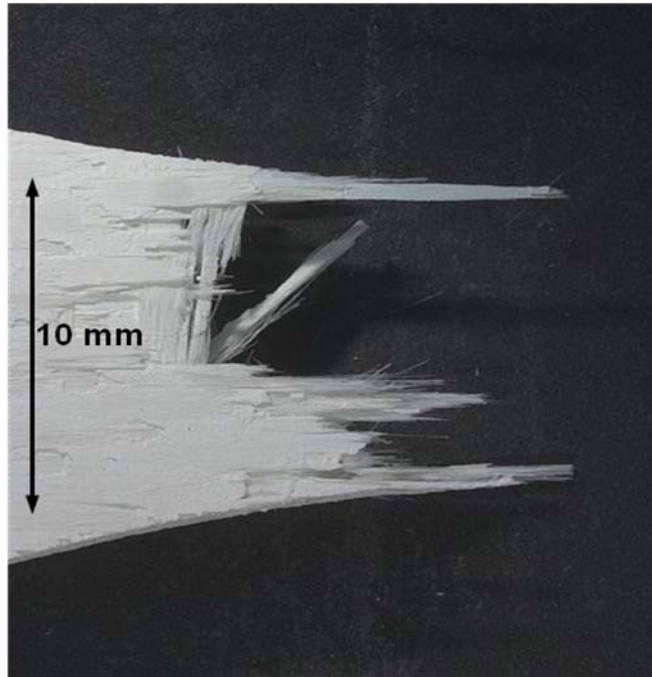


Figure 567. Fracture surface of the N720/AM specimen tested in creep at 131 MPa in laboratory air at 1100°C.

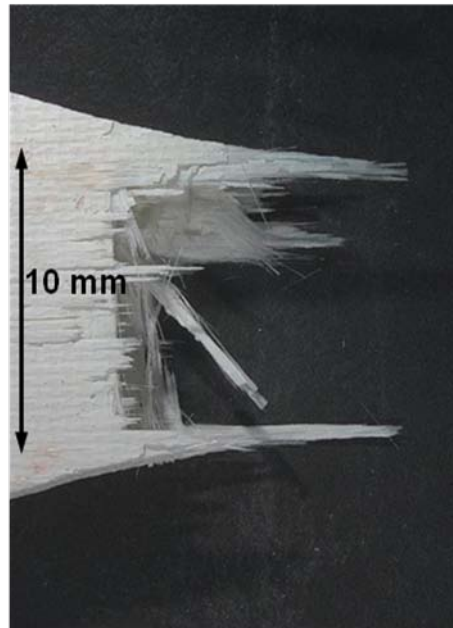


Figure 568. Fracture surface of the N720/AM specimen tested in creep at 131 MPa in laboratory air at 1100°C.

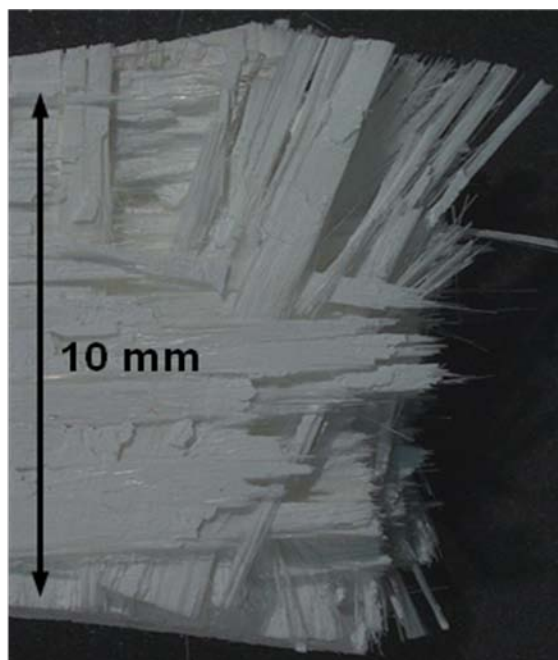


Figure 569. Fracture surface of the N720/AM specimen tested in creep at 131 MPa in laboratory air at 1100°C.

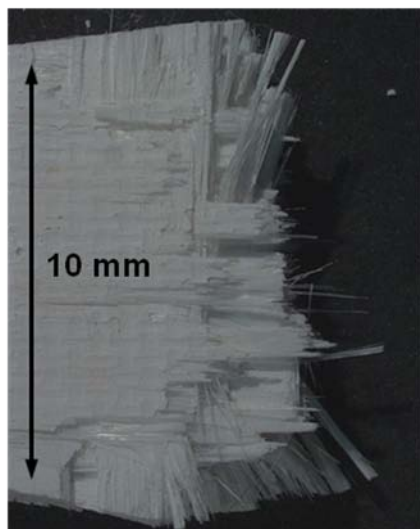


Figure 570. Fracture surface of the N720/AM specimen tested in creep at 131 MPa in laboratory air at 1100°C.



Figure 571. Fracture surface of the N720/AM specimen tested in creep at 131 MPa in laboratory air at 1100°C (side view).

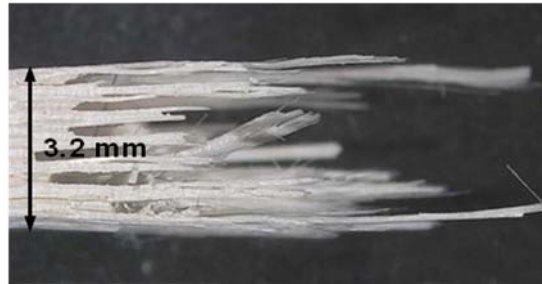


Figure 572. Fracture surface of the N720/AM specimen tested in creep at 131 MPa in laboratory air at 1100°C (side view).



Figure 573. Fracture surface of the N720/AM specimen tested in creep at 131 MPa in laboratory air at 1100°C (side view).



Figure 574. Fracture surface of the N720/AM specimen tested in creep at 131 MPa in laboratory air at 1100°C (side view).

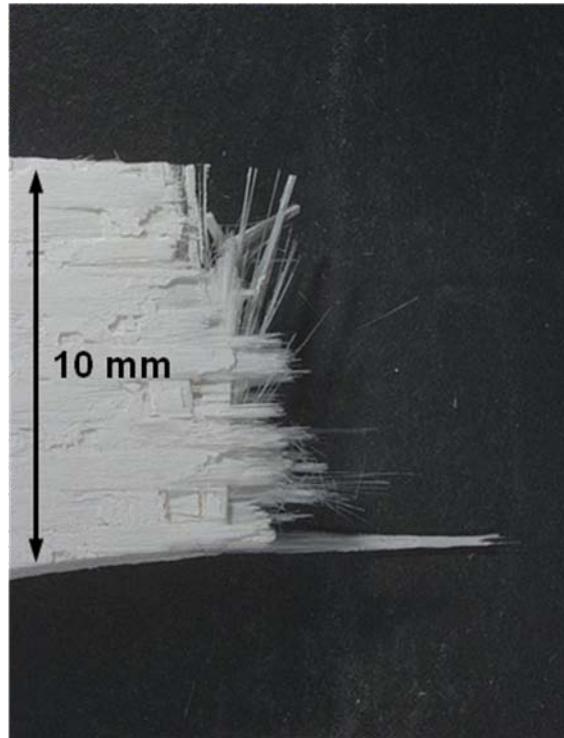


Figure 575. Fracture surface of the N720/AM specimen tested in creep at 131 MPa in steam at 1100°C.

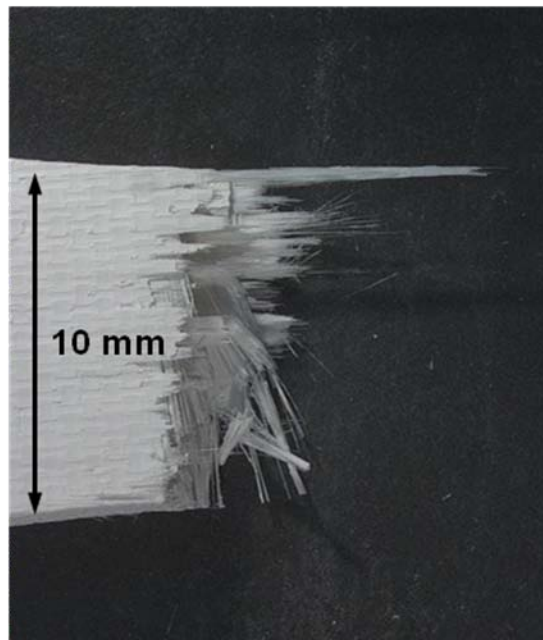


Figure 576. Fracture surface of the N720/AM specimen tested in creep at 131 MPa in steam at 1100°C.

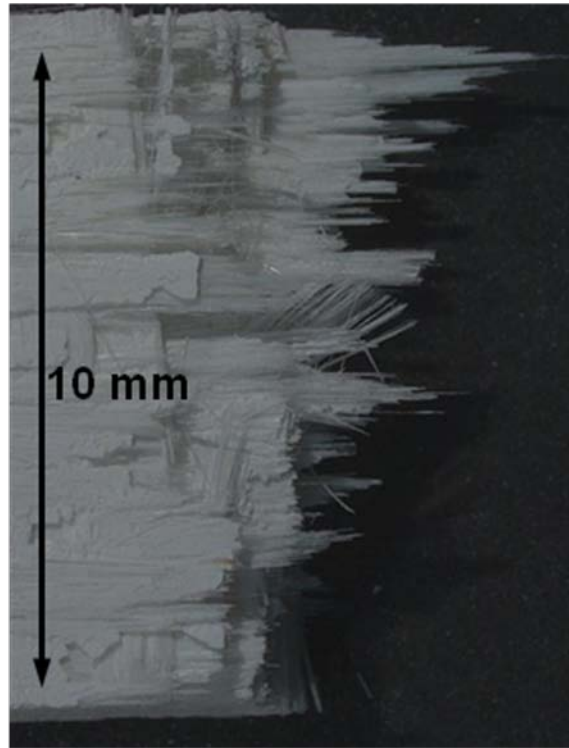


Figure 577. Fracture surface of the N720/AM specimen tested in creep at 131 MPa in steam at 1100°C.

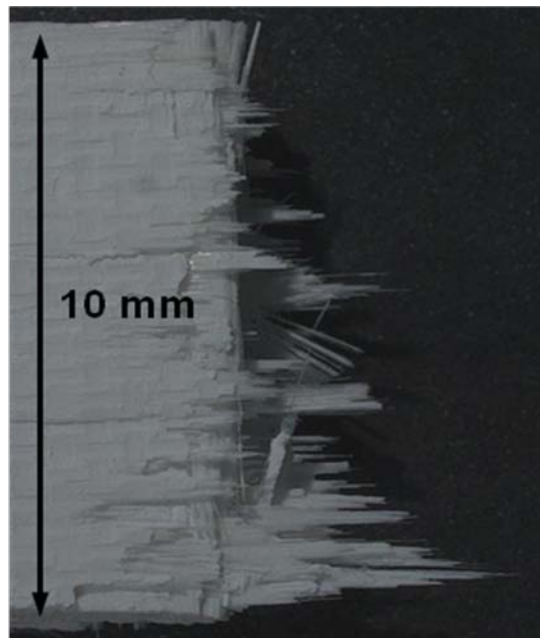


Figure 578. Fracture surface of the N720/AM specimen tested in creep at 131 MPa in steam at 1100°C.



Figure 579. Fracture surface of the N720/AM specimen tested in creep at 131 MPa in steam at 1100°C (side view).

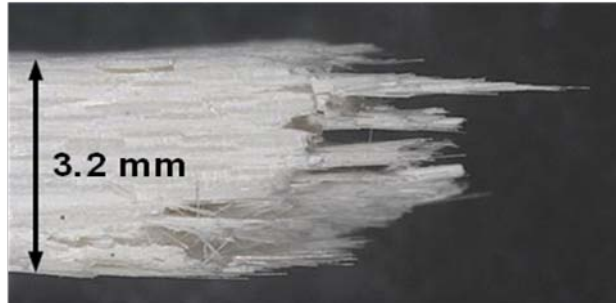


Figure 580. Fracture surface of the N720/AM specimen tested in creep at 131 MPa in steam at 1100°C (side view).

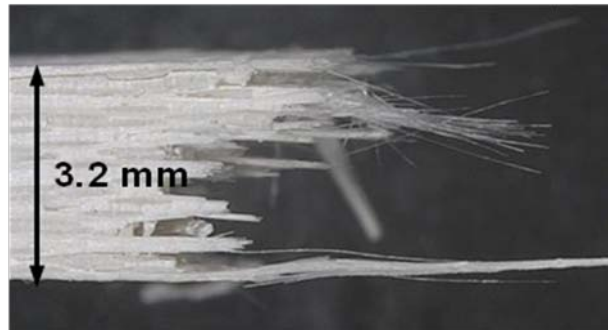


Figure 581. Fracture surface of the N720/AM specimen tested in creep at 131 MPa in steam at 1100°C (side view).

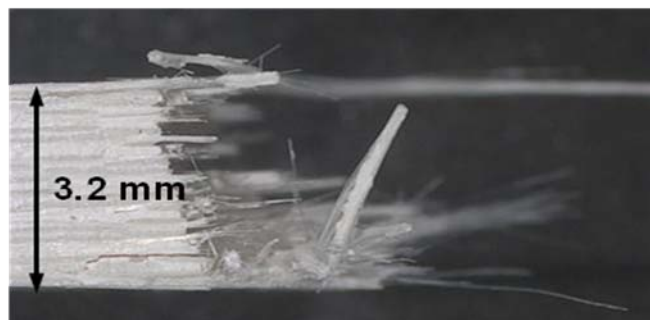


Figure 582. Fracture surface of the N720/AM specimen tested in creep at 131 MPa in steam at 1100°C (side view).

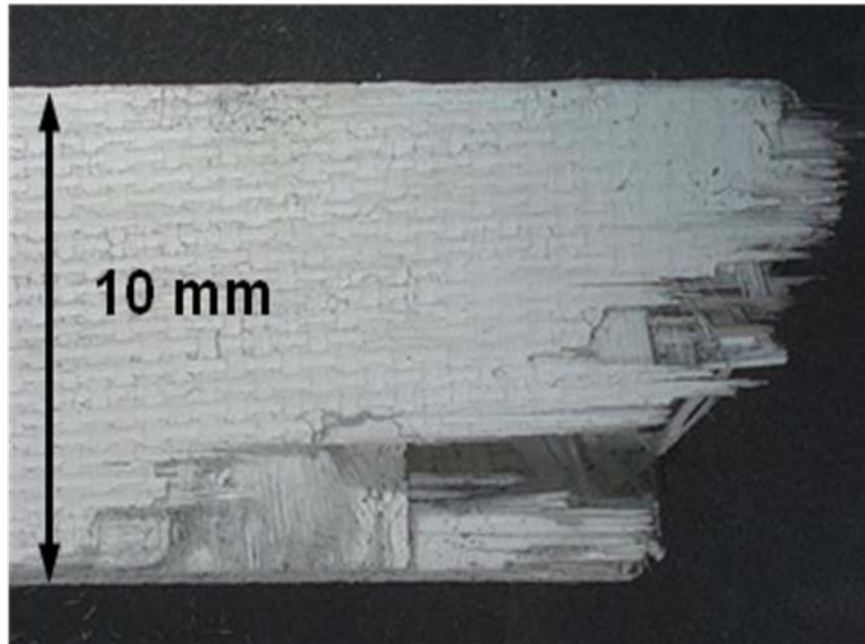


Figure 583. Fracture surface of the N720/AM specimen tested in creep at 109 MPa in steam at 1100°C.

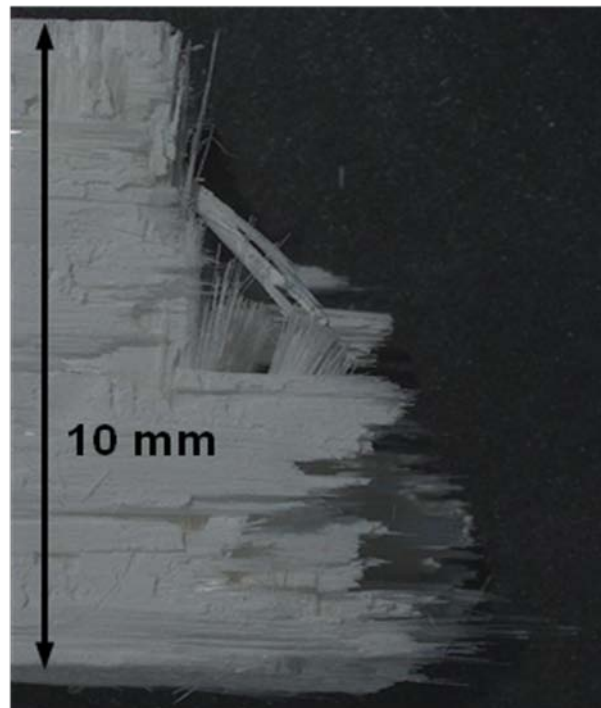


Figure 584. Fracture surface of the N720/AM specimen tested in creep at 109 MPa in steam at 1100°C.

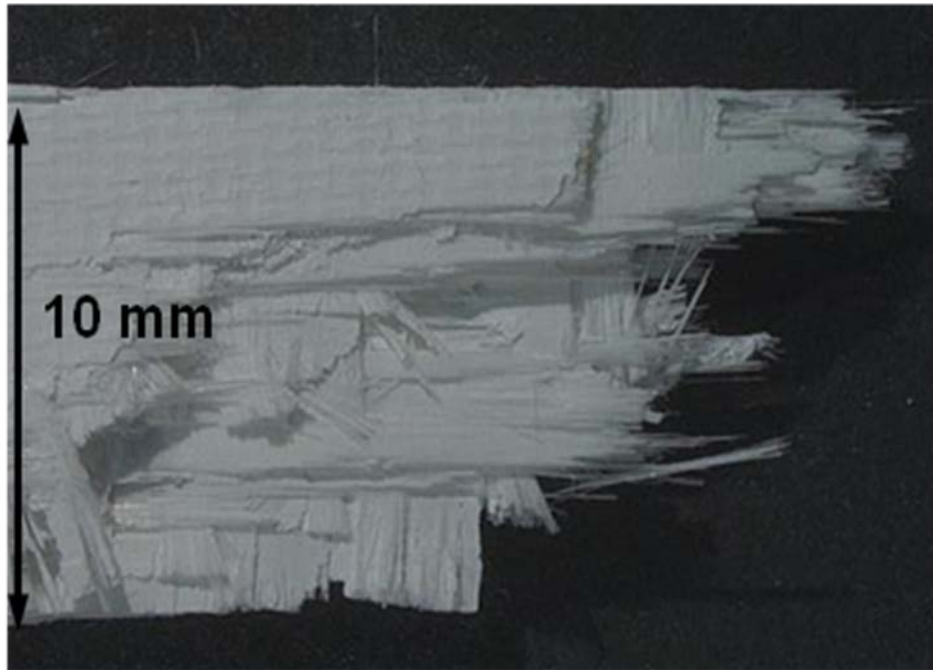


Figure 585. Fracture surface of the N720/AM specimen tested in creep at 109 MPa in steam at 1100°C.

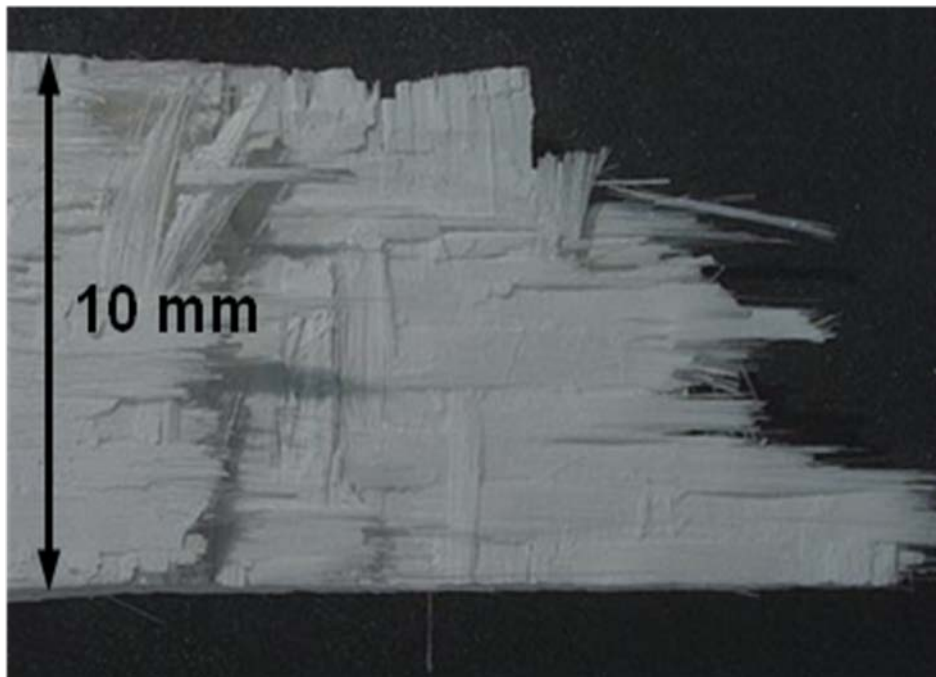


Figure 586. Fracture surface of the N720/AM specimen tested in creep at 109 MPa in steam at 1100°C.

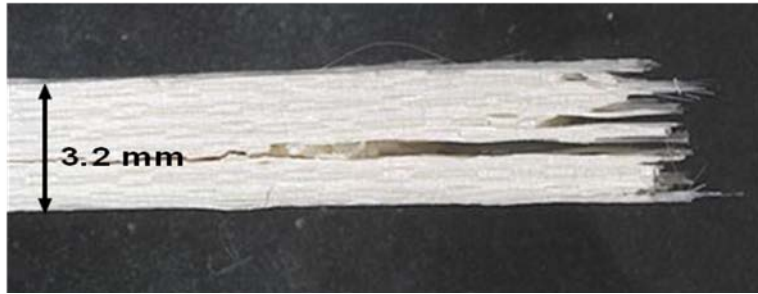


Figure 587. Fracture surface of the N720/AM specimen tested in creep at 109 MPa in steam at 1100°C (side view).



Figure 588. Fracture surface of the N720/AM specimen tested in creep at 109 MPa in steam at 1100°C (side view).



Figure 589. Fracture surface of the N720/AM specimen tested in creep at 109 MPa in steam at 1100°C (side view).



Figure 590. Fracture surface of the N720/AM specimen tested in creep at 109 MPa in steam at 1100°C (side view).

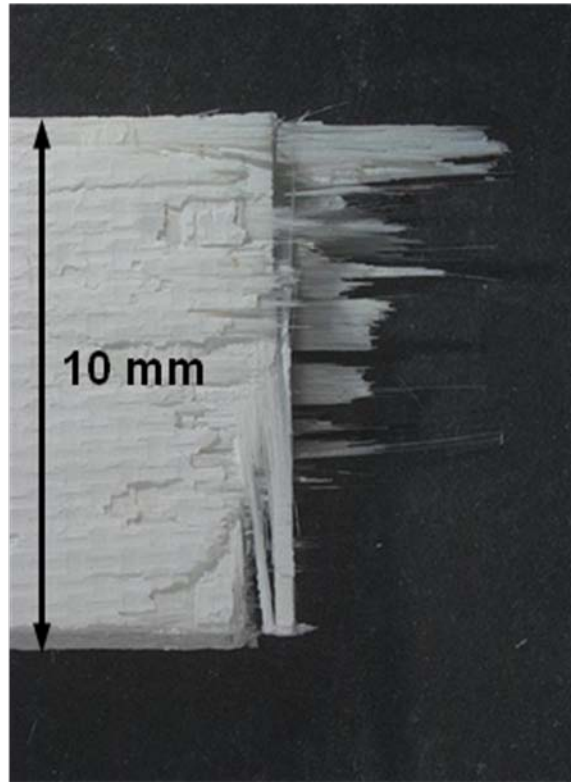


Figure 591. Fracture surface of the N720/AM specimen tested in creep at 87.5 MPa in steam at 1100°C.

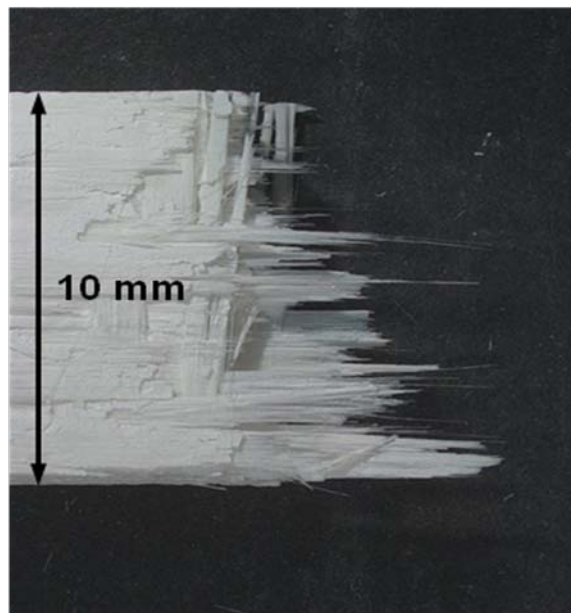


Figure 592. Fracture surface of the N720/AM specimen tested in creep at 87.5 MPa in steam at 1100°C.

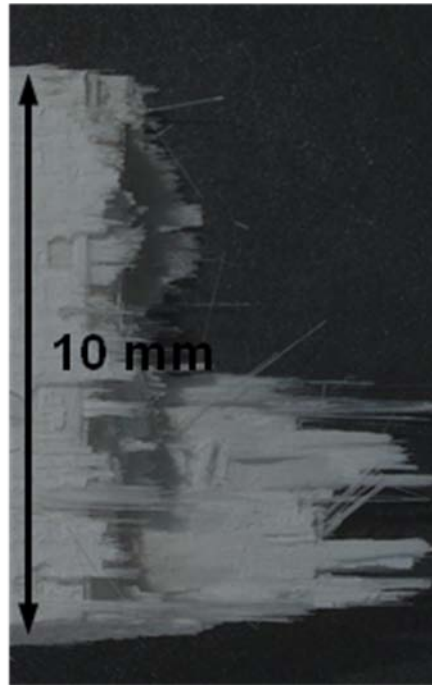


Figure 593. Fracture surface of the N720/AM specimen tested in creep at 87.5 MPa in steam at 1100°C.

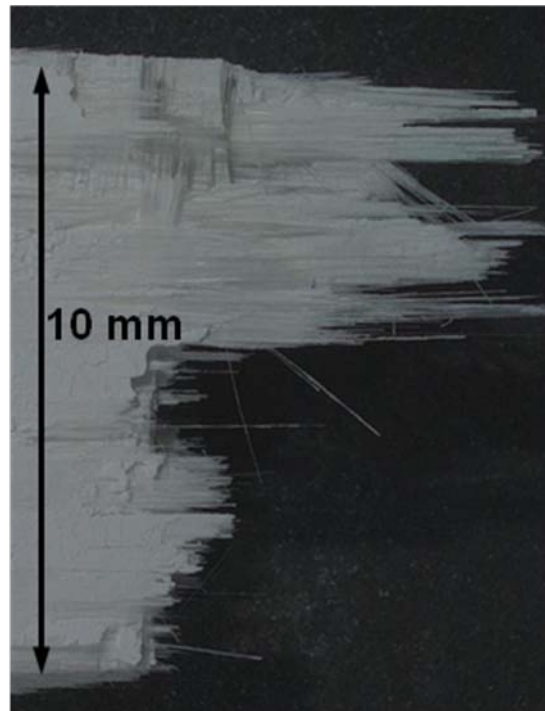


Figure 594. Fracture surface of the N720/AM specimen tested in creep at 87.5 MPa in steam at 1100°C.



Figure 595. Fracture surface of the N720/AM specimen tested in creep at 87.5 MPa in steam at 1100°C (side view).



Figure 596. Fracture surface of the N720/AM specimen tested in creep at 87.5 MPa in steam at 1100°C (side view).

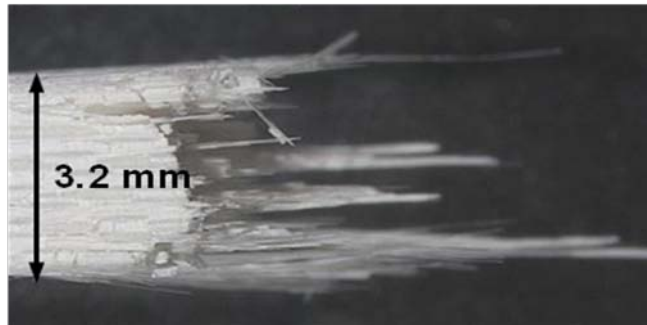


Figure 597. Fracture surface of the N720/AM specimen tested in creep at 87.5 MPa in steam at 1100°C (side view).

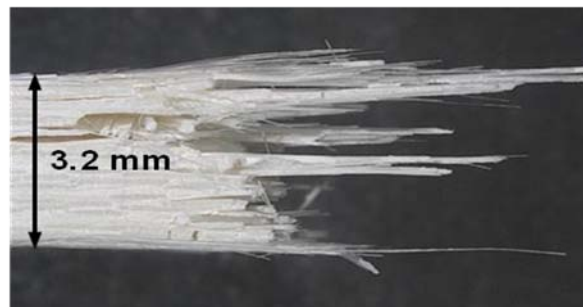


Figure 598. Fracture surface of the N720/AM specimen tested in creep at 87.5 MPa in steam at 1100°C (side view).

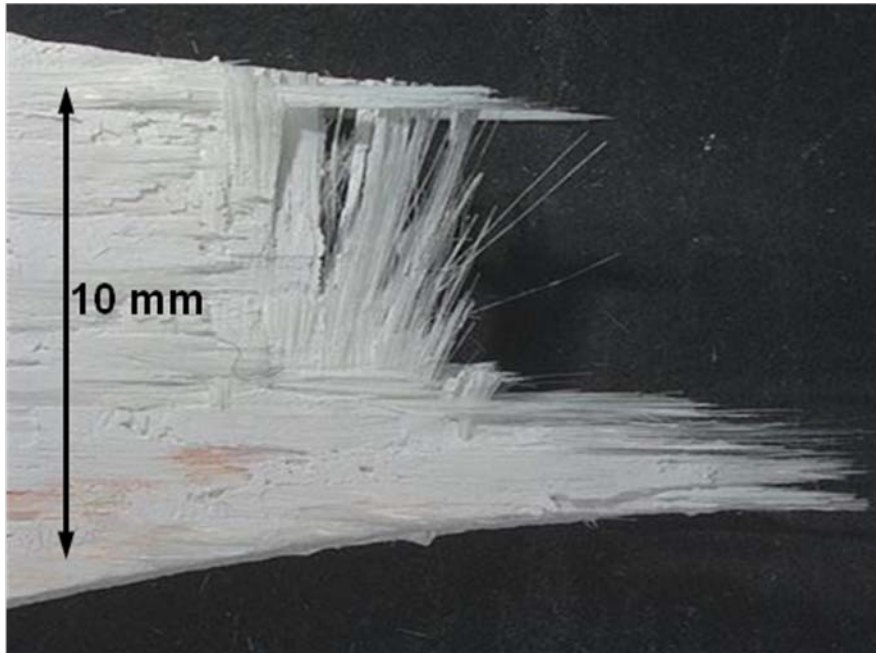


Figure 599. Fracture surface of the N720/AM specimen tested in creep at 131 MPa in steam at 1000°C.

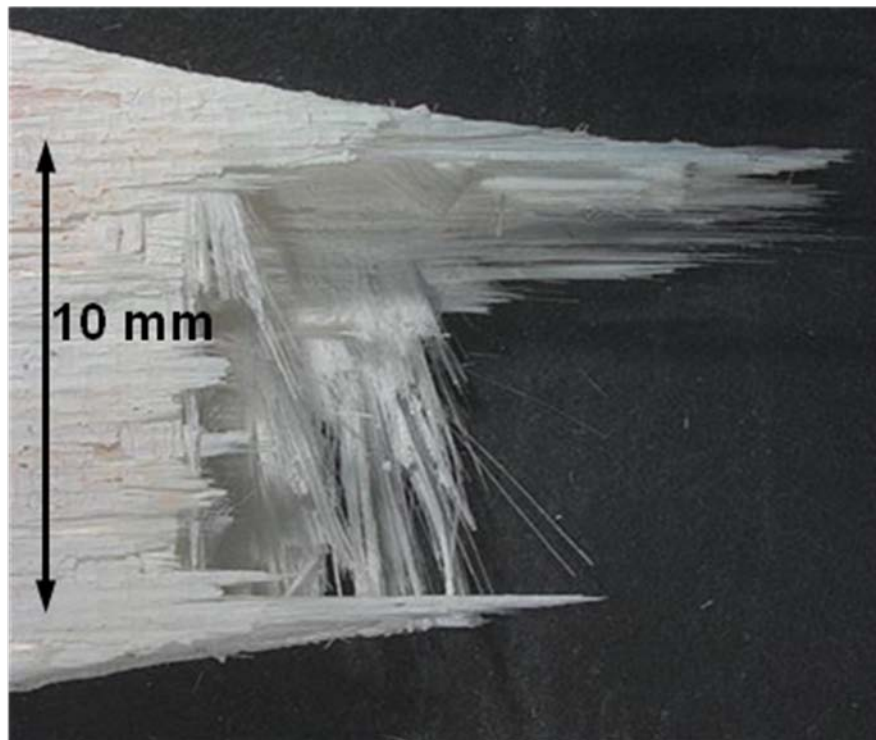


Figure 600. Fracture surface of the N720/AM specimen tested in creep at 131 MPa in steam at 1000°C.

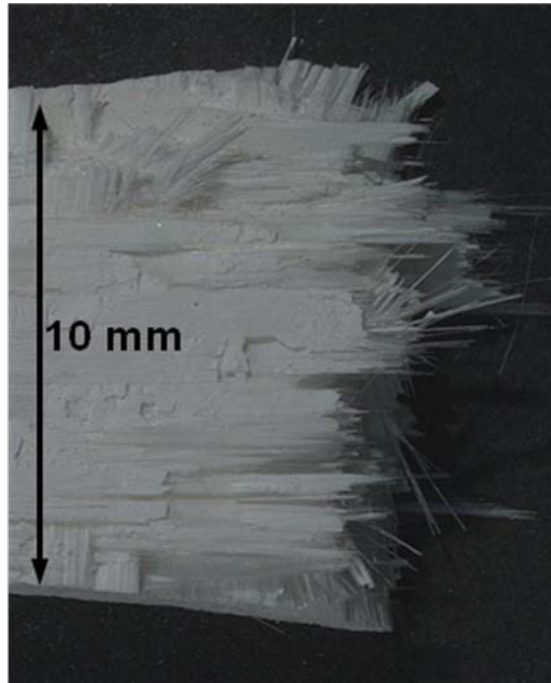


Figure 601. Fracture surface of the N720/AM specimen tested in creep at 131 MPa in steam at 1000°C.

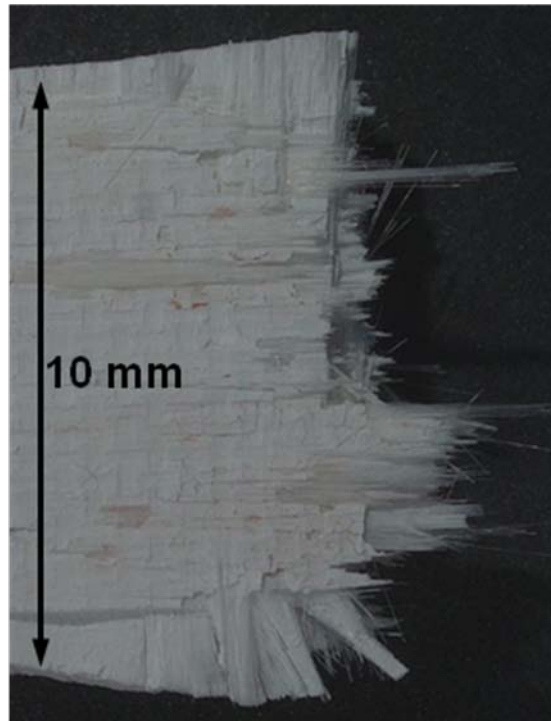


Figure 602. Fracture surface of the N720/AM specimen tested in creep at 131 MPa in steam at 1000°C.

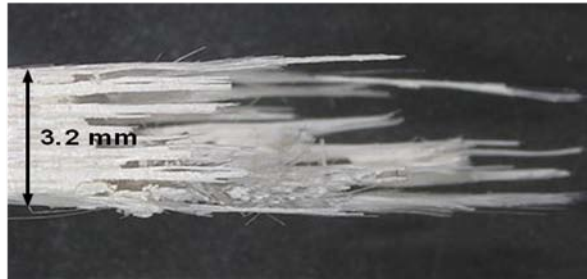


Figure 603. Fracture surface of the N720/AM specimen tested in creep at 131 MPa in steam at 1000°C (side view).



Figure 604. Fracture surface of the N720/AM specimen tested in creep at 131 MPa in steam at 1000°C (side view).



Figure 605. Fracture surface of the N720/AM specimen tested in creep at 131 MPa in steam at 1000°C (side view).



Figure 606. Fracture surface of the N720/AM specimen tested in creep at 131 MPa in steam at 1000°C (side view).

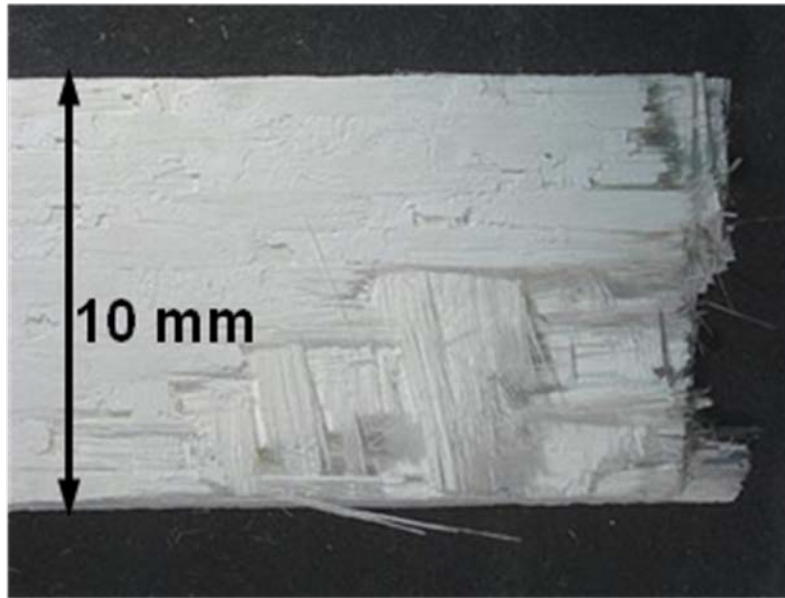


Figure 607. Fracture surface of the N720/AM specimen tested in creep at 140 MPa in steam at 1000°C.

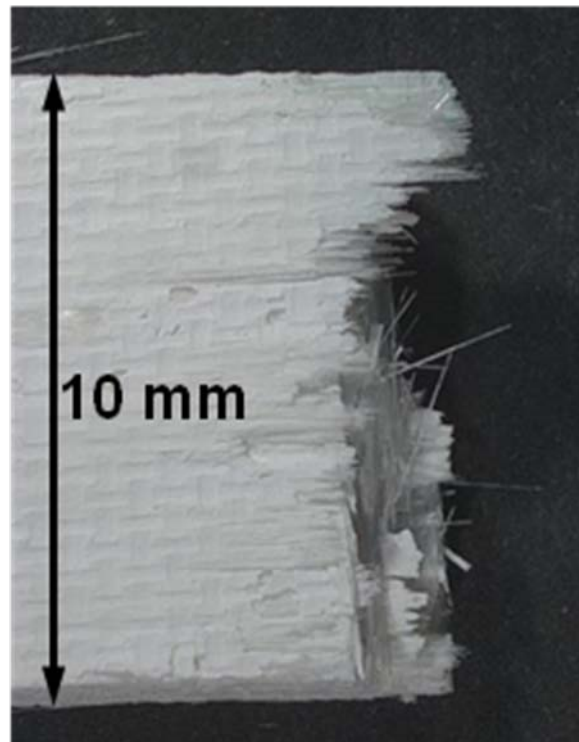


Figure 608. Fracture surface of the N720/AM specimen tested in creep at 140 MPa in steam at 1000°C.

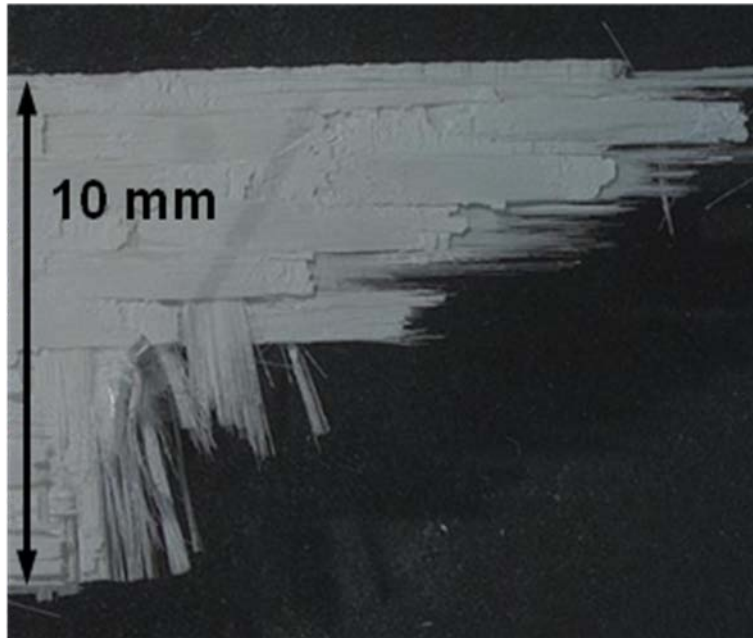


Figure 609. Fracture surface of the N720/AM specimen tested in creep at 140 MPa in steam at 1000°C.

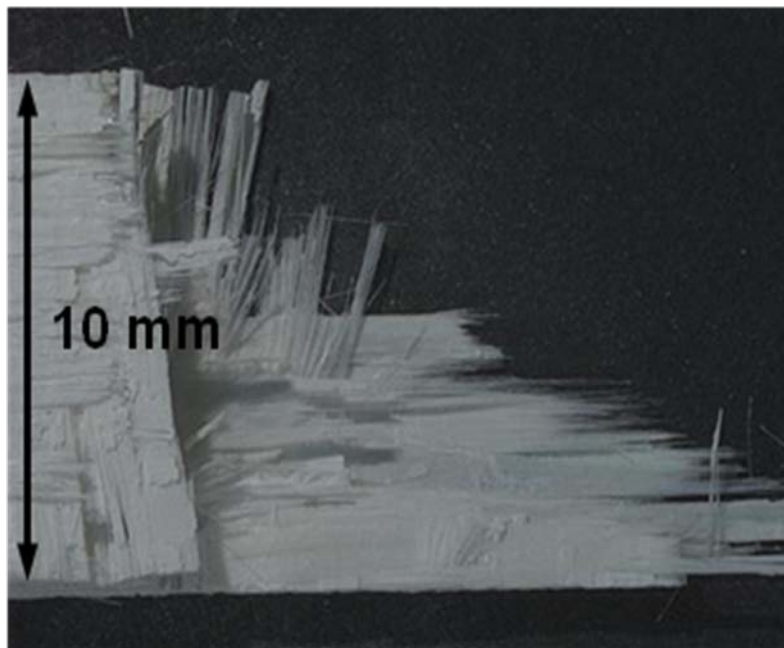


Figure 610. Fracture surface of the N720/AM specimen tested in creep at 140 MPa in steam at 1000°C.

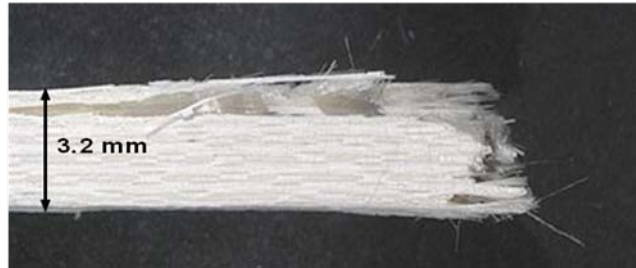


Figure 611. Fracture surface of the N720/AM specimen tested in creep at 140 MPa in steam at 1000°C (side view).

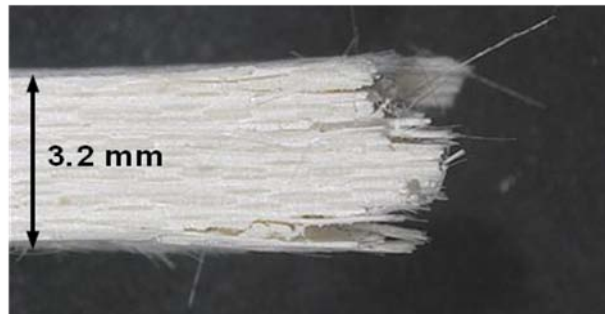


Figure 612. Fracture surface of the N720/AM specimen tested in creep at 140 MPa in steam at 1000°C (side view).

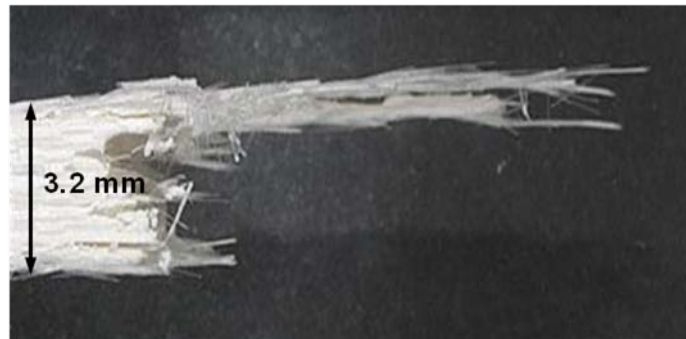


Figure 613. Fracture surface of the N720/AM specimen tested in creep at 140 MPa in steam at 1000°C (side view).

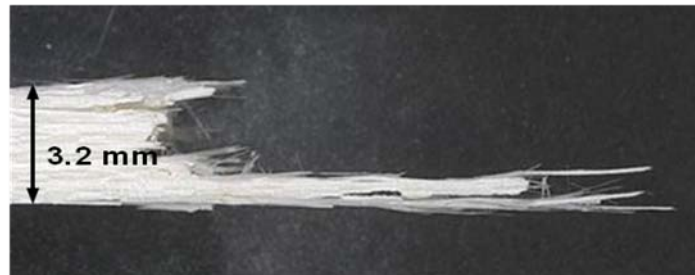


Figure 614. Fracture surface of the N720/AM specimen tested in creep at 140 MPa in steam at 1000°C (side view).

Bibliography

1. Narottam P .Bansal, *Handbook of ceramic composites*, Kluwer Academic Publishers
2. L.P.Zawada, J.STaehler, S.Steel, J.Am. Ceram. Soc. 86(8) (2003) 1282-1291
3. Chawla, K.K. *Ceramic Matrix Composites* (2nd Edition). Boston: Kluwer Academic Publishers, 2003.
4. Ralf Riedel and Li-Wei Chen, *Ceramics Science and Technology* (Volume 1 Structures).
5. Saruhan Bilge, *Oxide-based fiber-reinforced ceramic-matrix-composites: principles and materials* : Boston: Kluwer Academic Publishers, c2003
6. Chawla, K. K. *Ceramic Matrix Composites*. London: Chapman and Hall, 1993.
7. Parlier, M. and Ritti, M.H. "State of the art and perspectives for oxide/oxide composites," *Aerospace Science and Technology*, 7: 211-221,(2003).
8. LaRochelle, K.J. *Tensile Stress Rupture Behavior of a Woven Ceramic Matrix Composite in Humid Environments at Intermediate Temperatures*. Ph.D. dissertation, AFIT/DS/ENY/05-01. School of Engineering and Management, Air Force Institute of Technology (AU), Wright-Patterson AFB, OH March 2005.
9. Lavaste, V., Berger, M.H. and Bunsell, A.R. *A comparison of high temperature behaviour and structural modifications of continuous alumina fibers*. Ceramics Adding the Value, International Ceramic Conference, Melbourne, Australia. CSIRO Publications, 1992
10. Ruggles-Wrenn, M.B, Koutsoukos, P, Baeck, S.S. "Effects of Environment on Creep Behavior of Two Oxide-Oxide Ceramic Matrix Composites at 1200°C," *Journal of Materials Science*, Vol. 43, No. 20, 2008, pp. 6734-6746.
11. Tressler, R.E. and DiCarlo, J.A. (1995) *Creep and rupture of advanced ceramic reinforcements*. Ceram. Trans., 57, 141-155.
12. Baker, A., Dutton, S., Kelly, D. *Composite Materials for Aircraft Structures* (Second Edition). Virginia: AIAA, 2004.

13. Mehrman, J.M., Ruggles-Wrenn, M.B., and Baek, S.S. "Influence of Hold Times on the Elevated-Temperature Fatigue Behavior of an Oxide-Oxide Ceramic Composite in Air and Steam Environment", *Composites Science and Technology*, 67 (2007) 1425-1438.
14. Ohnabe, H., Masaki, S., Onozuka, M., Miyahara, K., Sasa, T. "Potential application of ceramic matrix composites to aero-engine components," *Composites: Part A, Applied Science and Manufacturing* 30: 489-496 (1999).
15. Schmidt, S., Beyer, S., Knabe, H., Immich, H., Mestring, R., and Gessler, A. "Advanced ceramic matrix composite materials for current and future propulsion technology applications," *Acta Astronautica*, 55: 409-420, 2004.
16. Genelin, Christopher L. *Effect of Environment on Creep Behavior of Nextel™720/Alumina-Mullite Ceramic Composite at 1200 °C*, MS thesis, AFIT/GAE/ENY/08-M11, School of Engineering and Management, Air Force Institute of Technology (AU), Wright-Patterson AFB, OH, March 2008.
17. Harlan, Lee B. *Creep-Rupture Behavior of an Oxide/Oxide Ceramic Matrix Composite at Elevated Temperatures in Air and Steam Environments*. MS thesis, AFIT/GA/ENY/05-M05. School of Engineering and Management, Air Force Institute of Technology (AU), Wright-Patterson AFB OH, March 2005.
18. Braun, Jason C. *Effects of Temperature and Environment on Creep Behavior of an Oxide-Oxide Ceramic Matrix Composite*. MS thesis, AFIT/GAE/ENY/07-M04, School of Engineering and Management, Air Force Institute of Technology (AU), Wright-Patterson AFB, OH, March 2007.
19. M. B. Ruggles-Wrenn and J. C. Braun, "Effects of Steam Environment on Creep Behavior of Nextel™720/Alumina Ceramic Composite at Elevated Temperature", *Materials Science and Engineering A*, Vol. 497, No. 1-2, 2008, pp. 101-110.
20. Siegert, Gregory T. *Effect of Environment on Creep Behavior of an Oxide/Oxide CFCC with ±45° Fiber Orientation*, MS thesis, AFIT/GAE/ENY/06-J15, School of Engineering and Management, Air Force Institute of Technology (AU), Wright-Patterson AFB, OH, June 2006.
21. Kaya, C., Butler, E.G., Selcuk, A., Boccaccini, A.R., and Lewis, M.H. "Mullite (Nextel™ 720) fibre-reinforced mullite matrix composites exhibiting favourable thermomechanical properties," *Journal of the European Ceramic Society*, 22: 2333-2342 (2002).

22. M.B. Ruggles-Wrenn and C.L. Genelin, “Creep of Nextel™720/alumina-mullite ceramic at 1200 °C in air, argon, and steam”, *Composites Science and Technology*, Vol. 69/2008, pp. 663-669.
23. http://en.wikipedia.org/wiki/Scanning_Electron_Microscope
24. M. B. Ruggles-Wrenn, G. T. Siegert, S. S. Baeck, “Creep Behavior of Nextel™720/Alumina Ceramic Composite with $\pm 45^\circ$ Fiber Orientation at 1200 °C”, *Composites Science and Technology*, Vol. 68, No. 6, 2008, pp. 1588-1595.

Vita

1st Lt. Tolga KUTSAL is an officer in Turkish Air Force. He graduated from Kocaeli Korfez Science High School in 1998. In same year he attended Turkish Air Force Academy and graduated as a 2nd Lt. with a Bachelor of Science degree in Aeronautical Engineering in 2002.

He attended pilot training school at 2nd Main Jet Base in Cigli, Izmir. He graduated as a jet pilot in 2004. He was trained with F-5 jet aircraft at 3rd Main Jet Base. Following that he took F-16 Jet Training Course at Oncel Training Squadron, 4th Main Jet Base, Ankara. He graduated as a war-ready fighter pilot at 2005. He was assigned to 151st SEAD Squadron (Vultures) where he flew for almost two years as a wingman before attending Graduate School of Engineering and Management, AFIT for master's degree program. Upon graduation, he will, again, be assigned to 151st fighter squadron in Merzifon.

REPORT DOCUMENTATION PAGE			Form Approved OMB No. 0704-0188		
<p>The public reporting burden for this collection of information is estimated to average 1 hour per response, including the time for reviewing instructions, searching existing data sources, gathering and maintaining the data needed, and completing and reviewing the collection of information. Send comments regarding this burden estimate or any other aspect of this collection of information, including suggestions for reducing this burden to Department of Defense, Washington Headquarters Services, Directorate for Information Operations and Reports (0704-0188), 1215 Jefferson Davis Highway, Suite 1204, Arlington, VA 22202-4302. Respondents should be aware that notwithstanding any other provision of law, no person shall be subject to any penalty for failing to comply with a collection of information if it does not display a currently valid OMB control number.</p> <p>PLEASE DO NOT RETURN YOUR FORM TO THE ABOVE ADDRESS.</p>					
1. REPORT DATE (DD-MM-YYYY) 26-03-2009		2. REPORT TYPE Master's Thesis		3. DATES COVERED (From — To) SEP 2008 - MAR 2009	
4. TITLE AND SUBTITLE Effect of Steam Environment on Creep Behavior of Nextel720/Alumina-Mullite Ceramic Matrix Composite at Elevated Temperature			5a. CONTRACT NUMBER		
			5b. GRANT NUMBER		
			5c. PROGRAM ELEMENT NUMBER		
6. AUTHOR(S) Tolga KUTSAL, 1 ST LT, TUAF			5d. PROJECT NUMBER ENY 08-107		
			5e. TASK NUMBER		
			5f. WORK UNIT NUMBER		
7. PERFORMING ORGANIZATION NAME(S) AND ADDRESS(ES) Air Force Institute of Technology Graduate School of Engineering and Management (AFIT/ENY) 2950 Hobson Way WPAFB OH 45433-7765			8. PERFORMING ORGANIZATION REPORT NUMBER AFIT/GSS/ENY/09-M03		
9. SPONSORING / MONITORING AGENCY NAME(S) AND ADDRESS(ES) Dr. Geoff E. Fair Air Force Research Laboratories (AFRL/RXLN) 2230 Tenth Street, Bldg 655 WPAFB OH 45433-7818			10. SPONSOR/MONITOR'S ACRONYM(S) AFRL/RXLN		
			11. SPONSOR/MONITOR'S REPORT NUMBER(S)		
12. DISTRIBUTION / AVAILABILITY STATEMENT APPROVED FOR PUBLIC RELEASE; DISTRIBUTION UNLIMITED					
13. SUPPLEMENTARY NOTES					
14. ABSTRACT The tensile creep behavior of an oxide-oxide ceramic matrix composite (CMC) was investigated at 1000 and 1100°C in laboratory air and steam. The oxide-oxide CMC studied in this research was Nextel TM 720/alumina-mullite (N720/AM). The composite consists of N720/ fibers with 0°/90° fiber orientation and a porous alumina-mullite matrix. Tensile-strain behavior was investigated and tensile properties measured at 900, 1000 and 1100°C. The effect of loading rate on tensile properties of N720/AM ceramic matrix composite at 1100°C in steam was also examined. Creep-rupture tests were performed at 1100°C in laboratory air and steam, and at 1000°C only in steam.					
15. SUBJECT TERMS Ceramic Matrix Composite (CMC), Nextel 720, Tensile, Creep, Air, Steam, Oxide-Oxide					
16. SECURITY CLASSIFICATION OF:			17. LIMITATION OF ABSTRACT	18. NUMBER OF PAGES	19a. NAME OF RESPONSIBLE PERSON
a. REPORT	b. ABSTRACT	c. THIS PAGE			19b. TELEPHONE NUMBER (Include Area Code)
U	U	U	UU	426	Dr. Marina B. Ruggles-Wrenn (937) 255-3636, ext4641; Marina.ruggles-wrenn@afit.edu